Frontiers in Orthopaedic Biomechanics

Cheng-Kung Cheng
Savio L-Y. Woo
Editors

Springer

Frontiers in Orthopaedic Biomechanics

Cheng-Kung Cheng • Savio L-Y. Woo
Editors

Frontiers in Orthopaedic Biomechanics

Springer

Editors
Cheng-Kung Cheng
School of Biomedical Engineering
Shanghai Jiao Tong University
Shanghai
China

Savio L-Y. Woo
Musculoskeletal Research Center,
Department of Bioengineering
University of Pittsburgh
Pittsburgh, PA
USA

ISBN 978-981-15-3158-3 ISBN 978-981-15-3159-0 (eBook)
https://doi.org/10.1007/978-981-15-3159-0

This Springer imprint is published by the registered company Springer Nature Singapore Pte Ltd.
The registered company address is: 152 Beach Road, #21-01/04 Gateway East, Singapore 189721, Singapore

Foreword

A good understanding of biomechanics is beneficial for orthopaedic surgeons as the majority of the diseases being treated start when the normal biomechanical environment in the body is disturbed. For this reason, orthopaedic surgeons are now required to undergo training in biomechanics, which is important for evaluating joint conditions, planning interventional treatments, and planning postoperative rehabilitation regimes. A number of textbooks have been published in recent years on the principles of orthopaedic biomechanics, but few texts to date have presented in-depth discussions of each area of the field of orthopaedics, from basic biomechanical principles through to direct clinical applications. The content of this book covers recent breakthroughs in the field of orthopaedic biomechanics, primarily focusing on clinically relevant developments and challenges in this field. I highly recommend this book be read by orthopaedic surgeons, biomedical engineers and researchers, and related personnel in the field of orthopaedic biomechanics. It is also my hope that this book will be a vital source of information on the latest advances in biomechanics for younger practitioners that may not yet have significant experience in the field.

Kerong Dai
Ninth People's Hospital
Shanghai, China

Shanghai Jiao Tong University School of Medicine
Shanghai, China

Contents

Introduction

The primary function of the musculoskeletal system is to produce force to move joints and limbs. It also serves to protect vital organs in the body. As such, the heavy burden placed on the system can often lead to injury and degeneration. Orthopaedics is a surgical discipline that is frequently used in conjunction with rehabilitation to manage musculoskeletal ailments.

About 50 years ago, a number of leading orthopaedic surgeons began to work with early bioengineers to introduce engineering practices to the medical field. These bioengineers introduced the principles of mechanics to the analysis of the structure and functional relationship of the musculoskeletal system, offered a better understanding on the mechanism of injuries, and collaborated to design new and more effective treatment procedures. Indeed, the contribution of orthopaedic biomechanics to advancing the management of musculoskeletal injuries has been significant and has greatly benefited patients around the world.

More recently, novel methods of production and processing of biomaterials, together with the application of advanced mechanical instrumentation, have revolutionized the development of orthopaedic devices, such as with customized anatomical prosthesis, implants with increased longevity, and arthroscopic and robot-assisted surgical instruments. Therefore, this book offers a systematic and comprehensive review of current clinical best practice as well as novel research on offer to further enhance patient outcomes.

This book is aimed towards younger orthopaedic surgeons, biomedical engineers, and rehabilitation scientists who are looking for a solid review of the current field of orthopaedic biomechanics. The book presents an in-depth analysis of the fundamental principles of orthopaedic biomechanics as well as the clinical applications across the musculoskeletal system—including fracture healing, design of customized orthopaedic implants, and evidence-based methods of orthopaedic rehabilitation. Moreover, the application of innovative biomaterials in clinical practice is also covered in this book. Thus, the main feature of the book is that it clearly shows the relationship between the musculoskeletal anatomy and design of orthopaedic and rehabilitation treatments. Sound mechanical theories are presented to

explain how the musculoskeletal system works, what causes musculoskeletal injuries, and how various treatment methods can improve the outcome.

There are 15 chapters in this book. Following Introduction, Chaps. 1–10 detail important biomechanical concepts relevant to surgical and clinical practice, including cartilage, muscles and tendons, ligaments, and joints. Chapter 11 introduces the biomechanics of human motion, and the following three chapters discuss various orthopaedic injuries and treatment methods. The last chapter focuses on orthopaedic bio-synthetics. Each chapter is contributed by experts in the respective research fields and presents advanced approaches to orthopaedic biomechanics. Key features of each chapter are highlighted as follows. The introductory section outlines the target and contents of the book. Chapter 1 discusses how mechanical biology and biomechanical signal transduction attenuate musculoskeletal degeneration, as knowledge of specific cellular responses is critical to understanding the underlying mechanism which has the potential to regulate bone and cartilage adaptation. Chapter 2 introduces the anatomy of muscles and tendons and demonstrates how these tissues act to produce mechanical force. Chapter 3 presents mechanical methods for measuring forces in ligaments, in addition to detailing the mechanism of ligament injury and treatment methods available. Chapter 4 provides a review of the anatomy and biomechanical function of the hand and wrist. This chapter also discusses the pathomechanics of the hand and wrist after injury, i.e. arthritis of the thumb, distal radius fracture, and malunion carpal tunnel syndrome. The functional and musculoskeletal anatomy of the elbow is illustrated with pictures in Chap. 5. This chapter also details the pathomechanics of the elbow, including elbow fracture and arthritis. Chapter 6 contains a systematical review of the musculoskeletal and functional anatomy of the shoulder, as well as a description of shoulder arthroplasty. Chapter 7 emphasizes on the repair of the lamina and related ligaments, using examples to illustrate the design of spinal arthroplasty to restore the function of the spine and improve the stability and longevity of implants. In Chap. 8, significant parameters relating to the function and kinematics of the hip are introduced, as well as an analysis of reaction forces in the hip joint. Chapter 9 focuses on knee disorders, namely knee osteoarthritis and osteotomy, and discusses the design of knee arthroplasties with the aim of restoring knee function. Chapter 10 includes a biomechanical assessment of the foot and ankle based on computational models, in addition to detailing methods of applying finite element analysis to the study of injuries, prosthetic design, surgical approaches, and orthotics. Chapter 11 discusses the structural anatomy that contributes to stability and mobility of joints. In this chapter, common pathologies and hip arthroplasties are introduced. Chapter 12 focuses on the introduction of fracture fixation methods. Biomechanical principles of screw and plate fixation for fracture healing are described comprehensively in this section. Chapter 13 introduces the concept of customized hip stems for individual patients based on their unique bone geometry, deformities, and pathological conditions. This chapter may be of interest to surgeons and researchers who regularly interact with such custom implants but need additional information on the development methods. Chapter 14 details methods for improving the effectiveness of orthopaedic rehabilitation. This section investigates the biomechanical principles of exercises as well as

appropriate assistive devices (splints, walkers, crutches, and canes) for orthopaedic rehabilitation. The final chapter, Chap. 15, focuses on the introduction of osteo-synthetics to the field of biomedical engineering. Design parameters such as implant microstructural and materials for osteo-synthetics are discussed, as well as a new design strategy termed Topology Optimization. This final chapter presents novel research that could readily be applied in clinical settings, such as materials that possess the solid-fluid bi-phasic properties of native bone.

We are truly grateful for the contributions made by all the authors of this book. Each is a distinguished leader in their respective areas of orthopaedic biomechanics. Their wealth of knowledge and experience makes this book a true representation of "the Frontiers in Orthopaedic Biomechanics". We thank each author for presenting the materials in each chapter in a comprehensive manner. We are also indebted to Springer Nature and the editorial team for their kind assistance with making this publication possible.

Shanghai, China — Cheng-Kung Cheng
Pittsburgh, PA, USA — Savio L-Y. Woo

Chapter 1
Biomechanics of Bone and Cartilage

Yi-Xian Qin, Minyi Hu, and Xiaofei Li

Abstract The use of mechanical biology and biomechanical signal transduction is a novel approach to attenuate musculoskeletal degeneration, whereas the understanding of specific cellular responses is critical to delineate the underlying mechanism. Dynamic mechanical signals with optimized loading signals, i.e., intensity and frequency, have been shown to have the potential to regulate bone and cartilage adaptation. Mechanotransduction pathways are of great interests in elucidating how mechanical signals produce such observed effects, including reduced bone loss, increased bone formation, and osteogenic cell differentiation. The objective of this review is to develop a molecular understanding of the mechanotransduction processes in tissue regeneration, which may provide new insights into bone physiology. In this chapter, we discuss the potential for mechanical loading to induce dynamic bone fluid flow, i.e., generated by the intramedullary pressure (ImP) and strains in bone, regulation of bone adaptation, and optimization of stimulation parameters in the loading regimen. The potential for mechanical loading to regulate bone fluid flow and microcirculation is also discussed. Particular attention is allotted to the responses of mechanical loading, including potential cellular and molecular pathways, osteocytes associated with Wnt signaling, the elevation of marrow stem cells and suppression of adipose cells, as well as the roles of LRP5 and microRNA. Altogether, these discussed data highlight the complex yet highly coordinated process of mechanotransduction in bone tissue regeneration.

Keywords Biomechanics and mechanobiology · Bone adaptation · Osteopenia Mechanical loading · Muscle atrophy · Stem cell differentiation · Loading frequency · Ultrasound treatment · Cartilage regeneration · Bone remodeling

Y.-X. Qin (✉) · M. Hu · X. Li
Stony Brook University, Stony Brook, NY, USA
e-mail: Yi-Xian.Qin@StonyBrook.edu

C.-K. Cheng, S. L-Y. Woo (eds.), *Frontiers in Orthopaedic Biomechanics*,
https://doi.org/10.1007/978-981-15-3159-0_1

1 Background

Bone mineral density (BMD) and muscle strength are highly biomechanically related to each other [1, 2]. High physical activity level has been associated with high bone mass and low fracture risks, and is therefore recommended to reduce fractures at old age [3–7]. As a direct consequence of exposure to microgravity, astronauts experience several physiological changes, which can have serious medical complications. Most immediate and significant are the musculoskeletal implications in bone and muscles [8–11]. Results of the joint Russian/US studies of the effect of microgravity on bone tissue from 4.5 to 14.5 month-long missions have demonstrated that bone mineral density (BMD, g/cm^2) and mineral content (BMC, g) are decayed in the whole body of the astronauts [12]. The greatest BMD losses have been observed in the skeleton of the lower body, i.e., in pelvic bones ($-11.99 \pm 1.22\%$) and in the femoral neck ($-8.17 \pm 1.24\%$), while there is no evitable decay found in the skull region. Overall changes in bone mass of the whole skeleton of male cosmonauts during the period of about 6 months on a mission made up $-1.41 \pm 0.41\%$ and suggest the mean balance of calcium over flight equals to -227 ± 62.8 mg/day. On average, the magnitude and rate of the loss are staggering; astronauts lose bone mineral in the lower appendicular skeleton at a rate approaching 2% per month with muscle atrophy [5, 6, 13–15]. In simulated or actual microgravity, human postural muscles undergo substantial atrophy: after about 270 days, the muscle mass attains a constant value of about 70% of the initial one. Most animal studies have reported preferential atrophy of slow-twitch fibers whose mechanical properties change towards the fast type. After microgravity, the maximal force of several muscle groups has showed a substantial decrease (6–25% of pre-flight values) [8, 10, 16–19]. The mechanism that explains both muscle and bone decays in the function disuse environment is still unclear. In recent years, considerable attention has focused on identifying particular parameters and exercise paradigms to ameliorate the deficits of muscle atrophy and bone density. Perhaps microcirculation and interstitial fluid flow that link with exercise and muscle contraction can identify the interrelationship between muscle and bone flow in response to loading and disuse environment. The headward shift of body fluids and the removal of gravitational loading from bone and muscles have led to progressive changes in the musculoskeletal systems. The underlying factor producing these changes may be primarily due to the fluid flow and circulations in both muscular and bone tissues.

The ability of musculoskeletal tissues to respond to changes in its functional milieu is one of the most intriguing aspects of such living tissue, and certainly contributes to its success as a structure. The ability of bone and muscle to rapidly accommodate changes in its functional environment ensures that sufficient skeletal mass is appropriately placed to withstand the rigors of functional activity, an attribute described as Wolff's law [20, 21]. This adaptive capability of musculoskeletal tissues suggests that biophysical stimuli may be able to provide a site-specific, exogenous treatment for controlling both bone mass and morphology. The premise

of a mechanical influence on bone morphology has become a basic tenet of bone physiology [22–26]. Absence of functional loading results in the loss of bone mass [22, 27–31], while exercise or increased activity results in increased bone mass [32–36].

Similarly, the increasing exercise of musculo-tissues can significantly increase blood flow, oxygen, and exchange fluid in muscle. During muscle contraction, several mechanisms regulate blood flow to ensure a close coupling between muscle oxygen delivery and metabolic demand [8, 10, 16–19, 37–44]. To define the formal relationship between the mechanical milieu, the adaptive response, and the relationship between muscle pump and interstitial fluid flow will prove instrumental in devising a mechanical intervention for musculoskeletal disorders, such as osteoporosis, muscle fatigue, and atrophy, designing biomechanical means to accelerate fracture healing, and promoting bony ingrowth.

2 Bone Structure, Physiology, and Basic Biomechanics

Similar to most of the biological tissues, bone has its unique structure and serves as a functional unit [45–47] (Fig. 1.1). In general, the basic structure of mature long bone includes both cortical (or compact) bone and trabecular (or cancellous) bone. Within the mature cortical bone, the skeleton shows the lamellar structure. Such a plate structure is centered with the Haversian canal, mostly aligned longitudinally and connected with the Volkmann's canals that is running horizontally in the cortex. These two conduits are rich in vascular tissue; two-thirds of the vascular supply is provided through the medullary cavity, and the other one-third is provided through the periosteum. Bone cells that present in the bone lacunae are interconnected by the canaliculi, tubules structure, and communicate with each other through the gap junction. Each concentric structure is consisted of a capillary tube, a concentric plate structure, lacuna, and canaliculi. Such a unique bone unit is called osteon.

The Haversian canals, canaliculi, and lacunae occupy 13.3% of the volume of the cortical bone [48, 49]. The rest solid portion is the matrix, which is occupied by mineral material containing the hydroxyapatite crystal and collagen fiber. The solid bone matrix of the bone contains pores of the order of 0.01–0.1 μm in diameter [48–52]. The primary constituents of an osteon are collagen (organic), hydroxyapatite (inorganic), and fluid. Fluid flows through the various microstructural spaces to transfer metabolites to the osteocytes, ensuring that bone tissue remains viable. This continuous perfusion allows the remodeling processes to continue in perpetuity. The requisite nutrition of the cells and essential disposal of their waste products are carried by this dynamic fluid stream. Because of the intricate microstructure of cortical bone, transportation between cells would be very poor if it relied solely on fluid diffusion. Indeed, a complex network of very thin (~1 μm) and quite long (up to 100 μm) canaliculi must employ a more active policy of nutrient allocation and signal dispersion [48–52].

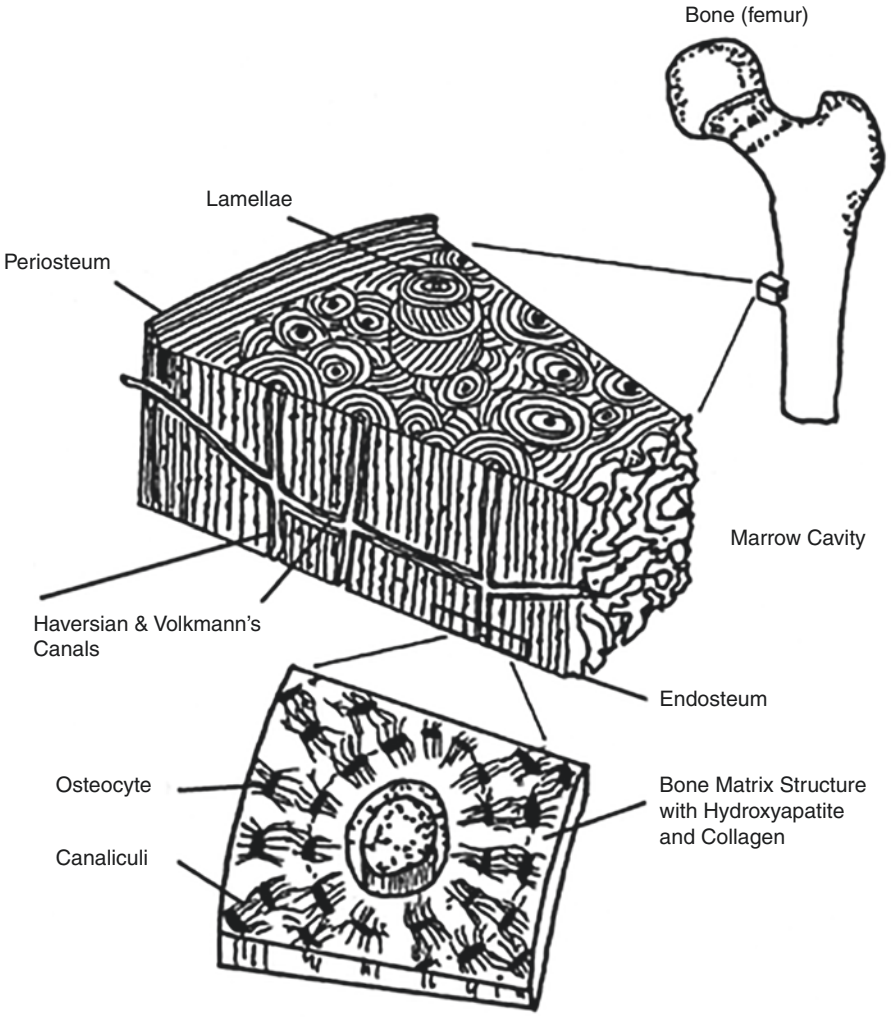

Fig. 1.1 Cortical bone and osteon structure. The general structure of cortical bone includes marrow cavity, periosteum, and endosteum. The microstructure includes Haversian Canals, Volkmann's canal, osteocyte, and lacuna and canaliculi system

Regarding the potential mechanotransduction in bone induced by fluid flow, Cowin [50, 51] summarized that there are three primary levels of bone porosities within cortical microstructure, which might mediate fluid flow. Firstly, an osteon, the basic structure of bone with dominant cylindrical structures of 100–150 μm radii running primarily along the long axes of bone, contains at its center an *osteonal canal* (OC), including blood vessels, a nerve, and surrounding fluid. There are cells attached on the walls of the OC. At the level of the osteon, fluid transduction from the Haversian canal to the cement line or its surrounding micropores, whether

via perfusion or convection, appears to be significantly influenced by the pathway of the fluid flow. Secondly, an osteon contains lacunae structure of 3–10 μm in radius surrounding the OC, which connects to the OC via canaliculi. Osteocytes (~2 μm radii) are contained within the lacunae. Thirdly, canaliculi, a capillary with 0.1–0.5 μm in radius, run radially, and surround and connect the lacunae, OC, and cement lines together. In addition, the microstructures of collagen-apatite porosity (100–300 Å) contain fluid in the collagen matrix. The cortical vascular supply begins primarily at the marrow cavity and passes through the endosteum, accommodating approximately 2/3 of the vascular supply in the cortex. These levels of porosities participate in and interact with each other in fluid diffusion/perfusion, and fluid pathways may include vascular canals, the lacunar-canalicular spaces, and collagen-apatite spaces.

3 Mechanical Properties and Characterization of Biological Tissues

The mechanical strength of biological tissue or a sample can be defined and quantified by its mechanical parameters, such as stress, strain, and modulus. These mechanical parameters are defined as follows.

3.1 Stress

In one-dimensional testing status, the stress is defined as the axial loading on the perpendicular cross-sectional area. The load and force per unit area is the response to externally applied loads on a structural section. In general, a unit point can experience three-dimensional loads. External forces and moments can be applied to the structure in different directions, resulting in tensile, compressive, bending, torsional, shear, and composite stresses. Fractures often clinically occur at the location where the principal stress exceeds the mechanical strength of the tissue. The unit of stress is defined as N/m^2 or Pa, MPa (10^6 Pa), and GPa (10^9 Pa).

3.2 Strain

External loading on a structure can induce the change of dimension of the structure, which is called deformation. The strain is defined as the structural deformation against the original shape of the structure caused by an applied load. There are two

types of strains, one of which is the normal strain, which causes a change in the length of the specimen, and another is the shear strain, which causes a change in the angular relationship within the structure. Strain has no unit quantity, but is usually expressed in %, ε, and με.

3.3 Elastic Modulus

It is the relation between strain and stress, such as the ratio of stress to strain, as the basic material constants that reflect the mechanical properties of a material. The relationship between stress and strain can be defined as stress/strain = elastic modulus, the value of which is the ratio of stress to strain. The unit of elastic modulus is also Pa, MPa, or GPa. The larger the value of elastic modulus, the higher the strength of the material (Fig. 1.2).

Bone intensity is referred to the ability of bone tissue to resist structural damage after being loaded. It is a comprehensive index that integrates bone structure, bone mass, and material properties.

The mechanical properties of the tissue can be quantified by various mechanical loading and evaluations. The mechanical strength testing instruments can be used to obtain the test results of the tissue strength, stiffness, hardness, and toughness. The mechanical properties of bone are usually assessed by mechanical testing of the

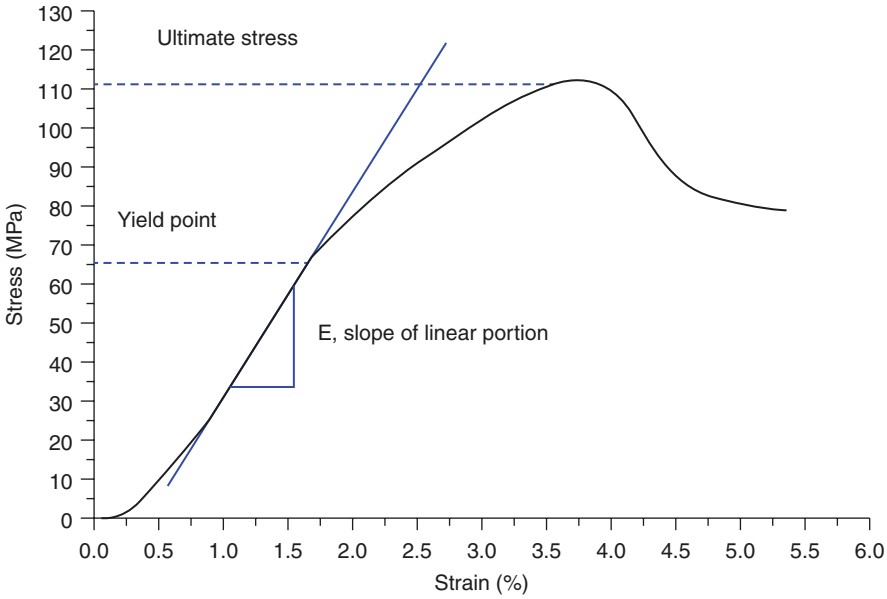

Fig. 1.2 Strain–stress relation under mechanical loading

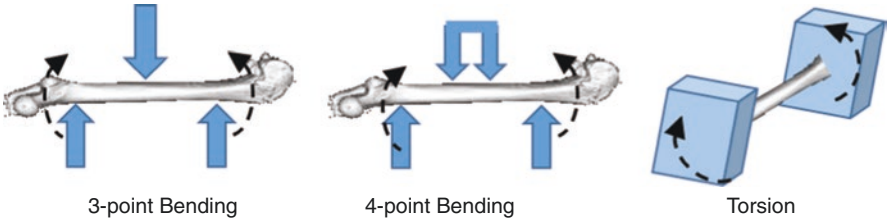

Fig. 1.3 Long bone under loading of 3-point bending, 4-point bending, and torsion

bone using a 3- or 4-point bending device (Fig. 1.3). The shear mechanical test of bone can be achieved by torsional testing (Fig. 1.3). The choice of the test type is determined by various technical and physiological factors. For example, in the study of healing of long bone fractures, bending and torsion tests are a logical choice because they can test the bending and torsional strength of the tissue. The torsional test subjects each cross-section of the bone to the same torque, while the 4-point bending test creates a uniform bending moment [53] for the entire epiphysis.

For the torsional test, an additional parameter, twisting to failure (fracture), can be used as a measure of the callus ductility. Although it can only be measured once for a given callus, it is possible to obtain multiple measurements on hardness and stiffness before reaching failure. Multilevel testing methods have been reported to test the loading model by performing a noninvasive load on bone. Within these methods, bending strength or torsional and compressive stiffness can be quantified in multiple planes.

4 Musculoskeletal Tissue Response to Dynamic Mechanical Signals

High physical activity level has been associated with high bone mass and low fracture risks, and is therefore recommended to reduce fractures [3, 4, 6]. The ability of musculoskeletal tissues to respond to changes in its functional milieu is one of the most intriguing aspects of such living tissue, and certainly contributes to its success as a structure. Bone and muscle rapidly accommodate changes in its functional environment to ensure that sufficient skeletal mass is appropriately placed to withstand the regions of functional activity, an attribute described as Wolff's law [20, 21]. This adaptive capability of musculoskeletal tissues suggests that biophysical stimuli may be able to provide a site-specific, exogenous treatment to control both bone mass and morphology. The premise of mechanical influence on bone morphology has become a basic tenet of bone physiology [24–26]. Based on the Muscle Pump Theory, vascular arteries and veins within skeletal muscles are compressed upon muscle contraction, and therefore increasing the arteriovenous pressure gradient and promoting capillary filtration [54–56].

Modeling (formation) and remodeling (coupling of resorption and formation) responses are sensitive only to dynamic (time-varying) strains; static strains are ignored as a source of osteogenic stimuli [57]. With that said, it is also clear the osteogenic potential of mechanical signals is defined by a strong interdependence between cycle number, strain magnitude, and frequency. In cortical bone, 2000 με induced at 0.5 Hz (one cycle every 2 s) maintains bone mass and achieves this with just four cycles of loading encompassing 8 s/day [30]. Reducing this strain to 1000 με at 1 Hz requires 100 cycles, and 100 s, to maintain bone mass [58]. Raising the loading frequency to 3 Hz, bone mass can be retained with 1800 cycles of only 800 με [53], while at 30 Hz, the same 600 s requires only 200 με to maintain cortical bone, a protocol employing 18,000 cycles of loading. Increasing the 30 Hz signal to 1 h/day (108,000 cycles), only 70 με is necessary to inhibit bone loss. These data demonstrate the sensitivity of bone to mechanical loading goes up quickly with the total number of loading cycles, which closely associated with the loading frequency, i.e., extremely low levels of strain will maintain bone mass if sufficient numbers induced by relatively higher frequency are applied. This relation between the loading cycle and resultant bone strain can be plotted in a nonlinear response curve [53] (Fig. 1.4). It is suggested that a nonlinear governing relationship between the daily

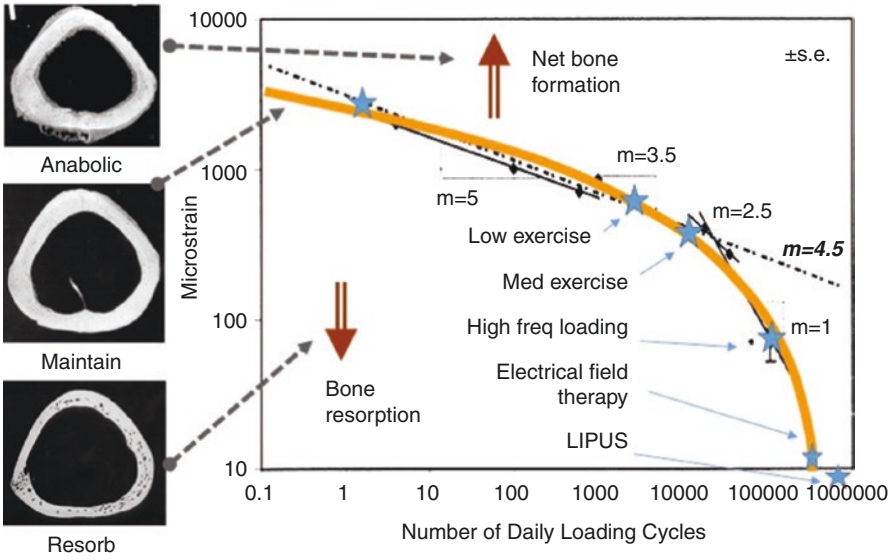

Fig. 1.4 Nonlinear interrelationship of cycle number and daily strain magnitude following a governing equation (Eq. 1.1). It appears that bone mass can be retained through a number of distinct strategies: (1) bone is preserved with extremely low daily loading cycles and extremely high frequency, i.e., 4 cycles per day of 2000 με, (2) bone mass is maintained with 100 cycles per day of 1000 με, or 10,000s of cycles of signals well below 100 με (each represented as a star), (3) bone is responded to extremely high frequency and extremely low strain magnitude, such as electrical field induced muscle contraction and low-intensity pulsed ultrasound (LIPUS). It is proposed that falling below this "daily strain energy" would stimulate bone loss, or any combination exceeding this relationship would stimulate net bone gain [53]

loading cycles and the peak bone strain magnitude generated in the body can be generated using curve fitting analysis [53].

$$S = 10^{2.28}\left(5.6 - log_{10}C\right)^{1.5} \tag{1.1}$$

where S represents the peak bone strain, and C represents the total daily loading cycles. Such higher loading cycles can be achieved using higher frequency daily loading regimen.

It is well accepted that overloading will damage the bone and lead to failure, just as too much light, noise, or pressure will overwhelm sight, hearing, and touch, respectively. Although the skeleton's primary responsibility is structural support in nature, its overall responsibilities are broader than first presumed, and even include, a critical role of the acoustic sensory organ in elephants [3]. Emphasizing this point, bone's adaptation to mechanical signals is nonlinear, such that it can be influenced by a very few high-magnitude strain events, or by many thousands of low-magnitude strain events.

To adapt to the changing demands of mechanics, bone mass and bone morphology can be regulated via bone remodeling at specific sites. This crucial process of structural remodeling of the bone involves bone resorption and the subsequent bone formation. However, difficulties to determine specific mechanical components will hamper our understanding of bone remodeling related diseases, as well as limiting our judgments on bone fractures and healing capacity. Therefore, continuous studies of the bone remodeling process, for example, to determine the mechanical model of this remodeling process, can ultimately benefit the intervention on prevention and treatment of musculoskeletal disorders.

5 Functional Disuse-Induced Bone Loss and Muscle Atrophy

Disuse osteoporosis is a common skeletal disorder in patients subjected to prolonged immobility or bed rest, e.g., fracture and spinal injury. In addition to bone loss, functional disuse and microgravity can cause muscle atrophy. These physiological changes generate additional health complications, including increased risk of falls and fracture, and poor long-term recovery. Analyses of spinal cord injury (SCI) patients showed a reduction in bone mineral density (BMD) in disused limbs [59–61] and a higher incidence of fracture [62–65]. More than 1 year after SCI, 30–40% of demineralization was observed in the femoral neck, distal femur, and proximal tibia [60]. It has been reported that SCI induced osteopenia/osteoporosis reaches the fracture threshold (BMD of 1 g/cm [66]) 1–5 years after the injury, with a fracture frequency of 5–34% [62, 67–69]. These patients were also observed to have significant reductions in muscle mass [70]. Analyses from space missions of 4–12 months duration have shown that weightlessness can induce 1–2% BMD loss per month in the spine, hip, and the lower extremities [5, 71]. The reduction in tra-

becular BMD in both hip and femur regions was greater than 2% per month, while there was only minimally decrease in cortical bone [72]. Similar results were observed in animal studies. Burr et al. [73] showed an increase in the bone turnover rate in cast-immobilized animals that received muscle stimulation for 17 days.

Lower extremity muscle volume was also altered by disuse. Exposure to a 6-month space mission resulted in a decrease in muscle volume of 10% in the quadriceps and 19% in the gastrocnemius and soleus [6, 74]. Computed tomography measurements of the muscle cross-sectional area (CSA) indicated a decrease of 10% in the gastrocnemius and 10–15% in the quadriceps after short-term missions [15, 75]. Similar results were concluded after SCI, where patients suffered significant 21%, 28%, and 39% reductions in CSA at the quadriceps femoris, soleus, and gastrocnemius muscles, respectively [76, 77]. In addition to the effects on whole muscle volume, muscle fiber characteristics were also modified due to inactivity [78–80]. There are two primary muscle fibers: slow (type I) fibers play an important role in maintaining body posture while fast (type II) fibers are responsive during physical activity. Under disuse conditions, all fiber types were decreased in size, 16% for type I and 23–36% for type II [79–81]. The atrophied soleus muscles also underwent a shift from type I (−8% in fiber numbers) to type II fibers [79, 81, 82].

Clinical muscle stimulation has been examined extensively in SCI patients to strengthen skeletal muscle and alleviate muscle atrophy with promising outcomes [83–86]. A few physical training studies further investigated this electrical stimulation technique to determine its effect on osteopenia. These studies showed mixed results with respect to bone density data [83, 87–90]. Using dual-energy X-ray absorptiometry (DXA), BeDell et al. found no change in BMD of the lumbar spine and femoral neck regions after functional electrical stimulation-induced cycling exercise, while Mohr et al. showed a 10% increase in BMD in the proximal tibia following 12 months of similar training [91–93]. In a 24-week study of SCI patients in whom 25 Hz electrical stimulation was applied to the quadriceps muscles daily, Belanger and colleagues reported a 28% recovery of BMD in the distal femur and proximal tibia, along with increased muscle strength [92]. A number of reported animal studies also indicated that muscle stimulation can not only enhance muscle mass, but bone mineral density as well [94, 95]. Both animal and human studies seem to strongly support that functional disuse can result in significant bone loss and muscle atrophy.

6 Frequency-Dependent Marrow Pressure and Bone Strain Generated by Muscle Stimulation

A recent study has revealed that induced marrow fluid pressure and bone strain by muscle stimulation were dependent on dynamic loading parameters and optimized at certain loading frequencies [96]. Adult Sprague Dawley retired breeder rats with a mean body weight of 387 ± 41 g (Taconic, NY) were used to measure the relationships between ImP, bone strain, and induced muscle contraction. Rats were anesthetized using standard isoflurane inhalation. A micro-cardiovascular pressure transducer (Millar Instruments, SPR-524, Houston, TX) was inserted into the femo-

ral marrow cavity, guided via a 16-gauge catheter. A single element strain gauge (120 Ω, factor 2.06, Kenkyojo Co., Tokyo) was firmly attached onto the lateral surface of the same femur at the mid-diaphyseal region, with minimal disruption to the quadriceps, for measuring bone strains during the loading. The MS was applied at various frequencies (1, 2.5, 5, 10, 15, 20, 30, 40, 50, 60, and 100 Hz) to induce muscle stimulation.

Normal heartbeat generated approximately 5 mmHg of ImP in the femur at a frequency of 5.37 ± 0.35 Hz. The ImP value (peak-peak) was increased significantly by dynamic MS at 5, 10, 15, 20, 30, and 40 Hz ($p < 0.05$ for 5, 10, 30, and 40 Hz, $p < 0.01$ for 15 and 20 Hz). The response trend of the ImP against frequency was nonlinear; the ImP reached a maximum value of 45 ± 9.3 mmHg (peak-peak) at 20 Hz (Fig. 1.5), although there was no significant difference between 10, 20, and

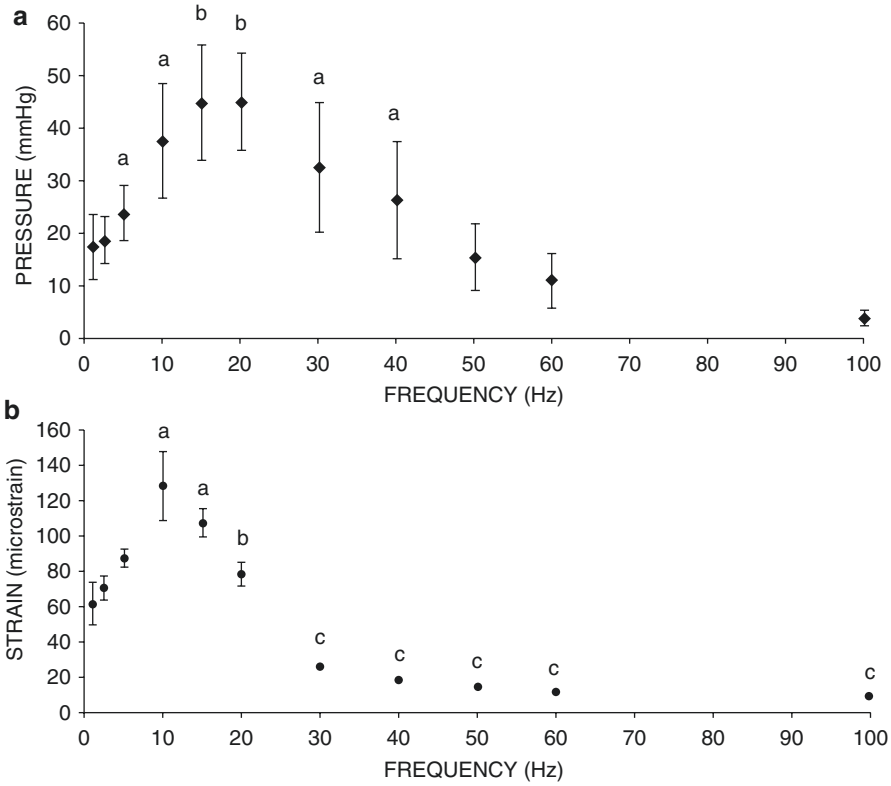

Fig. 1.5 (**a**) ImP in rat femur increased significantly with electrical frequency at 5, 10, 15, 20, 30, and 40 Hz. In the loading spectrum from 1 to 100 Hz, stimulation at 1 Hz generated an ImP of 18 mmHg. A maximum ImP of 45 mmHg was measured at 20 Hz, which was 2.5-folds higher than 1 Hz. [a]$p < 0.05$ vs. baseline ImP; [b]$p < 0.01$ vs. baseline ImP. (**b**) Bone surface strain measurement. Dynamic muscle stimulation applied at various frequencies significantly increased bone strain. In the loading spectrum from 1 to 100 Hz, stimulation at 1 Hz produced a strain of 62 με. Peak strain of 128 με was recorded at 10 Hz stimulation. The strain magnitude was reduced by >75% of the peak strain for stimulation frequencies greater than 30 Hz. [a]$p < 0.01$ vs. 1, 2.5, and 5 Hz; [b]$p < 0.01$ vs. 10 Hz; [c]$p < 0.001$ vs. stimulation 20 Hz and below

30 Hz. In the range from 5 to 40 Hz, the ImP was shown approximately 60% of the maximum ImP. The MS generated ImP in the marrow cavity with values of 17.4 ± 6.2, 24 ± 5.4, 37.5 ± 11.0, 26.3 ± 11.1, and 3.7 ± 1.5 mmHg at frequencies of 1, 5, 10, 40, and 100 Hz, respectively.

The response of matrix strain to the MS frequency also was nonlinear (Fig. 1.5). The MS generated femoral matrix strains of 61.8 ± 6.2, 87.5 ± 5.1, 128.4 ± 19.2, 78.3 ± 6.8, 18.7 ± 1.3, and 10.1 ± 1.8 με at frequencies of 1, 5, 10, 20, 40, and 100 Hz, respectively. While the ImP trend indicated that the peak ImP value was observed at 20 Hz, the maximum matrix strain was measured at 10 Hz. Bone strain induced by MS at 10 Hz was significantly different ($p < 0.01$) comparing to all other stimulations with the exception of 15 Hz. In addition, the strains generated by MS above 30 Hz were significantly lower than those values loaded at and below 20 Hz ($p < 0.005$), in which matrix strains, when loaded above 30 Hz, decreased by more than 75% of the peak strain measured at 10 Hz. For frequencies from 40 to 100 Hz, MS induced matrix strain were less than 20 με. These results suggest that MS with a relatively high rate and small magnitude can trigger significant fluid pressure in the skeleton.

7 Dynamic Muscle Stimulation Induced Attenuation of Bone Loss

These findings were verified in an *in vivo* experiment under functional disuse conditions [97]. Fifty-six 6-month-old female Sprague-Dawley retired breeder rats (Taconic, NY) were used to investigate the effects of frequency-dependent dynamic muscle stimulation (MS) on skeletal adaptation under disuse environment. Animals were randomly assigned to seven groups with $n = 8$ per group: (1) baseline control, (2) age-matched control, (3) HLS, (4) HLS + 1 Hz MS, (5) HLS + 20 Hz MS, (6) HLS + 50 Hz MS, and (7) HLS + 100 Hz MS. Functional disuse was induced by an HLS, setup modified from Morey-Holton and Globus [98, 99]. An approximately 30° head-down tilt was set to prevent contact of the animal's hind limbs with the cage bottom. The body weight of each animal was weighed 3 times per week throughout the study.

Throughout the entire experimental period, the body weights were not significantly different between groups at the beginning of the study, with an average of 320 ± 47 g. Age-matched control animals were able to maintain a steady body weight throughout the study, with only a −0.15% difference between the start and end date. Animals subjected to 4-week functional disuse lost a significant amount of body mass. These weight reductions were similar in HLS and HLS + MS groups, with −10% for HLS ($p < 0.05$), −8% for 1 Hz ($p = 0.07$), −9% for 20 Hz ($p < 0.05$), −11% for 50 Hz ($p < 0.01$), and −8% for 100 Hz ($p = 0.09$).

Trabecular bone structure changes by MS stimulation seem to be sensitive to the fluid pressure magnitude experienced by the tissue, where a larger response occurred at the region near the marrow cavity, and attenuated at the region near the growth

plate. For example, M1 is the distal metaphyseal region 1.5 mm above the growth plate. The lack of weight-bearing activity for 4 weeks significantly reduced trabecular bone quantity and quality, demonstrated by a 70% decreases in BV/TV, an 86% decrease in Conn.D, a 28% decrease in Tb.N, a 57% increases in SMI, and a 43% increase in Tb.Sp compared with baseline ($p < 0.001$). Similar results were observed when compared with age-matched control ($p < 0.001$); decreases in BV/TV (66%), Conn.D (86%), and Tb.N (26%), as well as increases in SMI (39%) and Tb.Sp (39%) were observed. Trabecular BV/TV in electrically stimulated animals, with the exception of 1 Hz, was significantly greater than that of disused bone. Animals with MS at 20 Hz and 50 Hz showed an increase in BV/TV by 143% ($p < 0.05$) and 147% ($p < 0.01$), respectively. Stimulation at 100 Hz showed an 86% increase in BV/TV, but this change was not statistically different from the HLS group. The other outcome measures of Conn.D, Tb.N, and Tb.Sp were also significantly affected by MS at 20, 50, and 100 Hz frequencies. There were up to 600% and 38% increases for Conn.D and Tb.N, and up to a 36% decrease for trabecular separation (20 Hz $p < 0.01$, 50 Hz $p < 0.001$, and 100 Hz $p < 0.05$). SMI and Tb.Th were not affected by the stimulus, regardless of its frequency. The animals subjected to 4 weeks of 1 Hz MS showed the same level of bone loss and structural deterioration as did the HLS animals without MS, and showed significant differences compared to stimulation at higher frequencies. M3, the distal metaphyseal portion directly above the growth plate, is a region with the most abundant trabecular network with 0.3 ± 0.05 BV/TV and 4.72 ± 0.64 Tb.N (Fig. 1.6). Disuse induced a 38% bone loss, 75% decrease in Conn.D, 30% reduction in Tb.N, and 43% more spacing within this region. Similar to the results reported for the M2 portion, 50 Hz MS resulted in the greatest preventive effects against disuse osteopenia, with increased BV/TV (40%; $p < 0.05$), Conn.D (305%; $p < 0.001$), and Tb.N (41%; $p < 0.001$), and reduced Tb.Sp (31%; $p < 0.001$). While BV/TV was not significantly altered by MS at 20 Hz (+26%) and 100 Hz (+20%), trabecular qualities, Conn.D, Tb.N, and Tb.Sp, were improved (up to 226%, 28%, and 24%, respectively, $p < 0.001$). Like the other metaphyseal regions, SMI and Tb.Th were not affected by the stimulation. With the exception of 1 Hz, stimulation frequencies at 20, 50, and 100 Hz had greater effects on the trabecular bone 2.25 cm away from the growth plate, closer to the diaphysis. Also, BV/TV inhibition at M1 was significantly higher ($p < 0.05$) than that of M3 with 20 Hz MS. Although following a trend similar to that of the above indices, at 50 and 20 Hz MS, the percent changes of the μCT measurements were not statistically significant between the three metaphyseal regions.

While trabecular bone responded to MS showing structural property changes, the epiphyseal trabecular bone was not significantly affected by the 4-week HLS. The percentage changes were minor versus the metaphyseal regions, with −5% BV/TV, −44% Conn.D, −7% Tb.N, and +4% Tb.Sp. In this region, MS did not induce any measurable effect on the bone volume and trabecular integrity at any stimulation frequency. All stimulated values were comparable to age-matched and HLS animals, with up to 10% greater in BV/TV, 8% greater in Tb.N, and a 9% reduction in Tb.Sp. These changes were not statistically significant.

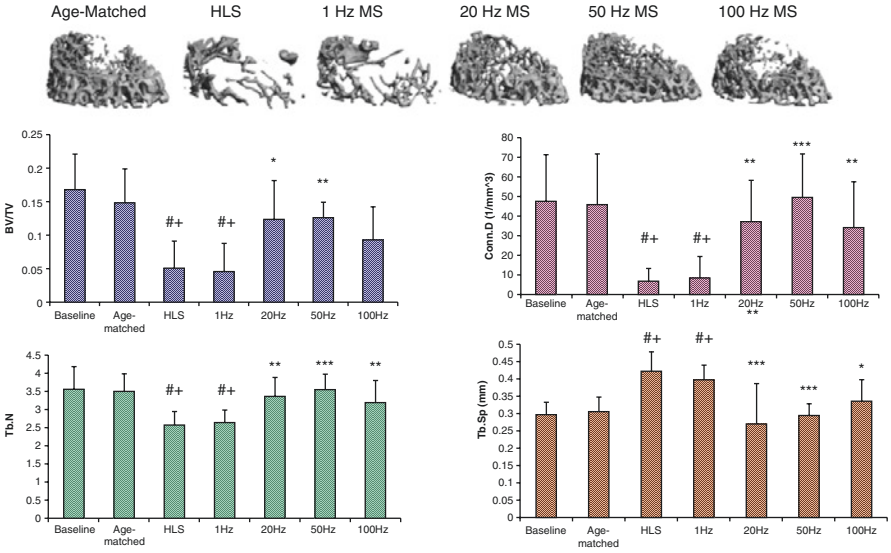

Fig. 1.6 MS induced ImP maintained bone mass at higher loading frequency, indicated by μCT images of trabecular bone in distal femur. Graphs show mean ± SD values for bone volume fraction (BV/TV, %), connectivity density (Conn.D, 1/mm^3), trabecular number (Tb.N, 1/mm), and separation (Tb.Sp, mm). MS at 50 Hz produced a significant change in all indices, compared to HLS. $^{\#}p < 0.001$ vs. baseline; $^{+}p < 0.001$ vs. age-matched; $^{*}p < 0.05$ vs. HLS and 1 Hz MS; $^{**}p < 0.01$ vs. HLS and 1 Hz MS; $^{***}p < 0.001$ vs. HLS and 1 Hz MS

The μCT data were correlated with the histomorphometry analyses. In the metaphyseal trabecular bone, BV/TV measured by the 2-D histomorphometric method was 43% lower in the HLS group than in age-matched controls ($p < 0.001$). Animals subjected to MS also experienced 22–29% of bone loss ($p < 0.01$). The result was correlated with the BV/TV values from the μCT analysis, giving an R^2 value of 0.84 ($p < 0.05$). In other bone formation indices, HLS animals also showed significant decline in MS/BS (76%, $p < 0.001$), MAR (80%, $p < 0.001$), and BFR/BS (92%, $p < 0.001$). Disuse had an insignificant effect on the trabecular BV/TV (−10%) at the epiphyseal region, similar to the results of the μCT analysis. Bone formation indices were reduced due to HLS (52% for MS/BS, 147% for MAR, and 59% for BFR/BS), and daily MS failed to prevent such reduction of bone formation activity.

These data imply that MS, applied at a high frequency with low magnitude and for a short duration, is able to mitigate bone loss induced by the functional disuse. There was, however, no evidence to suggest that such loading would enhance overall new bone formation, e.g., the total bone mass was less than age-match animals. However, further studies related to cellular activities, e.g., osteoclast and osteoblast, and linked either bone resorption and bone formation, may be necessary to further explore the balance of resorption and formation in such functional disuse model.

8 Cellular and Molecular Pathways of Bone in Response to Mechanical Loading

Bone remodeling involves all related cell types, i.e., osteoblast, osteoclast, osteocyte, T-cells, B-cells, megakaryocyte, and lining cells. Thus, all these cells are potentially mechano-sensitive and even interrelated. These cells respond to mechanical loading and can express specific molecular pathways. This section will discuss several potential pathways involved in mechanical stimulation induced adaptation.

8.1 Basic Multicellular Units (BMU)

To explore the interrelation among overall bone cells, a cluster of bone forming and bone resorption cells among dynamic and temporal adaptation structures are proposed, known as "basic multicellular units" (BMUs) [100]. Bone adaptation occurs constantly and each cycle may take over several weeks. Such processes are performed with a combination of resorption and formation. Each phase can involve targeted molecular and gene activations. An active BMU consists of a leading front of bone-resorbing osteoclasts. Reversal cells, of unclear phenotype, follow the osteoclasts, covering the newly exposed bone surface, and prepare it for deposition of replacement bone, following deposition of an unmineralized bone matrix known as osteoid. Related molecular factors are represented in this temporal sequence (Fig. 1.7).

In response to mechanical loading, the first stage of remodeling reflects the detection of initiating triggering signals such as fluid flow and any other of physical stimulation, e.g., pressure, electrical, and acoustic waves. Prior to activation, the resting bone surface is covered with bone-lining cells, including preosteoblasts. B cells are present in the bone marrow and secrete osteoprotegerin (OPG), which suppresses osteoclastogenesis.

During the *Activation* phase, the endocrine bone-remodeling signal parathyroid hormone (PTH) binds to the PTH receptor on preosteoblasts. Damage to the mineralized bone matrix results in localized osteocyte apoptosis, reducing the local transforming growth factor β (TGF-β) concentration and its inhibition of osteoclastogenesis.

In the *resorption* phase, in response to PTH signaling, preosteoclasts are recruited to the bone surface. Additionally, osteoblast expression of OPG is decreased, and the production of CSF-1 and RANKL is increased to promote the proliferation of osteoclast precursors and differentiation of mature osteoclasts. Mature osteoclasts anchor to RGD-binding sites, creating a localized microenvironment (sealed zone) that facilitates degradation of the mineralized bone matrix.

In the *Reversal* phase, reversal cells engulf and remove demineralized undigested collagen from the bone surface. Transition signals are generated that halt bone resorption and stimulate the bone formation process.

During the *Formation* phase, formation signals and molecules arise from the degraded bone matrix, mature osteoclasts, and potentially reversal cells. PTH and

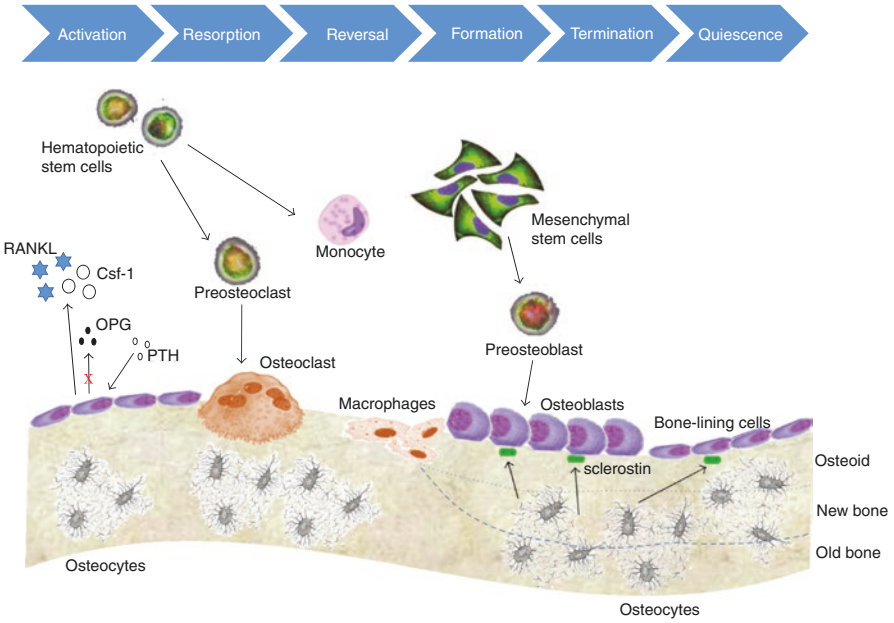

Fig. 1.7 Bone remodeling cycle and its associated molecular pathways. Three primary cell types are involved in bone modeling and remodeling, including osteoblast, osteoclast, and osteocyte. The remodeling cycle of bone is composed of sequential phases of resorption and formation, including the activation of precursor cells, osteoclasts activation generating bone resorption, bone formation by osteoblasts after mineral removal and reversal, and mineralization. The osteoblasts that are buried within the newly formed mineral matrix yield to osteocytes. Other osteoblasts that rest on the bone surface become bone lining cells [47]

mechanical activation of osteocytes reduce sclerostin expression, allowing for Wnt-directed bone formation to occur.

Finally, in the *Termination* phase, sclerostin expression likely returns, and bone formation ceases. The newly deposited osteoid is mineralized, the bone surfaces return to a resting state with bone-lining cells intercalated with osteomacs, and the remodeling cycle concludes.

Mechanical stimulation is likely involved in each of these phases and eventually regulates related molecular and genetic factors. This unique spatial and temporal arrangement of cells within the BMU is critical to bone remodeling, ensuring coordination of the distinct and sequential phases of this process: activation, resorption, reversal, formation, and termination.

9 Mechanical Signal Induced Marrow Stem Cell Elevation and Adipose Cell Suppression

The data from disuse osteopenia and clinical osteoporosis have shown significant reduction of bone density and structural integrity, culminating in an elevated risk of skeletal fracture. Concurrently, a marked reduction in the available bone-marrow-

derived population of mesenchymal stem cells (MSCs) [101] jeopardizes the regenerative potential that is critical to recovery from bone loss, musculoskeletal injury, and diseases. A potential way to combat the deterioration involves harnessing the sensitivity of bone to mechanical signals, which is crucial in defining, maintaining, and recovering bone mass. As discussed above, bone cells, i.e., osteoblast, osteoclast, and osteocyte, may sense external mechanical loading directly and perform the balance of formation and resorption in the remodeling process; specific mechanotransductive signals may also bias MSC differentiation towards osteoblastogenesis and away from adipogenesis. Mechanical targeting of the bone marrow stem-cell pool might, therefore, represent a novel, drug-free means of slowing the age-related decline of the musculoskeletal system.

Considering the importance of exercise in stemming both osteoporosis and obesity, combined with the fact that MSCs are progenitors of both osteoblasts and adipocytes (fat cells), as well as the anabolic response of the skeletal system to mechanical loadings, it was hypothesized that mechanical signals anabolic to bone would invariably cause a parallel decrease in fat production. In an *in vivo* setting, 7-week-old C57BL/6J mice on a normal chow diet were randomized to undergo low magnitude high-frequency loading (90 Hz at 0.2 g for 15 min/day) or placebo treatment [102]. At 15 weeks, with no differences in food consumption between groups, *in vivo* CT scans showed that the abdominal fat volume of mice subjected to loading was 27% lower than that of controls ($p < 0.01$) [103, 104]. Wet weights of visceral and subcutaneous fat deposits in loading mice were correspondingly lower. Confirmed by fluorescent labeling and flow cytometry studies [103, 104], these data indicated that mechanical signals influence not only the resident bone cell (osteoblast/osteocyte) population, but also their progenitors, biasing MSC differentiation towards bone (osteoblastogenesis) and away from fat (adipogenesis). In a follow-up test of this hypothesis, mice fed on a high-fat diet were subjected to low magnitude loading or placebo treatment [103, 104]. Suppression of adiposity by the mechanical signals was accompanied by a "mechanistic response" at the molecular level showing that loading significantly influenced MSC commitment to either an osteogenic (Runx2, a transcription factor central to osteoblastogenesis) or adipogenic (peroxisome proliferator-activated receptor [PPAR]γ, a transcription factor central to adipogenesis) fate. Runx2 expression was greater and PPARγ expression was decreased in mice that underwent LMMs compared with controls. The PPARγ transcription factor, when absent or present as a single copy, facilitates osteogenesis at least partly through enhanced canonical Wnt signaling [105, 106], a pathway critically important to MSC entry into the osteogenic lineage and expansion of the osteoprogenitor pool. Notably, low magnitude mechanical loading treatment also resulted in a 46% increase in the size of the MSC pool ($p < 0.05$) [103, 104]. These experiments, although not obviating a role for the osteoblast/osteocyte syncytium, provide evidence that bone marrow stem cells are capable of sensing exogenous mechanical signals and responding with an alteration in cell fate that ultimately influences both the bone and fat phenotype. Importantly, the inverse correlation of bone and fat phenotype has increasing support in the clinical literature. Although controversial, and despite the presumption that conditions such as obesity will inherently protect the skeleton owing to increased loading events, data in humans evaluating bone–fat interactions indicate that an ever-increasing adipose burden comes at the cost of bone structure and increased risk of fracture [107].

10 Osteocyte and Its Response to Mechanical Signals Coupled with Wnt Signaling

Osteocytes, cells embedded within the mineralized matrix of bone, are becoming the target of intensive investigation [100, 108–110]. Osteoblasts are defined as cells that make bone matrix, and are thought to translate mechanical loading into biochemical signals that affect bone modeling and remodeling. The interrelationship between osteoblasts and osteocytes would be expected to have the same lineage, yet these cells also have distinct differences, particularly in their responses to mechanical loading and utilization of the various biochemical pathways to accomplish their respective functions. Among many factors, Wnt/β-catenin signaling pathway may be recognized as an important regulator of bone mass and bone cell functions [100, 110]. While osteocytes are embedded within the mineral matrix, Wnt/β-catenin signaling pathway may serve as a transmitter to transfer mechanical signals sensed by osteocytes to the surface of bone. Further, new data suggest that the Wnt/β-catenin pathway in osteocytes may be triggered by crosstalk with the prostaglandin pathway in response to loading which then leads to a decrease in expression of negative regulators of the pathway such as Sclerostin (Sost) and Dickkopf-related protein 1 (Dkk-1) [66, 110]. Figure 1.8 indicates the potential pathway in response to mechanical loading.

It has been shown that the Wnt pathway is closely involved in bone cell differentiation, proliferation, and apoptosis [110, 111]. Regulation of the Wnt/β-catenin signaling pathway is vested largely in proteins that either act as competitive binders of Wnts, notably the secreted frizzled-related proteins (sFRP) family, or act at the level of low-density lipoprotein receptor-related protein 5 (LRP5), including the osteocyte-specific protein, sclerostin (the Sost gene product), and the Dkk proteins, particularly Dkk-1 and Dkk-2 [110–114]. Sclerostin has been shown to be made by mature osteocytes and inhibits Wnt/β-catenin signaling by binding to LRP5 and preventing the binding of Wnt. Dkk-1 is highly expressed in osteocytes [112–114]. Clinical trial studies using antibodies to sclerostin have also shown increased bone mass, suggesting that targeting of these negative regulators of Wnt/β-catenin signaling pathway might be anabolic treatments for diseases such as osteoporosis [112]. Finally, mechanical loading has been shown to reduce sclerostin levels in bone [112], suggesting that one of the targets of the pathways, activated by the early events after mechanical loading, is the genes encoding these negative modulators of the Wnt/β-catenin signaling pathway.

There is still much to be learned regarding how the bone cells, i.e., osteocyte, sense and transmit signals in response to or absence of loading and further elevate the activity of other cells. Although fluid shear stress is proposed as a triggering force, the identity of these particular mechanical signals is still a challenging area to study. The osteocyte is joining the osteoblast and osteoclast as targets for therapeutics to treat or prevent bone disease. Clearly targeting the Wnt/β-catenin pathway in osteocytes because of its central role in bone mass regulation and bone formation in response to mechanical loading may prove useful for designing new paradigms and pharmaceuticals to treat bone disease in the future.

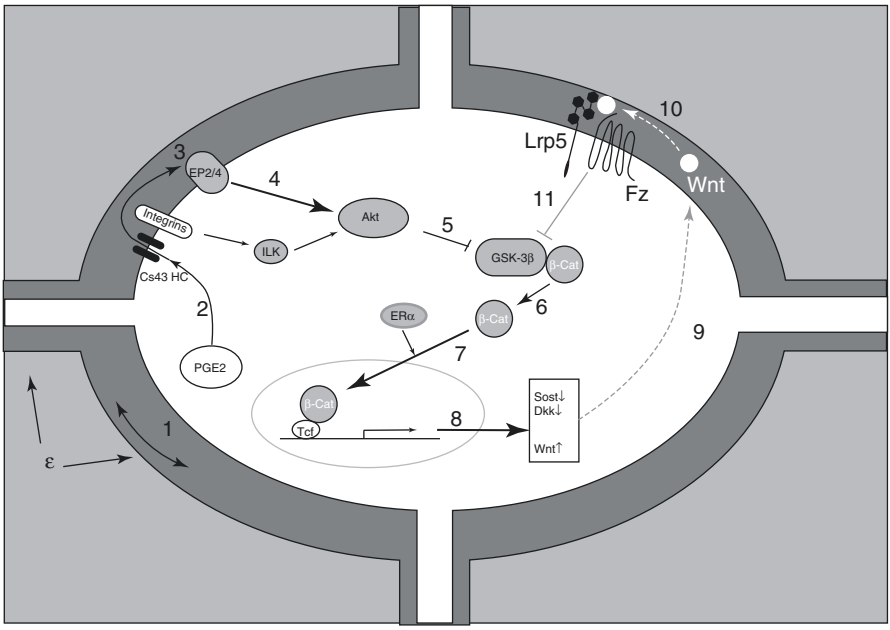

Fig. 1.8 Mechanical loading, e.g., fluid shear stress, induced Wnt signaling activation [110]. The mechanical load applied to bone (ε) is perceived by the osteocyte through an unknown mechanism, although fluid flow induced through the lacunar-canalicular system may be a critical component of this perception, "step **1**." Perception of load (strain) triggers a number of intracellular responses including the release of PGE2, "**2**" through a poorly understood mechanism into the lacunar-canalicular fluid where it can act in an autocrine and/or paracrine fashion. Connexin-43 hemichannels (CX43 HC) in this PGE2 and integrin proteins appear to be involved. Binding of PGE2 to its EP2 and/or EP4 receptor, "**3**," leads to a downstream inhibition of GSK-3β, "**5**" (likely mediated by Akt, "**4**") and the intracellular accumulation of free β-catenin, "**6**." (Integrin activation can also lead to Akt activation and GSK-3β inhibition.) New evidence suggests that ER may participate in the nuclear translocation of β-catenin, "**7**" which leads to changes in the expression of a number of key target genes "**8**." One of the apparent consequences is the reduction in sclerostin and Dkk1, "**9**" with increased expression of Wnt, "**10**" (which one or ones is unknown). The net result of these changes is to create a permissive environment for the binding of Wnt to Lrp5-Fz and amplification of the load signal, "**11**." (With permission of Bone)

10.1 The Role of LRP5 in Bone Responding to Mechanical Loading

LRP5 has been shown to have important functions in the mammalian skeleton. Experimental evidence has pointed LRP5 as a critical factor in translating mechanical signals into the proper skeletal response. For example, loss-of-function mutations in LRP5 have been reported to cause the autosomal recessive human disease Osteoporosis-Pseudoglioma syndrome (OPPG), which leads to a significant reduction of BMD, and are more susceptible to skeletal fracture and deformity [115–

117]. Moreover, the mechanical importance of LRP5 has been demonstrated in LRP5−/− mice, which were found with an almost complete ablation in the ulnar loading-induced bone formation compared to wild-type controls [117, 118]. Multiple single nucleotide polymorphisms (SNPs), located in exons 18 and 10, have been reported, which can significantly affect the interconnection between physical activity and bone mass [117, 119]. A high bone mass (HBM) phenotype in humans was reported to be caused by certain missense mutations near the N-terminus of LRP5 [120, 121]. An LRP5 overexpression mutation is, on the other hand, associated with high bone mass and induced osteoblast proliferation [120]. Increased sensitivity to load due to a lower threshold for initiating bone formation was also reported with this mouse [121]. A recent study done by Zhong et al. showed that *in vitro* tension on MC3T3-E1 cells increased LRP5 gene expression at 1, 3, and 5 h of loading [122].

10.2 MicroRNA and Its Role in Mechanotransduction in Tissue

The newly discovered MicroRNAs (miRNAs) are short noncoding RNAs, which can be complementary to messenger RNA (mRNA) sequences to silence gene expression by either degradation or inhibitory translation of target transcripts [123, 124]. Regulation of Runx2, bone morphogenic protein (BMP), and Wnt signaling pathways is by far the most well-studied miRNA-related osteoblast function. Positive and negative regulations of miRNAs on Runx2 expression have been shown to affect skeletal morphogenesis and osteoblastogenesis [125]. Inhibition of osteoblastogenesis can result from miRNA-135 and miRNA-26a regulated BMP-2/Smad signaling pathway [126]. Activation of Wnt signaling through miRNA-29a-targeted Wnt inhibitors is upregulated during osteoblast differentiation [127]. In addition, studies have been done to investigate the miRNA function on self-renewal and lineage determination for tissue regeneration via human stromal stem cells [128, 129]. Moreover, extensive studies have also been done to access the effects of miRNAs on osteogenic functions in committed cell lines including osteoprogenitors, osteoblasts, and osteocytic cell lines. In general, actions of miRNA may affect bone cell differentiation in either positive or negative ways [123, 129].

Recent research has gained interests in studying the transcription and microRNA regulation to better understand gene expression regulation in a mechanical loading model. Transcription factors can bind to motifs in the promoter of genes and directly affect their expression; therefore, mechanotransduction in bone may result in transcription factors alteration for regulation. Using a predictive bioinformatics algorithm, a recent study investigated the time-dependent regulatory mechanisms that governed mechanical loading-induced gene expression in bone. Axial loading was performed on the right forelimb in rodents. A linear model of gene expression was created and 44 transcription factor binding motifs and 29 microRNA binding sites were identified to predict the regulated gene expression across the time course. It

may be important in controlling the loading-induced bone formation process via the time-dependent regulatory mechanisms.

10.3 Mechanotransductive Implication in Bone Tissue Engineering

Development of artificial scaffold for musculoskeletal applications could take advantages of the mechanotransduction phenomena to achieve its integrity and function, which can lead to tissue healing. Mechanical signals delivered to bone cells may be interfered by the scaffold deformation, and should be taken into account. Fortunately, mechanotransduction could be used to control the proliferation and differentiation of bone cells [130–134]. Fluid flow has been proposed as an important mechanical aspect to be considered when developing bone scaffolds [132–136]. Studies using bioreactors have helped us understand the phenomena of mechanotransduction used in scaffold design [130]. For example, rotating bioreactors, flow perfusion bioreactors, and other mechanical stimuli such as strain have been designed to increase mass transfer by inducing dynamic flow conditions in culture, to create osteoinductive factors on mesenchymal stem cells by the generated fluid shear stress [137], and to induce the osteogenic differentiation of mesenchymal stem cells [138], respectively. Among all, mimicking the natural bone strain to favor osteogenesis is one of the most rational aims for scaffold development. Matching of the strain histograms of a scaffold and the actual bone can be performed using microCT measurements and finite element method [132, 139, 140].

11 Biomechanics of Articular Cartilage

11.1 The Composition of Articular Cartilage

As a kind of connective tissue, articular cartilage is a white, smooth, and thin layer that covers the surfaces of bones in diarthrodial joints [94]. Its primary function is to bear physical stress, distribute the mechanical load, absorb the shock, and lubricate the friction between bones in a joint during daily activities [141–143].

Articular cartilage has a highly organized layered structure. And it can be divided into four zones based on the cell shape, size, and collagen direction (as shown in Fig. 1.9) [142, 143]: (1) superficial zone (10–20%), elongated chondrocytes and thin collagen fibrils are parallel to the surface of joints in this zone; (2) middle zone (40–60%), spherical chondrocytes and larger collagen fibrils are randomly oriented; (3) deep zone (30–40%), spherical chondrocytes and larger collagen fibrils are perpendicular to the joint surface; (4) calcified zone (5%), the main components of the calcified zone are calcium salts deposition without chondrocytes or collagens [143].

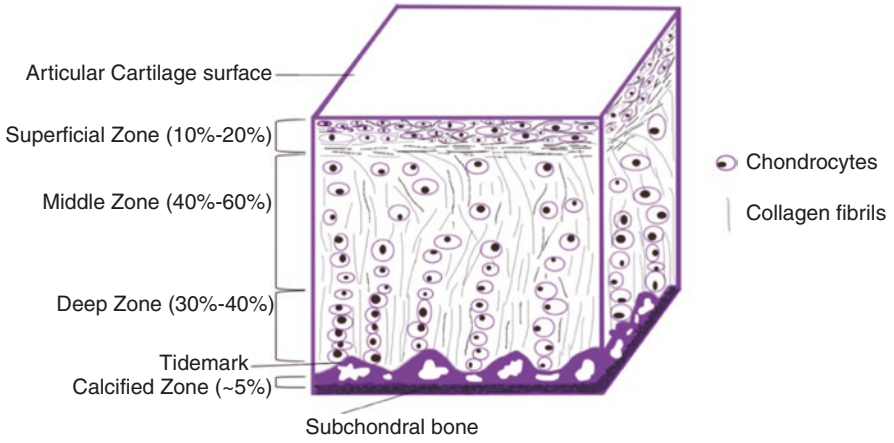

Fig. 1.9 The stratified structure of articular cartilage and the arrangement of chondrocytes and collagen fibrils in each zone. There are three primary layers in normal articular cartilage. The cell shapes are shown specific shapes in various zones, e.g., flat in the superficial zone, round in the middle zone, and column-like in the deep zone

Articular cartilage consists of chondrocytes and an extracellular matrix (ECM) [144, 145]. Chondrocytes are the sole type of cells in articular cartilage, and only make up 2% of the volume of articular cartilage [141–143]. They originate from mesenchymal stem cells (MSCs), and are highly specialized cells. And they vary in shape, size, and number in different zones of articular cartilage [141–143].

ECM is mainly composed of macromolecules including proteoglycans (PGs) (5–10% wet weight), collagen (10–20% wet weight), and water (60–80%) [142, 145]. Almost 90% Collagen in ECM is type II collagen, and they form a firm collagen network in articular cartilage [141–145]. Collagen types I, IV, V, VI, IX, and XI contribute only a minor proportion. PGs primarily exist as aggregates formed by a high density of negative charge sulfated glycosaminoglycan (sGAG) [146] (as shown in Fig. 1.10).

11.2 The Effect of Mechanical Load on the Metabolism of Articular Cartilage

Compared with other tissues such as bone and muscle, articular cartilage in diarthrodial joints does not contain blood vessels, lymphatic vessels, and nerves, and therefore the nutrients are transported to the chondrocytes from the synovial fluid in joint movements. The capacity of articular cartilage self-repair is very limited, and could not be able to heal on its own. During daily activities, articular cartilage experiences the mechanical environment changes caused by joint movements. And it can respond to a variety of mechanical stress, strain, and pressure generated by normal load-bearing activities in the walking, running, and other daily exercises [145]. The

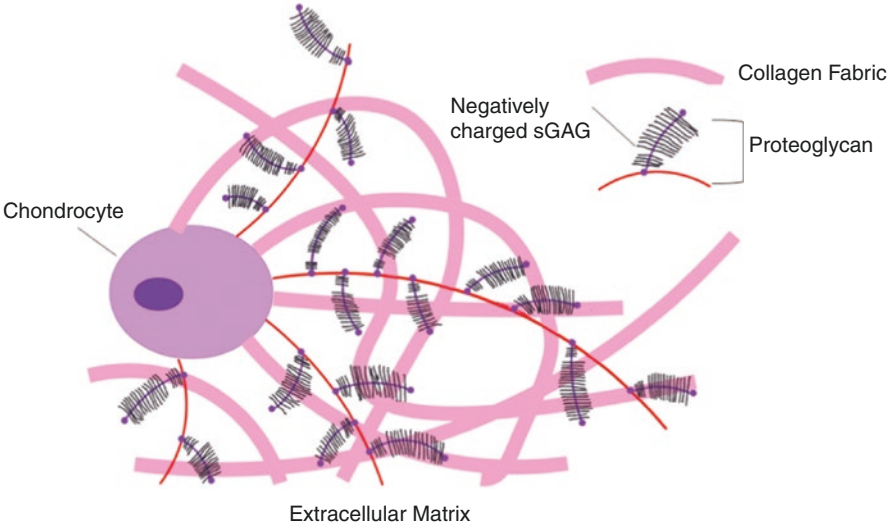

Fig. 1.10 The proteoglycan, collagen, and chondrocyte in the extracellular matrix of the articular cartilage

chondrocytes and ECM play a unique role in the anabolism and catabolism of articular cartilage, and are responsible for the maintenance of the structural integrity and mechanical function of articular cartilage.

Chondrocytes are sparsely embedded in the ECM [141–143, 145]. They have a low level of metabolic activity and replication due to the limited nutrition transportation from the synovial fluid [145]. For each chondrocyte, it can establish its microenvironment and trap itself in its matrix, which could prevent their migration to the adjacent area of cartilage. And the communication between cells and direct cell-to-cell signal transduction is limited under this microenvironment trap. The survival of chondrocytes in ECM mainly depends on the mechanical and chemical environment provided by articular cartilage, and they can regulate ECM in their vicinity area by sensing the mechanical force in their surrounding microenvironment and responding to mechanical stimuli caused by the physical load of joints, such as compressive, tensile, and shear stress.

Moreover, the negatively charged sGAG in ECM can attract ions, and provide articular cartilage with the osmotic imbalance in the ionic interstitial fluid, which leads to absorb water and induces a swelling pressure to resist compression loads [143, 145]. The collagen network in ECM enables articular cartilage to resist tension and shear forces. The mechanical balance between sGAG and collagen in ECM is responsible for the stable micromechanical environment for chondrocytes [143, 145]. Taken together, the chondrocytes could sense mechanical signals to synthesize and maintain the turnover of ECM. In turn, the ECM could protect chondrocytes from potentially damaging biomechanical forces and enables articular cartilage to support the physical load in our daily life. The interactions between chondrocytes and ECM are crucial for the homeostasis of articular cartilage.

11.3 The Degeneration of Articular Cartilage Caused by Joint Overuse/Disuse

Articular cartilage could maintain its structural integrity and mechanical function under joint normal loading conditions during routine daily activity. However, the homeostasis of articular cartilage is interrupted when it is exposed to insufficient or excessive mechanical loading conditions, and could cause cartilage degeneration with a consequence of joint diseases, such as osteoarthritis. Previous studies have found that the synthesis of proteoglycan decreased and cartilage degeneration was observed under joint overuse conditions in marathon runners or animal with running exercises (as shown in Table 1.1) [147–153]. Besides, prolonged joint disuse or joint immobilization can cause joint atrophy and AC degeneration [153–157]. Progressive thinning of AC and the degradation of the extracellular matrix (ECM) has been reported in both immobilized patients and unload animal models [153–157]. And the animal studies also demonstrated that the thickness of cartilage became thinner and the underlying subchondral bone increased in osteoarthritis group induced by anterior cruciate ligament transection; moreover, in hind limb suspension group, the irregular and lose distributions of chondrocytes in cartilage were found due to mechanical functional disuse. However, low-intensity ultrasound stimulation could generate acoustic pressure waves with mechanical energy, and it could mitigate the cartilage degeneration [5, 143, 145] (as shown in Fig. 1.11).

Table 1.1 Safranin O intensity of cartilage in the lateral middle section of tibia (ratio = experimental/control) [147]

	Immobilization/remobilization			Running		
Cartilage zones	Immobilization for 11 weeks	Remobilization for 15 weeks	Remobilization for 50 weeks	Moderate (4 km/day, 15 weeks)	Strenuous (20 km/day, 15 weeks)	Endurance (40 km/day, 15 weeks)
Superficial zone	0.58*	0.82	0.81	0.81	0.95	0.62**
Middle zone	0.80	1.00	0.81	0.90	1.02	1.00
Deep zone	0.82	0.95	0.93	0.90	1.00	1.00
Calcified zone	1.00	1.00	0.80	1.20	1.01	0.98

Changes of Safranin O intensity in different cartilage zones of the canine knee joints in the intermediate section of the latéral condyle of the tibia under immobilization/remobilization conditions and running conditions. The two-tailed Mann-Whitney U-test or Wilcoxon's matched-pairs signed-ranks tests was used for statistical analysis

*$p < 0.05$

**$p < 0.01$

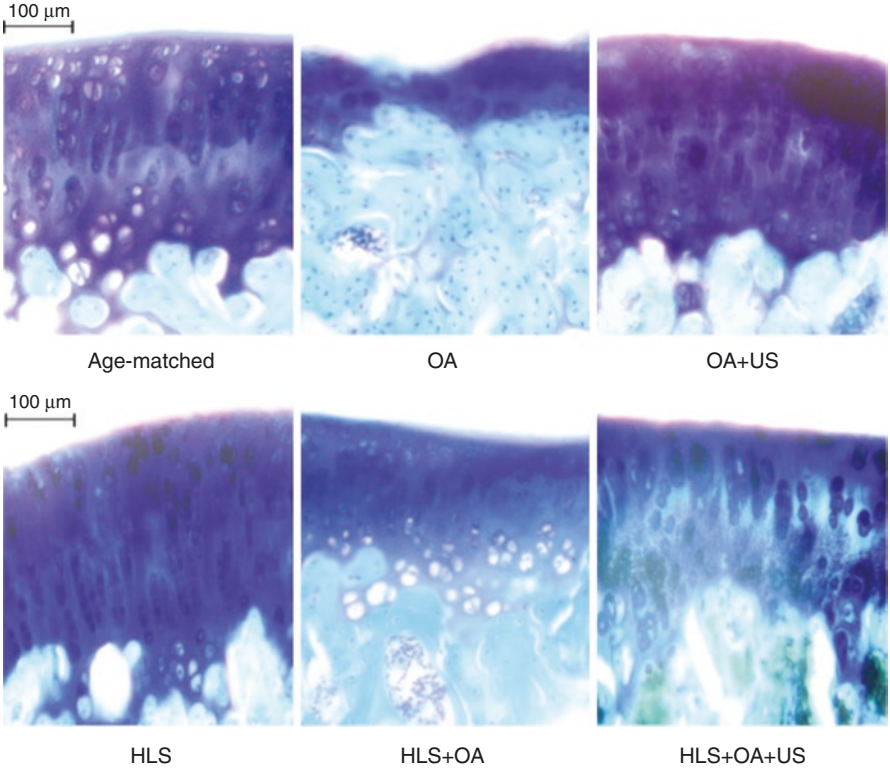

Fig. 1.11 The toluidine blue and fast green staining of cartilage in right tibial plateau in different groups (*OA* osteoarthritis, *US* ultrasound, *HLS* hind limb suspension) [158]

12 Discussion

These data have suggested that dynamic stimulation generates fluid pressure in bone with simultaneously low-level bone strain. MS adjacent to the rat femur induces a peak ImP at 20–30 Hz. The increase in bone fluid pressure suggests that hypertension in the skeletal nutrient vessels may increase ImP and regulate fluid flow in bone [56]. Similarly, the bone strain was highest at approximately 10 Hz. Stimulus-induced bone fluid and matrix deformation are dependent on stimulation frequency. It appears that the oscillatory MS stimulates relatively high fluid pressure at the frequency range between 20 Hz and 50 Hz in the tested frequencies up to 100 Hz. In such optimized loading rate (e.g., 20–50 Hz), relatively high ImP and relatively low bone strain were observed in response to the MS loading, which may be critical to regulating fluid flow, and adaptation in bone as a functional loading frequency-dependent manner. It is also noted that both ImP and strain at 10 Hz and 20 Hz are

higher than the value at a lower frequency, i.e., 1 Hz. There is a significant strain difference between 10 Hz and 20 Hz, while no significant ImP difference was observed between 10 Hz and 20 Hz. At an optimal frequency, MS can produce high fluid pressure gradients within the femoral marrow cavity and a high strain value in bone. It is possible that loading generated matrix strain and fluid pressure in bone may have combined effects in adaptation if loaded at relatively high frequencies.

Dynamic muscle stimulation was able to inhibit bone loss and trabecular architectural deterioration caused by a lack of daily weight-bearing activities. The importance of selecting an effective loading regimen was investigated in this study, in which a wide range of stimulation frequencies was tested to determine their effects on skeletal adaptive responses. Throughout this study, we have referred 1 Hz as low frequency, 20 Hz and 50 Hz as mid frequency, and 100 Hz as high frequency. From our results, we concluded that the effectiveness of dynamic MS was greatly dependent on the stimulation frequency. The optimized frequency, which resulted in a strong adaptive response in the disuse osteopenia model, was in the range of 50 Hz. While the strain level generated at 50 Hz by MS was relatively low, e.g., approximately 10 με, the adaptive response may be mainly contributed by induced fluid flow, and uncoupled to strain [159]. The degree of effectiveness of MS in attenuating bone loss varied in different regions of the distal femur. Such spatial response may also depend on the fluid pressure generated in the local region as a dose-dependent manner. While low-frequency MS was unsuccessful in preventing osteopenia, mid-frequency MS applied to the quadriceps was able to maintain trabecular bone mass.

These results were consistent with previous *in vivo* results in which mechanical loading at frequencies between 20 Hz and 50 Hz was shown to be anti-catabolic to bone [53, 160–162]. This sensitivity was even more apparent in trabecular bone, perhaps due to the increased surface area in the trabecular network, which exposes it to rapid changes in fluid pressure [163]. For example, trabecular osteoblast surface in the tibia was increased by 26% when an MS protocol at 10 Hz was applied for 3 weeks [162]. Likewise, whole body vibration at 45 Hz increased the rate of formation of the growing skeleton by 30% [164].

Both ImP and matrix strain have indicated a nonlinear response in the MS spectrum between 1 Hz and 100 Hz, though peaked differently at 20 Hz (ImP) and 10 Hz (strain). While no obvious muscle fatigue was observed, perhaps due to the rest period during the stimulation, the mechanism behind such a nonlinear response is not clear. From the characteristics of tissue material point of view, e.g., the viscoelastic property of the tissues, both muscle and bone could quickly dampen the response at high frequencies through the MS loading. But, due to the difference in densities and viscosities between muscle and bone, MS induced ImP, and matrix strain could result in different frequency responses or optimized/resonant patterns for different tissues against the loading. In addition, mechanotransduction of MS through different connective tissues may attenuate the high-frequency response in bone, e.g., via the connective pathway from muscle, tendon to bone, thus resulting in peak strain and peak ImP at varied frequencies. Future research on such complex interrelations between muscle kinematics, bone fluid flow, and matrix strain is necessary to elucidate the mechanism further.

Even in the absence of bone matrix strain, previous data have shown that ImP alone can induce bone adaptation [161]. Using a turkey ulna osteotomy model, disuse alone resulted in a 5.7% loss of cortical bone. Direct fluid loading at 20 Hz for 4 weeks increased cortical bone mass by 18% by enhancing the formation of bone at both periosteal and endosteal surfaces [161]. Transcortical fluid pressure gradient and total bone formation were strongly and positively correlated. Bone fluid flow plays an important role in triggering bone remodeling [165–167]. Strong evidence suggests that interstitial fluid flow in bone interacts strongly with external muscular activities via various mechanisms [168, 169]. According to a muscle pump hypothesis, an arteriovenous pressure gradient enhances muscle perfusion [54, 170]. This process may, in turn, increase the hydraulic pressure in skeletal nutrient vessels and amplify the capillary filtration in bone tissue [54–56].

As a clinical application, MS on spinal cord-injured patients can cause a partial reversal of disuse osteopenia and recovery of muscular strength [92]. Other *in vivo* studies have also reported positive effects of using muscle stimulation to inhibit muscle atrophy. Immobilization studies using MS at 50–100 Hz have shown to minimize the reduction of the cross-sectional area of muscle fiber and to restore mechanical properties [171, 172]. Previous data showed that stimulation of distal nerve stumps had similar action potential response between normal and innervated muscle [173]. Although the response of ImP and bone mass by MS under such periphery nerve block conditions still remains unknown, MS could serve as a mitigating agent to retain bone mass under chronic nerve damage conditions, e.g., spinal cord injury. Taken together with the results from our current study, dynamic MS may be applied as both a skeletal therapy and a muscular therapy to prevent osteopenia and sarcopenia.

Loading-induced fluid flow in the musculoskeletal tissues may ultimately enhance interstitial flow and mechanotransduction in bone. Furthermore, dynamic loading, if applied at an optimal frequency, has been shown to have preventive potential in osteopenia in a functional disuse environment as a biomechanically based intervention for preventing and treating osteoporosis and muscle atrophy.

Acknowledgments This research was supported by the National Institutes of Health (R01 AR52379, AR61821, and AR49286), and the National Space Biomedical Research Institute through a NASA Cooperative Agreement NCC 9-58. The authors are grateful to Ms. Alyssa Tuthill for her technical assistance and all the members in the Orthopaedic Bioengineering Research Lab, particularly for their tireless assistance in the study.

References

1. Ozdurak RH, Duz S, Arsal G, Akinci Y, Kablan N, Isikli S, Korkusuz F. Quantitative forearm muscle strength influences radial bone mineral density in osteoporotic and healthy males. Technol Health Care. 2003;11:253–61.
2. Srinivasan S, Weimer DA, Agans SC, Bain SD, Gross TS. Low-magnitude mechanical loading becomes osteogenic when rest is inserted between each load cycle. J Bone Miner Res. 2002;17:1613–20.

3. Gerdhem P, Ringsberg KA, Akesson K, Obrant KJ. Influence of muscle strength, physical activity and weight on bone mass in a population-based sample of 1004 elderly women. Osteoporos Int. 2003;14:768–72.
4. Gerdhem P, Ringsberg KA, Magnusson H, Obrant KJ, Akesson K. Bone mass cannot be predicted by estimations of frailty in elderly ambulatory women. Gerontology. 2003;49:168–72.
5. LeBlanc A. Summary of research issues in human studies. Bone. 1998;22:117S–8S.
6. LeBlanc A, Lin C, Shackelford L, Sinitsyn V, Evans H, Belichenko O, Schenkman B, Kozlovskaya I, Oganov V, Bakulin A, Hedrick T, Feeback D. Muscle volume, MRI relaxation times (T2), and body composition after spaceflight. J Appl Physiol. 2000;89:2158–64.
7. LeBlanc AD, Evans HJ, Johnson PC, Jhingran S. Changes in total body calcium balance with exercise in the rat. J Appl Physiol. 1983;55:201–4.
8. Convertino VA, Sandler H. Exercise countermeasures for spaceflight. Acta Astronaut. 1995;35:253–70.
9. Fluckey JD, Dupont-Versteegden EE, Montague DC, Knox M, Tesch P, Peterson CA, Gaddy-Kurten D. A rat resistance exercise regimen attenuates losses of musculoskeletal mass during hindlimb suspension. Acta Physiol Scand. 2002;176:293–300.
10. Keller TS, Strauss AM, Szpalski M. Prevention of bone loss and muscle atrophy during manned space flight. Microgravity Q. 1992;2:89–102.
11. McPhee JC, White RJ. Physiology, medicine, long-duration space flight and the NSBRI. Acta Astronaut. 2003;53:239–48.
12. Grigoriev A, Morukov B, Stupakov G, Bobrovnik E. Influence of bisphosphonates on calcium metabolism and bone tissue during simulation of the physiological effects of microgravity. J Gravit Physiol. 1998;5:69–70.
13. LeBlanc A, Marsh C, Evans H, Johnson P, Schneider V, Jhingran S. Bone and muscle atrophy with suspension of the rat. J Appl Physiol. 1985;58:1669–75.
14. LeBlanc A, Schneider V. Countermeasures against space flight related bone loss. Acta Astronaut. 1992;27:89–92.
15. LeBlanc A, Rowe R, Schneider V, Evans H, Hedrick T. Regional muscle loss after short duration spaceflight. Aviat Space Environ Med. 1995;66:1151–4.
16. Convertino VA. Mechanisms of microgravity induced orthostatic intolerance: implications for effective countermeasures. J Gravit Physiol. 2002;9:1–13.
17. Serova LV. Microgravity and aging of animals. J Gravit Physiol. 2001;8:137–8.
18. Mayet-Sornay MH, Hoppeler H, Shenkman BS, Desplanches D. Structural changes in arm muscles after microgravity. J Gravit Physiol. 2000;7:S43–4.
19. Larina IM, Tcheglova IA, Shenkman BS, Nemirovskaya TL. Muscle atrophy and hormonal regulation in women in 120 day bed rest. J Gravit Physiol. 1997;4:121–2.
20. Wolff J. Das Gesetz Der Transformation Der Knochen. Berlin, Hirschwald; 1892.
21. Wolff J. The law of bone remodeling. Berlin: Springer; 1986.
22. Evans FG. The mechanical properties of bone. Artif Limbs. 1969;13:37–48.
23. Evans FG. Factors affecting the mechanical properties of bone. Bull N Y Acad Med. 1973;49:751–64.
24. Evans FG, Vincentelli R. Relations of the compressive properties of human cortical bone to histological structure and calcification. J Biomech. 1974;7:1–10.
25. Martin RB, Burr DB. Structure, function and adaptation of compact bone. New York: Raven; 1989.
26. Stokes IA. Analysis of symmetry of vertebral body loading consequent to lateral spinal curvature. Spine. 1997;22:2495–503.
27. Donaldson CL, Hulley SB, Vogel JM, Hattner RS, Bayers JH, McMillan DE. Effect of prolonged bed rest on bone mineral. Metabolism. 1970;19:1071–84.
28. Gross TS, Edwards JL, McLeod KJ, Rubin CT. Strain gradients correlate with sites of periosteal bone formation. J Bone Miner Res. 1997;12:982–8.
29. Qin YX, Otter MW, Rubin CT, McLeod KJ. The influence of intramedullary hydrostatic pressure on transcortical fluid flow patterns in bone. Trans Ortho Res Soc. 1997;22:885.

30. Rubin CT, Lanyon LE. Regulation of bone formation by applied dynamic loads. J Bone Joint Surg Am. 1984;66:397–402.
31. Turner CH. Site-specific skeletal effects of exercise: importance of interstitial fluid pressure. Bone. 1999;24:161–2.
32. Jones HH, Priest JD, Hayes WC, Tichenor CC, Nagel DA. Humeral hypertrophy in response to exercise. J Bone Joint Surg Am. 1977;59:204–8.
33. Judex S, Zernicke RF. High-impact exercise and growing bone: relation between high strain rates and enhanced bone formation. J Appl Physiol. 2000;88:2183–91.
34. Krolner B, Toft B, Pors NS, Tondevold E. Physical exercise as prophylaxis against involutional vertebral bone loss: a controlled trial. Clin Sci (Lond). 1983;64:541–6.
35. Nilsson BE, Westlin NE. Bone density in athletes. Clin Orthop. 1971;77:179–82.
36. Stokes IA, Aronsson DD, Spence H, Iatridis JC. Mechanical modulation of intervertebral disc thickness in growing rat tails. J Spinal Disord. 1998;11:261–5.
37. Joyner MJ, Lennon RL, Wedel DJ, Rose SH, Shepherd JT. Blood flow to contracting human muscles: influence of increased sympathetic activity. J Appl Physiol. 1990;68:1453–7.
38. Joyner MJ. Does the pressor response to ischemic exercise improve blood flow to contracting muscles in humans? J Appl Physiol. 1991;71:1496–501.
39. Joyner MJ, Nauss LA, Warner MA, Warner DO. Sympathetic modulation of blood flow and O2 uptake in rhythmically contracting human forearm muscles. Am J Physiol. 1992;263:H1078–83.
40. Joyner MJ, Wieling W. Increased muscle perfusion reduces muscle sympathetic nerve activity during handgripping. J Appl Physiol. 1993;75:2450–5.
41. Joyner MJ, Dietz NM. Nitric oxide and vasodilation in human limbs. J Appl Physiol. 1997;83:1785–96.
42. Joyner MJ, Proctor DN. Muscle blood flow during exercise: the limits of reductionism. Med Sci Sports Exerc. 1999;31:1036–40.
43. Joyner MJ. Blood pressure and exercise: failing the acid test. J Physiol. 2001;537:331.
44. Hicks A, McGill S, Hughson RL. Tissue oxygenation by near-infrared spectroscopy and muscle blood flow during isometric contractions of the forearm. Can J Appl Physiol. 1999;24:216–30.
45. Mak AF, Huang L, Wang Q. A biphasic poroelastic analysis of the flow dependent subcutaneous tissue pressure and compaction due to epidermal loadings: issues in pressure sore. J Biomech Eng. 1994;116:421–9.
46. Qin YX, Lin W, Rubin C. The pathway of bone fluid flow as defined by in vivo intramedullary pressure and streaming potential measurements. Ann Biomed Eng. 2002;30(5):693–2.
47. Qin YX, Hu M. Mechanotransduction in musculoskeletal tissue regeneration: effects of fluid flow, loading, and cellular-molecular pathways. Biomed Res Int. 2014;2014:863421.
48. Frost HM. Intermediary organization of the skeleton. Boca Raton, FL: CRC Press; 1986.
49. Frost HM. Bone's mechanostat: a 2003 update. Anat Rec. 2003;275A:1081–101.
50. Cowin SC. Bone mechanics. Boca Raton, FL: CRC Press; 1989.
51. Cowin SC. Bone poroelasticity. J Biomech. 1999;32:217–38.
52. Piekarski K, Demetriades D, Mackenzie A. Osteogenetic stimulation by externally applied dc current. Acta Orthop Scand. 1978;49:113–20.
53. Qin Y-X, Rubin CT, McLeod KJ. Non-linear dependence of loading intensity and cycle number in the maintenance of bone mass and morphology. J Orthop Res. 1998;16:482–9.
54. Laughlin MH. The muscle pump: what question do we want to answer? J Appl Physiol. 2005;99:774.
55. Otter MW, Qin YX, Rubin CT, McLeod KJ. Does bone perfusion/reperfusion initiate bone remodeling and the stress fracture syndrome? Med Hypotheses. 1999;53:363–8.
56. Winet H. A bone fluid flow hypothesis for muscle pump-driven capillary filtration: II. Proposed role for exercise in erodible scaffold implant incorporation. Eur Cell Mater. 2003;6:1–10.

57. Lanyon LE, Rubin CT. Static vs dynamic loads as an influence on bone remodelling. J Biomech. 1984;17:897–905.
58. Rubin CT, Lanyon LE. Kappa Delta Award paper. Osteoregulatory nature of mechanical stimuli: function as a determinant for adaptive remodeling in bone. J Orthop Res. 1987;5:300–10.
59. Biering-Sorensen F, Bohr HH, Schaadt OP. Longitudinal study of bone mineral content in the lumbar spine, the forearm and the lower extremities after spinal cord injury. Eur J Clin Invest. 1990;20:330–5.
60. Dauty M, Perrouin VB, Maugars Y, Dubois C, Mathe JF. Supralesional and sublesional bone mineral density in spinal cord-injured patients. Bone. 2000;27:305–9.
61. Garland DE, Adkins RH, Stewart CA, Ashford R, Vigil D. Regional osteoporosis in women who have a complete spinal cord injury. J Bone Joint Surg Am. 2001;83-A:1195–200.
62. Lazo MG, Shirazi P, Sam M, Giobbie-Hurder A, Blacconiere MJ, Muppidi M. Osteoporosis and risk of fracture in men with spinal cord injury. Spinal Cord. 2001;39:208–14.
63. Ryg J, Rejnmark L, Overgaard S, Brixen K, Vestergaard P. Hip fracture patients at risk of second hip fracture: a nationwide population-based cohort study of 169,145 cases during 1977-2001. J Bone Miner Res. 2009;24:1299–307.
64. Vestergaard P, Krogh K, Rejnmark L, Mosekilde L. Fracture rates and risk factors for fractures in patients with spinal cord injury. Spinal Cord. 1998;36:790–6.
65. Vestergaard P, Rejnmark L, Mosekilde L. Osteoarthritis and risk of fractures. Calcif Tissue Int. 2009;84:249–56.
66. Armstrong VJ, Muzylak M, Sunters A, Zaman G, Saxon LK, Price JS, Lanyon LE. Wnt/beta-catenin signaling is a component of osteoblastic bone cell early responses to load-bearing and requires estrogen receptor alpha. J Biol Chem. 2007;282:20715–27.
67. Heaney RP. Pathophysiology of osteoporosis. Endocrinol Metab Clin North Am. 1998;27:255–65.
68. Ingram RR, Suman RK, Freeman PA. Lower limb fractures in the chronic spinal cord injured patient. Paraplegia. 1989;27:133–9.
69. Szollar SM, Martin EM, Sartoris DJ, Parthemore JG, Deftos LJ. Bone mineral density and indexes of bone metabolism in spinal cord injury. Am J Phys Med Rehabil. 1998;77:28–35.
70. Macdonald JH, Evans SF, Davie MW, Sharp CA. Muscle mass deficits are associated with bone mineral density in men with idiopathic vertebral fracture. Osteoporos Int. 2007;18:1371–8.
71. McCarthy I, Goodship A, Herzog R, Oganov V, Stussi E, Vahlensieck M. Investigation of bone changes in microgravity during long and short duration space flight: comparison of techniques. Eur J Clin Invest. 2000;30:1044–54.
72. Lang T, LeBlanc A, Evans H, Lu Y, Genant H, Yu A. Cortical and trabecular bone mineral loss from the spine and hip in long-duration spaceflight. J Bone Miner Res. 2004;19:1006–12.
73. Burr DB, Frederickson RG, Pavlinch C, Sickles M, Burkart S. Intracast muscle stimulation prevents bone and cartilage deterioration in cast-immobilized rabbits. Clin Orthop. 1984;189:264–78.
74. LeBlanc A, Rowe R, Evans H, West S, Shackelford L, Schneider V. Muscle atrophy during long duration bed rest. Int J Sports Med. 1997;18(Suppl 4):S283–5.
75. Narici M, Kayser B, Barattini P, Cerretelli P. Effects of 17-day spaceflight on electrically evoked torque and cross-sectional area of the human triceps surae. Eur J Appl Physiol. 2003;90:275–82.
76. Gorgey AS, Dudley GA. Skeletal muscle atrophy and increased intramuscular fat after incomplete spinal cord injury. Spinal Cord. 2007;45:304–9.
77. Shah PK, Stevens JE, Gregory CM, Pathare NC, Jayaraman A, Bickel SC, Bowden M, Behrman AL, Walter GA, Dudley GA, Vandenborne K. Lower-extremity muscle cross-sectional area after incomplete spinal cord injury. Arch Phys Med Rehabil. 2006;87:772–8.
78. Riley DA, Slocum GR, Bain JL, Sedlak FR, Sowa TE, Mellender JW. Rat hindlimb unloading: soleus histochemistry, ultrastructure, and electromyography. J Appl Physiol. 1990;69:58–66.

79. Roy RR, Pierotti DJ, Garfinkel A, Zhong H, Baldwin KM, Edgerton VR. Persistence of motor unit and muscle fiber types in the presence of inactivity. J Exp Biol. 2008;211:1041–9.
80. Zhong H, Roy RR, Siengthai B, Edgerton VR. Effects of inactivity on fiber size and myonuclear number in rat soleus muscle. J Appl Physiol. 2005;99:1494–9.
81. Stewart BG, Tarnopolsky MA, Hicks AL, McCartney N, Mahoney DJ, Staron RS, Phillips SM. Treadmill training-induced adaptations in muscle phenotype in persons with incomplete spinal cord injury. Muscle Nerve. 2004;30:61–8.
82. Zhou MY, Klitgaard H, Saltin B, Roy RR, Edgerton VR, Gollnick PD. Myosin heavy chain isoforms of human muscle after short-term spaceflight. J Appl Physiol. 1995;78: 1740–4.
83. Griffin L, Decker MJ, Hwang JY, Wang B, Kitchen K, Ding Z, Ivy JL. Functional electrical stimulation cycling improves body composition, metabolic and neural factors in persons with spinal cord injury. J Electromyogr Kinesiol. 2009;19:614–22.
84. Lim PA, Tow AM. Recovery and regeneration after spinal cord injury: a review and summary of recent literature. Ann Acad Med Singapore. 2007;36:49–57.
85. Rodgers MM, Glaser RM, Figoni SF, Hooker SP, Ezenwa BN, Collins SR, Mathews T, Suryaprasad AG, Gupta SC. Musculoskeletal responses of spinal cord injured individuals to functional neuromuscular stimulation-induced knee extension exercise training. J Rehabil Res Dev. 1991;28:19–26.
86. Shields RK, Dudley-Javoroski S. Musculoskeletal adaptations in chronic spinal cord injury: effects of long-term soleus electrical stimulation training. Neurorehabil Neural Repair. 2007;21:169–79.
87. Dudley-Javoroski S, Littmann AE, Iguchi M, Shields RK. Doublet stimulation protocol to minimize musculoskeletal stress during paralyzed quadriceps muscle testing. J Appl Physiol. 2008;104:1574–82.
88. Dudley-Javoroski S, Shields RK. Muscle and bone plasticity after spinal cord injury: review of adaptations to disuse and to electrical muscle stimulation. J Rehabil Res Dev. 2008;45:283–96.
89. Dudley-Javoroski S, Shields RK. Dose estimation and surveillance of mechanical loading interventions for bone loss after spinal cord injury. Phys Ther. 2008;88:387–96.
90. Yang YS, Koontz AM, Triolo RJ, Cooper RA, Boninger ML. Biomechanical analysis of functional electrical stimulation on trunk musculature during wheelchair propulsion. Neurorehabil Neural Repair. 2009;23:717–25.
91. BeDell KK, Scremin AM, Perell KL, Kunkel CF. Effects of functional electrical stimulation-induced lower extremity cycling on bone density of spinal cord-injured patients. Am J Phys Med Rehabil. 1996;75:29–34.
92. Belanger M, Stein RB, Wheeler GD, Gordon T, Leduc B. Electrical stimulation: can it increase muscle strength and reverse osteopenia in spinal cord injured individuals? Arch Phys Med Rehabil. 2000;81:1090–8.
93. Mohr T. [Electric stimulation in muscle training of the lower extremities in persons with spinal cord injuries]. Ugeskr Laeger. 2000;162:2190–4.
94. Allen MR, Hogan HA, Bloomfield SA. Differential bone and muscle recovery following hindlimb unloading in skeletally mature male rats. J Musculoskelet Neuronal Interact. 2006;6:217–25.
95. Swift JM, Nilsson MI, Hogan HA, Sumner LR, Bloomfield SA. Simulated resistance training during hindlimb unloading abolishes disuse bone loss and maintains muscle strength. J Bone Miner Res. 2010;25:564–74.
96. Qin YX, Lam H. Intramedullary pressure and matrix strain induced by oscillatory skeletal muscle stimulation and its potential in adaptation. J Biomech. 2009;42:140–5.
97. Lam H, Qin YX. The effects of frequency-dependent dynamic muscle stimulation on inhibition of trabecular bone loss in a disuse model. Bone. 2008;43:1093–100.
98. Morey-Holton ER, Globus RK. Hindlimb unloading of growing rats: a model for predicting skeletal changes during space flight. Bone. 1998;22:83S–8S.

99. Morey-Holton ER, Globus RK. Hindlimb unloading rodent model: technical aspects. J Appl Physiol. 2002;92:1367–77.
100. Raggatt LJ, Partridge NC. Cellular and molecular mechanisms of bone remodeling. J Biol Chem. 2010;285:25103–8.
101. Ozcivici E, Luu YK, Adler B, Qin YX, Rubin J, Judex S, Rubin CT. Mechanical signals as anabolic agents in bone. Nat Rev Rheumatol. 2010;6:50–9.
102. Rubin CT, Capilla E, Luu YK, Busa B, Crawford H, Nolan DJ, Mittal V, Rosen CJ, Pessin JE, Judex S. Adipogenesis is inhibited by brief, daily exposure to high-frequency, extremely low-magnitude mechanical signals. Proc Natl Acad Sci U S A. 2007;104:17879–84.
103. Luu YK, Pessin JE, Judex S, Rubin J, Rubin CT. Mechanical signals as a non-invasive means to influence mesenchymal stem cell fate, promoting bone and suppressing the fat phenotype. Bonekey Osteovision. 2009;6:132–49.
104. Luu YK, Capilla E, Rosen CJ, Gilsanz V, Pessin JE, Judex S, Rubin CT. Mechanical stimulation of mesenchymal stem cell proliferation and differentiation promotes osteogenesis while preventing dietary-induced obesity. J Bone Miner Res. 2009;24:50–61.
105. Kawaguchi H, Akune T, Yamaguchi M, Ohba S, Ogata N, Chung UI, Kubota N, Terauchi Y, Kadowaki T, Nakamura K. Distinct effects of PPARgamma insufficiency on bone marrow cells, osteoblasts, and osteoclastic cells. J Bone Miner Metab. 2005;23:275–9.
106. Liu J, Wang Y, Pan Q, Su Y, Zhang Z, Han J, Zhu X, Tang C, Hu D. Wnt/beta-catenin pathway forms a negative feedback loop during TGF-beta1 induced human normal skin fibroblast-to-myofibroblast transition. J Dermatol Sci. 2012;65:38–49.
107. Taes YE, Lapauw B, Vanbillemont G, Bogaert V, De Bacquer D, Zmierczak H, Goemaere S, Kaufman JM. Fat mass is negatively associated with cortical bone size in young healthy male siblings. J Clin Endocrinol Metab. 2009;94:2325–31.
108. Bonewald LF. Osteocytes: a proposed multifunctional bone cell. J Musculoskelet Neuronal Interact. 2002;2:239–41.
109. Bonewald LF. Osteocytes as dynamic multifunctional cells. Ann N Y Acad Sci. 2007;1116:281–90.
110. Bonewald LF, Johnson ML. Osteocytes, mechanosensing and Wnt signaling. Bone. 2008;42:606–15.
111. Robinson JA, Chatterjee-Kishore M, Yaworsky PJ, Cullen DM, Zhao W, Li C, Kharode Y, Sauter L, Babij P, Brown EL, Hill AA, Akhter MP, Johnson ML, Recker RR, Komm BS, Bex FJ. Wnt/beta-catenin signaling is a normal physiological response to mechanical loading in bone. J Biol Chem. 2006;281:31720–8.
112. Ke HZ, Richards WG, Li X, Ominsky MS. Sclerostin and Dickkopf-1 as therapeutic targets in bone diseases. Endocr Rev. 2012;33:747–83.
113. Li X, Zhang Y, Kang H, Liu W, Liu P, Zhang J, Harris SE, Wu D. Sclerostin binds to LRP5/6 and antagonizes canonical Wnt signaling. J Biol Chem. 2005;280:19883–7.
114. Li X, Liu P, Liu W, Maye P, Zhang J, Zhang Y, Hurley M, Guo C, Boskey A, Sun L, Harris SE, Rowe DW, Ke HZ, Wu D. Dkk2 has a role in terminal osteoblast differentiation and mineralized matrix formation. Nat Genet. 2005;37:945–52.
115. Gong Y, Slee RB, Fukai N, Rawadi G, Roman-Roman S, Reginato AM, Wang H, Cundy T, Glorieux FH, Lev D, Zacharin M, Oexle K, Marcelino J, Suwairi W, Heeger S, Sabatakos G, Apte S, Adkins WN, Allgrove J, Arslan-Kirchner M, Batch JA, Beighton P, Black GC, Boles RG, Boon LM, Borrone C, Brunner HG, Carle GF, Dallapiccola B, De Paepe A, Floege B, Halfhide ML, Hall B, Hennekam RC, Hirose T, Jans A, Juppner H, Kim CA, Keppler-Noreuil K, Kohlschuetter A, LaCombe D, Lambert M, Lemyre E, Letteboer T, Peltonen L, Ramesar RS, Romanengo M, Somer H, Steichen-Gersdorf E, Steinmann B, Sullivan B, Superti-Furga A, Swoboda W, van den Boogaard MJ, Van Hul W, Vikkula M, Votruba M, Zabel B, Garcia T, Baron R, Olsen BR, Warman ML. LDL receptor-related protein 5 (LRP5) affects bone accrual and eye development. Cell. 2001;107:513–23.
116. Robling AG, Turner CH. Mechanotransduction in bone: genetic effects on mechanosensitivity in mice. Bone. 2002;31:562–9.

117. Robling AG, Turner CH. Mechanical signaling for bone modeling and remodeling. Crit Rev Eukaryot Gene Expr. 2009;19:319–38.
118. Sawakami K, Robling AG, Ai M, Pitner ND, Liu D, Warden SJ, Li J, Maye P, Rowe DW, Duncan RL, Warman ML, Turner CH. The Wnt co-receptor LRP5 is essential for skeletal mechanotransduction but not for the anabolic bone response to parathyroid hormone treatment. J Biol Chem. 2006;281:23698–711.
119. Kiel DP, Hannan MT, Barton BA, Bouxsein ML, Lang TF, Brown KM, Shane E, Magaziner J, Zimmerman S, Rubin CT. Insights from the conduct of a device trial in older persons: low magnitude mechanical stimulation for musculoskeletal health. Clin Trials. 2010;7:354–67.
120. Little RD, Carulli JP, Del Mastro RG, Dupuis J, Osborne M, Folz C, Manning SP, Swain PM, Zhao SC, Eustace B, Lappe MM, Spitzer L, Zweier S, Braunschweiger K, Benchekroun Y, Hu X, Adair R, Chee L, FitzGerald MG, Tulig C, Caruso A, Tzellas N, Bawa A, Franklin B, McGuire S, Nogues X, Gong G, Allen KM, Anisowicz A, Morales AJ, Lomedico PT, Recker SM, Van Eerdewegh P, Recker RR, Johnson ML. A mutation in the LDL receptor-related protein 5 gene results in the autosomal dominant high-bone-mass trait. Am J Hum Genet. 2002;70:11–9.
121. Niziolek PJ, Warman ML, Robling AG. Mechanotransduction in bone tissue: The A214V and G171V mutations in Lrp5 enhance load-induced osteogenesis in a surface-selective manner. Bone. 2012;51:459–65.
122. Zhong Z, Zeng XL, Ni JH, Huang XF. Comparison of the biological response of osteoblasts after tension and compression. Eur J Orthod. 2013;35:59–65.
123. Lisse TS, Chun RF, Rieger S, Adams JS, Hewison M. Vitamin D activation of functionally distinct regulatory miRNAs in primary human osteoblasts. J Bone Miner Res. 2013;28:1478–88.
124. Sengul A, Santisuk R, Xing W, Kesavan C. Systemic administration of an antagomir designed to inhibit miR-92, a regulator of angiogenesis, failed to modulate skeletal anabolic response to mechanical loading. Physiol Res. 2013;62:221–6.
125. Lian JB, Stein GS, van Wijnen AJ, Stein JL, Hassan MQ, Gaur T, Zhang Y. MicroRNA control of bone formation and homeostasis. Nat Rev Endocrinol. 2012;8:212–27.
126. Luzi E, Marini F, Sala SC, Tognarini I, Galli G, Brandi ML. Osteogenic differentiation of human adipose tissue-derived stem cells is modulated by the miR-26a targeting of the SMAD1 transcription factor. J Bone Miner Res. 2008;23:287–95.
127. Kapinas K, Kessler CB, Delany AM. miR-29 suppression of osteonectin in osteoblasts: regulation during differentiation and by canonical Wnt signaling. J Cell Biochem. 2009;108:216–24.
128. Mizuno Y, Yagi K, Tokuzawa Y, Kanesaki-Yatsuka Y, Suda T, Katagiri T, Fukuda T, Maruyama M, Okuda A, Amemiya T, Kondoh Y, Tashiro H, Okazaki Y. miR-125b inhibits osteoblastic differentiation by down-regulation of cell proliferation. Biochem Biophys Res Commun. 2008;368:267–72.
129. Zhang JF, Fu WM, He ML, Xie WD, Lv Q, Wan G, Li G, Wang H, Lu G, Hu X, Jiang S, Li JN, Lin MC, Zhang YO, Kung HF. MiRNA-20a promotes osteogenic differentiation of human mesenchymal stem cells by co-regulating BMP signaling. RNA Biol. 2011;8:829–38.
130. Klein-Nulend J, Bacabac RG, Mullender MG. Mechanobiology of bone tissue. Pathol Biol (Paris). 2005;53:576–80.
131. Sikavitsas VI, Temenoff JS, Mikos AG. Biomaterials and bone mechanotransduction. Biomaterials. 2001;22:2581–93.
132. Ferreri SL, Talish R, Trandafir T, Qin YX. Mitigation of bone loss with ultrasound induced dynamic mechanical signals in an OVX induced rat model of osteopenia. Bone. 2011;48:1095–102.
133. Hu M, Cheng J, Qin YX. Dynamic hydraulic flow stimulation on mitigation of trabecular bone loss in a rat functional disuse model. Bone. 2012;51:819–25.
134. Uddin SMZ, Cheng J, Lin W, Qin YX. Low-intensity amplitude modulated ultrasound increases osteoblastic mineralization. Cell Mol Bioeng. 2011;4:81–90.
135. Hu M, Serra-Hsu F, Bethel N, Lin L, Ferreri S, Cheng J, Qin YX. Dynamic hydraulic fluid stimulation regulated intramedullary pressure. Bone. 2013;57(1):137–41.

136. Qin YX, Lam H, Ferreri S, Rubin C. Dynamic skeletal muscle stimulation and its potential in bone adaptation. J Musculoskelet Neuronal Interact. 2010;10:12–24.
137. Datta N, Pham QP, Sharma U, Sikavitsas VI, Jansen JA, Mikos AG. In vitro generated extracellular matrix and fluid shear stress synergistically enhance 3D osteoblastic differentiation. Proc Natl Acad Sci U S A. 2006;103:2488–93.
138. Mauney JR, Sjostorm S, Blumberg J, Horan R, O'Leary JP, Vunjak-Novakovic G, Volloch V, Kaplan DL. Mechanical stimulation promotes osteogenic differentiation of human bone marrow stromal cells on 3-D partially demineralized bone scaffolds in vitro. Calcif Tissue Int. 2004;74:458–68.
139. Milan JL, Planell JA, Lacroix D. Computational modelling of the mechanical environment of osteogenesis within a polylactic acid-calcium phosphate glass scaffold. Biomaterials. 2009;30:4219–26.
140. Pioletti DP. Biomechanics and tissue engineering. Osteoporos Int. 2011;22:2027–31.
141. Corvelli M, Che B, Saeui C, Singh A, Elisseeff J. Biodynamic performance of hyaluronic acid versus synovial fluid of the knee in osteoarthritis. Methods. 2015;84:90–8.
142. Sophia Fox AJ, Bedi A, Rodeo SA. The basic science of articular cartilage: structure, composition, and function. Sports Health. 2009;1:461–8.
143. Steward AJ, Liu Y, Wagner DR. Engineering cell attachments to scaffolds in cartilage tissue engineering. JOM. 2011;63:77–82.
144. Kurz B, Lemke AK, Fay J, Pufe T, Grodzinsky AJ, Schunke M. Pathomechanisms of cartilage destruction by mechanical injury. Ann Anat. 2005;187:473–85.
145. Pearle AD, Warren RF, Rodeo SA. Basic science of articular cartilage and osteoarthritis. Clin Sports Med. 2005;24:1–12.
146. Bansal PN, Joshi NS, Entezari V, Grinstaff MW, Snyder BD. Contrast enhanced computed tomography can predict the glycosaminoglycan content and biomechanical properties of articular cartilage. Osteoarthritis Cartilage. 2010;18:184–91.
147. Arokoski JP, Jurvelin JS, Vaatainen U, Helminen HJ. Normal and pathological adaptations of articular cartilage to joint loading. Scand J Med Sci Sports. 2000;10:186–98.
148. Guilak F, Nims RJ, Dicks A, Wu CL, Meulenbelt I. Osteoarthritis as a disease of the cartilage pericellular matrix. Matrix Biol. 2018;71–72:40–50.
149. Hunter DJ, Arden N, Conaghan PG, Eckstein F, Gold G, Grainger A, Guermazi A, Harvey W, Jones G, Hellio Le Graverand MP, Laredo JD, Lo G, Losina E, Mosher TJ, Roemer F, Zhang W. Definition of osteoarthritis on MRI: results of a Delphi exercise. Osteoarthritis Cartilage. 2011;19:963–9.
150. Hunter DJ, Beavers DP, Eckstein F, Guermazi A, Loeser RF, Nicklas BJ, Mihalko SL, Miller GD, Lyles M, Devita P, Legault C, Carr JJ, Williamson JD, Messier SP. The Intensive Diet and Exercise for Arthritis (IDEA) trial: 18-month radiographic and MRI outcomes. Osteoarthritis Cartilage. 2015;23:1090–8.
151. Jorgensen AEM, Kjaer M, Heinemeier KM. The effect of aging and mechanical loading on the metabolism of articular cartilage. J Rheumatol. 2017;44:410–7.
152. Mazor M, Best TM, Cesaro A, Lespessailles E, Toumi H. Osteoarthritis biomarker responses and cartilage adaptation to exercise: a review of animal and human models. Scand J Med Sci Sports. 2019;29:1072–82.
153. Guilak F. Biomechanical factors in osteoarthritis. Best Pract Res Clin Rheumatol. 2011;25:815–23.
154. Guilak F, Butler DL, Goldstein SA, Baaijens FP. Biomechanics and mechanobiology in functional tissue engineering. J Biomech. 2014;47:1933–40.
155. Sun HB. Mechanical loading, cartilage degradation, and arthritis. Ann N Y Acad Sci. 2010;1211:37–50.
156. Trudel G, Uhthoff H, Laneuville O. Knee joint immobility induces Mcl-1 gene expression in articular chondrocytes. Biochem Biophys Res Commun. 2005;333:247–52.
157. Vanwanseele B, Lucchinetti E, Stussi E. The effects of immobilization on the characteristics of articular cartilage: current concepts and future directions. Osteoarthritis Cartilage. 2002;10:408–19.

158. Li X, Sun Y, Zhou Z, Zhang D, Jiao J, Hu M, Hassan CR, Qin YX. Mitigation of articular cartilage degeneration and subchondral bone sclerosis in osteoarthritis progression using low-intensity ultrasound stimulation. Ultrasound Med Biol. 2019;45:148–59.
159. Caulkins C, Ebramzadeh E, Winet H. Skeletal muscle contractions uncoupled from gravitational loading directly increase cortical bone blood flow rates in vivo. J Orthop Res. 2009;27:651–6.
160. Garman R, Gaudette G, Donahue LR, Rubin C, Judex S. Low-level accelerations applied in the absence of weight bearing can enhance trabecular bone formation. J Orthop Res. 2007;25:732–40.
161. Qin YX, Kaplan T, Saldanha A, Rubin C. Fluid pressure gradients, arising from oscillations in intramedullary pressure, are correlated with the formation of bone and inhibition of intracortical porosity. J Biomech. 2003;36:1427–37.
162. Zerath E, Canon F, Guezennec CY, Holy X, Renault S, Andre C. Electrical stimulation of leg muscles increases tibial trabecular bone formation in unloaded rats. J Appl Physiol. 1995;79:1889–94.
163. Qin YX, Lin W, Rubin CT. Load-induced bone fluid flow pathway as defined by in-vivo intramedullary pressure and streaming potentials measurements. Ann Biomed Eng. 2002;30:693–702.
164. Xie L, Jacobson JM, Choi ES, Busa B, Donahue LR, Miller LM, Rubin CT, Judex S. Low-level mechanical vibrations can influence bone resorption and bone formation in the growing skeleton. Bone. 2006;39:1059–66.
165. Wang L, Fritton SP, Cowin SC, Weinbaum S. Fluid pressure relaxation depends upon osteonal microstructure: modeling an oscillatory bending experiment. J Biomech. 1999;32:663–72.
166. Wang L, Fritton SP, Weinbaum S, Cowin SC. On bone adaptation due to venous stasis. J Biomech. 2003;36:1439–51.
167. Wang L, Ciani C, Doty SB, Fritton SP. Delineating bone's interstitial fluid pathway in vivo. Bone. 2004;34:499–509.
168. Stevens HY, Meays DR, Frangos JA. Pressure gradients and transport in the murine femur upon hindlimb suspension. Bone. 2006;39:565–72.
169. Valic Z, Buckwalter JB, Clifford PS. Muscle blood flow response to contraction: influence of venous pressure. J Appl Physiol. 2005;98:72–6.
170. Laughlin MH, Joyner M. Closer to the edge? Contractions, pressures, waterfalls and blood flow to contracting skeletal muscle. J Appl Physiol. 2003;94:3–5.
171. Kim SJ, Roy RR, Zhong H, Suzuki H, Ambartsumyan L, Haddad F, Baldwin KM, Edgerton VR. Electromechanical stimulation ameliorates inactivity-induced adaptations in the medial gastrocnemius of adult rats. J Appl Physiol. 2007;103:195–205.
172. Qin L, Appell HJ, Chan KM, Maffulli N. Electrical stimulation prevents immobilization atrophy in skeletal muscle of rabbits. Arch Phys Med Rehabil. 1997;78:512–7.
173. O'Gara T, Urban W, Polishchuk D, Pierre-Louis A, Stewart M. Continuous stimulation of transected distal nerves fails to prolong action potential propagation. Clin Orthop Relat Res. 2006;447:209–13.

Chapter 2
Biomechanics of Skeletal Muscle and Tendon

Yuan-Hung Chao and Jui-Sheng Sun

Abstract Skeletal muscle is the biological tissue able to transform chemical energy to mechanical energy. Skeletal muscle has three basic performance parameters that describe its function: structure and composition, force production, and movement production. From a mechanical perspective, the musculotendinous unit behaves as an elastic-contractile component (muscle fibers) in series with another elastic component (tendons) to move human body. Due to their unique hierarchical structure and composition, tendons possess characteristic biomechanical properties, including high mechanical strength and viscoelasticity, which enable them to carry and transmit mechanical loads (muscular forces) effectively. Tendons are also mechanoresponsive by adaptively changing their structure and function in response to altered mechanical loading conditions. The production of movement and force is the mechanical outcome of skeletal muscle contraction. The focus of this chapter is on the biomechanical behavior of skeletal muscle and tendon as they contribute to function of the musculoskeletal system.

Keywords Skeletal muscle · Tendon · Structure and composition
Extracellular matrix · Viscoelastic behavior · Active muscles force production
Mechanotransduction

Y.-H. Chao
School and Graduate Institute of Physical Therapy, College of Medicine, National Taiwan University, Taipei City, Taiwan
e-mail: yuanhungchao@ntu.edu.tw

J.-S. Sun (✉)
Department of Orthopedic Surgery, College of Medicine, National Taiwan University, Taipei City, Taiwan

Department of Orthopedic Surgery, National Taiwan University Hospital, Taipei City, Taiwan

C.-K. Cheng, S. L-Y. Woo (eds.), *Frontiers in Orthopaedic Biomechanics*,
https://doi.org/10.1007/978-981-15-3159-0_2

1 Skeletal Muscle

1.1 Structure and Composition

1.1.1 Muscle Fiber

The fiber of the skeletal muscle is a long, cylindrical, multinucleated cell that is filled with smaller units of filaments. The largest of the filaments is the myofibril, which is composed of the sarcomeres that are arranged from end to end through the length of the myofibril. Each sarcomere also contains filaments, which is known as myofilaments. There are two types of myofilaments within each sarcomere, namely, thicker myofilaments and thinner myofilaments. The thicker one is composed of myosin protein molecules. The thinner one is composed of molecules of the protein actin. Sliding of the actin myofilament on the myosin chain is the basic mechanism of muscle contraction.

Connective tissue within the muscle, called intramuscular connective structure (IMCT), consists of predominantly collagen protein and proteoglycans [1]. It covers skeletal muscle fiber in layers, providing mechanical support for blood vessels and nerves deep in every muscle fiber. As muscle fiber generates mechanical tension, the IMCT transmits muscular passive force [2–4]. Extending from tendon, epimysium embraces every individual muscle. Fascicles within the muscle are layered by the perimysium, and individual muscle fibers are covered by the endomysium. IMCT comprises various proportion of collagen fiber, proteoglycans, and other substances. According to the location and ingredients, IMCT plays various functional roles. Endomysium with better elasticity can adapt with more deformation. Perimysium with better stiffness can transmit force produced by muscle fibers more efficiently.

Endomysium is directly in contact with the sarcolemma and muscle fiber, accounting for only 0.47–1.2% of the muscle dry weight. The main collagen fiber type of endomysium is type III, IV, V, and lesser percentage of type I is also found. Due to lesser proportion of type I collagen, endomysium is more elastic and less stiff for transmitting force. When force is produced by muscle fibers, the adjacent endomysium adapts itself with various angle between collagen fibers of endomysium and muscle fibers. Because of this adaptation, the endomysium can resist elongation deformation up to 150% change of its original physiological length. This adaptation and continuity of endomysium let muscle fibers not recruited during a movement render tendon transmitting force without changing length.

Different with endomysium, perimysium is multilayered, consisting of collagen fibers type I, III, IV, V, VI, and XII and proteoglycans, elastin fiber [1, 4]. Due to collagen fiber type I, perimysium is able to resist more traction force and has an important role in transmitting force. According to studies on bovine muscle, perimysium accounts for 0.4–4.8% muscle dry weight with different functions. The ratio of weight of perimysium in different muscles is more various than endomysium. This variance may indicate that perimysium plays a main role in defining functional differences in multiple muscle groups [1].

The epimysium, formed by collagen fibers type I and III, with larger diameter is thicker than endo- and perimysium [3]. It covers all muscle belly and consists of two layers of wavy collagen fibrils in contact with tendon surface [1, 4]. When tension takes place along the direction of the fiber, epimysium provides resistance. When the force is orthogonal, the epimysium will show a discrete yielding. When epimysium of two different muscles connects, it provides a membrane for vessels and nerves to transport into muscles and a surface for sliding in all directions when muscle contracts. Epimysium receives forces directly from perimysium and muscle fibers sometimes, and transmits the force to the tendons or the aponeurotic expansions. In conjunction with different muscles, it provides a fluent phase for sliding.

1.1.2 Mononuclear Cells

Fibroblast is the primary mononuclear cell in normal muscle ECM which is responsible for producing collagen, fibronectin, MMPs, and PGs [5]. Being sensitive to mechanical loading, fibroblasts are responsible for transforming mechanical signals into altered gene expression. Once experienced an altered mechanical environment, fibroblasts proximal to the myotendinous junction signal for increased collagen production to help in the development and maintenance of tendon. Laminins and talins are also produced to link the ends of muscle fibers to the basement membrane at the myotendinous junction [6]. A recent study by Archile-Contreras et al. showed that fibroblasts isolated from different muscle types possess distinct in vitro growth capability and express different levels of MMP-2 [5]. In this animal study, fibroblasts cultured from semitendinosus and sternomandibularis muscles showed higher growth capacity compared to that of longissimus dorsi. Active MMP-2 expression was highest in semitendinosus fibroblast cultures and lowest in sternomandibularis fibroblast cultures. The mechanical properties and collagen content were not analyzed in these muscles; therefore, these observed differences could not be correlated with muscle function or ECM turnover.

Satellite cells (SCs) are shown by Guerin et al. to be capable of synthesizing and secreting MMP-2 and MMP-9. This study suggested the skeletal muscle cells could participate in remodeling the ECM during myogenesis and the regeneration of skeletal muscle through assisting MMPs' migration through the ECM to muscle injury site [7]. A recent study by Hoedt et al. even showed that myogenic differentiation factor (myoD) could be induced by erythropoietin (Epo) treatment to prevent apoptosis of satellite cells in murine and in vitro models. In addition, satellite cell content in type II myofibers as well as the content of MyoD+ SCs increased through endurance training. Epo receptor mRNA expression in human SCs also suggested that Epo treatment could regulate human SCs in vivo [8]. Crameri et al. showed that a single bout of high intensity exercise could induce SCs re-entry into the cell growth cycle though a single bout was not sufficient for the SCs to undergo terminal differentiation [9].

1.1.3 Extracellular Matrix (ECM)

Skeletal muscle collagens, which accounts for 1–10% of muscle dry weight mass, is the major structural protein in skeletal muscle ECM. In the various types of collagens, type I and III predominate in adult endo-, peri-, and epimysium with type I being the predominant collagen in perimysium and type III evenly distributed between endomysium [10]. Type V collagen forms a core for type I collagen fibrils in peri- and endomysium [11]. Type XII and XIV collagen are fibril-associated collagens with interrupted triple helices (FACITS) localized primarily to perimysium and appeared to link fibrillary collagen to other ECM components without precisely known function [12]. Muscle basement membrane consists mainly of type I collagen network though type VI, XV, and XVIII are also present [13]. Types XV and XVIII are multiplexins that can bind growth factors and assist in linking the basement membranes of glycoproteins and endomysium [14]. The basement membrane and endomysium are closely connected, involving in the transmission of force from the myofiber to the tendon [15].

Many of the proteoglycans (PGs) in muscle ECM belong to the family of small leucine-rich proteoglycans (SLRPs), including decorin, biglycan, fibromodulin, and lumican with decorin and biglycan being the most abundant. Other PGs comprised approximately 30% in muscle ECM includes the heparin sulfate PGs collagen XVIII, perlecan, and agrin which bind to growth factors. Growth factors can be stored and released by negatively charged glycosaminoglycans (GAGs) in the basement membrane and endomysium surrounding muscle fibers. Enzymes in the ECM cleave the GAG chains with their associated growth factors allowing interaction in cell signaling and mechanotransduction [16, 17].

Comprising the major structure of ECM, collagen and proteoglycans interacts uniquely to maintain the structure and organization of the matrix. Decorin, the major PG in the perimysium, has been proposed to be a regulator of type I collagen fibrillogenesis due to its binding interaction with type I collagen. It inhibits the lateral growth of collagen fibrils through its core protein presumably. Biglycan also binds to type I collagen in a similar way with decorin. The binding and the location of collagen crosslinks might be key factors determining the structural organization of the ECM since collagen fibril diameter in tendon becomes irregular in the absence of these two materials. In mice absent of biglycan, mild muscular dystrophic phenotype is found implicating that these PGs are vital in maintaining normal tissue function and mechanical properties [18].

Various glycoproteins in the ECM functions in linking type IV collagen (basement membrane) and sarcolemma (muscle fiber membrane). Laminins are bound by intergrins and α-dystroglycan where integrins are bound to fibronectin [13]. Laminins are also bound to type IV collagen directly and indirectly linked to fibronectin or nidogen. These glycoproteins interact to provide lateral force transmissions from the myofiber, and with the network formed with type IV collagen, form the basic structure of basement membrane [19].

Matricellular proteins in skeletal muscle include osteopontin, secreted protein acidic and rich in cysteine (SPARC), thrombospondin, and tenascin-C. Osteopontin

possesses cytokine-like functions that appears during muscle regeneration but seldom observed in normal skeletal muscle. It is typically secreted by inflammatory cells and may also be secreted by myoblasts [20]. SPARC has been observed to bind collagen and accompany its interaction in extracellular matrix [21]. The role of thrombospondin is assumed to prevent excessive capillary formation in skeletal muscle ECM as evidenced in the mice model [22]. Tenascin-C is indicated to play a role in maintaining neuromuscular junction architecture by binding to perlecan and agrin [23]. The major function of these proteins is not structural, but they are vital in ECM signaling and maintaining ECM organization.

Skeletal muscle ECM composition and its mechanical properties are regulated by matrix remodeling enzymes. Matrix metalloproteinase (MMP) levels are generally low in uninjured muscle. In this, MMP-2 and MMP-9 are gelatinases expressed in muscle that degrade type IV collagen, fibronectin, proteoglycans, and laminin. Collagenases MMP-1 and MMP-13 degrade types I and III collagens. Membrane type I MMP not only activates MMP-2 but also functions proteolytically near muscle cell surface. Tissue inhibitors of matrix metalloproteinases (TIMPs) 1–3 bind to active MMPs or stabilize inactive MMPs to inhibit their enzymatic activities. Through these enzymes, ECM of skeletal muscle is strictly regulated [13].

To define ECM mechanical properties, Meyer et al. first showed in their study that isolated muscle fiber stress–strain behavior was linear, and that of muscle bundle was nonlinear. To further differentiate and distinguish the source of nonlinearity (ECM itself vs. numerous individual muscle fibers with different linear material properties), numerous single fibers were isolated from ECM and grouped into a bundle to compare among groups of multiple muscle fibers with and without ECM. The results showed that the modulus of a fiber group was nearly the same as that of single fibers while the modulus of bundle was about five times higher. These results demonstrate that ECM is inherently stiffer than muscle fibers and its material properties are highly nonlinear [24].

1.2 Passive Muscles

1.2.1 Elastic Behavior

The property of elasticity has a central role in a diverse range of physiological and pathophysiological processes in skeletal muscle. Skeletal muscle is anisotropic due to its microstructural arrangement. Its structure is divided into many levels—epimysium, perimysium, and endomysium, as stated. Each muscle fiber contains actin, myosin, and titin filaments. According to the sliding filament theory, muscle contraction occurs when actin and myosin interacts with a cross-bridge, and consume one ATP (adenosine triphosphate) per cross-bridge cycle.

Elasticity describes a material property in which the material returns to its original shape after stress applied and then removed. Muscle elastic behavior is nonlinear. There are three main features to its viscoelasticity: First, when the muscle is

stretched and relaxed, the tension decreases over time until the muscle reaches a new steady state (stress relaxation). Second, when the muscle is stretched with a constant tension, the length of muscle increases over time until it reaches a new steady state (creep). Third, muscle exhibits different length–tension relationship curve if repeatedly stretched. This is called "effect of cyclic loading" [25].

A relaxed skeletal muscle, referring to the passive muscle, will act as a deformable body when stretched beyond the resting length. However, the muscle deformation in response to the stretching does not follow Hooke's law, which means it is not linear. The passive muscle elasticity is mainly attributed to the connective tissues content within the muscle [26]. The more proportion of the connective tissue within the muscle, the stiffer the muscle will become [27]. Thus, lower extremity muscles, containing more intramuscular connective tissue, are usually stiffer, compared to the muscles from upper extremity. In addition, the muscles derived in vitro is usually shorter than the natural muscle length in vivo because of the lack of muscle tone from neural supply and the difference in intrinsic mechanical properties.

When muscle is stretched to more than its resting length, it will exhibit passive resistance to the stretching force without any metabolic energy requirement. The resistance to deform is mainly from the following three structural components: connective tissue within and around the muscle, intramuscular cross-links, and the noncontractile proteins [26, 28]. The connective tissues provide general support of the muscle structure. The binding sites of the cross-bridges between the actin and myosin filaments provide the resistance to stretching during attached state. The giant protein molecules such as titin help to maintain the integrity of sarcomere. By keeping the myosin in the center between the Z discs, the proteins form the elastic connections of the myosin and the Z-line. The part close to the fiber ends of the sarcomere is less deformable than that at other sites. The length of the sarcomere can be extended to a maximum of 3.5–4.0 μm [29].

However, from a macro perspective in joint motion, the changes in muscle–tendon complex length are much more than in the muscle length itself because the tendons will generate little resistance to stretch in the toe region of the stress–strain curve. On average, tendon changes account for almost more than half of the muscle–tendon complex length changes [30]. Moreover, the passive resistance in joints can be the interaction results of two components, including the joint angle and the displacement. The passive resistance produced regarding the joint angle is negligible in the middle range of the motion, but significantly increase around the end range of the motion [26]. The relationship between the passive resistance and the joint angle is presented as the following equation:

$$T = \begin{cases} k\left(\mathrm{e}^{l(\alpha-\alpha_0)}-1\right), & \text{if } \alpha \geq \alpha_0 \\ 0, & \text{if } \alpha < \alpha_0 \end{cases}$$

where T refers to the passive joint torque, k and l are constants, α is the joint angle, and α_0 is the joint angle threshold; joint angles below this value are slack and do not produce much passive resistance. On the other hand, the antagonist muscle, such as

the triceps brachialis when performing elbow flexion, will not contribute much resistance to the deformation during joint motion. Although the antagonist muscle does not activate, a little tension exerted by the muscle tone still contains energy for elastic deformation, which stores some space for structural extensibility without generating too much resistance to deformation.

1.2.2 Viscoelastic Behavior

Passive muscles are viscoelastic material that exhibit both viscous and elastic characteristics when subjected to tensile and compressive deformation [31]. Viscoelasticity is the stress and strain experienced in the passive muscle dependent on the rate of loading; hence, the timing of the force application affects the strain response of the passive muscle. The viscoelasticity displayed during tensile loading is contributed by the passive properties of the protein titin [32, 33]. Lengthening velocity affects the passive properties of muscle fibers significantly [34]. As lengthening rate increases, the peak transient stress within the muscle fiber also increases, even at very slow velocities. In passive muscles, a high rate of stretch results in a higher stiffness than a slow stretch. This is one of the reasons that slow stretching exercises are capable of minimizing the increase in force in the muscle–tendon unit for a given amount of stretch.

There are other important properties of viscoelastic materials, including creep, stress relaxation, and hysteresis. Hysteresis is the phenomenon that a stretched passive muscle returns to its pre-stretched length. It is found when length–tension characteristics of passive muscle differ during loading (imposition of an external force) and unloading response [35]. The hysteresis area between the loading and unloading represents the amount of mechanical energy loss (dissipated to heat) in the recovery from that stretch.

The more mechanical energy dissipated, the more obvious the hysteresis phenomenon. In general, the relation between hysteresis and muscle stretch speed (or rhythmic deformation frequency) can be presented as:

$$E = k\omega^n$$

where E is the dissipated mechanical energy (the hysteresis area), ω is the oscillation frequency, and k and n are empirical constants. If $n = 1$, the dissipated energy is proportional to velocity, and when $n = 0$, the dissipated energy is velocity independent. In the latter case, the resistance acts like friction and is the same at any velocity. In human joints, the exponent n is typically close to zero. Therefore, muscle hysteresis is relatively independent of oscillation frequency compared to "classic" viscoelastic bodies, such as rubber. This indicates that the amount of mechanical energy converted to heat is relatively independent of the rate of muscle length change. Recent study has examined the effects of aging and gender on muscular viscoelastic characteristics in athletes [36]. Increased tone and muscular stiffness are found associated with aging, which can potentially lead to increased risk of falls,

injuries, general muscle performance deficits, and a consequent limitation of the ability to perform daily activities.

When a constant load is applied for a sufficiently long period, the muscle exhibits creep (lengthening relaxation) [37]. Rapid elongation occurs initially followed by a slower increase in deformation. Stress relaxation is the declination of resistance (the tension recorded at the muscle end) over time when a constant deformation is applied [38]. For example, holding a static stretch at a specific joint position results in a gradual decrease in tension in the muscle from stress relaxation. Creep and stress relaxation have important implications for stretching and risk of injury in repetitive tasks.

Muscles also possess thixotropic, or sticky friction, properties which is distinct from muscle's elastic and viscous properties and which is contraction history dependent [39]. Thixotropy appears as semisolid fluids under resting conditions but temporarily becomes more fluid when it is shaken or stirred to decrease its viscosity. Thixotropy is a consequence of long-term stable cross-bridges between the myofilaments of both extrafusal and intrafusal muscle fibers. Synovial fluid (found in human joints) contains thixotropic property as well. Under some conditions, the proprioception, including the senses of limb position, limb movement and muscle force are subjected to the influence of thixotropy as evidenced [40]. The influence of muscle and joint thixotropy in our daily life may appear in morning stiffness, especially in seniors and in patients with rheumatoid arthritis. Several movements are required when waking up in the morning, to make joints more flexible. Thixotropy increases as muscle fatigues. Moreover, a recent study showed that a movement-dependent change in passive ankle stiffness is caused by thixotropic properties of the calf muscle, which may increase the levels of ankle sway [41].

Shear modulus is used to calculate the tissue modules. The shear modulus's equation is presented as:

$$\mu = \rho v^2 \lambda^2$$

where μ is the shear modulus, ρ is the density of the tissue, v is frequency of the vibration, λ is the local wavelength.

Elastography is a newly developed image-based technique for measuring passive mechanical properties of skeletal muscles. Using MRI or ultrasound, stiffness and elastic properties are determined based on one of the following two principles: (1) For a given stress (force), stiffer tissue strains (deforms) less. (2) Mechanical waves (specifically shear waves) travel (wave propagation) faster through stiffer tissue. In vivo methods for measuring muscle mechanical properties are developing. There are inverse finite analysis (FEA) for determining muscle mechanical properties in human [42] and 3-in-1 Whole Animal Muscle System (Aurora Scientific) for measuring in vivo, in situ, and in vitro muscle function. However, there are still some uncertainties and limitations to these methods such that further studies are needed. Understanding the normal mechanical properties of muscle is beneficial to differentiate the abnormal pattern and figure out the problems. This must be especially

considered in long-term therapy to provide the appropriate stimulus for normal muscle mechanical properties.

1.3 Active Muscles

1.3.1 Muscle Force Production

The relationship between muscle force production and movement speed has been described by Hill [43]. As pushing and lifting speed varies with the mass of the object under fixed amount of force. Equation established by Hill simulates the thermic generation during muscle contraction. This formation is: $(v + b)(F + a) = b(F_0 + a)$, where F means the tension in the muscle, v means the velocity of the contraction of the muscle, a is the Hill's coefficient which correlated with the heat generated during muscle shortening, and F_0 means the tension of the muscle when the contraction velocity is zero (isometric contraction).

In this model, where a and b are constant, the tension of the muscle and the velocity of the contraction are inversely proportional. In fast contraction, the tension generated by the muscle would be less than that in slow contraction under the same environmental setting. While in vivo, the environment varies and influenced by many factors. So, Hill-type model has been widely studied and modified into different models implicated in different situations for more accurate simulation throughout the years; however, the accuracy of the model in vivo remains unknown [44]. Biewener and his colleagues demonstrated a two-element Hill-type model in goats' gastrocnemius muscles with EMG and found this model more accurate at predicting muscle forces [44]. Further research to investigate more accurate models to simulate the muscle force–velocity relationship within different situations is required since it is multifactorial.

Features of muscle force–velocity in different types of muscle contractions are distinguished. In concentric contraction, the maximal force production decreases as the muscle contraction velocity increases. In isometric contraction, the length of the muscle stays unchanged. Therefore, the velocity of muscle contraction is zero. The eccentric contraction means the length change of the muscle is positive during muscle contraction. The amount of force production increases while the contraction velocity increases, which is converse to the situation in concentric contraction. The maximum force generated by the eccentric contraction is about 1.5 times the value of isometric contraction, and the plateau speed is also higher on isolated frog muscles [45]. However, the experiment showed that the phenomenon did not have the same effect on voluntary eccentric contraction on human body. In addition, EMG activation did not change much while the eccentric velocity changes; it is even lower than concentric contraction. Westling and his colleagues thought that might be due to a protective neural inhibitory mechanism from too much tension on the muscle [46]. Voukelatos et al. used electrical stimulation to train quadriceps muscles for 3 weeks and found the overall torque output in eccentric contraction

increases [47]. The results might indicate that the protective mechanism is changeable. However, the enhancement of the peak value of voluntary eccentric contraction did not correlate with the increasing of angular velocity, which, to some extent, might be due to the protective mechanism, though the mechanism remained unclear.

Typically, Hill-type model contains three elements: a contractile element with force-length and force–velocity relations, a serial and a parallel elastic element. For simulating the proper biomechanics in eccentric contraction, based on Hill-type model, Haeufle et al. established a four-element model composed of a contractile element, a parallel elastic element, a series elastic element, and a serial damping element. This model considered serial damping and eccentric force–velocity relation. Thus, it is thought to be more suitable for simulating eccentric contraction in human movements [48].

The decreasing of isometric force, maximum velocity of muscle shortening, and an increase curvature of the force–velocity relationship are three main factors contributing to the power loss in mammalian muscles after fatigue. The underlying mechanism of muscle physiologic change needs further exploration. Jones [49] reviewed recent articles and found there were two main discussion aspects: First, the relationship between excitation-contraction coupling and force, and the other is the slowing of contractile properties [50]. The contraction velocity was found slowing down when muscle was fatigued comparing to the same force output generated by non-fatigue muscle. On the other hand, under the same amount of velocity, the force output was also decreased [51].

1.3.2 Muscle Size and Force Production

Normal muscle contraction, no matter the length or types of muscle contraction, undergoes respective mechanisms. Multiple factors, such as physical property, neural activation, motor control, environment, and even psychology, affect force production. However, the muscle strength is directly associated with muscle size (physical property) in general. Skeletal muscle changes in size and in ways including weight, circumference, and length during muscle growth. Two major sources of muscle weight increment are water and protein content. Human fetal muscle contains about 90% water. It decreased to about 78.5% by 4–7 months of age before attaining about 76% in the adult. There are major changes in the protein content of muscle during muscle growth [52]. The more portion of fibrillar protein in skeletal muscle is, the greater the muscle strength can be produced during muscle contraction.

Muscle strength is also proposed to be closely related to changes in fiber cross-sectional area, especially the maximal strength. Tonson et al. found that maximal isometric strength exerted by the forearm muscles in human is proportional to their size whatever the age [53]. Muscle fiber circumference can increase with newly synthesized myofibrils located near or at the surface of the fibers through use, a phenomenon called hypertrophy. Overall, increase in muscle strength are accompanied by more fiber cross-sectional area in muscle although Krivickas et al. mentioned that force is proportional to fiber diameter, rather than to cross-sectional area [54].

Muscle fascicle length is the other way of measuring muscle force. Arnold et al. stated that the length and velocity of muscle fibers can have a large effect on muscle force generation [55]. As muscle fibers increase in length, the number of sarcomeres added to the ends of the myofiber increases. With longer muscle fascicle length, more sarcomeres with cross-bridges produce more force.

Besides muscle growth with age, the influence of exercise on muscle plays an important role between muscle size and muscle strength. In general, immobilization can reduce muscle size and mass within 1–2 weeks. Kawakami et al. found that subjects who performed isometric and bilateral leg extension exercise every day after bed ridden for 20 days suffered less decrease in muscle strength and fiber cross-sectional area [56]. The fiber cross-sectional area decreased in control group by −7.8% while in exercise group it showed a lower tendency of −3.8% decrement. This implies that exercise can reduce muscle atrophy and influence muscle size.

For more accurate evaluation of the change in muscle circumference (muscle size), fiber cross-sectional area is usually employed. It can be measured using anthropometric measurements or magnetic resonance imaging (MRI), with the latter being more accurate [53]. Therefore, MRI becomes the major tool for measuring the fiber cross-sectional area.

1.3.3 Force Production and Muscle's Moment Arm

Body movements depend on the contraction of muscles and the consequent motion of the bone moving through the joint. When muscle contracts, the force produced acts on muscle attachment (usually attached to bone). After receiving the force, the bone starts moving around the joint. The relation between moment arm and force can be simplified in the equation: $T = \mathbf{F} \times \mathbf{R}$ (Fig. 2.1), where T means the torque, **F** means the force (N), **R** means movement arm, the perpendicular distance from the pivot (rotation center) to the line of force **F**.

$$T = \mathbf{F} \times \mathbf{R}$$

When it comes to body (a three-dimensional structure) movement, the force becomes force vector and movement arm becomes movement arm vector to define muscle movement model of moment of force vector. In the human muscle contraction model (3D model), moment of force vector (Mt) is obtained as a cross product

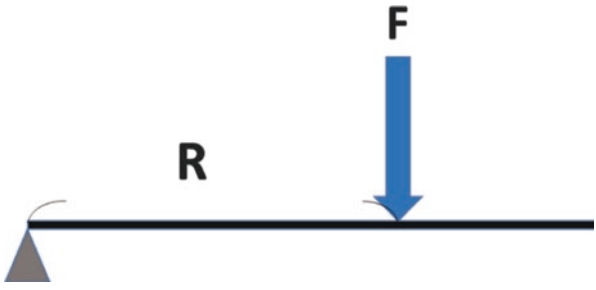

Fig. 2.1 Definition of torque (T)

of force vector (**F**) and the position vector (**r**), which is from pivot to any point along the line of **F**.

$$\mathrm{Mt} = \mathbf{F} \times \mathbf{r}$$

Force vector (**F**) could be divided into magnitude force (**f**) and unit force vector (**u**).

$$\mathbf{F} = \mathbf{fu}$$

$$\mathrm{Mt} = \mathbf{fu} \times \mathbf{r} = \mathbf{f}\left(\mathbf{u} \times \mathbf{r}\right)$$

Moment arm vector (**d**) comes from the cross of unit force vector (**u**) and position vector (**r**). In this equation, moment arm vector (**d**), also called normalized moment vector, means moment of force vector per unit scalar of force acts on the bone. The direction of moment arm vector (**d**) can be defined by right-hand rule. When circling the right hand second to fourth finger from the direction of position vector (**r**) to the direction of unit force vector (**u**), the direction of the right-hand thumb is the same as the direction of vector **d**.

In the muscle movement model, the magnitude of moment arm vector (d) was equal to the perpendicular distance from the pivot (joint center) to the line of force. However, when the force line was not perpendicular to the position vector (**r**), the magnitude of moment arm vector (d) is equal to $r \sin \theta$, θ means the angle between vectors **r** and **u** (when the force line is perpendicular to **r**, θ is 90° and $\sin\theta = 1$). In the below picture, vector **r** and **u** are on the same plate **o**. **d** is moment arm vector. As the cross production of $\mathbf{r} \times \mathbf{u}$, moment arm vector **d** is perpendicular to the **r** and **u** simultaneously. The direction of **d** is counterclockwise which can be defined by right-hand rule (Fig. 2.2).

$$\mathrm{Mt} = \mathbf{fd}$$
$$\mathbf{d} = \left(\mathbf{r} \times \mathbf{u}\right)$$
$$d = r \sin\theta$$

When it comes to human movement, *XYZ* 3D system can be used to analyze the muscle and joint action. Below is an elbow flexion example. Take elbow joint as a

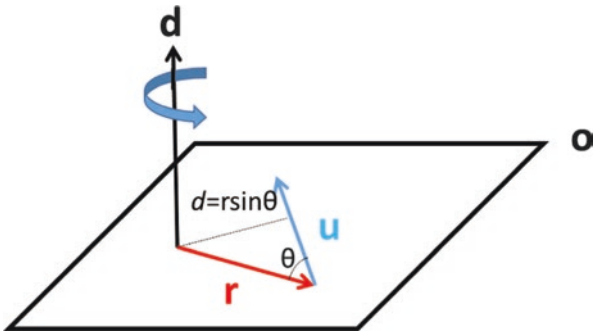

Fig. 2.2 Definition of moment arm vector (d)

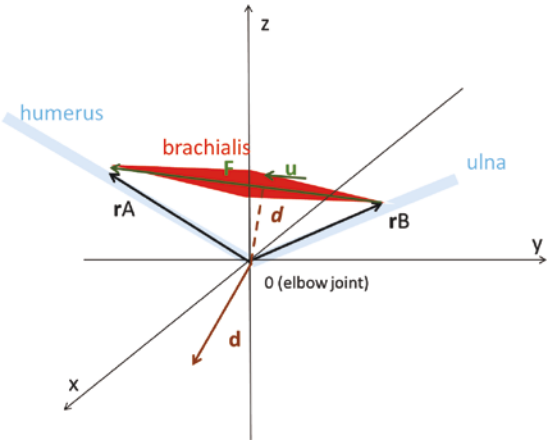

Fig. 2.3 Analysis of the muscle and joint action during human movement

center of 3D model, the movement arc produced by brachialis on humerus and ulna bone is then defined. **r**A and **r**B are the position vectors of the brachialis origin and insertion. **F** is the contraction force line and direction of the brachialis. **u** is the unit force vector of **F**. **d** is the moment arm vector of the brachialis on elbow joint. *d* is the magnitude of moment arm vector and it is equal to the length of the shortest distance from center (elbow joint) to the brachialis (Fig. 2.3).

u can be calculated by brachialis position vector (**r**A − **r**B) and the length of brachialis (|**r**A − **r**B|).

$$\vec{\mathbf{u}} = \frac{\overrightarrow{\mathbf{r}\mathrm{A}} - \overrightarrow{\mathbf{r}\mathrm{B}}}{\left|\overrightarrow{\mathbf{r}\mathrm{A}} - \overrightarrow{\mathbf{r}\mathrm{B}}\right|}$$

In the movement of elbow contraction, humerus bone and body is considered to be immobilized. The real moving bone is ulna bone. Thus, moment arm of action is **r**B. Moment arm vector **d** is the cross product of **r**B and **u**. Its direction can be defined by right-hand rule through **u** and **r**. The moment of force vector of brachialis on elbow joint can be calculated by Mt = **fd**.

In this 3D model, moment arm vector is continuously changing in the whole movement. When the brachialis keeps shortening, the angle between ulna and hummer bone becomes smaller, and the direction of the force vector **F** keep changing at the same time. Since we assume the force of muscle does not change in the whole movement, the length of muscle, moving traction of the bone, and the angle of the joint will influence the moment arm instantly.

The length of movement arm depends on the muscle attachment of the bone. The shorter movement arm is, the faster the joint movement than the longer movement arm muscle may produce under the same speed. Shorter movement arm may have a shorter angular excursion. When the joint comes to the rotation angle of θ, the moving distance of shorter movement arm is shorter than the longer movement arm one (when circling around the same angle θ, long radius circle has a longer arc length). The muscle with shorter movement arm can induce larger angular excursions than

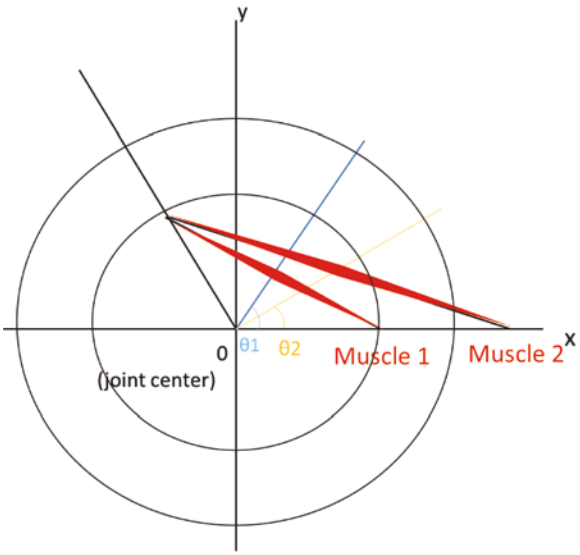

Fig. 2.4 Determination of the length of movement arm during human movement

the muscle with longer movement arm at the same shortened length of muscle contraction (Fig. 2.4).

In the figure, $\theta 1$ is the angle produced by the contraction of muscle 1. When the muscle is relaxed, the bone is lying on the X-axis ($X = 0$). The blue line is the bone situation when muscle 1 shortens (half of initial length). The yellow line is the bone situation when the muscle 2 shortens (half of initial length), which has a longer movement arm. Under the same shortening ratio (half of initial length in figure), $\theta 1$ is larger than $\theta 2$. Thus, if muscle 1 and muscle 2 have similar shortening speed, muscle 1 can induce more angular excursions than muscle 2.

However, the interaction between the muscle force and the movement arm length should be considered when discussing muscle function on joint movement in real life. The force produced by muscle relies on the type and the number of muscle fiber. In general, the muscle with more muscle fiber can produce larger force with contraction. Muscle types can be morphologically divided into parallel and pennate types. Parallel type muscle has liner muscle fiber. Parallel type has two subgroups, fusiform and strap type. Because the parallel type muscle is composed of long fibers, they can shorten more than the pennate muscle. More shortened length is able to induce larger angular excursion. However, the pennate type muscle is easy to induce large force in contraction. The movement arm could be confirmed with anatomical analyzation or the calculation of movement arm vector.

The method of measuring movement arm can be simply divided into geometric models and functional model. In early studies, geometric model was employed using cadaver and anatomical approach that may not apply to the living models and their complex movements. With technological advancement, high performance computer, and precise imaging system (X-ray, MRI), the measurement of movement arm improved. Thus, 3D geometric models and imaging geometric models

occurred. Researchers can observe muscle movement in the living situation, and calculation through the computer software can be done. In functional model, the actual movement arm is not important. The effective moment arm could be defined through calculation of the equation. The effective moment arm could be defined through calculation from the equation, Moment of Force = Force × Moment Arm. Functional model applies when the joint type, muscle structure, muscle length, joint angle are too complex to measure by geometric model.

The muscle moment arm vector is important in studying biomechanics and kinesiology. Combining the muscle force, contraction speed joint angle, and muscle moment arm human body movement can be analyzed precisely and in detail. Advance theory of biomechanics and kinesiology could be thus derived.

1.3.4 Force Production and Level of Recruitment of Motor Units

Motor unit is considered the functional unit of the neuromuscular system which work together to coordinate the contractions of a single muscle. A motor unit consists of a motor neuron and the skeletal muscle fibers innervated by that motor neuron's axonal terminals [57]. A group of motor units within a muscle is called motor pool. In human, there are no direct measures of the number of motor neurons innervating any muscle [58]. It can be counted by anatomical [59] or electrophysiological [60] method, but with some error. The number of muscle fibers within a single motor unit varies both within a particular muscle and from muscle to muscle as well. Muscles that act on the larger body masses usually contain more muscle fibers and hence more motor units [57]. For example, triceps brachii muscle has more muscle fibers in each motor unit than brachioradialis muscle.

Muscle produces force by regulating recruitment of motor units and by modulating the firing rates of recruited motor units [61]. Force production is controlled by three neuromuscular mechanisms: the number and type of recruited motor unit and their firing rate [62]. Increasing speed, force, or duration of movement involves progressive recruitment of motor units with larger size and higher activation thresholds. In 1965, Henneman et al. proposed a size principle of motor units recruitment [63]. Neurons within the central nervous system vary widely in size. The larger cell has larger surface area, and it should have some correlation with function. Finally, they found the motor units were recruited from the smallest to the largest based on the size of the load. As a result, the order is from slow twitch, low-force, fatigue-resistant muscle fibers to fast twitch, high-force, and less fatigue-resistant muscle fibers. The size principle is discussed in relation to the organization of the motor neuron pools. "Fractionation," "discharge zone," "subliminal fringe," "facilitation," and "occlusion" are redefined abbreviated terms of the sizes and excitabilities of the cells in a pool. Cell size is assumed to be the determinant of the overall frequency of discharge or usage of a motor neuron [63].

The relation between the recruitment and firing rate of motor units is organized in an inverse hierarchical structure—the onion skin scheme [61]. Hence, the firing rates of earlier-recruited motor units have a greater value than those of the

later-recruited motor units at any time and force during an isometric muscle contraction [64–66]. Also, the same pool of all the motor units of a muscle receives a common excited signal, known as common drive [64], and modulates their firing rate in unison. The later-recruited, higher-threshold motor units have shorter-duration, higher-amplitude force twitches compared with the earlier-recruited, lower-threshold motor units. The higher threshold motor units were driven by lower firing rate because of the nature of fatigue. It seems that the neuromuscular system is designed to optimize some combination of force and duration over which the force is sustained. The firing rate has a large range from very low frequencies to produce a series of single twitch contractions to high frequencies to produce a fused tetanic contraction. In general, there will be a 2 to 4-fold change in force. The firing rate of each individual motor unit increases with increased muscular effort until a maximum rate is reached [67].

As each individual level of analysis of the neuromuscular system structure has a unique frequency, there are also robust relations in the frequency domain between different levels [68]. Elble and Randall found a strong coherence between force output and EMG at 8–12 Hz, and they also found coherence at a similar frequency between single motor units and EMG [69]. Farmer et al. have found coherence between motor units in 1–12 and 16–32 Hz bandwidths during volitional force output [70].

1.3.5 Force Production and Fiber Type

Skeletal muscles are categorized into: (1) slow oxidative fibers, (2) fast oxidative–glycolytic fibers, and (3) fast glycolytic fibers, in terms of energy utilization. They can also be classified as type I fibers, type IIA fibers, and type IIB fibers, respectively. Most skeletal muscles contain a mixture of all three fiber types. Their proportions vary with the typical action of the muscle. Each type of muscle fiber harbors a unique feature. Slow oxidative fibers are the smallest in diameter and the least powerful type of muscle fibers. Fast oxidative–glycolytic fibers are intermediate in diameter between the other two types of fibers. Fast glycolytic fibers are the largest in diameter and produce most power. Other characteristics include myoglobin content, color, contraction velocity, method for generating ATP, fatigue resistance, order of recruitment, and primary functions [71].

The above classification classifies muscle fiber types as being fast or slow based on the speed of shortening and utilization of aerobic/anaerobic cellular respiration. Muscle fibers can also be typed using two other different methods: (1) histochemical staining for myosin ATPase and (2) myosin heavy chain isoform identification [72]. Classification for myosin ATPase staining, which based on staining intensities and differences in pH sensitivity, leads to 7 muscle fiber types. According to the speed of muscle contraction (from the slowest to the fastest): types I, IC, IIC, IIAC, IIA, IIAB, and IIB. Difference of myosin heavy chain isoform in muscle is also used to distinguish different muscle type. Although the human genome contains at least 10 genes for myosin heavy chains, only three are expressed in adult human limb

muscles [73]. MHC I, MHC IIA, and MHC IIB correspond to the isoforms identified by the speed of muscle shortening as types I, IIA, and IIB, respectively.

Skeletal muscle can be typed into different categories in different ways. However, skeletal muscle not only changes in size in response to demands, but also converts from one type to another (muscle fiber plasticity). Fiber conversions between type IIB and type IIA are the most common, but type I to type II conversions are possible in pathologic conditions. Aging can also influence the conversion between the proportion of muscle fiber type. Older muscle was found to have a greater percentage of fibers that co-express MHC I and MHC IIA (28.5%) compared with younger muscle (5–10%) [74]. Exercise, the common prescription in physical therapy, is the other way to change the proportion of muscle fiber type.

2 Tendon

2.1 Structure and Composition

Tendon is a highly dense connective tissue, composed of a range of multiple hierarchical components, which connect and transmit force from muscle to bone. The minimum unit of tendon is called tropocollagen molecules, which are then cross-linked into collagen molecules. Collagen molecules aggregate into microfibrils and lead to the formation of collagen fibrils. Coupling with multiple collagen fibrils, collagen fiber, the basic unit of a tendon, is formed. Each collagen fiber is surrounded by a connective tissue compartment named the endotenon, sometimes referred to as the interfascicular matrix (IFM). The well-established function of endotenon is to allow collagen fiber to glide with each other and to provide a canal with the supplement of vessels, nerves, and lymphatics into the deeper portion of tendon [75]. Then, the collagen fibers packed together to form primary fiber bundles, also termed subfascicles. Fascicles, secondary fiber bundles, are visible groups of collagen fibers with a wide variety of shapes and diameters, ranges from 150 to 500 μm [76]. Above this layer, groups of fascicles constitute the whole tendon, that is, the tertiary bundle, with a diameter of 1000–3000 μm surrounded by the epitenon [75]. These highly aligned collagen bundles arrange in a longitudinal axis parallel to the direction of mechanical stretch and allow tendon to withstand high tensile strength.

2.1.1 Cell Population within Tendon

Tendon cells, also named tenocytes, are the foremost fibroblast-like cells reside between either the intrafascicles or the interfascicles. With a highly developed endoplasmic reticulum, tenocytes are responsible to sense and respond to the changes of the microenvironment, including synthesis and degradation of the extracellular matrix (ECM) [77]. Although tendon cells seem to have a similar morphology, the

diversity of tenocytes is classified into several types according to their location and cell morphology. The first type is the “chondrocytic” type. The chondrocytic type presents in the entheses, where tendon attaches to bone. This type of tenocyte is characterized with round nuclei with the ability to produce chondrocyte-like matrix, such as type II collagen and aggrecan [78, 79]. The second type is the “external” type. The external-type tenocytes are more similar to the synovial cells; they reside in epitenon and interfascicles of endotenon and paratenon. Thus, they can provide adequate lubrication to facilitate the gliding of collagen bundles [80]. Another type is the “internal” type. The internal-type tendon cells can be found between the collagen fibers; they have fusiform morphology and a spindle-shaped nucleus that are responsible for producing the collagenous and non-collagenous ECM [80, 81]. Till now, the role of different cell populations on tendon healing is still in debate. After laceration of the flexor profundus tendons from adult monkeys, tenocytes from the epitenon first migrated and proliferated to the wound site at day 4 while the response of cells from the endotenon was postponed to day 9. Both cells demonstrated the ability to synthesize type I procollagen [82]. Gelberman et al. revealed the epitenon fibroblasts migrated to the injured spot and removed the cellular debris and collagen fragments through phagocytosis while the collagen anabolism occurred within the endotenon cell layer [83]. Recently, Cadby et al. indicated that both cells from peritenon and endotenon had multi-differentiated potency; the peritenon-derived cells migrated and proliferated more quickly with increased expression of alpha-smooth muscle actin (α-SMA), a specific gene marker of myofibroblast [84]. From the above information, tendon is consisted of multiple fibroblasts with different morphologies and biochemical characteristics, and it has the ability of intrinsic healing.

In this decade, tendon stem/progenitor cells (TSPCs) were first named and isolated from human and mouse tendons. These cells account for only 3–4% of total cells and possess divergent characteristics compared with tendon cells. TSPCs harbor several criteria of stem cells, including clonogenicity, multipotency, and self-renewal. Besides differentiating into tenocytes, TSPCs have the differentiating potential toward osteogenesis, adipogenesis, and chondrogenesis. Consequently, TSPCs are also named tendon-derived mesenchymal stem cells [85]. Similar to tendon cells, TSPCs can be classified into several types depending on the designated niches. In the study of Mienaltowski, tendon stem cells were isolated from the Achilles tendon and the surrounding peritenon (paratenon and epitenon) of C57Bl/6 mice. Interestingly, stem cells from tendon portion had higher colony forming units and a higher expression of tendon-related gene markers, such as tenomodulin (Tnmd) and scleraxis (Scx). Stem cells from peritenon displayed a higher level of endomucin (Emcn), a vascular endothelial marker, as well as Cd133 and Musashi-1 (Msi1), pericyte stem cell markers. These findings indicated that tendon tissue contains separate progenitor pools with distinct features. Thus, different kinds of TSPCs may play distinct role in tendon healing. For example, intrinsic healing is related to the expression of tendon-related gene markers while extrinsic repairing is achieved through recruiting the perivascular cells from peritenon [86]. Although the application of TSPCs into the research of tendon regeneration has drawn much interest, the use of TSPCSs still has several dilemmas. Due to their scarcity and the tendency to

lose their phenotype and function with passaging, several factors have been found to maintain their stemness [87]. For instance, matrix composition, substrate conformation, growth factor and cytokine supplement, mechanical loading as well as oxygen tension may affect their differentiated trend [88]. Thus, more studies are needed for further investigation of TSPCs in tendon pathology and tissue engineering.

2.1.2 Extracellular Matrix

In human body, collagen is the most plentiful protein with 25 subtypes. Among them, fibrillar types I, III, V, and XI collagen are essential for providing the connective tissue with its original stiffness and strength [76, 89]. In tendon, collagen composes 60–85% of tendon dry weight and type I collagen accounts for 95% of total collagen [90]. Besides type I collagen, there is little and varied amount of other collagens, including type III, V, VI, XI, XII, and XIV [76]. Type I collagen is a triple helix structure which comprises two α1 chains and one α2 chain. Thus, it is encoded by two genes: Col1a1 and Col1a2. During collagen synthesis, procollagen is translated and folded into triple helix in the rough endoplasmic reticulum and then transported to the Golgi apparatus. Next, procollagen is modified into bundles and packed into secretory vacuoles and then secreted to the extracellular matrix [91].

Type III collagen accounts for the remaining 5% of total collagen. Pertaining to the fibrillar type collagen, the structure of type III collagen is similar to type I collagen, wherein the difference is that type III collagen is composed by homotrimeric molecules; type I collagen consists of heterotrimeric units. Coinciding with type I collagen, Type III collagen is well known for its regulatory role in type I collagen fibrogenesis. The interaction between type I and III collagen modulates the diameter of collagen fibrils. Through tendon maturation, type III collagen assembles and gathers into the endotenon or tendon sheath [91]. Increased type III collagen was observed during tendon regeneration [92, 93].

Proteoglycans are a category of glycoprotein consisting of a core protein to which at least one glycosaminoglycan (GAG) chain is attached. PGs can be divided into two classes. One is the small leucine-rich proteoglycans (SLRPs), such as decorin (Dcn), biglycan (Bgn), fibromodulin (Fmod), and lumican. The other type is the large PGs, including aggrecan and versican [94]. Decorin is the most plentiful PGs in tendon, accounting for 80% of total PGs content. It is a horse-hoof like protein constituted by three domains. An N-terminal region is attached by a single dermatan or chondroitin sulfate side chain. A central region is composed of ten leucine-rich repeats which harbor a binding site of other proteins, including type I, II, III, VI collagen, and TGF-β, etc. A C-terminal region contains several cysteine residues [94, 95]. The central portion binds to the collagen fibril with the GAG side chain lying parallel or perpendicular to the axis of the collagen fibril. By doing so, the GAG side chain can interact with the other side chain of another Dcn molecule which binds to a collagen fibril nearby, connecting to adjacent collagen fibril with an inter-fibrillar bridge [96]. This is the way that Dcn maintains the spatial arrangement of collagen fibrils and regulates the diameter of collagen fibrils. $Dcn^{-/-}$ mice

showed disability in the regulation of collagen fibril diameter with increasing presence of enormous fibrils. In the studies of Halper and Reed et al., the packing of collagen fibrils was sabotaged, thus resulting in a decrease of tendon mechanical properties. These findings suggested that Dcn regulated the diameter of collagen fibrils through inhibiting abnormal lateral fusion of collagen fibrils [94, 95]. With two chondroitin or dermatan sulfate side chains, biglycan shares a similar collagen binding site with Dcn. Knockout of Bgn or Dcn leads to morphological defects of collagen fibrils. However, the lack of Bgn losses its ability to suppress bone morphogenetic protein-2 (BMP-2), resulting in ectopic tendon ossification [18, 94]. With keratin side chains, lumican and fibromodulin share the same binding site on fibrillar collagen, different from the binding site of Dcn and Bgn [94, 96].

Glycoproteins are a variety of proteins which are covalently attached by carbohydrate groups. The glycoproteins mainly found in tendon include tenomodulin (Tnmd), tenascin-C (Tnc), collagen oligomeric matrix component (COMP), and lubricin. As a potential candidate for tendon markers, tenomodulin is a type II transmembrane glycoprotein which highly presents in late developing and mature tendons. $Tnmd^{-/-}$ mice demonstrated a decrease in tendon cell density. Also, a reduce in cell proliferation was found without the presence of cell apoptosis. As a regulator of collagen architecture and fibrogenesis, $Tnmd^{-/-}$ mice showed uneven fibrillar surfaces and abnormally increased diameter of collagen fibrils [97]. Knockout of Tnmd in TSPCs inhibited self-renew capacity, and tendon stem cells tended to cease cell cycle inducing early cellular senescence [98].

As a hexameric extracellular matrix glycoprotein, tenascin-C (Tnc) is highly presented in the circumstances below. High concentration of Tnc was found during the embryogenesis of the musculoskeletal system, containing tendon, skin, ligament, muscle, articular cartilage, and bone [99, 100]. However, the $Tnc^{-/-}$ mice did not express a particular phenotype and revealed an ordinary wound healing process in skin and nerve tissues [101, 102]. Interestingly, upregulation of Tnc was discovered in mechanosensitive tissues that transmit forces from muscle to bone, such as myotendinous junction and osteotendinous junction [100, 103]. Therefore, the expression of Tnc is modulated by mechanical stimulus and has been postulated with the increase of elasticity in the ECM [104].

2.2 Basic Mechanics

2.2.1 Elastic Behavior

Elasticity is the tendency of tissue to resist deformation with an applied force [105]. Tendon is made up of collagen fibrils with highly consistent alignment. The collagen fibrils are the basic load-bearing units. Traditional material testing can be used to test the elasticity of the tendon. By fixing an isolated tendon specimen to a material testing machine, recording the loading of tensile stretch applied to the tendon and the amount of tendon elongation under each load, the elasticity of the tendon

can be calculated. Stiffness is an extensive property of a matter, which is calculated by dividing the tensile force by the amount of extension of the tendon. Elastic modulus, which is an intensive property of a matter, is the ratio of stress to strain. In tendon, the stress is the ratio of the force to the cross-sectional area, and the strain is the ratio of the change in length to the original length. When a tendon specimen is stretched, the length–tension relationship is nearly linear only at the mid-tension portion before tissue damage and failure. At the beginning, there is a toe-region because of the crimp structure of the collagen fibrils. The waviness of the fibrils is first straightened and then start to behave their elasticity [106].

Muscle–tendon unit should be viewed as a whole since tendon is connected to the muscle and caused by muscle contractions in real life. Therefore, when it comes to the elastic behavior of the tendon in vivo, the condition of the muscle is not negligible.

One of the methods for measuring tendon elasticity in vivo is through measuring the lengthening of the tendon or deep aponeurosis during maximal voluntary isometric contraction (MVIC) [107]. Force acting on the tendon is calculable using the moment arm length and torque data. Fitting the force and tendon elongation to a linear regression equation, the slope of the equation is considered to be an index of the tendon stiffness [107]. Another feasible method for measuring tendon elasticity in vivo is strain elastography. In this, tendon tissue is manually compressed. However, manual compression is not quantifiable; therefore, it provides only qualitative information (i.e., relative elasticity). Shear wave elastography produces shear wave into the tissue through its excitation transducer [108]. The information about shear wave propagation velocity can be collected by detectors and imaging transducers. Shear modulus can then be calculated by the following equation [109]:

$$\mu = c^2 \rho$$

where μ is the shear modulus, c is the shear wave propagation velocity, and ρ is the density of the tissue. The density of all soft tissue can be assumed to be 1000 kg/m^3.

Ultrasound and magnetic resonance imaging (MRI) are imaging modalities that can also be used to detect shear waves [108]. When force is imposed on a stiffer tendon, it will shorten rapidly and bear less load. A stiffer tendon will transmit more of the imposed force to the muscle, while a more compliant tendon will be more prone to involuntary oscillations. Tendon stiffness is influential by diet. In an animal experiment, the rats fed on diets containing advanced glycation end products (AGEs) for 88 days had stiffer tendons than those in the control group. Glycation has effect on collagen cross-linking, and this may result in change in integrity and elastic property of tendon tissue [110].

The slack of the muscle–tendon unit may influence the elastic behavior of tendon. Fukutani et al. applied supramaximal electrical stimulation at the tibial nerves of eight young healthy male volunteers [111]. The joint torque (plantar-flexion) was significantly larger when the ankle joint was positioned in 20° of dorsiflexion than positioned in 20° of plantar-flexion. However, the magnitude of Achilles tendon elongation measured by ultrasound was significantly smaller in the 20° dorsiflexed position.

Assuming a 20° dorsiflexed position, the influence of the slack is zero and the tendon elongation was resulted from muscle force only; at 20° plantar-flexed position, 20% of the tendon elongation was resulted from muscle force, and 80% of tendon elongation could be caused by elimination of slack due to different positioning [111].

Konow et al. investigated the lateral gastrocnemius muscle–tendon interaction during landing, and found that the muscle–tendon unit lengthened significantly during the last one-third of landing with increased range of motion of the joints, while the muscle fascicles behaved isometrically during the first two-thirds of landing without any observable muscle–tendon unit lengthening [112]. This result indicates that during the first two-thirds of landing, the tendon lengthened rapidly, storing the energy through elongation, and it recoiled, releasing the energy and lengthened the muscle fascicles during the last one-third of the landing. In such situations, tendon plays a role in power attenuation, which may be a protective mechanism that reduces the risk of muscle fascicle damage during rapid lengthening [112].

Farris et al. recruited young male participants to observe the muscle–tendon interaction during walking with constant speed and walking with acceleration. The amount of triceps surae muscle fascicles shortening was larger in early stance phase during the accelerative walking than during the constant walking, and the amount of fascicle shortening was not consistent to the muscle–tendon unit length change. This indicates that the energy produced by the fascicle shortening was stored in the tendon through elongation. In other words, the contractile work was stored in series elastic elements in the form of elastic energy [113]. The tendon then released the energy for the movement of the desired tasks. In the task of two-legged hopping, both adults and children presented maximal tendon excursion and minimal muscle excursion at their preferred self-selected hopping speed, which is in consistent with the optimal energy-saving strategy in theory [114]. This experimental result implies that elastic behavior of tendon plays an important role in movement efficiency.

2.2.2 Viscoelastic Behavior

Tendon is viscoelastic, meaning that their mechanical properties such as stiffness are time-dependent. Viscoelastic materials exhibit phenomena such as creep and stress-relaxation. Creep is strain increase (not large enough to cause any structural damage) over time with constant application of stress. This phenomenon exhibits most significantly early and reached plateau gradually during muscle contraction.

Stress-relaxation is a phenomenon presented as decreased stress over time with constantly applied strain. Both creep and relaxation are properties presented as a nondestructive change in tendon. If given sufficient time to recovery, and the load and strain removed, the tendon will return to the initial condition. The viscoelastic materials also demonstrate a variation between the loading and unloading curves, which is called hysteresis, wherein energy absorbed during loading is greater than dissipated during unloading [115].

An accurate measurement is crucial to understand the mechanical properties of tendon. Recently, ultrasound-based testing is widely used, because it is a noninva-

sive method and applicable under physiological condition. In vivo experiment, B-mode ultrasonography is mostly used to document tendon deformation during a ramp isometric contraction, and tendon force is calculated simultaneously. The load-deformation relationship is obtained in consequence. However, this measurement uses manual tracking to analyze, and manual tracking is extreme depending on the consistency of delineating in these patterns [116]. Shear wave elastography is considered a more accurate method to detect local change in tendon since it detects the velocity of transverse wave with established methodology [117].

O'Brien et al. reported that human patellar tendon with a 22-N peak load showed a 42% drop after 15 min, and with a 66-N peak load, a 35% drop was showed [118]. In contrast, Graf et al. reported the primate patellar tendon with a 39.6 ± 5.1 N of peak load and showed a 69.8% drop after 10 min [118]. Such differences may be due to species variation. However, Shepherd et al. reported species variation is less influential than functional requirement in determining fascicle fatigue behavior [119]. Different types of tendon were differentiated based on their function: the positional tendon (position joints and facilitate movement) and the energy-storing tendon (store high stresses when stretched, e.g., loading). Positional tendon tends to exhibit higher failure strength than energy-storing tendon. However, when fatigue properties were taken into consideration, energy-storing tendon showed significantly greater lifetimes under the same cyclic loading [119]. Furthermore, the strain distributions are varied among tendons. One study showed that the insertional regions of Achilles tendon are more capable of withstanding high strains than other regions without failing [120]. However, Suydam et al. showed that the cross-sectional area of tendon is unrelated to either the shear or viscosity modulus [121]. The exact factors affecting tendon behavior remain unknown.

In cyclic stress relaxation test, after 300, 900, and 1800 cycles, human semitendinosus showed stress decrease by 29.11%, 35.11%, and 38.5%, respectively, and cyclic creep test showed significant damage particularly in 900–1200 cycles. During cyclic creep, fiber bundles of the tendon are stretched out progressively, and the progressive recruitment pattern would not occur under stress relaxation [119]. Cyclic loading is seen to be more close to the mechanism of tendon injury. When tendon fibers responded to creep loading, isolated fiber kinks exhibited in low-level fatigue. In the case of moderate-level fatigue similar changes occurred but in a larger distribution. The situation of high-level fatigue showed severe matrix disruption [122]. Furthermore, Wren et al. found that tendon lifetime under cyclic loading was related to the magnitude of stress and the amount of initial strain [120].

Low hysteresis is beneficial for tendon, because it makes high elastic energy return and makes heat damage minimal [123]. Peltonen et al. reported hysteresis of Achilles tendon to be on an average of 5 ± 2% between 10–80% of maximum voluntary contraction [123]. However, hysteresis would increase after cyclic load the change may be caused by progressive extension of toe region and increasing cyclic energy dissipation [120]. In addition, hysteresis of tendon depends on the physiological capability of stress resistance in which high-stressed tendon (e.g., Achilles and patella tendon) showed higher fatigue resistance over low-stressed tendon. This is due to a functional requirement that these tendons are of different materials.

Several factors alter tendon viscoelastic properties, such as strengthening and stretching, and the physiological conditions like aging or preconditioning. Plyometric training reduces hysteresis without significant alteration in the cross-sectional area of Achilles tendon. This implies that regular engagement in physical activities could help to achieve or maintain a low hysteresis in Achilles tendon [123]. Stretching can also reduce hysteresis and stiffness. The change depends primarily on the duration rather than the number of stretches without alteration in maximum voluntary contraction. The present results suggest that stretching could decrease viscosity, but increase elasticity in tendon structure [115]. Stretching, in consequence, is considered an effective way to improve reused energy during exercise.

Preconditioning in the primate model is proved to reduce the acute tendon tension loss in the graft due to viscoelastic relaxation. Graf et al. showed that isometric conditioning is as effective as cyclic stretching for preconditioning [118]. Bed rest is another factor of increased hysteresis. Kubo et al. showed that 20 days bed rest reduced stiffness and increased hysteresis of vastus lateralis tendon. However, these changes were not found in plantar flexor [124]. Finally, research showed that age did not have significant effect on viscoelastic properties of the patellar tendon. The authors inferred that may be because patellar tendon is high loading dependent in daily activities; therefore, it harbors the properties that are not easily weakened [125].

2.3 Mechano-responses of Tendon

2.3.1 Physiological Mechano-responses

Adequate mechanical loading is essential for the maintenance of tendon homeostasis and enhancement of the biomechanical properties of tendon. For instance, uphill running exercise for 12 weeks significantly increased the modulus and failure stress per body weight in rat Achilles tendons [126]. In addition, swimming exercise for 8 weeks markedly increased the maximum tension, maximum force, and modulus of the rat Achilles tendons [127]. Since increase in modulus represents smaller deformation with a stationary mechanical stress in tendon; thus, a higher modulus indicates a stiffer tendon as a material [128]. Moreover, tendon can alter its structure in response to the mechanical loading to which it withstands. Treadmill exercise for 8 weeks increased the cross-sectional area (CSA) of collagen fibril of rat Achilles tendon [129]. Treadmill exercise for 4 weeks can also enhance the alignment of collagen fibril through the reorganization of the ECM into a close-packed condition [130, 131].

While appropriate exercise leads to the enhancement of tendon mechanical properties, we may consider the increase in tendon biomechanics, which is essentially related to the concentration and cross-links of collagen fiber. Curwin et al. showed a 46% increase in collagen deposition and a 50% decrease in pyridinoline cross-links, following 8-week strenuous treadmill exercise in the Achilles tendons of

premature roosters [132]. These findings indicated the turnover of collagen enhancement but a decrease in quality after strenuous endurance exercise of collagen fiber. A 12-week uphill running exercise increased the expression of type III collagen and insulin-like growth factor I (IGF-I). Type III collagen forms thinner and disorganized fiber. Increased type III collagen can be found in tendon lesion site [133, 134]. IGF-I is an effective stimulator of collagen anabolism and cell proliferation [135, 136]. These results indicate that exercise promotes metabolism of the ECM while the following mechanical consequences still need to be defined.

Several models were employed to mimic the mechanical stimulus during the locomotion of the body segment. In addition, tendons were loaded and unloaded, causing changes in the influx and extrusion of the interstitial fluid, and the interstitial fluid flow toward the organized extracellular matrix with low permeability [137]. Thus, fluid shear stress was used to mimic the shear force the tendon withstood. Shear stress at 1666 μm/s, approximately 0.02–0.1 Pa, increased the intracellular calcium concentration. Combining shear stress and uniaxial tension strain at 4% enhanced the percentage of tenocytes exhibiting transient calcium response [137]. Shear stress at 0.41 Pa reduced the expression of Col I, Col III and several profibrotic factors in rat palmar flexor tendon cells. Shear stress also downregulated TGF-β2, TGF-β3 and TGF-β receptors, except for TGF-β1. Increase in the expression of vascular endothelial growth factor (VEGF) as well as MMPs, and decrease in the expression of TIMPs, MMP inhibitors, were found under shear stress condition. These findings suggested shear stress had an antifibrotic effect and promoted tendon catabolism [138].

Besides shear stress, tensile loading has been exerted to evaluate how tenocytes regulated cell behaviors and homeostasis of the ECM in response to tensile strain. Yang et al. investigated the effect of cyclic mechanical stretching on the proliferation and collagen mRNA expression and protein production of human patellar tendon fibroblasts under serum-free condition [139]. The role of TGF-β1 in collagen production by cyclically stretched tendon fibroblasts was also investigated. The results suggest that increase in the cellular production of collagen type I is at least in part mediated by TGF-β1. Uniaxial cyclic strain at the parameter of 4%, 0.5 Hz enhanced the expression of tendon-related genes in TSCs, such as Col1 and Tnmd, while 8%, 0.5 Hz strain upregulated the expression of LPL, Sox-9, and Runx2, which, respectively, represented a specific gene marker of adipocytes, chondrocytes, and osteocytes. The findings were in accordance with the in vivo treadmill running model. Moderated treadmill running elevated the expression of tendon-related genes, including Col1 and Tnmd. The expression of IGF-1 was enhanced and TSCs proliferation increased with moderate exercise as well. Additionally, intensive exercise induced tendon anabolism through the expression of Col1 and Tnmd with the concomitant increase of non-tendon-related genes [140, 141]. This suggested that proper mechanical loading promoted the maintenance of tendon phenotype and facilitated TSCs differentiation into tendon lineage.

On the contrary, the following studies show different types of tendons and different tendon tissue response under unloading or detraining. Kubo et al. found that the tendon structure and collagen content of Achilles tendon showed gradual improvement

after 3 months of isometric training (15 repetitions of 80% MVC, 4 times/week). After another subsequent 3 months of detraining, the tendon experienced rapid decrease in tendon elongation and stiffness. With a significant detraining change showed in MRI, but not the ultrasound echo-intensity, the authors deduced the effect of detraining is more significant on tendon structure, but the tendon cell number may preserve to an amount [142].

In recent studies, compressive loads are under investigations because the compression effect on tendon grafts fixed to the bone via suture anchors is unneglectable. In an animal study, flexor digitorum tendons were harvested and subjected to compressive loads. Results showed that, the tendon had geometric changes with a volume decrease of up to 30%, mainly from extracellular water excretion. The tendon itself also experienced indirect elongation of 5–10% due to compressive force [143]. This result offers the clinical implication of preloading the tendon as a preparation to avoid post-surgical failure of grafting tendon tissues.

Recently, tendon mechanobiological studies gain more and more attention. With advanced technological conditions, scientists are able to investigate tenocyte reaction under various modes of external forces. Be it tensile, compressive, shear load or even unloading, tendon cells or extracellular matrix seems to have good response on healing and proliferate under various external forces. Although under external loading, tissue quality often has a better result, the biochemical strength seems to show no difference among various circumstances. With heterogeneous results shown in various conditions, it is crucial to continue study the dose of external loads under specific conditions of tendon for further in-depth knowledge of tendon mechanobiology.

2.3.2 Pathological Mechano-responses

It is well established that appropriate mechanical loads are beneficial to enhance the mechanical properties of the tendon. However, excessive mechanical loads on tendons may result in tendon injuries. Tendon injuries are classified into acute and chronic injury. Lacerations and ruptures are two common acute injuries. As for the chronic tendon injury, tendinopathy can be the representative [144].

Tendinopathy, which is usually termed tendinitis, tendinosis, and paratenonitis, has been found to be a result of a failed healing response according to recent histopathological studies [145]. It may cause degenerative changes with increased levels of prostaglandin E2 (PGE2), deoxyribonucleic acid, and protein synthesis in vitro within tendon [146, 147]. Every single microtrauma a tendon experienced may accumulate over time and cause tendinopathy. Previous study has found that loading on the tendon fibroblasts will increase PGE2 and leukotriene B4 expression. The correlation of tendon breakdown and the enhanced activities of vascular endothelial growth factor (VEGF) and matrix metalloproteinase (MMP) was evidenced in the study of Schwartz [148]. When comparing the histological characteristics of tendinopathy to those of the normal tendons, it shows an increased number of tenocytes and concentration of glycosaminoglycans in the ground substance, and disorganiza-

tion and fragmentation of the collagen, and neovascularization [145]. Moreover, the increased expression of type III collagen, fibronectin, tenascin C, aggrecan, and biglycan are the molecular changes found in the patients with chronic Achilles tendinopathy. These changes might be an adaptive response to changes in mechanical loading [149].

Overloading might be the cause of tendinopathy. Human patella tendon fibroblasts underwent cyclic uniaxial stretching of strain conditions: 4%, 8%, 12% randomly for 4 h and rested 4 h to observe the inflammatory response of mediators PGE_2 and LTB_4. Results showed that, under higher stress loads (12%) PGE_2 and LTB_4 levels were higher with significant difference. This may imply the possible mechanism of overuse inflammatory tendinitis [150, 151]. In tendon cells, repetitive, small-magnitude stretching, e.g., 4% strain at a frequency of 0.5 Hz, increased Col I, TGF-β production and reduced inflammatory mediators through downregulation of the expression of COX-2 and PGE_2. Whereas large-magnitude stretching, e.g., 8% strain at a frequency of 0.5 Hz, also increased Col I, TGF-β and MMP-1 production but had a pro-inflammatory effect [139, 152, 153]. The above studies indicated change in tendon anabolism with excessive mechanical loading may have a pathological inference on tendinopathy.

Insufficient mechanical loads, such as disuse or immobilization can also have some effects on tendons [146]. Immobilization has been associated with decreased levels of extracellular matrix protein expression, alterations in tenocyte morphology, and loss of normal extracellular matrix architecture, resulting in impaired function and healing capacity [154–158]. Deprived of stress, tendon tissues underwent dramatic changes in tendon cell shape, cell number, and collagen fiber alignment, and eventually caused tendon degeneration [155]. Stress deprivation-initiated metabolic alterations, such as decrease in anabolic activities but increase in catabolic activities of the tendon matrix are likely responsible for certain degenerative changes in tendons [159].

Non-physiological loading may induce tendinopathy as well, by altering TSPC function and fate at both the proliferation and differentiation levels. Tendon stem/progenitor cells (TSPCs) is responsible for preserving adequate tenocyte numbers in the tissue throughout life and replenishing them after injury. Studies supported that mechanical loading critically affects the fate of TSPCs. An in vitro study showed that mechanical loading at physiological levels promoted TSPC proliferation and differentiation into tenocytes, while excessive levels of loading led TSPCs to differentiate into non-tenocytes, such as adipocytes, chondrocytes, and osteocytes, in addition to tenocytes [159]. An in vivo study using treadmill running further found that tendons subjected to repetitive strenuous mechanical loading produced high levels of PGE_2, which was associated with decreased TSPC proliferation and induced TSPCs to differentiate into adipocytes and osteocytes [160]. These studies suggest that non-physiological loading may induce tendinopathy by altering TSPC function and fate at both the proliferation and differentiation levels. Better understanding of these mechanisms may provide a new strategy for the prevention and treatment of tendinopathy.

Aging accounts for tendinopathy as well which is termed “age-related tendinopathy.” Morphologically, increased lipid deposition and ossification and PGE_2

accumulation are characterized in aging tendon [146]. Altered morphology of tendon fibroblasts from aging was observed [161]. Cell nuclei are flattened in tendon cells and the shape of the tendon cell nuclei elongated significantly with age, especially at 3 and 12 months in rat [162]. Functional deficit in the biomechanical properties of tendons resulted from aging was reported by Ensey et al. In this study, tendons from aging rats showed lower Young's modulus and lower total strain than younger ones and have higher tensile modulus [163]. Moreover, the exposure to repetitive mechanical loading also had an effect on their biomechanical properties [162]. However, one study found that the modulus was not significantly different between 1 and 4–5 years old rabbits. Both normal and repaired tissues exhibited non-linear stress–strain curves, which are typical of collagenous materials [164]. The results of the mechano-response of aging tendons are heterogenous which require further elucidation.

2.3.3 Mechanotransduction

Tenocytes are mechanoresponsive through mechanotransduction mechanisms by which tenocytes convert mechanical signals into a series of biological events such as expression of numerous genes, including those responsible for extracellular matrix. In vitro, the earliest responses to mechanical stimuli are recorded at the proximities of the cell–ECM contacts; these include the opening of stretch-activated ion channels, the phosphorylation of focal adhesion kinase (FAK), the activation of small guanosine triphosphatases (GTPases), and generation of reactive oxygen species [165]. Multiple intracellular signaling pathways are subsequently triggered such as mitogen-activated protein kinases (MAPKs), protein kinase C, and NF-kB [166–170]. As a result, an ECM component could be regulated at the gene transcription level.

One candidate for mechanotransduction mechanisms are stretch-activated ion channels (SACs), which are suggested to interact directly with cytoskeleton and thus can sense the cell stretch [171]. Opening of SACs causes an increase in intracellular Ca^{2+} concentration and other ions (e.g., sodium and potassium) to influx followed by membrane depolarization. Tendon and ligament fibroblasts respond to mechanical loads by increasing their intracellular Ca^{2+} levels. Ligament fibroblasts subjected to mechanical stretch propagated Ca^{2+} wave better than cells that were not subjected to mechanical stretch [172]. In human flexor digitorum profundus tendon cells, transient increase in intracellular calcium level was found under fluid-induced shear stimuli [173, 174]. While tensile stretch at 0.5 Hz, 4% for 10 cycles increased the percentage of tendon cells with transient calcium response. When combining fluid shear stress and cyclic mechanical stretch, greater calcium activity was generated compared to the single model application [137]. In human mesenchymal stem cells, uniaxial mechanical stretch at 1 Hz, 8% for 6, 24, 48, and 72 h enhanced the production of ECM proteins and expression of tendon-related gene markers, including Scx, tenascin-C, tenomodulin, decorin, Col I, and Col III. However, these effects were eliminated by inhibiting the SACs with gadolinium [175]. The above findings

suggested that tendon cell responded to tensile mechanical stimuli through increasing the intracellular calcium level via the SACs. Taken together, these studies suggest that calcium is an important mediator in cellular mechanotransduction.

MAPKs constitute key steps in many intracellular signaling pathways. They usually function as final effectors of signal transduction pathways directly to activate transcription factors in the cytoplasm and nucleus. MAPKs are serine/threonine-specific protein kinases that respond to extracellular stimuli (mitogens) and regulate various cellular activities such as gene expression, mitosis, differentiation, and cell survival/apoptosis. MAPK is crucial for the conversion of mechanical load to tissue adaptation inducing signaling from the cytosol to the nucleus. It is well described that several cell types and subsets of MAPKs such as extracellular signal-regulated kinase 1 and 2 (ERK1/2), MAPK-p38, and stress-activated protein kinases/c-*jun* NH2-terminal kinase (SAPK/JNK) can be activated by mechanical stress, as well as by lowered pH, growth factors, hormones, and reactive oxygen species [1]. ERK-mediated pathways are mostly involved in proliferation and differentiation and generally considered anti-apoptotic. JNK and p38-signaling pathways are activated by stress stimuli, many of which induce apoptosis, but in some cellular systems they have been implicated in proliferation and differentiation as well. Each is proved to have major roles in the regulation of intracellular metabolism and gene expression and integral actions in many areas including growth and development, disease, apoptosis, and cellular responses to external stresses [176]. For example, cyclic strain resulted in an immediate activation of JNK in patellar tendon fibroblasts which was regulated by a magnitude-dependent response and appeared to be mediated through a calcium-dependent mechanotransduction pathway [177]. Our recent study demonstrated that mechanical stretch with 8% strain at 1 Hz rate improves tenocyte characteristics via reversing the fibroblast-to-adipocyte phenotypic transition induced by high glucose through inhibition of Akt and activation of ERK [178].

References

1. Kjaer M. Role of extracellular matrix in adaptation of tendon and skeletal muscle to mechanical loading. Physiol Rev. 2004;84(2):649–98.
2. McCormick RJ. The flexibility of the collagen compartment of muscle. Meat Sci. 1994;36(1–2):79–91.
3. Purslow PP. The structure and functional significance of variations in the connective tissue within muscle. Comp Biochem Physiol A Mol Integr Physiol. 2002;133(4):947–66.
4. Turrina A, Martinez-Gonzalez MA, Stecco C. The muscular force transmission system: role of the intramuscular connective tissue. J Bodyw Mov Ther. 2013;17(1):95–102.
5. Archile-Contreras AC, Mandell IB, Purslow PP. Phenotypic differences in matrix metalloproteinase 2 activity between fibroblasts from 3 bovine muscles. J Anim Sci. 2010;88(12):4006–15.
6. Chiquet M, Gelman L, Lutz R, Maier S. From mechanotransduction to extracellular matrix gene expression in fibroblasts. Biochim Biophys Acta. 2009;1793(5):911–20.
7. Guerin CW, Holland PC. Synthesis and secretion of matrix-degrading metalloproteases by human skeletal muscle satellite cells. Dev Dyn. 1995;202(1):91–9.

8. Hoedt A, Christensen B, Nellemann B, Mikkelsen UR, Hansen M, Schjerling P, et al. Satellite cell response to erythropoietin treatment and endurance training in healthy young men. J Physiol. 2016;594(3):727–43.
9. Crameri RM, Langberg H, Magnusson P, Jensen CH, Schroder HD, Olesen JL, et al. Changes in satellite cells in human skeletal muscle after a single bout of high intensity exercise. J Physiol. 2004;558(Pt 1):333–40.
10. Light N, Champion AE. Characterization of muscle epimysium, perimysium and endomysium collagens. Biochem J. 1984;219(3):1017–26.
11. Fitch JM, Gross J, Mayne R, Johnson-Wint B, Linsenmayer TF. Organization of collagen types I and V in the embryonic chicken cornea: monoclonal antibody studies. Proc Natl Acad Sci U S A. 1984;81(9):2791–5.
12. Listrat A, Lethias C, Hocquette JF, Renand G, Menissier F, Geay Y, et al. Age-related changes and location of types I, III, XII and XIV collagen during development of skeletal muscles from genetically different animals. Histochem J. 2000;32(6):349–56.
13. Gillies AR, Lieber RL. Structure and function of the skeletal muscle extracellular matrix. Muscle Nerve. 2011;44(3):318–31.
14. Eklund L, Piuhola J, Komulainen J, Sormunen R, Ongvarrasopone C, Fassler R, et al. Lack of type XV collagen causes a skeletal myopathy and cardiovascular defects in mice. Proc Natl Acad Sci U S A. 2001;98(3):1194–9.
15. Grounds MD, Sorokin L, White J. Strength at the extracellular matrix-muscle interface. Scand J Med Sci Sports. 2005;15(6):381–91.
16. Whitelock JM, Murdoch AD, Iozzo RV, Underwood PA. The degradation of human endothelial cell-derived perlecan and release of bound basic fibroblast growth factor by stromelysin, collagenase, plasmin, and heparanases. J Biol Chem. 1996;271(17):10079–86.
17. Hedbom E, Heinegard D. Binding of fibromodulin and decorin to separate sites on fibrillar collagens. J Biol Chem. 1993;268(36):27307–12.
18. Ameye L, Young MF. Mice deficient in small leucine-rich proteoglycans: novel in vivo models for osteoporosis, osteoarthritis, Ehlers-Danlos syndrome, muscular dystrophy, and corneal diseases. Glycobiology. 2002;12(9):107R–16R.
19. Sanes JR. The basement membrane/basal lamina of skeletal muscle. J Biol Chem. 2003;278(15):12601–4.
20. Uaesoontrachoon K, Yoo HJ, Tudor EM, Pike RN, Mackie EJ, Pagel CN. Osteopontin and skeletal muscle myoblasts: association with muscle regeneration and regulation of myoblast function in vitro. Int J Biochem Cell Biol. 2008;40(10):2303–14.
21. Bradshaw AD. The role of SPARC in extracellular matrix assembly. J Cell Commun Signal. 2009;3(3–4):239–46.
22. Malek MH, Olfert IM. Global deletion of thrombospondin-1 increases cardiac and skeletal muscle capillarity and exercise capacity in mice. Exp Physiol. 2009;94(6):749–60.
23. Cotman SL, Halfter W, Cole GJ. Identification of extracellular matrix ligands for the heparan sulfate proteoglycan agrin. Exp Cell Res. 1999;249(1):54–64.
24. Meyer GA, Lieber RL. Elucidation of extracellular matrix mechanics from muscle fibers and fiber bundles. J Biomech. 2011;44(4):771–3.
25. Herbert R. The passive mechanical properties of muscle and their adaptations to altered patterns of use. Aust J Physiother. 1988;34(3):141–9.
26. Magnusson SP. Passive properties of human skeletal muscle during stretch maneuvers. A review. Scand J Med Sci Sports. 1998;8(2):65–77.
27. Nordez A, Gennisson JL, Casari P, Catheline S, Cornu C. Characterization of muscle belly elastic properties during passive stretching using transient elastography. J Biomech. 2008;41(10):2305–11.
28. Gajdosik RL. Passive extensibility of skeletal muscle: review of the literature with clinical implications. Clin Biomech (Bristol, Avon). 2001;16(2):87–101.
29. Lieber RL, Ward SR. Skeletal muscle design to meet functional demands. Philos Trans R Soc Lond B Biol Sci. 2011;366(1570):1466–76.

30. Herbert RD, Moseley AM, Butler JE, Gandevia SC. Change in length of relaxed muscle fascicles and tendons with knee and ankle movement in humans. J Physiol. 2002;539(Pt 2):637–45.
31. Zatsiorsky VM, Prilutsky BI. Biomechanics of skeletal muscles. Champaign, IL: Human Kinetics; 2012.
32. Wang K, McCarter R, Wright J, Beverly J, Ramirez-Mitchell R. Viscoelasticity of the sarcomere matrix of skeletal muscles. The titin-myosin composite filament is a dual-stage molecular spring. Biophys J. 1993;64(4):1161–77.
33. Toursel T, Stevens L, Granzier H, Mounier Y. Passive tension of rat skeletal soleus muscle fibers: effects of unloading conditions. J Appl Physiol (Bethesda, MD: 1985). 2002;92(4):1465–72.
34. Rehorn MR, Schroer AK, Blemker SS. The passive properties of muscle fibers are velocity dependent. J Biomech. 2014;47(3):687–93.
35. Ramos J, Lynch S, Jones D, Degens H. Hysteresis in muscle. Int J Bifurc Chaos. 2017;27(1):1730003.
36. Gervasi M, Sisti D, Amatori S, Andreazza M, Benelli P, Sestili P, et al. Muscular viscoelastic characteristics of athletes participating in the European Master Indoor Athletics Championship. Eur J Appl Physiol. 2017;117(8):1739–46.
37. Ryan ED, Herda TJ, Costa PB, Walter AA, Hoge KM, Stout JR, et al. Viscoelastic creep in the human skeletal muscle–tendon unit. Eur J Appl Physiol. 2010;108(1):207–11.
38. Knudson D. Fundamentals of biomechanics. J Sports Sci Med. 2007;6(3):384.
39. Proske U, Morgan DL, Gregory JE. Thixotropy in skeletal muscle and in muscle spindles: a review. Prog Neurobiol. 1993;41(6):705–21.
40. Proske U, Tsay A, Allen T. Muscle thixotropy as a tool in the study of proprioception. Exp Brain Res. 2014;232(11):3397–412.
41. Sakanaka TE, Lakie M, Reynolds RF. Sway-dependent changes in standing ankle stiffness caused by muscle thixotropy. J Physiol. 2016;594(3):781–93.
42. Silva MET, Brandao S, Parente MPL, Mascarenhas T, Natal Jorge RM. Biomechanical properties of the pelvic floor muscles of continent and incontinent women using an inverse finite element analysis. Comput Methods Biomech Biomed Eng. 2017;20(8):842–52.
43. Hill AV. The heat of shortening and the dynamic constants of muscle. Proc R Soc Lond B Biol Sci. 1938;126(843):136–95.
44. Biewener AA, Wakeling JM, Lee SS, Arnold AS. Validation of Hill-type muscle models in relation to neuromuscular recruitment and force-velocity properties: predicting patterns of in vivo muscle force. Integr Comp Biol. 2014;54(6):1072–83.
45. Harry JD, Ward AW, Heglund NC, Morgan DL, McMahon TA. Cross-bridge cycling theories cannot explain high-speed lengthening behavior in frog muscle. Biophys J. 1990;57(2):201–8.
46. Westing SH, Seger JY, Thorstensson A. Effects of electrical stimulation on eccentric and concentric torque-velocity relationships during knee extension in man. Acta Physiol Scand. 1990;140(1):17–22.
47. Voukelatos D, Kirkland M, Pain MTG. Training induced changes in quadriceps activation during maximal eccentric contractions. J Biomech. 2018;73:66–72.
48. Haeufle DF, Gunther M, Bayer A, Schmitt S. Hill-type muscle model with serial damping and eccentric force-velocity relation. J Biomech. 2014;47(6):1531–6.
49. Jones DA. Changes in the force-velocity relationship of fatigued muscle: implications for power production and possible causes. J Physiol. 2010;588(Pt 16):2977–86.
50. Allen DG, Lamb GD, Westerblad H. Skeletal muscle fatigue: cellular mechanisms. Physiol Rev. 2008;88(1):287–332.
51. Ruiter CJ, Didden WJ, Jones DA, Haan AD. The force-velocity relationship of human adductor pollicis muscle during stretch and the effects of fatigue. J Physiol. 2000;526(Pt 3):671–81.
52. Pearson AM. Muscle growth and exercise. Crit Rev Food Sci Nutr. 1990;29(3):167–96.
53. Tonson A, Ratel S, Le Fur Y, Cozzone P, Bendahan D. Effect of maturation on the relationship between muscle size and force production. Med Sci Sports Exerc. 2008;40(5):918–25.

54. Krivickas LS, Dorer DJ, Ochala J, Frontera WR. Relationship between force and size in human single muscle fibres. Exp Physiol. 2011;96(5):539–47.
55. Arnold EM, Hamner SR, Seth A, Millard M, Delp SL. How muscle fiber lengths and velocities affect muscle force generation as humans walk and run at different speeds. J Exp Biol. 2013;216(Pt 11):2150–60.
56. Kawakami Y, Akima H, Kubo K, Muraoka Y, Hasegawa H, Kouzaki M, et al. Changes in muscle size, architecture, and neural activation after 20 days of bed rest with and without resistance exercise. Eur J Appl Physiol. 2001;84(1–2):7–12.
57. Buchthal F, Schmalbruch H. Motor unit of mammalian muscle. Physiol Rev. 1980;60(1):90–142.
58. Fuglevand AJ. Mechanical properties and neural control of human hand motor units. J Physiol. 2011;589(Pt 23):5595–602.
59. Feinstein B, Lindegard B, Nyman E, Wohlfart G. Morphologic studies of motor units in normal human muscles. Acta Anat (Basel). 1955;23(2):127–42.
60. McComas AJ, Fawcett PR, Campbell MJ, Sica RE. Electrophysiological estimation of the number of motor units within a human muscle. J Neurol Neurosurg Psychiatry. 1971;34(2):121–31.
61. De Luca CJ, Erim Z. Common drive of motor units in regulation of muscle force. Trends Neurosci. 1994;17(7):299–305.
62. Akataki K, Mita K, Watakabe M, Ito K. Age-related change in motor unit activation strategy in force production: a mechanomyographic investigation. Muscle Nerve. 2002;25(4):505–12.
63. Henneman E, Somjen G, Carpenter DO. Functional significance of cell size in spinal motoneurons. J Neurophysiol. 1965;28:560–80.
64. De Luca CJ, LeFever RS, McCue MP, Xenakis AP. Control scheme governing concurrently active human motor units during voluntary contractions. J Physiol. 1982;329:129–42.
65. De Luca CJ, Contessa P. Hierarchical control of motor units in voluntary contractions. J Neurophysiol. 2012;107(1):178–95.
66. De Luca CJ, Hostage EC. Relationship between firing rate and recruitment threshold of motoneurons in voluntary isometric contractions. J Neurophysiol. 2010;104(2):1034–46.
67. De Luca CJ. Control properties of motor units. J Exp Biol. 1985;115:125–36.
68. Sosnoff JJ, Vaillancourt DE, Larsson L, Newell KM. Coherence of EMG activity and single motor unit discharge patterns in human rhythmical force production. Behav Brain Res. 2005;158(2):301–10.
69. Elble RJ, Randall JE. Motor-unit activity responsible for 8- to 12-Hz component of human physiological finger tremor. J Neurophysiol. 1976;39(2):370–83.
70. Farmer SF, Bremner FD, Halliday DM, Rosenberg JR, Stephens JA. The frequency content of common synaptic inputs to motoneurones studied during voluntary isometric contraction in man. J Physiol. 1993;470:127–55.
71. Scott W, Stevens J, Binder-Macleod SA. Human skeletal muscle fiber type classifications. Phys Ther. 2001;81(11):1810–6.
72. Roy RR, Talmadge RJ, Hodgson JA, Oishi Y, Baldwin KM, Edgerton VR. Differential response of fast hindlimb extensor and flexor muscles to exercise in adult spinalized cats. Muscle Nerve. 1999;22(2):230–41.
73. Andersen JL, Terzis G, Kryger A. Increase in the degree of coexpression of myosin heavy chain isoforms in skeletal muscle fibers of the very old. Muscle Nerve. 1999;22(4):449–54.
74. Staron RS. Human skeletal muscle fiber types: delineation, development, and distribution. Can J Appl Physiol. 1997;22(4):307–27.
75. Nickisch F. Anatomy of the achilles tendon. In: Nunley JA, editor. The achilles tendon: treatment and rehabilitation. New York: Springer New York; 2009. p. 2–16.
76. Thorpe CT, Birch HL, Clegg PD, Screen HRC. Chapter 1—Tendon physiology and mechanical behavior: structure–function relationships. Tendon regeneration. Boston, MA: Academic Press; 2015. p. 3–39.

77. Liu W, Wang B, Cao Y. Chapter 14—Engineered tendon repair and regeneration. Tendon regeneration. Boston, MA: Academic Press; 2015. p. 381–412.
78. Benjamin M, Ralphs JR. Fibrocartilage in tendons and ligaments—an adaptation to compressive load. J Anat. 1998;193(Pt 4):481–94.
79. Smith RKW, Goodship AE. Chapter 2.3—Tendon and ligament physiology: responses to exercise and training A2—Hinchcliff, Kenneth W. In: Geor RJ, Kaneps AJ, editors. Equine exercise physiology. Edinburgh: W.B. Saunders; 2008. p. 106–31.
80. Banes AJ, Donlon K, Link GW, Gillespie Y, Bevin AG, Peterson HD, et al. Cell populations of tendon: a simplified method for isolation of synovial cells and internal fibroblasts: confirmation of origin and biologic properties. J Orthop Res. 1988;6(1):83–94.
81. Goodship AE, Birch HL, Wilson AM. The pathobiology and repair of tendon and ligament injury. Vet Clin North Am Equine Pract. 1994;10(2):323–49.
82. Russell JE, Manske PR. Collagen synthesis during primate flexor tendon repair in vitro. J Orthop Res. 1990;8(1):13–20.
83. Gelberman RH, Manske PR, Vande Berg JS, Lesker PA, Akeson WH. Flexor tendon repair in vitro: a comparative histologic study of the rabbit, chicken, dog, and monkey. J Orthop Res. 1984;2(1):39–48.
84. Cadby JA, Buehler E, Godbout C, van Weeren PR, Snedeker JG. Differences between the cell populations from the peritenon and the tendon core with regard to their potential implication in tendon repair. PLoS One. 2014;9(3):e92474.
85. Bi Y, Ehirchiou D, Kilts TM, Inkson CA, Embree MC, Sonoyama W, et al. Identification of tendon stem/progenitor cells and the role of the extracellular matrix in their niche. Nat Med. 2007;13(10):1219–27.
86. Mienaltowski MJ, Adams SM, Birk DE. Regional differences in stem cell/progenitor cell populations from the mouse achilles tendon. Tissue Eng A. 2013;19(1–2):199–210.
87. Tan Q, Lui PP, Rui YF. Effect of in vitro passaging on the stem cell-related properties of tendon-derived stem cells-implications in tissue engineering. Stem Cells Dev. 2012;21(5):790–800.
88. Gaspar D, Spanoudes K, Holladay C, Pandit A, Zeugolis D. Progress in cell-based therapies for tendon repair. Adv Drug Deliv Rev. 2015;84:240–56.
89. Humphrey JD, Dufresne ER, Schwartz MA. Mechanotransduction and extracellular matrix homeostasis. Nat Rev Mol Cell Biol. 2014;15(12):802–12.
90. Kastelic J, Galeski A, Baer E. The multicomposite structure of tendon. Connect Tissue Res. 1978;6(1):11–23.
91. Banos CC, Thomas AH, Kuo CK. Collagen fibrillogenesis in tendon development: current models and regulation of fibril assembly. Birth Defects Res C Embryo Today Rev. 2008;84(3):228–44.
92. Ahmed AS, Schizas N, Li J, Ahmed M, Ostenson CG, Salo P, et al. Type 2 diabetes impairs tendon repair after injury in a rat model. J Appl Physiol (Bethesda, MD: 1985). 2012;113(11):1784–91.
93. Eriksen HA, Pajala A, Leppilahti J, Risteli J. Increased content of type III collagen at the rupture site of human Achilles tendon. J Orthop Res. 2002;20(6):1352–7.
94. Halper J. Proteoglycans and diseases of soft tissues. Adv Exp Med Biol. 2014;802:49–58.
95. Reed CC, Iozzo RV. The role of decorin in collagen fibrillogenesis and skin homeostasis. Glycoconj J. 2002;19(4–5):249–55.
96. Thorpe CT, Birch HL, Clegg PD, Screen HR. The role of the non-collagenous matrix in tendon function. Int J Exp Pathol. 2013;94(4):248–59.
97. Docheva D, Hunziker EB, Fassler R, Brandau O. Tenomodulin is necessary for tenocyte proliferation and tendon maturation. Mol Cell Biol. 2005;25(2):699–705.
98. Alberton P, Dex S, Popov C, Shukunami C, Schieker M, Docheva D. Loss of tenomodulin results in reduced self-renewal and augmented senescence of tendon stem/progenitor cells. Stem Cells Dev. 2015;24(5):597–609.
99. Kardon G. Muscle and tendon morphogenesis in the avian hind limb. Development (Cambridge, England). 1998;125(20):4019–32.

100. Jarvinen TA, Kannus P, Jarvinen TL, Jozsa L, Kalimo H, Jarvinen M. Tenascin-C in the pathobiology and healing process of musculoskeletal tissue injury. Scand J Med Sci Sports. 2000;10(6):376–82.
101. Forsberg E, Hirsch E, Frohlich L, Meyer M, Ekblom P, Aszodi A, et al. Skin wounds and severed nerves heal normally in mice lacking tenascin-C. Proc Natl Acad Sci U S A. 1996;93(13):6594–9.
102. Erickson HP. A tenascin knockout with a phenotype. Nat Genet. 1997;17(1):5–7.
103. Kannus P, Jozsa L, Jarvinen TA, Jarvinen TL, Kvist M, Natri A, et al. Location and distribution of non-collagenous matrix proteins in musculoskeletal tissues of rat. Histochem J. 1998;30(11):799–810.
104. Riley GP, Harrall RL, Cawston TE, Hazleman BL, Mackie EJ. Tenascin-C and human tendon degeneration. Am J Pathol. 1996;149(3):933–43.
105. Sigrist RMS, Liau J, Kaffas AE, Chammas MC, Willmann JK. Ultrasound elastography: review of techniques and clinical applications. Theranostics. 2017;7(5):1303–29.
106. Proske U, Morgan DL. Tendon stiffness: methods of measurement and significance for the control of movement. A review. J Biomech. 1987;20(1):75–82.
107. Kubo K, Kanehisa H, Fukunaga T. Effects of different duration isometric contractions on tendon elasticity in human quadriceps muscles. J Physiol. 2001;536(Pt 2):649–55.
108. Sarvazyan AP, Rudenko OV, Swanson SD, Fowlkes JB, Emelianov SY. Shear wave elasticity imaging: a new ultrasonic technology of medical diagnostics. Ultrasound Med Biol. 1998;24(9):1419–35.
109. Eby SF, Song P, Chen S, Chen Q, Greenleaf JF, An KN. Validation of shear wave elastography in skeletal muscle. J Biomech. 2013;46(14):2381–7.
110. Grasa J, Calvo B, Delgado-Andrade C, Navarro MP. Variations in tendon stiffness due to diets with different glycotoxins affect mechanical properties in the muscle-tendon unit. Ann Biomed Eng. 2013;41(3):488–96.
111. Fukutani A, Misaki J, Isaka T. Relationship between joint torque and muscle fascicle shortening at various joint angles and intensities in the plantar flexors. Sci Rep. 2017;7(1):290.
112. Konow N, Azizi E, Roberts TJ. Muscle power attenuation by tendon during energy dissipation. Proc Biol Sci. 2012;279(1731):1108–13.
113. Farris DJ, Raiteri BJ. Elastic ankle muscle-tendon interactions are adjusted to produce acceleration during walking in humans. J Exp Biol. 2017;220(Pt 22):4252–60.
114. Waugh CM, Korff T, Blazevich AJ. Developmental differences in dynamic muscle-tendon behaviour: implications for movement efficiency. J Exp Biol. 2017;220(Pt 7):1287–94.
115. Kubo K, Kanehisa H, Kawakami Y, Fukunaga T. Influence of static stretching on viscoelastic properties of human tendon structures in vivo. J Appl Physiol (1985). 2001;90(2):520–7.
116. Seynnes OR, Bojsen-Moller J, Albracht K, Arndt A, Cronin NJ, Finni T, et al. Ultrasound-based testing of tendon mechanical properties: a critical evaluation. J Appl Physiol (1985). 2015;118(2):133–41.
117. Cortes DH, Suydam SM, Silbernagel KG, Buchanan TS, Elliott DM. Continuous shear wave elastography: a new method to measure viscoelastic properties of tendons in vivo. Ultrasound Med Biol. 2015;41(6):1518–29.
118. Graf BK, Vanderby R Jr, Ulm MJ, Rogalski RP, Thielke RJ. Effect of preconditioning on the viscoelastic response of primate patellar tendon. Arthroscopy. 1994;10(1):90–6.
119. Shepherd JH, Legerlotz K, Demirci T, Klemt C, Riley GP, Screen HR. Functionally distinct tendon fascicles exhibit different creep and stress relaxation behaviour. Proc Inst Mech Eng H. 2014;228(1):49–59.
120. Wren TAL, Lindsey DP, Beaupré GS, Carter DR. Effects of creep and cyclic loading on the mechanical properties and failure of human achilles tendons. Ann Biomed Eng. 2003;31(6):710–7.
121. Suydam SM, Soulas EM, Elliott DM, Silbernagel KG, Buchanan TS, Cortes DH. Viscoelastic properties of healthy achilles tendon are independent of isometric plantar flexion strength and cross-sectional area. J Orthop Res. 2015;33(6):926–31.

122. Neviaser A, Andarawis-Puri N, Flatow E. Basic mechanisms of tendon fatigue damage. J Shoulder Elbow Surg. 2012;21(2):158–63.
123. Peltonen J, Cronin NJ, Stenroth L, Finni T, Avela J. Viscoelastic properties of the Achilles tendon in vivo. Springerplus. 2013;2(1):212.
124. Kubo K, Akima H, Ushiyama J, Tabata I, Fukuoka H, Kanehisa H, et al. Effects of 20 days of bed rest on the viscoelastic properties of tendon structures in lower limb muscles. Br J Sports Med. 2004;38(3):324–30.
125. Johnson GA, Tramaglini DM, Levine RE, Ohno K, Choi NY, Woo SL. Tensile and viscoelastic properties of human patellar tendon. J Orthop Res. 1994;12(6):796–803.
126. Heinemeier KM, Skovgaard D, Bayer ML, Qvortrup K, Kjaer A, Kjaer M, et al. Uphill running improves rat Achilles tendon tissue mechanical properties and alters gene expression without inducing pathological changes. J Appl Physiol (Bethesda, MD: 1985). 2012;113(5):827–36.
127. Bezerra MA, Santos de Lira KD, Coutinho MP, de Mesquita GN, Novaes KA, da Silva RT, et al. Biomechanical and structural parameters of tendons in rats subjected to swimming exercise. Int J Sports Med. 2013;34(12):1070–3.
128. Heinemeier KM, Kjaer M. In vivo investigation of tendon responses to mechanical loading. J Musculoskel Neuronal Interact. 2011;11(2):115–23.
129. Enwemeka CS, Maxwell LC, Fernandes G. Ultrastructural morphometry of matrical changes induced by exercise and food restriction in the rat calcaneal tendon. Tissue Cell. 1992;24(4):499–510.
130. Vilarta R, Vidal Bde C. Anisotropic and biomechanical properties of tendons modified by exercise and denervation: aggregation and macromolecular order in collagen bundles. Matrix (Stuttgart, Germany). 1989;9(1):55–61.
131. Buchanan CI, Marsh RL. Effects of exercise on the biomechanical, biochemical and structural properties of tendons. Comp Biochem Physiol A Mol Integr Physiol. 2002;133(4):1101–7.
132. Curwin SL, Vailas AC, Wood J. Immature tendon adaptation to strenuous exercise. J Appl Physiol (Bethesda, MD: 1985). 1988;65(5):2297–301.
133. Lapiere CM, Nusgens B, Pierard GE. Interaction between collagen type I and type III in conditioning bundles organization. Connect Tissue Res. 1977;5(1):21–9.
134. Pajala A, Melkko J, Leppilahti J, Ohtonen P, Soini Y, Risteli J. Tenascin-C and type I and III collagen expression in total Achilles tendon rupture. An immunohistochemical study. Histol Histopathol. 2009;24(10):1207–11.
135. Abrahamsson SO, Lundborg G, Lohmander LS. Recombinant human insulin-like growth factor-I stimulates in vitro matrix synthesis and cell proliferation in rabbit flexor tendon. J Orthop Res. 1991;9(4):495–502.
136. Simmons JG, Pucilowska JB, Keku TO, Lund PK. IGF-I and TGF-beta1 have distinct effects on phenotype and proliferation of intestinal fibroblasts. Am J Physiol Gastrointest Liver Physiol. 2002;283(3):G809–18.
137. Maeda E, Hagiwara Y, Wang JH, Ohashi T. A new experimental system for simultaneous application of cyclic tensile strain and fluid shear stress to tenocytes in vitro. Biomed Microdevices. 2013;15(6):1067–75.
138. Fong KD, Trindade MC, Wang Z, Nacamuli RP, Pham H, Fang TD, et al. Microarray analysis of mechanical shear effects on flexor tendon cells. Plast Reconstr Surg. 2005;116(5):1393–404; discussion 405–6.
139. Yang G, Crawford RC, Wang JH. Proliferation and collagen production of human patellar tendon fibroblasts in response to cyclic uniaxial stretching in serum-free conditions. J Biomech. 2004;37(10):1543–50.
140. Zhang J, Wang JH. Moderate exercise mitigates the detrimental effects of aging on tendon stem cells. PLoS One. 2015;10(6):e0130454.
141. Zhang J, Wang JH. The effects of mechanical loading on tendons—an in vivo and in vitro model study. PLoS One. 2013;8(8):e71740.
142. Kubo K, Ikebukuro T, Maki A, Yata H, Tsunoda N. Time course of changes in the human Achilles tendon properties and metabolism during training and detraining in vivo. Eur J Appl Physiol. 2012;112(7):2679–91.

143. Meyer D, Snedeker J, Weinert-Aplin R, Farshad M. Viscoelastic adaptation of tendon graft material to compression: biomechanical quantification of graft preconditioning. Arch Orthop Trauma Surg. 2012;132(9):1315–20.
144. Kannus P, Jozsa L. Histopathological changes preceding spontaneous rupture of a tendon. A controlled study of 891 patients. J Bone Joint Surg Am. 1991;73(10):1507–25.
145. Li HY, Hua YH. Achilles tendinopathy: current concepts about the basic science and clinical treatments. Biomed Res Int. 2016;2016:6492597.
146. Wang JH, Guo Q, Li B. Tendon biomechanics and mechanobiology—a minireview of basic concepts and recent advancements. J Hand Ther. 2012;25(2):133–40; quiz 41.
147. Uchihashi K, Tsuruta T, Mine H, Aoki S, Nishijima-Matsunobu A, Yamamoto M, et al. Histopathology of tenosynovium in trigger fingers. Pathol Int. 2014;64(6):276–82.
148. Schwartz A, Watson JN, Hutchinson MR. Patellar tendinopathy. Sports Health. 2015;7(5):415–20.
149. Kader D, Saxena A, Movin T, Maffulli N. Achilles tendinopathy: some aspects of basic science and clinical management. Br J Sports Med. 2002;36(4):239–49.
150. Li Z, Yang G, Khan M, Stone D, Woo S, Wang J. Inflammatory response of human tendon fibroblasts to cyclic mechanical stretching. Am J Sports Med. 2004;32(2):435–40.
151. Wang J, Jia F, Yang G, Yang S, Campbell B, Stone D, et al. Cyclic mechanical stretching of human tendon fibroblasts increases the production of prostaglandin E 2 and levels of cyclooxygenase expression: a novel in vitro model study. Connect Tissue Res. 2003;44(3–4):128–33.
152. Wang JH, Jia F, Yang G, Yang S, Campbell BH, Stone D, et al. Cyclic mechanical stretching of human tendon fibroblasts increases the production of prostaglandin E2 and levels of cyclooxygenase expression: a novel in vitro model study. Connect Tissue Res. 2003;44(3–4):128–33.
153. Yang G, Im HJ, Wang JH. Repetitive mechanical stretching modulates IL-1beta induced COX-2, MMP-1 expression, and PGE2 production in human patellar tendon fibroblasts. Gene. 2005;363:166–72.
154. Wang JH. Mechanobiology of tendon. J Biomech. 2006;39(9):1563–82.
155. Reeves ND, Maganaris CN, Ferretti G, Narici MV. Influence of 90-day simulated microgravity on human tendon mechanical properties and the effect of resistive countermeasures. J Appl Physiol (1985). 2005;98(6):2278–86.
156. Yasuda T, Kinoshita M, Abe M, Shibayama Y. Unfavorable effect of knee immobilization on Achilles tendon healing in rabbits. Acta Orthop Scand. 2000;71(1):69–73.
157. Yamamoto N, Ohno K, Hayashi K, Kuriyama H, Yasuda K, Kaneda K. Effects of stress shielding on the mechanical properties of rabbit patellar tendon. J Biomech Eng. 1993;115(1):23–8.
158. Maganaris CN, Paul JP. In vivo human tendinous tissue stretch upon maximum muscle force generation. J Biomech. 2000;33(11):1453–9.
159. Zhang J, Wang JH. Mechanobiological response of tendon stem cells: implications of tendon homeostasis and pathogenesis of tendinopathy. J Orthop Res. 2010;28(5):639–43.
160. Zhang J, Wang JH. Production of PGE(2) increases in tendons subjected to repetitive mechanical loading and induces differentiation of tendon stem cells into non-tenocytes. J Orthop Res. 2010;28(2):198–203.
161. Arnesen SM, Lawson MA. Age-related changes in focal adhesions lead to altered cell behavior in tendon fibroblasts. Mech Ageing Dev. 2006;127(9):726–32.
162. Zhou B, Zhou Y, Tang K. An overview of structure, mechanical properties, and treatment for age-related tendinopathy. J Nutr Health Aging. 2014;18:441–8.
163. Ensey JS, Hollander MS, Wu JZ, Kashon ML, Baker BB, Cutlip RG. Response of tibialis anterior tendon to a chronic exposure of stretch-shortening cycles: age effects. Biomed Eng Online. 2009;8:12.
164. Dressler MR, Butler DL, Boivin GP. Age-related changes in the biomechanics of healing patellar tendon. J Biomech. 2006;39(12):2205–12.
165. Sarasa-Renedo A, Chiquet M. Mechanical signals regulating extracellular matrix gene expression in fibroblasts. Scand J Med Sci Sports. 2005;15(4):223–30.

166. Chiquet M. Regulation of extracellular matrix gene expression by mechanical stress. Matrix Biol. 1999;18(5):417–26.
167. Fluck M, Carson JA, Gordon SE, Ziemiecki A, Booth FW. Focal adhesion proteins FAK and paxillin increase in hypertrophied skeletal muscle. Am J Physiol. 1999;277(1 Pt 1):C152–62.
168. Fluck M, Tunc-Civelek V, Chiquet M. Rapid and reciprocal regulation of tenascin-C and tenascin-Y expression by loading of skeletal muscle. J Cell Sci. 2000;113(Pt 20):3583–91.
169. Goodyear LJ, Chang PY, Sherwood DJ, Dufresne SD, Moller DE. Effects of exercise and insulin on mitogen-activated protein kinase signaling pathways in rat skeletal muscle. Am J Physiol. 1996;271(2 Pt 1):E403–8.
170. Milanini J, Vinals F, Pouyssegur J, Pages G. p42/p44 MAP kinase module plays a key role in the transcriptional regulation of the vascular endothelial growth factor gene in fibroblasts. J Biol Chem. 1998;273(29):18165–72.
171. Sackin H. Mechanosensitive channels. Annu Rev Physiol. 1995;57:333–53.
172. Jones BF, Wall ME, Carroll RL, Washburn S, Banes AJ. Ligament cells stretch-adapted on a microgrooved substrate increase intercellular communication in response to a mechanical stimulus. J Biomech. 2005;38(8):1653–64.
173. Wall ME, Banes AJ. Early responses to mechanical load in tendon: role for calcium signaling, gap junctions and intercellular communication. J Musculoskel Neuronal Interact. 2005;5(1):70–84.
174. Wall ME, Dyment NA, Bodle J, Volmer J, Loboa E, Cederlund A, et al. Cell signaling in tenocytes: response to load and ligands in health and disease. Adv Exp Med Biol. 2016;920:79–95.
175. Nam HY, Balaji Raghavendran HR, Pingguan-Murphy B, Abbas AA, Merican AM, Kamarul T. Fate of tenogenic differentiation potential of human bone marrow stromal cells by uniaxial stretching affected by stretch-activated calcium channel agonist gadolinium. PLoS One. 2017;12(6):e0178117.
176. Cowan KJ, Storey KB. Mitogen-activated protein kinases: new signaling pathways functioning in cellular responses to environmental stress. J Exp Biol. 2003;206(Pt 7):1107–15.
177. Arnoczky SP, Tian T, Lavagnino M, Gardner K, Schuler P, Morse P. Activation of stress-activated protein kinases (SAPK) in tendon cells following cyclic strain: the effects of strain frequency, strain magnitude, and cytosolic calcium. J Orthop Res. 2002;20(5):947–52.
178. Wu YF, Huang YT, Wang HK, Yao CJ, Sun JS, Chao YH. Hyperglycemia augments the adipogenic transdifferentiation potential of tenocytes and is alleviated by cyclic mechanical stretch. Int J Mol Sci. 2017;19(1):E90.

Chapter 3
Biomechanics of Ligaments

Jie Yao, Zizhan Lian, Bin Yang, and Yubo Fan

Abstract The ligaments are important tissues that connect the bones in the human body. The main function is to transmit the tensile load by playing an important role in maintaining the stability and restraint excessive joint motion in musculoskeletal system. Their unique composition and structure let ligaments to guide joints to articulate smoothly and to protect other soft tissues in and around the joints. These ligaments have biomechanical properties designed for this important function. As such, understanding the biomechanical behavior of ligaments is important. Also, these fundamental knowledges are helpful in preventing ligament injury and improving the treatment method. In this chapter, the ligament composition, structure, and function are introduced. Then the biomechanical properties of the ligaments and the method to obtain them are described by using the anterior cruciate ligament (ACL) of the knee as an example. And finally, injury, as well as current surgical treatment and postoperative rehabilitation, is reviewed.

J. Yao · Z. Lian
Key Laboratory for Biomechanics and Mechanobiology of Ministry of Education, School of Biological Science and Medical Engineering, Beihang University, Beijing, China

Advanced Innovation Center for Biomedical Engineering, Beihang University, Beijing, China

B. Yang
Orthopedics Department, Peking University International Hospital, Beijing, China

Y. Fan (✉)
Key Laboratory for Biomechanics and Mechanobiology of Ministry of Education, School of Biological Science and Medical Engineering, Beihang University, Beijing, China

Advanced Innovation Center for Biomedical Engineering, Beihang University, Beijing, China

National Research Center for Rehabilitation Technical Aids, Beijing, China
e-mail: yubofan@buaa.edu.cn

C.-K. Cheng, S. L-Y. Woo (eds.), *Frontiers in Orthopaedic Biomechanics*,
https://doi.org/10.1007/978-981-15-3159-0_3

Keywords Ligaments · Anterior cruciate ligament · Tensile properties
Viscoelastic properties · Injury · Reconstruction

1 Ligament Composition, Structure, and Function

1.1 Composition

The ligament is a fibrous connective tissue that is mainly composed of fibroblasts. Its extracellular matrix is rich in collagen, proteoglycans, and water, which determines the biomechanical characteristics of the ligament. Water accounts for about 60–70% of the mass of the cytoplasmic matrix. Collagen accounts for about 70–80% of its dry weight, and is a most important component of bearing loading. In addition, other components such as elastin and proteoglycan are also included in the cytoplasmic matrix [1, 2].

Collagen is the main component of the ligament extracellular matrix and is mainly composed of type I collagen. In addition, type II, type III, type V, and type XI collagen also account for a certain proportion. For example, Type II collagen usually exists at the junction of the ligament and bone; the proportion of type III collagen in the ligament gradually decreases as the embryo develops. A small amount of type V and type XI collagen is often accompanied by type I, II, and III collagen in fibrous cell surfaceome [3, 4].

The content of elastin varies among different types of ligaments, generally less than 1% of dry weight. It can impart ligament elasticity and tensile strength together with collagen. There is no continuous repetitive cycle throughout the peptide chain in its amino acid sequence structure. But there are alternating hydrophobic and hydrophilic segments [5]. Proteoglycans consist of small amounts of protein bound to negatively charged polysaccharide chains referred to as GAGs. Proteoglycans account for a small proportion of ligaments, about 0.5%. It can bind to water and improve the stability and strength between ligament fibers. In addition, there are a variety of other chemicals, including intracellular DNA, proteases, lipoproteins, etc., which together maintain the survival of cells in the ligament.

The distribution of the biochemical components that make up the ligament is nonuniform. For example, the collagen proportions of the four ligaments (anterior cruciate ligament (ACL), posterior cruciate ligament (PCL), medial collateral ligament (MCL), and lateral collateral ligament (LCL)) in knee joint are different, the hydroxyproline densities are: 15.1 ± 0.4, 18.3 ± 0.3, 17.6 ± 0.4, 17.6 ± 0.4 mg/μm^3. On the same ligament, the collagen distribution is nonuniform. The collagen proportion in the anterior sites of the above four ligaments is higher than the posterior sites. Along the longitudinal axis of ACL and PCL, the collagen proportions at the middle regions are greater than those at both ends near the bone [6]. Furthermore, there are also capillaries in the ligament, which provide blood for the growth of the ligament, as well as the repair after injury. Blood vessels growing in some ligaments can also nourish surrounding bones and other soft tissues.

1.2 Structure

Microscopically, the collagen of the ligament is a layered structure. The triple helix-shaped collagen molecules aggregate to form collagen fibers. Macroscopically, the ligaments can be divided into visceral ligament and joint ligament. They are distributed in different locations, which makes their structure varying. The visceral ligament is formed by a single layer or double layers of peritoneal folds. It is connected to the visceral layer of the liver, kidneys, and other organs. The ends of the joint ligament are attached to the surface of the bone or fused to the joint capsule. At the ligament's insertion site on the bone, the collagen fibers bind to the bone cells and form the skeletal junction of the ligament. The middle part of the ligament is a dense connective tissue composed of a large number of fiber bundles. The length and thickness of the fiber bundles are nonuniformly and irregularly distributed. The fiber bundles interact with each other, and each bundle of fibers is at an angle of 0–30° to the longitudinal direction of the ligament.

Take the PCL as an example. 95% of the fiber bundles are aligned and distributed consistent with the longitudinal axis of the ligament. The other 5% is arranged obliquely from the proximal posterior end to distal medial, at an angle of 15–20° to the longitudinal axis of the ligament. The fiber bundles in the middle part of the ligament are tightly connected to each other, and looks like a twisted rope. The fiber bundles near the femoral and tibial attachments are relatively loose and can be separated. These fiber bundles are composed of elastin and collagen, which are intertwined to form the overall structure of PCL.

1.3 Function

Physiological functions of the ligament include transmitting loads and limiting excessive movement. The ligaments are distributed in and around the joint cavity, and between the body's organs and the peritoneum. Due to the difference in anatomical location and structure, the ligaments' functions vary.

The joint ligament is connected to the bones. The joint tracking is mostly determined by the restraints of ligament and articular cartilages. The ligament can prevent the joint from over-extension and over-flexion, and generally bears the load within its elastic limit to ensure the joint is stable. Injury occurs when the ligament is extended to its yield stress. The consequences of ligament injury include joint instability, dislocation, and changes in the mechanical environment of the joint, and will lead to subsequent joint tissue injury, arthritis, and other symptoms. In addition, the visceral ligament fixes the internal organs in a normal position and limits their range of motion, thereby protecting the organs. The composition and structure of the ligaments make it exhibit typical nonlinear anisotropic mechanical behavior. For example, when the loading is small, the collagen fibers in the ligament are in a "crimp" state, and the ligament is relatively compliant, which is represented by the

"toe" region of the loading-elongation curve. When the load is increased, the collagen fibers are elongated, and the sliding between each other is reduced, the stiffness of the ligament is increased. Ligament maintains approximately linear elastic until the collagen fibers reach the yield threshold. In addition, the mutual sliding action between the fiber bundles can contribute to the viscoelastic effect of the ligament. All these characteristics provide the basis for the physiological function of the ligament: at low loads, guide the path of joint motion; at high loads, restrict excessive motion (displacement) between bones to protect other soft tissue.

2 Biomechanical Properties of Ligaments

2.1 Tensile Properties

The main function of the ligament is to withstand the tensile loads. Therefore, quantification of the mechanical properties of the ligament in response to different loading condition is important for understanding its function as well as the mechanism of ligament injury healing. The uniaxial tensile test is usually used to measure the tensile properties of the ligament [1]. Taking the anterior cruciate ligament of New Zealand rabbits as an example, the general procedure is as follows:

After sacrifice of the subject, the knee joint is taken, including the femur and tibia. Because subject's ACL is short and difficult to fix, the "femur-ACL-tibia" specimen is prepared. The skin, muscle, fat, meniscus, and other ligamentous tissues are carefully removed. In order to facilitate the fixation of the sample, the proximal femur and the distal tibia are fixed in a standard mold with resin material (Fig. 3.1). The stiffness of the mold, resin, and bone has been tested to be much greater than ACL, and thus their deformations could be neglected compared with the ACL. Since the mechanical properties of ACL are significantly correlated with water proportion, saline is used to keep ACL moist in both the preparation process and the subsequent experimental procedures.

The Femur-ACL-Tibia specimen is loaded and measured using a dynamic mechanical testing machine (Instron E10000, Illinois Tool Works Inc., USA) with a sensor range of 250 N. ACL is kept coinciding with the load axis. ACL length under 1.0 N loading is measured as the initial length. First, a cycle loading is performed. A loading magnitude of 1% in the nominal strain and a loading frequency of 1 Hz are applied for 20 cycles. Second, a tensile test with a strain rate of 0.1%/s is applied. To calculate the nominal stress, the entire ACL is embedded in paraffin. The average cross-sectional area is calculated from five positions along the longitudinal axis of the ligament. The nominal stress is calculated as the ratio of loading to the cross-sectional area. The nominal strain is calculated as the change in length per unit of the original length of the ligament.

The force-displacement curve of ACL is shown in Fig. 3.2. ACL exhibits typical hyperelasticity under the uniaxial tension. The force-displacement curve can be divided into toe region, linear region, and yield region. When the load is small, the

Fig. 3.1 Femur-ACL-Tibia specimen

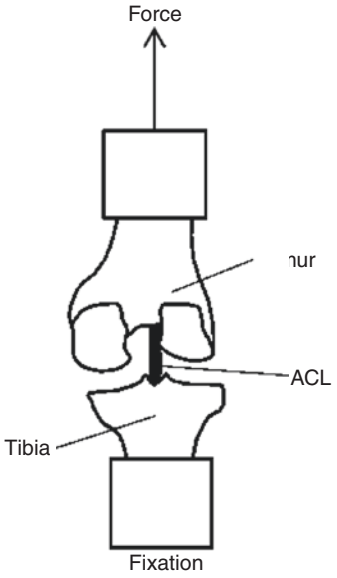

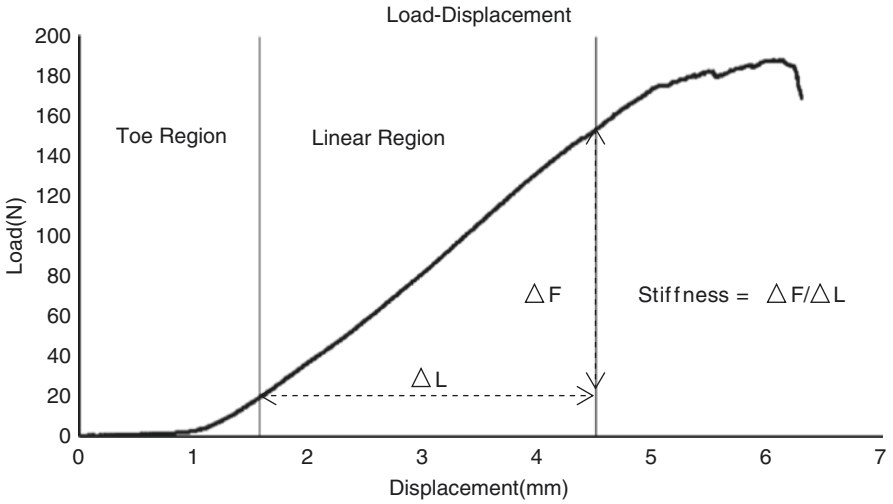

Fig. 3.2 Load-displacement curve of ligament under uniaxial tension

fiber bundles in the ligament are not fully stretched, and the ligament is relatively flexible, which is in the toe region in the figure. The modulus of elasticity in the toe region increases continuously, but it is at a smaller level than that in linear region. As the stress increases, all the fiber bundles turn into the tension state, which is in the linear region in the figure. Linear region is the main functional region of ligament. Compared with the toe region, the modulus of linear region is greater and nearly constant. As the load continues to increase, some fiber bundles break, and the

ligament is damaged. Plastic deformation occurred in the region. With the increase of the fiber bundles broken, the ligament modulus decreases.

The critical point between the toe region and the linear region is called the toe region point. The larger the stress in the toe region, the larger the degree of curling of the fiber bundle in the relaxed state. This is instructive for the setting of preloading in ligament reconstruction. The normal functional region of the ligament is linear region. Therefore, the elastic modulus of the linear region is an important parameter of the biomechanical property of the ligament, which is used to represent the stiffness of different ligaments. In the above experiment, the rabbit ACL elastic modulus was about 61.3 MPa. The point between the linear region and the yield region is called the elastic limit. When the ligament exceeds the elastic limit, the ligament begins to injury. In the stress-strain curve, the point at which the stress reaches the maximum value is called the tensile strength. When the ligament is stretched exceeding its strength, the ligament is completely torn. Therefore, strength refers to the ability of the ligament to resist damage. The acute injury to the ligament is mostly due to the load exceeding the strength of the ligament.

The mechanical properties of the ligament are related to age. Taking the human ACL as an example, the linear region stiffness and ultimate load will decrease with age [7]. The cadaveric study indicated that the linear region stiffness of young group (20–35 years old) (242 ± 28 N/mm) was 10% higher than that of the middle-aged group (40–50 years old) (220 ± 24 N/mm), and was 34% higher than that of elderly group (60–97 years old) (180 ± 25 N/mm). The ultimate load of young group (2160 ± 157 N) was 44% higher than that of the middle-aged group (1503 ± 83 N) and 228% higher than that of the elderly group (658 ± 129 N). In addition, the energy absorbed by the ligament injury has the similar tendency as the linear stiffness. Ligaments of young group absorb more energy when destroyed than those of older groups. In the elderly group, the incidence of collagen ligament destruction in the middle of the ligament (12/18, 67%) was higher than that in the young group (5/18, 28%) and the middle-age group (8/18, 44%). In the young group, the skeletal avulsion at the ligament was the highest (9/18, 50%). Possible causes include: Older donors' knee joints have fewer types and amounts of daily activity than younger donors, resulting in changes in joint geometry and ligament material properties.

In complex in vivo mechanical environments, the loading direction of the joint is often not parallel to the longitudinal axis of the ligament, and thus also affects the mechanical response of the ligament. Take the ACL as an example. The stiffness of the femoral-ACL-tibia specimen parallel to the longitudinal axis of the ACL was 242 ± 28 N/mm, and the stiffness of the specimen parallel to the tibia shaft was reduced to 218 ± 27 N/mm. The ultimate load of the specimen in the direction of the longitudinal axis of the ACL is 35% higher than the direction of the tibia shaft. The experimental results imply that the influence of the tensile direction of the specimen plays a role in the mechanical properties of the ligament. In fact, the various parts of the ligament have different lengths. Therefore, the entire ligament is not uniformly elongated during the stretching. There are also differences in the way the ligaments yield in different directions of stretching. When the ligament is loaded in the

direction of the longitudinal axis, the deformations of elastic fibers are relatively uniform under the tensile load. The ultimate load in this direction can more accurately reflect the strength of the ligament. Therefore, when testing the mechanical properties of the ligament, it is necessary to ensure that the longitudinal axis of the ligament coincides with the loading axis.

2.2 Viscoelastic Properties

The complex interaction of collagen, elastin, proteoglycan, and water in the ligament results in a viscoelastic property of the ligament. This is manifested in the fact that the mechanical response is related to the rate of loading and exhibits hysteresis, creep, and stress relaxation. The viscoelastic properties of the ligaments are generally measured by uniaxial tensile tests at different loading rates. Taking the measurement of ACL of New Zealand rabbits as an example, the general procedure is as follows:

Femur-ACL-tibia specimens are prepared and fixed in the dynamic mechanical testing machine (Instron E10000, Illinois Tool Works Inc., USA). The ligament is kept in line with the loading direction. In daily joint motion, the ligaments generally perform a periodic stretching motion at approximate 0.1–1 Hz. Therefore, a sinusoidal test of 1% strain amplitude is performed at a frequency of 0.1 Hz and 1 Hz, and each frequency was performed for 20 cycles. Each set of specimens is recovered for 60 min at 0% strain between trials, eliminating the effects of historical deformation.

In the test, the soft tissue strain was large; therefore the true strain and true stress were calculated:

$$\varepsilon = \ln\left(L / L_0\right) \tag{3.1}$$

$$\delta = \frac{F}{A_0}\frac{L}{A_0} \tag{3.2}$$

where L is the measured length, L_0 is the initial length, F is the measured tensile force, and A_0 is the cross-sectional area. The data is then fitted to the stress and strain data of the sinusoidal test:

$$z = A\sin\left(2\pi ft + \varphi\right) + z_0 \tag{3.3}$$

where z is stress or strain, A is amplitude, z_0 is the constant parameter, f is frequency, and φ is phase. The phase difference is defined as the difference between the stress and the strain phase. The viscosity increased with the phase difference. As a result, the ligament had a phase difference of 3.22 at 0.1 Hz and a phase difference of 6.20 at 1 Hz, which means that the ligaments exhibit higher viscosity characteristics at high loading rates.

There are several methods of quantifying the viscoelastic properties of the ligament. The parameter "supplementary stress" can also describe this property [8]. Define the "supplementary stress" variable as:

$$\text{Supplementary stress} = \frac{\sigma_y - \sigma_{0.1}}{\sigma_y}$$

where y indicates a different strain rate value. σ_y indicates the stress at y%/s strain rate, and $\sigma_{0.1}$ indicates the stress at 0.1%/s strain rate. The supplementary stress represents the percentage of stress at a high strain rate at a strain rate greater than 0.1%/s strain rate at the same strain level. The shape of the stress-strain curve does not change with increasing strain rate, except that the toe region appears in the lower strain range. As the strain rate increases, the "supplemental stress" increases significantly. When the strain rate is 40%/s, the "supplemental stress" value can reach 70%. This phenomenon of bovine ACL is similar to the conclusion obtained from the rabbit ACL test.

The viscoelastic effect of the ligament is closely related to its physiological function. When the joint movement speed is low, the ligament has a low strain rate and is relatively flexible, then the muscle plays a greater role in stability and restraint of joint. As the speed of joint motion increases, the stiffness of the ligament increases, which can compensate the delay of the muscle response.

In addition, the toe region modulus is also one of the methods to reflect viscoelastic properties [9]. In the uniaxial tensile tests with different loading rates, the ratio of stress to strain at the critical point between the toe region and the linear region is defined as the toe region modulus. The viscosity increases with the difference of the toe modulus at different strain rates. By this method, the change in viscosity of the xenograft porcine superflexor tendon (pSFT) used in ACL reconstruction before and after decellularization was measured. The natural pSFT has a significant difference in the toe modulus (29.7, 104.3, 139.8 MPa) under the three different strain rates (1%/s, 10%/s, 100%/s). However, there is no such difference in the toe modulus (48.8, 63.1, and 68.1 MPa) after decellularization. This indicates that pSFT after decellularization results in a decrease in viscosity.

3 Ligament Injury, Treatment, and Rehabilitation

3.1 Injury

There are many factors contributing to the injury of the ligament. Most ligament injuries are caused by violent, traumatic, non-physiological activities, especially joint ligaments. For example, medial collateral ligament may tear under violent knee valgus, and ACL may tear under knee internal rotation. When external factors cause the ligament to reach the elastic limit and exceed its tolerance, the ligament is

injured. The injury may occur in the middle or the attachments of the ligament. Damage to the joint ligaments can contribute to dislocation, maltracking, and instability of the joints, and lead to subsequent diseases of other soft tissue and bone, such as osteoarthritis. In addition, genetic, endocrine, and microbial infections can lead to ligamentous lesions that gradually damage the ligaments.

The risk of ligament injury is also related to the physiological structure of the musculoskeletal system and the external environment. Taking ACL injury as an example, the probability of ACL injury in the subject with narrow intercondylar notch is greater. Since ACL is located in the joint cavity of the tibiofemoral joint, and is sandwiched by the medial and lateral femoral condyles, when the knee joint is subjected to internal and external loads, the two femoral condyles will press the ACL, causing additional lateral force on the ACL and increasing the chance of ACL tear [10–12]. In addition, ACL footprints are at the anteromedial aspect of the intercondylar area on the tibial plateau and the posteromedial aspect of the lateral femoral condyle. For individuals with an anterior medial aspect of the tibial plateau that is higher than the posterior lateral aspect, when the knee joint is subjected to a vertical load, the tibia will be additionally subjected to the forward and medial loading, thereby causing additional in situ force in ACL, and increasing the probability of ACL injury. A number of statistical studies have reported the correlation between this knee anatomical feature and ACL injury [13–15].

Under different sports types and ground conditions, the injury rate of ACL is also different. Renstrom et al. reported the rate of ACL injury in basketball, ice hockey, football, and gymnastics. The ACL injury rate of women's basketball and women's gymnastics was the highest, reaching nearly 5%, while the ACL injury rate for men's basketball and women's ice hockey was only 0.7% [16]. At the same time, a number of statistical studies have analyzed the correlation between ground environment and ACL injury rate; selecting the appropriate site according to the type of exercise can reduce the probability of ACL injury [17–20]. In addition, Lambson et al. found that different sole materials and textures provide different grips (such as lateral, longitudinal, and torsional resistance) and have an impact on ACL injury [21].

3.2 Treatment

The treatment of ligament injury mainly includes conservative treatment and surgical treatment. The choice of the treatment methods mainly depends on the type and severity of the ligament injury. For example, nearly 90% of knee joint ligament injuries are ACL and MCL injuries [22]. MCL injuries usually heal spontaneous, although scar tissue will appear between MCL and bones, resulting in nonideal changes in MCL mechanical properties. However, the clinical treatment is usually conservative, and the MCL will be repaired by resting. In contrast, ACL tears often require surgery because ACL has fewer blood vessels and poor healing ability. If nonsurgical conservative treatment is used, it may lead to subsequent meniscus and cartilage lesions, resulting in severe instability of the knee joint.

ACL reconstruction surgery assisted by arthroscope is the main method to treat ACL tear in clinic at present. Essentially, the procedure aims to replace the damaged ACL with an autologous or allogeneic ligament graft and maintain the restraint function for the knee joint. The success of the operation depends on whether the knee joint can return to normal motion and mechanical environment after surgery, or more accurately depends on whether the ligament graft can reconstruct the biomechanical function of normal ACL. The basic steps in ACL reconstruction include: graft preparation, bone tunnel creation, and graft fixation.

Autologous ligament grafts are commonly used in clinics. Currently used autologous ligament grafts include patellar tendon, quadriceps tendon, and hamstring tendon. Taking the patellar tendon as an example, the surgery cuts the middle third bundles of the patellar tendon, about 9–10 mm wide. The incision is parallel to the fiber direction of the patellar ligament and continues to the tibia and patella. The cut ligament graft with the bones at both ends have a total length of about 95 mm, and each end contains about 20 mm of wedge-shaped bone. The redundant soft tissue on the graft is then removed, the wedge-shaped bone is trimmed, and the sutures are connected on the bones at both ends, which can be used to pull the ligament graft into the bone tunnel and apply pretension.

After arthroscopic removal of the injured ACL stump, bone tunnels are created on the tibia and femur for fixation of the ligament graft. To create the tibial bone tunnel, the ACL tibial footprint is determined on the tibial plateau using an aimer. A small tunnel is drilled from the medial site of the tibia tuberosity with a 2.4 mm drill guide pin, and to the center of the ACL tibial footprint. The angle between the guide pin and the tibial plateau is approximately 55°. The diameter of the bone tunnel is then expanded to 7–9 mm using a reamer. Then the bone tunnel of the femur is created. The knee joint was flexed to approximately 120°, and the ACL femoral footprint is determined on the medial side of the lateral femoral condyle. The drilled guide pin is drilled from the medial site of the patellar tendon and passed through the ACL femoral footprint, to the lateral femoral cortex. The reamer is then used to create a bone tunnel about 35 mm deep and 9 mm in diameter along the guide wire on the femur.

Finally, the implant is fixed in the bone tunnel. The suture of the femoral end of the ligament graft is used to pull it from the distal end of the tibial bone tunnel into the joint cavity, and finally the bone blocks at both ends are located in the bone tunnel of the tibia and femur. In order to fix the ligament graft at the femoral end, the knee joint is flexed, and the interface screw is used to fix the bone block of the femoral end of the ligament graft in the bone tunnel. The knee joint is then subjected to 20–30 flexion-extension, and a pretension of about 45 N is applied by using the suture of the tibial end of the ligament graft. The bone graft of the ligament graft is fixed in the tibial tunnel at the 30° position of the knee by placing the interface screw at the distal end of the tibial tunnel.

In addition, allografts are also used in clinical procedures. Xenografts and synthetic grafts have also been used in clinical procedures, but due to their durability and biocompatibility issues, they are currently used in small quantities. With the study of the ACL double-bundle anatomy, double-bundle reconstruction is getting

increasing attention. Additional tunnels will be created in the double-bundle reconstruction. Compared to single-bundle reconstruction, double-bundle ACL reconstruction can better restore knee stability, but at the same time may cause greater bone volume loss.

3.3 ACL Reconstruction Animal Model

Animal model is often researched for the improvement of ACL reconstruction. Take rabbit ACL reconstruction as an example (Fig. 3.3). ACL reconstruction is performed on the left knee joint. After preoperative anesthesia, the right ankle joint and the left knee joint are shaved and wiped with iodophor and alcohol. Then the epidermis of the right Achilles tendon is cut open, one-third of the total width is cut as the graft. Two sutures are connected at both ends of the graft and placed in physiological saline for use. The left knee joint epidermis and joint cavity are then dissected, the original ACL is removed. The knee joint is bent to the maximum knee flexion angle. To create the femoral tunnel, the 1 o'clock position of the femoral intercondylar notch is used as the pin insertion point. The 2.5-gauge Kirschner wire is used to drill the tunnel through the anterior and lateral femur. To create the tibial tunnel, the ACL tibial footprint is used as the pin insertion point. The tunnel is drilled into the anterior medial aspect of the tibia using a 2.5-gauge

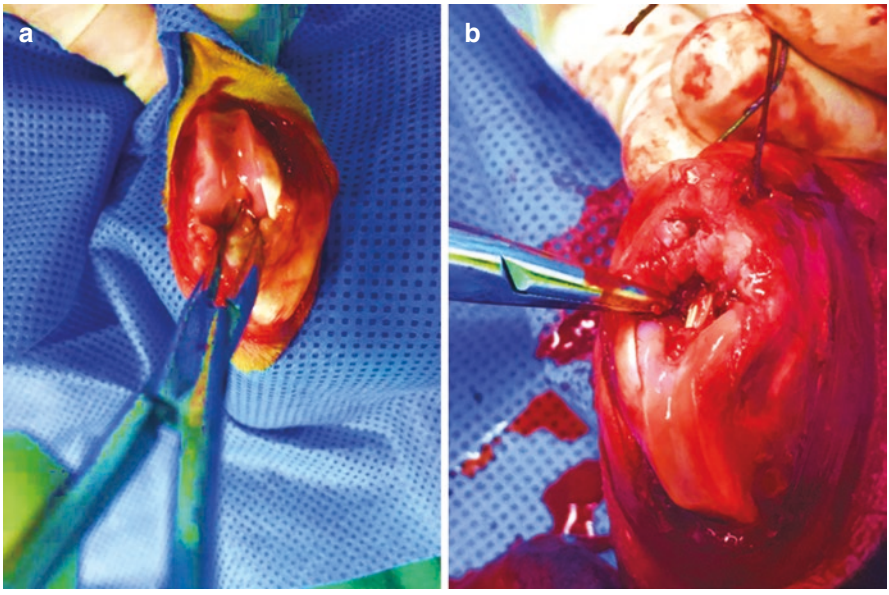

Fig. 3.3 Rabbit ACL reconstruction. (**a**) Rabbit knee joint before ACL reconstruction. (**b**) Rabbit knee joint after ACL reconstruction

needle. The sutures at both ends of the graft are respectively passed through the tunnel, and the graft is pulled into the tunnel. The joint stability is assessed according to the tibiofemoral anterior-posterior translation. Finally, the sutures at both ends of the graft were tied to the proximal femur and the distal end of the tibia. The knee joint capsule and the epidermal incision were sutured and placed in the cage after being injected with antibiotics.

3.4 Rehabilitation

Different ligament injuries have different rehabilitation methods. For example, patients with ankle ligament injury are not recommended to perform functional exercise immediately after surgery to avoid delayed or secondary injury. It is generally recommended to use a fixed shoe or cast gypsum for 6 weeks after the repair of the proximal deltoid ligament injury. When the medial collateral ligament of the knee is injured, the knee joint will be fixed by a bracket to reduce the joint motion and external loading; a 30 days rest is usually suggested.

Rehabilitation after ACL reconstruction is critical to the postoperative outcome. Passive knee-flexion training within 90° is required within 1 week after surgery, and ankle and foot training is also required to enhance the calf muscle strength. In the second week after surgery, appropriate active knee flexion, straight leg elevation, and hip abduction-adduction training should also be performed. In the third week after surgery, a protective semi-squat training can be performed appropriately, and the flexion and extension should be less than 45°.

4 Summary

The biomechanical properties of the ligaments are closely related to their physiological functions. Therefore, the ligaments' composition, structure, as well as their biochemical and mechanical interactions with the surrounding tissue are varying in different locations of the human body. Illustrating the relationship between the biochemical and mechanical characters of ligaments is critical for understanding the mechanism of ligament injury and improving the treatment strategies. This will become an important direction for future research and will bring profound significance to clinical application.

Statement on the Animal Benefit All animal treatments were approved by the Animal Care Committee of Beihang University in accordance with the Regulation of Administration of Affairs Concerning Experimental Animals of State Science and Technology Commission of China.

Acknowledgement The authors would like to convey their appreciation to Prof. Savio L-Y. Woo for his precious suggestions.

References

1. Woo SL, Abramowitch SD, Kilger R, Liang R. Biomechanics of knee ligaments: injury, healing, and repair. J Biomech. 2006;39(1):1–20.
2. Mienaltowski MJ, Birk DE. Structure, physiology, and biochemistry of collagens. In: Progress heritable soft connective tissue diseases, vol. 802. Dordrecht: Springer; 2014. p. 5–29.
3. Milz S, Jakob J, Buttner A, Tischer T, Putz R, Benjamin M. The structure of the coracoacromial ligament: fibrocartilage differentiation does not necessarily mean pathology. Scand J Med Sci Sports. 2008;18(1):16–22.
4. Smith SM, Thomas CE, Birk DE. Pericellular proteins of the developing mouse tendon: a proteomic analysis. Connect Tissue Res. 2012;53(1):2–13.
5. Quapp KM. Material characterization of human medical collateral. Ligament. 1997;
6. Mommersteeg TJ, Blankevoort L, Kooloos JG, Hendriks JC, Kauer JM, Huiskes R. Nonuniform distribution of collagen density in human knee ligaments. J Orthop Res. 1994;12(2):238–45.
7. Woo SL-Y, Hollis JM, Adams DJ, Lyon RM, Takai S. Tensile properties of the human femur-anterior cruciate ligament-tibia complex. The effects of specimen age and orientation. Am J Sports Med. 1991;19(3):217–25.
8. Pioletti DP, Rakotomanana LR, Leyvraz PF. Strain rate effect on the mechanical behavior of the anterior cruciate ligament-bone complex. Med Eng Phys. 1999;21(2):95–100.
9. Edwards JH, Ingham E, Herbert A. Decellularisation affects the strain rate dependent and dynamic mechanical properties of a xenogeneic tendon intended for anterior cruciate ligament replacement. J Mech Behav Biomed Mater. 2019;91:18–23.
10. Souryal TO, Freeman TR. Intercondylar notch size and anterior cruciate ligament injuries in athletes. A prospective study. Am J Sports Med. 1993;21(4):535–9.
11. Lund-Hanssen H, Gannon J, Engebretsen L, Holen KJ, Anda S, Vatten L. Intercondylar notch width and the risk for anterior cruciate ligament rupture. A case-control study in 46 female handball players. Acta Orthop Scand. 1994;65(5):529–32.
12. Souryal TO, Moore HA, Evans JP. Bilaterality in anterior cruciate ligament injuries: associated intercondylar notch stenosis. Am J Sports Med. 1988;16(5):449–54.
13. Hashemi J, Chandrashekar N, Mansouri H, Gill B, Slauterbeck JR, Schutt RC, et al. Shallow medial tibial plateau and steep medial and lateral tibial slopes new risk factors for anterior cruciate ligament injuries. Am J Sport Med. 2010;38(1):54–62.
14. Todd MS, Lalliss S, Garcia E, DeBerardino TM, Cameron KL. The relationship between posterior tibial slope and anterior cruciate ligament injuries. Am J Sport Med. 2010;38(1):63–7.
15. Khan MS, Seon JK, Song EK. Risk factors for anterior cruciate ligament injury: assessment of tibial plateau anatomic variables on conventional MRI using a new combined method. Int Orthop. 2011;35(8):1251–6.
16. Renstrom P, Ljungqvist A, Arendt E, Beynnon B, Fukubayashi T, Garrett W, et al. Non-contact ACL injuries in female athletes: an International Olympic Committee current concepts statement. Br J Sport Med. 2008;42(6):394–412.
17. Orchard J, Seward H, McGivern J, Hood S. Rainfall, evaporation and the risk of non-contact anterior cruciate ligament injury in the Australian Football League. Med J Aust. 1999;170(7):304–6.
18. Olsen OE, Myklebust G, Engebretsen L, Holme I, Bahr R. Relationship between floor type and risk of ACL injury in team handball. Scand J Med Sci Sports. 2003;13(5):299–304.
19. Orchard JW, Powell JW. Risk of knee and ankle: sprains under various weather conditions in american football. Med Sci Sports Exerc. 2003;35(7):1118–23.
20. Orchard JW, Chivers I, Aldous D, Bennell K, Seward H. Rye grass is associated with fewer non-contact anterior cruciate ligament injuries than Bermuda grass. Br J Sport Med. 2005;39(10):704–9.
21. Lambson RB, Barnhill BS, Higgins RW. Football cleat design and its effect on anterior cruciate ligament injuries. A three-year prospective study. Am J Sports Med. 1996;24(2):155–9.
22. Woo SL-Y, Debski RE, Zeminski J, Abramowitch SD, Saw SS, Fenwick JA. Injury and repair of ligaments and tendons. Annu Rev Biomed Eng. 2000;2:83–118.

Chapter 4
Hand and Wrist Biomechanics

Steven Regal, Steven Maschke, and Zong-Ming Li

Abstract The biomechanical function of the human hand and wrist is closely related to the intricacy of its anatomy. The arrangement of the bones, ligament, and muscles in the hand allows a complex array of tasks to be performed. This chapter provides a brief review of the anatomy of the hand and wrist, normal biomechanical function, and examples of pathomechanics.

Keywords Hand · Wrist · Biomechanics · Pathomechanics

The human hand and wrist are a set of complex anatomic tools that forms a tactile connection to the world. The intricacies of hand and wrist anatomy permit a multitude of different functions including the ability to grip an object, let go, flex and extend and to allow the precise movements required for writing, playing sport, and innumerable other actions. This chapter will briefly review some skeletal and ligamentous anatomy of the hand and wrist and then describe the complex biomechanics of the muscles, ligaments, and joints. Lastly, a few examples of pathomechanics are provided, including arthritic condition of the first carpometacarpal joint, distal radius fracture, and carpal tunnel syndrome.

S. Regal · S. Maschke
Department of Orthopedic Surgery, Cleveland Clinic, Cleveland, OH, USA
e-mail: regals@ccf.org; maschks@ccf.org

Z.-M. Li (✉)
Department of Orthopedic Surgery, Cleveland Clinic, Cleveland, OH, USA

Department of Biomedical Engineering, Cleveland Clinic, Cleveland, OH, USA

Department of Physical Medicine and Rehabilitation, Cleveland Clinic, Cleveland, OH, USA
e-mail: liz4@ccf.org

C.-K. Cheng, S. L-Y. Woo (eds.), *Frontiers in Orthopaedic Biomechanics*,
https://doi.org/10.1007/978-981-15-3159-0_4

1 Skeletal and Ligamentous Anatomy

The human hand comprises 27 bones (14 phalanges, 5 metacarpals, and 8 carpal bones) that form the distal portion of the wrist joint. The "wrist joint," or more accurately "wrist joint complex," contains numerous articulations linking the distal forearm to the hand and consists of the distal radius and ulna articulating with the multi-articular carpal bones which then articulate with the metacarpals. The carpal bones have been classically divided into proximal and distal rows based upon their kinematic behavior during wrist motion. The distal row contains the trapezium, trapezoid, capitate, and hamate which are tightly bound to each other by stout intercarpal ligaments that allow minimal motion. The scaphoid, lunate, triquetrum, and pisiform form the proximal carpal row and is described as an intercalated segment because no tendons insert on them and their motion is dependent on mechanical forces from their adjacent articulations [1, 2].

Taleisnik [3] divided the carpal ligaments into intrinsic and extrinsic groups determined by the anatomical origination and insertion of the ligament. The extrinsic ligaments of the wrist bridge the carpal bones to the radius, ulna, or metacarpals. The dorsal extrinsic ligaments consist of the dorsal radiocarpal (radiotriquetral) ligament and the dorsal intercarpal ligament that form a sideways V. Both ligaments have attachments to the lunate and are important secondary stabilizers of the scapholunate joint [1]. The palmar extrinsic ligaments of the wrist have been shown to provide the most restraint in dorsal/palmar translation of the carpus and include the radioscaphoid-capitate, long radiolunate, short radiolunate, ulnotriquetral, ulnolunate, and ulnocapitate ligaments [4]. The space of Poirier is an area of capsular weakness that is clinically important in dislocations about the lunate and is located between the radioscaphocapitate and long radiolunate ligaments (Fig. 4.1). The radioscapholunate ligament is not a true ligament but is a vascular conduit to the lunate [5, 6].

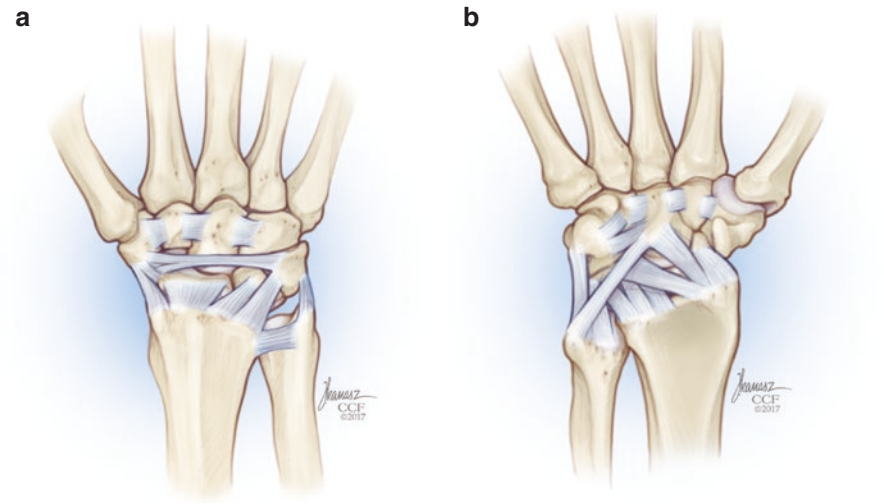

Fig. 4.1 (**a**, **b**) Wrist dorsal

There are nine intrinsic ligaments of the wrist that originate and insert on adjacent carpal bones. The two most important intrinsic ligaments are the scapholunate and lunotriquetral ligaments which can be divided into dorsal, proximal, and palmar parts. The thickest and strongest part of the scapholunate ligament is the dorsal portion whereas the thickest and strongest part of the lunotriquetral ligament is located palmarly.

2 Biomechanics

The hand and wrist contain four different types of synovial joints—plane, pivot, ellipsoidal, and saddle. Plane joints allow simple gliding motion between flat articular surfaces such as in the intercarpal, intermetacarpal, and carpometacarpal joints of the second to fourth digits. The interphalangeal joints of the digits are hinge joints and only allow motion to occur in one plane 90° to the bones to permit flexion and extension. An ellipsoidal joint formed by oval-shaped condyle and ellipsoidal cavity allows motion in two planes, flexion/extension and abduction/adduction secondary to their reciprocal concave/convex articular surfaces like those found in the radiocarpal and metacarpophalangeal joints. A saddle joint is formed by bones with concave and convex articular surfaces and only occurs in the carpometacarpal joint of the thumb, allowing motion in flexion/extension, abduction/adduction, and circumduction [7].

2.1 Wrist Motion

Normal wrist range of motion in the sagittal plan is about 65° of flexion and 55° of extension while in the coronal plane there is 15° of radial deviation and 35° of ulnar deviation. Research on the specifics of carpal motion and wrist kinematics date back to the nineteenth century and several theories have been proposed. The eight carpal bones of the wrist are commonly described as containing a proximal and distal row; however, when discussing carpal kinematics, it is much more complex. Navarro described the columnar theory in 1921 dividing the wrist into three columns. The lateral column contained the scaphoid, trapezium, and trapezoid; the central column contained the lunate, capitate, and hamate; and the medial column contained the triquetrum and pisiform [8]. Taleisnik later modified this theory in 1976 and stated only the scaphoid was in the lateral column while the central column now consisted of the trapezium, trapezoid, lunate, capitate, and hamate. In both theories, the central column moved concurrently during flexion/extension and the medial and lateral columns rotated around the central column in radial/ulnar deviation [3]. Years later, Craigen and Stanley proposed that carpal motion is complex and variable and can be accounted for by both the row and columnar theories [9].

The proximal carpal row has no direct tendon attachment and moves passively when muscle contraction initiates movement at the distal carpal row. In normal wrists, there is very little motion between the bones in the distal carpal row which essentially moves as one functional unit. During wrist flexion, the distal carpal row synchronously flexes accompanied by a small amount of ulnar deviation. Conversely, during wrist extension the distal row rotates into extension and radial deviation. During radioulnar deviation, the proximal carpal row moves from a flexed position in radial deviation to an extended position in ulnar deviation. More recently, studies of carpal motion have been performed in vivo with computed tomography and magnetic resonance imaging. Moojen et al. [10] quantified in vivo carpal kinematics and compared their results to in vitro studies. Their in vivo results were consistent with prior studies in that that the majority of wrist flexion and extension occur at the radiocarpal joint. Their results showed that in 60° of wrist flexion and extension, the scaphoid contributes to 62% and 87% of the in-plane motion, respectively, while the lunate contributes 31% and 66%. Kaufmann et al. [11] showed that the midcarpal joint is responsible for 86% of radial deviation and 66% of ulnar deviation. In radioulnar deviation, the scaphoid flexes and extends, respectively, while in wrist flexion/extension the scaphoid moves in the same plane of motion. A combination of these motions, radiodorsal/ulnopalmar, has been described as the dart thrower's motion and has been portrayed as the most frequently used motion during activities of daily living [12–14]. A three-dimensional motion analysis of the carpal bones during the dart thrower's motion found that the majority of the motion occurs at the midcarpal joint and that there is minimal motion between the scaphoid and lunate [13, 15, 16].

2.2 Muscular Biomechanics

Hand and wrist motion is multifaceted and relies not only on the bony articulations but also on a dynamic balance of muscular forces. The hand is merely a functional puppet that follows the brain's desire to perform a specific task; the brain sends signals to the hand via nerves and activates precise muscles to contract or relax with instantaneous sensory feedback from visual cues and sensory receptors. This complex, coordinated interaction happens constantly at a subconscious level. Anatomically and functionally, the wrist is powered by 3 extensors and 3 flexor muscles while the hand is powered by 9 extrinsic muscles and 17 intrinsic muscles (Table 4.1). The amount of force a muscle can produce is somewhat proportional to its cross-sectional area and the mechanical effect on a joint is determined by its insertion and origin; the flexors insert on the volar aspect of the bone while the extensors insert dorsally. The muscles of the hand and wrist are in constant harmonious balance of synergism and antagonism. When the wrist is passively extended, the finger flexor muscles are lengthened and involuntarily finger flexion occurs. In contrast, passive wrist flexion causes reciprocal finger extension. The combination of these motions has been termed "the tenodesis effect" and is a clinically useful

Table 4.1 Muscles of the wrist

Muscle	Action
Muscles of the wrist	
Wrist flexors	
Flexor carpi radialis	Flexion of wrist, radial deviation
Flexor carpi ulnaris	Flexion of wrist, ulnar deviation
Palmaris longus	Flexion of wrist
Wrist extensors	
Extensor carpi radialis longus and brevis	Extension of wrist, radial deviation
Extensor carpi ulnaris	Flexion of wrist, ulnar deviation
Muscles of the hand	
Extrinsic muscles	
Hand flexors	
Flexor pollicis longus	Flexion of MCP and IP joints of thumb
Flexor digitorum profundus	Flexion of MCP, PIP, and DIP joints
Flexor digitorum superficialis	Flexion of MCP and PIP joints
Hand extensors	
Extensor pollicis longus	Extension of MCP and IP joint of thumb
Extensor pollicis brevis	Extension of MCP joint of thumb
Abductor pollicis longus	Abduction of thumb
Extensor indicis proprius	Extension of index finger
Extensor digitorum communis	Extension of fingers
Extensor digiti quinti	Extension of small finger
Intrinsic muscles	
Dorsal interossei (4)	Abduction of fingers
Palmar interossei (3)	Adduction of fingers
Lumbricals (4)	Flexion of MCP joint and extension of PIP and DIP joints
Abductor pollicis brevis	Abduction of thumb
Flexor pollicis brevis	Flexion of thumb
Opponens pollicis	Flexion and abduction of thumb
Abductor digiti quinti	Abduction of small finger
Flexor digiti quinti	Flexion of small finger
Adductor pollicis	Adduction of thumb

exam technique when evaluating flexor tendon injuries [17]. Furthermore, position of the wrist affects the amount of peak force that can be generated by the flexor tendons [18, 19]. Using electromyography, Volz et al. [20] found that the greatest grip strength was with the wrist in 20° of extension and weakest in 40° of flexion. Hazelton et al. [18] found the highest force production at the interphalangeal joints were greatest with the wrist in ulnar deviation, followed by extension and weakest with wrist in flexion. Muscular action and joint forces will be further discussed during the description of specific joints of the hand and wrist.

2.3 Carpometacarpal Joints

There are five carpometacarpal (CMC) joints in the hand that consist of articulations between the distal carpal row and the bases of the metacarpals. While there are similarities between the joints of the thumb and the joints of the fingers, the thumb is discussed separately for its function and motion differ significantly. The second through fourth CMC joints are synovial joints with motion in one plane, flexion and extension, while the fifth CMC joint is a saddle-like joint with 2 degrees of freedom; flexion-extension and abduction-adduction. The second and third CMC joint are immobile while the fifth CMC joint can move as much as 20° due to the bony configuration of the base of the fifth metacarpal and hamate. The immobility of the second and third CMC joint is a functional adaptation that facilitates the function of the wrist extensors and radial wrist flexor (extensor carpi radialis longus and brevis, flexor carpi radialis). These muscles insert on the bases of the second and third metacarpals and with their rigid attachment to the carpals, the lever arm of the muscle is increased.

A critical function of the CMC joints of the hand is its contribution to the palmar arches. The hand consists of a longitudinal and two transverse arches that are essential in power grip and pinch as well as the ability to cup and flatten the hand (Fig. 4.2). The intermetacarpal and the deep transverse metacarpal ligaments of the proximal and distal portions of the metacarpal, respectively, are necessary to maintain these arches [21, 22]. The longitudinal arch is fixed due to the immobility of the second and third CMC joints while the transverse arches facilitate conforming the hand to the shape of an object being held. The proximal transverse arch is maintained by the shape of the carpal bones as well as their encompassing ligaments, the flexor retinaculum (or transverse carpal ligament) and the transverse intercarpal ligaments. The bony carpal arch and the flexor retinaculum comprise what is known as the carpal tunnel. The carpal tunnel not only allows the palm to increase its contact area with objects, it also protects the finger flexors and median nerve. When the flexor retinaculum is incised during a carpal tunnel release, there is widening of the arch but overall transverse stability is maintained due to the intact transverse intercarpal ligaments [23].

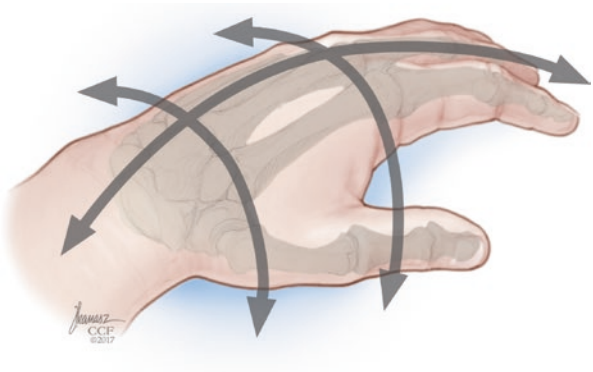

Fig. 4.2 Arches

2.4 CMC Joint of the Thumb

The first CMC joint is an articulation between the trapezium and the first metacarpal and has been described as a saddle joint that is concave in the sagittal plane and convex in the coronal plane (Fig. 4.3). This unique joint allows flexion-extension, abduction-adduction, and pronation-supination with the net effect of these motions allowing circumduction or opposition-reposition. Though there is motion in three anatomic planes, the first CMC joint is commonly considered to have 2 degrees of freedom. The flexion-extension axis is through the trapezium and the abduction-adduction axis run through the metacarpal base; both are constant through a range of motion. Because these axes are not perpendicular to each other, for any position of flexion-extension/abduction-adduction, a set degree of pronation-supination occurs [24, 25]. The bony configuration of the thumb allows for increased range of motion required for opposition. Opposition is the sequential movements of abduction, flexion, and adduction of the first metacarpal with concurrent rotation. This compound movement brings the thumb out of the palm and rotates the metacarpal to put the thumb into a position to grip an object together with a finger.

Stability of the first CMC joint is provided by seven ligaments, the dorsoradial ligament, the posterior oblique ligament, the superficial and deep palmar oblique ligament, the ulnar collateral ligament, the volar and dorsal first metacarpal ulnar base–second metacarpal radial base intermetacarpal ligaments. The palmar oblique ligament, also referred to as the beak ligament, originates on the palmar tubercle of the trapezium and inserts on the ulnar side of the metacarpal base. As a result of its intracapsular location, it plays a major role in CMC stabilization and resists

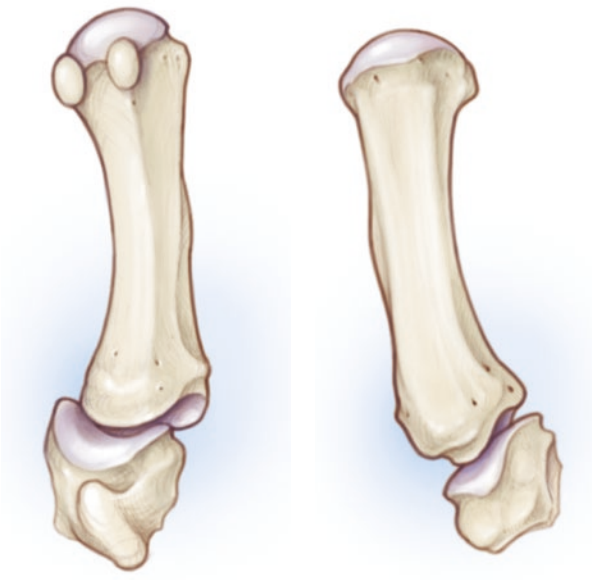

Fig. 4.3 (**a**, **b**) Metatarsal joint

abduction, extension, and pronation forces. Progressive degeneration of the palmar oblique ligament has been shown to correlate with the stages of osteoarthritis. The dorsoradial ligament is the thickest and strongest ligament of the CMC joint and is the primary restraint to dorsal dislocation [26]. Dynamic stability is provided by three thenar muscles (abductor pollicis brevis, flexor pollicis brevis, and opponens pollicis) and six extrinsic muscles (flexor pollicis longus, adductor pollicis, abductor pollicis longus, extensor pollicis brevis, extensor pollicis longus, and the first dorsal interosseous muscle). The thenar muscles are active in grasping activities while the extrinsic muscles function mainly to return the thumb to extension from its position in the palm.

2.5 Metacarpophalangeal Joints

The metacarpophalangeal (MCP) joints have a convex, asymmetric metacarpal head proximally and a concave proximal phalanx distally. This joint has 3 degrees of freedom, flexion-extension, abduction-adduction, and slight pronation-supination. The normal range of motion of the MCP joint is 0–90° of flexion, though some individuals may have up to 20° of hyperextension. Though the bony joint is incongruent, it achieves stability with its fibrous capsule, thick volar plate, and collateral ligaments. The radial and ulnar collateral ligaments are dorsal to the center of rotation of the MCP joint and are lax in extension. The volar surface of the metacarpal head is longer and broader than its dorsal surface, so when the joint is flexed, a cam effect occurs and the collateral ligaments becomes taut (Fig. 4.4). Movement of the MCP joint is indirectly through the extrinsic finger flexors and extensors (flexor digitorum superficialis/profundus, extensor digitorum indicis/proprius/quinti) as well directly by the intrinsic muscles. The sagittal bands, retinacular tissue that surround the metacarpal head, stabilize the extensor mechanism centrally over the digit and extend the MCP joint with its insertion onto the volar plate. The lumbricals and interossei provide MCP flexion, abduction, and adduction through their insertions into the extensor hood and proximal phalanx [27] (Fig. 4.5).

2.6 Proximal and Distal Interphalangeal Joints

The interphalangeal joints of the hand are ginglymus, or hinge joints, comprised of two phalanges with congruous articular surfaces that allow up to 10° of hyperextension and 100° of flexion [28]. The interphalangeal joints achieve stability from the bony architecture as well as from the volar plate and collateral ligaments. On the proximal interphalangeal joint, the proper collateral ligament (PCL) originates from the proximal and dorsal sides of the proximal phalanx and inserts via Sharpey's fibers on the middle phalanx. The fibers at the origin are parallel to the phalanx and the insertional fibers are more oblique, giving the ligament a fan-shaped appearance.

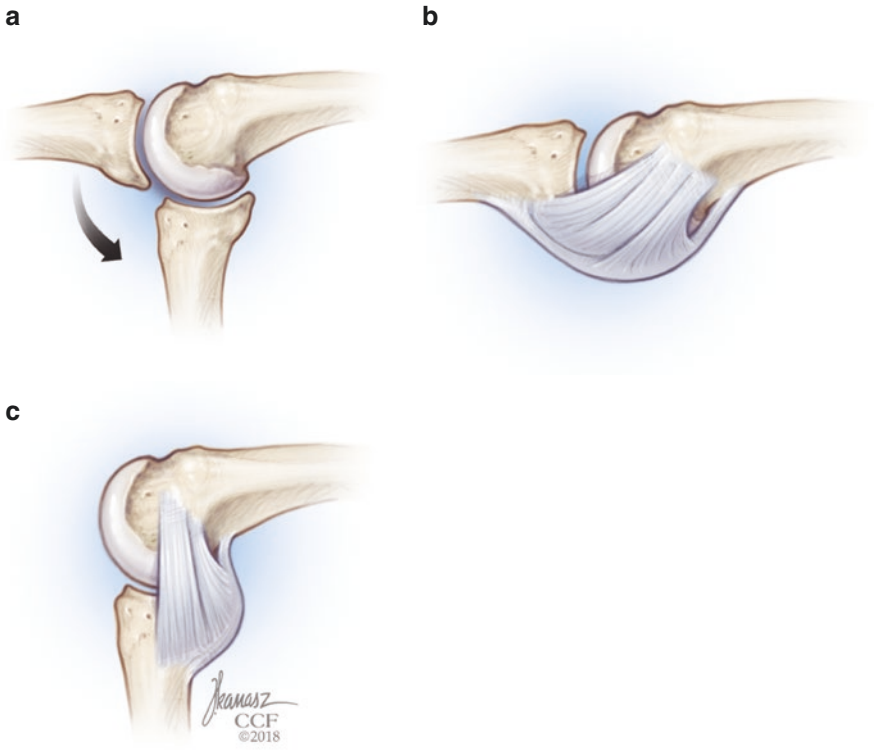

Fig. 4.4 (**a**–**c**) Volar plate

Fig. 4.5 (**a**, **b**) Tendon

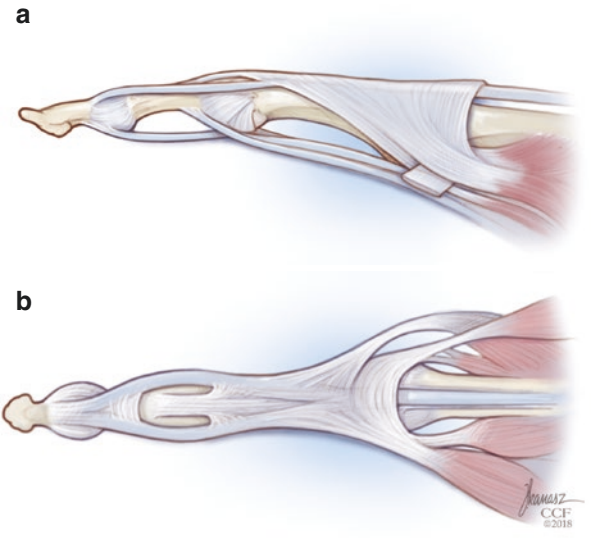

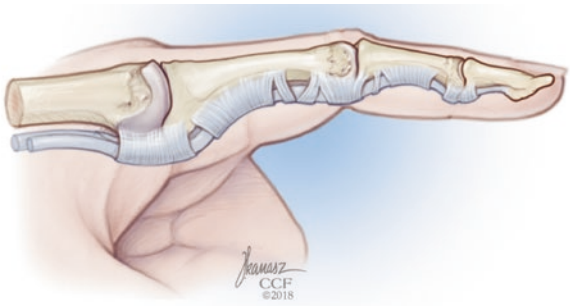

Fig. 4.6 Pulleys

The accessory collateral ligament (ACL) originates on the volar portion of the PCL and inserts distally on dorsolateral side of the volar plate on the middle phalanx [29]. A recent three-dimensional computed tomography study of the proximal interphalangeal joint found that the dorsal portion of the PCL increased in length as the joint went from 0° to 90° of flexion and was the most stabilizing structure while the joint was in flexion. The volar portion of the PCL and distal portion of the ACL provided joint stability while in extension [30].

Motion of the fingers is a dynamic balance between the extrinsic and intrinsic muscles of the hand. The extrinsic muscles, those that originate proximal to the hand, include the flexor digitorum profundus, flexor digitorum superficialis, extensor digitorum communis, extensor indices proprius, and extensor digitorum minimi. The lumbricals and interossei comprise the intrinsic muscles. The flexor tendons are held closely to the volar surface of the phalanges by five annular pulleys and three cruciate pulleys. Not only are these pulleys biomechanically critical to prevent bowstringing, they transmit force during finger flexion. The flexor digitorum profundus inserts on the proximal portion of the distal phalanx; when the muscle belly contracts, force is emitted along the tendon and flexion at the distal interphalangeal joint follows. Flexion at the joint creates an angled pathway for the profundus tendon as it exits the A4 pulley which transmits force to the middle phalanx and resultant flexion of the proximal interphalangeal joint. The profundus tendon creates a similar force as it exits the A2 pulley and causes a flexion moment at the metacarpophalangeal joint [7] (Fig. 4.6).

3 Pathological Biomechanics

A thorough understanding of normal hand and wrist biomechanics is helpful in studying disease etiology and treatment. With daily activities, the hand and wrist are put through an enumerable amount of complex and coordinated movements that place mechanical loads on the surrounding muscles, ligaments, and joints. With injury or overuse, the mechanical loads may be altered and lead to degeneration or

instability. Pathologic motion ensues which often leads to disability and pain. With knowledge of normal biomechanics, treatment can be made to manipulate the mechanical environment or recreate it.

3.1 Arthritis of the Thumb CMC Joint

The thumb CMC joint is the second most common site for osteoarthritis (OA) in the hand and is the most common joint in the upper extremity to undergo surgical reconstruction for OA. Arthritis of the thumb CMC joint, also known as basal joint arthritis or trapeziometacarpal arthritis, can be a debilitating disorder that results in pain, decreased motion, and reduced strength. Basal joint arthritis affects 1 in 4 women and 1 in 12 men; such a gender factor is thought to be related to ligament hypermobility secondary to hormonal differences or possibly to subtle differences in trapezium morphology [26]. The etiology of basal joint arthritis is multifactorial but it is widely believed to involve the loss of the integrity of the palmar oblique ligament for multiple cadaveric studies have shown a direct correlation between the stages of OA and integrity of the ligament [31]. As attenuation or hyperlaxity of the ligament ensues, increased shear forces are placed on the joint leading to inflammation (synovitis) and degeneration. With progressive disease, the thumb becomes adducted and subsequently often be dorsoradially subluxated due to the distal pull of the adductor pollicus muscle. With the thumb adducted, the hand is at a mechanical disadvantage to grip objects and will often pathologically compensate with fixed metacarpophalangeal hyperextension, the so-called "Z-deformity" (Fig. 4.7) [32]. Patients with basal joint arthritis often experience pain, at times severe, and difficulty performing daily activities such as hand writing or opening jars. Commonly, patients complain of functional limitations secondarily to decreased strength and motion. A recent three-dimensional motion analysis found that patients with OA at the thumb CMC joint had a 50.6% decrease in the circumduction envelope compared to those without arthritis [33].

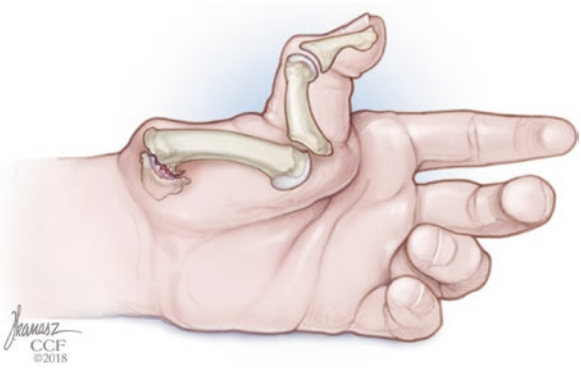

Fig. 4.7 Z deformity

Nonsurgical treatment for OA of the thumb CMC joint include activity modification, nonsteroidal anti-inflammatories, splinting, and corticosteroid injections. Surgical options include trapeziectomy with/without volar ligament reconstruction and with/without tendon interposition, metacarpal extension osteotomy, arthroscopy, resection arthroplasty, implant arthroplasty, and arthrodesis (bone fusion). The surgical procedure is chosen by extent of disease, age and activity level of patient, and surgeon preference. For early disease, ligament reconstruction and metacarpal extension osteotomy are common procedures. Ligament reconstruction is frequently performed with a strip of the flexor carpi radialis passed through a drill hole in the first metacarpal and sutured to itself, recreating the volar oblique and dorsoradial ligaments. Koff et al. [34] performed a cadaveric biomechanical study that found ligament reconstruction to reduce laxity in the dorsovolar, radioulnar, and pronosupination directions. Limited evidence is available for metacarpal extension osteotomy but the biomechanical rationale of its clinical success is shifting the joint contact forces to non-arthritic cartilage and reducing joint laxity [35].

Trapeziectomy with/without volar ligament reconstruction and with/without tendon interposition, arthroplasty, and arthrodesis are common surgical options for more severe disease. All options provide pain relief and improve function though their biomechanical implications are varied. The native 2 degrees of freedom (DoF) the trapeziometacarapal joint has is altered with surgical reconstruction. When arthrodesis is performed, the joint has 0 DoF in contrast to arthroplasty procedures such as ligament reconstruction tendon interposition (LRTI) and ball and socket implant have 3 DoF. The change in DoF impacts the joint reaction forces at this CMC joint. Comparing the above procedures in a biomechanical study, the arthroplasty group (3 DoF) had 12 times the joint reaction force than the native joint while the fusion group (0 DoF) showed the lowest amount of joint forces [24]. Another biomechanical study found that LRTI had kinematics similar to a native joint though the pivot point and center of rotation were different. This same study found that the ball and socket arthroplasty has a fixed axis of rotation which could possibly lead to a higher rate of wear and loosening [36]. Though the treatment of basal joint arthritis is varied, surgical reconstruction improves pain, increases function, and reliably produces good to excellent outcomes in 90–95% of cases [32].

3.2 Distal Radius Fracture Malunion

Distal radius fractures account for one-sixth of all emergency visits and up to 46% of all skeletal fractures seen in a primary care setting. One of the most common complications after a distal radius fracture is malunion, as high as 24% in those treated in a cast [37]. A malunion is when a fractured bone heals in an abnormal position. Numerous studies have evaluated the biomechanical effects and load mechanics of radial shortening, loss of radial inclination and abnormal volar or dorsal angulation. In the non-fractured distal radius with neutral ulnar variance,

79% of the mechanical load of the wrist joint is through the radius and 21% is transmitted across the ulna [38]. Wrists with 2 mm or more of ulnar plus variance showed 69% of the transmitted load through the radius and 31% of the load through the ulna [37]. Pogue et al. [39] showed that greater than 2 mm of radial shortening resulted in a significant increase in lunate contact area, and at 6–8 mm of radial shortening, the ulna was noted to impinge on the triquetrum and/or the ulnar aspect of the lunate. Palmer and Werner [38] found a 25% increase in load to the ulna with a positive 1 mm change to the ulnar variance.

Malalignment of distal radius fracture in the sagittal plane cause abnormal wrist biomechanics and decreased functional results in patients [39, 40]. Fernandez [40] reported that distal radius fracture malunions with greater than 25° dorsal angulation were more likely to be symptomatic and the scaphoid/lunate fossa had increased loads and more dorsal contact areas compared to the normal wrist. As the distal radius articular surface moves from its native 10° volar tilt to 45° of dorsal angulation, load through the ulna increases from 21% to 67% of the total load. Additionally, it has been reported that malunited distal radius fractures may cause dynamic midcarpal instability, increased strain on the triangular fibrocartilage, decreased grip strength, and median nerve neuropathy [41].

Treatment of distal radius malunions should be reserved for only those who are symptomatic rather than just treating radiographic findings. Surgical options include corrective osteotomy, wrist denervation, and wrist fusion. In a study with 195 corrective osteotomies for dorsal malunion of the distal radius, the flexion-extension arc improved by 49° and there was an increase in prono-supination and increase in grip strength from 29 to 40 kg [41].

3.3 Carpal Tunnel Syndrome

Carpal tunnel syndrome (CTS) is the most common compressive neuropathy of the upper extremity with a prevalence of 2.6–5.8% in the general adult population. There are more than 500,000 surgical procedures performed each year in the United States with an economic impact exceeding 2 billion dollars. The carpal tunnel is formed by the carpal bones dorsally and the transverse carpal ligament (TCL) volarly, with nine flexor tendons and the median nerve passing through the tunnel. The median nerve is vulnerable to compression due to the unyielding borders of the tunnel; when the median nerve experiences compression, its blood flow is reduced and symptoms of pain and paresthesias ensue in the median nerve distribution. Most cases of CTS are idiopathic or unknown; however some cases have been attributed to trauma, fluid overload states (pregnancy, renal disease, congestive heart failure), and space occupying lesions in the carpal tunnel (ganglion cyst, anomalous tendon, lipoma), all with the common pathway of compression on the median nerve [42].

Surgical release of the TCL is the standard treatment of choice for CTS when nonoperative measures fail. When the TCL is released open or endoscopically, there are many known and even more unknown biomechanical consequences. In an endo-

scopic carpal tunnel release, the incision is performed from within the carpal tunnel and only the TCL is incised, whereas in an open release, the skin, fat, and superficial fascial layer are incised. The intact TCL helps maintain the concavity of the carpal arch and acts as a pulley for the flexor tendons of the hand. After surgical release of the TCL, the volume of the carpal tunnel is increased, thus decreasing the compression on the median nerve. Magnetic resonance imaging (MRI) studies have shown the contents of the carpal tunnel to be displaced volarly after carpal tunnel release (CTR). With anterior displacement of the flexor tendons, their moment arm is effectively increased which theoretically may result in decreased grip strength. Several in vitro biomechanical studies found that flexor tendon excursion was significantly increased, as much as 26%, after CTR [43, 44]. Some surgeons lengthen and reconstruct the TCL after a CTR; small clinical studies have shown less volar displacement of carpal tunnel contents as well as earlier improved grip and pinch strength compared to CTR without reconstruction. These results are perceived to be caused by the mechanical advantage of the restoring the flexor pulley [45, 46].

Carpal arch flattening and widening of the carpal bones is another known consequence of CTR, though not all authors agree on the extent of widening or its clinical effects. Kwon et al. [47] compared carpal arch widths with radiographs before and 6 months after open CTR and found the carpal arch widened on average 1.8 mm after surgery while previous MRI studies found as much as 2.7 mm of carpal arch widening after release of the TCL. In a finite element study, Guo et al. [48] reported after TCL release and an axial load was placed, all carpal bones became more radially deviated and the contact forces at the midcarpal joint were altered, and yet long-term biomechanics and its clinical effects of dividing the TCL remain unclear. Recently, Li and colleagues proposed a nonsurgical treatment of carpal tunnel syndrome by biomechanically manipulating the carpal arch width as a means to expand carpal tunnel area and decompress the median nerve [49–51].

References

1. Kijima Y, Viegas SF. Wrist anatomy and biomechanics. J Hand Surg Am. 2009;34(8):1555–63.
2. Kuo CE, Wolfe SW. Scapholunate instability: current concepts in diagnosis and management. J Hand Surg Am. 2008;33(6):998–1013.
3. Taleisnik J. The ligaments of the wrist. J Hand Surg Am. 1976;1(2):110–8.
4. Katz DA, Green JK, Werner FW, Loftus JB. Capsuloligamentous restraints to dorsal and palmar carpal translation. J Hand Surg Am. 2003;28(4):610–3.
5. Berger RA. The ligaments of the wrist. A current overview of anatomy with considerations of their potential functions. Hand Clin. 1997;13(1):63–82.
6. Lamas C, Carrera A, Proubasta I, Llusa M, Majo J, Mir X. The anatomy and vascularity of the lunate: considerations applied to Kienbock's disease. Chir Main. 2007;26(1):13–20.
7. Gonzalez MH, Mohan V, Elhassan B, Amirouche F. Biomechanics of the digit. J Am Soc Surg Hand. 2005;5(1):48–60.
8. Navarro A. Luxaciones del carpo. Anales de la Facultad de Medicina. 1921;6:113–41.
9. Craigen MA, Stanley JK. Wrist kinematics. Row, column or both? J Hand Surg Br. 1995;20(2):165–70.

10. Moojen TM, Snel JG, Ritt MJ, Venema HW, Kauer JM, Bos KE. In vivo analysis of carpal kinematics and comparative review of the literature. J Hand Surg Am. 2003;28(1):81–7.
11. Kaufmann R, Pfaeffle J, Blankenhorn B, Stabile K, Robertson D, Goitz R. Kinematics of the midcarpal and radiocarpal joints in radioulnar deviation: an in vitro study. J Hand Surg Am. 2005;30(5):937–42.
12. Li ZM, Kuxhaus L, Fisk JA, Christophel TH. Coupling between wrist flexion-extension and radial-ulnar deviation. Clin Biomech. 2005;20(2):177–83.
13. Moritomo H, Apergis EP, Garcia-Elias M, Werner FW, Wolfe SW. International Federation of Societies for Surgery of the Hand 2013 Committee's report on wrist dart-throwing motion. J Hand Surg Am. 2014;39(7):1433–9.
14. Wolfe SW, Crisco JJ, Orr CM, Marzke MW. The dart-throwing motion of the wrist: is it unique to humans? J Hand Surg Am. 2006;31(9):1429–37.
15. Crisco JJ, Coburn JC, Moore DC, Akelman E, Weiss AP, Wolfe SW. In vivo radiocarpal kinematics and the dart thrower's motion. J Bone Joint Surg Am. 2005;87(12):2729–40.
16. Werner FW, Green JK, Short WH, Masaoka S. Scaphoid and lunate motion during a wrist dart throw motion. J Hand Surg Am. 2004;29(3):418–22.
17. Shah KN, Hodax JD, Katarincic JA. Evaluating a flexor tendon laceration with the tenodesis effect. J Pediatr. 2016;176:214–214.e1.
18. Hazelton FT, Smidt GL, Flatt AE, Stephens RI. The influence of wrist position on the force produced by the finger flexors. J Biomech. 1975;8(5):301–6.
19. Li ZM. The influence of wrist position on individual finger forces during forceful grip. J Hand Surg Am. 2002;27(5):886–96.
20. Volz RG, Lieb M, Benjamin J. Biomechanics of the wrist. Clin Orthop Relat Res. 1980;149:112–7.
21. Bade H, Schubert M, Koebke J. Functional morphology of the deep transverse metacarpal ligament. Ann Anat. 1994;176(5):443–50.
22. Dzwierzynski WW, Matloub HS, Yan JG, Deng S, Sanger JR, Yousif NJ. Anatomy of the intermetacarpal ligaments of the carpometacarpal joints of the fingers. J Hand Surg Am. 1997;22(5):931–4.
23. Garcia-Elias M, An KN, Cooney WP 3rd, Linscheid RL, Chao EY. Stability of the transverse carpal arch: an experimental study. J Hand Surg Am. 1989;14(2 Pt 1):277–82.
24. Domalain MF, Seitz WH, Evans PJ, Li ZM. Biomechanical effect of increasing or decreasing degrees of freedom for surgery of trapeziometacarpal joint arthritis: a simulation study. J Orthop Res. 2011;29(11):1675–81.
25. Hollister A, Buford WL, Myers LM, Giurintano DJ, Novick A. The axes of rotation of the thumb carpometacarpal joint. J Orthop Res. 1992;10(3):454–60.
26. Van Heest AE, Kallemeier P. Thumb carpal metacarpal arthritis. J Am Acad Orthop Surg. 2008;16(3):140–51.
27. Abboud JA, Beredjiklian PK, Bozentka DJ. Metacarpophalangeal joint arthroplasty in rheumatoid arthritis. J Am Acad Orthop Surg. 2003;11(3):184–91.
28. Bain GI, Polites N, Higgs BG, Heptinstall RJ, McGrath AM. The functional range of motion of the finger joints. J Hand Surg Eur Vol. 2015;40(4):406–11.
29. Allison DM. Anatomy of the collateral ligaments of the proximal interphalangeal joint. J Hand Surg Am. 2005;30(5):1026–31.
30. Chen J, Tan J, Zhang AX. In vivo length changes of the proximal interphalangeal joint proper and accessory collateral ligaments during flexion. J Hand Surg Am. 2015;40(6):1130–7.
31. Halilaj E, Rainbow MJ, Moore DC, Laidlaw DH, Weiss AP, Ladd AL, Crisco JJ. In vivo recruitment patterns in the anterior oblique and dorsoradial ligaments of the first carpometacarpal joint. J Biomech. 2015;48(10):1893–8.
32. Barron OA, Glickel SZ, Eaton RG. Basal joint arthritis of the thumb. J Am Acad Orthop Surg. 2000;8(5):314–23.
33. Gehrmann SV, Tang J, Li ZM, Goitz RJ, Windolf J, Kaufmann RA. Motion deficit of the thumb in CMC joint arthritis. J Hand Surg Am. 2010;35(9):1449–53.

34. Koff MF, Shrivastava N, Gardner TR, Rosenwasser MP, Mow VC, Strauch RJ. An in vitro analysis of ligament reconstruction or extension osteotomy on trapeziometacarpal joint stability and contact area. J Hand Surg Am. 2006;31(3):429–39.
35. Ladd AL, Crisco JJ, Hagert E, Rose J, Weiss AP. The 2014 ABJS Nicolas Andry Award: The puzzle of the thumb: mobility, stability, and demands in opposition. Clin Orthop Relat Res. 2014;472(12):3605–22.
36. Imaeda T, Cooney WP, Niebur GL, Linscheid RL, An KN. Kinematics of the trapeziometacarpal joint: a biomechanical analysis comparing tendon interposition arthroplasty and total-joint arthroplasty. J Hand Surg Am. 1996;21(4):544–53.
37. Bu J, Patterson RM, Morris R, Yang J, Viegas SF. The effect of radial shortening on wrist joint mechanics in cadaver specimens with inherent differences in ulnar variance. J Hand Surg Am. 2006;31(10):1594–600.
38. Palmer AK, Werner FW. Biomechanics of the distal radiulnar joint. Clin Orthop. 1984;187:26–35.
39. Pogue DJ, Viegas SF, Patterson RM, Peterson PD, Jenkins DK, Sweo TD, Hokanson JA. Effects of distal radius fracture malunion on wrist joint mechanics. J Hand Surg Am. 1990;15(5):721–7.
40. Fernandez DL. Correction of post-traumatic wrist deformity in adults by osteotomy, bone-grafting, and internal fixation. J Bone Joint Surg Am. 1982;64(8):1164–78.
41. Prommersberger KJ, Pillukat T, Muhldorfer M, van Schoonhoven J. Malunion of the distal radius. Arch Orthop Trauma Surg. 2012;132(5):693–702.
42. Cranford CS, Ho JY, Kalainov DM, Hartigan BJ. Carpal tunnel syndrome. J Am Acad Orthop Surg. 2007;15(9):537–48.
43. Brown RK, Peimer CA. Changes in digital flexor tendon mechanics after endoscopic and open carpal tunnel releases in cadaver wrists. J Hand Surg Am. 2000;25(1):112–9.
44. Kiritsis PG, Kline SC. Biomechanical changes after carpal tunnel release: a cadaveric model for comparing open, endoscopic, and step-cut lengthening techniques. J Hand Surg Am. 1995;20(2):173–80.
45. Netscher D, Mosharrafa A, Lee M, Polsen C, Choi H, Steadman AK, Thornby J. Transverse carpal ligament: its effect on flexor tendon excursion, morphologic changes of the carpal canal, and on pinch and grip strengths after open carpal tunnel release. Plast Reconstr Surg. 1997;100(3):636–42.
46. Seitz, WH, A. Lallb Open carpal tunnel release with median neurolysis and Z-plasty reconstruction of the transverse carpal ligament. Current Orthopaedic Practice. 2013;24(1):53–7.
47. Kwon YE, Gong HS, Shin HS, Lee HR, Kim KH, Baek GH. Evaluation of carpal arch widening and outcomes after carpal tunnel release. J Hand Surg Am. 2017;42(2):113–7.
48. Guo X, Fan Y, Li ZM. Effects of dividing the transverse carpal ligament on the mechanical behavior of the carpal bones under axial compressive load: a finite element study. Med Eng Phys. 2009;31(2):188–94.
49. Li ZM, Tang J, Chakan M, Kaz R. Carpal tunnel expansion by palmarly directed forces to the transverse carpal ligament. J Biomech Eng. 2009;131(8):081011.
50. Li ZM, Gabra JN, Marquardt TL, Kim DH. Narrowing carpal arch width to increase cross sectional area of carpal tunnel—a cadaveric study. Clin Biomech. 2013;28(4):402–7.
51. Marquardt TL, Evans PJ, Seitz WH Jr, Li ZM. Carpal arch and median nerve changes during radioulnar wrist compression in carpal tunnel syndrome patients. J Orthop Res. 2016;34(7):1234–40.

Chapter 5
Biomechanics of the Elbow

Su-Ya Lee and Fong-Chin Su

Abstract This chapter introduces the anatomy, function, and pathomechanics of the elbow. First, the bone, joints, muscles, tendons, ligaments, and joint capsules in the elbow are reviewed. The normal functions of the elbow are introduced from aspects of kinematics, kinetics and joint stability and constraint. The elbow joint configuration, joint motion, and joint force are integrated to provide joint stability. The understanding of normal elbow function provides information and applications in investigation of the pathomechanics of the elbow. The abnormal joint motion and instability including valgus instability, posterolateral rotatory instability, varus posteromedial rotatory instability, elbow dislocation, elbow fracture, and elbow joint arthritis are examined. The tendinopathy and cubital tunnel syndrome are also important to be explained from pathomechanics point of view.

Keywords Elbow · Biomechanics · Anatomy · Function · Kinematics · Kinetics Stability · Constraint · Pathomechanics

1 Anatomy

1.1 Bone and Joints in the Elbow

The elbow, a complex joint, is composed of the ulna, the radial, and the distal humerus. The elbow joint is formed by the three articulations, which include ulnohumeral, radiocapitellar, and proximal radioulnar joint in the elbow (Fig. 5.1a, b). The distal humerus has several important anatomical landmarks including trochlea, capitellum, medial epicondyle, lateral epicondyle, coronoid fossa, radial fossa, and coronoid process in the anterior view (Fig. 5.1c) and coronoid process in the posterior view. These anatomical landmarks in the distal humerus play an important role

S.-Y. Lee · F.-C. Su (✉)
Department of Biomedical Engineering, National Cheng Kung University, Tainan, Taiwan
e-mail: fcsu@mail.ncku.edu.tw

C.-K. Cheng, S. L-Y. Woo (eds.), *Frontiers in Orthopaedic Biomechanics*,
https://doi.org/10.1007/978-981-15-3159-0_5

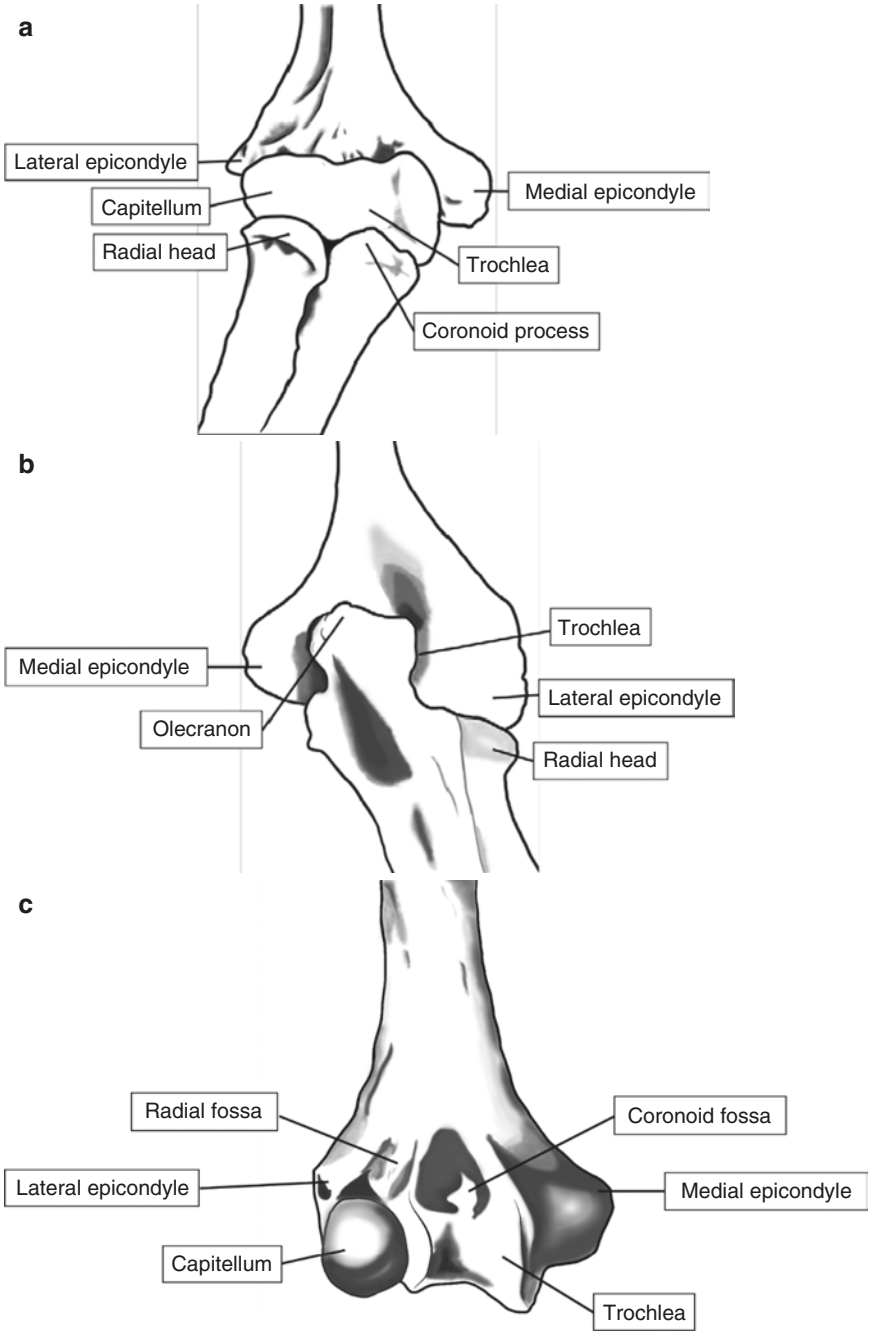

Fig. 5.1 (**a**) Anterior view of elbow joint. (**b**) Posterior view of elbow joint. (**c**) Anterior view of distal humerus

to stabilize the elbow joint during the elbow extension and flexion with a wide range of motion. The coronoid fossa and radial fossa provide the osseous stability and prevent anterior impingement during flexion of the elbow joint. The olecranon fossa also provides the osseous stability and prevent posterior impingement during extension of the elbow joint.

The ulnohumeral joint is formed by the trochlea of the humerus and olecranon of the ulna (Fig. 5.2a) to stabilize the elbow joint during extension and prevent posterior translation. The function of the ulnohumeral joint, hinge joint, is the movement of flexion and extension of the arm. The radiohumeral joint, ball-and-socket joint, is formed by the convex structure of capitellum and concave structure of the radial head (Fig. 5.2b) to stabilize the elbow joint during flexion and be a valgus stabilizer of the elbow joint. The proximal radioulnar joint is formed by the lesser sigmoid notch of ulna and the margin of the radial head. The function of the proximal radioulnar joint and the radiocapitellar joint is the movement of supination and pronation of the forearm. The radial head is covered with the large area of articular cartilage which is nearly 270–280° along the proximal radioulnar joint and the radiocapitellar joint.

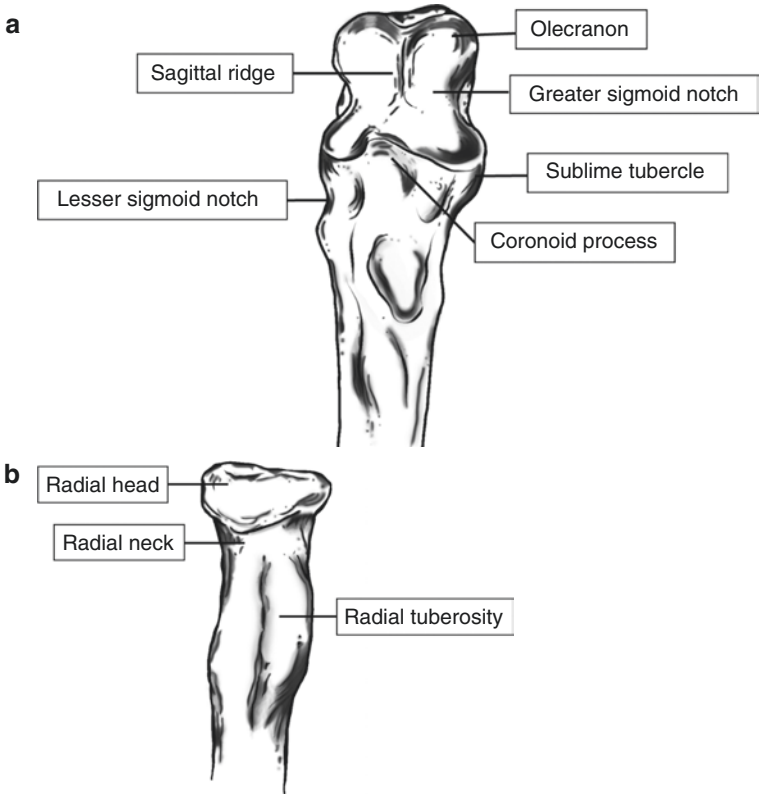

Fig. 5.2 (**a**) Anterior view of ulna. (**b**) Anterior view of radial

Carrying angle, a small degree of cubitus valgus, occurred at the forearm full extension and supination due to the noncollinearity between the long axis of ulnar and long axis of humerus. The average carrying angle is 13–16° for women and 11–14° for men. During the movement of elbow joint flexion, the carrying angle will decrease and disappear due to the colinearity between the long axis of ulnar and long axis of humerus.

1.2 Muscles, Their Innervation and Tendons

According to movement functions of muscles around the elbow, they can be classified into the elbow extensor muscles, elbow flexor muscles, wrist flexor muscles, and wrist extensor muscles. These muscles play an important role in the dynamic stabilizers to prevent the elbow subluxation and reinforce the osseous stability of the elbow. These muscles are innervated by the median nerve, radial nerve, ulnar nerve, and musculocutaneous nerve (C5–C7), respectively.

The elbow extensor muscles are triceps brachii muscles and anconeus muscle. The triceps brachii muscle is the main elbow flexor muscle and its maximal muscle is efficient when elbow is flexed at 20–30°. The anconeus muscle has an assistant elbow extensor role during the elbow extension and a major dynamic stabilizer to restrain the posterolateral and varus force on the elbow joint. The elbow flexors are brachialis, brachioradialis, biceps brachii, and pronator teres. The short head of biceps brachii is a main elbow flexor muscle and a stronger elbow flexor muscle compared to the brachialis muscle. Brachioradialis has a great mechanical advantage of any elbow flexor muscles; however, brachialis has a poor mechanical advantage as it is near the axis of rotation. The common extensor tendon, which is the origin of the wrist extensor muscles, consists of the extensor carpi radialis brevis, extensor carpi ulnaris, extensor digitorum communis, and extensor digiti minimi. The wrist flexor muscles in the medial side of elbow are flexor carpi radialis, flexor carpi ulnaris, flexor digitorum superficialis, and flexor digitorum profundus. The common extensor tendon, which is the major wrist extensor muscles, consists of the flexor carpi radialis, flexor carpi ulnaris, flexor digitorum superficialis, pronator teres, and palmaris longus. The wrist extensor muscles in the lateral side of elbow are extensor carpi radialis longus, extensor carpi radialis brevis, extensor carpi ulnaris, extensor digitorum communis, extensor digiti minimi, and anconeus. The forearm pronation muscle is pronator teres and the forearm supination muscles are supinator and long head of biceps brachii. When the arm is the extreme supination posture, brachioradialis can assist in the pronation of the forearm.

All of wrist flexor and pronator teres are innervated by the median nerve, except for the flexor carpi ulnaris and little and ring finger flexor digitorum profundus, which are innervated by the ulnar nerve (Fig. 5.3a). The elbow extensor muscles include triceps brachii in the lateral and medial heads and anconeus. All of wrist extensor muscles, brachioradialis and supinator are innervated by the radial nerve (Fig. 5.3b). Biceps brachii is innerved by the musculocutaneous nerve (C5–C7) and brachialis is innerved by the musculocutaneous nerve (C5–C6).

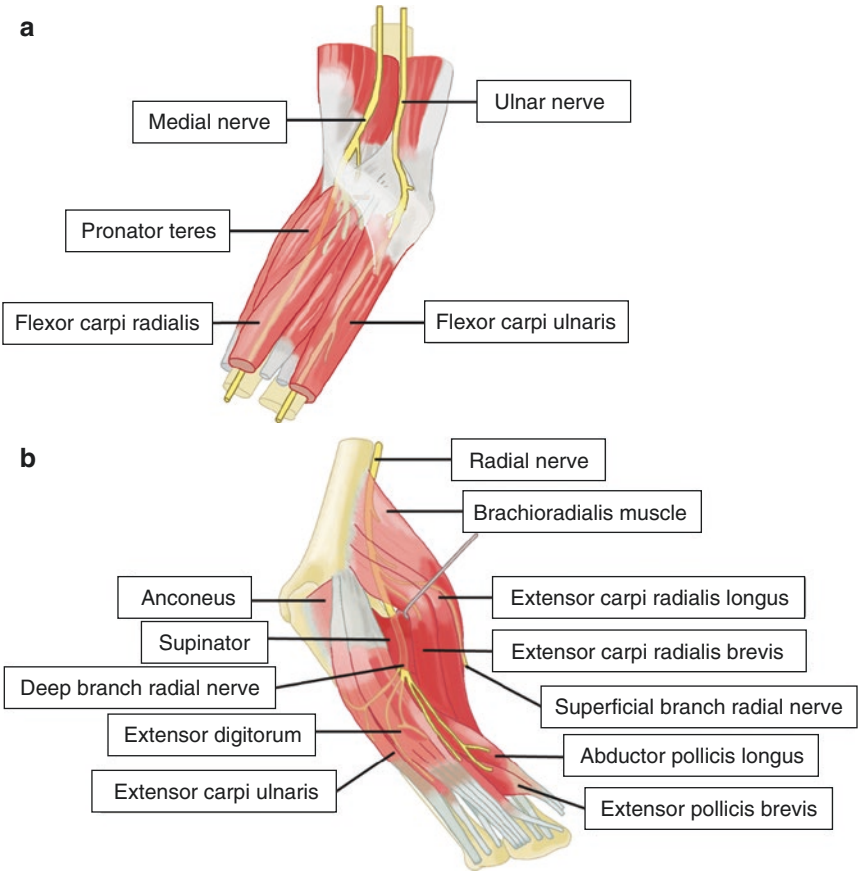

Fig. 5.3 (**a**, **b**) Motor innervation of wrist flexors

1.3 Ligaments and Joint Capsules in the Elbow

The elbow joint is enclosed by the joint capsule, which is surrounded around the olecranon, the coronoid fossa, and the radial fossa, except for the humeral epicondyle (Fig. 5.4). The joint capsule, a secondary static stabilizer, has a laxity on the anterior and posterior side of elbow joint to provide the appropriate movement of elbow joint during the flexion and extension. The brachialis muscle and triceps brachialis muscles can prevent the joint capsule to pinching in the joint and maintain the sufficient tension on the capsule during extension and flexion.

The collateral ligaments are fused with the joint capsules and can be divided into the lateral collateral ligament and medial collateral ligament. The collateral ligaments, a primary static stabilizer, cross the articular joints of elbow. The collateral ligaments have the tension to restrict the varus motion, the valgus motion, and the axial rotation motion. The function of lateral collateral ligament complex is to maintain the stability during the posterolateral force on the elbow joint and hinder

varus stress on the elbow joint. The function of medial collateral ligament is to maintain the stability during the posteromedial force on the elbow joint and hinder valgus stress on the elbow joint. The lateral collateral ligament complex is composed of lateral ulnar ligament, the radial collateral ligament, and the annular ligament (Fig. 5.5). The annular ligament, one of the lateral collateral ligament complex,

Fig. 5.4 Anterior view of the joint capsule

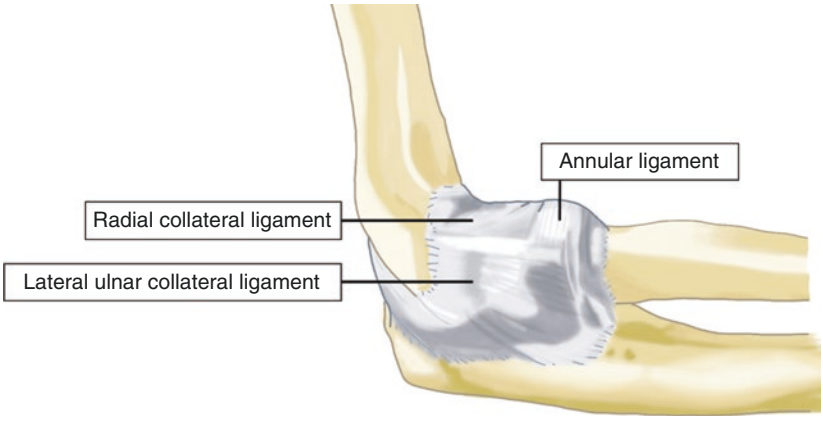

Fig. 5.5 Lateral collateral ligament complex

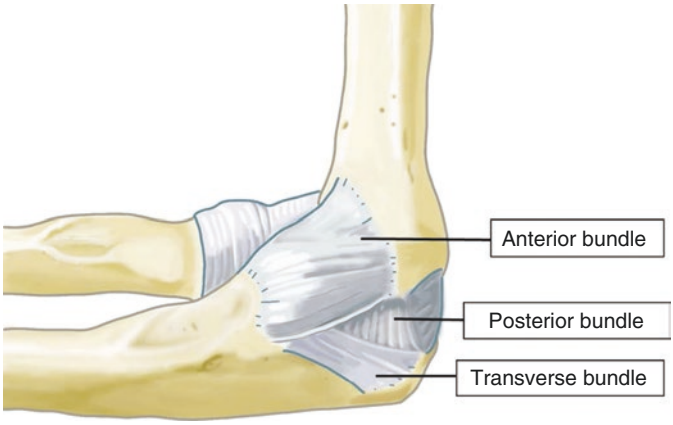

Fig. 5.6 Medial collateral ligament complex

enclosed the radial head, and the insertion/origin of the annular ligament is located at the ulna to maintain the stability of forearm rotation.

The medial collateral ligament complex is formed by the anterior bundle, posterior bundle, and transverse ligament (Cooper ligament) (Fig. 5.6). The anterior bundle of the medial collateral ligament is formed by thick parallel fibers [1], the posterior bundle of the medial collateral ligament is formed by the fan-shaped capsular fibers [2], and the transverse ligament is formed by the horizontal capsular fibers [3]. The anterior bundle of the medial collateral ligament is attached to the antero-inferior aspect of the medial epicondyle and provide the constant tension during the elbow flexion and extension. The anterior bundle can be further separated to the anterior band and posterior band. The anterior band of the anterior bundle of medial collateral ligament shows an isometric strain pattern during the elbow flexion and the posterior band of the anterior bundle of medial collateral ligament has increased its strain value with the increase of elbow flexion [4]. The difference in strain pattern between the anterior and posterior bands of the anterior bundle of the medial collateral ligament is due to the insertion point in the elbow joint [4]. The posterior bundle of the medial collateral ligament has a tension during the elbow flexion to restrain the valgus stress [5].

2 Function

2.1 Kinematics of the Elbow

The elbow joint consists of three articulations including ulnohumeral, radiocapitellar, and proximal radioulnar articulations. The ulnohumeral, principal articulation, allows the motion of flexion-extension in the nearly sagittal plane. The normal range

of motion for the elbow joint consists of 0° full extension and 146° extension. The functional range of motion for the elbow joint consists of 30° flexion and 130° extension. Recently, researchers have investigated the kinematics of elbow joint by noninvasive three-dimensional technique [6–9]. The instant screw axis of rotation of elbow flexion-extension is a changeable circular path with the elbow flexion. During the movement of elbow flexion, the path of axis of rotation showed a counterclockwise pattern and a conical shape on the lateral condyle and this path of axis of rotation crossed and converged at the medial facet of the trochlea [6]. The average axis of elbow flexion-extension is a line from the anterior aspect of the medial epicondyle to the center of trochlea and the capitellum which has 4–8° valgus relative to the long axis of the humerus. During the movement of flexion, ulna changes its position with the anterior glide, lateral shift, and varus rotation relative to the humerus [7, 8]. The ulna has the internal rotation from the full extension to 90° flexion and external rotation from the 90° flexion to the full flexion relative to the humerus [7, 8]. During the movement of extension, particularly in the last 5–10°, the ulna has the posterior glide relative to the humerus. The humerus has significant compression force on the ulna with the elbow 90° flexion because the greater sigmoid notch has a nearly posterior 30° respective to the axis of the ulna (Fig. 5.7) and the capitellum/trochlea has a near anterior 30° respective to the axis of the humerus [10, 11].

The proximal radioulnar and radiocapitellar articulations allow motion of forearm pronation and supination in the transverse plane. The normal range of motion for the forearm pronation-supination consists of 71° pronation and 81° supination. The axis of forearm rotation is a line from the center of the radial head to the distal ulna. The forearm pronation-supination plays an important role in the daily activity which required 50° pronation and 50° supination to perform the functional movement. Previous studies investigated the motion of radius and ulna during the movement of forearm pronation-supination via two-dimensional computed tomography [12] and three-dimensional computational model [9]. From supination to pronation, the radius showed a varus rotation, internal rotation, and extension relative to humerus and ulna showed a valgus rotation [9]. The center of radial head has anterior, proximal, and lateral translation with the forearm pronation. The con-

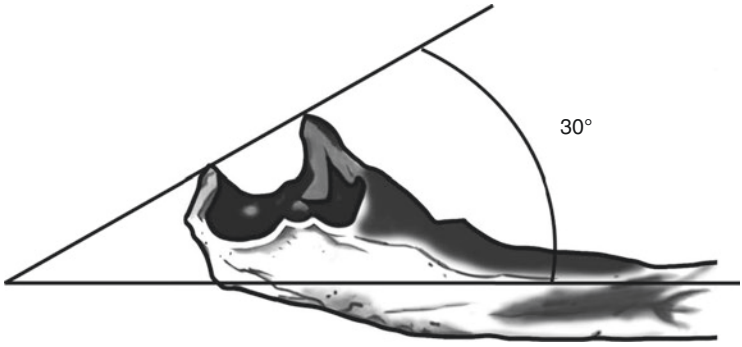

Fig. 5.7 Angle between greater sigmoid notch and axis of the ulna

tact area of radiocapitellar has a large congruency in the forearm pronation and the contact area of proximal radioulnar joint has a large congruency in the forearm supination [9].

2.2 Kinetics of the Elbow

2.2.1 Elbow Joint Forces

The elbow joint plays an important role in the daily activity of the upper extremity. Understanding the force distribution in the elbow joint is essential to design joint replacement and investigate the effect of osteotomy. With the 15° elbow flexion with full pronation and wrist extension, the axial compressive load of 100 N transmitted to the radiocapitellar joint is approximately 61% loading distribution [13]. With the increasing weight of axial loading, the axial load distribution through the radiocapitellar joint has decreased to 55% [13]. When the axial compressive load of 160 N is transmitted to the radiocapitellar, there is nearly 90 mm^2 contact area at the radiocapitellar joint at 0° of flexion [14]. The contact area at the ulnohumeral joint increased from the elbow extension to elbow flexion [15, 16]. The contact area at the radiocapitellar joint increased with the increase of angle of elbow flexion [17]. In general, the peak contact pressure of radial head does not exceed 5 MPa and the daily activities applied approximately 100 N force at the radiocapitellar articulation [18]. The contact pressure of the humeroulnar joint increased from the elbow extension to elbow flexion [15, 16].

2.2.2 Joint Reaction Forces at the Elbow

The free-body diagram is used to estimate the joint reaction force by the equilibrium equations. The equilibrium equations assume that the sum of forces and sum of moments acting on the elbow joint are zero. The calculation of elbow joint reaction force needs to consider the weight of external object, weight of forearm and arm, the distance between center of mass of forearm/arm and the center of rotation of the joint, the line of action of muscle, and the angle of forearm and arm in the free-body diagram. The biceps and brachialis muscle was considered as the primary elbow flexors and the triceps is considered as the primary elbow extensor [10, 19]. Regarding the dynamic movement that generates the acceleration in the limbs, the joint force and joint moment at the elbow can be calculated by the inverse Newton-Euler method. Recently, most of the studies investigated the joint force and moment at the elbow joint during performing the daily activities of the upper extremity [20, 21]. The block to head height generates the flexion moment and external rotation moment of the elbow joint and the elbow joint force along the humeral longitudinal axis and rotation axis that is perpendicular to the humeral longitudinal axis than other upper extremity activities [21]. The reach to head side and back are the high demand of elbow flexion, forearm pronation, elbow extension moment, and elbow internal rotation moment [21].

2.3 Stability and Constraints of the Elbow

A stable joint provides the normal functional activity of the elbow. The dynamic and static factors contribute to the joint stability by anatomy of the joint, surrounding ligament, joint capsule, and muscles. The bony geometry of elbow joint contributes much to the joint stability due to its congruous articulation. The radial head and coronoid process are the major articulation stabilizers to prevent the posterior subluxation or dislocation. A previous study showed that at least 50% coronoid height is needed to provide the stability of elbow joint under the valgus force and foramen supination [22]. The radial head is the minor articulation stabilizer relative to the coronoid process [11]. The ligament, joint capsule, and articulation form the static stabilizer of the elbow joint. The primary static stabilizer consists of ulnohumeral joint and anterior bundle of medial collateral ligament and the secondary stabilizer consists of radiocapitellar joint, common flexor tendon, common extensor tendon, and the joint capsule. The anterior joint capsule can be against the joint distraction, joint hyperextension, valgus stress, and the posterior joint capsule can against the joint hyperflexion and posterior directed force [19]. Muscles are the dynamic stabilizer across the elbow joint because muscle contraction can generate the compressive force. The elbow flexors can generate the varus moment to resist the valgus force and elbow extensors can resist the varus force of elbow joint [23]. The muscles contributing for the valgus stability are flexor carpi ulnaris and flexor digitorum superficialis muscle [24].

Collateral ligaments are the important soft tissue of the elbow joint to act as the static stabilizer of elbow joint. In the medial side of elbow joint, the medial collateral ligament is composed of multiple bundles against the valgus force and posteromedial (internal) rotatory instability. The anterior bundle of the medial collateral ligament is the strongest bundle of the medial collateral ligament to prevent the valgus and posteromedial rotatory instability [5, 25]. Additionally, the anterior bundle of the medial collateral ligament is the priority reconstruction of the medial collateral ligament in clinics because it is the primary restrain and stabilizer [25, 26]. The anterior bundle of medial collateral ligament is composed of the anterior and posterior bands. The anterior band of anterior bundle of the medial collateral ligament is the primary restraint to provide the stability in the valgus force [2]. At 120° elbow flexion, the anterior and posterior bands of the anterior bundle of medial collateral ligament are the co-primary restraints when applying the valgus force [5]. Therefore, the anterior band of anterior bundle of medial collateral ligament may have isolated injury between 0° and 90° elbow flexion. When the elbow flexion is greater than 90°, both the anterior and posterior bands of anterior bundle of medial collateral ligament may be injured at the same time [5]. Recently, the poster bundle of medial collateral ligament has been considered as a stabilizer, independent of the integrity of anterior bundle of medial collateral ligament, in the posteromedial elbow instability. After transection of posterior bundle of medial collateral ligament, the proximal ulnohumeral joint gapping and torsion angle of ulnohumeral joint increase as the elbow flexion increases [27] with the intact anterior bundle of medial collateral ligament.

In the lateral side of elbow joint, the lateral ulnar collateral ligament is attached to the superior crest of the ulna, which is blended with the distal annular ligament at the proximal of ulna [3]. The lateral ulnar collateral ligament is the primary constraint in the lateral collateral ligaments to provide the stability of the ulnohumeral joint during the varus force and external rotated force [28]. A previous study showed that one of the distal sections of lateral ulnar collateral ligament or annular ligament was dissected which generates minor laxity of the elbow joint during the applied varus and external rotated forces [29]. Both the lateral collateral ligament and lateral radial collateral ligament were dissected which result in the significant rotatory laxity [29]. The entire transection of the lateral collateral ligament at the insertion or origin causes the maximal laxity [29]. The maximal external rotatory laxity was 20.6° at the 110° elbow flexion [29]. According to a previous study, the anterior portion of the lateral collateral ligament causes the significant laxity when applied the varus and external rotational forces at 80° elbow flexion [30].

To sum up, previous studies showed that articulation is the primary stabilizer under varus stress and the medial collateral ligament is the primary stabilizer under valgus stress in elbow flexion [11, 19, 26]. The lateral collateral ligament, capsule, and osseous structure provide 9%, 13%, and 75%, respectively, for resisting the varus force in the 90° flexion of elbow joint [31]. The medial collateral ligament, anterior capsule, and articulation provide 54%, 10%, and 36%, respectively, for resisting the valgus force in the 90° flexion of elbow joint [31]. The anterior bundle of medial collateral ligament is the primary stabilizer and the radial head is a secondary stabilizer of the elbow to resist the valgus force [26]. In the elbow extension, articulation is the primary stabilizer during the applied varus force of the elbow joint, and medial collateral ligament, capsule, and articulation have a similar contribution to stabilize the elbow joint during the applied valgus force of the elbow joint [11, 19, 26]. The medial collateral ligament, anterior capsule, and articulation provide 31%, 38%, and 31%, respectively, for resisting the valgus force in the full extension of elbow joint [31]. The lateral collateral ligament, capsule, and osseous structure provide 14%, 32%, and 55%, respectively, for resisting the varus force in the full extension of elbow joint [31].

3 Pathomechanics of Elbow

3.1 Abnormal Joint Motion and Instability

3.1.1 Valgus Instability, Posterolateral Rotatory Instability, Varus Posteromedial Rotatory Instability, and Elbow Dislocation

The valgus and varus loads influence the pattern of contact in the elbow joint, which is importance for the valgus instability, posterolateral instability, and varus posteromedial instability in the clinics. Elbow instability pattern is based on the injury duration, involvement of articulation, the direction of laxity, the extent of laxity, and

with or without fracture of elbow joint [32]. The injury of medial collateral ligament, especially anterior bundle, causes the valgus instability after the overuse injury (chronic injury) [33] or single acute traumatic injury [34]. The disruption of lateral collateral ligament is the main factor to cause the posterolateral rotatory instability under an axial load combining valgus load and the forearm supination after a traumatic injury [33]. The resultant force transmits from the lateral side to medial side causing the progressive structure injury of the elbow joint. The posterolateral rotatory instability is the frequent recurrent instability of the elbow [33]. The varus posteromedial rotatory instability is associated with the anteromedial facet of the coronoid fracture, a rupture of the lateral collateral ligament and posterior bundle of the medial collateral ligament under a varus load with the forearm pronation [35, 36]. Therefore, it is important to understand the contributions of soft tissues and bony geometry in the stability of elbow joint.

Previous studies have used the cadaver to investigate the extent of valgus laxity at the specific joint angle by sectioning the different degree of medial collateral ligament and articulation of elbow [2, 26]. Table 5.1 shows the relationship between valgus laxity and medial collateral ligament, radial head, and muscle force of the elbow joint. The maximum valgus laxity occurred at the 70–90° elbow flexion with anterior bundle of medial collateral ligament release and radial head intact [37]. The entire medial collateral ligament release with the radial head intact causes the 31.2 valgus laxity at the 90° elbow flexion [2]. Additionally, the entire medial collateral ligament release with radial head removal results in the gross valgus and internal rotational instability [26].

Posterolateral rotatory instability is a recurrent injury and the most common pattern of elbow instability [32, 38, 39]. Posterolateral rotatory instability commonly occurs at the tear or disruption from the lateral collateral ligament to the ulnar collateral ligament leading to the elbow dislocation after a traumatic injury [30]. The tennis elbow or iatrogenic injury from prior lateral elbow surgery may be factors to cause the posterolateral rotatory instability. Posterolateral rotatory instability is associated with the posterolateral subluxation or dislocation of the radial head and proximal ulna away from the humerus due to the laxity of the lateral collateral ligament [40]. Posterolateral rotatory instability can be further divided into three stages according to the degree of soft tissue disruption and displacement of elbow joint (Table 5.2).

Posteromedial rotatory instability occurred under the varus load and is associated with the subluxation and dislocation of the elbow joint [41]. The posteromedial rotatory instability causes the articular incongruity because the radius and ulnar rotate posteromedially which is off the articulation of humerus and this injury can in turn cause the increase of contact pressure in the coronoid surface [41]. The anteromedial facet fracture [42–44], tear of the lateral ulnar collateral ligament injury [41], and posterior bundle of the medial collateral ligament injury [27] are associated with the posteromedial rotatory instability. A previous study indicated that the isolated sectioning of the posterior bundle of the medial collateral ligament can cause the increase of 4.5 and 2.7 ulnar rotations at 60° and 90° elbow flexion, respectively, to generate the posteromedial instability of the elbow joint [27].

Table 5.1 The relationship between valgus laxity and medial collateral ligament, radial head, and muscle force of the elbow joint

UCL intact	Radial head intact	Without muscle loading	5 Normal valgus laxity	10–20° elbow flexion [26]
UCL intact	Radial head intact	With muscle loading	2.6 Valgus laxity	[26]
AOL release	Radial head intact		• 14 Valgus laxity • Maximum internal rotational laxity	• 70° elbow flexion [26] • 60° elbow flexion [2]
AOL release	Radial head removal		50 Valgus laxity	[26]
AB of AOL release	Radial head intact		• 11.7 Valgus laxity • Maximal internal rotational laxity	• 30° elbow flexion [2] • 40° elbow flexion [2]
PB of AOL release	Radial head intact		Little change in valgus and internal rotation	[2]
UCL intact	Radial head removal		Little change in valgus and internal rotation	
POL release	Radial head removal or not		Little change in valgus and internal rotation	[26]
AB release + POL release	Radial head intact		Did not induce more laxity	[2]
AOL release + POL release	Radial head intact		• Completely unstable • 31.2 Valgus laxity	90° elbow flexion (full flexion and full extension can confer some stability with joint surface) [2]
Entire UCL release	Radial head removal		Gross valgus and internal rotational instability	• Increase of internal rotational laxity • Increase of elbow flexion [26]
Entire UCL release	Radial head removal	Muscle force	Restore some stability (compared to a UCL-deficient elbow)	[26]

Table 5.2 The classification of the PLRS [39]

Stage		Soft tissues	Elbow joint
1	Posterolateral rotatory instability	1. Detach or tear lateral collateral ligament	Posterolateral subluxation
2	Subluxation	1. Progresses anteriorly and posteriorly around the elbow to the medial side 2. Detach or tear capsule	Greater displacement
3a and 3b	Posterior dislocation	1. Involve the medial collateral ligament and detach	Fully dislocates
3c	Posterior dislocation	1. Detach or tear the common flexor pronator origin	Grossly unstable elbow

Besides, the ulnohumeral joint gapping increase with the increase of elbow flexion after the sectioning of the posterior bundle of the medial collateral ligament. According to the findings of contact pressure of the coronoid surface, the anteromedial fracture with the lesion of lateral collateral ligament which is the involvement of posteromedial rotatory instability has the high contact pressure value at the edge of coronoid fracture with lower contact area compared to the intact elbow [41]. The anteromedial fracture with the posteromedial rotatory instability and tear of lateral collateral ligament causes a significant subluxation and decreases of elbow flexion compared to the coronoid fracture with lesion of posterior medial collateral ligament [41]. Therefore, the lateral collateral ligament is an important factor for preventing the subluxation in the posteromedial rotatory instability. According to previous studies, posterior medial collateral ligament can contribute part of the stability under the resistance of varus and internal rotational instability (posteromedial elbow instability) [27, 45].

3.1.2 Elbow Fracture

Elbow is the second dislocated major joint of the upper extremity in adults [46] after a traumatic injury. Posterior dislocation, a common disorder in the elbow joint, causes the injury of soft tissues including tear of lateral collateral ligament, the different extent injury of the ulnar collateral ligament and flexor-pronator muscles of elbow joint [42]. The valgus posterolateral rotatory load is a more common mechanism to cause the elbow dislocation and fracture than varus posteromedial rotatory load [47]. When the greater sigmoid notch has posterior and inferior subluxation under a valgus posterolateral rotatory load, a shearing force transmits to the tip of coronoid to induce the coronoid fracture [48, 49]. The severe valgus posterolateral rotatory injury eventually results in the terrible triad injury, which causes the elbow dislocation with radial head and coronoid fractures and ruptures the medial collateral ligament.

Radial head fracture (Fig. 5.8) is associated with the posterior dislocation of the elbow joint. The 10–15% patients with posterior dislocation have combined with the radial head fracture or coronoid fracture [50]. Coronoid fracture which is a frequent fracture type of the elbow joint [51] can be divided into three types including transverse fractures of the tip, fracture involving the anteromedial facet, and fractures at the coronoid base [43] (Fig. 5.9). In the transverse coronoid fracture with tip subtype II and 50% coronoid height of the elbow joint, the transection of posterior bundle of the medial collateral ligament causes the significant increase of ulnohumeral joint gapping during the elbow flexion [52]. However, the reconstruction of the posterior bundle of the medial collateral ligament only can decrease the ulnohumeral joint gapping and forearm rotation at 90° elbow flexion to restore posteromedial stability [52]. It indicated that the intact posterior bundle of the medial collateral ligament can provide some of the posteromedial stability after coronoid fracture without fixing [52]. The anteromedial fracture of the coronoid can be further subdivide to three subtypes according to the injury site of the anteromedial coronoid face

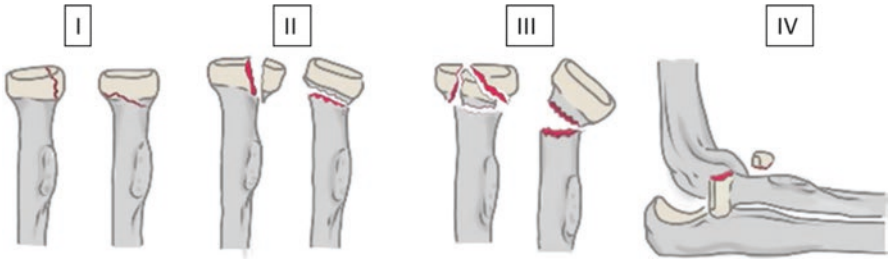

Fig. 5.8 Type of radial head fracture

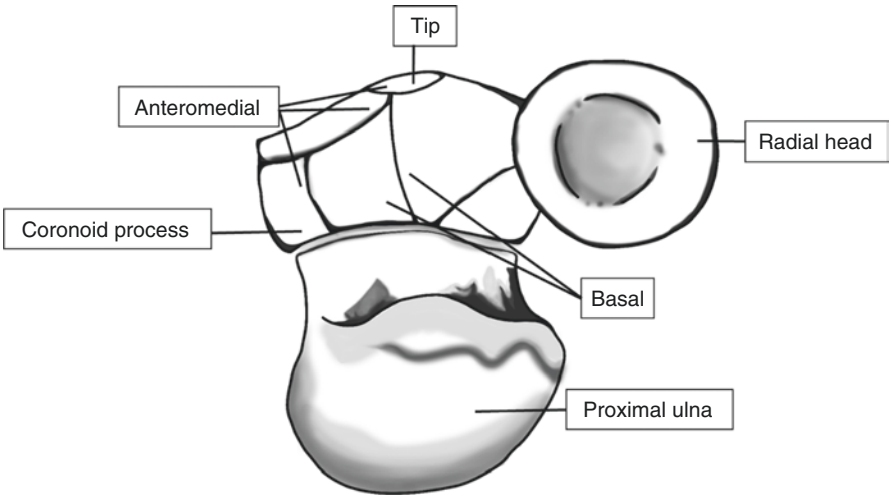

Fig. 5.9 Type of coronoid fracture

including (1) injury of the anteromedial rim, (2) injury of the anteromedial rim and tip, (3) injury of the anteromedial rim, tip, and the whole sublime tubercle [43] (Fig. 5.6). Both the lateral collateral ligament and the posterior bundle of the medial collateral ligament have tear associated with the anteromedial fractures [43, 44, 53]. The coronoid fracture can increase the forearm rotation angle, which is associated with the posteromedial instability of the elbow joint [43, 44, 52]. Recently, many researchers have investigated the effect of extent injury of anteromedial fractures with lesions of lateral collateral ligament or the posterior bundle of the medial collateral ligament on the posteromedial elbow instability [43, 44].

In clinics, the appropriate reconstruction and fixation can restore the range of motion and stability of elbow joint, increase the functional outcomes, and reduce the pain. The valgus posterolateral rotatory injury, terrible triad injury, causes the elbow dislocation combined with the lateral collateral ligament rupture and radial head and coronoid process fraction. The management of the valgus posterolateral rotatory includes fixation of the coronoid, fixation or replacement of the radial head, repair of the lateral ulnar collateral ligament, possible repair of the medial

collateral ligament, and external fixation of elbow as elbow remains unstable. The coronoid fracture can be repaired by the suture lasso technique for the small fragment of coronoid and by the lag screws with/without mini fragment plate for the large fragments of the coronoid [49]. The partial radial head fracture can be fixed with the screws [54, 55] or mini fragment plate [56]. The radial head replacement can be used to fix the radial head for more than three fragments and the prosthesis of radial head needs 2 mm distal to the coronoid [57]. In clinics, the lateral collateral ligament was commonly reconstructed by grasping type stitch to restore the elbow stability and prevent the subluxation under a valgus force [58] because the valgus posterolateral rotatory injury causes the detachment and avulsion of lateral collateral ligament from its attachment in the humerus. Recently, some researchers have indicated that the soft tissue injury may occur initially from the medial side of elbow joint [47, 59]. According to the MRI findings, posterolateral direction results in distractive injury to cause the displacement of the soft tissue in the ulnar side from the insertion point and detachment of soft tissue in the lateral side near the original point [47]. Therefore, the anterior bundle of medial collateral ligament may be the initial injury site at some acute injury situation with posterolateral dislocation [59].

The varus posteromedial rotatory injury causes the avulsion of the lateral collateral ligament and fracture of anteromedial facet of the coronoid. The surgical fixation was commonly used to repair the anteromedial facet fracture by internal fixation [44] through buttress plate and screw to fix the anteromedial facet fragment. There are many surgical approaches including flexor carpi ulnaris-splitting approach, over-the-top approach [60], posterior incision following the development of a medial skin flap [61], and the floor of the cubital tunnel approach following transportation of the ulnar nerve to repair the anteromedial facet fracture [62].

Anterior olecranon fracture dislocation is a high-energy injury in a dorsal aspect of the forearm at the elbow 90° flexion, causing the anterior dislocation of the radius and ulnar [63] with a large simple coronoid fragment [35]. Posterior Monteggia fracture is a low-energy injury causing the fracture at the base of the coronoid process. About 50% patients with posterior Monteggia fracture has combined with radial head fracture and avulsion of the lateral collateral ligament complex [64].

3.1.3 Elbow Joint Arthritis

The osteoarthritic elbow is a degenerative disease that cause osteophytes at the coronoid, olecranon, and radial head, decrease of the joint space of the ulnotrochlear and radiocapitellar, loose bodies, soft tissue contracture, and synovitis [65, 66]. The post-traumatic osteoarthritic elbow is in majority of osteoarthritic elbow due to the elbow dislocation, radial head fracture, and coronoid fracture to cause the cartilage lesion and post-traumatic deformity [67]. The post-traumatic osteoarthritic elbow commonly begins from the radiocapitellar joint to ulnohumeral joint with soft tissue destruction [65, 68, 69]. The osteoarthritic elbow can result in the joint deformity to

restrict the joint mobility and elbow stiffness in the advanced stage [66, 68, 69]. The treatment of osteoarthritic elbow includes the conservative treatment and surgical treatment. The conservative treatment is the first choice and the surgical treatment is used when there is failure of nonsurgical treatment [70] and significant impairment of the daily actives (range of motion of elbow less than 30–130°) [68]. The surgical treatment of osteoarthritic elbow includes arthroscopic approaches [70–72] and open techniques to restore the joint mobility and relieve the pain. The arthroscopic debridement focuses on removing the osteophytes, inflamed soft tissue, and loose bodies, releasing the tight capsular, and resecting the radial head [70, 71]. The arthroscopic debridement can restore the functional elbow mobility, improve the clinical scores, decrease the severity of elbow stiffness, and relieve the pain for primary and post-traumatic osteoarthritic elbow [71]. According to previous studies, the early and mild osteoarthritic elbow with the joint congruence can use the arthroscopy treatment and this treatment can provide the good postoperative functional and clinical outcomes at follow-up 24 months [70, 71, 73]. The radial head excision is commonly used in the patients with osteoarthritic elbow involved in the radiocapitellar arthritis. Patients who underwent radial head excision alone had a greater return of range of motion and clinical outcomes after mean follow-up 52 months [74]. However, the radial head plays an important role in the valgus stability. The resection of the radial head decrease valgus instability and increase ulnohumeral joint pressure under an axial load, eventually leading to the degenerative changes [13, 75, 76]. The effect of radial head excision has recently been investigated on the progression of ulnohumeral articular surface damage in the arthroscopic debridement [77]. A previous study showed that the patients with moderate and severe radiocapitellar chondral loss can improve elbow motion (flexion, extension, pronation, and supination) and relieve the pain after arthroscopic debridement of the arthritic elbow without radial head excision [77]. Additionally, a previous study showed that the shortening osteotomy of proximal radial of 2.5 mm, in the radiocapitellar osteoarthritis, can preserve the intact radial head to decrease the radiocapitellar contact pressure under a 250 N axial loading and remain the valgus stability during the elbow movement [13]. The shortening osteotomy of radial head might delay the ulnohumeral degeneration [13].

The prosthetic replacement may be considered in patients with severe osteoarthritic elbow and joint incongruence or elbow fracture-dislocation. Radiocapitellar replacement is used as the failure of repairing the radial head by the internal fixation. The radialcapitellar replacement has the metallic monopolar and bipolar flexed-neck prosthesis, which have demonstrated good clinical outcomes in repairing the elbow fracture dislocation [78–81]. In regard to the stability of elbow joint, monopolar implant significantly improves the ulnohumeral laxity and radiocapitellar joint subluxation compared to the bipolar implant in the terrible triad models [82, 83]. The lateral collateral ligament of elbow is the varus stabilizer; therefore, the integrity of the lateral collateral is an important factor to affect the elbow stability of the radialcapitellar replacement [84]. A previous study indicated that both monopolar and bipolar prosthesis would improve the stability of the elbow joint in the coronal plan and axial rotation loading as the adequate lateral collateral liga-

ment construction and intact medial collateral ligament [85]. The radiocapitellar replacement has been used in patients with osteoarthritic elbow who have the asymmetry elbow joint [86]. The degenerative and inflamed condition of osteoarthritic elbow commonly involved the lateral side [87]. The radiocapitellar replacement can restore the joint mobility, improve the clinical outcomes, and relieve the pain in patients with primary and post-traumatic arthritis after postoperative 22 months [86]. Although the orientation of the radial head cannot affect the kinematics of ulnohumeral joint, it can affect the force transmission in the radiocapitellar joint [88]. Therefore, the design of accurate orientation of radial head is necessary. Total elbow arthroplasty has been developed from the constrained articulated prosthesis to the semiconstrained and nonconstrained prostheses to reduce loosing [89]. Total elbow arthroplasty is indicated in the rheumatoid arthritis patients, patients with highly comminuted fracture of the distal humerus [90], or primary and post-traumatic osteoarthritis with the failure reconstruction [91, 92]. The limitation of total arthroplasty is the lifting weight restriction (5-lb) during a lifetime to ensure the durability and ultimate satisfactory function [89]. Additionally, the semiconstrained total elbow arthroplasty cause the impaired proprioception of elbow joint [93]. The correct positioning of the prostheses [94], ligament integrity, and prosthesis design remains challenging to improve the stability of elbow joint after total elbow arthroplasty.

3.2 Repetitive Soft Tissue Injury in the Elbow

3.2.1 Tendinopathy of Elbow

Tendinopathy of elbow can occur on the lateral side and medial side of the elbow. The lateral tendinopathy of elbow, tennis elbow, causes the tenderness of the origin of common extensor tendon and pain at the lateral side of the elbow [95]. The repetitive wrist extension and supination is the major pathomechanics to cause the degenerative condition of the common extensor tendon [96, 97]. According to previous studies, the contact pressure between the extensor carpi radialis brevis and capitellum increases with the wrist supination and elbow extension during backhand strokes [98–100]. Therefore, the repetitive loading of common tendon is a factor to cause the lateral tendinopathy of elbow. In regard to functional outcomes, patient with tennis elbow decreases the grip force and isokinetic performances of wrist extensors [101]. The primary treatment in patients with the tennis elbow is the nonsurgical management by physical therapy, activity modification, nonsteroidal anti-inflammatory drugs, and injections for the relief of lateral-sided elbow pain [96, 102, 103]. Surgical management is indicated in patients with tennis elbow when nonsurgical management fails [104]. Surgical management includes percutaneous, arthroscopic, and open approaches to release of the affected extensor muscles

[104, 105]. Recently, ultrasound has been used to diagnosis tennis elbow [106, 107]. Previous studies found that patients with tennis elbow has not only focal hypoechoic areas and calcification but also alternation of tendon stiffness by sonoelastography measurement [108, 109].

The medial tendinopathy of elbow, golfer's elbow, causes the tenderness of the origin of common flexor tendon and pain at the medial side of the elbow [110, 111]. The repetitive eccentric loading of the flexor muscles is a main pathomechanism to cause the golfer's elbow, especially in the wrist flexion and forearm pronation with valgus stress at the elbow joint [112]. This long-term repetitive loading cause the degeneration and microtrauma of tendon to result in the fibrosis and calcification within the tendon [113]. The sonoelastography has been used to evaluate the common flexor tendon and sonoelastography is correlated with the histological findings of the common flexor tendon [113]. As in the tennis elbow, nonsurgical management is a primary treatment in patients with the golfer's elbow for the relief of medial-sided elbow pain [112, 114]. Surgical management is indicated after patients receive nonsurgical therapy for 4–6 months and remain persistent symptoms [115, 116].

3.2.2 Cubital Tunnel Syndrome

Cubital tunnel syndrome, a compressive neuropathy, causes the impairment of sensation and muscle weakness. Cubital tunnel is composed of (1) the flexor carpi ulnaris fascia and Osborne's ligament (roof), (2) posterior and transverse bands of medial collateral ligament and elbow joint capsule (floor), and (3) medial epicondyle and olecranon (walls). The ulnar nerve is commonly compressed by the soft tissue, which includes the arcade of Struthers, Osborne ligament, flexor carpi ulnaris, and flexor digitorum superficialis. The sensation of ring finger and little finger has altered. Cubital tunnel syndrome exacerbated its symptoms during the prolonged elbow flexion. The pathologic of Osborne ligament results in the decrease of gliding of ulnar nerve during the elbow flexion and extension [117]. During the elbow flexion, the ulnar nerve has 2.2 cm excursion and 15% strain within the cubital tunnel [118]. The intra-neural pressure of the ulnar nerve has the low value at 40–50° elbow flexion and increases the value with the increase of angle [119]. Cubital tunnel syndrome would occur after the elbow dislocation and distal humerus fracture [120–122] due to the joint deformity, thickening of the cubital tunnel, swelling, and scarring. Nonsurgical management is indicated in patients with the mild to moderate cubital tunnel syndrome by using splint to limit elbow flexion to reduce the compressive and tensile load on the ulnar nerve [123, 124]. Surgical management is indicated in patients with severe cubital tunnel syndrome, impairment of two-point sensibility, and muscle atrophy by simple decompression [125], medial epicondylectomy [126], and anterior transposition to release the fascial structures [127].

References

1. Cage DJ, Abrams RA, Callahan JJ, Botte MJ. Soft tissue attachments of the ulnar coronoid process. An anatomic study with radiographic correlation. Clin Orthop Relat Res. 1995;320:154–8.
2. Floris S, Olsen BS, Dalstra M, Sojbjerg JO, Sneppen O. The medial collateral ligament of the elbow joint: anatomy and kinematics. J Shoulder Elbow Surg. 1998;7(4):345–51.
3. Morrey BF, An KN. Functional anatomy of the ligaments of the elbow. Clin Orthop Relat Res. 1985;201:84–90.
4. Jackson TJ, Jarrell SE, Adamson GJ, Chung KC, Lee TQ. Biomechanical differences of the anterior and posterior bands of the ulnar collateral ligament of the elbow. Knee Surg Sports Traumatol Arthrosc. 2016;24(7):2319–23. https://doi.org/10.1007/s00167-014-3482-7.
5. Callaway GH, Field LD, Deng XH, Torzilli PA, O'Brien SJ, Altchek DW, Warren RF. Biomechanical evaluation of the medial collateral ligament of the elbow. J Bone Joint Surg Am. 1997;79(8):1223–31.
6. Goto A, Moritomo H, Murase T, Oka K, Sugamoto K, Arimura T, et al. In vivo elbow biomechanical analysis during flexion: three-dimensional motion analysis using magnetic resonance imaging. J Shoulder Elbow Surg. 2004;13(4):441–7. https://doi.org/10.1016/S1058274604000394.
7. Goto A, Murase T, Moritomo H, Oka K, Sugamoto K, Yoshikawa H. Three-dimensional in vivo kinematics during elbow flexion in patients with lateral humeral condyle nonunion by an image-matching technique. J Shoulder Elbow Surg. 2014;23(3):318–26. https://doi.org/10.1016/j.jse.2013.11.010.
8. Miyake J, Shimada K, Moritomo H, Kataoka T, Murase T, Sugamoto K. Kinematic changes in elbow osteoarthritis: in vivo and 3-dimensional analysis using computed tomographic data. J Hand Surg Am. 2013;38(5):957–64. https://doi.org/10.1016/j.jhsa.2013.02.006.
9. Omori S, Miyake J, Oka K, Tanaka H, Yoshikawa H, Murase T. In vivo three-dimensional elbow biomechanics during forearm rotation. J Shoulder Elbow Surg. 2016;25(1):112–9. https://doi.org/10.1016/j.jse.2015.07.002.
10. Bryce CD, Armstrong AD. Anatomy and biomechanics of the elbow. Orthop Clin North Am. 2008;39(2):141–54, v. https://doi.org/10.1016/j.ocl.2007.12.001.
11. Morrey BF, An KN. Stability of the elbow: osseous constraints. J Shoulder Elbow Surg. 2005;14(1 Suppl S):174S–8S. https://doi.org/10.1016/j.jse.2004.09.031.
12. Kim HJ, Yi JH, Jung JW, Cho DW, van Riet R, Jeon IH. Influence of forearm rotation on proximal radioulnar joint congruency and translational motion using computed tomography and computer-aided design technologies. J Hand Surg Am. 2011;36(5):811–5. https://doi.org/10.1016/j.jhsa.2011.01.043.
13. Hackl M, Wegmann K, Kahmann SL, Heinze N, Staat M, Neiss WF, et al. Radial shortening osteotomy reduces radiocapitellar contact pressures while preserving valgus stability of the elbow. Knee Surg Sports Traumatol Arthrosc. 2017;25(7):2280–8. https://doi.org/10.1007/s00167-017-4468-z.
14. Bachman DR, Thaveepunsan S, Park S, Fitzsimmons JS, An KN, O'Driscoll SW. The effect of prosthetic radial head geometry on the distribution and magnitude of radiocapitellar joint contact pressures. J Hand Surg Am. 2015;40(2):281–8. https://doi.org/10.1016/j.jhsa.2014.11.005.
15. Ahmad CS, Park MC, Elattrache NS. Elbow medial ulnar collateral ligament insufficiency alters posteromedial olecranon contact. Am J Sports Med. 2004;32(7):1607–12. https://doi.org/10.1177/0363546503263149.
16. Hassan SE, Parks BG, Douoguih WA, Osbahr DC. Effect of distal ulnar collateral ligament tear pattern on contact forces and valgus stability in the posteromedial compartment of the elbow. Am J Sports Med. 2015;43(2):447–52. https://doi.org/10.1177/0363546514557239.

17. Sahu D, Holmes DM, Fitzsimmons JS, Thoreson AR, Berglund LJ, An KN, O'Driscoll SW. Influence of radial head prosthetic design on radiocapitellar joint contact mechanics. J Shoulder Elbow Surg. 2014;23(4):456–62. https://doi.org/10.1016/j.jse.2013.11.028.
18. Chen CT, Bhargava M, Lin PM, Torzilli PA. Time, stress, and location dependent chondrocyte death and collagen damage in cyclically loaded articular cartilage. J Orthop Res. 2003;21(5):888–98. https://doi.org/10.1016/S0736-0266(03)00050-0.
19. Safran MR, Baillargeon D. Soft-tissue stabilizers of the elbow. J Shoulder Elbow Surg. 2005;14(1 Suppl S):179S–85S. https://doi.org/10.1016/j.jse.2004.09.032.
20. Buckley MA, Yardley A, Johnson GR, Carus DA. Dynamics of the upper limb during performance of the tasks of everyday living—a review of the current knowledge base. Proc Inst Mech Eng H. 1996;210(4):241–7. https://doi.org/10.1243/PIME_PROC_1996_210_420_02.
21. Murray IA, Johnson GR. A study of the external forces and moments at the shoulder and elbow while performing every day tasks. Clin Biomech (Bristol, Avon). 2004;19(6):586–94. https://doi.org/10.1016/j.clinbiomech.2004.03.004.
22. Closkey RF, Goode JR, Kirschenbaum D, Cody RP. The role of the coronoid process in elbow stability. A biomechanical analysis of axial loading. J Bone Joint Surg Am. 2000;82-A(12):1749–53.
23. An KN, Hui FC, Morrey BF, Linscheid RL, Chao EY. Muscles across the elbow joint: a biomechanical analysis. J Biomech. 1981;14(10):659–69.
24. Park MC, Ahmad CS. Dynamic contributions of the flexor-pronator mass to elbow valgus stability. J Bone Joint Surg Am. 2004;86-A(10):2268–74.
25. Regan WD, Korinek SL, Morrey BF, An KN. Biomechanical study of ligaments around the elbow joint. Clin Orthop Relat Res. 1991;271:170–9.
26. Morrey BF, Tanaka S, An KN. Valgus stability of the elbow. A definition of primary and secondary constraints. Clin Orthop Relat Res. 1991;265:187–95.
27. Golan EJ, Shukla DR, Nasser P, Hausman M. Isolated ligamentous injury can cause posteromedial elbow instability: a cadaveric study. J Shoulder Elbow Surg. 2016;25(12):2019–24. https://doi.org/10.1016/j.jse.2016.04.022.
28. Hannouche D, Begue T. Functional anatomy of the lateral collateral ligament complex of the elbow. Surg Radiol Anat. 1999;21(3):187–91.
29. Olsen BS, Sojbjerg JO, Dalstra M, Sneppen O. Kinematics of the lateral ligamentous constraints of the elbow joint. J Shoulder Elbow Surg. 1996;5(5):333–41.
30. Seki A, Olsen BS, Jensen SL, Eygendaal D, Sojbjerg JO. Functional anatomy of the lateral collateral ligament complex of the elbow: configuration of Y and its role. J Shoulder Elbow Surg. 2002;11(1):53–9. https://doi.org/10.1067/mse.2002.119389.
31. Morrey BF, An KN. Articular and ligamentous contributions to the stability of the elbow joint. Am J Sports Med. 1983;11(5):315–9. https://doi.org/10.1177/036354658301100506.
32. O'Driscoll SW. Classification and evaluation of recurrent instability of the elbow. Clin Orthop Relat Res. 2000;370:34–43.
33. Karbach LE, Elfar J. Elbow instability: anatomy, biomechanics, diagnostic maneuvers, and testing. J Hand Surg Am. 2017;42(2):118–26. https://doi.org/10.1016/j.jhsa.2016.11.025.
34. Chung CB, Stanley AJ, Gentili A. Magnetic resonance imaging of elbow instability. Semin Musculoskelet Radiol. 2005;9(1):67–76. https://doi.org/10.1055/s-2005-867,104.
35. Ebrahimzadeh MH, Amadzadeh-Chabock H, Ring D. Traumatic elbow instability. J Hand Surg Am. 2010;35(7):1220–5. https://doi.org/10.1016/j.jhsa.2010.05.002.
36. Wyrick JD, Dailey SK, Gunzenhaeuser JM, Casstevens EC. Management of complex elbow dislocations: a mechanistic approach. J Am Acad Orthop Surg. 2015;23(5):297–306. https://doi.org/10.5435/JAAOS-D-14-00023.
37. Eygendaal D, Olsen BS, Jensen SL, Seki A, Sojbjerg JO. Kinematics of partial and total ruptures of the medial collateral ligament of the elbow. J Shoulder Elbow Surg. 1999;8(6):612–6.
38. O'Driscoll SW, Bell DF, Morrey BF. Posterolateral rotatory instability of the elbow. J Bone Joint Surg Am. 1991;73(3):440–6.

39. O'Driscoll SW, Morrey BF, Korinek S, An KN. Elbow subluxation and dislocation. A spectrum of instability. Clin Orthop Relat Res. 1992;280:186–97.
40. Camp CL, Smith J, O'Driscoll SW. Posterolateral rotatory instability of the elbow: part I. Mechanism of injury and the posterolateral rotatory drawer test. Arthrosc Tech. 2017;6(2):e401–5. https://doi.org/10.1016/j.eats.2016.10.016.
41. Bellato E, Kim Y, Fitzsimmons JS, Hooke AW, Berglund LJ, Bachman DR, O'Driscoll SW. Role of the lateral collateral ligament in posteromedial rotatory instability of the elbow. J Shoulder Elbow Surg. 2017;26(9):1636–43. https://doi.org/10.1016/j.jse.2017.04.011.
42. Mellema JJ, Doornberg JN, Dyer GS, Ring D. Distribution of coronoid fracture lines by specific patterns of traumatic elbow instability. J Hand Surg Am. 2014;39(10):2041–6. https://doi.org/10.1016/j.jhsa.2014.06.123.
43. O'Driscoll SW, Jupiter JB, Cohen MS, Ring D, McKee MD. Difficult elbow fractures: pearls and pitfalls. Instr Course Lect. 2003;52:113–34.
44. Pollock JW, Brownhill J, Ferreira L, McDonald CP, Johnson J, King G. The effect of anteromedial facet fractures of the coronoid and lateral collateral ligament injury on elbow stability and kinematics. J Bone Joint Surg Am. 2009;91(6):1448–58. https://doi.org/10.2106/JBJS.H.00222.
45. Pollock JW, Brownhill J, Ferreira LM, McDonald CP, Johnson JA, King GJ. Effect of the posterior bundle of the medial collateral ligament on elbow stability. J Hand Surg Am. 2009;34(1):116–23. https://doi.org/10.1016/j.jhsa.2008.09.016.
46. Stoneback JW, Owens BD, Sykes J, Athwal GS, Pointer L, Wolf JM. Incidence of elbow dislocations in the United States population. J Bone Joint Surg Am. 2012;94(3):240–5. https://doi.org/10.2106/JBJS.J.01663.
47. Rhyou IH, Kim YS. New mechanism of the posterior elbow dislocation. Knee Surg Sports Traumatol Arthrosc. 2012;20(12):2535–41. https://doi.org/10.1007/s00167-011-1872-7.
48. Doornberg JN, Ring D. Coronoid fracture patterns. J Hand Surg Am. 2006;31(1):45–52. https://doi.org/10.1016/j.jhsa.2005.08.014.
49. Garrigues GE, Wray WH 3rd, Lindenhovius AL, Ring DC, Ruch DS. Fixation of the coronoid process in elbow fracture-dislocations. J Bone Joint Surg Am. 2011;93(20):1873–81. https://doi.org/10.2106/JBJS.I.01673.
50. Ring D, Jupiter JB. Fracture-dislocation of the elbow. J Bone Joint Surg Am. 1998;80(4):566–80.
51. Doornberg JN, van Duijn J, Ring D. Coronoid fracture height in terrible-triad injuries. J Hand Surg Am. 2006;31(5):794–7. https://doi.org/10.1016/j.jhsa.2006.01.004.
52. Shukla DR, Golan E, Weiser MC, Nasser P, Choueka J, Hausman M. The posterior bundle's effect on posteromedial elbow instability after a transverse coronoid fracture: a biomechanical study. J Hand Surg Am. 2017. https://doi.org/10.1016/j.jhsa.2017.09.018.
53. Steinmann SP. Coronoid process fracture. J Am Acad Orthop Surg. 2008;16(9):519–29.
54. Leigh WB, Ball CM. Radial head reconstruction versus replacement in the treatment of terrible triad injuries of the elbow. J Shoulder Elbow Surg. 2012;21(10):1336–41. https://doi.org/10.1016/j.jse.2012.03.005.
55. Watters TS, Garrigues GE, Ring D, Ruch DS. Fixation versus replacement of radial head in terrible triad: is there a difference in elbow stability and prognosis? Clin Orthop Relat Res. 2014;472(7):2128–35. https://doi.org/10.1007/s11999-013-3331-x.
56. Kuhn S, Burkhart KJ, Schneider J, Muelbert BK, Hartmann F, Mueller LP, Rommens PM. The anatomy of the proximal radius: implications on fracture implant design. J Shoulder Elbow Surg. 2012;21(9):1247–54. https://doi.org/10.1016/j.jse.2011.11.008.
57. Rowland AS, Athwal GS, MacDermid JC, King GJ. Lateral ulnohumeral joint space widening is not diagnostic of radial head arthroplasty overstuffing. J Hand Surg Am. 2007;32(5):637–41. https://doi.org/10.1016/j.jhsa.2007.02.024.
58. Arrigoni P, D'Ambrosi R, Nicoletti S, Randelli P. Arthroscopic reinsertion of lateral collateral ligament, anterior capsular plication, and coronoid tunneling technique for chronic elbow

posterolateral rotatory instability. Arthrosc Tech. 2016;5(3):e471–5. https://doi.org/10.1016/j.eats.2016.01.031.
59. Schreiber JJ, Warren RF, Hotchkiss RN, Daluiski A. An online video investigation into the mechanism of elbow dislocation. J Hand Surg Am. 2013;38(3):488–94. https://doi.org/10.1016/j.jhsa.2012.12.017.
60. Huh J, Krueger CA, Medvecky MJ, Hsu JR, Skeletal Trauma Research Consortium. Medial elbow exposure for coronoid fractures: FCU-split versus over-the-top. J Orthop Trauma. 2013;27(12):730–4. https://doi.org/10.1097/BOT.0b013e31828ba91c.
61. Doornberg JN, Ring DC. Fracture of the anteromedial facet of the coronoid process. J Bone Joint Surg Am. 2006;88(10):2216–24. https://doi.org/10.2106/JBJS.E.01127.
62. Cheung EV, Steinmann SP. Surgical approaches to the elbow. J Am Acad Orthop Surg. 2009;17(5):325–33.
63. Ring D, Jupiter JB. Fracture-dislocation of the elbow. Hand Clin. 2002;18(1):55–63.
64. Ring D, Jupiter JB, Simpson NS. Monteggia fractures in adults. J Bone Joint Surg Am. 1998;80(12):1733–44.
65. Dalal S, Bull M, Stanley D. Radiographic changes at the elbow in primary osteoarthritis: a comparison with normal aging of the elbow joint. J Shoulder Elbow Surg. 2007;16(3):358–61. https://doi.org/10.1016/j.jse.2006.08.005.
66. O'Driscoll SW. Operative treatment of elbow arthritis. Curr Opin Rheumatol. 1995;7(2):103–6.
67. Lapner PC, Leith JM, Regan WD. Arthroscopic debridement of the elbow for arthrofibrosis resulting from nondisplaced fracture of the radial head. Arthroscopy. 2005;21(12):1492. https://doi.org/10.1016/j.arthro.2005.09.016.
68. Morrey BF, Askew LJ, Chao EY. A biomechanical study of normal functional elbow motion. J Bone Joint Surg Am. 1981;63(6):872–7.
69. Morrey BF, Bryan RS, Dobyns JH, Linscheid RL. Total elbow arthroplasty. A five-year experience at the Mayo Clinic. J Bone Joint Surg Am. 1981;63(7):1050–63.
70. Lim TK, Koh KH, Lee HI, Shim JW, Park MJ. Arthroscopic debridement for primary osteoarthritis of the elbow: analysis of preoperative factors affecting outcome. J Shoulder Elbow Surg. 2014;23(9):1381–7. https://doi.org/10.1016/j.jse.2014.01.009.
71. Merolla G, Buononato C, Chillemi C, Paladini P, Porcellini G. Arthroscopic joint debridement and capsular release in primary and post-traumatic elbow osteoarthritis: a retrospective blinded cohort study with minimum 24-month follow-up. Musculoskelet Surg. 2015;99(Suppl 1):S83–90. https://doi.org/10.1007/s12306-015-0365-0.
72. Savoie FH 3rd, Nunley PD, Field LD. Arthroscopic management of the arthritic elbow: indications, technique, and results. J Shoulder Elbow Surg. 1999;8(3):214–9.
73. Kelly EW, Morrey BF, O'Driscoll SW. Complications of elbow arthroscopy. J Bone Joint Surg Am. 2001;83-A(1):25–34.
74. McLaughlin RE 2nd, Savoie FH 3rd, Field LD, Ramsey JR. Arthroscopic treatment of the arthritic elbow due to primary radiocapitellar arthritis. Arthroscopy. 2006;22(1):63–9. https://doi.org/10.1016/j.arthro.2005.10.013.
75. Beingessner DM, Dunning CE, Gordon KD, Johnson JA, King GJ. The effect of radial head excision and arthroplasty on elbow kinematics and stability. J Bone Joint Surg Am. 2004;86-A(8):1730–9.
76. Yalcinkaya M, Bagatur AE, Erdogan S, Zorer G. Resection arthroplasty for Mason type III radial head fractures yield good clinical but poor radiological results in the long term. Orthopedics. 2013;36(11):e1358–64. https://doi.org/10.3928/01477447-20,131,021-15.
77. Kelly EW, Bryce R, Coghlan J, Bell S. Arthroscopic debridement without radial head excision of the osteoarthritic elbow. Arthroscopy. 2007;23(2):151–6. https://doi.org/10.1016/j.arthro.2006.10.008.
78. Berschback JC, Lynch TS, Kalainov DM, Wysocki RW, Merk BR, Cohen MS. Clinical and radiographic comparisons of two different radial head implant designs. J Shoulder Elbow Surg. 2013;22(8):1108–20. https://doi.org/10.1016/j.jse.2013.02.011.

79. Harrington IJ, Sekyi-Otu A, Barrington TW, Evans DC, Tuli V. The functional outcome with metallic radial head implants in the treatment of unstable elbow fractures: a long-term review. J Trauma. 2001;50(1):46–52.
80. Popovic N, Lemaire R, Georis P, Gillet P. Midterm results with a bipolar radial head prosthesis: radiographic evidence of loosening at the bone-cement interface. J Bone Joint Surg Am. 2007;89(11):2469–76. https://doi.org/10.2106/JBJS.F.00723.
81. Zunkiewicz MR, Clemente JS, Miller MC, Baratz ME, Wysocki RW, Cohen MS. Radial head replacement with a bipolar system: a minimum 2-year follow-up. J Shoulder Elbow Surg. 2012;21(1):98–104. https://doi.org/10.1016/j.jse.2011.05.012.
82. Pomianowski S, Morrey BF, Neale PG, Park MJ, O'Driscoll SW, An KN. Contribution of monoblock and bipolar radial head prostheses to valgus stability of the elbow. J Bone Joint Surg Am. 2001;83-A(12):1829–34.
83. Schneeberger AG, Sadowski MM, Jacob HA. Coronoid process and radial head as posterolateral rotatory stabilizers of the elbow. J Bone Joint Surg Am. 2004;86-A(5):975–82.
84. Chanlalit C, Shukla DR, Fitzsimmons JS, Thoreson AR, An KN, O'Driscoll SW. Radiocapitellar stability: the effect of soft tissue integrity on bipolar versus monopolar radial head prostheses. J Shoulder Elbow Surg. 2011;20(2):219–25. https://doi.org/10.1016/j.jse.2010.10.033.
85. Hartzler RU, Morrey BF, Steinmann SP, Llusa-Perez M, Sanchez-Sotelo J. Radial head reconstruction in elbow fracture-dislocation: monopolar or bipolar prosthesis? Clin Orthop Relat Res. 2014;472(7):2144–50. https://doi.org/10.1007/s11999-014-3672-0.
86. Giannicola G, Angeloni R, Mantovani A, Rebuzzi E, Merolla G, Greco A, et al. Open debridement and radiocapitellar replacement in primary and post-traumatic arthritis of the elbow: a multicenter study. J Shoulder Elbow Surg. 2012;21(4):456–63. https://doi.org/10.1016/j.jse.2011.08.071.
87. Ahrens PM, Redfern DR, Forester AJ. Patterns of articular wear in the cadaveric elbow joint. J Shoulder Elbow Surg. 2001;10(1):52–6. https://doi.org/10.1067/mse.2001.109382.
88. van Riet RP, Van Glabbeek F, Baumfeld JA, Neale PG, Morrey BF, O'Driscoll SW, An KN. The effect of the orientation of the radial head on the kinematics of the ulnohumeral joint and force transmission through the radiocapitellar joint. Clin Biomech (Bristol, Avon). 2006;21(6):554–9. https://doi.org/10.1016/j.clinbiomech.2006.01.006.
89. Bennett JB, Mehlhoff TL. Total elbow arthroplasty: surgical technique. J Hand Surg Am. 2009;34(5):933–9. https://doi.org/10.1016/j.jhsa.2009.02.021.
90. Kamineni S, Morrey BF. Distal humeral fractures treated with noncustom total elbow replacement. Surgical technique. J Bone Joint Surg Am. 2005;87 Suppl 1(Pt 1):41–50. https://doi.org/10.2106/JBJS.D.02871.
91. Antuna SA, Morrey BF, Adams RA, O'Driscoll SW. Ulnohumeral arthroplasty for primary degenerative arthritis of the elbow: long-term outcome and complications. J Bone Joint Surg Am. 2002;84-A(12):2168–73.
92. Cheung EV, Adams R, Morrey BF. Primary osteoarthritis of the elbow: current treatment options. J Am Acad Orthop Surg. 2008;16(2):77–87.
93. Siqueira GSL, Amaral MVG, Schiefer M, Schlee G, Schultz-Wenk TF, de Almeida MN, et al. Proprioceptive deficit after total elbow arthroplasty: an observational study. J Shoulder Elbow Surg. 2017;26(11):2017–22. https://doi.org/10.1016/j.jse.2017.07.003.
94. King GJ, Glauser SJ, Westreich A, Morrey BF, An KN. In vitro stability of an unconstrained total elbow prosthesis. Influence of axial loading and joint flexion angle. J Arthroplasty. 1993;8(3):291–8.
95. Walz DM, Newman JS, Konin GP, Ross G. Epicondylitis: pathogenesis, imaging, and treatment. Radiographics. 2010;30(1):167–84. https://doi.org/10.1148/rg.301095078.
96. Calfee RP, Patel A, DaSilva MF, Akelman E. Management of lateral epicondylitis: current concepts. J Am Acad Orthop Surg. 2008;16(1):19–29.
97. Lee SY, Chieh HF, Lin CJ, Jou IM, Kuo LC, Su FC. The potential risk factors relevant to lateral epicondylitis by wrist coupling posture. PLoS One. 2016;11(5):e0155379. https://doi.org/10.1371/journal.pone.0155379.

98. Bunata RE, Brown DS, Capelo R. Anatomic factors related to the cause of tennis elbow. J Bone Joint Surg Am. 2007;89(9):1955–63. https://doi.org/10.2106/JBJS.F.00727.
99. Orchard J, Kountouris A. The management of tennis elbow. BMJ. 2011;342:d2687. https://doi.org/10.1136/bmj.d2687.
100. Tanaka Y, Aoki M, Izumi T, Wada T, Fujimiya M, Yamashita T. Effect of elbow and forearm position on contact pressure between the extensor origin and the lateral side of the capitellum. J Hand Surg Am. 2011;36(1):81–8. https://doi.org/10.1016/j.jhsa.2010.10.005.
101. Unyo C, Chaler J, Rojas-Martinez M, Pujol E, Muller B, Garreta R, Mananas MA. A cross-sectional study comparing strength profile of dorsal and palmar flexor muscles of the wrist in epicondylitis and healthy men. Eur J Phys Rehabil Med. 2013;49(4):507–15.
102. Gosens T, Peerbooms JC, van Laar W, den Oudsten BL. Ongoing positive effect of platelet-rich plasma versus corticosteroid injection in lateral epicondylitis: a double-blind randomized controlled trial with 2-year follow-up. Am J Sports Med. 2011;39(6):1200–8. https://doi.org/10.1177/0363546510397173.
103. Tyler TF, Thomas GC, Nicholas SJ, McHugh MP. Addition of isolated wrist extensor eccentric exercise to standard treatment for chronic lateral epicondylosis: a prospective randomized trial. J Shoulder Elbow Surg. 2010;19(6):917–22. https://doi.org/10.1016/j.jse.2010.04.041.
104. Othman AM. Arthroscopic versus percutaneous release of common extensor origin for treatment of chronic tennis elbow. Arch Orthop Trauma Surg. 2011;131(3):383–8. https://doi.org/10.1007/s00402-011-1260-2.
105. Dunkow PD, Jatti M, Muddu BN. A comparison of open and percutaneous techniques in the surgical treatment of tennis elbow. J Bone Joint Surg Br. 2004;86(5):701–4.
106. Connell D, Burke F, Coombes P, McNealy S, Freeman D, Pryde D, Hoy G. Sonographic examination of lateral epicondylitis. AJR Am J Roentgenol. 2001;176(3):777–82. https://doi.org/10.2214/ajr.176.3.1760777.
107. Jaen-Diaz JI, Cerezo-Lopez E, Lopez-de Castro F, Mata-Castrillo M, Barcelo-Galindez JP, De la Fuente J, Balius-Mata R. Sonographic findings for the common extensor tendon of the elbow in the general population. J Ultrasound Med. 2010;29(12):1717–24.
108. Galletti S, Oliva F, Masiero S, Frizziero A, Galletti R, Schiavone C, et al. Sonoelastography in the diagnosis of tendinopathies: an added value. Muscles Ligaments Tendons J. 2015;5(4):325–30. https://doi.org/10.11138/mltj/2015.5.4.325.
109. Klauser AS, Pamminger M, Halpern EJ, Abd Ellah MMH, Moriggl B, Taljanovic MS, et al. Extensor tendinopathy of the elbow assessed with sonoelastography: histologic correlation. Eur Radiol. 2017;27(8):3460–6. https://doi.org/10.1007/s00330-016-4711-x.
110. Shiri R, Viikari-Juntura E, Varonen H, Heliovaara M. Prevalence and determinants of lateral and medial epicondylitis: a population study. Am J Epidemiol. 2006;164(11):1065–74. https://doi.org/10.1093/aje/kwj325.
111. Wolf JM, Mountcastle S, Burks R, Sturdivant RX, Owens BD. Epidemiology of lateral and medial epicondylitis in a military population. Mil Med. 2010;175(5):336–9.
112. Ciccotti MG, Ramani MN. Medial epicondylitis. Tech Hand Up Extrem Surg. 2003;7(4):190–6.
113. Klauser AS, Pamminger MJ, Halpern EJ, Abd Ellah MMH, Moriggl B, Taljanovic MS, et al. Sonoelastography of the common flexor tendon of the elbow with histologic agreement: a cadaveric study. Radiology. 2017;283(2):486–91. https://doi.org/10.1148/radiol.2016160139.
114. Harada M, Takahara M, Hirayama T, Sasaki J, Mura N, Ogino T. Outcome of nonoperative treatment for humeral medial epicondylar fragmentation before epiphyseal closure in young baseball players. Am J Sports Med. 2012;40(7):1583–90. https://doi.org/10.1177/0363546512443807.
115. Amin NH, Kumar NS, Schickendantz MS. Medial epicondylitis: evaluation and management. J Am Acad Orthop Surg. 2015;23(6):348–55. https://doi.org/10.5435/JAAOS-D-14-00145.
116. Mishra A, Pirolo JM, Gosens T. Treatment of medial epicondylar tendinopathy in athletes. Sports Med Arthrosc Rev. 2014;22(3):164–8. https://doi.org/10.1097/JSA.0000000000000031.
117. Macchi V, Tiengo C, Porzionato A, Stecco C, Sarasin G, Tubbs S, et al. The cubital tunnel: a radiologic and histotopographic study. J Anat. 2014;225(2):262–9. https://doi.org/10.1111/joa.12206.

118. Wright TW, Glowczewskie F Jr, Cowin D, Wheeler DL. Ulnar nerve excursion and strain at the elbow and wrist associated with upper extremity motion. J Hand Surg Am. 2001;26(4):655–62. https://doi.org/10.1053/jhsu.2001.26140.
119. Gelberman RH, Yamaguchi K, Hollstien SB, Winn SS, Heidenreich FP Jr, Bindra RR, et al. Changes in interstitial pressure and cross-sectional area of the cubital tunnel and of the ulnar nerve with flexion of the elbow. An experimental study in human cadavera. J Bone Joint Surg Am. 1998;80(4):492–501.
120. Buehler MJ, Thayer DT. The elbow flexion test. A clinical test for the cubital tunnel syndrome. Clin Orthop Relat Res. 1988;233:213–6.
121. Mehlhoff TL, Noble PC, Bennett JB, Tullos HS. Simple dislocation of the elbow in the adult. Results after closed treatment. J Bone Joint Surg Am. 1988;70(2):244–9.
122. Robinson CM, Hill RM, Jacobs N, Dall G, Court-Brown CM. Adult distal humeral metaphyseal fractures: epidemiology and results of treatment. J Orthop Trauma. 2003;17(1):38–47.
123. Shah CM, Calfee RP, Gelberman RH, Goldfarb CA. Outcomes of rigid night splinting and activity modification in the treatment of cubital tunnel syndrome. J Hand Surg Am. 2013;38(6):1125–30, e1121. https://doi.org/10.1016/j.jhsa.2013.02.039.
124. Svernlov B, Larsson M, Rehn K, Adolfsson L. Conservative treatment of the cubital tunnel syndrome. J Hand Surg Eur Vol. 2009;34(2):201–7. https://doi.org/10.1177/1753193408098480.
125. Krogue JD, Aleem AW, Osei DA, Goldfarb CA, Calfee RP. Predictors of surgical revision after in situ decompression of the ulnar nerve. J Shoulder Elbow Surg. 2015;24(4):634–9. https://doi.org/10.1016/j.jse.2014.12.015.
126. Osei DA, Padegimas EM, Calfee RP, Gelberman RH. Outcomes following modified oblique medial epicondylectomy for treatment of cubital tunnel syndrome. J Hand Surg Am. 2013;38(2):336–43. https://doi.org/10.1016/j.jhsa.2012.11.006.
127. Bartels RH, Verhagen WI, van der Wilt GJ, Meulstee J, van Rossum LG, Grotenhuis JA. Prospective randomized controlled study comparing simple decompression versus anterior subcutaneous transposition for idiopathic neuropathy of the ulnar nerve at the elbow: part 1. Neurosurgery. 2005;56(3):522–30; discussion 522–30.

Chapter 6
Biomechanics of the Shoulder

Min Zhang and Chih-Hwa Chen

Abstract The glenohumeral (GH) joint is a complex and unstable articulation. The interaction between various structures of the shoulder caused by mechanical stimuli and motion provides multiple degrees of shoulder motion. The static stability of the shoulder is supported by the articulation of the humeral head and the glenoid with additional GH ligaments, capsule, and labrum. The rotator cuff muscles surrounding the shoulder joint provide dynamic stability. The combination of these factors forms the biomechanical system that can respond in accordance with the arm movement. Different pathological processes and injuries may result in similar clinical manifestations. It is crucial to know the etiology of these different pathological factors from the viewpoint of the shoulder joint biomechanics to provide the most effective and curable treatments for patients suffering from shoulder diseases and disorders.

Keywords Shoulder stability · Biomechanics · Rotator cuff · Glenohumeral joint Shoulder instability

1 Introduction

The shoulder motion is subject to the reaction to the shoulder structure stimuli. Due to the mismatch between the humeral head and the articular surface of the glenoid, the stabilization of the shoulder is compensated by static and dynamic stabilizers.

M. Zhang
Beijing Advanced Innovation Center for Biomedical Engineering, Beihang University, Beijing, China

Key Laboratory for Biomechanics and Mechanobiology of Ministry of Education, School of Biological Science and Medical Engineering, Beihang University, Beijing, China

C.-H. Chen (✉)
Department of Orthopedics, Taipei Medical University—Shuang Ho Hospital, Taipei, Taiwan

School of Medicine, College of Medicine, Taipei Medical University, Taipei, Taiwan

School of Biomedical Engineering, College of Biomedical Engineering, Taipei Medical University, Taipei, Taiwan

Research Center of Biomedical Devices, Taipei Medical University, Taipei, Taiwan

C.-K. Cheng, S. L-Y. Woo (eds.), *Frontiers in Orthopaedic Biomechanics*,
https://doi.org/10.1007/978-981-15-3159-0_6

The static stabilizers include the glenohumeral (GH) ligaments, the labrum, and the constrained capsule. The dynamic stability is provided by the rotator cuff (RC) muscles surrounding the shoulder joint. The combined effect of the stabilizers is to support the multiple degrees of motion within the GH joint. The scapulothoracic (ST) joint provides additional mobility and stability to the shoulder.

2 Musculoskeletal and Functional Anatomy of Shoulder

The human shoulder is composed of bones as well as associated muscles, ligaments, and tendons. It is the connection between the neck and the upper limb.

2.1 Bony Structure of the Shoulder

The skeletal structure of the shoulder includes the humerus, the scapula, and the clavicle.

2.1.1 Humerus

The humerus is located on the upper limb and is articulated with the glenoid fossa at the glenohumeral joint. The head of the humerus is elliptical and inclines between 120° and 145° [1] as well as a retroversion within a range of 60° [2]. There are two bulges on the lateral and anterior sides of the humeral head. They are greater and lesser tubercles. These two tubercles are separated by intertubercular groove and are origins to subscapularis, teres minor, infraspinatus, and supraspinatus muscles. The humerus has two necks: surgical and anatomical necks. The surgical neck is a constriction below the tubercles of the greater tubercle and lesser tubercle, and above the deltoid tuberosity. The anatomical neck is obliquely directed, forming an obtuse angle with the body. It provides the attachment to the articular capsule.

2.1.2 Scapula

The scapula is located on the posterior chest wall and is in an inverted triangular shape. It inclines approximately 40° anteriorly to the coronal plane [3]. There is a broad concavity on the anterior surface of the scapula and it forms the origin of the subscapularis muscle. The posterior surface of the scapula consists of the infraspinatus and supraspinal fossae, which is separated by the scapular spine provide the origins to the infraspinatus and supraspinatus muscles. Further, the scapula is com-

posed of three corners and three sides, namely the lateral, superior, and inferior angles, and the medial, superior, and lateral borders, respectively. Next to the lateral angle, the glenoid is a shallow and pear-shape cavity. It inclines 3–5° superiorly [4] and 2.5–12.5° posteriorly [5].

2.1.3 Clavicle

The clavicle is an elongated bone in an S-shaped and connects the upper limb to the torso. The lateral and medial end of the clavicle is flat and thick, respectively. The clavicle transmits forces from the trunk to the upper limb. The articulation between the clavicle and the manubrium of the sternum is a sternoclavicular (SC) joint. The articulation between the clavicle and the acromion of the scapula is the acromioclavicular (AC) joint.

2.2 Articulation of the Shoulder

The shoulder joint is composed of four joints (SC joint, AC joint, GH joint, and ST articulation) with bony and soft-tissue structures. These articulations provide a high degree of shoulder motion. The arm can reach an elevation angle of 180°, internal and external rotations of approximately 150°, and flexion and extension of 170° [6].

2.2.1 Sternoclavicular Joint

The articulation between the manubrium sterni and the medial end of the clavicle is the SC joint. It connects the thorax to the upper limb and allows approximately 35° of elevation and 50° of axial rotation [6]. The intrinsic bony stability of the SC joint is mainly supported by the anterior and posterior SC ligaments, the interclavicular ligament, the costoclavicular ligament, and the articular disc.

2.2.2 Acromioclavicular Joint

The AC joint is composed of the acromion and the clavicle surfaces, which transmits forces from the upper extremity to the chest musculature. The AC articulation is stabilized by the coracoclavicular and the AC ligaments. The coracoacromial ligament spans between the lateral aspect of the coracoid process and the anterior facet of the acromion. It is to restraint the superior-inferior migration of the clavicle [7, 8]. The AC ligament is to restrain the anterior-posterior translation of the clavicle [7, 8] and provides scapular and synchronous clavicular rotation [9].

2.2.3 Glenohumeral Joint

The GH joint is a flexible and unstable articulation composed of the scapula glenoid fossa and humeral head. The glenoid cavity accounts for 25–30% of the humeral head and can move relatively to the humerus [9]. The glenoid-humerus contact area varies in degrees during the shoulder motion. Its stability is mainly supported by the articular capsule, the labrum, and the surrounding muscles [10]. The capsular-ligamentous complex includes the superior, the medial, and the inferior GH ligaments. The superior and the medial GH ligaments are both single-band structures and reach the lesser tubercle and the humeral neck, respectively. The inferior GH ligament complex consists of anterior and posterior bands and inserts on the humerus beyond the lesser tuberosity [11]. The glenoid labrum is a circumferential and fibrocartilaginous ring attaching to the glenoid rim. The glenoid labrum serves as a bumper during the shoulder motion and an attachment site of the GH ligaments. The muscles supplying the stability of the GH joint refers to the RC, which will be described in Sect. 2.3.

2.2.4 Scapulothoracic Articulation

The ST articulation is composed of the anterior surface of the scapula and the posterior surface of the thoracic [12]. The neurovascular, muscular, and bursal structures allow smooth motion of the scapula on the thorax. The ST articulation allows 30° of abduction internal rotation, respectively. It increases the shoulder movement after the initial 120°, which is supplied by the GH joint [12].

2.3 Functional Muscles of the Shoulder

The shoulder muscles supply athletic ability and dynamic stability. The function of muscles are subjected to its origin and endpoint. The muscles and their functions on the shoulder complex are described below.

The anterior outer layer muscles on the shoulder complex involve the pectoralis major and the deltoid muscles. The pectoralis major muscle has two heads (sternocostal and clavicular heads) and is located above the anterior chest wall. The sternocostal head originates from the anterior sternum surface, the superior six costal cartilages, and the external oblique muscle aponeurosis. In contrast, the clavicular head originates from the medial clavicle anterior surface. Both the sternocostal and clavicular heads insert to the crest of the greater tubercle of the humerus and serve the elevation and adduction of the arm. The deltoid muscle is composed of the anterior, the intermediate, and the posterior fibers. The anterior fibers originate from the upper surface and the anterior border of the lateral third of the clavicle and serve the

flexion and internal rotation of the arm. The intermediate fibers originate from the acromion process and the spine of the scapula and serve the abduction of the arm after the initial 15° of arm rotation [6]. The posterior section of the deltoid originates from the spine of the scapula. It serves the external rotation and the extension of the humerus. All the fibers of the deltoid muscle insert into the deltoid tuberosity of the humerus.

The inner muscles involve the pectoralis minor, the subclavius, and the subscapularis muscles. The pectoralis minor plays an important stabilizing role on the scapula. The subclavian muscle is located underneath the clavicle and contributes to the clavicular movement. The subscapularis muscle, which is located in the anterior scapula, functions as the arm rotator.

The posterior outer layer muscles involve the latissimus dorsi, the trapezius, the serratus anterior, and the posterior deltoid muscles. The latissimus dorsi muscle arises from the thoracic vertebrae and inserts into the intertubercular groove of the humerus. It works in collaboration with the pectoralis major to contribute to the adduction and medial rotation of the humerus. The trapezius muscle is one of the broadest back muscles. It arises from the occipital bone, the ligamentum nuchae, and the spinous processes of T01–T12 and inserts into the third clavicle lateral, as well as the acromion and scapular spine. The trapezius muscle contributes to the shoulder elevation and rotation and also acts in head/neck extension [13]. The serratus anterior muscle arises from the anterior surfaces of the eighth upper ribs and inserts into the inner medial border of the scapula. The serratus anterior muscle allows the forward rotation of the arm and to pull the scapula forward and around the rib cage.

The posterior inner layer muscle below the superficial muscles (the trapezius and deltoid muscles) includes the supraspinatus, infraspinatus, teres minor, and teres major muscles. The origin of the supraspinatus muscle is the supraspinatus fossa. The muscle tracks laterally underneath the acromion and goes on the insertion at the greater tuberosity [14]. Thus, the supraspinatus muscle assists in the arm abduction and humerus stabilization [6]. The infraspinatus muscle originates from the infraspinous fossa of the scapula and inserts at the greater tuberosity. The origin of the teres minor muscle is at the lateral margin of the scapula. The muscle inserts at the most posterior and inferior facet of the greater tuberosity. Both the teres minor and the infraspinatus muscles assist the stability and rotation of the humerus. The subscapularis muscle is trapezoidal and origins from the anterior scapula aspect and inserts at the lesser tuberosity [15]. The teres major muscle arises from the inferior angle of the scapula and passes laterally and superiorly to the bicipital groove. It contributes to the extension and rotation of the humerus.

The RC is formed by the subscapularis, the infraspinatus, the teres minor, the supraspinatus muscles, and their associated tendons. The RC muscles contribute to the abduction and rotation of the humerus and also provide a compressive force to centralize the humeral head on the glenoid. In the case of a massive rotator cuff tear, the loss of enough passive muscle tension and dynamic contraction leads to exces-

sive superior translation of the humerus to the glenoid cavity. The translation can reach 12 mm in some cases [9]. It may result in subacromial impingement and the erosions of surrounding bone and articulations (i.e., the glenoid, the acromioclavicular joint, and the anterior acromion) (the severe RC tear is described further in Sect. 4.2.1).

2.4 Summary

The GH joint is an enarthrodial socket-to-ball joint and supports the polyaxial arm motions. It includes abduction/adduction around the sagittal axis, flexion/extension around the frontal axis, and external/internal rotation around a longitudinal-humeral axis.

GH joint kinematics is not precisely equivalent to enarthrodial kinematics. Numerous studies have reported the exact determination of the GH joint kinematics and the founding is controversial. Due to different methodological approaches in different studies, it is difficult to compare the results. In general, the humeral head translates approximately 1.1 mm inferiorly during the whole abduction and 2.4 mm anteriorly before the abduction of 90° and 1.4 mm posteriorly during the abduction of 90–150° [16].

The GH joint maintains stability in utilizing static and dynamic restraints. These static stabilizers dynamic restraint involve ligamentous, capsular, cartilaginous, and bony structures, as well as musculature structure of the shoulder, respectively. The GH ligament stabilizes the GH joint by preventing excessive movements of the humeral head relative to the glenoid cavity in the extremes of motion [17]. A competent sealed capsule of appropriate volume, minimal joint fluid, and an intact congruent glenoid labrum provides the stability of the GH articulation [18]. Neuromuscular control primarily provides dynamic stability between the RC muscles and ST musculature. The functional ST musculature can ideally release the instability of the shoulder joint and the neural feedback from the GH ligaments and RC muscles, which are used to prevent pathologic translation of the GH joint.

Dynamic stabilizers may contribute to joint stability by the muscle contraction, which leads to compression of the articular surfaces, and the passive muscle tension from the bulk effect of the muscles [17]. The contraction of the RC muscles compresses the humeral head on the glenoid cavity and the asymmetric contraction leads to the humeral head rotation during the shoulder motion. The interaction of the RC muscles works in conjunction with other muscles in the shoulder girdle [19].

The shoulder joint kinematics relies on the ST and deltoid muscles, as well as the RC muscles interaction. The subscapularis and infraspinatus muscles act as a transverse force couple generating compressive forces. Also, the supraspinatus muscle plays a significant role in the concavity compression during early abduction [20].

3 Mechanical Properties and Glenoid Architecture

The mechanical parameters of the glenoid relate to bone architecture [21–23]. As illustrated in Fig. 6.1, the subchondral bone from the sagittal plane view is formed by the superoinferior, which oriented parallel to the trabeculae in the peripheral regions and honeycomb-fashion struts in the center of the glenoid [24]. In the transverse view, the trabeculae are plate-like and generally perpendicular to the glenoid surface (Fig. 6.1b). In the posterior and anterior regions, the thin rods directly connect the semi-circular cortical base to the subchondral plate and present low porosity, while the trabeculae in the middle portion distribute partially and present high porosity [21, 24].

As a result of the partial distribution of trabeculae in the center of the glenoid and high alignments of trabeculae in the anterior and posterior portions, the bone in the center of the glenoid presents a lesser strength, low stiffness, and isotropic characteristic with reference to the bone in the peripheral glenoid [22, 25]. The scapula bone from the lateral to the medial is orderly the subchondral bone, trabecular bone, and compact bone. In conformity with the architecture of the scapula, the strength of the scapula bone reduces significantly beneath the subchondral layer and then increases to the cortical bone layer [23]. In a regional test, the posterosuperior and anteroinferior glenoid shows the strongest and weakest bones, respectively [21, 22, 25, 26]. The porous trabecular bone at the center of the glenoid enables the heavy loads from the articular surface to be absorbed and conveyed, and the dense bone in the peripheral glenoid enables the compressive stresses generated during the arm motion to be absorbed [24]. The studies shows the individual glenoid present that the glenoid trabecular bone Young's modulus varies between 99 and 264 MPa and

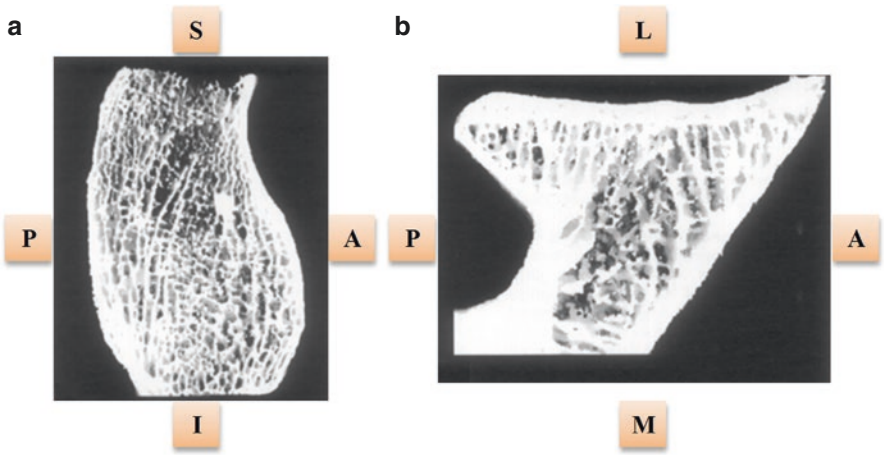

Fig. 6.1 The glenoid bone (**a**) sagittal view; (**b**) transverse view. *L* lateral, *M* medial, *P* posterior, *A* anterior, *I* inferior, *S* superior. (Adapted from Frich et al., 1998)

the strength ranges from 26 to 110 MPa [21, 23, 25]. Young's modulus and strength values are related to many factors such as health conditions, gender, and ages [23, 27, 28].

4 Shoulder Joint Arthroplasty

Shoulder joint arthroplasty is a surgical way to alleviate shoulder pain and restore the shoulder function. This section introduces the shoulder joint replacements from the following sections: (1) the types of shoulder joint arthroplasty; (2) clinical indications of shoulder joint arthroplasty; and (3) knowledge-based related to the shoulder joint arthroplasty.

4.1 Types of Shoulder Arthroplasty

The artificial shoulder joint arthroplasty can be classified into (1) anatomical and reverse shoulder arthroplasties, (2) total shoulder arthroplasty (TSA) and prosthetic humeral hemiarthroplasty (HA), and (3) stemmed and resurfacing shoulder arthroplasties.

4.1.1 Anatomical and Reverse Shoulder Arthroplasties

The structure of anatomical shoulder arthroplasty is similar to that of a natural shoulder joint and composed of a ball replacing the humeral head and a socket replacing the glenoid fossa. In contrast, the design of reverse shoulder arthroplasty (RSA) is different. Thus, in prosthesis type, the glenoid fossa is replaced with a ball and the humeral head is replaced with a socket. Anatomical shoulder arthroplasty is mainly used for the treatment of the incongruent osseous surface, moderate and severe osteoarthritis (OA), and inflammatory arthritis [29]. Primary indications of the reverse total shoulder arthroplasty (RTSA) are arthritis with massive RC tear. (Detail information on the advantages of RSA for severe RC treatment are shown in Sect. 4.2.1.)

4.1.2 Humeral Hemiarthroplasty and Total Shoulder Arthroplasty

In humeral HA (Fig. 6.2a), only the proximal humerus was replaced by an artificial device, while in the TSA, both the humerus and the glenoid are reconstructed. In the surgical technique of HA, the entire glenoid can be preserved and the complications associating with the glenoid component in the TSA can be avoided. HA is used for patients with intact articular cartilage surfaces. When the cartilage is damaged or the glenoid erosion is severe, TSA is usually preferred.

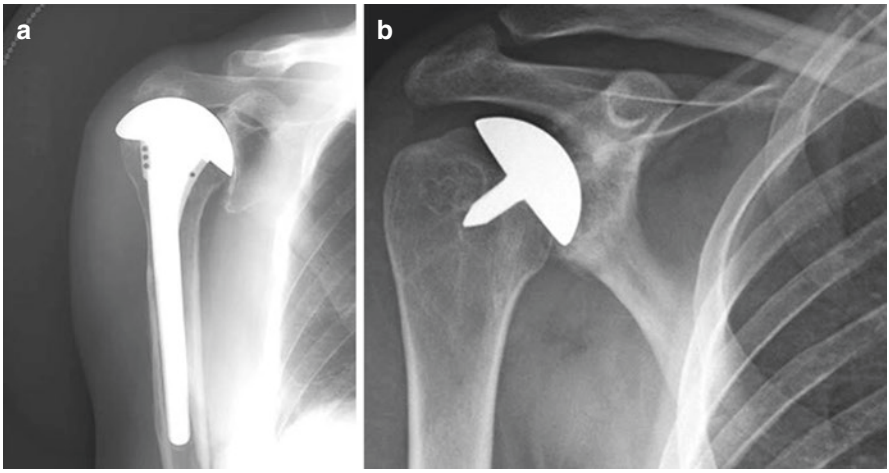

Fig. 6.2 (**a**) Radiograph of a hemiarthroplasty and (**b**) prosthesis resurfacing

4.1.3 Resurfacing and Stemmed Shoulder Arthroplasties

Prosthesis resurfacing (Fig. 6.2b) refers to the surgical technique in which only the damaged surface of the humeral head is reconstructed. This technique can preserve the native inclination and offset of the humerus as well as the head shaft angle. Prosthesis resurfacing is usually used for the treatments of young and active patients [30, 31]. The contact between the glenoid bone and the stiff metallic humeral resurfacing device may lead to late glenoid arthrosis and need a revision to a TSA [30].

4.2 Clinical Indications of Shoulder Joint Arthroplasty

The indications for shoulder joint replacements involve cuff tear arthropathy (CTA), primary OA, rheumatoid arthritis, humeral fracture, and the failed shoulder joint arthroplasty [29].

4.2.1 Cuff Tear Arthropathy

CTA is a common shoulder disease referring to shoulder arthritis with RC tears [32]. Besides the loss of the shoulder cartilage function, severe CTA also leads to the dysfunction of RC tendons. This type of shoulder disease is often accompanied by synovial fluid leakage, GH articular cartilage atrophy, and subchondral osteoporosis on the humeral head [32]. In Sect. 2.3, the RC acts as a dynamic stabilizer. The dysfunction of these muscles may lead to the migration of the humeral head

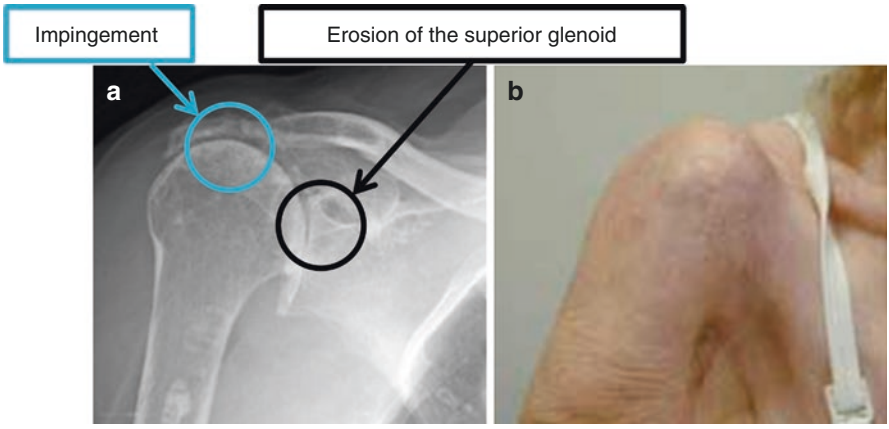

Fig. 6.3 (**a**) A radiograph of the RC arthropathy. (Adapted from http://www.djosurgical.com/patient/rsp/index.htm). (**b**) Photograph of a patient with CTA

and subacromial impingement. Meanwhile, it may also induce pseudocyesis, pain, and loss of shoulder function. CTA may be developed after surgical treatments. It is reported that RC tears were observed in 47% of patients who had TSA from 2004 to 2007 [33] (Fig. 6.3).

CTA is generally treated with RTSA or HA. If the CTA is mild and the shoulders are stable, HA is recommended [34, 35]. Further, if the shoulder is unstable, RSA treatment is generally used [29]. The application of TSA for CTA treatment is not an ideal approach [29]. Biomechanical analyses for these reasons are described below. In the case of severe CTA, the deltoid muscle force may lead to the superior movement of the humerus and could cause the subacromial impingement and other indications of CTA (Fig. 6.4a). When the TSA is applied for CTA treatment (Fig. 6.4b), the GH joint cannot be stabilized, and the humeral head may still be translated superiorly under the deltoid muscle force. Moreover, it may lead to eccentric loading on the glenoid socket and finally result in glenoid loosening. When the RSA is used for the treatment of CTA, the center of rotation of the humerus is secured on the glenoid and the arm can rotate under the deltoid muscle force (Fig. 6.4c). RSA is currently the only recommended treatment for the elderly adults (≥65 years) with pseudoparalysis and pain, due to the high long-term implant failure rate [36–38].

4.2.2 Osteoarthritis

OA is a disorder in which the biomechanical properties of the articular cartilage are gradually degraded. The OA starts from the articular cartilage wearing. When the wear leads to the direct bone contact of the two parts of the GH joint, OA may cause osteophytes, subchondral bone thickening, motion restriction, swelling, and pain

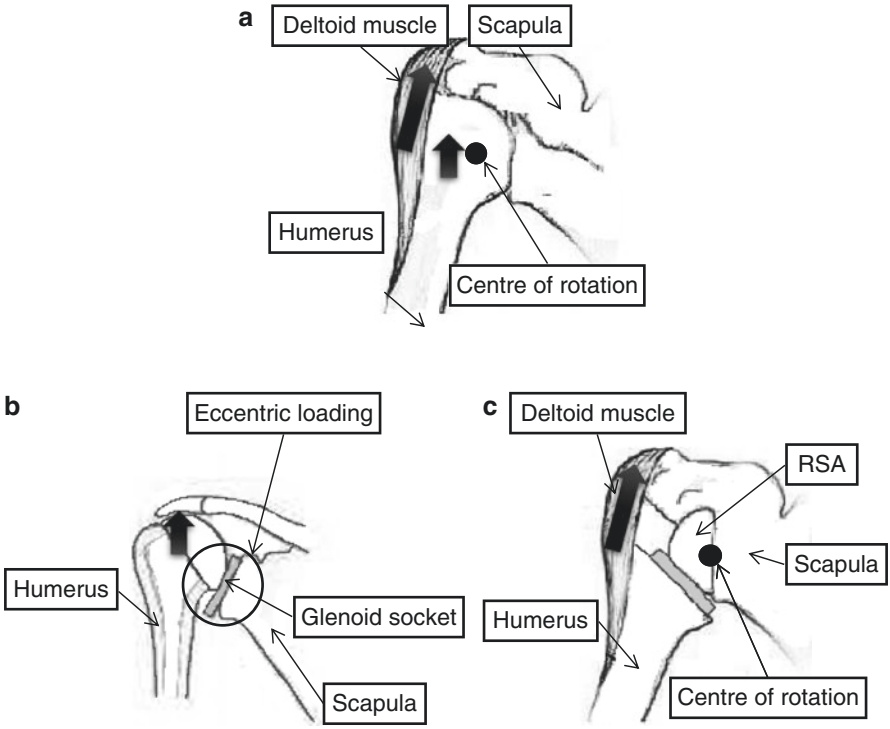

Fig. 6.4 Schematic diagram of the CTA in (**a**) the anatomical shoulder; (**b**) the TSA and (**c**) the RSA

[39]. The mild OA is usually treated with a nonsurgical method (i.e., local injections, medications, and physical therapy [40]). When OA is severe, HA or TSA is usually recommended [41–43].

4.2.3 Rheumatoid Arthritis

Rheumatoid arthritis is an autoimmune-related disease, which is associated with the breakdown of articular cartilage, synovial membranes thickening, and inflammation. Thus, patients with rheumatoid arthritis usually suffer from bone ossification or fusing and limited motion. The treatment depends on the integrity of the RC. When the RC is irreparable, RSA is recommended. If the RC is intact, TSA or resurfacing HA is used, depending on the degree of glenoid erosion [44].

4.2.4 Proximal Humerus Fractures

There are four types of proximal humeral fractures (Fig. 6.5). Type 1 (Fig. 6.5a) refers to the fracture with collapse or necrosis on the humeral head; Type 2

(Fig. 6.5b) refers to the fracture with irreducible dislocations; Type 3 (Fig. 6.5c) refers to the facture with completely broken surgical neck; Type 4 (Fig. 6.5d) is the fracture with severe tuberosity malunions. For Type 1 and Type 2, TSA treatment is recommended. For Types 3 and 4, the treatment depends on the degree of RC deficiency. HA treatment is recommended for patients with intact RC, and RSA treatment is used for patients over the age of 65-years-old with massive RC tear [29].

4.2.5 Revision

The revision of the shoulder arthroplasty is usually recommended for the treatments of implant problems (i.e., loosening, wearing, improper sizing, and malposition), osseous problem (i.e., bone loss, glenoid arthrosis), and soft-tissue deficiency. It is reported that the application of RSA for the failed HA can increase the American Shoulder and Elbow Surgeons (ASES) score to 30, and improve the forward elevation from 38.1° to 72.7° [45].

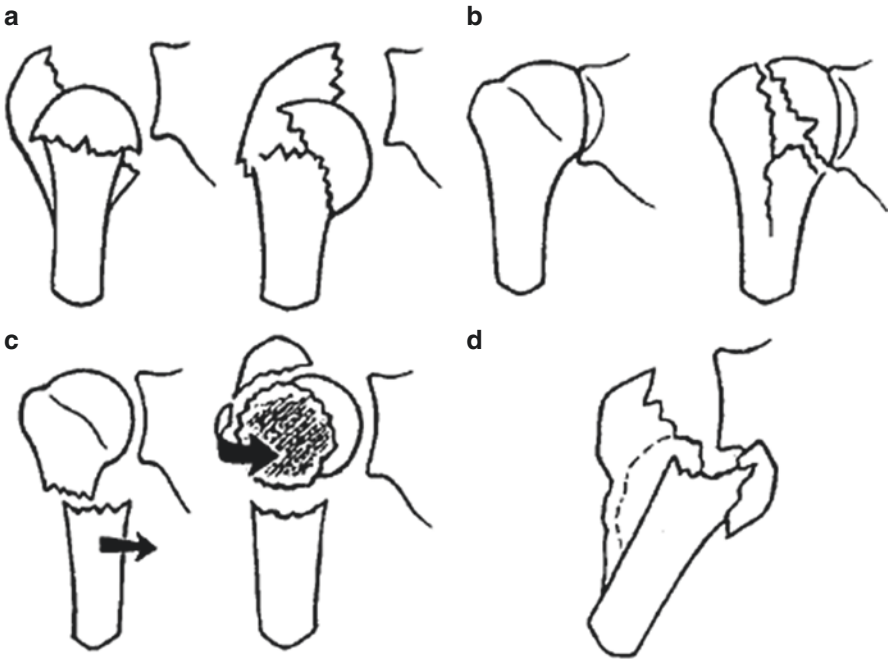

Fig. 6.5 (**a**) Type 1 proximal humeral fracture; (**b**) Type 2 proximal humeral fracture; (**c**) Type 3 proximal humeral fracture; (**d**) Type 4 proximal humeral fracture

5 Conclusions

The GH joint is an articulation with the compensation of a series of static and dynamic stabilizers. The static and dynamic stabilizers cooperate with each other to support the stability of the whole shoulder joint and achieve the shoulder motion. Once the stabilizing structure is disrupted, it may lead to clinical manifestations of the shoulder pain or instability. Therefore, treatments to the shoulder diseases and disorders are subjected to a clear understanding of the etiology of the shoulder problem and the designs of the shoulder arthroplasties.

References

1. Iannotti JP, Gabriel JP, Schneck S, Evans B, Misra S. The normal glenohumeral relationships. An anatomical study of one hundred and forty shoulders. JBJS. 1992;74(4):491–500.
2. Roberts S, Foley A, Swallow H, Wallace W, Coughlan D. The geometry of the humeral head and the design of prostheses. Bone Joint J. 1991;73(4):647–50.
3. Saha A, Das A, Dutta S. Mechanism of shoulder movements and a plea for the recognition of "zero position" of glenohumeral joint. Clin Orthop Relat Res. 1983;173:3–10.
4. Basmajian JV, Bazant FJ. Factors preventing downward dislocation of the adducted shoulder joint: an electromyographic and morphological study. JBJS. 1959;41(7):1182–6.
5. Friedman RJ, Hawthorne K, Genez B. The use of computerized tomography in the measurement of glenoid version. JBJS. 1992;74(7):1032–7.
6. Inman VT, Abbott LC. Observations on the function of the shoulder joint. JBJS. 1944; 26(1):1–30.
7. Su WR, Budoff JE, Luo ZP. The effect of coracoacromial ligament excision and acromioplasty on superior and anterosuperior glenohumeral stability. Arthroscopy. 2009;25(1):13–8.
8. Lee KW, Debski RE, Chen CH, Woo SL, Fu FH. Functional evaluation of the ligaments at the acromioclavicular joint during anteroposterior and superoinferior translation. Am J Sports Med. 1997;25(6):858–62.
9. Anthony AS, Brian DB. Sports medicine. Philadelphia, PA: Lippincott Williams & Wilkins; 2006.
10. Lucas DB. Biomechanics of the shoulder joint. Arch Surg. 1973;107(3):425–32.
11. O'Brien SJ, Neves MC, Arnoczky SP, Rozbruck SR, Dicarlo EF, Warren RF, et al. The anatomy and histology of the inferior glenohumeral ligament complex of the shoulder. Am J Sports Med. 1990;18(5):449–56.
12. Terry GC, Chopp TM. Functional anatomy of the shoulder. J Athl Train. 2000;35(3):248.
13. Martini FH, Nath JL, Bartholomew EF. Fundamentals of anatomy & physiology. New York: Pearson Education, Inc.; 2006.
14. Mochizuki T, Sugaya H, Uomizu M, Maeda K, Matsuki K, Sekiya I, et al. Humeral insertion of the supraspinatus and infraspinatus: new anatomical findings regarding the footprint of the rotator cuff. JBJS. 2008;90(5):962–9.
15. Richards DP, Burkhart SS, Tehrany AM, Wirth MA. The subscapularis footprint: an anatomic description of its insertion site. Arthroscopy. 2007;23(3):251–4.
16. Sahara W, Sugamoto K, Murai M, Tanaka H, Yoshikawa H. The three-dimensional motions of glenohumeral joint under semi-loaded condition during arm abduction using vertically open MRI. Clin Biomech. 2007;22(3):304–12.
17. Abboud JA, Soslowsky LJ. Interplay of the static and dynamic restraints in glenohumeral instability. Clin Orthop Relat Res. 2002;400:48–57.

18. Soslowsky LJ, Flatow EL, Bigliani LU, Mow VC. Articular geometry of the glenohumeral joint. Clin Orthop Relat Res. 1992;285:181–90.
19. Frankle MA, Teramoto A, Luo ZP, Levy JC, Pupello D. Glenoid morphology in reverse shoulder arthroplasty: classification and surgical implications. J Shoulder Elbow Surg. 2009;18(6):874–85.
20. Apreleva M, Parsons I IV, Warner JJ, Fu FH, Woo SL-Y. Experimental investigation of reaction forces at the glenohumeral joint during active abduction. J Shoulder Elbow Surg. 2000;9(5):409–17.
21. Mimar R, Limb D, Hall RM. Evaluation of the mechanical and architectural properties of glenoid bone. J Shoulder Elbow Surg. 2008;17(2):336–41.
22. Mansat P, Barea C, Hobatho MC, Darmana R, Mansat M. Anatomic variation of the mechanical properties of the glenoid. J Shoulder Elbow Surg. 1998;7(2):109–15.
23. Anglin C, Tolhurst P, Wyss UP, Pichora DR. Glenoid cancellous bone strength and modulus. J Biomech. 1999;32(10):1091–7.
24. Frich LH, Odgaard A, Dalstra M. Glenoid bone architecture. J Shoulder Elbow Surg. 1998;7(4):356–61.
25. Frich LH, Jensen NC, Odgaard A, Pedersen CM, Søjbjerg JO, Dalstra M. Bone strength and material properties of the glenoid. J Shoulder Elbow Surg. 1997;6(2):97–104.
26. Lehtinen JT, Tingart MJ, Apreleva M, Warner JJP. Total, trabecular, and cortical bone mineral density in different regions of the glenoid. J Shoulder Elbow Surg. 2004;13(3):344–8.
27. Kalouche I, Abdelmoumen S, Crepin J, Mitton D, Guillot G, Gagey O. Mechanical properties of glenoid cancellous bone. In: 16th ESB congress, London, UK; 2008.
28. Keaveny TM, Hayes WC. A 20-year perspective on the mechanical-properties of trabecular bone. J Biomech Eng T ASME. 1993;115(4):534–42.
29. Wiater MJ, Fabing MH. Shoulder arthroplasty: prosthetic options and indications. JAAOS. 2009;17(7):415–25.
30. Bailie DS, Llinas PJ, Ellenbecker TS. Cementless humeral resurfacing arthroplasty in active patients less than fifty-five years of age. JBJS. 2008;90(1):110–7.
31. Levy O, Copeland SA. Cementless surface replacement arthroplasty (Copeland CSRA) for osteoarthritis of the shoulder. J Shoulder Elbow Surg. 2004;13(3):266–71.
32. Craig E, Fukuda H. Cuff-tear arthropathy. JBJS. 1983;65(9):1232–44.
33. Joshi D. Reverse shoulder replacement soaring popularity. Orthopedics. 2009;5(22):23–6.
34. Sanchez-Sotelo J, Cofield R, Rowland C. Shoulder hemiarthroplasty for glenohumeral arthritis associated with severe rotator cuff deficiency. JBJS. 2001;83-A:1814–22.
35. Williams GR Jr, Rockwood CA Jr. Hemiarthroplasty in rotator cuff-deficient shoulders. J Shoulder Elbow Surg. 1996;5(5):362–7.
36. Boileau P. Neer award 2005: the Grammont reverse shoulder prosthesis: results in cuff tear arthritis, fracture sequelae, and revision arthroplasty. J Shoulder Elbow Surg. 2006;15(5): 527–40.
37. Guery J, Favard L, Sirveaux F, Oudet D, Mole D, Walch G. Reverse total shoulder arthroplasty: survivorship analysis of eighty replacements followed for five to ten years. JBJS. 2006;88:1742–7.
38. Sirveaux F, Favard L, Oudet D, Huquet D, Walch G, Mole D. Gammont inverted total shoulder arthroplasty in the treatment of glenohumeral osteoarthritis with massive rupture of the cuff: results of a multicentre study of 80 shoulders. Bone Joint J. 2004;86(3):388–95.
39. Susan BH. Basic biomechanics. Boston, MA: McGraw-Hill; 2007.
40. Michael L, Kelley T. Nonsurgical management of osteoarthritis of the knee. JAAPA. 2006;19(1):26–32.
41. Edwards TB, Kadakia NR, Boulahia A, Kempf J-F, Boileau P, Némoz C, et al. A comparison of hemiarthroplasty and total shoulder arthroplasty in the treatment of primary glenohumeral osteoarthritis: results of a multicenter study. J Shoulder Elbow Surg. 2003;12(3):207–13.
42. Lo IK, Litchfield RB, Griffin S, Faber K, Patterson SD, Kirkley A. Quality-of-life outcome following hemiarthroplasty or total shoulder arthroplasty in patients with osteoarthritis: a prospective, randomized trial. JBJS. 2005;87(10):2178–85.

43. Radnay CS, Setter KJ, Chambers L, Levine WN, Bigliani LU, Ahmad CS. Total shoulder replacement compared with humeral head replacement for the treatment of primary glenohumeral osteoarthritis: a systematic review. J Shoulder Elbow Surg. 2007;16(4):396–402.
44. Hedtmann A, Werner A. Shoulder arthroplasty in rheumatoid arthritis. Der Orthopade. 2007;36(11):1050–61.
45. Levy JC, Virani N, Pupello D, Frankle M. Use of the reverse shoulder prosthesis for the treatment of failed hemiarthroplasty in patients with glenohumeral arthritis and rotator cuff deficiency. Bone Joint J. 2007;89(2):189–95.

Chapter 7
Biomechanics of Spine

Lizhen Wang, Zhongjun Mo, Yuanjun Zhu, Enze Zhou, and Yubo Fan

Abstract Spinal disease including primary and secondary tumors occurs in various tissues such as nerve root, blood vessel, spinal cord, and so on. There was about 9.7 patient with spinal tumor in every 1 million. Spine laminectomy has usually been applied in treating the spinal cord tumor. Spinal instability after spine surgery was observed with high occurrence rate, due to excision of posterior structures. Total disc replacement (TDR) is an effective surgical method as well as anterior cervical discectomy and fusion (ACDF) to decompressing neural elements and restore disc height. With regard to keeping cervical spine's normal kinematics, TDR is more feasible and widely accepted than ACDF for treating degenerative cervical disc disease. It is important to investigate the biomechanical performances of ligament and vertebral on the spine stability in repair surgery, which would provide the theoretical

L. Wang · Y. Zhu · E. Zhou
Key Laboratory for Biomechanics and Mechanobiology of Ministry of Education, School of Biological Science and Medical Engineering, Beihang University, Beijing, China

Beijing Advanced Innovation Center for Biomedical Engineering, Beihang University, Beijing, China

Z. Mo
Beijing Key Laboratory of Rehabilitation Technical Aids for Old-Age Disability, Key Laboratory of Technical Aids Analysis and Identification of Ministry of Civil Affairs, National Research Centre for Rehabilitation Technical Aids, Beijing, China

Y. Fan (✉)
Key Laboratory for Biomechanics and Mechanobiology of Ministry of Education, School of Biological Science and Medical Engineering, Beihang University, Beijing, China

Beijing Advanced Innovation Center for Biomedical Engineering, Beihang University, Beijing, China

Beijing Key Laboratory of Rehabilitation Technical Aids for Old-Age Disability, Key Laboratory of Technical Aids Analysis and Identification of Ministry of Civil Affairs, National Research Centre for Rehabilitation Technical Aids, Beijing, China
e-mail: yubofan@buaa.edu.cn

C.-K. Cheng, S. L-Y. Woo (eds.), *Frontiers in Orthopaedic Biomechanics*,
https://doi.org/10.1007/978-981-15-3159-0_7

suggestion to disc or cage design. In this chapter, the cervical spine (C2–C7) with lamina repair surgery was studied at C3–C6 segments. The spinal stability in the adjacent segments with posterior ligaments excised was worse than the one with posterior ligament repaired. Repairing or preserving the posterior ligaments in the lamina repair surgery is benefit to spinal integrity and stability. On the other hand, the design of disc and the placement location of it were important factors for the postoperative rehabilitation, especially for the ROM (range of motion) of flexion/extension and the stress of implant. Therefore, reserving the range of motion and avoiding adverse problems should be taken into consideration, and more attentions also should be paid to a proper implant position along the anterior-posterior direction in ADR surgery.

Keywords Lamina repair · Ligament repair · Replacement · Disc design · Spinal biomechanics

1 Biomechanical Effect of Posterior Ligament Repair in Lamina Repair Surgery

Spinal tumors including primary and secondary tumors occurs in various tissues such as nerve root, blood vessel, spinal cord, and so on. The incidence rate of spinal tumor was 9.7 in 1 million [1]. Cervical laminectomy has usually been applied in treating cervical spinal cord tumor [2]. However, the occurrence rate of spinal instability after laminectomy was reportedly 20% in adults [3] and up to 45% in children [4], since the posterior structures of vertebrae, including interspinous ligament, supraspinous ligament, flaval ligament, and spinous process, also was excised with laminectomy [5]. Excision of posterior structures causes movement of the anterior vertebrae body, which induces declination and torsion of vertebral body, resulting in spinal instability [6, 7]. Previous studies reported the increase in ROM after laminectomies, which was likely to result in developing spinal kyphosis or other deformity [8–16]. Spinal deformity following laminectomy would oppress spinal cord or nerve root, and subsequently result in neurological symptoms as back pain and radiculopathy.

In order to avoid the complications caused by laminectomy, lamina repairment was firstly applied in clinics to treat intraspinal lesions in 1976 [17]. Since then, repairing of the excised lamina simultaneously with excision of the neoplasm was advocated to maintaining spinal stability and preserving daily activities of the spine [2, 18]. Good clinical results were found in the follow-up of the patients after lamina repairment surgery, which can maintain spinal integrity, and prevent postoperative instability, subluxation, and kyphotic deformities [19–22].

Nowadays, the resected ligamentum flavum (LF) and interspinous ligament (ISL) have not been repaired during lamina repair surgery. However, the posterior structures, including the vertebral arch, supraspinous ligament, and interspinal ligament, are believed to play important roles in tethering or tension constraint during anterior flexion [21]. Hotta [23] demonstrated the importance of ISL in the enhancement of spinal flexion stability. So, Sano [24] and Joson [25] proposed new methods to conserve ISL during laminectomy. Hirofuji [26] also suggested to reconstruct ISL by using artificial ligament. However, is there apparent benefits in terms of biomechanical performance with posterior ligament repairment in lamina repair surgery than that without posterior ligament repairment? In the present study, a finite element model of cervical spine (C2–C7) was constructed and used to simulate the lamina repairment surgery with and without lamina ligament repairment at C3–C6 segments, to explore the biomechanical effects of ligament repair on the cervical spinal stability in lamina repair surgery.

1.1 Construct a Healthy Cervical Model (C2–C7)

To develop the finite element model of the intact cervical spine (C2–C7), computerized tomographies (CT) of a healthy volunteer (male, 28 years, 60 kg, 173 cm) were achieved by CT scanner (Brilliance iCT, Philips, the Netherlands). The corresponding ethical committee has approved this research plan (No. IRB00006761-L2010021), and the participant signed the informed consent form. The CT scan images were imported into medical image-processing software (Mimics 15.1, Materialise Inc., Belgium) to rebuild the vertebrae's geometry. The intervertebral space was filled with a solid block as disc, which was divided into nucleus pulposus and annulus ground substance in a ratio of 4.3:5.7 [27, 28] by CAD software (Solidworks 2012, Dassault Inc., France). The vertebrae and intervertebral disc were meshed into tetrahedral elements and hexahedral elements, respectively, by using Hypermesh (12.0, Altair Inc., America). Finally, all the meshed vertebrae and discs were imported into finite element software (ABAQUS 6.14, Simulia Inc., USA) as separated solid volumes. A layer of shell with a thickness of 0.4 mm was generated by sharing the common nodes with the solid vertebrae volume (cancellous bone), and partitioned into cortical shell and endplate region. A layer of netlike truss elements (annulus fiber) were attached on the circumferential surface of the ground substance to simulate annulus fibrosus by sharing the common nodes. Intervertebral ligaments, including anterior longitudinal ligament (ALL), capsular ligament (CL), posterior longitudinal ligament (PLL), ligamentum flavum (LF), and interspinous ligaments (ISL), were simulated using tension-only nonlinear truss element (Fig. 7.1). In the healthy model of cervical spine, the total numbers of nodes and elements are 47,068 and 176,373, respectively. The material properties and mesh type of cervical components [29, 30] are listed in Table 7.1.

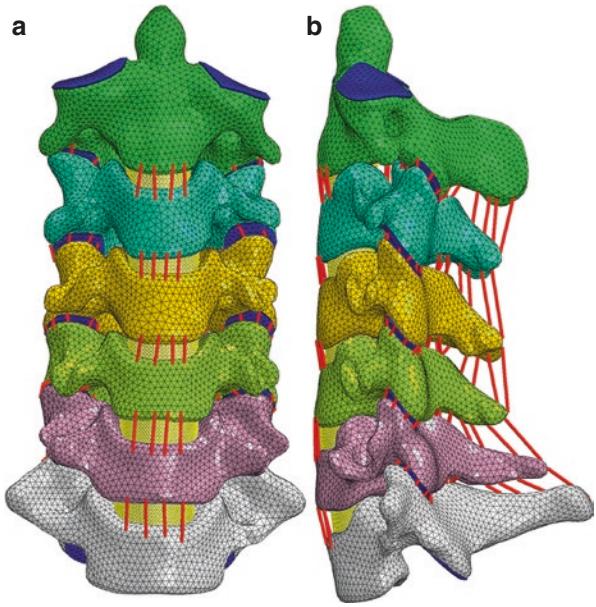

Fig. 7.1 Finite element model of C2–7 cervical spine: (**a**) anterior view and (**b**) sagittal view

Table 7.1 Mesh types and material properties of the cervical spine components

Components		Element type	Young modulus (MPa)	Poisson ratio	Cross section area (mm^2)
Cortical bone		S3	12,000.0	0.30	–
Cancellous bone		C3D4	450.0	0.30	–
Endplate		S3	1000.0	0.40	–
Articular cartilage		C3D6	10.0	0.30	–
Annulus fiber		T3D2	450.0	0.30	–
Annulus ground substance		C3D8	3.4	0.40	–
Nucleus pulposus		C3D8	1.0	0.49	–
Mini-plate and screw					
C2–C5	ALL	T3D2	26.3	0.40	11
	PLL	T3D2	22.2	0.40	11
	FL	T3D2	3.1	0.40	46
	CL	T3D2	3.3	0.40	42
	ISL	T3D2	4.9	0.40	13
C5–C7	ALL	T3D2	28.2	0.40	12
	PLL	T3D2	23.0	0.40	14
	FL	T3D2	3.5	0.40	49
	CL	T3D2	4.8	0.40	50
	ISL	T3D2	5.0	0.40	13

1.2 Construct the Lamina Repair and Lamina Ligament Repair Models

Based on the healthy model, all the FL and ISL at C2–C3 and C6–C7 levels were removed, and both the left and right sides of the laminas at C3–C6 were cut by gaps with 2 mm width, and then titanium alloy mini-plate is used to fix the lamina and spinous process to simulate the lamina repairment surgery (Fig. 7.2). The lamina ligament repair model (LLRM) was based on the lamina repair model (LRM) by reconstructing the FL and ISL at C2–C3 and C6–C7 segments. The metal components in the titanium mini-plate and screw were made of Ti6Al4V with the sizes of the mini-plate as 10 × 2 × 0.5 mm (length × width × height) and the screw as 4 × 1.6 mm (length × diameter).

1.3 Load and Boundary Conditions

The ligaments were inserted in corresponding position and attached on the adjacent vertebrae, to which the intervertebral disc was also adhered. The interaction between the facet joint cartilages was defined as surface-to-surface contact formulation with 0.1 friction coefficient. The bone-implant interface was assigned with a tie constraint to simulate thorough osseointegration. All models were immobilized at the

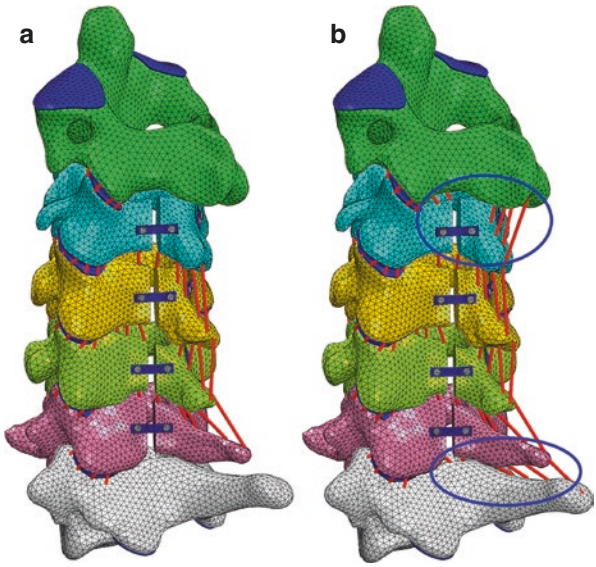

Fig. 7.2 Finite element model: (**a**) lamina repair and (**b**) lamina ligaments repair

C7 inferior endplate with 6 degrees of freedom. A pure moment of 1.5 Nm was applied at the top of the superior surface of the C2 vertebral body in all six principal directions to simulate flexion, extension, left and right axial rotation, and left and right lateral-bending motions in the healthy cervical spine. Subsequently, the pure moments of 1.5 Nm was also applied to the LRM and LLRM at the top of the superior surface of the C2 vertebral body.

1.4 ROM and Stress in the Healthy Cervical Spine

The ROM of each motion segment in the healthy model subjected to the pure moments of 1.5 Nm is shown in Fig. 7.3. The ROM was in agreement with the in vitro experimental data from the literature [31–33].

1.4.1 ROM in the LRM and LLRM

Compared with the healthy model, in the LRM, the ROM of C2–C3 in flexion, lateral bending, and axial rotation increased by 113.6%, 23.6%, and 28.5%, while that of C6–C7 increased by 88.9%, 12.8%, and 20.7%, and change of ROM in other segments under different conditions was less than 9.2%. The change of ROM at the corresponding levels in LLRM was lower than 7.2% compared to the healthy model (Fig. 7.4).

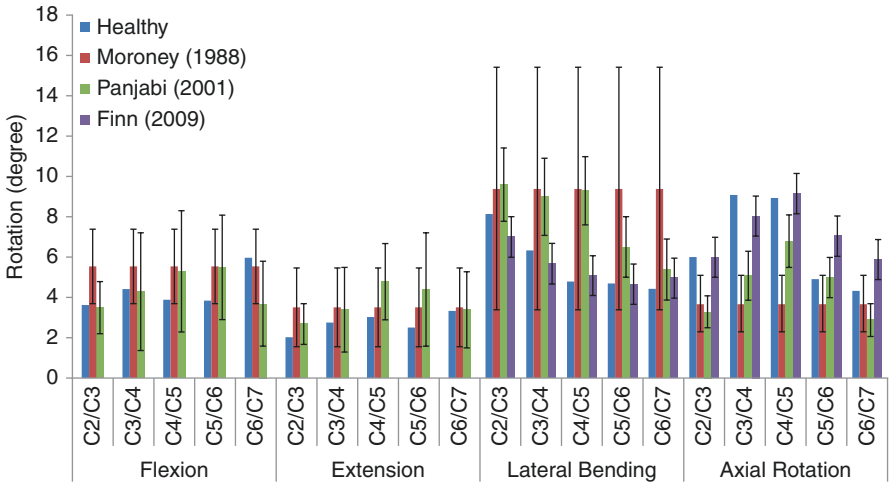

Fig. 7.3 Comparison of ROM in healthy cervical spine and data reported in the literature

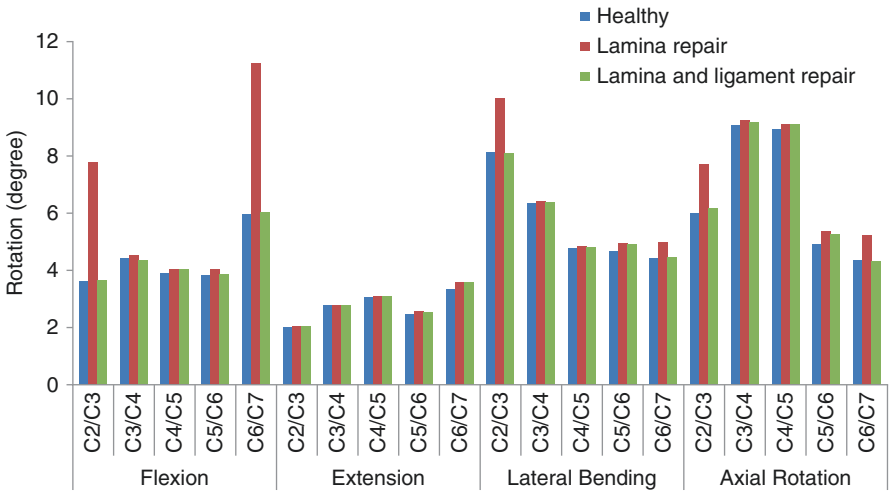

Fig. 7.4 ROM comparison of the healthy cervical spine and surgical models

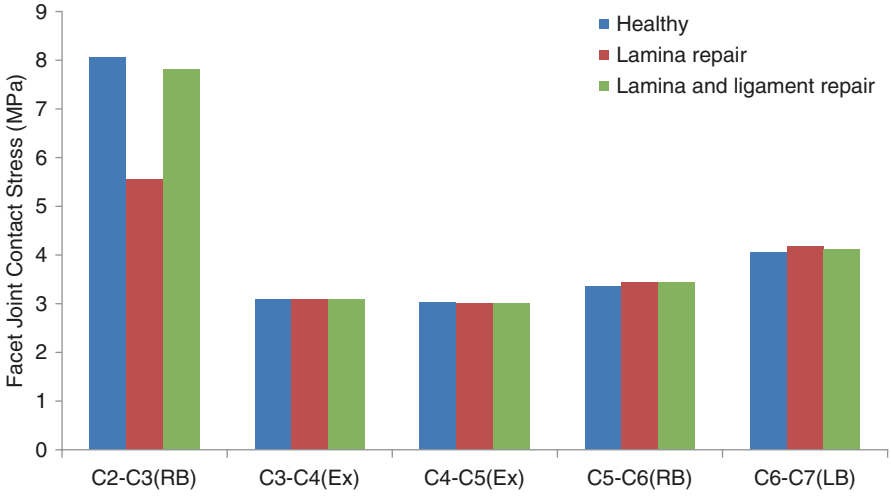

Fig. 7.5 Contact stress in facet joint in the healthy cervical spine and surgical models

1.4.2 Facet Joint Contact Stress

The maximal contact stress in the facet joint in each motion segment is shown in Fig. 7.5. In the LRM, the facet cartilage at C2–C3 was in a zero-stress state in flexion. Compared to healthy model, the maximal contact stresses of C2–C3 decreased by 31.0% in right bending. Compared to healthy model, the change of the maximal contact stresses in the LLRM was less than 3.0% in each motion segment.

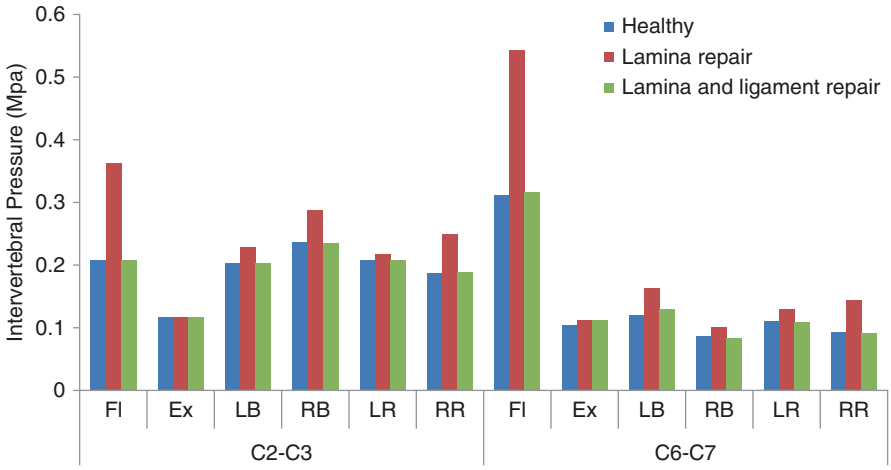

Fig. 7.6 Intradiscal pressure in the healthy cervical spine and surgical models

1.4.3 Intradiscal Pressure

The intradiscal pressure during different loading conditions in LRM increased by 4.1–73.7% at C2–C3 and 7.8–73.7% at C6–C7 segment compared with the normal model, and the greatest intervertebral pressure was detected during flexion. In the LLRM, the change of pressure were less than 11.5% in all loading conditions as shown in Fig. 7.6.

1.4.4 Stress of Capsular Ligament

In the LRM, the stress of capsular ligament under different loading conditions increased by 4.5–168.6% at C2–C3 and 9.5–115.6% at C6–C7 compared with the healthy model. However, in the LLRM, the change of the stresses (C2–C3, C6–C7) in all conditions was lower than 4.4% as shown in Fig. 7.7.

1.4.5 Stress on Bone-Screw Interface and Screw-Plate System

The stresses on the bone-screw interface and in the screw-plate system of C3–C6 are listed in Table 7.2. In the two kinds of surgical models, the differences of maximum stresses on screw and bone-screw interface was less than 6 MPa (C4 and C5) and 106 MPa (C3 and C6), respectively.

1.5 Comparison of with or Without Ligament After Repairment

Since lamina repairment was firstly proposed to treat intraspinal lesions by Raimondi, it is being gradually used widely. In many postoperative follow-ups, it was found that lamina repairment can maintain spinal stability and integrity, and

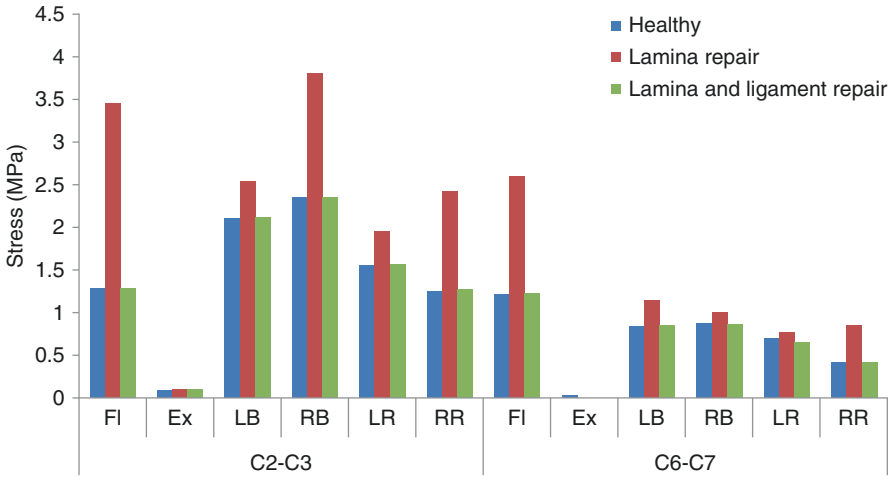

Fig. 7.7 Stress in the CL in the healthy cervical spine and surgical models

Table 7.2 Maximum Von Mises stress on bone-screw interface and screw-plate system (MPa)

	Model	C3	C4	C5	C6
Screw	LRM	144.6	115.9	130.4	116.2
	LLRM	112.9	115.1	133.9	164.8
Titanium plate	LRM	259.3	166.5	220.5	257.4
	LLRM	153.6	173.8	214.6	359.8
Bone-screw interface	LRM	1.458	1.45	2.085	1.844
	LLRM	1.69	1.389	2.105	1.654

prevent the development of spinal instability and kyphosis [20–23]. Nong et al. [34] performed a cadaveric study and proved that the lamina repairment surgery brought more stability than laminectomy. Healy et al. [35] also performed a cadaveric study to explore the effect of ISL on the spinal stability, and found that after excision of the ISL between C2–C3 and C7–T1, the ROM of C2–T1 increased by 7.9%, 2.4%, and 5.6% in flexion, bending, and rotation, while the ROM of C2–C3 and C7–T1 increased by 36.5% and 25.4% in flexion. Other studies demonstrated the importance of the ISL in the enhancement of spinal flexion stability, and they proposed methods to conserve or repair the posterior ligament during laminectomy [23–26].

In the present study, a healthy cervical model (C2–C7), a lamina repair model, and a lamina ligament repair model were built. The ROM of C2–C3 and C6–C7 in LRM had an obvious increase which range from 12.8% to 113.6% compared to the healthy model, whereas the ROM of C2–C3 and C6–C7 in LLRM were close to the healthy model (<7.2%). The significant difference of ROM in the adjacent segments (C2–C3 and C6–C7) in LRM and LLRM was due to whether the posterior ligaments existing. Since the physiologic role of ISL and FL include a tethering or tension constraint during anterior flexion [21], without ISL and FL can lead to a significant increase of the ROM, which was consistent with the experimental results

by Healy [35]. However, the changes of ROM at C3–C4, C4–C5, and C5–C6 in LRM and LLRM were not apparent in comparison with healthy model (<9.2%).

In LRM, the maximal contact stress in facet joint at C2–C3 was 0 MPa in flexion due to the absence of posterior ligaments, in comparison with healthy model, but the maximal stress of C2–C3 decreased by 31.0% in right bending. Nevertheless, there's no obvious change of maximal facet contact stress at each adjacent segments in the LLRM (<2.9%).

There is an evident increase of intradiscal pressure at C2–C3 and C6–C7 up to 73.7% in LRM, while the change at the corresponding segments in LLRM was not obvious (<11.5%). In LRM, the intradiscal pressure at C2–C3 and C6–C7 both increased by 73.7% in flexion, because the excision of posterior structures causes movement of the anterior part of vertebrae around the nucleus pulposus [6, 7], and the posterior ligaments had not been repaired in LRM; therefore, the disks in C2–C3 and C6–C7 have suffered much higher intradiscal pressure in flexion. The increase in intradiscal pressure is related to adjacent segment degenerations.

Compared to the healthy model, the maximal stresses in capsular ligament at C2–C3, C6–C7 in LRM increased obviously by up to 168.6%. Exaggerated stresses do harm to the ligaments and may affect long-term clinical results. However, the change of stresses at each motion segments in LLRM was small (<4.4%).

In LRM and LLRM, the difference of stresses on bone-screw interface and screw-plate system in C4, C5 was less than 6 MPa (2.7%), but the difference in C3, C6 was up to 105.7 MPa (41.8%).

Compared with the healthy model, the ROM, intervertebral pressure, facet joint contact stress, stresses of capsular ligament at C2–C3, C6–C7 had significant changes under different loading conditions in LRM. However, those parameters in LLRM were close to healthy cervical spine. In addition, the stresses on bone-screw interface and screw-plate system (C3, C6) between LRM and LLRM had great differences, because of the integrity of posterior ligaments. Besides, the variation tendency between LRM and LLRM was almost same in terms of ROM, intervertebral pressure, contact stress in facet joint, stresses in capsular ligament, and stresses on bone-screw interface and in screw-plate system (C3–C4, C4–C5, C5–C6). It meant that lamina repairment with posterior structure preserved can maintain stability of the cervical segments.

The study focused on the effect of with and without posterior ligaments in lamina repair surgery, and explored the biomechanical properties of cervical spine such as ROM, intervertebral pressure, facet joint contact stress, stresses of capsular ligament, etc. However, the soft tissues in maintaining the cervical spine stability is important; therefore, as part of this study to improve the accuracy of the cervical spine model, a more complete model with soft tissues (muscles) will be built in future study.

The spinal stability in the adjacent segments with posterior ligaments excised was worse than the one with posterior ligament repaired. Repairing or preserving the posterior ligaments in the lamina repair surgery is benefit to spinal integrity and stability. It is suggested to conserve or reconstruct the posterior ligaments in lamina repair surgery if the operation technology is realizable.

2 Sensitivity Study on Different ProDisc-C Arthroplasty Designs After Implanted

Total disc replacement (TDR) is an effective surgical method as well as anterior cervical discectomy and fusion (ACDF) to decompressing neural elements and restore disc height. With regard to keeping cervical spine's normal kinematics, TDR is more feasible and widely accepted than ACDF for treating degenerative cervical disc disease [36]. Various prostheses of cervical disc, such as the Bryan cervical disc, PCM prosthesis, Frenchay artificial cervical joint, Prestige II implant, and the ProDisc-C, are in commercial application or clinical trials. In 2008, Galbusera et al. [37] reviewed a number of biomechanical studies about total disc replacement, aiming to figure out the relationship between the geometrical, mechanical, and material properties of the various cervical disc prostheses. The study suggested that the biomechanics of the implanted spine was affected by the concepts of different design, which thus influence the clinical outcome.

Among the available devices, "ball-and-socket" shape is commonly employed for the prosthesis designs [38]. ProDisc-C (Synthes Inc., West Chester, PA, USA) is one of the typical ball-and-socket disc prostheses. It was composed of a hemispherical ball and a matched socket, over which the ball can roll. Therefore, the gliding spherical joint will be critical in the survival and biomechanics of the implanted spine. Rousseau et al. investigate two types of posterior geometric center simulated disc models with large radius and small radius and one type of anterior geometric center simulated disc with large radius to study the biomechanical changes in different geometrical parameter designs of a ball-and-socket disc prosthesis [39]. The result indicated that the ROM of all prostheses is basically same. The mean center of rotation and the force transmitted through the facet joints was primarily affected by the position of the geometric center and the radius of curvature, and the lowest facet forces were observed in the disc prostheses with posterior center and large radius design. However, the study has some limitations: only two radiuses of curvature (6 and 10 mm) and two positions of disc geometric center (0 or 3 mm posterior to the center of the endplate), which cannot exclude the accidental factors for lacking gradient variations [40].

Given the importance of the implantation position of the prosthesis on the biomechanics of the cervical spine, Galbusera et al. used the Monte Carlo method to study the effects of positional changes and generated random input parameters [41]. The results showed that the axial and anteroposterior position of the rotation center were the important factors affecting the flexibility of the spine, while the effect of the lateral position was not significant. The authors investigated the biomechanical effects of shape (oval vs. spherical ball) and location (inferior vs. superior ball) of various cervical artificial disc replacements. No major kinematic was observed in the design of the disc, but biomechanically, the oval design with an inferior ball component appeared to be closest to the intact spine.

Over all, a comprehensive biomechanical evaluation on the disc parameter variations is still lacking, especially considering the combination of radius of curvature

and positions. Therefore, the purpose of our study is to investigate biomechanical differences by changing the radius of curvature and the inserted position along the anteroposterior direction and lateral direction.

2.1 Model of Cervical Spine and Different Artificial Discs

2.1.1 Development of FE Model of Cervical Spine and Different Artificial Discs

The geometry model of the vertebrae was reconstructed based on the computed tomography (CT) scan images with the slice of 0.625 mm from a healthy male (32 years, 68 kg, 170 cm) through a commercial software MIMICS (Materialise, Belgium). Then a 3D nonlinear finite element model of the cervical spine was established using software ABAQUS 6.11 (Simulia Inc.). The intact FE model consists of intervertebral disc, endplate, and five groups of ligaments (anterior longitudinal, posterior longitudinal, capsular, ligamentum flavum, and interspinous ligaments). A layer of 0.4 mm thick shell was used to model the cortical bone surrounding the cancellous core. A nonlinear 3D contact was set to the facet joint. The intervertebral disc consists of the nucleus pulposus and the annulus fibrosus. The nucleus pulposus accounts for 33% of the total disc volume surrounded by the annulus fibrosus. Three-node link elements were used to simulate the annulus fibers, which were placed approximately 30 from the horizontal plane. Truss elements were used to reconstruct the ligaments and resisted tension only [40]. The detailed information about material properties and element types used to reconstruct the FE model of the cervical spine is described below (Table 7.1).

The basic ball-and-socket disc prostheses were constructed in ABAQUS 6.11 (Simulia Inc.). The geometry parameters were obtained from the product called Prodisc-C (Synthes Inc., West Chester, PA, USA). The Prodisc size M (width 15 mm, depth 12 mm, height 5 mm) with 5 mm radius of curvature was chosen to fit the specimen properly, and which was named as ProC-R5 [40].

Similarly, ProC-R4 with 4 mm radius of curvature and ProC-R6 with 6 mm radius of curvature were generated. The heights of the three models are consistent, and the superior endplate "socket" was altered for fitting the "ball" component with different radius of curvature (Fig. 7.8). The material properties of the cobalt-chromium-molybdenum endplates (Alloy of CoCrMo) and polyethylene core (UHMWPE) were set as linearly elastic materials (E = 220,000 MPa, υ = 0.32; E = 1000 MPa, υ = 0.49). The spherical joint between the two components was set as face-to-face contact with no friction to model the kinematical behavior. Then three FE models of different radiuses of curvature were generated and meshed into tetrahedron elements [40].

To simulating the anterior arthroplasty, the anterior longitudinal ligaments and intervertebral disc at C5–6 level were deleted. Each prostheses of intervertebral disc had 5 implantation sites that vary along the anteroposterior direction and lateral direction. And then these three types of prostheses were implanted at C5–6 level commonly

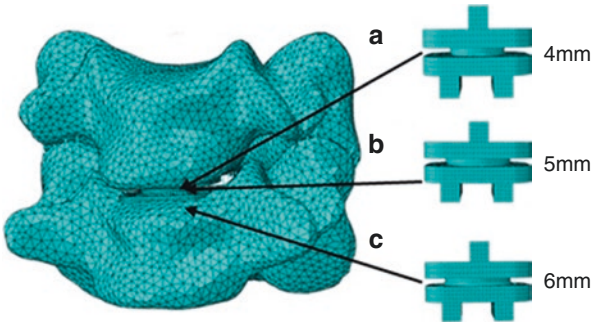

Fig. 7.8 The ball components of (**a**) ProC-R4, (**b**) ProC-R5, (**c**) ProC-R6 disc design

applied in surgery. As some studies had demonstrated the finite axes of rotation were sited below the disc and posterior to the endplate center [40, 42]. The center of the prostheses was set at a position called neutral position, and we named them N4, N5, N6 (4, 5, 6 for radius of curvature, N for neutral), respectively. The models implanted 2 mm anterior to the neutral position were named A4, A5, A6 (A means anterior). In the same way, other implanted models were built named P4, P5, P6 (1.2 mm Posterior to the neutral position; note that, the moving distance was different because the neutral position wasn't at central location of endplate), L4, L5, L6 (1 mm Left to the neutral position), and R4, R5, R6 (1 mm Right to the neutral position). Apart from the anterior position (15° from the horizontal plane), all prostheses were implanted at an angle of 12° to the horizontal for fitting the super-inferior endplate of this model well [40].

2.1.2 Loading and Boundary Conditions

For validation of the FE model, we constrained all degrees of freedom of C6 inferior endplate, and applied 74 N (an axial compression preload) at C5 superior surface's center, which was also applied 1.8 Nm (a pure moment) to simulate cervical spine movement: flexion, extension, bilateral bending, and axial rotation. Under the loading conditions, we calculated the range of motion (ROM) of the C5–C6 (an intact motion unit) and compared it with previous studies to validate the FE model [43]. Through validation, the intact FE model was established as containing 21,839 nodes and 112,117 elements.

After the validity of the intact FE model, the same boundary and loading conditions as described above was set to the models implanted with different types of Prodisc-C prostheses. The range of motion (ROM), the contact force of the facet joints, the stress of ligament, and the stress on Polyethylene core were recorded separately under respective loading conditions [40].

2.1.3 Validation of the Intact FE Model

The ROM of the C5–6 intact model in flexion//extension, lateral bending, and axial rotation was 7.41°, 4.23°, and 5.49°, respectively [40]. Compared with the previous studies [42], the ROM of the intact model was consistent with the published data

above. In addition to the validation, Lee et al. reviewed and summed up the ROM data from previous FE researches and in vitro experiments, finding that ROM of C5–6 segment ranged from 7.2° to 9.9° for flexion/extension in sagittal plane, ROM of C5–6 segment ranged from 3.1° to 15.4° for bilateral bending in coronal plane, and ROM of C5–6 segment ranged from 2.3° to 13.3° for axial rotation in transverse plane. Based on the fact that all the ROMs of C5–6 segment were within the range of results, we considered the motion unit of the 3D finite element model was valid.

2.1.4 Range of Motion After Implanted

7.41°, 4.23°, and 5.49° were observed in the ROM of the intact model in sagittal plane, coronal plane, and transverse plane, respectively. Compared with the intact FE model, both the ROM of the FE models implanted with different Prodisc-C prostheses and positions were all rose under the same external loading conditions. In flexion/extension load, the ROMs of ProC-R4 and ProC-R5 were approximately the same (difference <3%), but a remarkable increase was observed in ROM compared with ProC-R4 and ProC-R5 in any position. In lateral bending and axial rotation load, no apparent differences were seen among ProC-R4, ProC-R5, and ProC-R6 (<2% change). We can also find that there was a trend that the posterior position caused higher level of ROM to the neutral, middle, left, and right positions under every loading condition. The closest ROM was observed in N5 (ProC-R5 model with neutral position) compared with intact model. The highest ROM was observed in P6 model (ProC-R6 with posterior position), which was 25.2% and 23.9% higher than P4 and P5, respectively. The ROM of the intact model and models implanted with different Prodisc-C prostheses is described in Table 7.3.

2.1.5 Facet Joint Force

In flexion, the force of facet joint was observed in all positions for the prosthesis with 4 mm radius of curvature (ProC-R4), and second one was ProC-R5, and the largest force of facet joint occurred in the ProC-R6. In terms of the positions, facet force was highest in posterior among all positions. P6 model showed the maximum facet force (47.1 N), increased by 106.9% to the intact model. Compared with the

Table 7.3 The ROM of the intact model and models implanted with different Prodisc-C prostheses

	Flexion&Extension (°)	Left&Right bending (°)	Axial torsion (°)
Intact model	7.41	4.23	5.49
Pro-C-M	9.14	4.58	6.13
Pro-C-A	9.07	4.67	6.54
Pro-C-P	12.44	6.06	8.36
Pro-C-L	11.46	5.73	8.05
Pro-C-R	11.80	5.93	8.20

intact model, an increase was observed in force transmitted through the facet joints in all cases under extension, left-right lateral bending, and right axial torsion. Similar facet joint force was also observed in prostheses with different radius size (4, 5, 6 mm) in all the conditions. However, the changes were significant with the variation of the positions of implant. In left axial torsion, all models except for the anterior position showed the decrease of the facet force, with the increase of the A4, A5, and A6 by 2.69%, 7.23%, and 2.34%, respectively.

2.1.6 Ligament Tensile Stress

In flexion, the stress of the posterior longitudinal ligament (PLL) tensile in the intact model was 2.577 MPa as shown in Table 7.4. The increased percentage was 10.48%, 20.14%, 34.69%, 25.81%, and 30.77% for the ProC-R4 models with neutral, anterior, posterior, left, and right positions, respectively; 5.63%, 10.48%, 45.67%, 33.14%, and 37.10% for the ProC-R4 models; and 42.18%, 45.36%, 80.05%, 79.71%, and 86.03% for the ProC-R6. The stress of the capsular ligament (CL) was

Table 7.4 Ligaments tensile stress in flexion, extension, left bending, right bending, left torsion, and right torsion for intact model, ProC-R4, ProC-R5, and ProC-R6

		PLL	CL	FL	SL
Flexion	Intact model	2.577	2.698	0.4802	0.4288
	ProC-R4	2.858	3.003	0.5233	0.4918
	ProC-R5	2.722	2.765	0.4792	0.4387
	ProC-R6	3.693	3.713	0.6099	0.5681
Extension	Intact model	0	0.7841	0	0
	ProC-R4	0.5302	1.882	0	0
	ProC-R5	0.585	1.987	0	0
	ProC-R6	0.5522	1.923	0	0
Left bending	Intact model	0.8529	2.297	0.1217	0.07164
	ProC-R4	1.133	2.897	0.1438	0.08785
	ProC-R5	1.166	2.908	0.1436	0.0894
	ProC-R6	1.175	2.914	0.1373	0.0894
Right bending	Intact model	0.8197	2.117	0.1761	0.09752
	ProC-R4	1.137	2.802	0.1957	0.1143
	ProC-R5	1.147	2.659	0.1944	0.1115
	ProC-R6	1.206	2.794	0.1838	0.1078
Left torsion	Intact model	0.5332	2.928	0.1151	0.03631
	ProC-R4	0.8837	3.448	0.1341	0.0475
	ProC-R5	0.8977	3.409	0.1313	0.0468
	ProC-R6	0.9331	3.466	0.1302	0.051
Right torsion	Intact model	0.6196	2.316	0.1768	0.09282
	ProC-R4	1.003	3.225	0.1983	0.1106
	ProC-R5	1.008	3.014	0.1988	0.107
	ProC-R6	1.034	3.213	0.1835	0.1018

2.698 MPa in flexion. The increased percentage was 5.74%, 18.35%, 34.40%, 14.53%, and 36.77% for the ProC-R4 models with neutral, anterior, posterior, left, and right positions, respectively; 2.48%, 7.15%, 43.66%, 19.46%, and 40.96% for the ProC-R4 models; and 39.66%, 42.18%, 87.88%, 67.27%, and 95.48% for the ProC-R6.

In extension, the tensile stress of PLL was zero, 0.438, 0.637, 0.987, and 0.874 MPa in the ProC-R4 models in five positions, respectively; 0.585, 0.864, 1.171, 1.008, and 1.334 MPa for the ProC-R5 models; and 0.519, 0.7662, 1.050, 0.969, and 1.292 MPa for the ProC-R6 models. Also, for the tensile stress of CL apparently increasement was seen in all models, which was up to 114.39–305.31% compared with the intact model.

In lateral bending and axial rotation, compared with the intact model, increasement was observed in all models for the tensile stress of PLL and CL. However, the ligament tensile stress of different radiuses and position models were similar, no marked changes observed.

2.1.7 Stress on the Ball Component

The stresses on the polyethylene (PE) ball component of different designs were measured under flexion, extension, bilateral bending, and axial rotation conditions, and the stresses were maximal in flexion compared with other loading conditions. In flexion, the stress of 93.96, 54.63, 127, 128.6, and 130.7 MPa were seen on polyethylene ball of ProC-R4 models with neutral, anterior, posterior, left, and right positions, respectively; 75.61, 84.75, 97.66, 87.91, and 111.7 MPa were seen on polyethylene ball of the ProC-R5 models; and 16.18, 16.77, 15.97, 18.3, and 19.55 MPa were seen on polyethylene ball of the ProC-R6 models, which decreased markedly. In all positions, the stresses distributions of ProC-R4 and ProC-R5 were concentrated on the part anterior to the PE ball and the maximum stresses—130.7 and 111.7 MPa—were observed in right position. As for the ProC-R6, the stress was distributed at the edge of the joint between the hemisphere and plate, and the maximum stress—19.55 MPa—was also observed in right position as shown in Table 7.5.

In this part, we investigated and quantified the theoretical effects on the spine biomechanics of the ball-and-socket TDR at the C5–6 level with prostheses of 3 designs and 5 implanted positions. These variations were related to not only design parameters (radius of curvature) but also surgical procedure (the positioning and insertion trajectory varied along the anteroposterior direction and lateral direction).

Table 7.5 Stress on the ball component in flexion, extension, left bending, right bending, left torsion, and right torsion for intact model, ProC-R4, ProC-R5, and ProC-R6

	Flexion	Extension	Left bending	Right bending	Left torsion	Right torsion
ProC-R4	144.2	29.52	16.72	16.93	17.2	16.59
ProC-R5	75.61	18.95	13.96	13.65	14.47	13.95
ProC-R6	12.06	17.39	4.932	5.144	5.661	4.885

We observed the major changes in ROM, stress on polyethylene ball, the force of the facet joint, and the tensile stress of ligament, which were influenced by the sizes of implant and the implanted position.

After the implantation of prostheses, the ROM data of C5–C6 finite element cervical model in this study presented an increase compared with the intact model. This result was in accordance with the previous study, in which ROM increased after replacing the disc with the semi-constrained ProDisc-C at the treated segment. Meanwhile, in flexion/extension there was increasement observed in the ROMs of ProC-R4, ProC-R5, and ProC-R6 and the increasement was lager in ProC-R6. However, we do not find the same phenomenon in lateral bending and axial rotation. These suggested that the influence of different radius of curvature on the ROM was not obvious apart from flexion/extension. Rousseau et al. [39] verified our results through the finite element analysis of three types of ball-and-socket designs (PL, PS, and CL), in which they found that the ROMs increased in flexion/extension but was consistent with the intact model in axial rotation and bilateral bending.

Most studies found the ROMs can preserve the general motion and similar to the physiological values, regardless of the various prosthesis designs, which mean prosthesis design more strongly related to the quality of motion, than to the quantity [41]. Some similar researches have indicated that the typical motion quality was the location of rotation axis [43, 44]. The mean center of rotation (MCR) was analyzed, finding that the intact model's MCR was at the posterior one-third of the lower vertebra endplate and varied in a certain area under flexion/extension [39]. With regard to different types of prostheses, MCR presented a trend to match the prosthesis center. It is a matter of course that the variation of the position of the implant accompanied by that of MCR based on this fact. Therefore, the larger ROM was seen in posterior position models, the rotation axis of which was adjacent to the actual center of rotation axis. Take the radius of curvature into account; in order to keep the height of the disc, the MCR of ProC-R4, ProC-R5, and ProC-R6 would change as the hemisphere moves up and down. Probabilistic variables were investigated in the center of rotation (COR). The intervertebral rotation was affected by the anteroposterior position of COR only in flexion/extension, but not being affected by the lateral position of the COR. In this part, it is really no apparent difference from left to right positions, but they all differed greatly from the neutral position. After the prosthesis being implanted, the force of the facet joint was observed to be less than that of ProC-R5 and ProC-R6 in most kinetic situations, and there were significant distinctions in flexion, with the value of P6 being the largest. It was also found that the maximum ROM was seen in ProC-R6 model with posterior position (P6) in flexion/extension. It seemed that the larger force of facet joint was caused by the lager ROM. Although some researches have pointed out this phenomenon [44], the relevance between ROM and force of facet joint still remained to be figured out. Womack et al. employed ProDisc-C models varying with 5-, 6-, and 7-mm implant heights to explore the effects of the size of implant, founding that the size of implant influenced contact force of facet without influencing the ROM [45]. It was demonstrated that the force of facet joint was vulnerable to the variation of implanted positions, but no tendency was observed.

The capsular ligament (CL) was associated with the force of facet joint and the related pain, so it was paid main attention in preview studies. In the part, increased tensile stress of CL was observed in all cases after implantation. And the ligament tensile stress of larger radius model with posterior position is the largest, while capsular ligament tension of model with neutral and anterior positions slightly reduced. The overmuch tensile stress companied by the force of facet joint may cause fatigue damage, and partially affected the adjacent ligament, finally had a bad impact on the long-term clinical results [40].

For each prosthesis implanted, the stress distribution on the core of PE is approximately similar, no matter how the position of implant varied, and the maximum value of stress was witnessed in flexion. The stress of ProC-R4 and ProC-R5 concentrated on the part anterior to the PE ball. In contrast, the pressure of ProC-R6 was lower and spread over the joint edge between plate and hemisphere. In view of this point, ProC-R6, a prosthesis having a larger curvature, seemingly could lower the stress of implant and avoid the concentration of stress. In the long run, this (large curvature) design may delay spherical bearing wear on surfaces, thereby avoiding the inflammatory reactions caused which wear debris led to. Speaking of wear debris, most studies primarily focused on osseointegration and biological response (to wear debris) at the interface between prosthesis and bone. A caprine model was used to assess the biomechanical characteristic. No evidence of wear particles or loosening implant (subluxation) was found, while it was reported that one patient implanted the PCM disc had a large amount of wear debris [40, 46].

Based on the observation, the ROM, force of facet joint and tension of capsule ligament were affected by the radius of implanted prosthesis, while the position had an influence on all these aspects under all loading conditions. These aspects (the ROM, force of facet joint and tension of capsule ligament) are sensitive to the position in anteroposterior direction. The disc having larger curvature has less stress on the polyethylene, which can avoid stress concentration, but bring adverse outcomes such as increased force of facet joint and tension of ligament. Therefore, the design of disc prosthesis should be considered retaining the range of motion as well as avoiding the adverse problems, so as not to affect the long-term clinical results [40].

In summary, surgical procedure such as repairing or preserving the posterior ligaments in the lamina repair surgery and better implant design are important factors for the postoperative rehabilitation, especially the range of motion (ROM) of flexion/extension and implant stress, and spinal integrity and stability. Thus, a proper implant design should consider reserving the range of motion as well as avoiding adverse problems, and a proper surgical procedure and implant position along the anterior-posterior direction ought to be paid more attentions in spine biomechanics.

Acknowledgement This work was supported by Beijing Municipal Science and Technology Project (No. 161100001016013).

References

1. Duetzmann S, Cole T, Ratliff JK. Cervical laminoplasty developments and trends, 2003–2013: a systematic review. J Neurosurg Spine. 2015;23:24–34.
2. Hirabayashi K, Watanabe K, Wakana KR, et al. Expansive open-door laminoplasty for cervical spinal stenotic myelopathy. Spine. 1983;8:693–9.
3. Katsum Y, Honma T, Nakamura T. Analysis of cervical instability resulting from laminectomies for removal of spinal cord tumor. Spine. 1989;14:1171–6.
4. Yeh JS, Sgouros S, Walsh AR, et al. Spinal sagittal malalignment following surgery for primary intramedullary tumours in children. Pediatr Neurosurg. 2001;35:318–24.
5. Haddadi A, Qazvini HR. Outcome after surgery of lumbar spinal stenosis: a randomized comparison of bilateral laminotomy, trumpet laminectomy, and conventional laminectomy. Front Surg. 2016;3:19. https://doi.org/10.3389/fsurg.2016.00019.
6. Kotani Y, Cunningham BW, Abumi K, et al. Biomechanical analysis of cervical stabilization systems: an assessment of transpedicular screw fixation in the cervical spine. Spine. 1994;19:2529–39.
7. McGirt MJ, Garces-Ambrossi GL, Parker SL, et al. Short-term progressive spinal deformity following laminoplasty versus laminectomy for resection of intradural spinal tumors: analysis of 238 patients. Neurosurgery. 2010;66:1005–12. https://doi.org/10.1227/01.NEU.0000367721.73220.C9.
8. Goel VK, Clark CR, Harris KG, et al. Kinematics of the cervical spine: effects of multiple total laminectomy and facet wiring. J Orthop Res. 1988;6:611–9.
9. Kode S, Kallemeyn NA, Smucker JD, et al. The effect of multi-level laminoplasty and laminectomy on the biomechanics of the cervical spine: a finite element study. Iowa Orthop J. 2014;34:150–7.
10. Tadepalli SC, Gandhi AA, Fredericks DC, et al. Cervical laminoplasty construct stability: an experimental and finite element investigation. Iowa Orthop J. 2011;31:207–14.
11. Xie T, Qian J, Lu Y, et al. Biomechanical comparison of laminectomy, hemilaminectomy and a new minimally invasive approach in the surgical treatment of multilevel cervical intradural tumour: a finite element analysis. Eur Spine J. 2013;22:2719–30. https://doi.org/10.1007/s00586-013-2992-1.
12. Saito T, Yamamuro T, Shikata J, et al. Analysis and prevention of spinal column deformity following cervical laminectomy. I. Pathogenetic analysis of postlaminectomy deformities. Spine. 1991;16:494–502.
13. Ng HW, Teo EC, Zhang QH. Influence of laminotomies and laminectomies on cervical spine biomechanics under combined flexion-extension. J Appl Biomech. 2004;20:243–59.
14. Ng HW, Teo EC, Zhang QH. Biomechanical effects of C2-C7 intersegmental stability due to laminectomy with unilateral and bilateral facetectomy. Spine. 2004;29:1737–45.
15. Ogden AT, Bresnahan L, Smith JS, et al. Biomechanical comparison of traditional and minimally invasive intradural tumor exposures using finite element analysis. Clin Biomech. 2009;24:143–7.
16. Ahmed R, Menezes AH, Awe OO, et al. Long-term incidence and risk factors for development of spinal deformity following resection of pediatric intramedullary spinal cord tumors. J Neurosurg Pediatr. 2014;13:613–21.
17. Raimondi AJ, Gutierrez FA, Di RC. Laminotomy and total reconstruction of the posterior spinal arch for spinal canal surgery in childhood. J Neurosurg. 1976;45:555–60.
18. Wiedemayer H, Schoch B, Stolke D. Osteoplastic laminotomy using titanium microplates for reconstruction of the laminar roof: a technical note. Neurosurg Rev. 1998;21:93–7.
19. Jeon SC, Chough CK, Park HK, et al. Surgical technique and long-term follow-up of cervical laminoplasty using titanium miniplates. J Korean Neurosurg. 2004;36:369–74.
20. Hida S, Naito M, Arimizu J, et al. The transverse placement laminoplasty using titanium miniplates for the reconstruction of the laminae in thoracic and lumbar lesion. Eur Spine J. 2006;15:1292–7. https://doi.org/10.1007/s00586-006-0099-7.

21. Menku A, Koc RK, Oktem IS, et al. Laminoplasty with miniplates for posterior approach in thoracic and lumbar intraspinal surgery. Turk Neurosurg. 2010;20:27–32.
22. Zhou D, Nong L, Gao G, et al. Application of lamina replantation with ARCH plate fixation in thoracic and lumbar intraspinal tumors. Exp Therap Med. 2013;6:596–600. https://doi.org/10.3892/etm.2013.1170.
23. Hotta H. An experimental study on stability of human spine, especially the role of the lumbar ligaments. J Jpn Orthop Assoc. 1976;50:1–14.
24. Sano S, Masuda A, Kabata K, et al. Laminectomy with spinous process reattachment—preliminary report. Orthop Surg Traumatol. 1983;26:1227–30.
25. Joson RM, McCormick KJ. Preservation of the supraspinous ligament for spinal stenosis: a technical note. Neurosurgery. 1987;21:420–2.
26. Hirofuji E, Tanaka K, Nakano A. Ligamentous reconstruction with artificial ligament to prevent the unstable lumbar spine. Clin Orthop Surg. 1990;25:501–6.
27. Zhao Y, Li Q, Mo Z, et al. Finite element analysis of cervical arthroplasty combined with fusion against 2-level fusion. J Spinal Disord Tech. 2013;26:347–50.
28. Mo Z, Zhao Y, Du C, et al. Does location of rotation center in artificial disc affect cervical biomechanics? Spine. 2015;40:E469–75.
29. Yoganandan N, Kumaresan S, Pintar FA. Geometric and mechanical properties of human cervical spine ligaments. J Biomech Eng. 2000;122:623–9.
30. Li Q, Mo Z, Fan Y. Biomechanical comparison of cervical arthroplasty with and without posterior longitudinal ligament resection: a finite element study. J Med Imaging Health Inf. 2016;6:1559–65. https://doi.org/10.1166/jmihi.2016.1848.
31. Panjabi MM, Crisco JJ, Vasavada A, et al. Mechanical properties of the human cervical spine as shown by three-dimensional load displacement curves. Spine. 2001;26:2692–700.
32. Finn MA, Brodke DS, Daubs M, et al. Local and global subaxial cervical spine biomechanics after single-level fusion or cervical arthroplasty. Eur Spine J. 2009;18:1520–7. https://doi.org/10.1007/s00586-009-1085-7.
33. Moroney SP, Schultz AB, Miller JAA, et al. Load-displacement properties of lower cervical spine motion segments. J Biomech. 1988;21:769–79.
34. Nong L, Zhou D, Xu N, et al. Lamina replacement with titanium plate fixation improves spinal stability after total lumbar laminectomy. Comput Methods Biomech Biomed Eng. 2014;18:1753–9.
35. Healy AT, Lubelski D, West JL, et al. Biomechanics of open-door laminoplasty with and without preservation of posterior structures. J Neurosurg Spine. 2016;24:1–6.
36. Park JJ, Quirno M, Cunningham MR, et al. Analysis of segmental cervical spine vertebral motion after prodisc-C cervical disc replacement. Spine. 2010;35(8):E285–9.
37. Galbusera F, Bellini CM, Brayda-Bruno M, et al. Biomechanical studies on cervical total disc arthroplasty: a literature review. Clin Biomech. 2008;23(9):1095–104.
38. Puttlitz CM, DiAngelo DJ. Cervical spine arthroplasty biomechanics. Neurosurg Clin N Am. 2005;16(4):589–94.
39. Rousseau MA, Bonnet X, Skalli W. Influence of the geometry of a ball-and-socket intervertebral prosthesis at the cervical spine: a finite element study. Spine. 2008;33(1):E10–4.
40. Tang Q, Wang L, Mo Z, et al. Biomechanical analysis of different prodisc-C arthroplasty designs after implantation: a numerical sensitivity study. J Mech Med Biol. 2015;15(1):1550007.
41. Galbusera F, Anasetti F, Bellini CM, et al. The influence of the axial, antero-posterior and lateral positions of the center of rotation of a ball-and-socket disc prosthesis on the cervical spine biomechanics. Clin Biomech. 2010;25(5):397–401.
42. Bogduk N, Mercer S. Biomechanics of the cervical spine. I: normal kinematics. Clin Biomech. 2000;15(9):633–48.
43. Ha SK. Finite element modeling of multi-level cervical spinal segments (C3–C6) and biomechanical analysis of an elastomer-type prosthetic disc. Med Eng Phys. 2006;28(6):534–41.
44. Ahn HS, DiAngelo DJ. A biomechanical study of artificial cervical discs using computer simulation. Spine. 2008;33(8):883–92.

45. Womack W, Leahy PD, Patel VV, et al. Finite element modeling of kinematic and load transmission alterations due to cervical intervertebral disc replacement. Spine. 2011;36(17):E1126–33.
46. Pitzen T, Kettler A, Drumm J, et al. Cervical spine disc prosthesis: radiographic, biomechanical and morphological post mortal findings 12 weeks after implantation. A retrieval example. Eur Spine J. 2007;16(7):1015–20.

Chapter 8
Biomechanics of the Hip

Bolun Liu, Jia Hua, and Cheng-Kung Cheng

Abstract The hip joint is a crucial support structure for the human body structure, second only to the knee in the terms of weight-bearing forces placed upon it, and is an essential joint for walking. A solid understanding of the anatomy and biomechanics of the hip joint is necessary for improving treatments for hip disorders and for the design of hip prostheses. In this chapter, the anatomy of the hip joint is introduced and is then followed by a more in-depth analysis of the kinetic and kinematic movements of the joint.

Keywords Hip joint · Anatomy · Biomechanics · Kinematics · Kinetics

1 Anatomy of the Hip

The femoral head and acetabulum form a ball-and-socket joint (Fig. 8.1), which is surrounded and protected by powerful muscles, tendons, and a ligamentous capsule. Both the femoral head and acetabulum are covered with articular cartilage and separated by a small volume of synovial fluid which is produced by the synovial membrane. The synovial fluid keeps the cartilage nourished and provides lubrication for the joint. The bones, muscles, tendons, ligaments, and synovial fluid work together to make the hip joint flexible, stable, and strong.

B. Liu
School of Biological Science and Medical Engineering, Beihang University, Beijing, China

J. Hua
Department of Nature Science, Faculty of Science and Technology, Middlesex University, London, UK

C.-K. Cheng (✉)
School of Biomedical Engineering, Shanghai Jiao Tong University, Shanghai, China
e-mail: ckcheng2020@sjtu.edu.cn

C.-K. Cheng, S. L-Y. Woo (eds.), *Frontiers in Orthopaedic Biomechanics*,
https://doi.org/10.1007/978-981-15-3159-0_8

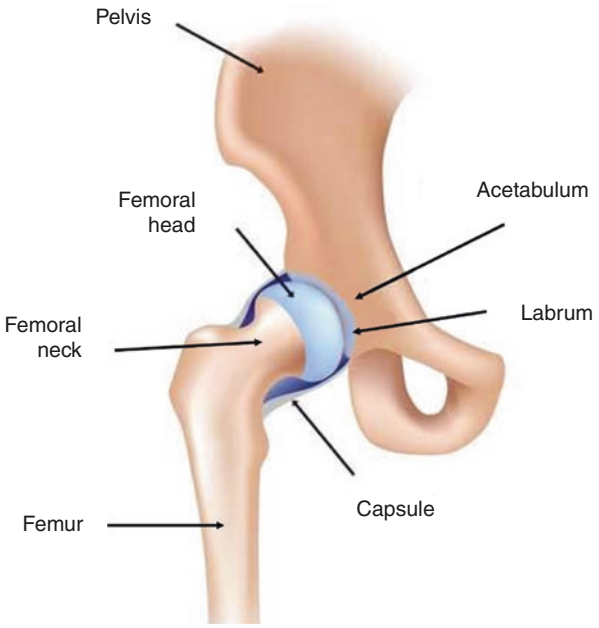

Fig. 8.1 Anatomy of the hip joint

1.1 Bony Structure

1.1.1 Acetabulum

The acetabulum resembles a concave hemisphere and is closely matched to the shapes of the femoral head.

The cup-shaped acetabulum is located at the intersection of three pelvic bones—the ilium (40% area of acetabulum), ischium (40%), and pubis (20%) [1]. These three bones are connected by cartilage by the time a person reaches the age of 14. The cartilage begins to ossify at around the age of 14–16 and ends at the age of 23 [2].

The acetabulum is oriented inferiorly, laterally, and anteriorly. The angle between the open plane of the acetabulum and the sagittal plane can be used to describe the level of anteversion of the acetabulum, which is critical for flexion stability of the hip joint. On a radiograph, the anteversion angle of the acetabulum is determined as the angle between a line drawn through the anterior and posterior edge of acetabulum and a line perpendicular to a line connecting the posterior pelvic margins at the level of the sciatic notch (Fig. 8.2). The anteversion angle of the acetabular (AV.A) is an index to measure the coverage of the femoral head by the acetabulum in the horizontal plane. The mean acetabular anteversion is about 23°. The acetabular anteversion increases slightly with age and the value in men is about 2.7° lower than that in women [3]. Excessive AV.A have been linked to greater joint instability and a greater prevalence of anterior dislocation of femoral head.

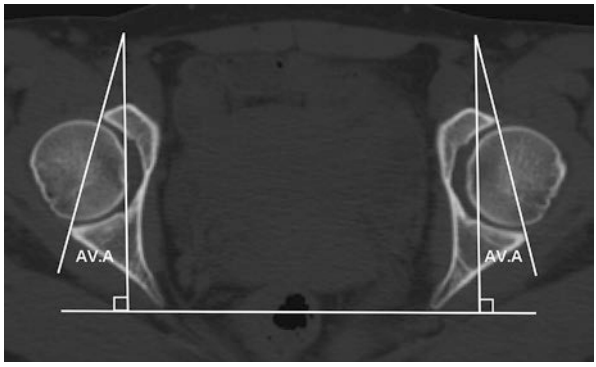

Fig. 8.2 Measurement of the anteversion angle of the acetabulum

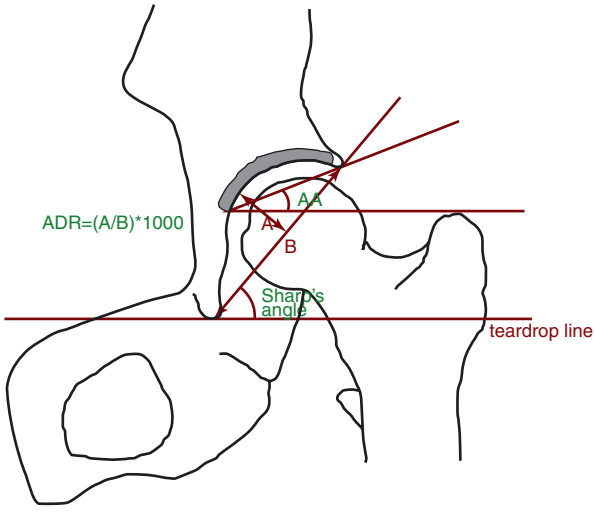

Fig. 8.3 Measurement of Sharp's angle, the acetabular roof angle (AA), and the acetabular depth-width ratio (ADR) [4] (Reprinted with permission from 'Skeletal Radiology'. License Number: 4567410923053)

The morphology of acetabulum is a primary factor cause of developmental dysplasia of the hip (DDH) and femoroacetabular impingement (FAI). Therefore, correctly evaluating the morphology of acetabulum is necessary for the clinical diagnosis of DDH and FAI. The indices, namely Sharp's angle, acetabular roof angle, acetabular depth-to-width ratio, center-edge angle, and femoral head extrusion index, are often used for describing the acetabular morphology and diagnosing DDH [4, 5].

The Sharp's angle, which is measured between the acetabular margin line and teardrop line on the coronal plane, is an index for reflecting lateral coverage of the femoral head (Fig. 8.3). The normal range of the Sharp's angle is between 33° and 38°, and an angle of greater than 42° is considered as dysplastic [6].

Tönnis detailed a method of using the acetabular roof angle to measure the inclination of the acetabular load-bearing surface on anterior-posterior radiographs of the hip [7]. The load-bearing surface of the acetabulum, also known as the acetabular sourcil, is an area of dense bone on the acetabular roof. The acetabular roof angle

is formed between a line connecting the medial sourcil and lateral rim of the acetabulum and a horizontal line between the lowest points of two teardrops (Fig. 8.3). The acetabular roof angle typically ranges from 0° to 10°, while greater than 10° can be considered as hip dysplasia. A larger angle generally means a more unstable hip joint, while an angle of less than 0° indicates that the acetabulum tends to overcover the femoral head [7].

The acetabular development can be evaluated by the acetabular depth-to-width ratio (ADR) [8], which is calculated by depth/width × 1000. The width of the acetabulum is measured as the distance between the tip of the inferior teardrop to the lateral rim of the acetabulum on the coronal plane (Fig. 8.3). The depth is the distance between the deepest point of the acetabulum to a line connecting the medial and lateral rim of the acetabulum [9]. A depth-to-width ratio of less than 250 is considered hip dysplasia [10].

The bony coverage of the femoral head by the acetabulum provides inherent stability for the hip joint. The center-edge angle (CE angle) was first proposed by Wiberg [11] to describe the relationship between the femoral head and acetabulum. The CE angle is formed by the intersection of a line through the center of femoral head and superolateral rim of acetabulum and a vertical line passing through the center of the femoral head (Fig. 8.4a). A CE angle of over 25° is normal in adults, lower than 20° is associated with DDH [11, 12], and an angle greater than 39° is considered as acetabular over-coverage, which often causes impingement.

Another index for measuring the bony coverage of the femoral head by the acetabulum is the femoral head extrusion index (FHEI). This index is calculated as the percentage of the uncovered portion of the femoral head to the width of the femoral head (Fig. 8.4b) and is useful in assessing developmental dysplasia as well as femoroacetabular impingement. Values between 17 and 27% are considered within the normal range. An FHEI of greater than 27% may be categorized as developmental dysplasia, while values lower than 17% can be considered as overcoverage [13].

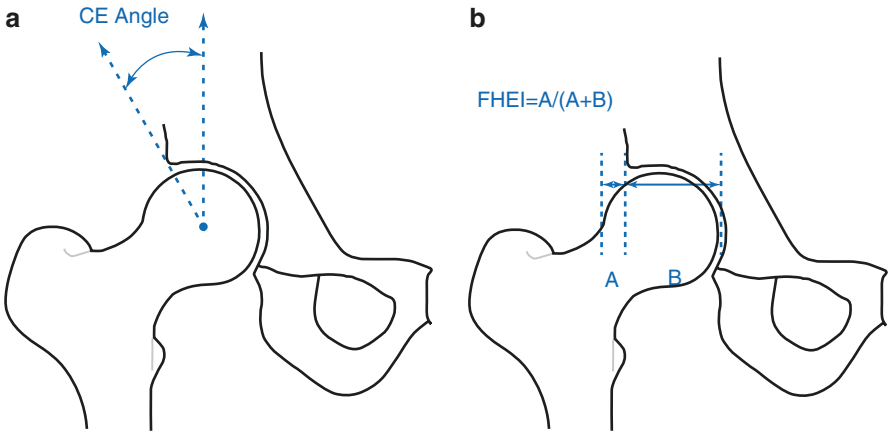

Fig. 8.4 Measurement of center-edge (CE) angle (**a**) and femoral head extrusion index (FHEI) (**b**)

1.1.2 The Acetabular Labrum

The acetabular labrum is a circular fibrocartilage structure with a triangular cross section which attaches directly to the bony edge of the acetabulum (Fig. 8.1). The labrum joins the transverse ligament at the lower rim of the acetabulum to form a continuous and complete sealing ring. An adult labrum has an average circumference of around 16 cm for males and 14 cm for females [14] and an average thickness is 2–3 mm [15].

It is one of the most important structures in the hip joint cavity [16]. The labrum forms a seal around the joint cavity to prevent leakage of the lubricant film that lies between the femoral head and the acetabular cartilage, ultimately reducing the occurrence of cartilage damage and osteoarthritis. This seal also has a suctioning effect on the joint through negative intra-articular pressure, which maintains the stability of the joint and makes it more difficult to dislocate [16].

The labrum also increases the contact area between the acetabulum and femoral head by 22% and increases the depth of the acetabulum. This increases the stability of the hip joint [17]. Studies have shown that a normal labrum shares 1–2% of the load on the hip joint, whereas the labrum of DDH patients bears 4–11% of the joint load [18, 19].

1.1.3 Femoral Head

The femoral head, consisting of a dense trabecular bone structure, is located at the proximal end of the femur and is supported by the femoral neck (Fig. 8.1). The femoral head is crucial for supporting the body as well as transmitting and absorbing loads generated during daily activities. The diameter of the femoral head is generally larger in men than in women [20].

The femoral head is approximately spherical with a smooth surface, and about 60–70% of the femoral head is covered by articular cartilage [21]. There is a small rough depression called the fovea capitis on the posterior and inferior part of the femoral head which acts as an attachment point for the ligamentum teres femoris. The strength and stiffness of the femoral head vary from region to region depending on the thickness of the surface cartilage. The cartilage is thickest around the area anterior to the zenith region [22]. Since the articular cartilage is viscoelastic, the load-bearing area of the femoral head changes in accordance with the magnitude of the load. As the load increases, the load-bearing area changes from the periphery of the femoral head to the center of the lunate surface and the anterior and posterior horns [23].

1.1.4 Femoral Neck

The femoral neck, projecting in a superior and medial direction, is a cylindrical bone which connects the femoral head to the long femoral shaft (Fig. 8.1). The main functions of the neck are to support the femoral head and to maintain the hip at the correct angle.

The femoral Neck-Shaft Angle (NSA) is the angle formed by the long axis of the femoral neck and the longitudinal axis of the femoral shaft. During infancy, the NSA has an angle of inclination of about 140–150°, and this decreases progressively as children get older to reach a value of about 125° at puberty (average 125 ± 5°). The NSA does not typically change again after this. When the angle exceeds 130° after growth has stopped, this condition is known as a coxa valgus deformity. In cases where the angle is less than 120°, this is known as a coxa varus deformity. Coxa valga is more likely to be found in patients with hip dysplasia [24, 25]. In contrast, coxa vara is more commonly associated with femoroacetabular impingement (FAI) [26].

Femoral neck anteversion (FNA) is the angle between the projection of the femoral head-neck axis on the transverse plane and on the coronal plane. If the head-neck axis is inclined forwards towards the transcondylar plane, then it is termed anteversion, and if the same is directed downwards and posterior, it is termed as retroversion. Anteversion reduces the coverage of the femoral head by the acetabulum, and thus the leg tends to rotate internally to prevent the femoral head from dislocating, whereas retroversion has the opposite effect. Femoral neck anteversion ranges from 30° to 40° in infancy and decreases progressively as the body grows. For adults, a normal anteversion angle ranges from 15° to 20°, with males having slightly less femoral anteversion than females [27]. Abnormal femoral neck anteversion and structural deformities cause lead to FAI, which is considered a precursor to osteoarthritis [28].

1.1.5 Femoral Calcar

The femoral calcar is an important component of the internal weight-bearing structure of the proximal femur located at the posteromedial conjunction of the femoral neck and shaft, and runs along the posterointernal margin of the femoral neck from the diaphysis towards the femoral head [29]. This ridge of dense bone is a result of the stress distributions in the proximal femur under physiological loading, which is a combination of compression, tension, and shear. The complex loading pattern is caused by the large bending moments and torsion around the femoral head. The femoral neck is equivalent to a cantilever beam, and the femoral calcar is located at the base of the cantilever beam, thus shortening the arm of force and reducing the bending moment of the femoral neck-shaft connection. The femoral calcar influences how load is transferred through the femur, reduces the load on the posterior and medial cortical bone [30], increases the load on the anterior and lateral cortical bone, and distributes the stress more evenly in the proximal femur. Due to high compressive loads placed on the region of the femoral calcar, the trabecular bone in this area is almost as hard and strong as the cortical bone. This is useful for THA as the dense bone acts to support the implant, thereby reducing loosening and subsidence.

1.2 Muscles and Ligaments

1.2.1 Muscles

The muscles of the hip, working together to provide force for movement and stability, are crucial for the normal functioning of the hip joint. By contracting various muscles, the hip joint is capable of moving through 6 degrees of freedom based on the femoral head center: flexion and extension around a transverse axis, abduction and adduction around a sagittal axis, external rotation and internal rotation around a longitudinal axis (Fig. 8.5).

The most powerful flexor of the hip joint is the iliopsoas, which is composed of the psoas major, iliacus, and psoas minor muscles. The psoas major (superficial layer) originates at the T12-L4 vertebrae and the iliacus originates at the iliac fossa. At the other end, both muscles have an insertion point on the lesser trochanter. Only about half of the population have a psoas minor muscle (deep layer), which originates from the costal processes of the L1 to L5 vertebrae and inserts at the iliopectineal arch. The rectus femoris, sartorius, and tensor fasciae latae are other flexors which assist the iliopsoas.

The gluteus maximus, as the largest muscle in the body, acts as the main extensor of the hip joint. The gluteus maximus mainly arises from the dorsal surface of the sacrum and gluteal surface of the ilium and then branches out as two fibers. The upper and lower fibers insert on the iliotibial tract and gluteal tuberosity, respectively. The force of the gluteus maximus also contributes when rotating the hip externally as well as maintaining the body's upright posture. Other main extensors of hip include the biceps femoris, semimembranosus, and semitendinosus.

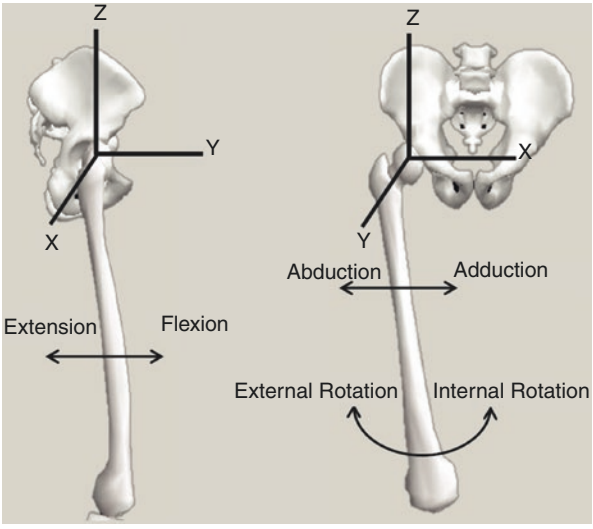

Fig. 8.5 Axis of rotation around the hip joint center and movements produced by the hip joint [31] (Reprinted with permission from 'Orthopaedics and Trauma'. License Number: 4570520375663)

The gluteus medius, gluteus minimus, and tensor fascia latae form the major abductors of the hip joint, assisted by the piriformis and sartorius. The gluteus medius and gluteus minimus originate at the gluteal surface of the ilium and insert at the lateral and anterolateral surface of the greater trochanter, respectively. The tensor fasciae latae originates from the anterior superior iliac spine and inserts at the iliotibial tract. The piriformis is located in the middle of the gluteal region; it arises from the surface of the sacrum and inserts at the greater trochanter.

Hip adduction is primarily accomplished by the adductor longus, brevis, and magnus muscles with assistance from the gracilis and pectineus muscles. The adductor longus, brevis, and gracilis also play roles in flexing the hip, whereas the adductor magnus and pectineus contribute to hip external rotation.

The primarily external rotators of the hip are obturator externus, quadratus femoris, and gemelli with assistance from the gluteus maximus, sartorius, and piriformis. The obturator externus originates from the external surface of the obturator membrane and the surrounding bony surface and inserts at the intertrochanteric fossa through the posterior part of the femoral neck. This muscle also plays a role as an adductor of the hip joint. The quadratus femoris arises from the lateral side of the ischial tuberosity and ends at the intertrochanteric crest of the femur.

Internal rotation of the hip joint is mainly accomplished by the actions of the tensor fascia latae, anterior fibers of the gluteus medius, and minimus muscles.

1.2.2 Capsule and Ligaments

The hip capsule helps maintain the stability of the hip joint. The capsule is composed of a strong and dense fibrous cylindrical sleeve originating from the acetabular margin 5–6 mm beyond the acetabular labrum and attaching anteriorly at the intertrochanteric line [32]. The femoral head and most of the femoral neck are enclosed in the joint capsule, whereas the lateral half of the femoral neck as well as the great trochanter and lesser trochanter are not enclosed in capsule. Because of the need to bear greater loads, the anterosuperior part of the hip joint capsule is thicker, whereas the posteroinferior part is thinner and looser. On the inside, a synovial membrane lines the inner surface of the capsule and produces synovial fluid to lubricate the articular surface and provide nutrition to the articular cartilage.

The stability of hip joint is strengthened by four ligaments, three extracapsular ligaments (iliofemoral ligament, ischiofemoral ligament, and pubofemoral ligament) and one intracapsular ligament (ligamentum teres femoris).

The iliofemoral ligament (also called Y-ligament) lies on the anterior side of the hip joint and resembles an inverted "Y." The ligament originates on the lower part of the AIIS (Anterior inferior iliac spine) and then divides into two branches which subsequently attach at the distal and proximal part of the intertrochanteric line, respectively. The iliofemoral ligament is the strongest ligament in the body with a tensile strength exceeding 350 N [1]. Its lateral branch limits excessive abduction and adduction of the hip joint. It also limits internal and external rotation when the hip joint is in extension and limits external rotation when the hip joint is in flexion.

The medial fibers of the iliofemoral ligament limit abduction and external rotation of the hip [1, 32].

The ischiofemoral ligament is located on the posterior superior side of the hip joint. It originates at the ischial portion of the acetabulum and then crosses the hip capsule as two fibers. The central fibers (superior ischiofemoral ligament) spiral superiorly around the neck of the femur from the posterior surface of the ischium to the medial surface of the greater trochanter of the femur. The lateral and medial inferior ischiofemoral ligaments attach to the neck of the femur and reinforce the posterior aspect of the joint capsule. The ischiofemoral ligament contributes over 60% of the restraining force required to limit excessive internal rotation in flexion and extension [33]. It is helpful for maintaining stability as well as reducing the amount of muscle energy required to maintain a standing position.

The pubofemoral ligament (also called pubocapsular ligament), located at the anterior inferior aspect of the hip joint, plays a role in supporting the joint capsule and maintaining the anterior and inferior stability of the hip joint. It originates at the iliopubic eminence, the pubic portion of the acetabular rim, superior aspect of the pubic ramus and the obturator crest, and inserts at the inferior surface of the femoral neck. The pubofemoral ligament restricts internal rotation once the hip is flexed beyond 30°, as well as restricting excessive abduction [34].

The ligamentum teres femoris (also called femoral head ligament) is a flat triangular fibrous band in the hip capsule. The base attaches to both sides of the transverse acetabular ligament and the edges of the acetabular notch, and the tip connects to the fovea capitis on the head of the femur. The femoral head ligament is covered by synovium with blood vessels passing through it. It is generally believed that this ligament has no restrictive effect on the motion of the hip joint [35].

2 Biomechanics of the Hip

2.1 Kinematics of the Hip Joint

Kinematics is the evaluation of motion and positioning, but does not consider the physical properties of the object itself or the forces imposed on it. In human motion analysis, joint angular displacement is the most common method for describing the relative motion between limbs. A comprehensive understanding of joint kinematics is important for the diagnosis and treatment of joint diseases.

Because of the congruency of the surface of the hip, almost all movement between the femoral head and the acetabulum is rotational, without detectable translation [36]. Usually, hip motion is described by the movement of the femur relative to the pelvis around the hip joint center. The hip joint can move through 3 degrees of freedom: flexion and extension in the sagittal plane, abduction and adduction in the frontal plane, and internal and external rotation in the transverse plane (Fig. 8.5).

Hip joint motion is achieved through the action of a series of muscles and connected tendons, and is limited by the bony structure of a hip joint, the acetabular labrum, and surrounding ligaments. The largest movement occurs in the sagittal plane, where the flexion angle ranges from 0° to 140° and the extension angle ranges from 0° to 20°. In the frontal plane, the range of abduction is from 0° to 50° and adduction is from 0° to 30° with the hip joint extended. When the hip joint is flexed to 90°, the abduction limit increases to 80° whereas the adduction limit decreases to 20°. In the transverse plane, the limits of external and internal rotation are 50° and 40°, respectively, with the hip flexed to 90°. When in the prone position with the hip extended, the external rotation limit decreases to 30° because of the restrictive actions of the soft tissues [37]. The ranges detailed above show the largest angles that the hip joint can safely reach, but the joint seldom reaches such extremes during daily activities.

Typical joint ranges of motion in daily activities can be used to evaluate a patient's functional movement in clinical settings. Common daily activities that require a large range of motion include trying shoes on the floor, sitting down on a chair or rising from it, and ascending or descending stairs. A study by Johnston and Smidt [38] measured the range of motion for 33 males performing these sample activities. It was found that the greatest motion in the sagittal plane occurred when squatting on the floor to tie shoes. In the frontal and transverse planes, the two greatest motions occurred when squatting to tie a shoe on the opposite foot across the thigh. These values indicate that for carrying out daily activities a flexion angle of at least 120° and an external rotation angle of at least 20° is necessary.

Walking is one of the most repetitive activities for the hip joint. Understanding the movement of the hip joint during walking is helpful for further understanding hip joint function. Compared with other joints, the hip has a larger range of motion in the frontal and transverse planes during level gait [39]. One single gait cycle is typically composed of an initial heel strike (0%) through to the second contact of the same foot (100%) and can be divided into two phases: stance phase and swing phase (Fig. 8.6). The stance phase refers to the period when the foot contacts with

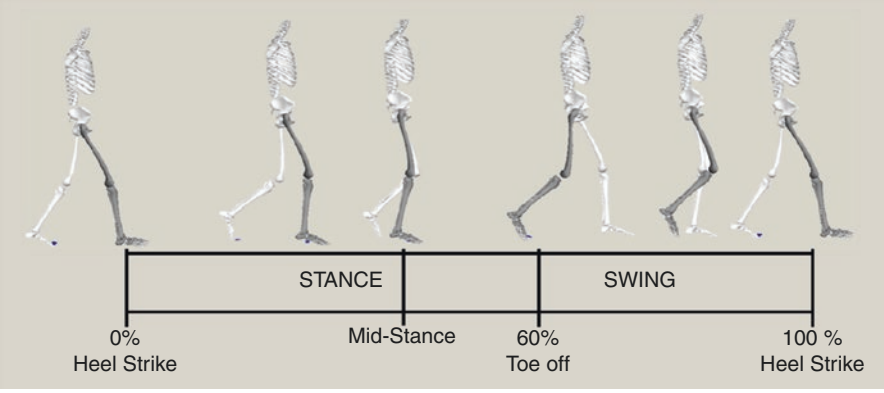

Fig. 8.6 Period of one gait cycle [31] (Reprinted with permission from 'Orthopaedics and Trauma'. License Number: 4567661288157)

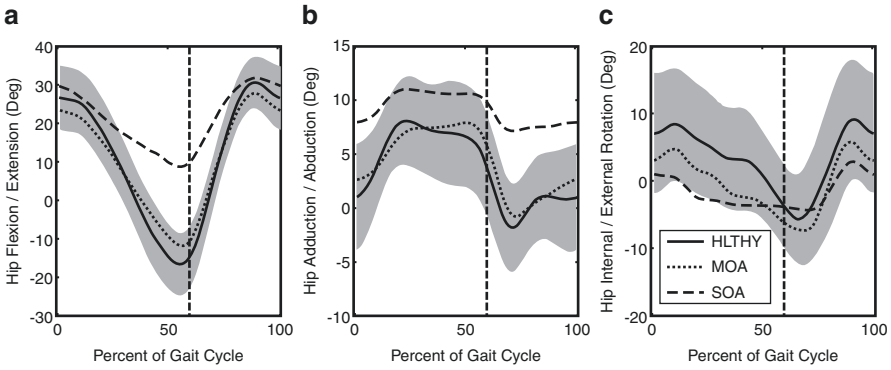

Fig. 8.7 Hip movements in the (**a**) sagittal, (**b**) frontal, and (**c**) transverse plane for nonexistent (solid), moderate (dotted), and severe hip osteoarthritis (dashed) groups. Flexion, adduction, and internal rotation are represented as positive angles. The shaded region represents 1SD above and below the healthy/non-OA group waveform and the vertical line represents the toe off period of the gait cycle [40] (Reprinted with permission from 'Journal of Electromyography and Kinesiology'. License Number: 4567410168348)

ground and accounts for about 60% of the gait cycle. The swing phase is the period when the limb is swinging forward and accounts for about 40% of the gait cycle.

The motions of the hip joint during gait are illustrated in Fig. 8.7 [40]. At heel strike (0% of gait cycle), the hip is flexed to 30–35° in the sagittal plane, before extending to a neutral position at midstance [39, 40]. The end of the stance phase is gauged by the "toe off" period at about 60% of the gait cycle, at which point the hip is extended to 10–15°. In the frontal plane, the hip joint is in an adducted position during the stance phase, and the maximum adduction angle occurs at about 20% of the whole gait. In the swing phase, the hip joint reverts to an abducted position, which continues until the middle of the swing phase. In the transverse plane, the hip is externally rotated in the stance phase and converts to internal rotation around the middle of the swing phase. The hip joint remains internally rotated until late in the following stance phase, at which point it rotates externally again.

Hip joint diseases such as osteoarthritis (OA) often have an influence on the range of motion of the hip joint. Moderate OA results in a considerable decrease in hip range of motion in the sagittal plane, but there is only a significant decrease in the range of motion in the frontal and transverse planes in patients with severe OA [40] (Fig. 8.7).

Total hip arthroplasty (THA) involves replacing a diseased or damaged hip joint with a prosthesis. THA is often performed in cases of severe joint pain, OA, avascular necrosis (AVN), and femoral neck fracture. However, numerous studies found that the range of motion of the hip in the sagittal plane was reduced after THA [41–44]. The achievable limit of hip extension is reduced after THA [41, 44–46], but it has been reported that the limit of hip flexion is not significantly impacted by THA [42, 47]. But, in contrast, Beaulieu et al. did find a reduction in peak flexion angle after THA [41]. The decrease in the extension limit may be related to the increased passive resistance of the flexors (i.e., a flexion contracture) [48].

2.2 *Kinetics of the Hip Joint*

Kinetic analysis of the hip joint focuses on the forces acting on the hip that cause motion. Hip motion is the result of the interaction between internal forces (muscles, joints, tendons, ligaments, and joint contact forces [49]) and external forces acting on the system (gravity, ground reaction forces, and inertia [49]). Such kinetic information is useful for evaluating hip motion and diseases, as well as developing treatment methods and designing hip prostheses.

2.2.1 Static Loading

The human body is an elaborate structure in which bones and soft tissues interact under static or dynamic conditions to maintain balance and generate motion. Static analysis of the hip joint is useful for evaluating changes in the anatomical structure or different treatment modalities on the hip joint reaction forces. Free-body diagrams, as shown in Figs. 8.8 and 8.9, can be used to illustrate contact forces during various loading conditions, such as single leg stance, double leg stance, and carrying external loads.

Single-Leg Stance

In a single leg stance, the human body can be considered as a lever-like structure with the femoral head acting as the fulcrum. A simplified free-body diagram can be used to calculate and illustrate the joint reaction force indirectly (Fig. 8.8). Since the weight of the non-supporting leg is included in the load acting on the load-bearing hip, the effective center of gravity of the body moves close to the non-supporting leg.

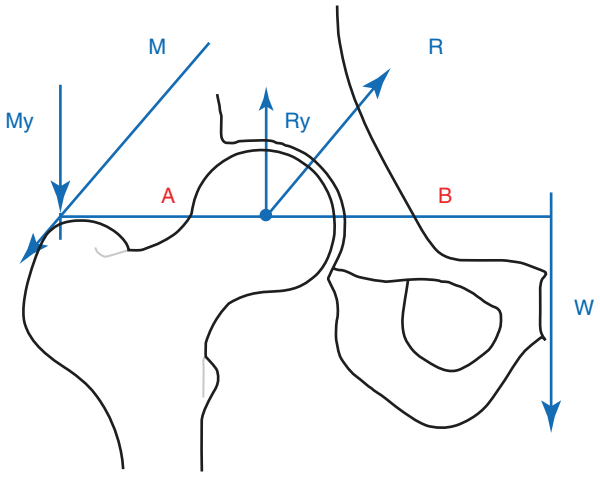

Fig. 8.8 Joint reaction force on the hip joint during single leg stance illustrated using a simplified free-body diagram

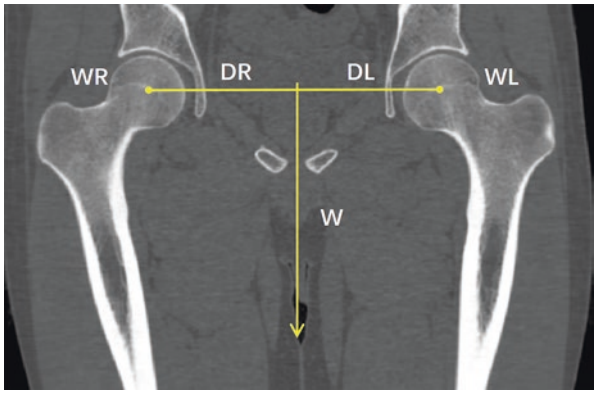

Fig. 8.9 Anterior view of the pelvis in erect double leg stance. DR = moment arm for the right hip, DL = moment arm for the left hip, WR = upper body weight act on right hip, WL = upper body weight act on left hip

As the lower extremities account for 1/3 of the full body weight, the non-supporting limb accounts for half of that, or 1/6 of the full body weight. Therefore, the gravitational force (*W*) acting on the load-bearing hip is 5/6 body weight (BW). This downward force will create a moment around the center of the femoral head, with the gravitational moment arm (*B*) being the distance between the center of the femoral head and the center of gravity of the body. To maintain balance, this moment is offset by a counteracting moment generated by the combined abductor muscle force (M) acting over a lever arm measured as the distance between the center of the femoral head and the insertion site of the abduct muscles on the greater trochanter.

To calculate the joint reaction force (*R*) in single leg stance, the sum of all moments acting on the joint equals zero:

$$\left(\mathrm{A}\times\mathrm{My}\right)-\left(\mathrm{B}\times 5/6\mathrm{W}\right)=0.$$

Usually the ratio between *B* and *A* (*B*:*A*) is about 2.5.
Thus, $My = 2.5W$,

$$\mathrm{Ry}=\mathrm{My}+\mathrm{W}=2.5\mathrm{W}+\mathrm{W}=3.5\mathrm{W}$$

$$\mathrm{R}=\mathrm{Ry}/\left(\cos 30^{\circ}\right)=3.5\mathrm{W}/\left(\cos 30^{\circ}\right)\approx 4\mathrm{W}$$

When the hip joint succumbs to disease or trauma, loading the joint can be extremely painful [21]. Reducing the hip joint reaction force can offer immediate pain relief. According to the above calculations, the joint reaction force can be reduced in two ways. One way is to reduce the moment generated by body weight. Since the moment is calculated as the force multiplied by the moment arm, the moment can be reduced by either reducing body weight or the length of the moment arm. For example, tilting the trunk towards the diseased hip will shift the center of gravity closer to the hip joint (this results in Trendelenburg gait), thereby reducing the body weight moment arm. Another way is to reduce the required hip abductor force. This can be achieved by increasing the moment arm of the abductor muscle

force. For example, in THA a femoral implant with a greater offset may be chosen or the acetabular component may be positioned medially. The effectiveness of offsetting the hip is illustrated by the fact that the reaction force on the hip in patients with coxa vara is 25% lower than the average hip joint, while the reaction force in patients with coxa valgus is 25% higher than the average hip joint [50]. This is due to the moment arm of the abductors decreasing; thus, more abductor muscle force is need to balance the body weight.

Using a cane in the hand contralateral to the diseased hip is also a way to lower the joint reaction force by reducing the body weight passing through the affected hip. The cane effectively creates a moment that counteracts the moments generated by body weight. Therefore, lower abductor muscle force is required and so the joint reaction force is reduced, which in turn alleviates pain in the affected hip. Since the force arm produced by cane is much larger than that of abductor muscles, even small forces on the cane can generate moments that are large enough to significantly reduce the force of abductors. It has been shown that applying about 15% of body weight to a cane can cut the joint reaction force by 50% [50].

Double-Leg Stance

In double leg stance, the upper body weight is distributed equally between the two femoral heads (WR = WL) with equivalent gravitational moment arms (DR = DL) (Fig. 8.9). The moment acting on each hip joint is equal in magnitude and opposite in direction. The pelvis is in balance in the coronal plane with negligible assistance from surrounding musculature. Therefore, if abductor muscles are not required to maintain balance in frontal plane and sagittal plane, there would be an equal force of 1/2 superimposed body weight (W). This force will be increased if the abductor muscle acts to maintain balance and stability.

Trabecular Bone System

As mentioned above, in standing or upright weight-bearing activities, over half of the weight of the HAT (superimposed body weight; head-arms-trunk) passes down through the pelvis to the femoral head. Correspondingly, the ground produces an opposing ground reaction force (GRF) acting on the femoral shaft. These two nearly parallel and opposite forces create a bending moment with a moment arm (MA) that is dependent on the angle and length of the femoral neck. Due to this bending moment, tensile and compressive stresses appear on the lateral and medial aspect of the femoral neck, respectively (Fig. 8.10).

Long-term load-bearing affects the micro-structure of bones. The trabecular structure of cancellous bone is arranged according to the trajectories of the principal

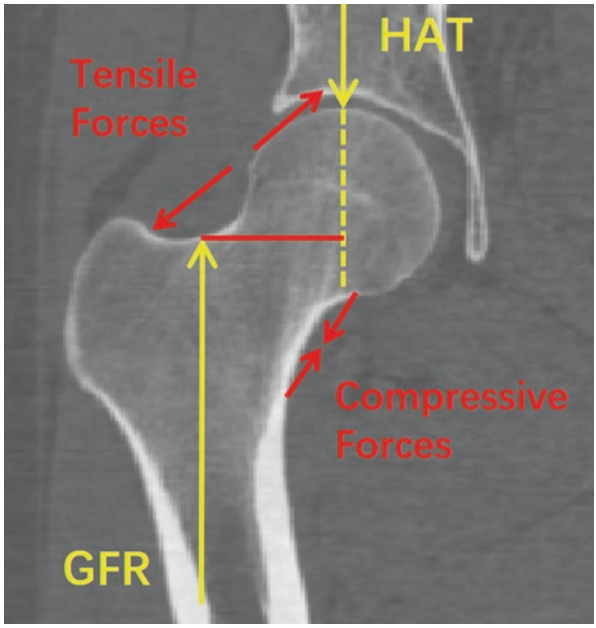

Fig. 8.10 The weight-bearing line of the head, arms, and trunk (HAT)

stresses in the bone [51]. This nonuniform arrangement increases the resistance to mechanical stress. The primary pathway of force transmission in the proximal femur is reflected by the appearance of the trabecular system.

2.2.2 Dynamic Loading

As detailed previously, free-body diagrams are a simple method for indirectly estimating hip contact forces. Knowing the real-time hip contact forces during daily dynamic activities (walking, running, squatting, etc.) is also necessary for better understanding the relevant muscle function and strength and the wear and stability of the hip joint. Dynamic hip contact forces (HCFs) may be measured using direct and indirect means. Direct measurements are carried in vivo using instrumented telemetric prostheses [52, 53]. This method is considered as the gold standard for measuring loading on the hip [54] and can be used to verify indirect measurement models. Indirect measurements may be performed using musculoskeletal models and inverse static optimization techniques to calculate muscle forces and hence joint loading [55, 56]. Some studies have claimed that results calculated using this indirect method are comparable to experimental data [53, 57–60].

Numerous studies have measured HCFs during dynamic activities [53, 54, 61–63], of which walking and running are the most two common activities. It has been shown that the typical peak force (BW) in gait ranges from 1.6 to 5.7 times body weight, but is influenced by physiological differences, gender, age, and walking

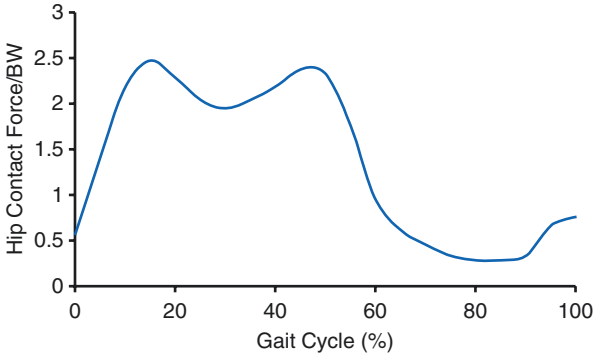

Fig. 8.11 Typical hip contact force (HCF) in healthy individuals during one gait cycle [52]

speed. Figure 8.11 details the typical HCF during one gait cycle, showing two peaks for hip contact force. The initial peak occurs during heel-strike and early midstance, and the second peak occurs just before toe-off.

The contact force is related to the walking speed, whereby increased speed results in an increased HCF [53, 54, 64]. A study [54] on musculoskeletal models calculated the HCFs for 20 young healthy adults and found that the peak HCF increased from 4.22 body weight to 5.41 body weight when the walking speed increased from 3 to 6 km/h. The greater force is because (1) the increased dynamic variation of ground reaction force with the walking speed in the heel-strike stage [65], and (2) the increased stride length corresponds to the increased velocity, which generates a greater offset of the ground reaction force from the joint axis and mobilizes more muscle activity to maintain balance. The HCF is also linearly and positively correlated with BMI, meaning that obese people generate a greater HCF during most of the stance period [57].

During running, there is only one peak HCF, which happens in the stance phase at 0–30% of the gait cycle [54]. As with walking, the HCF is positively correlated with speed.

Bergmann et al. has measured hip contact forces using instrumented total hip implants [52]. The results of his study are illustrated in Fig. 8.12. The graph demonstrates that the greatest contact force was measured during jogging, reaching about 4.1 times body weight, and walking down stairs generated the second greatest force. The lowest joint contact force was produced during cycling.

There are also other unpredictable loads placed on the joints that can generate substantial force, such as the peak HCF during stumbling being recorded at 7.2–8.7 times body weight [61, 66]. Therefore, it should be emphasized that after THA patients should pay attention not only to daily activities that generate relatively low HCFs, but also to unexpected events such as stumbling or unstable periods when standing on one leg which may produce a resultant force in excess of 8 times body weight.

Furthermore, it should also be noted that direct measurements using instrumented telemetric prostheses can only be performed in patients who need THA. Such methods cannot evaluate the physiological condition of healthy joints.

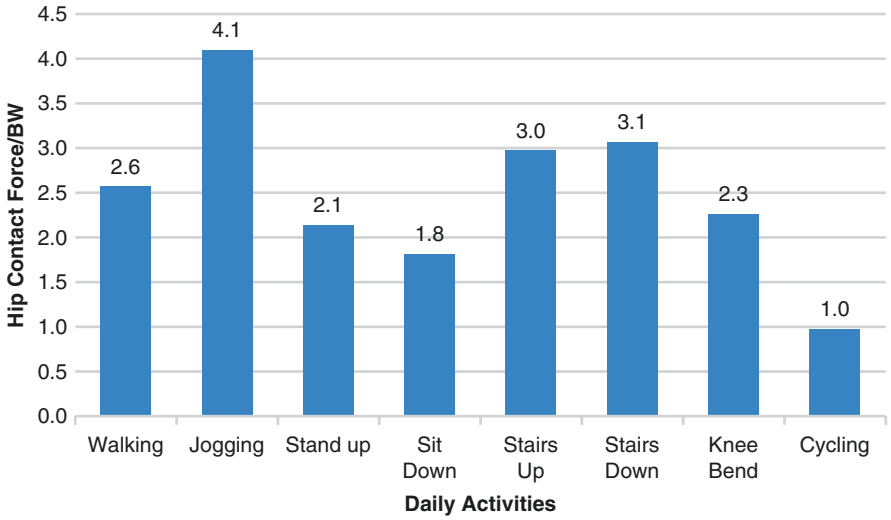

Fig. 8.12 Hip contact force (resultant forces) during different activities [52]

3 Summary

The mechanical conditions of the hip joint are determined and reflected by its anatomical features. This chapter provides essential information on a normal hip joint based on an evaluation of its bony structure and surrounding muscles and ligaments, in addition to their roles in hip functionality and related static and dynamic conditions of the hip joint. However, when the hip joint undergoes pathological changes such as osteoarthritis or trauma, these mechanical conditions of the hip may be altered. This needs to be taken into consideration when considering a suitable clinical treatment such as total hip replacement or other surgery.

References

1. Schünke M, Schulte E, Schumacher U, Ross LM, Lamperti ED. Thieme atlas of anatomy: latin nomenclature: general anatomy and musculoskeletal system. New York: Thieme; 2006.
2. Moore KL, Dalley AF, Agur AM. Clinically oriented anatomy. Philadelphia, PA: Lippincott Williams & Wilkins; 2013.
3. Stem ES, O'Connor MI, Kransdorf MJ, Crook J. Computed tomography analysis of acetabular anteversion and abduction. Skelet Radiol. 2006;35:385–9.
4. Engesæter IØ, Laborie LB, Lehmann TG, Sera F, Fevang J, Pedersen D, et al. Radiological findings for hip dysplasia at skeletal maturity. Validation of digital and manual measurement techniques. Skelet Radiol. 2012;41:775–85.
5. Laborie LB, Engesæter IØ, Lehmann TG, Sera F, Dezateux C, Engesæter LB, et al. Radiographic measurements of hip dysplasia at skeletal maturity—new reference intervals based on 2,038 19-year-old Norwegians. Skelet Radiol. 2013;42:925–35.

6. Mannava S, Geeslin AG, Frangiamore SJ, Cinque ME, Geeslin MG, Chahla J, et al. Comprehensive clinical evaluation of femoroacetabular impingement: part 2, plain radiography. Arthrosc Tech. 2017;6:e2003–9.
7. Tönnis D. Normal Values of the Hip Joint for the Evaluation of X-rays in Children and Adults. Clin Orthop Relat Res. 1976;119:39–47.
8. Cooperman DR, Wallensten R, Stulberg SD. Acetabular dysplasia in the adult. Clin Orthop Relat Res. 1983;175:79–85.
9. Zeng Y, Wang Y, Zhu Z, Tang T, Dai K, Qiu S. Differences in acetabular morphology related to side and sex in a Chinese population. J Anat. 2012;220:256–62.
10. Jacobsen S, Sonne-Holm S, Søballe K, Gebuhr P, Lund B. Hip dysplasia and osteoarthrosis: a survey of 4 151 subjects from the Osteoarthrosis Substudy of the Copenhagen City heart study. Acta Orthop. 2005;76:149–58.
11. Wiberg G. Studies on dysplastic acetabulum and congenital subluxation of the hip joint with special reference to the complications of osteoarthritis. Acta Chir Scand. 1939;83:58.
12. Bouttier R, Morvan J, Mazieres B, Rat A-C, Ziegler LE, Fardellone P, et al. Reproducibility of radiographic hip measurements in adults. Joint Bone Spine. 2013;80:52–6.
13. Tannast M, Hanke MS, Zheng G, Steppacher SD, Siebenrock KA. What are the radiographic reference values for acetabular under-and overcoverage? Clin Orthop Relat Res. 2015;473:1234–46.
14. Karns MR, Patel SH, Kolaczko J, Liu RW, Mather RC, White BJ, et al. Acetabular rim length: an anatomical study to determine reasonable graft sizes for labral reconstruction. J Hip Preserv Surg. 2017;4:106–12.
15. Groh MM, Herrera J. A comprehensive review of hip labral tears. Curr Rev Musculoskelet Med. 2009;2:105–17.
16. Bsat S, Frei H, Beaulé P. The acetabular labrum: a review of its function. Bone Joint J. 2016;98:730–5.
17. Philippon MJ, Nepple JJ, Campbell KJ, Dornan GJ, Jansson KS, LaPrade RF, et al. The hip fluid seal—part I: the effect of an acetabular labral tear, repair, resection, and reconstruction on hip fluid pressurization. Knee Surg Sports Traumatol Arthrosc. 2014;22:722–9.
18. Henak CR, Ellis BJ, Harris MD, Anderson AE, Peters CL, Weiss JA. Role of the acetabular labrum in load support across the hip joint. J Biomech. 2011;44:2201–6.
19. Seldes R, Tan V, Hunt J, Katz M, Winiarsky R, Fitzgerald RJ. Anatomy, histologic features, and vascularity of the adult acetabular labrum. Clin Orthop Relat Res. 2001;382:232–40.
20. Bartoska R. Measurement of femoral head diameter: a clinical study. Acta Chir Orthop Traumatol Cechoslov. 2009;76:133–6.
21. Byrne DP, Mulhall KJ, Baker JF. Anatomy & biomechanics of the hip. Open Sports Med J. 2010;4:51–7.
22. Armstrong C, Gardner D. Thickness and distribution of human femoral head articular cartilage. Changes with age. Ann Rheum Dis. 1977;36:407–12.
23. von Eisenhart-Rothe R, Eckstein F, Müller-Gerbl M, Landgraf J, Rock C, Putz R. Direct comparison of contact areas, contact stress and subchondral mineralization in human hip joint specimens. Anat Embryol. 1997;195:279–88.
24. Clohisy JC, Nunley RM, Carlisle JC, Schoenecker PL. Incidence and characteristics of femoral deformities in the dysplastic hip. Clin Orthop Relat Res. 2009;467:128–34.
25. Fabry G, Macewen GD, Shands A Jr. Torsion of the femur: a follow-up study in normal and abnormal conditions. JBJS. 1973;55:1726–38.
26. Beall DP, Sweet CF, Martin HD, Lastine CL, Grayson DE, Ly JQ, et al. Imaging findings of femoroacetabular impingement syndrome. Skelet Radiol. 2005;34:691–701.
27. Pollard TC, Villar RN, Norton MR, Fern ED, Williams MR, Simpson DJ, et al. Femoroacetabular impingement and classification of the cam deformity: the reference interval in normal hips. Acta Orthop. 2010;81:134–41.
28. Maheshwari AV, Malik A, Dorr LD. Impingement of the native hip joint. JBJS. 2007;89:2508–18.
29. Li B, Aspden R. Material properties of bone from the femoral neck and calcar femorale of patients with osteoporosis or osteoarthritis. Osteoporos Int. 1997;7:450–6.

30. Zhang Q, Chen W, Liu HJ, Li ZY, Song ZH, Pan JS, et al. The role of the calcar femorale in stress distribution in the proximal femur. Orthop Surg. 2009;1:311–6.
31. Lunn DE, Lampropoulos A, Stewart TD. Basic biomechanics of the hip. Orthop Trauma. 2016;30:239–46.
32. Gray H, Standring S. Gray's anatomy. London: Arcturus Publishing; 2008.
33. Martin HD, Savage A, Braly BA, Palmer IJ, Beall DP, Kelly B. The function of the hip capsular ligaments: a quantitative report. Arthroscopy. 2008;24:188–95.
34. Martin HD, Khoury AN, Schröder R, Johnson E, Gómez-Hoyos J, Campos S, et al. Contribution of the pubofemoral ligament to hip stability: a biomechanical study. Arthroscopy. 2017;33:305–13.
35. Perumal V, Woodley SJ, Nicholson HD. Ligament of the head of femur: a comprehensive review of its anatomy, embryology, and potential function. Clin Anat. 2016;29:247–55.
36. Bowman KF Jr, Fox J, Sekiya JK. A clinically relevant review of hip biomechanics. Arthroscopy. 2010;26:1118–29.
37. Nordin M, Frankel VH. Basic biomechanics of the musculoskeletal system. Philadelphia, PA: Lippincott Williams & Wilkins; 2001.
38. Johnston RC, Smidt GL. Hip motion measurements for selected activities of daily living. Clin Orthop Relat Res. 1970;72:205–15.
39. Bovi G, Rabuffetti M, Mazzoleni P, Ferrarin M. A multiple-task gait analysis approach: kinematic, kinetic and EMG reference data for healthy young and adult subjects. Gait Posture. 2011;33:6–13.
40. Rutherford DJ, Moreside J, Wong I. Hip joint motion and gluteal muscle activation differences between healthy controls and those with varying degrees of hip osteoarthritis during walking. J Electromyogr Kinesiol. 2015;25:944–50.
41. Beaulieu ML, Lamontagne M, Beaulé PE. Lower limb biomechanics during gait do not return to normal following total hip arthroplasty. Gait Posture. 2010;32:269–73.
42. Kiss RM, Illyés Á. Comparison of gait parameters in patients following total hip arthroplasty with a direct-lateral or antero-lateral surgical approach. Hum Mov Sci. 2012;31:1302–16.
43. Madsen MS, Ritter MA, Morris HH, Meding JB, Berend ME, Faris PM, et al. The effect of total hip arthroplasty surgical approach on gait. J Orthop Res. 2004;22:44–50.
44. Varin D, Lamontagne M, Beaulé PE. Does the anterior approach for THA provide closer-to-normal lower-limb motion? J Arthroplast. 2013;28:1401–7.
45. Perron M, Malouin F, Moffet H, McFadyen BJ. Three-dimensional gait analysis in women with a total hip arthroplasty. Clin Biomech. 2000;15:504–15.
46. Sander K, Layher F, Babisch J, Roth A. Evaluation of results after total hip replacement using a minimally invasive and a conventional approach. Clinical scores and gait analysis. Zeitschrift fur Orthopadie und Unfallchirurgie. 2011;149:191–9.
47. Tateuchi H, Tsukagoshi R, Fukumoto Y, Oda S, Ichihashi N. Dynamic hip joint stiffness in individuals with total hip arthroplasty: relationships between hip impairments and dynamics of the other joints. Clin Biomech. 2011;26:598–604.
48. Kolk S, Minten MJ, van Bon GE, Rijnen WH, Geurts AC, Verdonschot N, et al. Gait and gait-related activities of daily living after total hip arthroplasty: a systematic review. Clin Biomech. 2014;29:705–18.
49. Chao E. Biomechanics of the human gait. In: Frontiers in biomechanics. New York: Springer; 1986. p. 225–44.
50. Pauwels F. Biomechanics of the normal and diseased hip: theoretical foundation, technique and results of treatment an atlas. Springer Science & Business Media; 2012.
51. Pugh J, Rose R, Radin E. A possible mechanism of Wolff's law: trabecular microfractures. Arch Int Physiol Biochim. 1973;81:27–40.
52. Bergmann G, Bender A, Dymke J, Duda G, Damm P. Standardized loads acting in hip implants. PLoS One. 2016;11:e0155612.
53. Bergmann G, Deuretzbacher G, Heller M, Graichen F, Rohlmann A, Strauss J, et al. Hip contact forces and gait patterns from routine activities. J Biomech. 2001;34:859–71.

54. Giarmatzis G, Jonkers I, Wesseling M, Van Rossom S, Verschueren S. Loading of hip measured by hip contact forces at different speeds of walking and running. J Bone Miner Res. 2015;30:1431–40.
55. Pedersen DR, Brand RA, Cheng C, Arora JS. Direct comparison of muscle force predictions using linear and nonlinear programming. J Biomech Eng. 1987;109:192–9.
56. Andrews JG, Cheng CK. The joint distribution problem with multiple articular contact forces. J Biomech Eng. 1990;112:364–6.
57. De Pieri E, Lunn D, Chapman G, Rasmussen K, Ferguson S, Redmond A. Patient characteristics affect hip contact forces during gait. Osteoarthr Cartil. 2019;27:895–905.
58. Heller M, Bergmann G, Deuretzbacher G, Dürselen L, Pohl M, Claes L, et al. Musculo-skeletal loading conditions at the hip during walking and stair climbing. J Biomech. 2001;34:883–93.
59. Lenaerts G, Mulier M, Spaepen A, Van der Perre G, Jonkers I. Aberrant pelvis and hip kinematics impair hip loading before and after total hip replacement. Gait Posture. 2009;30:296–302.
60. Stansfield B, Nicol A, Paul J, Kelly I, Graichen F, Bergmann G. Direct comparison of calculated hip joint contact forces with those measured using instrumented implants. An evaluation of a three-dimensional mathematical model of the lower limb. J Biomech. 2003;36:929–36.
61. Bergmann G, Graichen F, Rohlmann A. Hip joint loading during walking and running, measured in two patients. J Biomech. 1993;26:969–90.
62. Bergmann G, Graichen F, Rohlmann A. Is staircase walking a risk for the fixation of hip implants? J Biomech. 1995;28:535–53.
63. Rydell NW. Forces acting on the femoral head-prosthesis: a study on strain gauge supplied prostheses in living persons. Acta Orthop Scand. 1966;37:1–132.
64. Weinhandl JT, Irmischer BS, Sievert ZA. Effects of gait speed of femoroacetabular joint forces. Appl Bionics Biomech. 2017;2017:6432969.
65. Chung M-J, Wang M-JJ. The change of gait parameters during walking at different percentage of preferred walking speed for healthy adults aged 20–60 years. Gait Posture. 2010;31:131–5.
66. Bergmann G, Graichen F, Rohlmann A. Hip joint contact forces during stumbling. Langenbeck's Arch Surg. 2004;389:53–9.

Chapter 9
Biomechanics of the Knee

Huizhi Wang, Bolun Liu, Xinzheng Qi, Savio L-Y. Woo, and Cheng-Kung Cheng

Abstract Composed of tibiofemoral and patellofemoral joints, the knee is a complex synovial joint in the human body, both in terms of anatomy and biomechanics. Common knee injuries include torn ligaments and tendons as well as menisci that could lead to cartilage degeneration and osteoarthritis. Therefore, a thorough understanding of the anatomy and biomechanical function of the knee is important for diagnosing any knee disorders, developing appropriate clinical treatments, and improving the design of joint replacement prostheses. In this chapter, the functional anatomy of the knee and the biomechanics and kinematics of both the tibiofemroal and patellofemoral joints will be reviewed. Then, the knee pathomechanics and corresponding clinical treatments will be presented and discussed.

Keywords Knee joint · Biomechanics · Implant

1 Functional Anatomy of the Knee Joint

The tibiofemoral joint and patellofemoral joint are the two articulating surfaces that constitute the knee joint and both are diarthrodial joints that consist of bones, hyaline cartilage, ligaments, tendons, as well as the musculature (Fig. 9.1). The tibiofemoral joint also has medial and lateral menisci between its surface to distribute

H. Wang · B. Liu · X. Qi
School of Biological Science and Medical Engineering, Beihang University, Beijing, China

S. L-Y. Woo
Musculoskeletal Research Center, University of Pittsburgh, Pittsburgh, PA, USA

C.-K. Cheng (✉)
School of Biomedical Engineering, Shanghai Jiao Tong University, Shanghai, China
e-mail: ckcheng2020@sjtu.edu.cn

C.-K. Cheng, S. L-Y. Woo (eds.), *Frontiers in Orthopaedic Biomechanics*,
https://doi.org/10.1007/978-981-15-3159-0_9

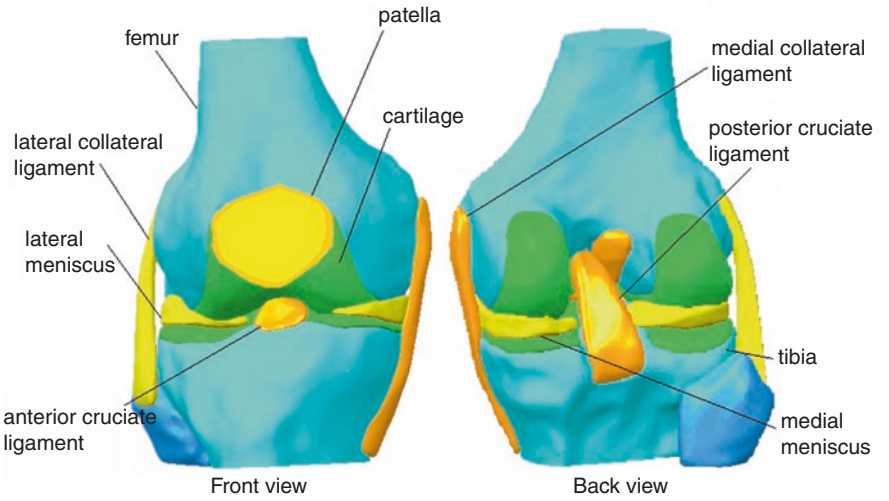

Fig. 9.1 Anatomy of the knee

the loads as well as to absorb impact forces on the joint. All these soft tissues work in synergy to stabilize the knee while the muscles power its motion.

Using the principles of biomechanics, the mechanical behavior and the function of the biological system, in this case the knee joint, can be analyzed and understood. The motion between two bony structures in a joint is known as kinematics. Normal kinematics of the knee is maintained by biomechanical functions of each joint component. Changing of any one of these components secondary to injury or diseases could alter the normal balance and synergy of the knee joint and introduce abnormal kinematics that could cause increased loading of other soft tissue structures and induce additional damages.

In this section, the anatomy and function of the knee components, as well as the joint kinematics, are presented.

1.1 Bones

As the femoral condyles are round while the tibial plateau is relatively flat, the conformity is reinforced by the menisci lying between them. In the sagittal view, the anterior section of the tibia is generally higher than its posterior section. Hashemi et al. [1] demonstrated that the posterior slope of the tibia ranged from −3° to 14°, and was steeper in females than the males. Also, in the coronal view, the tibial plateau is oriented upward in a medial-to-lateral direction. The coronal tibial slope ranged from −1° to 6° and was less steep in females. Besides, there is typically a valgus angle of 7–10° between the tibia and femur. The medial condyle of the distal femur projects more distally than the lateral condyle [2].

The patella is a sesamoid bone and has the appearance of an inverted triangle. The cartilage of the patella is also the thickest in the human body [3].

1.2 Hyaline Cartilage

The hyaline cartilage in the knee joint is a layer of elastic tissue which covers the contact surfaces of the bones along which the joint moves. Hyaline cartilage is mainly composed of a matrix of proteoglycans and collagen traversed with interstitial water. This cartilage layer serves numerous functions, including providing a smooth surface for joint movement, buffering compressive loads, and protecting the underlying bone. With a thickness of between 1.69 and 2.55 mm, the hyaline cartilage in the knee is significantly thicker than in the hip (1.35–2.00 mm) and ankle joints (1.00–1.62 mm) [4].

The micro-structure of hyaline cartilage has low permeability, which acts to trap water within the matrix during loading. This pressurizes the cartilage and increases the stiffness by up to ten times that of the intrinsic modulus of the solid matrix [5]. The increased stiffness of the matrix means there is very little deformation, and the cartilage can take up to 90 min to recover after loading [6]. It has been shown that the thickest regions of the knee cartilage on the femur and tibia are aligned at full knee extension, suggesting an adaption of the cartilage to high loading such as during the heel strike phase of gait [7]. In contrast, under conditions of reduced loading, such as immobilization following surgery, the hyaline cartilage suffers atrophy. However, a sudden change in the loading pattern on the knee (for example, a knee with a ruptured ACL could cause a redistribution of loading on the articular surface) does not produce a significant increase in cartilage thickness, but may in fact initiate degeneration of the cartilage [7]. It has been reported that regular cyclic loading enhances the synthesis of proteoglycans which makes the cartilage stiffer, but continuous compressive loading hinders the synthesis of proteoglycans, which causes damage to the cartilage through necrosis [5].

1.3 Menisci

The crescent-shaped menisci are fibrocartilaginous structures lying between the contact surfaces of the tibiofemoral joint, plugging the gap between the femur and the tibia. To conform to the shape of the femoral condyle and the tibial plateau, the menisci are wedge-shaped in the coronal view, and have a concave upper surface that allows them to “hold” or stabilize the convex femoral condyles. The medial meniscus has a longer span in the A-P direction, while the lateral meniscus has a more rounded shape (Fig. 9.2). The menisci are connected to the tibia primarily by ligaments located at the four horns of the menisci, which restrict their movement relative to the tibial plateau but do allow some limited movement.

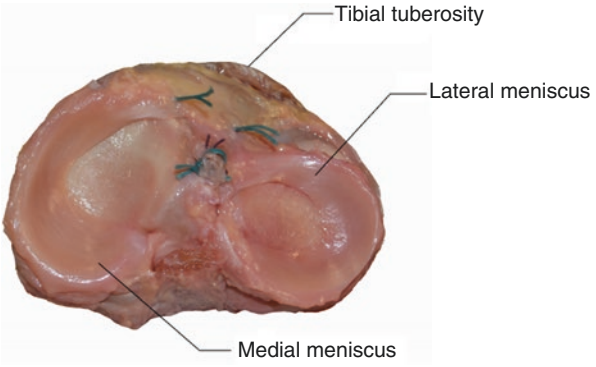

Fig. 9.2 Anatomy of the menisci

As the knee moves, the menisci deform to share and buffer forces in the joint and indirectly increase the articular contact area, thus stabilizing the knee and decreasing stresses on the hyaline cartilage of the tibia and femur. Studies have demonstrated that up to 70% of the loading on the lateral compartment of the knee is carried by the lateral meniscus while 50% of the loading on the medial compartment is borne by the medial meniscus [8].

The menisci also work with the hyaline cartilage to lubricate the knee joint and allow smooth motion between the articular contact surfaces. McCann et al. conducted cadaveric testing on bovine knees and demonstrated that removal of the menisci resulted in an increased friction coefficient on the joint [9].

Undue femoral gliding on the tibia plateau is also restrained by the menisci, making them particularly important for a knee with ACL deficiency. Previous studies have shown greater loading on the menisci following resection of the ACL [10].

1.4 Ligaments

Four major ligaments in the tibiofemoral joint are: the anterior and posterior cruciate ligaments (ACL and PCL), and the medial and lateral collateral ligaments (MCL and LCL). The ACL and PCL are intra-articular ligaments while the MCL and LCL are extra-articular (Fig. 9.1).

The bone insertions of the ACL are located at the medial posterior side of the lateral femoral condyle and the anterior side of the tibial plateau. Both insertion sites have a considerably larger cross section than the midsubstance of the ligament [11]. For biomechanical purposes, some researchers [11] have proposed dividing the ACL into two bundles according to the anatomical location of its tibial insertion: the anteromedial (AM) and posterolateral (PL) bundles. Length of the AM bundle is relatively constant through joint flexion angles from 0° to 90°, while the PL bundle is more stretched in extension [12]. However, pursuing this approach even further, other studies [13] have proposed dividing the ACL into three bundles (the anteromedial, intermediate, and posterolateral bundles).

The ACL plays an important role in constraining anterior tibial translation, thus preventing the femur from posterior luxation, while also helping to avoid excessive internal and valgus rotations of the tibia [14–16]. As the knee flexes, the femur initially rolls back along the tibial plateau during early flexion, before converting to anterior sliding due to the drag force from the ACL. Besides, previous studies [17] also showed an increased ACL force under a combined loading of axial compressive force and anterior tibial load, comparing with using an anterior tibial load alone, indicating a biomechanical role of ACL in resisting compressive joint impact.

The PCL inserts at the lateral posterior side of the medial condyle of the femur and stretches to the inferior posterior side of the tibial plateau. As with the ACL, the PCL may also be divided into two functional bundles, which are named according to the location of their femoral attachments [12]. Both the AL bundle and the PM bundle have increased lengths with flexion [12].

In contrast to the ACL, the PCL prevents the tibia from undue posterior translation, which decreases the risk of anterior luxation of the femur [18]. During knee extension, the PCL forces the femur to slide back along the tibial surface as it rolls forward. Besides, the PCL has been reported to prevent excessive external tibial rotation, especially for the joint flexion angles beyond 60° [19].

The MCL and LCL are located at the medial and lateral side of the knee, respectively. The LCL inserts at the lateral femoral condyle and the lateral superior side of the fibular head, while the MCL attaches to the medial femoral condyle and the inferior medial side of the tibial plateau.

The MCL and LCL function together to constrain the knee joint from excessive internal-external and varus-valgus rotations. The MCL cooperates with the ACL in constraining anterior tibial translation. This partnership is clearly evident in cases of ACL injury, which often result in a decrease in joint stability and an increase in the MCL force, subsequently placing the MCL at a greater risk of injury [20].

1.5 Muscle System

There are two major muscle groups primarily responsible for the extension and flexion of the knee: the quadriceps muscles, located at the front of the femur, which contract to extend the knee; and the hamstring muscles, located the back of the femur, which contract for knee flexion.

The quadriceps muscles consist of the vastus lateralis, rectus femoris, vastus intermedius, and vastus medialis muscles, all of which are controlled by the femoral nerve [21]. The rectus femoris muscle inserts at the hip bone and the tibia, while the other three muscles insert at the femur and connect to the quadriceps tendon.

The quadriceps muscles, mainly serving as a knee extensor, form a large fleshy mass which covers the front and sides of the femur. The rectus femoris muscle also acts as a flexor of the hip due to its attachment to the ilium [22]. As the knee extensor, the quadriceps muscles are crucial for most daily activities (walking, running, jumping, etc.) and serve to stabilize the knee. Weak quadriceps muscles are reported

to compromise knee stability [23]. The lever arm of the quadriceps muscle is increased by the presence of the patella, which is discussed in more detail in Sect. 1.7.

The hamstring muscles consist of the semimembranosus, biceps femoris muscles, and semitendinosus, all of which are controlled by the sciatic nerve. The short head of the biceps femoris inserts at the trochanter of the femur and the lateral side of the fibular head, while the long head originates at the sciatic tuberosities and has the same fibular insertion point as the short head. The semitendinosus and semimembranosus muscles both originate from the sciatic tuberosities and insert at the medial side of the tibia.

The hamstring muscles act to flex the knee, while also function to extend the hip except for the short head of the biceps femoris [24]. The short head of the biceps femoris crosses only the knee joint and is therefore not involved in hip extension. The biceps femoris is an external rotator of the tibia, while the semitendinosus and semimembranosus muscles function to rotate the tibia internally [25]. As an antagonist to the quadriceps muscles, the hamstring muscles also function to control the joint motion during daily activities.

1.6 Biomechanics of the Tibiofemoral Joint

Motion and biomechanics of the tibiofemoral joint are greatly influenced by the morphology of the articular surfaces, and of course the integrity of all the joint structures [16]. The posterior tibial slope is considered an important characteristic for producing anterior shear forces on the tibia. Wang et al. suggested that in knee arthroplasty surgery, the posterior tibial slope has a significant effect on postoperative kinematics of the joint and thus the slope angle should be highly scrutinized intraoperatively [26]. Woo et al. found that increasing the posterior tibial slope caused an increased anterior tibial translation which could stabilize the knee with a deficient PCL. In contrast, decreasing the posterior slope may be considered for a knee with ACL deficiency [27]. Females have a deeper posterior tibial slope than males, resulting in a greater anterior tibial force, especially when in the posture of weight-bearing, placing females at greater risk of ACL rupture than males [1, 28]. Conversely, the lateral section of the tibial plateau is generally located higher (more proximal) than the medial section, forming a slope which is larger in males than in females, but the effect of this coronal slope on joint mechanics is not yet clear [1]. However, while the link between slop angle and knee mechanics has been widely studied, large differences between individuals means there is a large degree of variation across the general population [1]. Thus, understanding this variation could be beneficial for developing more accurate subject-specific implants that could better replicate normal knee biomechanics.

The tibiofemoral joint has 6 degrees of freedom (DOFs) of motion: three (anterior-posterior, proximal-distal, and medial-lateral) translations, as well as three (flexion-extension, varus-valgus, and internal-external) rotations (Fig. 9.3). Because the femoral

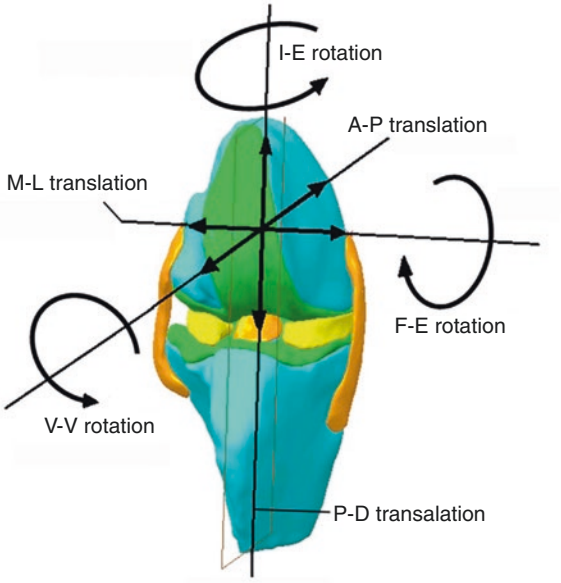

Fig. 9.3 Joint motions in 6 degrees of freedom

condyles have a circular shape and the tibial plateau is relatively flat, the tibiofemoral joint has good rotational flexibility in terms of flexion-extension (0–165°) [29].

The flexion movement of the knee joint can be divided into three functional phases, comprising the screw-home arc, the functional active arc, and the passive flexion arc [30]. The first phase is defined to represent joint activity through joint flexions from 0° to 20°, during which the joint motions are mainly determined by the morphology of the tibial plateau and the femoral condyles. Because of the asymmetry between the distal regions of the lateral and medial femoral condyles, the tibia undergoes internal rotation during this phase. The second phase represents joint activity from 20° to 120° of flexion, during which there is little axial rotation of the tibia. The final phase is defined as joint flexion over 120°. During this phase, the medial femoral condyle moves proximally because of its contact with the posterior section of the medial meniscus; this might explain why the posterior horn of the medial meniscus is typically ruptured during deep joint flexion [31]. Meanwhile, the lateral femoral condyle continues to move posteriorly during the passive flexion arc, resulting in a subluxation at the end of this phase.

During normal gait, the knee has a flexion angle of 0–10° at heel strike, then flexes to 15–20° at 15–20% of the gait cycle, followed by an extension during 20–40% of the gait cycle, and then flexes to around 60° in the swing phase [32]. Meanwhile, the knee undergoes internal-external rotation of up to 5° and varus-valgus rotation of up to 4°, combined with medial-lateral translation of up to 12 mm, proximal-distal translation of up to 14 mm, and anterior-posterior tibial translation of up to 7 mm [33]. As the knee is flexed, the medial condyle of the femur has little anterior-posterior movement but the lateral condyle rolls backward on the tibia, resulting in a coupled internal tibial rotation [34].

During normal gait, axial compression on the articular contact surface of the knee ranges from 0 to 3.2 times body weight (BW) [35]. The greatest axial compression occurs at around 50% of the gait cycle, just before the toe-off phase, and most of the joint forces are distributed on the medial tibial plateau. Loading in the A-P and M-L directions is much lower than the axial loading, ranging from 0 to 0.28 BW and 0 to 0.14 BW, respectively. Internal-external moments range from 0 to 0.02 Nm per BW.

1.7 Biomechanics of the Patellofemoral (PF) Joint

As the name suggests, the PF joint mainly consists of the patella and the femur. The quadriceps tendon inserts at proximal patella which connects the patella to quadriceps femoris muscle. On the distal side, the patellar tendon attaches directly to the tibial bone. As a gliding joint, the patella slides along the femoral trochlea during knee flexion/extension. The primary function of the PF joint is to increase the lever arm of the quadriceps muscles and thus to enhance the efficiency of extending the knee [36].

During flexion, the patella moves posteriorly and distally with respect to the femur condyles, following a "C"–shaped pattern (Fig. 9.4). Movement of the patella outside the sagittal plane is minor by comparison, tilting and twisting by less than 15° [37]. The lateral facet of the patella has been reported to bear greater contact forces than the medial facet during knee flexion [37]. Contact between the articular surfaces of the PF joint reach a peak when the joint flexes to 90°. Past 90°, the patella starts to rotate laterally and contacts the femur at the medial side. During deep flexion (around 140°), the patella falls into the femoral notch and the contact area is greatly reduced (termed the "odd facet"), resulting in high localized stresses. Therefore, patellar chondromalacia and patellofemoral pain syndrome are often experienced during this "odd facet" stage [38].

To have a better understanding on the biomechanics of the PF joint, the quadriceps angle (Q angle) needs to be introduced first. As shown in Fig. 9.5, the Q angle

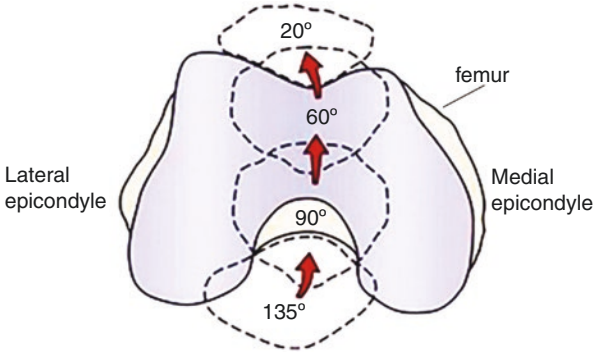

Fig. 9.4 Movement track of the patella during knee flexion

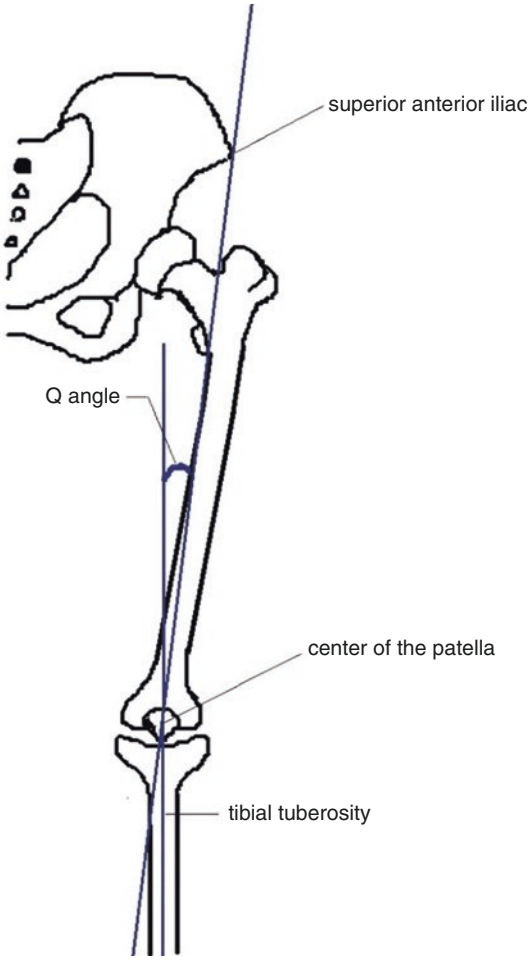

Fig. 9.5 Quadriceps angle

is the angle between a line that connects the center of the patella and the superior anterior iliac and another line that goes through the center of the patella and the tuberosity of the tibia. However, there is a significant difference in Q angle between males and females. For males, the Q angle at full knee extension ranges from 0° to 19°, while that for females is larger, ranging from 6° to 27° [39]. This is mainly due to the larger pelvis in females. Changes in the Q angle can help with understanding the mechanics of knee motions and patellar traction. During knee extension, the tibia gradually rotates externally and as a result the Q angle increases. Inversely, the Q angle decreases during knee flexion when the patella is pulled into the trochlea of the femur by a traction of horizontal forces from the oblique muscle. Thus, stability of the patella is largely dependent on the value of the Q angle and strength of the oblique muscle. Loss of stability may result in the patella tilting externally, resulting in wearing of the lateral patellar cartilage. The size of the Q angle can be affected

by some factors, such as the size of the pelvic bone and connection between joint structures [40]. Abnormal joint structure such as excessive anterior tilt of the femoral head, excessive knee abduction, and other irregular rotations of the tibiofemoral joint could all result in an increased Q angle.

2 Pathomechanics of the Knee Joint and Clinical Treatment

2.1 ACL Injury and Clinical Treatments

2.1.1 ACL Injury

The ACL is frequently injured because of its critical role in constraining joint motion [41]. Most ACL injuries occurred in the absence of physical contact, and frequently during sport activities such as skiing, football, and basketball [41–43]. Females also have a higher incidence of injury than males [28]. Serious damage to the ACL can have a considerable impact on absence from work and the life quality. Long-term complications of ACL injury include secondary injuries to other knee structures such as meniscal tear, MCL injury that could induce degenerative changes to the cartilage both without and with surgical reconstruction [44, 45].

More than 75% of ACL tears are a complete rupture of the ligament, while the remaining 25% are partial tears [46]. Generally speaking, 1/3 of the patients had ACL reconstruction surgery, while a second 1/3 had delayed surgery. The remaining 1/3 would not require surgery. For the latter group, the ACL healed and the knee functions as well as those following surgery.

2.1.2 Conservative Treatment

Conservative treatments for ACL injury include plaster fixation, cryotherapy, muscle training, and strengthening of coordination [47]. With limited ACL function, anterior translation of the tibia may be restricted if there is adequate proprioception to contract the hamstring muscles [47]. However, although such conservative treatments are noninvasive and less stressful for the patient, the clinical outcome is relatively unpredictable and remains controversial. In a clinical report at 10–13 years after surgery, the ACL reconstruction group was reported to perform significantly better than the nonoperative group (conservative treatments) in maintaining involvement in sports [48]. In contrast, other studies have shown good patient satisfaction after 20 years following conservative treatments, though the objective measures indicated increasing knee degeneration [47]. When treated by conservative means alone, Noyes [49] reported that tears across one-quarter of the ACL body did not usually progress further, while one-half tears progressed in 50% of people and three-quarter tears progressed in 86% of people, eventually becoming a complete deficiency 7 years after treatment. Thus, the initial size of the ACL tear might be important for evaluating the expected clinical outcome of conservative treatment.

2.1.3 ACL Repair

The first attempts at repairing ruptured ACLs involved reconnecting the ligament remnants by sutures (termed a primary repair) to facilitate healing. However, in a 5-year clinical follow-up study on ACL primary repair, 53% of the patients had a reinjury, 94% suffered instability, and 71% had pain [50]. It was generally concluded that the poor results of primary repair could be attributed to the poor healing capacity of the ACL [51, 52].

Functional tissue engineering was introduced in the 1980s as a novel method to "grow tissues or organs from a single cell taken from an individual" [53]. With developments in functional tissue engineering, biological scaffolds such as extracellular matrix (ECM) have been used to reinforce ACL healing [54, 55]. ECM bioscaffolds serve to bridge the gap between the ACL remnants to facilitate the migration and proliferation of the cells and formation of the blood vessels, as well as the transportation of wastes, and thus consequently accelerate tissue formation and improve the healing of the ACL. Woo et al. [55] used ECM in sheet and gel forms to repair a transected goat ACL. The results showed continuous formation of neotissue in the ECM group while there was limited tissue growth in the control group (suture only). Also, the stiffness of the femur-ACL-tibia complex for the group using ECM was 2–3 times that of the group using suture repair alone.

Mechanical augmentation for ACL repair has also shown positive results for improving ACL healing. Fleming et al. introduced a form of suture augmentation where the sutures were fixed directly to the bone to reinforce the repaired ACL and reduce anterior laxity of the joint [56]. Fisher et al. [10] showed that, in comparison to traditional suture repair, mechanical augmentation of ruptured ACLs with sutures resulted in improved joint stability, higher load in the repaired ACL, and lower load in the medial meniscus, demonstrating the effectiveness of suture augmentation for restoring joint stability and protecting the medial meniscus. The subsequent introduction of biodegradable ACL grafts allowed for early reinforcement of the repaired ACL and gradual transferring of loading to the ACL as it heals, along with the concurrent dissolution of the graft [57]. Similarly, a degradable magnesium ring device was designed and used by Farraro et al. as mechanical reinforcement which was combined with biological reinforcement (ECM scaffold) for ACL repair to restore joint stability and to load the femoral insertion site to prevent disuse atrophy throughout the ligament healing [58].

2.1.4 ACL Reconstruction

Because of the bad capacity of healing of the ACL and the unsatisfying clinical outcomes of conservative treatments and repair surgeries, ACL reconstruction has remained the gold standard for treating ACL ruptures [59]. This involves replacement of the original ACL with a graft that is fixed into femoral and tibial tunnels to restore joint stability. There are a variety of sources for the graft, with the choice of using an allograft, autograft, or artificial graft. The bone-patellar tendon-bone complex (BPTB) and four-strand hamstring tendon (HS) have become the two most

commonly used autografts, and the LARS artificial graft (LARS Company, France) is the most popular synthetic graft, with a market history of over 20 years [60, 61].

Satisfactory outcomes have been reported in the short term following ACL reconstruction. Previous study displayed no loss in range of motion of the knee 2 years after the surgery and limited postsurgical complications [62]. Another recent study [63] reported that 1 year following ACL reconstruction, the rate of graft failure was 6.5% for HS and 2.1% for BPTB, while the rate of returning to sports was 71% when using a HS graft and 78% when using a BPTB graft.

However, although ACL reconstruction shows positive results in the short term, long-term complications have been reported. First, the complex anatomy of the ACL insertions cannot be restored, and thus the rotational joint stability cannot be totally restored. Tashman et al. [64] measured knee kinematics during downhill running 4–12 months following ACL reconstruction and found that the anterior tibial translation for the reconstructed knee had no significant difference with the uninjured knee, but the reconstructed knee had larger external rotation (3.8° larger on average) and varus rotation (2.8° larger on average). Second, there could be donor site morbidity when using autografts. In a study by Salmon et al. [65], donor site related complications were reported to appear in 42% of the patients 13 years after ACL reconstruction, while 45% of patients suffered pain when kneeling. Third, there have been reports of enlargement of the bone tunnels and rupture of the grafts, which have an incidence of up to 72% and 22%, respectively [66, 67]. Bone tunnel enlargement can cause graft loosening, fixation failure, knee instability, and osteoarthritis, while a graft rupture directly calls for follow-up surgery. Other potential complications include loss of proprioception, graft wear, graft laxity [68], extension loss, and long-term osteoarthritis [69, 70]. A recent study reported an incidence of knee osteoarthritis of nearly 20% at 12 years following ACL reconstruction [45].

2.2 Meniscal Tear and Clinical Treatments

2.2.1 Meniscal Tear

A tear in the meniscus is a relatively common soft-tissue injury. A meniscal tear can cause pain, swelling, and joint instability, and long term could induce knee osteoarthritis due to increased stresses on the hyaline cartilage. Englund et al. [71] assessed the integrity of the menisci in 991 subjects using a 1.5 T MRI and found that 19% of females and 56% of males had some level of tearing, and over 60% of subjects with osteoarthritis had a meniscal tear. Among the subjects without any symptoms of knee pain, aching, or stiffness, 60% were found to have a meniscal tear.

There are a variety of types of meniscal tear which may be characterized based on the location and appearance: horizontal tear, flap tear, radial tear, root tear, vertical tear, oblique tear, and complex tear.

Horizontal tears are defined as occurring parallel to the tibial plateau in the region that divides the meniscus into superior and inferior halves. A flap tear occurs

where there are displacements of torn fragments toward the articular space. A radial tear is vertical to the tibial plateau and transects the longitudinal collagen bundle. This type of meniscal tear impairs the axial strength of meniscus and might increase the risk of meniscal extrusion [72]. A meniscal root tear is defined when a radial tear happens within 1 cm of the bony tibial attachment. A vertical tear runs parallel to the longitudinal collagen bundle and divides the meniscus into peripheral and central portions. Oblique tears are oriented oblique to the longitudinal collagen fibers. Complex tears are defined as a combination of two or more types of tears occurring simultaneously. According to Englund et al. [71], among 308 subjects with meniscal tear, 40% were horizontal tears, 37% were complex tears, 15% were radial tears, 12% were oblique tears, 7% were longitudinal (vertical) tears, and 1% were root tears.

2.2.2 Meniscal Repair

Where appropriate, repairing the meniscus with sutures is often a good option for restoring normal mechanical function while maintaining proprioception and vascularity. In a 2-year follow-up study on 280 meniscal repairs [73], successful results were obtained in 252 knees, with a total failure rate of 10%. Of those patients that were deemed successful, there was an absence of any tenderness of the joint line, blocking or swelling. However, whether to perform a meniscal repair could be largely dependent on the tear type and the surgeon's individual ability and experience. Vascularity is only provided at the periphery of the menisci (up to 25% of the width, termed the red-red zone) (Fig. 9.6) as well as at its horn attachments [74], and thus the capacity of healing of the meniscus is rather poor in the middle portion (termed the white-white zone) (Fig. 9.6). Previous studies demonstrated how tears on the posterior root of the medial meniscus could be repaired to restore the normal joint loading profile [75]. If a vertical tear is located peripherally, meniscal repair using sutures is usually the preferred treatment [76]. Other types of meniscal tears, particularly radial tears, are more difficult to repair and heal. For these difficult

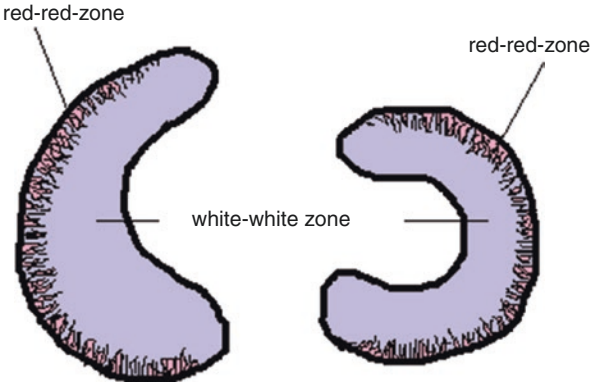

Fig. 9.6 Illustration of the red-red and white-white zones of the menisci

tears, meniscectomy or meniscal replacement may be a more suitable option. It was reported that around 25% of meniscal tears could be repaired in patients younger than 40 years old [77].

2.2.3 Meniscectomy

Meniscectomy is a surgical procedure to partially or completely remove a damaged meniscus. A clinical follow-up study by Roos showed that undergoing meniscectomy increased the risk of tibiofemoral osteoarthritis by 14 times at 21 years after the surgery [78]. Ihn et al. performed cadaveric testing using pressure films [79] and found that following meniscectomy, the peak contact stress in the knee joint increased because of the reduced contact area.

Compared with partial meniscectomy, total meniscectomy could result in a smaller articular contact area, which may speed the development of osteoarthritis. Meniscectomy could also have a considerable effect on the ligaments, with one study [65] reporting a sixfold increase in graft rupture 13 years after undergoing meniscectomy and ACL reconstruction. Conversely, forces in the meniscus could be doubled after transecting the ACL [80].

In comparison to medial meniscectomy, lateral meniscectomy is reported to have more postoperative complications [81]. As mentioned previously, the lateral meniscus shares more load for the knee compartments. Thus, removal of the lateral meniscus could be expected to have a more pronounced effect on stress distribution in the joint. Also, the lateral tibial plateau is convex in contrary to the concave medial plateau; therefore, removal of the lateral meniscus would cause more point contacts and increase the peak articular contact stress. A clinical study [82] on meniscectomy reported good results in 80% of the patients following medial meniscectomy while only 47% of patients who underwent lateral meniscectomy reported similar results.

2.2.4 Meniscal Replacement

If a patient develops complications such as joint pain from early degeneration after meniscectomy, they may be considered as a candidate for meniscal replacement.

Allograft

Meniscal allografts are obtained from donors and should contain no living cells [77]. If donor cellular material remains in the graft, a dense cartilage matrix would be used to lock the materials so that the allograft does not elicit any immune response.

Meniscal replacement was first introduced in the 1980s [83]. A previous study [84] reported a total failure rate of 29% for allograft transplants 13 years after the replacement surgery, while the overall Lysholm score improved from 36 to 61

comparing with the preoperative situation, showing a promising potential for relieving pain and postponing the need for knee arthroplasty in younger patients [85]. Similar results have been reported by other researchers [86], whereby meniscal replacement has been shown to prevent further narrowing of the joint space, reduce knee pain, and halt further degeneration of the cartilage.

Meniscal Bioscaffold

The red-red zone of the meniscus has a vascular supply while the middle section (white-white zone) does not. In a partial meniscectomy, if the red-red zone is well preserved, an artificial scaffold can be sutured to replace the missing tissue and restore the mechanical function of the meniscus.

The Menaflex Collagen Meniscal Scaffold (Regen Biologics Inc., New Jersey, USA) and the Actifit Scaffold (Orteq, London, UK) are two of the most commonly used meniscal scaffolds on the market. The former is made of Achilles tendon of bovine that is pressure heat molded into the shape of a meniscus. A clinical follow-up study demonstrated significantly increased tissue formation with the use of this scaffold over a partial meniscectomy [87], and more activity was regained postoperatively in the scaffold group than the meniscectomy group. The Actifit scaffold is a porous biodegradable scaffold made of polyurethane that allows neo-tissue to gradually replace the scaffold material over time. A 1-year biopsy study showed viable "meniscus-like" tissue replacing the scaffold material and a considerable reduction in patient pain [77].

2.3 Knee Osteoarthritis and Treatment Options

2.3.1 Knee Osteoarthritis

Knee osteoarthritis is a common disease in middle-aged and older people, presenting as progressive degeneration of the joint cartilage, including osteophytes formation, cartilage loss, sclerosis of subchondral bone, degeneration of menisci, laxity of ligaments and alterations in the synovium and fat pad [23]. There are numerous factors that may lead a person to develop osteoarthritis, to name a few, cumulative high weight-bearing, poor posture during gait, muscle weakness, and sudden temperature changes [88–90]. With knee osteoarthritis, people suffer from stiffness, pain, and loss of knee function.

For patients in the early stages of arthritis, basic and conservative treatments are often used, such as nonsteroidal anti-inflammatory medication, localized corticosteroid injections, and weight loss [91]. As the osteoarthritis progresses, destruction of the matrix occurs and the external loads exceed the physiological limit of the cartilage, resulting in asymmetric wearing of the cartilage and subsequent bone loss. Generally, once the pain reaches a certain level, the patient and physician may opt

for surgical knee osteotomy. This may be a high tibial osteotomy or fibular osteotomy. However, under severe loss of cartilage and/or bone and consequent intolerable pain and dysfunction of the knee joint, the only viable option is to undergo knee arthroplasty, during which the joint surfaces are replaced by prosthetic components. The ultimate goal of knee arthroplasty is to replace the problematic knee joint with a prosthetic knee in order to restore the joint functionality and relieve the pain.

2.3.2 High Tibial Osteotomy (HTO)

Although osteoarthritis can present in any of the knee compartments, a large portion of the cases reported occur in the medial compartment of the tibiofemoral joint [92], with fewer cases being reported for the lateral side or the patellofemoral joint [93]. When osteoarthritis appears in the medial side, the medial joint space is usually narrowed because of the loss of cartilage and bone, resulting in abnormal force transmission along the lower limb.

For patients who are younger and more active, high tibial osteotomy (HTO) is often chosen for early and moderate osteoarthritis. In this case, part of the tibial bone is removed to relocate the joint surface and to restore joint alignment. For medial arthritis, more bone would be removed at the medial side, changing the joint alignment from varus to be slightly valgus, thus decreasing medial joint pressure and slowing down the degeneration of the medial cartilage. This may postpone or avoid the necessity for knee arthroplasty. Previous studies comparing clinical results of HTO and unicompartmental knee arthroplasty (UKA) concluded that UKA presents lower revision rates, less postoperative complications, and less postoperative pain. However, HTO allowed for a better range of motion, which could be more satisfactory for highly active patients [94].

2.3.3 Fibular Osteotomy

The fibula bone is generally considered to be less critical for joint functionality than the other long bones of the lower limb. The fibula provides an origin for several muscles of the knee joint and carries axial weight-bearing loads ranging from 6.4% [95] to 16.7% [96]. It has been freely used as a source for grafts and as a vascularized transplant to bridge large bony defects for conditions such as congenital pseudarthrosis of the tibia [97], tumor resection [98], nonunion [99] and grafting operations in case of femoral head necrosis [100].

Proximal fibulectomy (fibular osteotomy) has been demonstrated by several studies to improve the restoration of joint functionality and reduce pain in patients with OA. It is a simple but effective procedure, with the number of patients with a fibulectomy in China surpassing 1000 in 2015 [101]. To perform a fibular osteotomy, the proximal part of the fibula is first exposed, followed by an osteotomy with a length of 2–4 cm at 7–8 cm from the proximal fibula head. In a follow-up study on 110 patients over a 2-year period, Yang et al. [102]

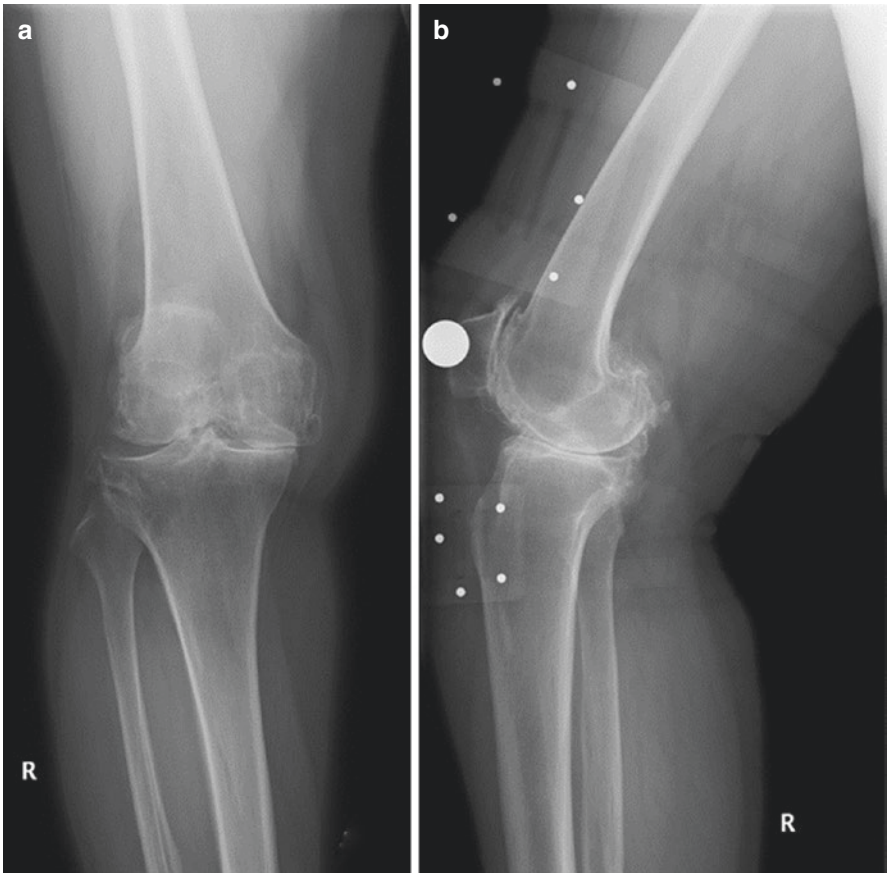

Fig. 9.7 Preoperative radiographs; anteroposterior (**a**) and lateral (**b**)

reported significant improvement in alignment (Figs. 9.7 and 9.8) and function of the knee, as well as relief of pain following the fibular osteotomy. Zou et al. [103] investigated 92 patients with varus knee OA treated by either fibular osteotomy or HTO and found that the outcomes of fibular osteotomy were superior to HTO in either short term or long term. Nie et al. [104] reported on 16 patients with knee OA in the medial compartment who underwent proximal fibulectomy and found that there were significant improvement in VAS pain and HSS score 1 day and 6 months after surgery. In addition, the hip-knee-angle (HKA) improved and remained stable for 3 months and there was an inverse relationship between the overall peak knee adduction moment (KAM) and HKA. Yazdi et al. [105] evaluated the effect of partial fibulectomy on the articular contact pressure in cadaver knees and it was demonstrated that partial fibulectomy decreased the medial articular pressure and increased that in the lateral compartment. Although the procedure is relatively simple and there are good clinical results, it may

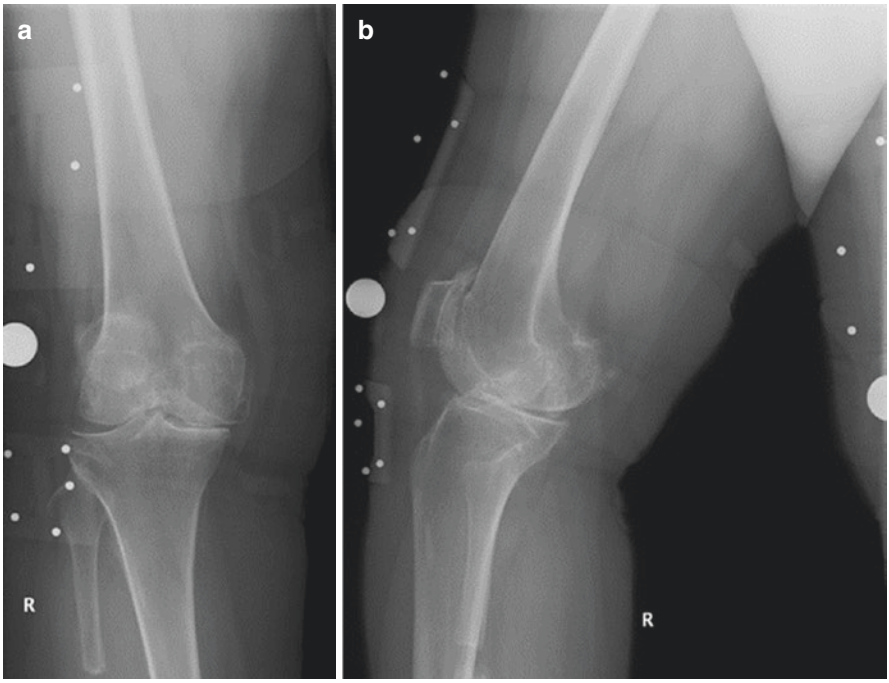

Fig. 9.8 Immediately postoperative radiographs; anteroposterior (**a**) and lateral (**b**)

cause adjacent peroneal nerve injury. Sandoval et al. [106] followed up 116 patients with proximal fibulectomy for 2 years and reported that only 9.4% suffered complications, mainly for neuropraxia of the peroneal nerve, hematoma of the wound and infection. While fibulectomy has generally been shown to be effective, it is not clear exactly how the procedure relieves knee pain. Zhang et al. [107] stated that nonuniform settlement and bilateral degeneration of the plateau leads to varus knee, while with an osteotomy of the fibula can modify this situation. Weakened support from the lateral fibula results in a correction of the varus deformity, and consequently shifted the loading from the medial compartment to the lateral, which eventually leads to relieved pain and restored joint functionality.

Qi et al. [108] hypothesized that a reduction in lateral muscle contraction after fibulectomy may cause a rebalance in the resultant joint moment, making the contact forces in the medial compartment shift laterally and decrease in magnitude.

According to Qi [108], the balance of joint forces in the coronal plane of a varus knee may be gauged by the following equations (Fig. 9.9):

$F_{LM} + F_B + F_{MM} = F_{JL} + F_{JM}$, where F_{JM} is the medial joint contact force, F_{JL} is the lateral joint contact force, F_{LM} is the lateral resultant muscle force, F_B is body weight due to the gravity, F_{MM} is the medial resultant muscle force, and F_{JM} can be ignored due to varus knee.

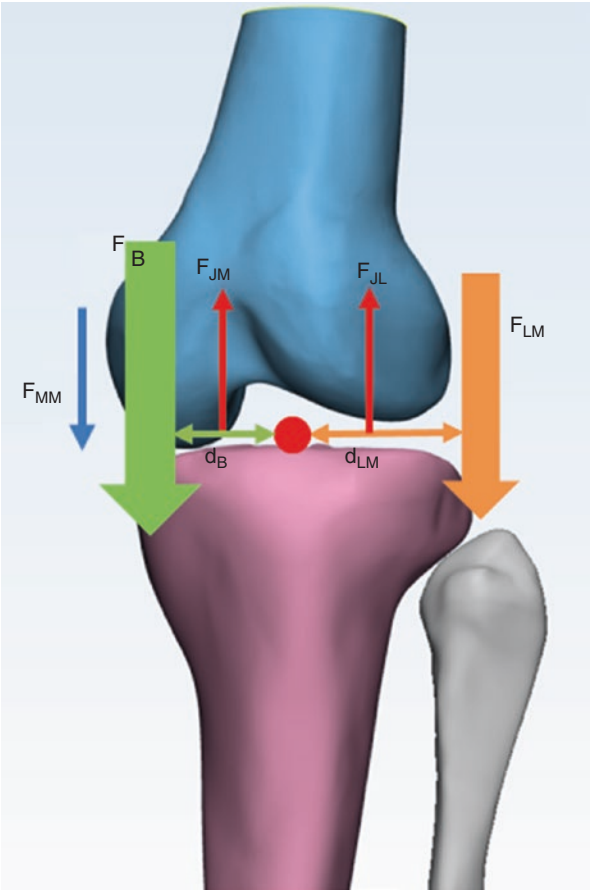

Fig. 9.9 Before operation

$d_{LM} \times F_{LM} = d_B \times F_B + d_{MM} \times F_{MM}$, where d_{LM} is the moment arm of lateral resultant muscle force to knee joint center, d_B is the moment arm of body weight to the knee joint center, and d_{MM} is the moment arm of medial resultant muscle force to the knee joint.

After removing a portion of the fibula (Fig. 9.10), the lateral muscle (F'_{LM}) is released which decreases the valgus moment ($d_{LM} \times F'_{LM} < d_B \times F_B$). To compensate, the varus resultant moment is reduced by shifting the body weight laterally which subsequently decreases the moment arm of body weight ($d'_B < d_B$). Meanwhile due to the decrease in the lateral muscle force (F'_{LM}), the overall knee joint forces also decrease ($F'_{LM} + F_B = F'_{JL} + F'_{JM}$).

In summary, proximal fibulectomy is an innovative procedure to treat medial knee OA without the need for resecting the knee joint. Studies performed to date lack sufficient quantitative biomechanical evidence to recommend using this procedure as standard practice. Further clinical follow-up studies and comparative analyses to other common treatment methods are required.

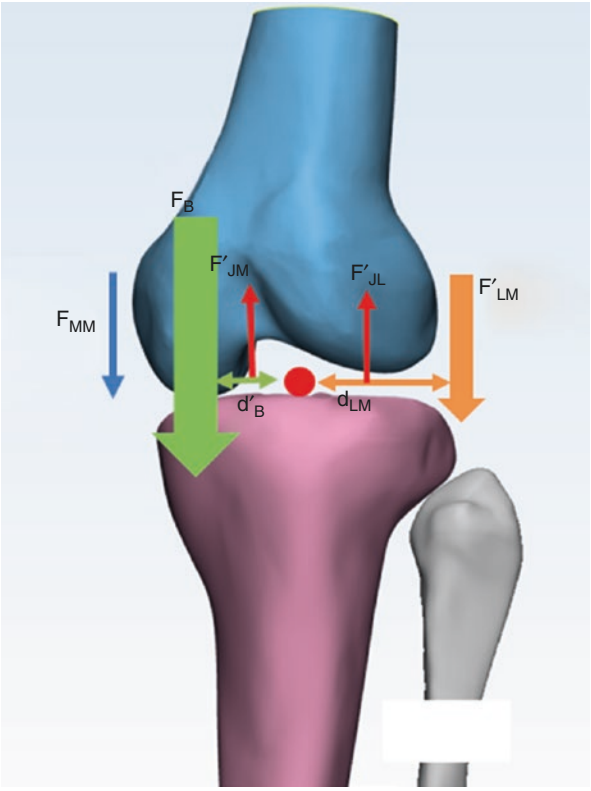

Fig. 9.10 After fibular osteotomy

2.3.4 Knee Arthroplasty

Knee arthroplasty is often considered when conservative treatments and less invasive bone osteotomies are either unsuccessful or are not considered a viable option because the natural cartilage has reached an irreparable state. Knee arthroplasty can offer pain relief and help regain normal joint function. The knee prosthesis generally consists of the femoral, tibial, and patellar components. The tibial component usually contains a polyethylene liner inserted into a metal baseplate.

Knee arthroplasty may be performed as a unicompartmental knee arthroplasty (UKA) or a total knee arthroplasty (TKA). For TKA, there are generally two types of knee prosthesis in clinical use: cruciate-retaining type (CR type) and posterior-stabilized type (PS type).

Unicompartmental Knee Arthroplasty (UKA)

UKA is an operation used to relieve arthritis by replacing the articular surface of either the medial or lateral condyle without sacrificing the cruciate ligaments and the patella, as opposed to total knee arthroplasty (TKA) which replaces both knee

compartments at the same time. In theory, because UKA retains more soft tissues, it can better restore knee functionality and stability than TKA and would allow the patient to retain a better ontological feel. In the early years following the introduction of unicompartmental procedures, the failure rate was quite high due to poor surgical techniques and poorly designed components. The average revision rate of UKA at 2 and 6 years has been reported at 20% and 28%, respectively, in 1970s [109, 110]. With successive improvements in the design of components, mature clinical techniques using minimally invasive surgery have significantly improved the clinical success rate with appropriate patient selection [111]. The survival rate of UKA at 2 and 5 year is 98.7% and 95.5%, respectively, and the knee function score remains satisfactory [112]. However, the long-term survival rate is significantly lower than that of TKA [113]. Failure rates of UKA vary across literature and for different regions [114–117]; 27% (10 years) in Finland, 12.1% (8 years) in UK, and 4.6% (10 years) in Japan. The success of UKA is dependent on many factors, including the age and activity of the patient, surgeon's experience, and the type of implant used.

UKA has been used in clinic for over 60 years. In the early 1950s, McKeever [118] inserted metal plates into a patient to replace the damaged articular cartilage surface, becoming one of the first documented cases of UKA. By the 1960s the procedure had reached mainstream practice thanks to improved designs and the use of alternative materials. Gunston [119] developed the first unilateral metal-on-PE bearing, which is still the most common material combination in use today. The 1970s saw the introduction of non-constrained prostheses that increased the activity of the joint and could achieve a greater joint range of motion than TKA prostheses [120]. In the 1980s, Goodfellow introduced the idea of an Oxford active platform into the design of single condyle prostheses (Oxford unicompartmental knee replacement, OUKR) which increased the articular contact area and reduced the contact stress [121]. In recent years, custom-made UKA prostheses (for example, iUni by ConforMIS Inc.) developed from CT scans and manufactured by 3D reconstruction and printing have been introduced. As the shape of the prosthesis is designed according to the individual anatomy of the femoral condyles, custom prostheses can provide better alignment and more natural movement. However, given that custom implants are a recent development, the long-term outcome is relatively unknown. According to the American Joint Replacement Registry [122], UKA accounted for about 3.2% of primary knee replacement procedures from 2012 to 2017, and there was a downward trend year on year. This same trend has also been observed in Australia [123] and Sweden [124], with the former showing a decrease in UKA from 14.5% in 2003 to 5.1% in 2016. However, since 2017 the trend has reversed and there has been a slight uptake in UKA procedures in Australia [123], Sweden [124], and Britain [125].

There are a number of potential causes of failure of unilateral knee prostheses, including degeneration of the adjacent tibiofemoral joint and patellofemoral joint, implant loosening, mechanical injury, malposition, and infection. Among them, aseptic loosening and joint disease (including contralateral arthritis) are the most common causes of failure [123–125]. Typical factors leading to loosening of the

prosthesis are malalignment of the components, undercorrection of a preexisting deformity, deficiency of the ACL, improper tibial slope, and dislocation of the bearing in mobile designs. Each of these factors may cause asymmetrical loading on the prosthesis and therefore produce more wear particles, leading to further osteolysis. Joint diseases after UKA, such as the progressing of OA in the other knee compartments, can be caused by overcorrection of the mechanical axis or impingement due to an oversized femoral component [126].

At present, biomechanical studies of unicondylar knee prostheses typically focus on the effect of the mechanical axis of the knee joint on the medial or lateral articular stress. If the stress of the articular surface is not evenly distributed, it may accelerate implant failure [127]. In general, the stability of ligaments and the amount of angular deformation must be carefully assessed preoperatively. Medial arthritis often first appears in the anteromedial region of the knee joint, and then gradually extends to the femoral condyles and intercondylar fossa. Inflammation of the knee caused by cartilage degeneration and the presence of intercondylar fossa osteophytes alters the biochemical and mechanical environment of the ACL. Degeneration of the ACL subsequently changes the kinematics of the knee joint, leading to further degeneration of the posteromedial region. In the early stages of medial knee arthritis, if the ACL does not display functional deficiencies, UKA can be chosen to slow down regression of the ACL and the contralateral compartment. However, if the functionality of the ACL is impaired, for example, through rupture or resection, then the stability of the knee joint may be affected. In such situations UKA is not a viable option.

Total Knee Arthroplasty (TKA)

In the operation of TKA, all of the articular surfaces in the knee are replaced with prosthetic components. The two most common types of total knee prostheses in clinical use today are cruciate-retaining (CR) and posterior-stabilized (PS). Both types require the removing of the ACL, but with CR prostheses the posterior cruciate ligament (PCL) is retained, while PS prostheses also require a resection of the PCL. With the PS knee, a femoral cam and a tibial post interact as a functional replacement for the PCL. When the femoral component slides anteriorly, the cam contacts the tibial post, forcing the femoral component to roll back along the tibia. This mechanism is designed to prevent excessive anterior femoral translation and help to maintain joint stability.

The anterior region of the tibial liner in TKA is often designed to be higher than the posterior part in order to avoid excessive anterior femoral translation and increase the contact area of the tibiofemoral joint. This stabilizes the knee and decreases contact stress on the components [128].

The polyethylene liner in the tibial component may be anatomically shaped ("anatomical design") (Fig. 9.11b) or be a simpler nonanatomical design (Fig. 9.11a). For the nonanatomical design, the medial and lateral part of the polyethylene liner are often symmetrical, concave, and have the same curvature radius [128]. In this case, the curvature of the femoral component may be also designed to conform to

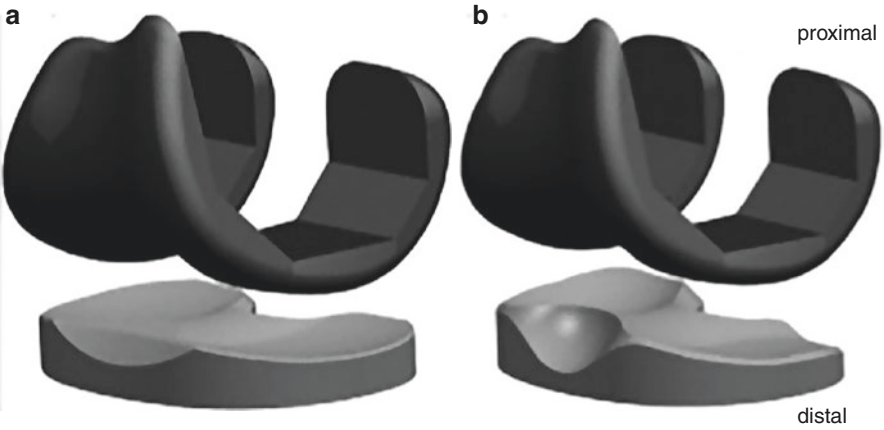

Fig. 9.11 Different designs of the polyethylene liner (**a**) nonanatomical design and (**b**) anatomical design [129] (Reprinted with permission from Elsevier, license number: 4687410127428)

the tibial liner in order to maintain the knee stability and prevent component dislocation [128]. However, the normal knee shape is asymmetrical and this nonanatomical design could induce abnormal knee kinematics such as inadequate rollback of the femur and insufficient internal rotation of the tibia. Thus, anatomical prosthesis designs aim to mimic the morphology of the intact knee to restore the kinematics of the knee. Liu et al. found that [129] changing the posterolateral region of the tibial liner to be convex could better restore the posterior translation of the lateral femoral condyle and the internal rotation of the tibia through joint flexion from 0° to 140°. A study by Moonot et al. [130] demonstrated that asymmetrical tibial liners with a highly conforming medial aspect and a moderately conforming lateral aspect could adequately restore the internal tibial rotation and reduce excessive anterior movement of the lateral femoral condyle, thus reducing wear on the liner and increasing implant longevity.

When considering the type of TKA implant to be used, it is still controversial whether the PCL needs to be retained for proper knee functionality [131]. CR knees require an intact and functioning PCL, and so this must be carefully evaluated beforehand. Otherwise, if the PCL is compromised then joint stability could be at risk. In this case a PS knee is more desirable. However, when using a PS design, joint stability is greatly affected by the design of the tibial post and the femoral cam, and this would also have a considerable effect on joint kinematics and kinetics.

If the cartilage on the patella is degraded and may compromise knee functionality, then there is the option of replacing the cartilage with a smooth polymer surface (patellar replacement). However, Cadambi et al. reported that replacing the patellar surface reduces the success rate of TKA [132]. Huang et al. also showed that tensile stress on the patellar bone increased after the surface was replaced [133]. Rand [134] stated that introduction of the patellar component could alleviate anterior knee pain of the patients. However, the revision rate of TKA is still relatively high because of the patellar component related complications, such as infection, fracture,

subluxation, wear, and loosening of the patellar component [135, 136]. Obese patients are also not recommended to undergo patellar arthroplasty because the higher loading could increase the risk of loosening and fracture [137].

3 Summary

In this chapter, the basic anatomy and functionality of bony structures, menisci, cartilage, tendons, and muscles in a normal knee joint were presented, accompanied by a discussion of the biomechanics of the patellofemoral and tibiofemoral joints. Pathological changes to the structures of the knee could alter the joint kinematics, which in long term could induce secondary injuries to the other surrounding tissues. Clinical treatments should be carefully chosen to best rebuild the normal biomechanics and functionality of the knee.

References

1. Hashemi J, Chandrashekar N, Gill B, Beynnon BD, Slauterbeck JR, Schutt RC, Mansouri H, Dabezies E. The geometry of the tibial plateau and its influence on the biomechanics of the tibiofemoral joint. J Bone Joint Surg. 2008;90:2724–34.
2. Flandry F, Hommel G. Normal anatomy and biomechanics of the knee. Sports Med Arthrosc Rev. 2011;19:82–92.
3. Sullivan NP, Robinson PW, Ansari A, Hassaballa M, Robinson JR, Porteous AJ, Eldridge JD, Murray JR. Bristol index of patellar width to thickness (BIPWiT): a reproducible measure of patellar thickness from adult MRI. Knee. 2014;21:1058–62.
4. Shepherd D, Seedhom B. Thickness of human articular cartilage in joints of the lower limb. Ann Rheum Dis. 1999;58:27–34.
5. Arokoski J, Jurvelin J, Väätäinen U, Helminen H. Normal and pathological adaptations of articular cartilage to joint loading. Scand J Med Sci Sports. 2000;10:186–98.
6. Eckstein F, Hudelmaier M, Putz R. The effects of exercise on human articular cartilage. J Anat. 2006;208:491–512.
7. Andriacchi TP, Mündermann A, Smith RL, Alexander EJ, Dyrby CO, Koo S. A framework for the in vivo pathomechanics of osteoarthritis at the knee. Ann Biomed Eng. 2004;32:447–57.
8. Seedhom B, Dowson D, Wright V. Proceedings: functions of the menisci. A preliminary study. Ann Rheum Dis. 1974;33:111.
9. McCann L, Ingham E, Jin Z, Fisher J. Influence of the meniscus on friction and degradation of cartilage in the natural knee joint. Osteoarthr Cartil. 2009;17:995–1000.
10. Fisher MB, Jung HJ, McMahon PJ, Woo SLY. Suture augmentation following ACL injury to restore the function of the ACL, MCL, and medial meniscus in the goat stifle joint. J Biomech. 2011;44:1530–5.
11. Harner CD, Baek GH, Vogrin TM, Carlin GJ, Kashiwaguchi S, Woo SLY. Quantitative analysis of human cruciate ligament insertions. Arthroscopy. 1999;15:741–9.
12. Li G, DeFrate LE, Sun H, Gill TJ. In vivo elongation of the anterior cruciate ligament and posterior cruciate ligament during knee flexion. Am J Sports Med. 2004;32:1415–20.
13. Otsubo H, Shino K, Suzuki D, Kamiya T, Suzuki T, Watanabe K, Fujimiya M, Iwahashi T, Yamashita T. The arrangement and the attachment areas of three ACL bundles. Knee Surg Sports Traumatol Arthrosc. 2012;20:127–34.

14. Kanamori A, Zeminski J, Rudy TW, Li G, Fu FH, Woo SLY. The effect of axial tibial torque on the function of the anterior cruciate ligament. Arthroscopy. 2002;18:394–8.
15. Fukuda Y, Woo SLY, Loh JC, Tsuda E, Tang P, Mcmahon PJ, Debski RE. A quantitative analysis of valgus torque on the ACL: a human cadaveric study. J Orthop Res. 2010;21:1107–12.
16. Woo SLY, Debski RE, Zeminski J, Abramowitch SD, Chan Saw SS, Fenwick JA. Injury and repair of ligaments and tendons. Annu Rev Biomed Eng. 2000;2:83–118.
17. Li G, Rudy TW, Allen C, Sakane M, Woo SLY. Effect of combined axial compressive and anterior tibial loads on in situ forces in the anterior cruciate ligament: a porcine study. J Orthop Res. 1998;16:122.
18. Voos JE, Mauro CS, Wente T, Warren RF, Wickiewicz TL. Posterior cruciate ligament: anatomy, biomechanics, and outcomes. Am J Sports Med. 2012;40:222–31.
19. Gill TJ, DeFrate LE, Wang C, Carey CT, Zayontz S, Zarins B, Li G. The biomechanical effect of posterior cruciate ligament reconstruction on knee joint function: kinematic response to simulated muscle loads. Am J Sports Med. 2003;31:530–6.
20. Inoue M, Mcgurk-Burleson E, Hollis JM, Woo SLY. Treatment of medial collateral ligament injury: I. The importance of anterior cruciate ligament on the varus-valgus knee laxity. Am J Sports Med. 1987;15:15–21.
21. Javier RF, Nicolas P. Recruitment order of quadriceps motor units: femoral nerve vs. direct quadriceps stimulation. Eur J Appl Physiol. 2013;113:3069–77.
22. Bell D, Trigsted S, Post E, Walden C. Hip strength in patients with quadriceps strength deficits after ACL reconstruction. Med Sci Sports Exerc. 2016;48:1886–92.
23. Segal NA, Glass NA. Is quadriceps muscle weakness a risk factor for incident or progressive knee osteoarthritis? Phys Sportsmed. 2011;39:44–50.
24. Ko HI, Jeon SY, Kim SH, Nam PK. Comparison of hip extensor muscle activity including the adductor magnus during three prone hip extension exercises. Physiother Theory Pract. 2019;35:451–7.
25. Cleather DJ. An important role of the biarticular hamstrings is to exert internal/external rotation moments on the tibia during vertical jumping. J Theor Biol. 2018;455:101–8.
26. Wang ZW, Liu YL, Lin KJ, Qu TB, Dong X, Cheng CK, Hai Y. The effects of implantation of tibio-femoral components in hyperextension on kinematics of TKA. Knee Surg Sports Traumatol Arthrosc. 2012;20:2032–8.
27. Giffin JR, Vogrin TM, Zantop T, Woo SLY, Harner CD. Effects of increasing tibial slope on the biomechanics of the knee. Am J Sports Med. 2004;32:376–82.
28. Arendt E, Dick R. Knee injury patterns among men and women in collegiate basketball and soccer: NCAA data and review of literature. Am J Sports Med. 1995;23:694–701.
29. Hefzy MS, Kelly BP, Cooke TD. Kinematics of the knee joint in deep flexion: a radiographic assessment. Med Eng Phys. 1998;20:302–7.
30. Hung CH, Wei HW, Chang ZW, Cheng CK. Anatomy and biomechanics of knee. In: Chan KM, editor. Practical arthroscopic surgery. Beijing: People's Medical Publishing House; 2008. p. 78–90.
31. Chung JY, Song HK, Jung MK, Oh HT, Kim JH, Yoon JS, Min BH. Larger medial femoral to tibial condylar dimension may trigger posterior root tear of medial meniscus. Knee Surg Sports Traumatol Arthrosc. 2016;24:1448–54.
32. Lafortune M, Cavanagh P, Sommer HJ, Kalenak A. Three-dimensional kinematics of the human knee during walking. J Biomech. 1992;25:347–57.
33. Zhang Y, Yao Z, Wang S, Huang W, Ma L, Huang H, Xia H. Motion analysis of Chinese normal knees during gait based on a novel portable system. Gait Posture. 2015;41:763–8.
34. Hollis JM, Takai S, Adams DJ, Horibe S, Woo SLY. The effects of knee motion and external loading on the length of the anterior cruciate ligament (ACL): a kinematic study. J Biomech Eng. 1991;113:208.
35. ASTM. Standard guide for total knee replacement loading profiles. West Conshohocken, PA: ASTM International; 2017. p. 1–33.
36. Fox AJ, Wanivenhaus F, Rodeo SA. The basic science of the patella: structure, composition, and function. J Knee Surg. 2012;25:127–42.

37. Akbarshahi M, Fernandez JW, Schache AG, Pandy MG. Subject-specific evaluation of patellofemoral joint biomechanics during functional activity. Med Eng Phys. 2014;36:1122–33.
38. Hsu RWW, Cheng CK, Yu SY, Chen TH. The laxity of knee joint in normal Chinese adults. Biomed Eng Appl Basis Commun. 1994;6:186–92.
39. Shultz SJ, Nguyen AD, Schmitz RJ. Differences in lower extremity anatomical and postural characteristics in males and females between maturation groups. J Orthop Sports Phys Ther. 2008;38:137–49.
40. Byl T, Cole JA, Livingston LA. What determines the magnitude of the Q angle? A preliminary study of selected skeletal and muscular measures. J Sport Rehabil. 2000;9:26–34.
41. Griffin LY, Albohm MJ, Arendt EA, Bahr R, Beynnon BD, DeMaio M, Dick RW, Engebretsen L, Garrett WE, Hannafin JA. Understanding and preventing noncontact anterior cruciate ligament injuries: a review of the Hunt Valley II meeting, January 2005. Am J Sports Med. 2006;34:1512–32.
42. Ali N, Rouhi G. Barriers to predicting the mechanisms and risk factors of non-contact anterior cruciate ligament injury. Open Biomed Eng J. 2010;4:178–89.
43. Shimokochi Y, Shultz SJ. Mechanisms of noncontact anterior cruciate ligament injury. J Athl Train. 2008;43:396–408.
44. Finsterbush A, Frankl U, Matan Y, Mann G. Secondary damage to the knee after isolated injury of the anterior cruciate ligament. Am J Sports Med. 1990;18:475–9.
45. Lecoq FA, Parienti JJ, Murison J, Ruiz N, Bouacida K, Besse J, Morin V, Padiolleau G, Cucurulo T, Graveleau N. Graft choice and the incidence of osteoarthritis after anterior cruciate ligament reconstruction: a causal analysis from a cohort of 541 patients. Am J Sports Med. 2018;46:2842–50.
46. Smith BA, Livesay GA, Woo SL. Biology and biomechanics of the anterior cruciate ligament. Clin Sports Med. 1993;12:637–70.
47. Gföller P, Abermann E, Runer A, Hoser C, Pflüglmayer M, Wierer G, Fink C. Non-operative treatment of ACL injury is associated with opposing subjective and objective outcomes over 20 years of follow-up. Knee Surg Sports Traumatol Arthrosc. 2019;27:2665–71.
48. Fink C, Hoser C, Hackl W, Navarro R, Benedetto K. Long-term outcome of operative or nonoperative treatment of anterior cruciate ligament rupture-is sports activity a determining variable? Int J Sports Med. 2001;22:304–9.
49. Noyes F, Mooar L, Moorman C, McGinniss G. Partial tears of the anterior cruciate ligament. Progression to complete ligament deficiency. J Bone Joint Surg Br Vol. 1989;71:825–33.
50. Feagin JA, Curl W. Isolated tear of the anterior cruciate ligament: 5-year follow-up study. Am J Sports Med. 1976;4:95–100.
51. Sandberg R, Balkfors B, Nilsson B, Westlin N. Operative versus non-operative treatment of recent injuries to the ligaments of the knee. A prospective randomized study. J Bone Joint Surg Am Vol. 1987;69:1120–6.
52. Feagin JA, Pierce CM, Geyer MR. ACL primary repair: what we did, the results, and how it helps today to tailor treatments to the patient and the pathology. In: The ACL-deficient knee. London: Springer; 2012. p. 97–104.
53. Sipe JD. Tissue engineering and reparative medicine. Ann N Y Acad Sci. 2002;961:1–9.
54. Badylak SF, Freytes DO, Gilbert TW. Extracellular matrix as a biological scaffold material: structure and function. Acta Biomater. 2009;5:1–13.
55. Fisher MB, Liang R, Jung HJ, Kim KE, Zamarra G, Almarza AJ, McMahon PJ, Woo SLY. Potential of healing a transected anterior cruciate ligament with genetically modified extracellular matrix bioscaffolds in a goat model. Knee Surg Sports Traumatol Arthrosc. 2012;20:1357–65.
56. Fleming BC, Carey JL, Spindler KP, Murray MM. Can suture repair of ACL transection restore normal anteroposterior laxity of the knee? An ex vivo study. J Orthop Res. 2008;26:1500–5.
57. Gisselfält K, Edberg B, Flodin P. Synthesis and properties of degradable poly (urethane urea) s to be used for ligament reconstructions. Biomacromolecules. 2002;3:951–8.

58. Farraro KF, Sasaki N, Woo SLY, Kim KE, Tei MM, Speziali A, McMahon PJ. Magnesium ring device to restore function of a transected anterior cruciate ligament in the goat stifle joint. J Orthop Res. 2016;34:2001–8.
59. Chambat P, Guier C, Sonnery-Cottet B, Fayard J-M, Thaunat M. The evolution of ACL reconstruction over the last fifty years. Int Orthop. 2013;37:181–6.
60. Parchi PD, Ciapini G, Paglialunga C, Giuntoli M, Picece C, Chiellini F, Lisanti M, Scaglione M. Anterior cruciate ligament reconstruction with LARS artificial ligament-clinical results after a long-term follow-up. Joints. 2018;6:75–9.
61. Barenius B, Nordlander M, Ponzer S, Tidermark J, Eriksson K. Quality of life and clinical outcome after anterior cruciate ligament reconstruction using patellar tendon graft or quadrupled semitendinosus graft: an 8-year follow-up of a randomized controlled trial. Am J Sports Med. 2010;38:1533–41.
62. Aune AK, Holm I, Risberg MA, Jensen HK, Steen H. Four-strand hamstring tendon autograft compared with patellar tendon-bone autograft for anterior cruciate ligament reconstruction: a randomized study with two-year follow-up. Am J Sports Med. 2001;29:722–8.
63. Laboute E, James-Belin E, Puig P, Trouve P, Verhaeghe E. Graft failure is more frequent after hamstring than patellar tendon autograft. Knee Surg Sports Traumatol Arthrosc. 2018;26:3537–46.
64. Tashman S, Collon D, Anderson K, Kolowich P, Anderst W. Abnormal rotational knee motion during running after anterior cruciate ligament reconstruction. Am J Sports Med. 2004;32:975–83.
65. Salmon LJ, Russell VJ, Refshauge K, Kader D, Connolly C, Linklater J, Pinczewski LA. Long-term outcome of endoscopic anterior cruciate ligament reconstruction with patellar tendon autograft: minimum 13-year review. Am J Sports Med. 2006;34:721–32.
66. Nebelung W, Becker R, Merkel M, Röpke M. Bone tunnel enlargement after anterior cruciate ligament reconstruction with semitendinosus tendon using endobutton fixation on the femoral side. Arthroscopy. 1998;14:810–5.
67. Lai CC, Ardern CL, Feller JA, Webster KE. Eighty-three per cent of elite athletes return to preinjury sport after anterior cruciate ligament reconstruction: a systematic review with meta-analysis of return to sport rates, graft rupture rates and performance outcomes. Br J Sports Med. 2018;52:128–38.
68. Chen CH, Chang CH, Su CI, Wang KC, Liu HT, Yu CM, Wong CB, Wang IC. Arthroscopic single-bundle anterior cruciate ligament reconstruction with periosteum-enveloping hamstring tendon graft: clinical outcome at 2 to 7 years. Arthroscopy. 2010;26:907–17.
69. Nagelli CV, Cook JL, Kuroki K, Bozynski C, Ma R, Hewett TE. Does anterior cruciate ligament innervation matter for joint function and development of osteoarthritis? J Knee Surg. 2017;30:364–71.
70. Guidoin MF, Marois Y, Bejui J, Poddevin N, King MW, Guidoin R. Analysis of retrieved polymer fiber based replacements for the ACL. Biomaterials. 2000;21:2461–74.
71. Englund M, Guermazi A, Gale D, Hunter DJ, Aliabadi P, Clancy M, Felson DT. Incidental meniscal findings on knee MRI in middle-aged and elderly persons. N Engl J Med. 2008;359:1108–15.
72. Zhang F, Kumm J, Svensson F, Turkiewicz A, Frobell R, Englund M. Risk factors for meniscal body extrusion on MRI in subjects free of radiographic knee osteoarthritis: longitudinal data from the osteoarthritis initiative. Osteoarthr Cartil. 2016;24:801–6.
73. Kalliakmanis A, Zourntos S, Bousgas D, Nikolaou P. Comparison of arthroscopic meniscal repair results using 3 different meniscal repair devices in anterior cruciate ligament reconstruction patients. Arthroscopy. 2008;24:810–6.
74. Arnoczky SP, Warren RF. The microvasculature of the meniscus and its response to injury: an experimental study in the dog. Am J Sports Med. 1983;11:131–41.
75. Allaire R, Muriuki M, Gilbertson L, Harner CD. Biomechanical consequences of a tear of the posterior root of the medial meniscus: similar to total meniscectomy. J Bone Joint Surg. 2008;90:1922–31.

76. Jarraya M, Roemer FW, Englund M, Crema MD, Gale HI, Hayashi D, Katz JN, Guermazi A. Meniscus morphology: does tear type matter? A narrative review with focus on relevance for osteoarthritis research. Semin Arthritis Rheum. 2017;46:552–61.
77. McDermott I. Meniscal tears, repairs and replacement: their relevance to osteoarthritis of the knee. Br J Sports Med. 2011;45:292–7.
78. Roos H, Laurén M, Adalberth T, Roos EM, Jonsson K, Lohmander LS. Knee osteoarthritis after meniscectomy: prevalence of radiographic changes after twenty-one years, compared with matched controls. Arthritis Rheum. 1998;41:687–93.
79. Ihn J, Kim S, Park I. In vitro study of contact area and pressure distribution in the human knee after partial and total meniscectomy. Int Orthop. 1993;17:214–8.
80. Papageorgiou CD, Gil JE, Kanamori A, Fenwick JA, Woo SL, Fu FH. The biomechanical interdependence between the anterior cruciate ligament replacement graft and the medial meniscus. Am J Sports Med. 2001;29:226–31.
81. Jorgensen U, Sonne-Holm S, Lauridsen F, Rosenklint A. Long-term follow-up of meniscectomy in athletes. A prospective longitudinal study. J Bone Joint Surg Br Vol. 1987;69:80–3.
82. McNicholas M, Rowley D, McGurty D, Adalberth T, Abdon P, Lindstrand A, Lohmander L. Total meniscectomy in adolescence: a thirty-year follow-up. J Bone Joint Surg Br Vol. 2000;82:217–21.
83. Milachowski K, Weismeier K, Wirth C. Homologous meniscus transplantation. Int Orthop. 1989;13:1–11.
84. van der Wal RJP, Thomassen BJW, van Arkel ERA. Long-term clinical outcome of open meniscal allograft transplantation. Am J Sports Med. 2009;37:2134–9.
85. Stone K, Adelson W, Pelsis J, Walgenbach A, Turek T. Long-term survival of concurrent meniscus allograft transplantation and repair of the articular cartilage: a prospective two-to 12-year follow-up report. J Bone Joint Surg Br Vol. 2010;92:941–8.
86. Verdonk PC, Verstraete KL, Almqvist KF, De Cuyper K, Veys EM, Verbruggen G, Verdonk R. Meniscal allograft transplantation: long-term clinical results with radiological and magnetic resonance imaging correlations. Knee Surg Sports Traumatol Arthrosc. 2006;14:694–706.
87. Rodkey WG, DeHaven KE, Montgomery WH, Baker CL, Beck CL, Hormel SE, Steadman R, Cole BJ, Briggs KK. Comparison of the collagen meniscus implant with partial meniscectomy: a prospective randomized trial. J Bone Joint Surg. 2008;90:1413–26.
88. Krishnasamy P, Hall M, Robbins S. The role of skeletal muscle in the pathophysiology and management of knee osteoarthritis. Rheumatology. 2018;57:iv22–33.
89. Miller RH. Joint loading in runners does not initiate knee osteoarthritis. Exerc Sport Sci Rev. 2017;45:87–95.
90. McAlindon T, Formica M, Schmid C, Fletcher J. Changes in barometric pressure and ambient temperature influence osteoarthritis pain. Am J Med. 2007;120:429–34.
91. Hofstede S, Vlieland TPV, Ende CH, Mheen PJM, Nelissen R, Bodegom-Vos L. Designing a strategy to implement optimal conservative treatments in patients with knee or hip osteoarthritis in orthopedic practice: a study protocol of the BART-OP study. Implement Sci. 2014;9:22–8.
92. Wise BL, Niu J, Mei Y, Lane NE, Harvey W, Felson DT, Hietpas J, Nevitt M, Sharma L, Torner J. Patterns of compartment involvement in tibiofemoral osteoarthritis in men and women and in Caucasians and African Americans: the multicenter osteoarthritis study. Arthritis Care Res. 2012;64:847–52.
93. Willis-Owen CA, Brust K, Alsop H, Miraldo M, Cobb JP. Unicondylar knee arthroplasty in the UK National Health Service: an analysis of candidacy, outcome and cost efficacy. Knee. 2009;16:473–8.
94. Cao Z, Mai X, Wang J, Feng E, Huang Y. Unicompartmental knee arthroplasty vs high tibial osteotomy for knee osteoarthritis: a systematic review and meta-analysis. J Arthroplasty. 2017;33:952–9.
95. Lambert KL. The weight-bearing function of the fibula. A strain gauge study. J Bone Joint Surg Am Vol. 1971;53:507–13.

96. Takebe K, Nakagawa A, Minami H, Kanazawa H, Hirohata K. Role of the fibula in weight-bearing. Clin Orthop Relat Res. 1984;184:289–92.
97. Pho RW, Levack B, Satku K, Patradul A. Free vascularised fibular graft in the treatment of congenital pseudarthrosis of the tibia. J Bone Joint Surg Br Vol. 1985;67:64–70.
98. Pho RW. Malignant giant-cell tumor of the distal end of the radius treated by a free vascularized fibular transplant. J Bone Joint Surg Am Vol. 1981;63:877–84.
99. Solonen KA. Free vascularized bone graft in the treatment of pseudarthrosis. Int Orthop. 1982;6:9–13.
100. Hall FM. Treatment of avascular necrosis of the femoral head. Hip. 1983;165:876–7.
101. Wang J, Wang K, Chen W, Wu T, Zhang F, Zhang Y. The influence of partial fibula osteotomy on hip knee and ankle joint. J Hei Bei Med Univ. 2015;36:84–5.
102. Yang ZY, Chen W, Li CX, Wang J, Shao DC, Hou ZY, Gao SJ, Wang F, Li JD, Hao JD. Medial compartment decompression by fibular osteotomy to treat medial compartment knee osteoarthritis: a pilot study. Orthopedics. 2015;38:e1110–e4.
103. Zou GP, Lan WB, Zeng YY, Xie JH, Chen SL, YR Q. Early clinical effect of proximal fibular osteotomy on knee osteoarthritis. Biomed Res. 2017;28:9291–4.
104. Nie Y, Ma J, Huang ZY, Xu B, Tang S, Shen B, Kraus VB, FX P. Upper partial fibulectomy improves knee biomechanics and function and decreases knee pain of osteoarthritis: a pilot and biomechanical study. J Biomech. 2018;71:22–9.
105. Yazdi H, Mallakzadeh M, Mohtajeb M, Farshidfar SS, Baghery A, Givehchian B. The effect of partial fibulectomy on contact pressure of the knee: a cadaveric study. Eur J Orthop Surg Traumatol. 2014;24:1285–9.
106. Sandoval EAP, Mesa AC, Valera DH, Pérez JAQ, Quiñones AD, Villanueva FS. Complications of proximal fibular ostectomy in patients with painful genu varum. Revista Cubana de Medicina Militar. 2018;47:1–9.
107. Zhang Y-Z. Innovations in orthopedics and traumatology in China. Chin Med J. 2015;128:2841.
108. Qi XZ, Chang CM, Tan CM, Zhang YZ, Cheng CK. Evaluation of unicondylar knee arthroplasty and fibulectomy from a biomechanical viewpoint. J Med Biomech. 2015;30:479–87.
109. Laskin RS. Unicompartmental tibiofemoral resurfacing arthroplasty. JBJS. 1978;60:182–5.
110. Insall J, Aglietti P. A five to seven-year follow-up of unicondylar arthroplasty. JBJS. 1980;62:1329–37.
111. Kulshrestha V, Datta B, Kumar S, Mittal G. Outcome of unicondylar knee arthroplasty vs total knee arthroplasty for early medial compartment arthritis: a randomized study. J Arthroplast. 2017;32:1460–9.
112. Smith JR, Robinson JR, Porteous AJ, Murray JR, Hassaballa MA, Artz N, Newman JH. Fixed bearing lateral unicompartmental knee arthroplasty—short to midterm survivorship and knee scores for 101 prostheses. Knee. 2014;21:843–7.
113. Howell RE, Lombardi AV Jr, Crilly R, Opolot S, Berend KR. Unicompartmental knee arthroplasty: does a selection bias exist? J Arthroplast. 2015;30:1740–2.
114. Koskinen E, Paavolainen P, Eskelinen A, Pulkkinen P, Remes V. Unicondylar knee replacement for primary osteoarthritis: a prospective follow-up study of 1,819 patients from the Finnish Arthroplasty Register. Acta Orthop. 2007;78:128–35.
115. Liddle A, Pandit H, Judge A, Murray D. Optimal usage of unicompartmental knee arthroplasty: a study of 41 986 cases from the National Joint Registry for England and Wales. Bone Joint J. 2015;97:1506–11.
116. Liddle AD, Pandit H, Judge A, Murray DW. Effect of surgical caseload on revision rate following total and unicompartmental knee replacement. JBJS. 2016;98:1–8.
117. Yoshida K, Tada M, Yoshida H, Takei S, Fukuoka S, Nakamura H. Oxford phase 3 unicompartmental knee arthroplasty in Japan—clinical results in greater than one thousand cases over ten years. J Arthroplast. 2013;28:168–71.
118. Mckeever DC. The choice of prosthetic materials and evaluation of results. Clin Orthop Relat Res. 1955;6:17–21.

119. Gunston FH. Prosthetic simulation of normal knee movement. J Bone Joint Surg Br Vol. 1971;53:272–7.
120. Marmor L. The modular knee. Clin Orthop Rel Res. 1973;94:242–8.
121. Goodfellow JW, O'Connor J. The mechanics of the knee and prosthesis design. J Bone Joint Surg Br Vol. 1978;60:358–69.
122. American Joint Replacement Registry. Annual report. 2018. http://www.ajrr.net/images/annual_reports/AAOS-AJRR-2018-Annual-Report-final.pdf.
123. Australian Orthopaedic Association National Joint Replacement Registry. Hip, knee & shoulder annual report. 2018. https://aoanjrr.sahmri.com/documents/10180/576950/Hip%2C%20Knee%20%26%20Shoulder%20Arthroplasty.
124. Swedish Knee Arthroplasty Register. Annual report. 2017. http://www.myknee.se/pdf/SVK_2017_Eng_1.0.pdf.
125. National Joint Registry. 15th Annual Report National Joint Registry for England. Wales, Northern Ireland and the Isle of Man. https://www.hqip.org.uk/wp-content/uploads/2018/11/NJR-15th-Annual-Report-2018.pdf.
126. Vasso M, Corona K, D'Apolito R, Mazzitelli G, Panni AS. Unicompartmental knee arthroplasty: modes of failure and conversion to total knee arthroplasty. Joints. 2017;5:44–50.
127. Riff AJ, Sah AP, Della Valle CJ. Outcomes and complications of unicondylar arthroplasty. Clin Sports Med. 2014;33:149–60.
128. Wang X-H, Song D-Y, Dong X, Suguro T, Cheng C-K. Motion type and knee articular conformity influenced mid-flexion stability of a single radius knee prosthesis. Knee Surg Sports Traumatol Arthrosc. 2019;27:1595–603.
129. Liu YL, Lin KJ, Huang CH, Chen WC, Chen CH, Chang TW, Lai YS, Cheng CK. Anatomic-like polyethylene insert could improve knee kinematics after total knee arthroplasty—a computational assessment. Clin Biomech. 2011;26:612–9.
130. Moonot P, Shang M, Railton GT, Field RE, Banks SA. In vivo weight-bearing kinematics with medial rotation knee arthroplasty. Knee. 2010;17:33–7.
131. Fang C-H, Chang C-M, Lai Y-S, Chen W-C, Song D-Y, McClean CJ, Kao H-Y, Qu T-B, Cheng C-K. Is the posterior cruciate ligament necessary for medial pivot knee prostheses with regard to postoperative kinematics? Knee Surg Sports Traumatol Arthrosc. 2015;23:3375–82.
132. Cadambi A, Engh GA, Dwyer KA, Vinh TN. Osteolysis of the distal femur after total knee arthroplasty. J Arthroplasty. 1994;9:579–94.
133. Huang CH, Hsu LI, Chang TK, Chuang TY, Shih SL, Lu YC, Chen CS, Huang CH. Stress distribution of the patellofemoral joint in the anatomic V-shape and curved dome-shape femoral component: a comparison of resurfaced and unresurfaced patellae. Knee Surg Sports Traumatol Arthrosc. 2017;25:263–71.
134. Chang MA, Rand JA, Trousdale RT. Patellectomy after total knee arthroplasty. Clin Orthop Rel Res (1976–2007). 2005;440:175–7.
135. Jan N, Fontaine C, Migaud H, Pasquier G, Valluy J, Saffarini M, Putman S. Patellofemoral design enhancements reduce long-term complications of postero-stabilized total knee arthroplasty. Knee Surg Sports Traumatol Arthrosc. 2019;27:1241–50.
136. Huang CH, Liau JJ, Ho FY, Lin CY, Young TH, Cheng CK. Polyethylene failure of the patellar component in New Jersey low-contact stress total knee arthroplasties. J Arthroplast. 2005;20:202–8.
137. Huang CH, Hsu LI, Lin KJ, Chang TK, Cheng CK, Lu YC, Chen CS, Huang CH. Patellofemoral kinematics during deep knee flexion after total knee replacement: a computational simulation. Knee Surg Sports Traumatol Arthrosc. 2014;22:3047–53.

Chapter 10
Biomechanics of Foot and Ankle

Duo Wai-Chi Wong, Ming Ni, Yan Wang, and Ming Zhang

Abstract The human foot-and-ankle is a highly developed, biomechanically complex structure which sustains the weight of the body and facilitates forces transmission during propulsion. Apart from 28 bones, the foot is composed of more than 30 joints surrounded by more than a hundred of muscles, tendons, and ligaments. The geometry of the foot and the balance-controlling mechanism of the body enabled us on a variety of motions, including walking, running, and jumping.

However, the high and complicated load on the foot impose risk of the foot injury, trauma, and other problems. Common foot disorders include hallux valgus, bunion, flatfoot, plantar fasciitis, heel pain, and Achilles tendonitis. Ankle fracture in elderly people is a major burden in developed countries with an aging population. There was a threefold increase in the incidence of ankle fractures in elderly people in the last century. Aging and overweight also contribute to the chance of foot problems. Besides, calcaneal fracture is common for young and physically active population and may turn into degenerative or traumatic arthritis after serious injuries.

D. W.-C. Wong · Y. Wang · M. Zhang (✉)
Department of Biomedical Engineering, The Hong Kong Polytechnic University, Hong Kong, China

Hong Kong Polytechnic University Shenzhen Research Institute, Shenzhen, China
e-mail: ming.zhang@polyu.edu.hk

M. Ni
Department of Biomedical Engineering, The Hong Kong Polytechnic University, Hong Kong, China

Tongji Hospital, Tongji University School of Medicine, Shanghai, China

Pudong New Area People's Hospital, Shanghai, China

C.-K. Cheng, S. L-Y. Woo (eds.), *Frontiers in Orthopaedic Biomechanics*,
https://doi.org/10.1007/978-981-15-3159-0_10

Both surgical and conservative methods have been adopted to treat foot problems and diseases. Most of the interventions targeted the treatment on the problem site but the effect of the foot problems could extend beyond the site to adjacent regions or the entire foot. Assessment and evaluation of the biomechanical environment and the variations before and after the intervention could help intervention design, planning and thus minimizes complications.

Experimental methodologies, such as motion capture analysis, pedobarography, and cadaveric experiments have been developed to quantify foot biomechanics. However, the internal biomechanics of the foot, such as the stress distributions within bones and soft tissues is not easy to measure by experiments. Computational methods or platforms such as the finite element (FE) analysis are useful tools to investigate biomechanics of the musculoskeletal structures. This evaluation method has been used to study injury mechanism, improve prosthetic and orthotic designs, and predict surgery outcome, in addition to promoting fundamental understanding of foot biomechanics. In this chapter, four common foot problems and interventions of the foot and ankle were analyzed by FE models including hallux valgus, ankle arthroplasty, tarsometatarsal joint fusion, and calcaneal fractures.

Keywords Hallux valgus · Ankle arthrodesis · Tarsometatarsal joint fusion
Calcaneal fracture · Finite element method · Foot and ankle

1 Biomechanics of First Ray Hypermobility and Hallux Valgus

Summary
Hallux valgus (or hallux abducto valgus) has been one of the most common foot problems and associated with functional disability. Clinical studies were conducted that featured the pathoanatomy and pathomechanics of hallux valgus. However, the effectiveness of current treatments remains unsatisfactory, while complications and recurrence rates are undeniable. It is pragmatically demanding to further understand the biomechanics of hallux valgus to improve intervention. This study constructed a three-dimensional foot model of the subject and simulated with hypermobility. Besides, partial models consisted of isolated first ray and were constructed and compared among the normal participant and hallux valgus scenario. The model participant was invited to participate in a gait analysis session to acquire the boundary and loading condition for the simulation of walking stance. The finite element (FE) analysis outcome suggested that the hypermobility case generated higher joint force at the metatarsocuneiform and metatarsophalangeal joint. In the medial-lateral direction, the metatarsocuneiform joint force switched sharply that could indicate a potential risk of metatarsus primus varus.

1.1 Background

Hallux valgus (or hallux abducto valgus) is represented by a lateral and medial deviation deformity of the hallux and the first metatarsal, respectively. The enlarged and swollen medial projected eminence is also a characteristics of hallux valgus and thus it is also known as the bunion. Hallux valgus imposes significant public health burden as supported by the incident rate of related foot surgery. There could also be secondary problems such as poor gait patterns and impaired coordination and stability that may lead to falling risks to the elderly population [1–5].

The prevalence of hallux valgus was found strongly associated with family history, while gender is also suggested to be a contributing factor [6]. The shape of the foot bones, arch height, and the level of hypermobility may be affected by heredity [7]. In fact, the incidence of hallux valgus on women is more than two times higher than that of men [8]. Similarly, the different sex presents different bone morphology and alignment, in addition to the level of hypermobility or laxity [9–11]. Other influencing factors included footwear, body weight, habit, and occupation [12].

In fact, hallux valgus ranks high in the list of common foot complaint. More than one-quarter of adults in the United Kingdom suffered from the problem [8], while nearly 15% of students reported hallux valgus as reported by Owoeye et al. [13]. The same study reported that 9% of the students with hallux valgus showed pain and 14% demonstrated difficulty in prolong walking. Survey on the elderly population reported even higher prevalence [14] which results in economic burden on hospitalization and society. More than 50 k surgeries were taken to treat hallux valgus which accounted for more than one-quarter of all forefoot surgeries [15]. More than 2 absent days are incurred by relevant surgery, resulting in more than AUS$3800 productivity loss and AUS$3700 hospitalization cost in Australia in 2008 [16–19].

Despite that surgical correction for hallux valgus are not few, the outcome remains unsatisfactory with failures, complications, and recurrence. The complication rates and recurrence rates can be up to 55% and 16%, respectively [20, 21], contributed by over-correction, avascular necrosis, etc. [22]. Surgery using soft tissue correction procedure produces even higher failure rates [22].

1.2 Biomechanical Study of Hallux Valgus

Biomechanical studies on hallux valgus and its intervention have been conducted to better understand the pathogenesis of the disease and improve treatment outcomes. The hypermobility of the first ray was first introduced by Morton and Lapidus which attracted debates on the appropriate interventions [23, 24]. Arthrodesis procedure was proposed aiming to address the problem of stability. The evaluation of stability was also included in other studies on the outcome of osteotomy of hallux valgus

[25]. Currently, mobility and stability are assessed by manual dorsal excursion [26], load-bearing radiographs [12], or custom-made mechanical devices [27]. Yet the quantification of hypermobility has been believed to be subjective and confined to static measurement [23].

Foot types and deformities are often classified using plantar pressure measurement [28]. Hallux valgus was found to impair the loading at the hallux region. The peak pressure of the forefoot was found shifting laterally [29], as evidenced by the heightened peak pressure and pressure time-integral at the central forefoot [30]. Conversely, some study discovered that the plantar pressure pattern moved medially [31, 32]. There could be other factors, including secondary deformities, that may influence the pressure pattern on the medial metatarsal region [33]. Hallux valgus patients shall have a persistent reduction in hallux loading compensated by the central metatarsal area [33].

Pedobarographic assessment has been used as a biomechanical tool to evaluate surgical interventions of hallux valgus. By expanding the contact area under hallux, Mittal et al. [34] suggested that McBride procedure could restore some of the hallux functions. Another operation carried out by Saro et al. [35] suggested that the operation did not produce positive biomechanical effect as indicated by the significant reduction in peak pressure under the hallux and heel region. Some studies compared different osteotomy procedures (Mitchell and Scarf) using plantar pressure distribution [36].

Since consensus was not reached on the interpretation of plantar pressure distribution towards clinical outcome of the surgeries, researchers endeavored to investigate how hallux valgus attenuates the biomechanical environment of the foot by means of manual examination and further plantar pressure studies. This approach has been achieved by the finite element (FE) simulations that could investigate the internal stress or strain pattern as well as the load transfer characteristics noninvasively [37]. A major extrinsic factor of hallux valgus, the wearing of high-heeled shoes, was considered in the study of Yu et al. [38] using FE model. In addition, a simplified first ray model was used to understand the linkage between first ray hypermobility and hallux valgus [39]. Meanwhile, we have constructed a FE model to imitate hallux valgus and simulated the walking stance. Five instants were extracted from the simulation findings and the outcome on stress, strain, and joint loading were used to evaluate the changes of kinematics and stability induced by hallux valgus.

1.3 Finite Element Model Development

1.3.1 Clinical Image Acquisition and Geometry Reconstruction

The model geometry of the normal foot and hallux valgus foot (asymptomatic) was reconstructed from magnetic resonance (MR) images of two female subjects. They were both aged 28, 165 cm tall, while the body weights were 54 kg and 56 kg, respectively, for the normal and hallux valgus foot participants. Both participants

reported no other musculoskeletal pathology, pain, or lower limb trauma or surgery within the past 6 months. Segmentation software were used to segment and process the MR images (Mimics v 10, Materalise, Leuven, Belgium and Rapidform XOR2, 3D INUS Technology Inc., Seoul, Korea). We constructed the encapsulated soft tissue and bony structures, including 30 bones and two sesamoids, using 3D solid, while the ligaments were modelled as 3D surfaces and muscles were modelled as 1D connectors.

1.3.2 Material Properties

The elastic modulus of the bone was 7300 MPa with the Poisson's ratio of 0.3 [40], and was assumed isotropic and homogeneous. The material of the encapsulated soft tissue was hyperelastic with data experimented by Lemmon et al. [41]. The supporting ground was bilayers. The bottom layer was rigid, while the upper layer was deformable (40 GPa), representing concrete ground. The elastic modulus of all ligaments was 264.8 MPa, which was the reported average elasticity of rearfoot ligaments [42]. The thickness of ligaments was 1.5 mm as reported by Milz et al. [43].

1.3.3 Load and Boundary Conditions

Ground reaction force (GRF) and tibial inclination from the gait experiment of the model subject was input as the loading and boundary conditions to simulate stance phase in five consecutive static steps named: heel strike (0% stance), GRF first peak (27% stance), GRF valley, (45% stance), initial push-off (60%), and GF second peak (75%). The magnitude of muscle forces was adopted from literature [44–46] based on the level of muscle activation and maximum capacity.

Frictionless contact was assigned at all joint facets. The coefficient of friction between the ground and tissue contact was 0.6 [47]. The constructed geometrical of the bony components were illustrated in Fig. 10.1, demonstrating a predicted metatarsophalangeal (MTP) dorsiflexion angle of 27.3° at 75% stance. The axial direction was defined as the longitudinal axis along the tibia and fibula segment. Both the direction of the metatarsocuneiform (MC) joint force and the MTP joint force were defined as acting from the proximal side to the distal side.

1.4 Study Design

The study was divided into two parts. The first part involved with the reconstruction of the entire foot and ankle model for the normal subject while comparing to that of the hypermobile foot. By weakening the deep transverse metatarsal ligament (DTML) between the first and second metatarsals, the hypermobility of the first ray

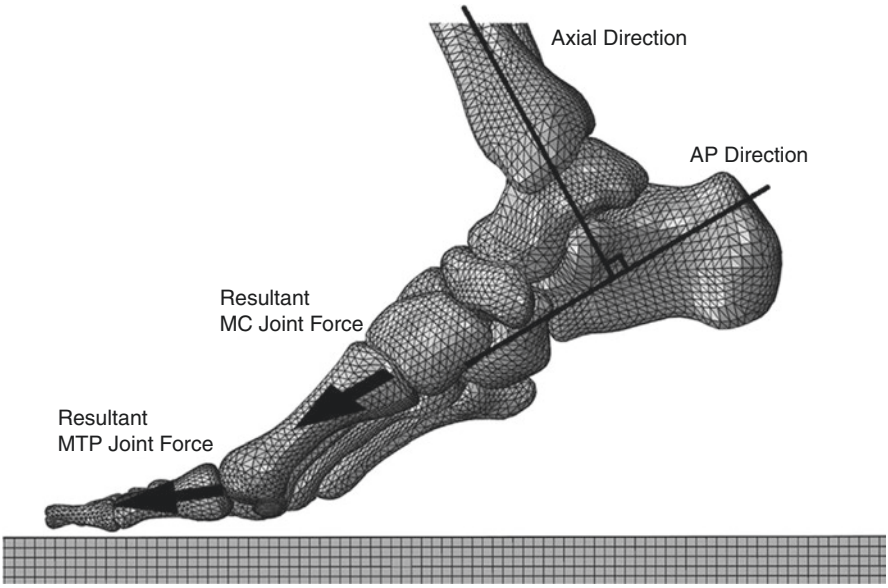

Fig. 10.1 Illustration of the joint forces and defined axes directions. (*Reprinted from Medical Engineering & Physics, 36, Wong et al., Biomechanics of first ray hypermobility: An investigation on the joint force during walking using finite element analysis, 1388–1393, Copyright (2014), with permission from Elsevier*)

was resembled on the normal foot [48]. The MC and MTP joint forces were output from the simulation. The second part of the study involved with the building of partial foot model (the first ray) for the normal and hallux valgus participant. The bone alignment and displacement were extracted for analysis.

1.5 Implications of the Finite Element Model

1.5.1 Model Validation

Model validation was performed by comparing the measured and predicted plantar pressure. The participant was asked to walk at their self-comfortable speed. An insole plantar pressure measurement system (F-Scan, Tekscan, USA) was utilized to assess the plantar pressure distribution. Figure 10.2 shows the comparison of prediction and measurement at the instant of GRF first peak and second peak. During GRF first peak, the predicted maximum peak pressure was 0.49 MPa, locating at the heel while the measurement value was 0.46 MPa. On the other hand, the plantar pressure was concentrated at the hallux, toes, and metatarsals at GRF second peak. The predicted and measured maximum peak pressures at the hallux region were 0.52 MPa and 0.46 MPa, respectively, which was generally agreeable.

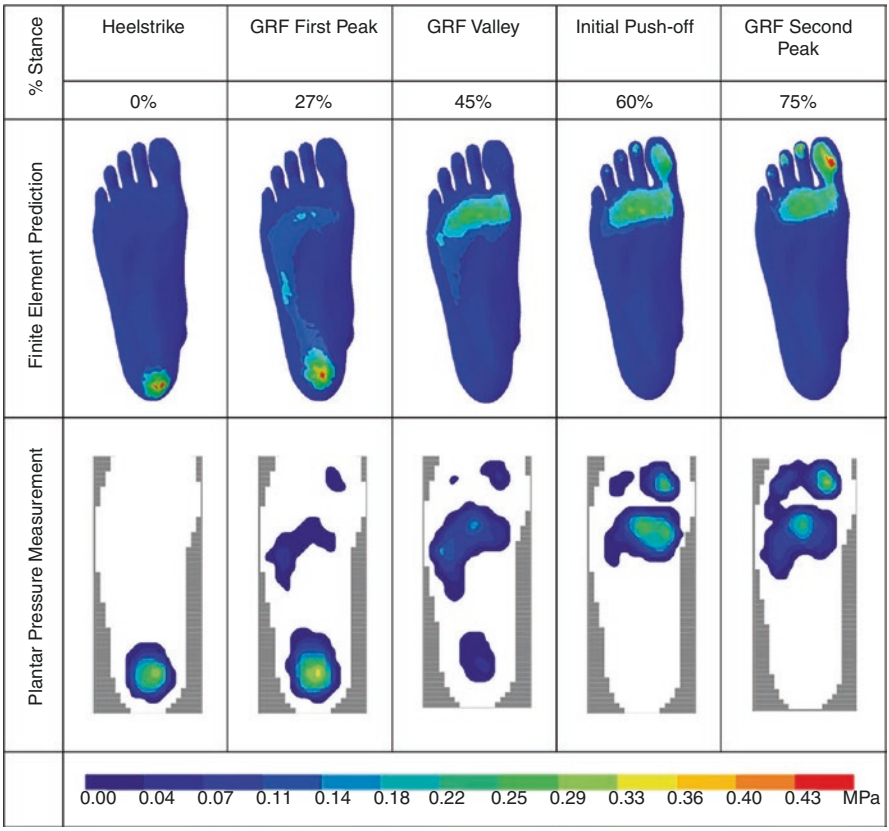

Fig. 10.2 Comparison of FE predicted and experimental result on plantar pressure distribution. (*Reprinted from Medical Engineering & Physics, 36, Wong et al., Biomechanics of first ray hypermobility: An investigation on the joint force during walking using finite element analysis, 1388–1393, Copyright (2014), with permission from Elsevier*)

1.5.2 Load Transfer Across the First Ray

The MC joint forces of the normal and the hypermobile foot in AP, axial, and mediolateral (ML) directions during stance are shown in Fig. 10.3. Before the instant of GRF first peak, joint forces in all directions were quite small, but increased apparently after the instant of GRF valley. On the other hand, the force in both axial and AP directions increased consistently until terminal stance, while that in medial-lateral direction switched laterally during late stance.

The deviation of MC joint force became prominent during late stance. There were about one-tenth leverage in the medial direction and one-fifth leverage in the axial and AP direction joint forces upon hypermobility during initial push-off. The increase was more than 25% at GRF second-peak instant in axial and AP directions, and skyrocketed to 200% in the medial direction.

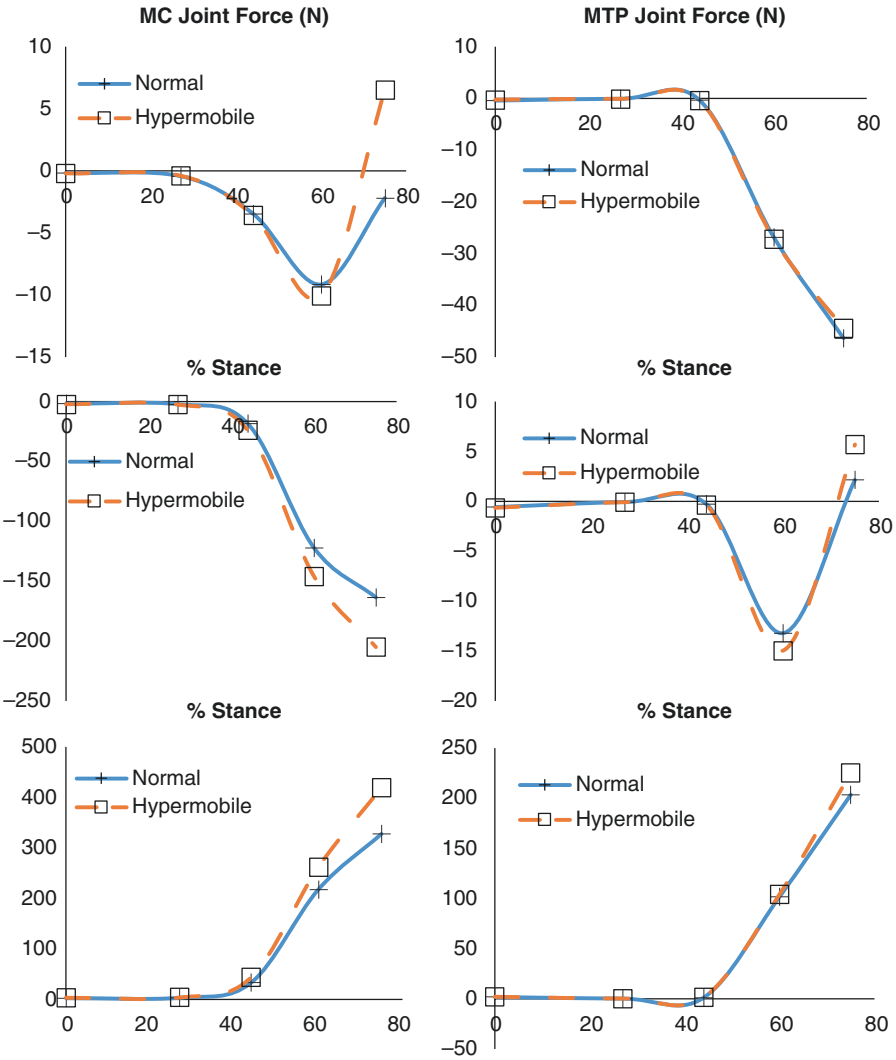

Fig. 10.3 Metatarsocuneiform (MC) and metatarsophalangeal (MTP) joint force comparing normal foot and foot with hypermobile first ray. ML direction (+ Medial), axial direction (+ Inferior), AP direction (+ Anterior). The dotted lines were interpolated from the results of the five instants for illustration. (*Reprinted from Medical Engineering & Physics, 36, Wong et al., Biomechanics of first ray hypermobility: An investigation on the joint force during walking using finite element analysis, 1388–1393, Copyright (2014), with permission from Elsevier*)

The MTP joint force demonstrated comparable trend as that of the MC joint force. Joint forces along the ML and AP directions advanced with time (percentage stance phase) and the deviation became obvious after the GRF valley instant. Notwithstanding, the joint force in the axial direction turned from superior to inferior at 75% stance. In fact, the MTP joint force differences among the normal and

hypermobile foot were generally less than that of the MC joint force, while the largest difference between the normal and hypermobile foot occurred in the axial direction.

MTP and MC joint force increase with hypermobility which could be due to the reduction in shock attenuation capacity of the arch. To maintain the stability and integrity of the foot, the load on the first ray may be increased. However, joint problems could be occurred with the burden of heavy joint force. The sharp change of the MC joint force direction could result in joint instability and may consequently lead to the malalignment of the first metatarsal. Since the attenuation of joint force primarily happened at the MC joint rather than the MTP joint, it was suggested that hallux abducto valgus deformity could be secondary to the metatarsus primus varus.

1.5.3 Bone Alignment and Displacement

The intermetatarsal angle (IMA) and the hallux valgus angle (HVA) were used to quantify bone alignment. The former parameter represents the angulation between the first and second metatarsal, while the latter was calculated by the intersection of the first metatarsal and phalanx axes. To estimate the alignment angles, we estimated the longitudinal axis of the bone shaft by means of regression algorithm and assumed that the bones were cylindrical. For normal condition, HVA and IMA were 9.1° and 15.0°, respectively. However, imposing a hallux valgus condition elevated these parameters to 10.4° and 25.7°, respectively. The angles advanced with increasing forefoot loading. Hallux valgus patients demonstrated higher deterioration of IMA, which was 20% higher than that of normal foot. The finding also supported the fact that hallux abducto valgus deformity could be secondary to the metatarsus primus varus.

1.6 Conclusion

The outcome on MC and MTP joint force provides insights on the development of hallux valgus upon the laxity effect constituted by first ray hypermobility. The increased joint loading may contribute to the risk of joint problems, whereas the abrupt change on the loading direction at the MC joint may indicate potential development of metatarsus primus varus.

2 Biomechanical Study of Ankle Arthrodesis

Summary
Ankle arthrodesis is considered as the standard treatment for some ankle problems, including degenerative deformity, traumatic arthritis. However, many complications

have been observed after ankle arthrodesis. An investigation on the biomechanical influence of ankle arthrodesis on the entire foot helps provide a baseline for the surgical plan. This study constructed a finite element (FE) model of the foot and ankle, and the biomechanical performances of a normal foot and a foot with ankle arthrodesis were compared. The results showed that ankle arthrodesis increased the peak plantar pressure and anterior movement of the center of pressure. The talonavicular joint and joints of the first to third rays also increased after ankle arthrodesis. The findings suggested that the subtalar joint contact force and pressure did not increase after arthrodesis that may indicate that the arthritic joint may not be result from the surgery and may be due to the ongoing degeneration. This study provides additional insights on the assessment of surgery outcome.

2.1 Background

Ankle arthritis is a common foot and ankle problem, while osteoarthritis (OA) secondary to fracture and trauma was highly prevalent. Survey indicated that about 15% of the people was affected by the disabling conditions and pain ascribed to OA and approximately 6% have OA of the ankle [49]. Another survey in the United Kingdom estimated that the number of ankle OA patients requiring hospitalization or clinical care was 47.7 per 100,000 [50].

Ankle arthritis is a prevalent disabling condition that impair one's physical function and quality of living. Glazebrook et al. [51] reported that patients with end-stage ankle arthritis scored significantly lower in the evaluation of function and quality of living. Further, the consequence with respect to mental and physical disability could be as severe as that of the end-stage hip arthrosis [52]. Ankle arthrodesis, firstly performed in 1879, was considered as the salvage procedure for end-stage ankle arthritis. Despite significant relief of pain and retaining plantigrade foot function, ankle arthrodesis is known to cause gait alterations as well as arthritic changes in the subtalar and other distal foot joints [53–56]. Existing retrospective clinical studies revealed that there was a high incidence rate of ipsilateral hind- and mid-foot arthritis associated with the deterioration [56, 57].

2.2 Biomechanical Research on Ankle Arthrodesis

The complication of ankle arthrodesis can be partly contributed to the changes of biomechanical behavior of the foot after the operation. A postoperative patient with an ankle arthrodesis may walk comparatively slower than a normal participant while the percentage duration of the stance phase may remain unchanged [56, 58–60]. Recognizing the influence of the ankle arthrodesis by considering the whole foot segment and the ankle joint is imperative to head for the optimization of the procedure and design.

Finite element (FE) approach aims to explore information of biomechanical environment of the human musculoskeletal system which provides valuable information such as contact pressure of articular joints, soft tissue deformation, and stresses of the bony structures. Nevertheless, relevant studies on ankle arthrodesis confined to the use of simplified FE models, such as that with partial geometries or two-dimensional models [61, 62]. A more precise representation using three-dimensional anatomically detailed FE models could further our understandings on the complex interactions among foot segments [63].

In the present study, a three-dimensional FE model with more precise anatomical structures will be reconstructed. We investigate the biomechanical responses of both the whole foot segment and the ankle joint upon arthrodesis which could be beneficial to identify risks and improve surgical protocols.

2.3 Computational Analysis

2.3.1 Geometry Construction

A normal adult (height 164 cm and body weight 54 kg) was recruited in the study. The MR images of her right foot were extracted under a setting of 0.625 mm pixel resolution and 2 mm slice interval. The three-dimensional FE model was reconstructed featuring the foot-and-ankle complex with 28 bony components, encapsulated soft tissue, 103 ligaments, plantar fascia, and major muscles [63, 64] (Fig. 10.4). The reconstruction process was carried out in the segmentation software, Mimics (Materialise, Leuven, Belgium), and meshed in the finite element package, Abaqus (Dassault Systèms Simulia Corp., Providence, RI, USA).

We resembled the ligaments and plantar fascia using wires that connected the insertions points on the bony structures and meshed them with tension-only truss elements. Nine major muscle groups were assumed by axial connectors. The bilayer ground plate consisted of an upper layer with high elastic modulus and a rigid lower layer. The coefficient of friction between the foot plantar surface and the ground support surface was set to 0.6 [47].

2.3.2 Material Property

Most of the components were assumed to be isotropic, linearly elastic, and homogeneous, including the osseous structure and soft tissue, and the Young's modulus and Poisson's ratio of these components were adopted from existing literature [42, 65–67]. The bulk soft tissue and skin were assigned as hyperelastic material with nonlinear properties. Most of the three-dimensional components were meshed as linear tetrahedral elements, while that of the plantar fascia and ligaments were meshed as truss. The mesh and material properties are shown in Table 10.1.

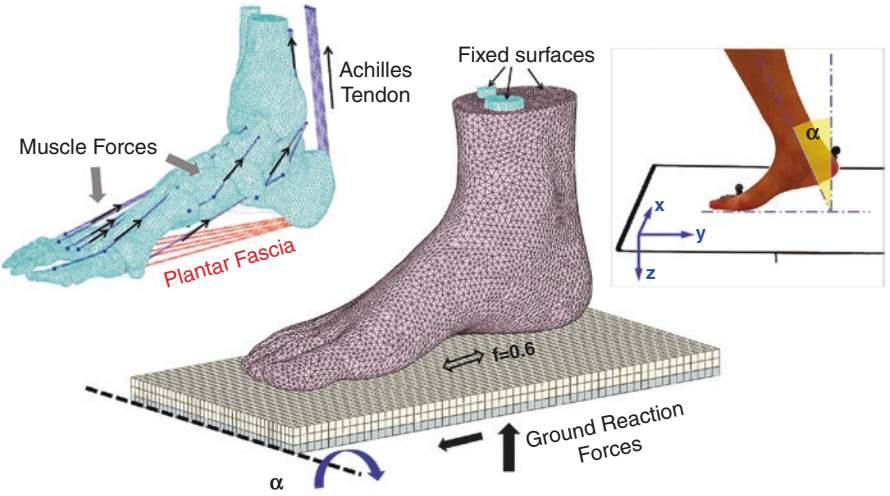

Fig. 10.4 The three-dimensional finite element model of the foot and ankle and application of boundary and loading conditions. (*Reprinted from PlosOne, Wang et al., Effects of Ankle Arthrodesis on Biomechanical Performance of the Entire Foot, e0134340 (2015), under CC-BY*)

Table 10.1 Material property and mesh element type for the foot model components

Component	Element type	Young's modulus *E* (MPa)	Poisson's ratio *v*	Cross-section area (mm^2)
Bone	C3D4	7300	0.3	–
Encapsulated soft tissue	C3D4 and S3	Hyperelastic	–	–
Cartilage	C3D4	1	0.4	
Ligaments	T3D2	260	–	18.4
Plantar fascia	T3D2	350	–	58.6
Ground	C3D8R	17,000	0.1	–

2.3.3 Boundary and Loading Conditions

The model participant was invited to conduct a gait analysis using the motion capture system (Vicon, Oxford Metrics, Oxford, UK) to obtain the boundary and loading conditions for the input of the FE analysis. We targeted on seven body segments with 16 retroreflective markers attached on the lower extremity of the participant. The participant stood on the force platform (AMTI, Watertown, MA, USA) to conduct the static calibration for the motion capture system. The orientation of the shank was defined by the three-dimensional angulation between the shank segment and the global system, denoted as α in Fig. 10.4 with the time series in Fig. 10.5. The force plate would detect the ground reaction force in the vertical, anterior-posterior, and medial-lateral directions. In Fig. 10.5, we extracted the first-peak, midstance, and second-peak instants of the ground reaction force curve in the vertical direction for further analysis.

The proximal side of the FE model was fixed, including the superior surfaces of the tibial, fibula, and the encapsulated soft tissue (Fig. 10.4). The ground reaction force was applied on the rigid ground plate to mimic the setting of the force platform. The foot-shank angle was applied through the rotational degree of freedom of the ground plate whereas the translational degree of freedom was not fixed. The muscle forces were approximated by the cross-sectional area, the normalized electromyography, and the muscle gain of the muscles during walking stance [46, 68, 69], and later adjusted based on another study [45].

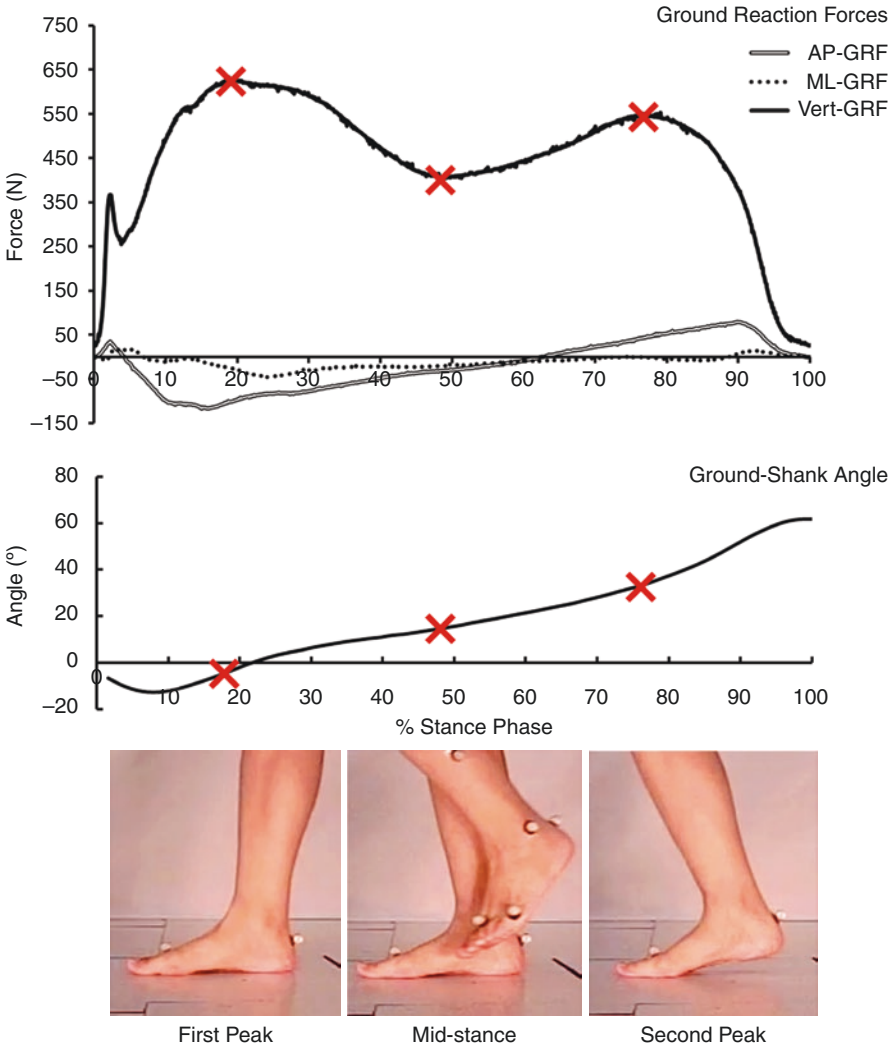

Fig. 10.5 Ground reaction forces and ground-shank angle recorded in the gait analysis and the three instants, first peak, midstance, and second peak, for simulation. The three instants were marked in the curves. (*Reprinted from PlosOne, Wang et al., Effects of Ankle Arthrodesis on Biomechanical Performance of the Entire Foot, e0134340 (2015), under CC-BY*)

2.4 *Effects of Ankle Arthrodesis on Foot Biomechanics*

2.4.1 Model Validation

Plantar pressure during balanced standing and walking stance was assessed and compared between the experiments and predictions from the FE model. Model validation was completed by comparing these findings. As shown in Fig. 10.6, the pressure pattern was generally agreeable with the peak pressure located at the heel region.

2.4.2 Plantar Pressure

Figure 10.7 shows the plantar pressure distribution of the intact foot and the foot after arthrodesis at the three stance instants (first peak, midstance, and second peak). At the first-peak instant, there was a slight difference in peak plantar pressure between the conditions, which was 0.33 MPa and 0.36 MPa for the intact foot and arthrodesis foot, respectively. The peak plantar pressures for the intact foot between the midstance and second-peak instant were both 0.68 MPa. However, that of the arthrodesis foot was higher and increased chronologically. The peak plantar pressure was 0.78 MPa and 0.93 MPa, respectively, for the midstance and second-peak condition for the arthrodesis foot. Compared to the intact condition, the center of pressure after arthrodesis has shifted slightly towards the medial side and appeared beneath the third metatarsal bone.

2.4.3 Joint Contact Pressure

Figure 10.8 summarizes the maximum contact pressure of the articular joints between the intact and arthrodesis condition at the first-peak, midstance, and second-peak instants. There were observable increases of maximum pressure at the talonavicular and intertarsal joints after the ankle arthrodesis procedure. In consideration of the average of the maximum contact pressure across the time instants, the talonavicular joint remained highest and was increased from 0.80 to 1.21 MPa; 1.14 to 1.59 MPa; and 2.00 to 2.14 MPa after surgery at the three instants.

The medial cuneonavicular joints carried higher maximum contact pressure compared with the other cuneonavicular joints. The maximum contact pressure of the joint increased from 0.60 to 0.79 MPa; from 0.97 to 1.20 MPa; and from 1.90 to 1.97 MPa after ankle arthrodesis, respectively, for the first-peak, midstance, and second-peak instants. However, the highest magnitude of the change due to the surgical procedure was evident at the lateral cuneonavicular joint. The percentage changes were 80.3%, 64.7%, and 11.6%, respectively, at the first-peak, midstance, and second-peak instants.

Distally, considering the tarsometatarsal joints, the second tarsometatarsal joint sustained the highest maximum contact pressure compared with the other

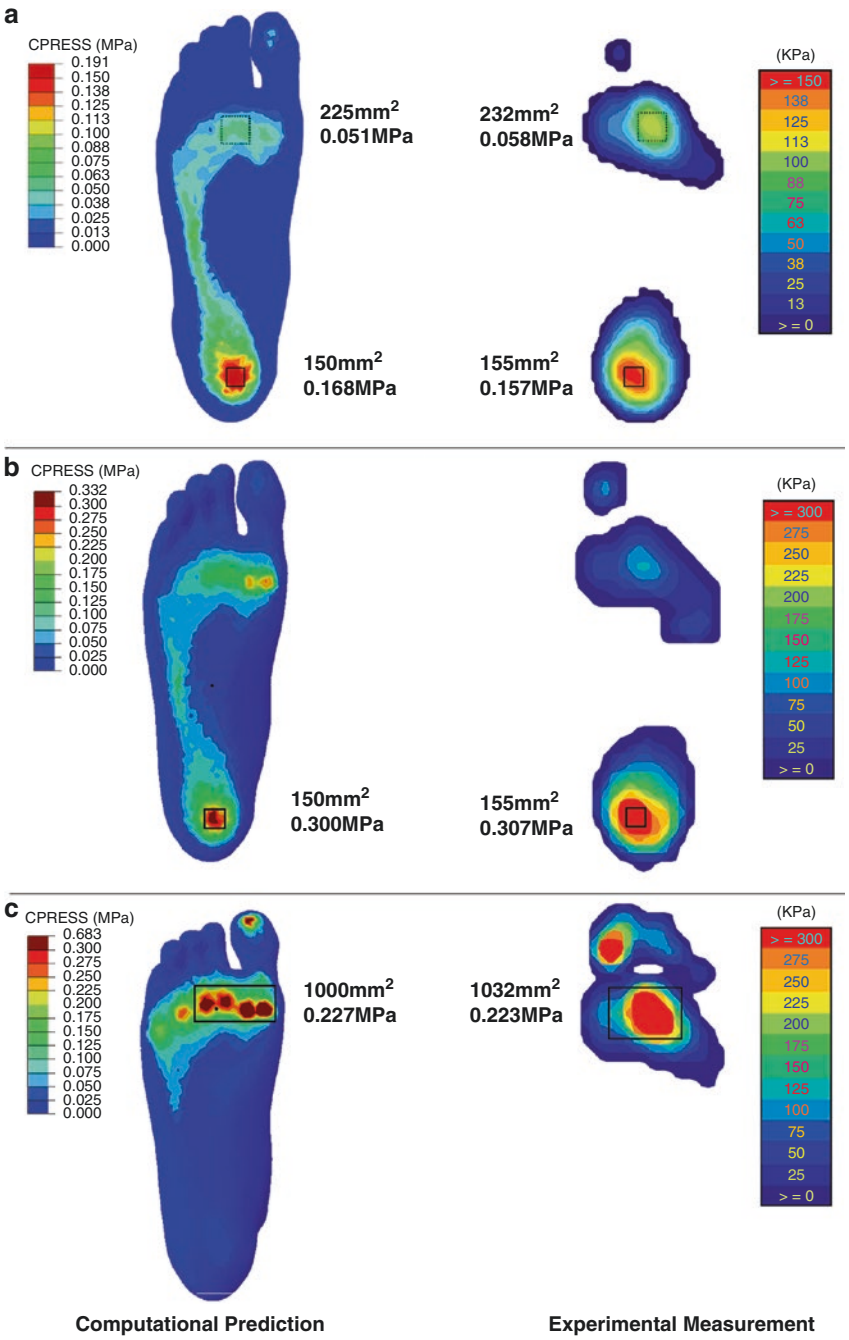

Fig. 10.6 Comparison of the plantar pressure between computational prediction and experimental measurement in (**a**) balanced standing position, (**b**) the first-peak instant, and (**c**) the second-peak instant for validation. (*Reprinted from PlosOne, Wang et al., Effects of Ankle Arthrodesis on Biomechanical Performance of the Entire Foot, e0134340 (2015), under CC-BY*)

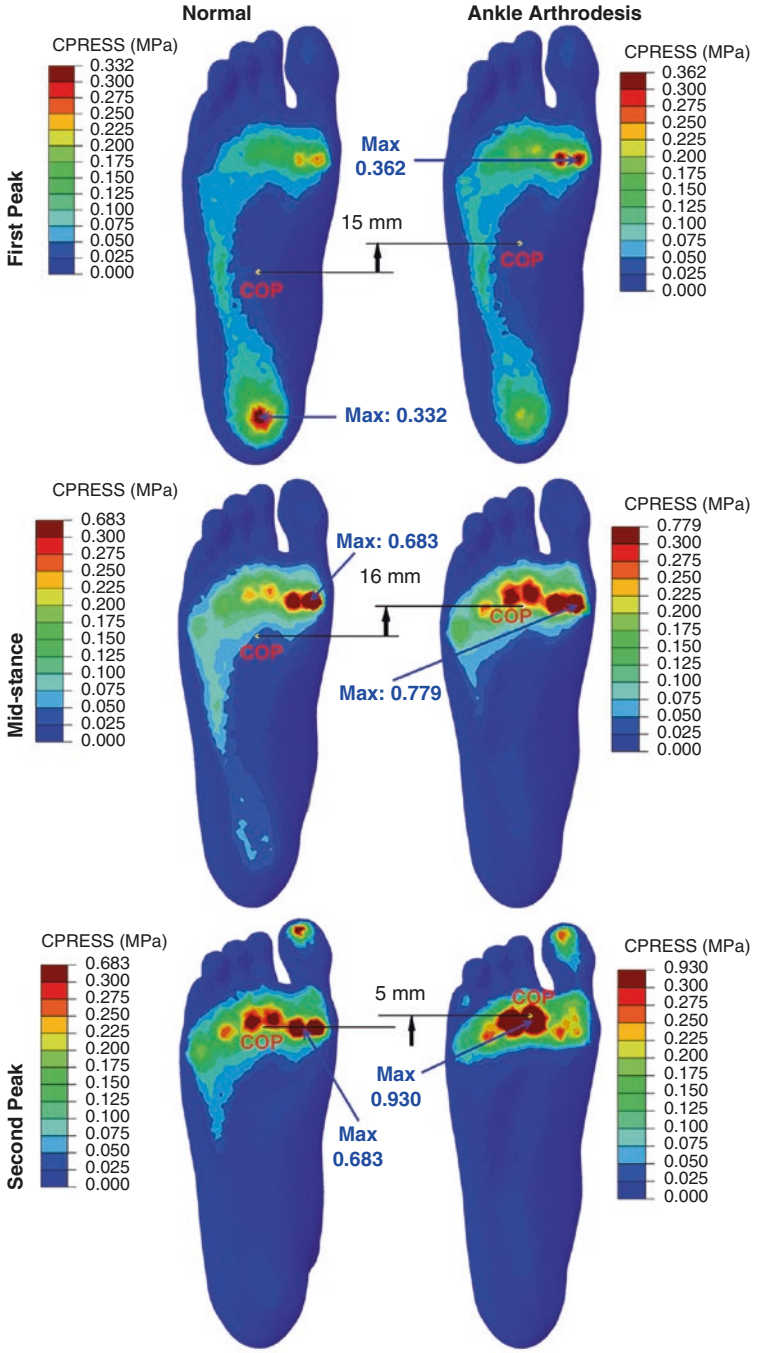

Fig. 10.7 Comparison of the plantar pressure distribution between normal foot model and ankle arthrodesis foot model at the three instants. (*Reprinted from PlosOne, Wang et al., Effects of Ankle Arthrodesis on Biomechanical Performance of the Entire Foot, e0134340 (2015), under CC-BY*)

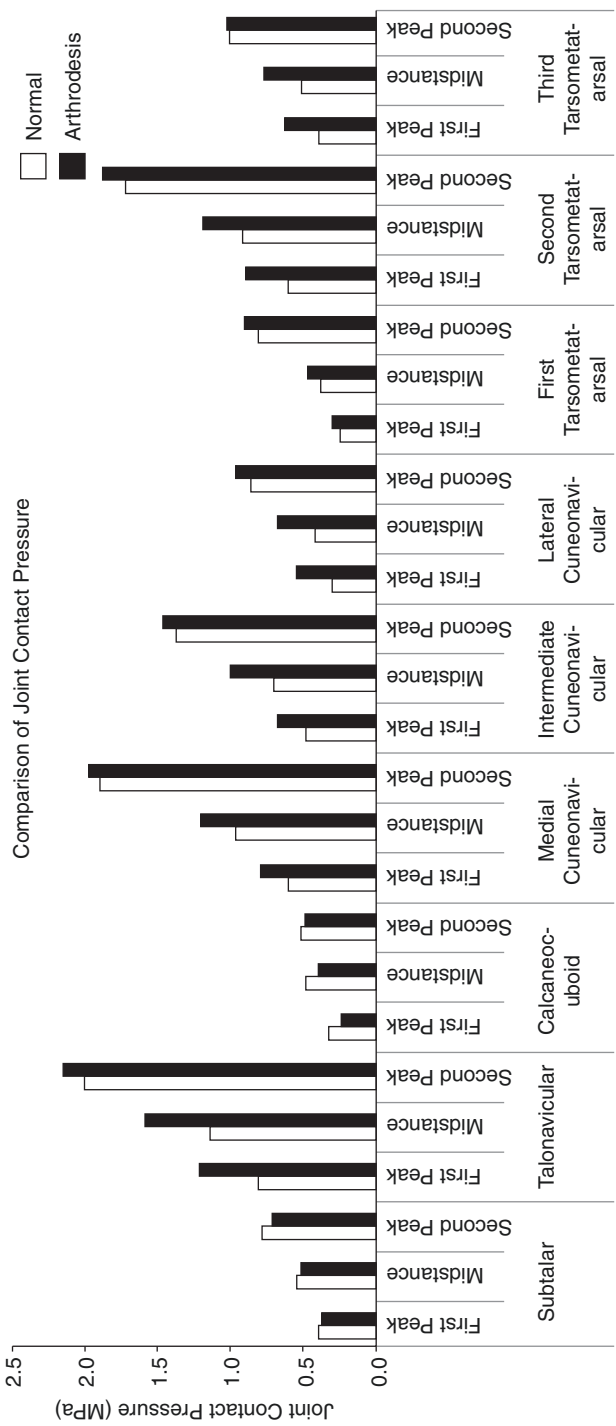

Fig. 10.8 Comparison of the contact pressure at nine joints in the hind- and mid-foot between the normal foot model and the ankle arthrodesis foot model at the first-peak, midstance, and second-peak instants. (*Reprinted from PlosOne, Wang et al., Effects of Ankle Arthrodesis on Biomechanical Performance of the Entire Foot, e0134340 (2015), under CC-BY*)

tarsometatarsal joints. The maximum contact pressure was increased from 0.60 to 0.90 MPa; from 0.91 to 1.19 MPa; and from 1.72 to 1.88 MPa after the ankle arthrodesis procedure, respectively, for the three stance instants. In fact, the surgical procedure imposed the largest influence of the third tarsometatarsal joint accounting for the percentage changes of 62.8%, 51.4%, and 2.0% at the three stance instants. The fourth and fifth tarsometatarsal joints did not demonstrate consistent trend throughout the stance instants. The former showed a maximum contact pressure reduction after surgery at the first peak and midstance, whereas the latter presented a reduction at the midstance and second-peak instant.

Ankle arthrodesis reduced the maximum contact pressure of the subtalar and calcaneocuboid joints. The maximum contact pressure of the calcaneocuboid joint was decreased from 0.32 to 0.24 MPa; from 0.48 to 0.39 MPa; and from 0.51 to 0.49 MPa after surgery at the three stance instants, respectively. Furthermore, the maximum contact pressure of the subtalar joint was decreased from 0.39 to 0.37 MPa; from 0.54 to 0.51 MPa; and from 0.78 to 0.70 MPa after surgery, respectively, at the three instants. The reduction of maximum contact pressure of the hindfoot joints may suggest that subtalar arthritis may not be a consequence of ankle arthrodesis. We speculated that the progression could be attributed to the pre-existing degenerative changes.

2.4.4 Joint Contact Force

Figure 10.9 compares the joint contact forces among the intact and surgery conditions at the selected instants of walking stance. The contact force elevated chronologically (first-peak, midstance, and then second-peak instants) for the talonavicular, cuneonavicular, and the first and second tarsometatarsal joints. Apparent change appeared at the first-peak instance whereas most of the joint presented their highest value at the second-peak instant.

The talonavicular joint acted as the highest load-bearing bone in the foot and ankle complex. The joint forces were 181 N, 259 N, and 514 N, respectively, at the first-peak, midstance, and second-peak instants. The forces were increased more than half for the first peak and midstance and reached to 578 N at the second peak which was slightly higher than the applied vertical ground reaction force (540 N). Conversely, the load transfer towards the calcaneocuboid declined after arthrodesis by 31%, 17%, and 8%, and reached to 33 N, 55 N, and 74 N, respectively, for the three instants of walking stance.

In general, the first ray sustained a higher contact force compared to that of the second and third ray. They experienced greater contact force at the second-peak instants. The medial cuneonavicular and first tarsometatarsal joints of the first ray increased by 31% and 75%, respectively, at the first-peak instant, while the intermediate cuneonavicular and second tarsometatarsal joints of the second ray increased by 52% and 79%, in addition to the 74% and 71% increase at the lateral cuneonavicular and third tarsometatarsal joints of the third ray.

Figure 10.10 demonstrates the differences in load transfer between the intact and arthrodesis model at the first-peak instant, which was more prominent compared to that of the other two instants. Approximately one-third of the body weight was

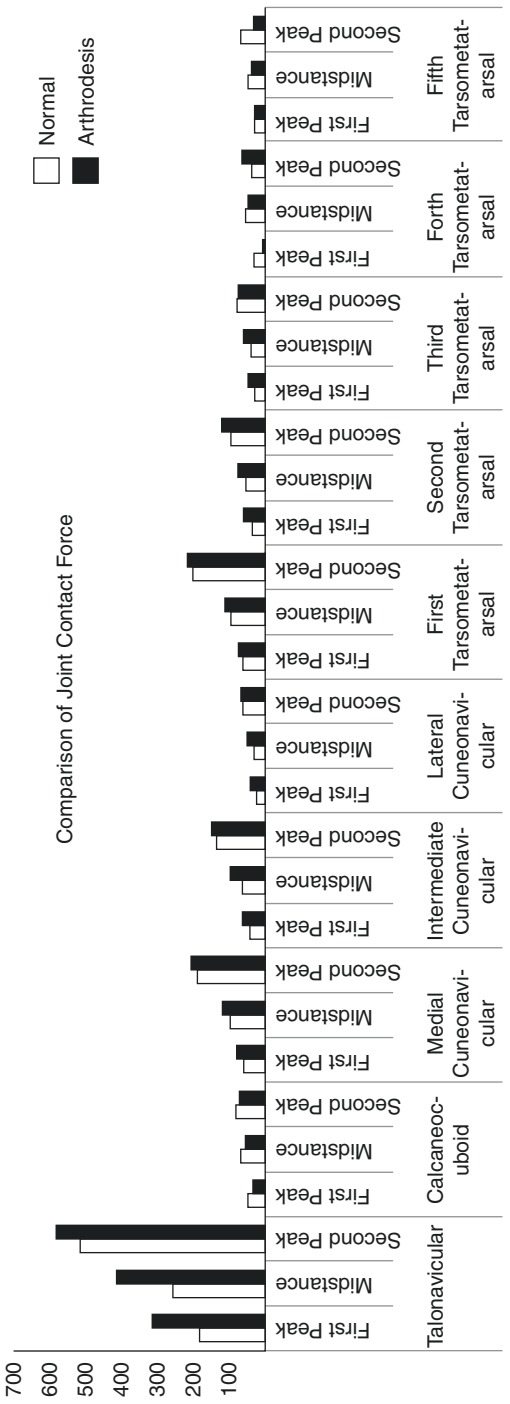

Fig. 10.9 Comparison of the contact forces at ten joints in the hind- and mid-foot between the normal foot model and ankle arthrodesis model at the first-peak, midstance, and second-peak instants. (*Reprinted from PlosOne, Wang et al., Effects of Ankle Arthrodesis on Biomechanical Performance of the Entire Foot, e0134340 (2015), under CC-BY*)

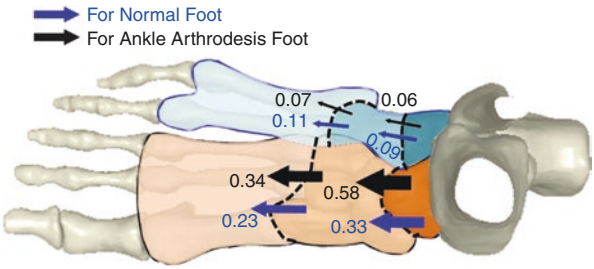

Fig. 10.10 Load transfer (times of body weight) in the normal and ankle arthrodesis foot model at the first-peak instant. (*Reprinted from PlosOne, Wang et al., Effects of Ankle Arthrodesis on Biomechanical Performance of the Entire Foot, e0134340 (2015), under CC-BY*)

transferred through the talonavicular joint to the medial joints while less than 10% of the body weight was transmitted through the calcaneocuboid joint to the fourth and fifth rays. From mid-foot to forefoot, 23% of the body weight was conveyed medially and 11% laterally. The ankle arthrodesis imposed additional burden on load transferred which was increased to 58% at the talonavicular joint and reduced that of the calcaneocuboid joint. Similarly, the midfoot-to-forefoot transfer increased to 34% in the medial three rays and decreased to 7% in the lateral two rays. The change in load transfer pattern may induce risk of foot pain the medial columns which may constitute to foot deformity in long term. Orthotic intervention such as wedge insole may help revise the load transfer pattern after surgery.

2.4.5 Bone Stress

As shown in Fig. 10.11, ankle arthrodesis increased the von Mises stress of the bone in general. At the first-peak instant, the von Mises stress increased apparently by 19% and 52%, respectively, in the first and third metatarsal bone, while the lateral metatarsal only processed small slight changes. However, all the metatarsal showed an obvious elevation in stress at the midstance and second-peak instants. The second metatarsal represented the part with the highest stress which was 42 MPa and 52 MPa, respectively, for the normal and arthrodesis condition. The third metatarsal comes after the second metatarsal. The stress was 20 MPa at midstance and increased to 34 MPa at the second-peak instant.

2.4.6 Foot Deformation at the Second-Peak Instant

As shown in Fig. 10.12, the predicted results showed different joint position and foot deformation between the intact and surgery conditions, particularly at the second-peak instant. The foot-shank angle for both conditions were 30°. However, the orientation angle was 28° for the intact foot and 44° for the arthrodesis foot, respectively, between the horizontal plane and the first ray axis at the second-peak instant.

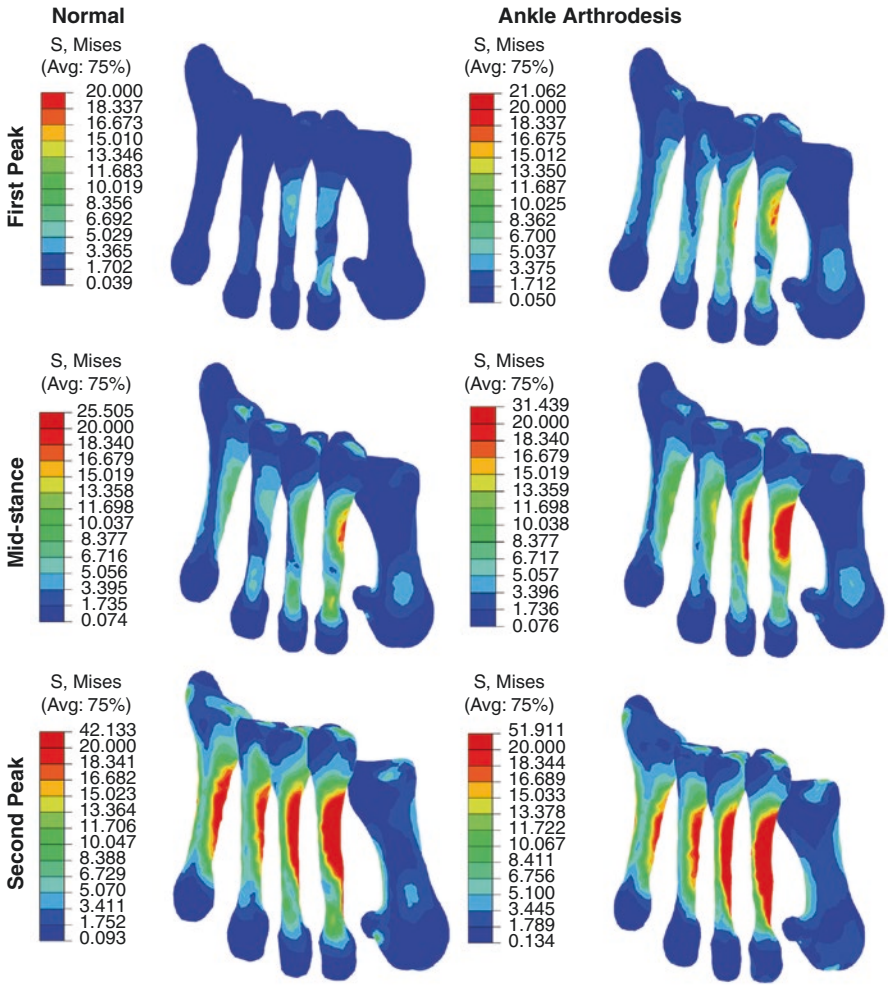

Fig. 10.11 Comparison of von Mises stress in five metatarsal bones in normal foot model and ankle arthrodesis foot model at three instants. (*Reprinted from PlosOne, Wang et al., Effects of Ankle Arthrodesis on Biomechanical Performance of the Entire Foot, e0134340 (2015), under CC-BY*)

2.4.7 Limitations

The FE model in this study inherited some simplifications and assumptions. The ankle arthrodesis was realized by constraining the contact at the ankle articulation rather than reconstructing and installing the models of the screws or pins. It would be better to reconstruct the screws to examine its behavior and influences. Besides, the suggested Young's modulus and Poisson's ratio was not relatively accurate [40]. It was derived from a weighted average elasticity of the cortical and trabecular based on their volumetric contribution [66]. Further model refinement shall be made to advance a more accurate model or material representation.

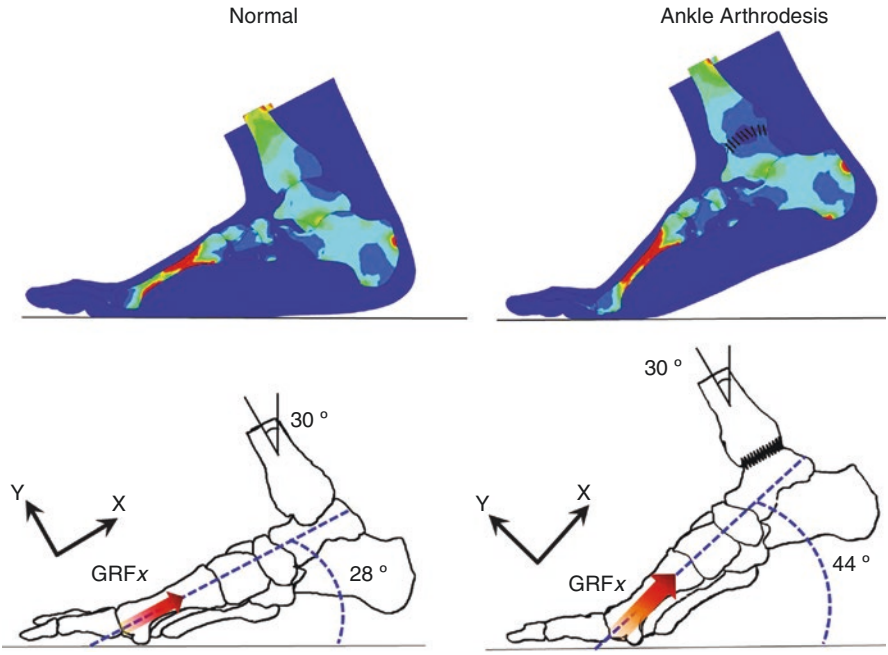

Fig. 10.12 Angular positions of normal foot and ankle arthrodesis foot at a second-peak instant in the sagittal plane. (*Reprinted from PlosOne, Wang et al., Effects of Ankle Arthrodesis on Biomechanical Performance of the Entire Foot, e0134340 (2015), under CC-BY*)

We anticipated that the influence of the simplifications and assumptions produced similar offset errors to the models of the two conditions. Therefore, due to the self-compare study design, we believe that the outcome in terms of trend or differences between the conditions were less affected by these limitations. On the other hand, another limitation of this study was that we assumed the gait pattern (boundary and loading conditions) between the normal and ankle arthrodesis conditions was similar. There are claims that the arthrodesis may not change the input boundary and loading conditions, despite that some patients may demonstrate change in spatiotemporal parameters.

2.5 Conclusions

Ankle arthrodesis is a common surgical procedure that aims at pain relief and function improvement for patients with ankle degeneration. However, the fusion and constraints on the ankle joint, which is the major foot joint, corrupt the normal biomechanics of both the ankle joint and the entire foot, leading to potential postoperative complications.

The biomechanical consequences of ankle arthrodesis are indicated by the differences in biomechanical parameters, including plantar pressure, contact

force, stresses, and deformation, which could explain the mechanism of some clinical findings. The high load on the medial rays may result in pain and deteriorate the arthritic condition, while the large stress on the second and third metatarsals could impose risk of bone fractures. There was a decrease in subtalar joint loading after ankle arthrodesis such that we believe the postoperative arthritis of the subtalar joint may not be a consequence of the ankle arthrodesis procedure.

The model used in this study was regarded as a representation of the normal physique and may be regarded as a baseline reference from a biomechanical point perspective. Foot in valgus position may lateralize the loading. In addition, orthotic intervention may help to relieve the negative effects of ankle arthrodesis. Further evaluations are required to decide the effectiveness of these interventions.

3 Biomechanical Study of Tarsometatarsal Joint Fusion

Summary
The Lisfranc joint complex is also named as the tarsometatarsal joint (TMT) and is recognized as a crucial connection that facilitates stability of the midfoot and forefoot. The joint comprises sophisticated osseous and capsuloligamentous structure such that the injury of the TMT joint may lead to disabling osteoarthritis (OA) requiring surgery. Acknowledging the effectiveness of surgical intervention and minimizing risk of complication are imperative in surgical design. Determining the internal biomechanical environment, such as plantar pressure distribution, stress of the bone, and deformation of soft tissue, attenuated by surgical intervention facilitates evaluation. In this study, we aimed to evaluate the influence of TMT joint fusion biomechanically using a finite element model of the foot and ankle complex, which consisted of 28 bony structures, 72 ligaments, plantar pressure, and an encapsulated bulk tissue. Our finite element prediction suggested that TMT joint fusion elevated the plantar pressure by 0.42, 19, and 37% in three featured time instants compared to the intact foot. In particular, the load transfer across the cuneonavicular and the fifth cuboideometatarsal joints were increased by 27% and 40%, respectively, at the second-peak instant that may impose risk of joint arthritis. On the other hand, the maximum stress of the second metatarsal bone was increased by more than 20% that may lead to vulnerability to stress fracture.

3.1 Background

The tarsometatarsal (TMT) joint, or the Lisfranc joint, is named after a French surgeon, Jacques Lisfranc (1790–1847), who served in the Napoleon's [70]. The TMT joint plays an important role in bridging the midfoot and the forefoot. In addition,

the arrangement of the five metatarsals on the distal side and the four midfoot bones (three cuneiforms and cuboid) facilitates structural support for the transverse arch along with the attaching ligamentous structures. The TMT joint is often divided into three columns along the anterior-posterior direction by the articulation of the second and third TMT joints. The TMT joint can have little sagittal plane motion with a range of 0.6 mm, 3.5 mm, and 13 mm, respectively, for the central, medial, and lateral columns [70, 71].

In the United States, fractures of the TMT joint accounted for 0.2% of all fractures, in which there was one fracture in every 55,000 persons each year [72]. The treatment to TMT joint injuries, however, remains no consensus. Nonoperative intervention could be indicated for nondisplaced fracture. Surgical methods using either closed or open reduction would be used to treat displaced fracture assisted with different implants, such as Kirschner wires, screws, plates, or suture-button devices. Correct reduction and alignment with sufficient stability is the key to satisfactory clinical outcome [73].

While joint fusion procedure aims to restore some normal foot functions, it may produce some undesirable biomechanical effects. The constraints on the joint may induce additional stress onto the bony structures leading to irritation, loosening of implants, and breakage. A mid-term follow-up on TMT joint fixation patients reported that more than 10% of them developed posttraumatic arthritis and nearly 3% developed subluxation [74]. In addition, approximately 7% of them developed flatfoot or severe symptoms that required a secondary surgery [74].

3.2 Biomechanical Study of Tarsometatarsal Joint Injury

It is imperative to evaluate the biomechanical performance and thus the effectiveness of the surgery to minimize potential complications. TMT joint plays an important role in load transfer from hindfoot to the forefoot that facilitates foot propulsion and body movement. TMT joint modulates load transfer by two different mechanisms depending on the magnitude of load. For small loads, TMT adjusts the joint contact area to regulate the contact area and contact pressure. For large loads, the group of joints in the TMT would be rearranged and redistribute the load among the group of joints [75].

Ankle joint and other foot joints work interdependently and synergistically to maintain balance and bring about ambulation. Therefore, a localized joint problem is likely to affect adjacent joints and subsequently impair the function of the foot and ankle complex. The internal stress and strain distribution could be an indicator reflecting the changes resulted from interventions yet difficult to be measured by physical experiment approach. Computer simulation via a FE approach represents a feasible alternative to explore the internal biomechanical environment of the foot and ankle. The strength of the approach is the capability in managing complex geometries, material properties, boundary, and loading conditions

that offer additional insights to the problem. In this study, we simulated a TMT joint fusion procedure on a comprehensive 3D FE foot and ankle model to evaluate the biomechanical performance of the intervention.

3.3 Finite Element Simulation of Tarsometatarsal Joint Fusion

3.3.1 Finite Element Model and Simulation of Joint Fusion

The FE model was reconstructed from the right foot of a female (54 kg, 1.64 m). The model consisted of a volume of encapsulated soft tissue embracing 28 body segments and other soft tissues [63, 64]. The first and second tarsometatarsal joint fusion procedure was realized in the simulation platform [76]. Clinically, the affected joint is linked by screws whereas the process was simplified in the simulation by fusing the articular contact interface among the medial and intermediate cuneiform, and the first and second metatarsal bones (Fig. 10.13).

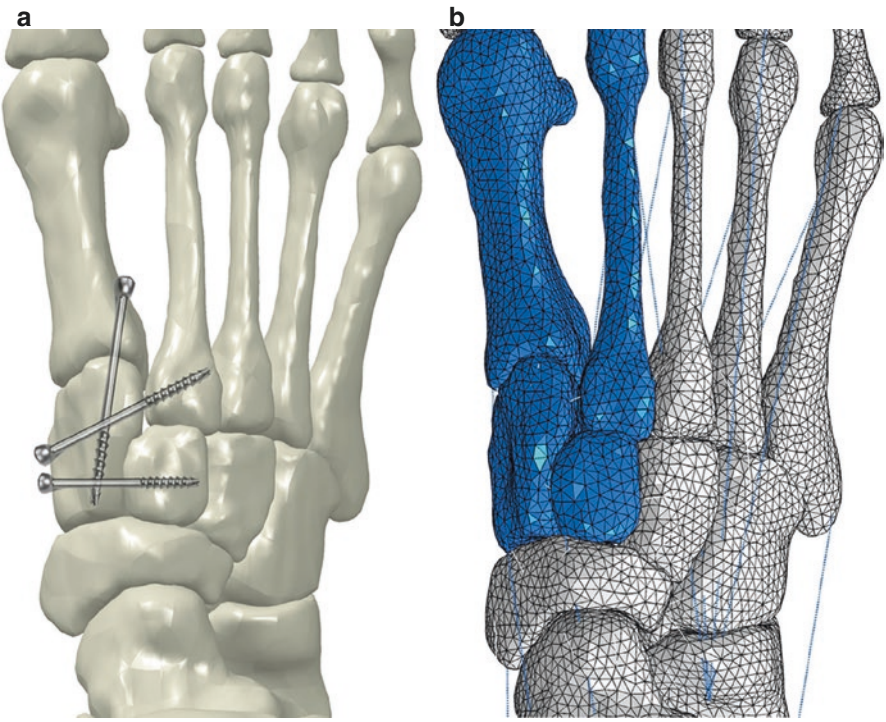

Fig. 10.13 Surgery of first and second tarsometatarsal joint fusion (**a**), and four tied bones in the model for simulation (**b**). Articular surfaces among the first and second metatarsal bones and medial and intermediate cuneiforms were tied together to simulate the fixed joints. (*Reprinted from Medical Engineering & Physics, 36, Wang et al., Biomechanical study of tarsometatarsal joint fusion using finite element analysis, 1394–1400, Copyright (2014), with permission from Elsevier*)

3.4 Boundary and Loading Conditions

The model subject was recruited to perform locomotion analysis using the motion capture system, as well as the force platform and electromyography. Reflective markers were attached to the interested body segments whereas the kinematic and kinetic information during gait were extracted. As shown in Fig. 10.14, the GRFs with time were obtained featuring the first-peak, midstance, and the second-peak instants.

The first peak of the vertical GRF happened at 25% stance phase while that of the second peak occurred at 70%. The midstance was defined as the valley of the curve and occurred between the first- and second-peak instants. Extrinsic muscle forces were estimated and applied according to the linear EMG-force assumption, measured EMG and suggested cross-sectional area of the muscles [68, 69]. The input of the boundary and loading conditions in the four simulated time instants are summarized in Table 10.2.

The muscles in the simulation were modelled as connectors jointing the relevant attachment points. Tendon Achilles were assumed by five axial connectors and forces were applied onto these connectors equally. Figure 10.15 illustrates the other

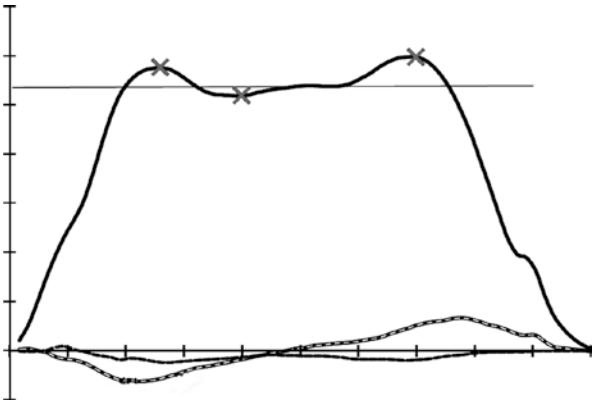

Fig. 10.14 The vertical ground reaction force and the three investigated gait instants

Table 10.2 Boundary conditions of the four simulated instants: balanced standing, first peak, midstance, and the second peak

Loadings	Balanced standing	First peak	Midstance	Second peak
GRF (N)	270	578.6	519.3	600
Ankle-shank angle (rad)	0	0.113	0.216	0.485
Tibialis anterior (N)	–	0	0	0
Tibialis posterior (N)	–	34	42.5	0
Achilles tendon (N)	135	500	900	1100
Extensor digitorum longus (N)	0	0	0	0
Flexor digitorum longus (N)	0	40	20	96
Flexor hallucis longus (N)	0	30	0	284
Peroneus longus (N)	0	0	41.25	0
Peroneus brevis (N)	0	20	22	91.8

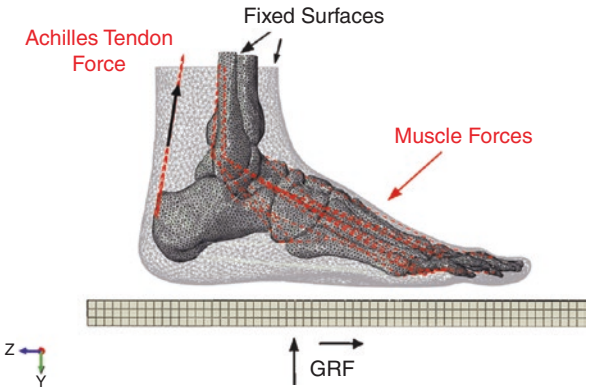

Fig. 10.15 Boundary and loading conditions for the simulation of gait instants. The superior surfaces of soft tissue, tibia and talus bones were fixed. Ground reaction forces of anteroposterior and vertical directions were applied. Muscle forces were applied to muscle representatives. (*Reprinted from Medical Engineering & Physics, 36, Wang et al., Biomechanical study of tarsometatarsal joint fusion using finite element analysis, 1394–1400, Copyright (2014), with permission from Elsevier*)

muscle construction represented by the red dotted lines. The proximal end of the encapsulated soft tissue, tibia, and fibula were fixed along with GRFs applied beneath the rigid ground plate. The ground plate was also rotated according to the foot-shank orientation profile sourced from the locomotion analysis. Besides, balanced walking was also mimicked with half body weight (270 N). It was also assumed that only Achilles tendon was activated and other muscle forces were negligible.

3.5 Biomechanical Effects of Tarsometatarsal Joint Fusion

Plantar pressure distribution, contact pressure of the articular joint at the midfoot and hindfoot, as well as the maximum von Mises stress of the metatarsal bones would be compared between the intact and the surgical conditions. In addition, model validation was carried out by comparing the plantar pressure and joint contact pressure between FE prediction and physical experiment which demonstrated a reasonable agreement.

3.5.1 Plantar Pressure Distribution

Figure 10.16 demonstrated that the plantar pressure distribution between the intact and surgical conditions were similar but the surgical model showed a larger peak pressure value. The peak plantar pressure was increased by 0.42%, 19%, and 37% after surgery, respectively, at the first-peak, midstance, and second-peak instants, which was more prominent during later stance. The corresponding peak pressure values from intact to surgical conditions were: from 0.50 to 0.51 MPa; from 0.60 to 0.72 MPa; and from 0.64 to 0.88 MPa.

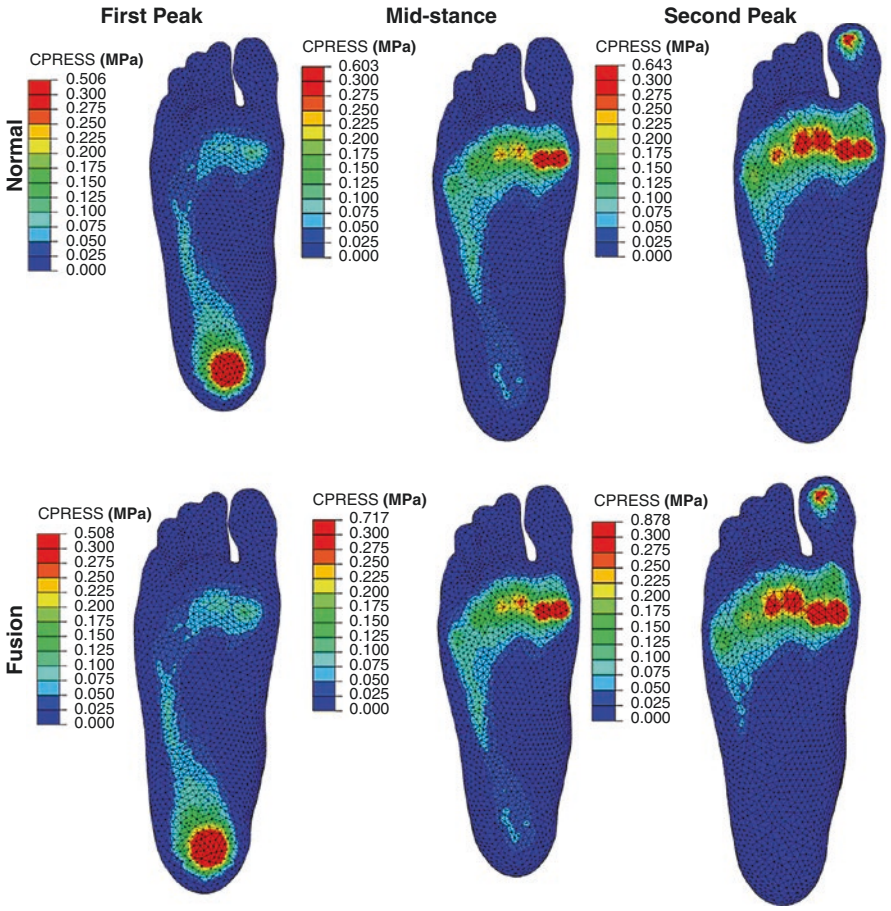

Fig. 10.16 Plantar pressure distributions in the normal and fused tarsometatarsal joint models in three instants. (*Reprinted from Medical Engineering & Physics, 36, Wang et al., Biomechanical study of tarsometatarsal joint fusion using finite element analysis, 1394–1400, Copyright (2014), with permission from Elsevier*)

Arch height stiffness and contact area are also determinants to contact pressure. The arch height stiffness was reflected by its flexibility which was quantified by the change in arch height during balanced standing (measured from the dorsal peak of intermediate cuneiform to the tuberosity of the calcaneus bone). Our study showed that the surgery reduced about a quarter flexibility compared to that of the intact foot.

3.5.2 Contact Pressure of Plantar Foot and Joints

The joint fusion surgery elevated the maximum contact pressure of the ankle, talonavicular, intermediate cuneonavicular, cuboideonavicular, and the fifth cuboideometatarsal joints. Figure 10.17 illustrates the maximum joint contact pressure normalized to that of the ankle joint during the first-peak instant.

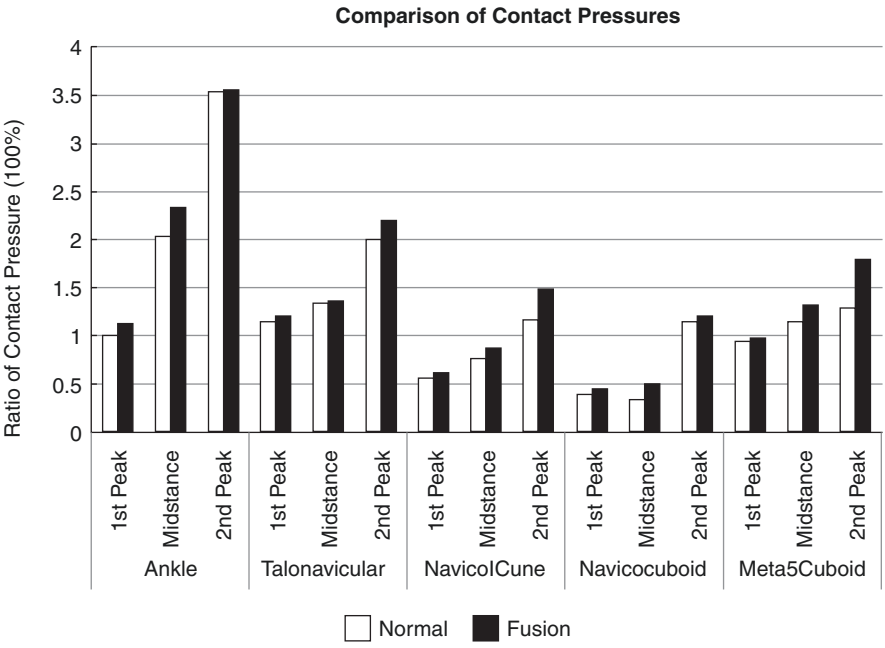

Fig. 10.17 Comparison of normalized contact pressure at five joints between normal foot and foot with two tarsometatarsal joint fusion. These five joints showed increased contact pressure after the joints fusion. All contact pressures were divided by that of the ankle joint during the first-peak instant. (*Reprinted from Medical Engineering & Physics, 36, Wang et al., Biomechanical study of tarsometatarsal joint fusion using finite element analysis, 1394–1400, Copyright (2014), with permission from Elsevier*)

Figure 10.17 shows that the maximum contact pressure progressed chronologically along the stance phase, particularly dominated by the ankle joint. The fusion surgery did not produce considerable change at the ankle joint with a percentage increase of 12%, 14%, and 0.58%, respectively, for the three stance instants. The joint between the navicular and cuboid bone presented the largest percentage change during midstance despite relatively small magnitude.

3.5.3 von Mises Stress in the Five Metatarsal Bones

Figure 10.18 illustrates the von Mises stress plot during midstance. While metatarsal bones were relatively more susceptible to fracture due to its long and thin shape with large load transfer, von Mises stress was believed to be one of the key predictors for stress fracture [77].

The maximum stress was located at the second metatarsal bone at midstance. The magnitude increased from 26 MPa under normal condition to 31 MPa under the fusion condition. Similarly, the stress was also elevated by 16% and 14%, respectively, during first peak and second peak. Besides, the maximum von Mises stress of the fifth metatarsal bone was increased by 5.1% and 9.5% after fusion, respectively,

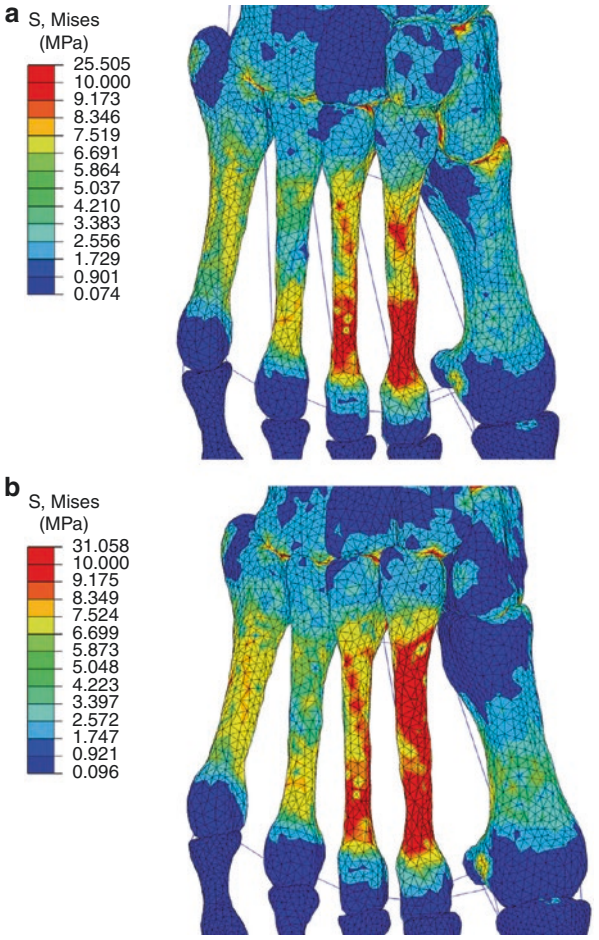

Fig. 10.18 Von Mises stress in the five metatarsal bones (**a**) in normal foot model and (**b**) model with the first and second tarsometatarsal joint fusion in midstance. The second metatarsal showed the maximum change during midstance instant. (*Reprinted from Medical Engineering & Physics, 36, Wang et al., Biomechanical study of tarsometatarsal joint fusion using finite element analysis, 1394–1400, Copyright (2014), with permission from Elsevier*)

during the first-peak and midstance instants. On the other hand, there were no substantial change of the maximum stress for the first and fourth metatarsal bone comparing the normal and the fusion conditions.

Stress fractures are more prevalent at the second and third metatarsals which was reported as one of the major complications after foot surgeries [78, 79]. With approximately one-fifth of stress increase, our prediction supported the fact that TMT joint fusion between the first and second rays induce risk of second metatarsal bone fracture.

3.6 Conclusions

TMT joint fusion could be a salvage procedure to repair severe flatfoot. The stiffening created by the fusion attenuated the internal stress and strain of bones and soft tissue, as well as the plantar pressure distribution. The peak plantar pressure increased in all simulated instants whereas the largest increase happened during push-off.

The surgical procedure produced relatively pronounced raise in the peak contact pressure between the navicular and cuboid joint, whereas increases in contact pressure were also predicted in other joints, including the ankle, talonavicular joint, the fifth cuboideometatarsal, and intermediate cuneonavicular joints. Based on the findings, we believed that the cuboideonavicular and the ankle joints were more susceptible to arthritis due to the large contact pressure. Likewise, the large von Mises stress on the second metatarsal induced by the procedure could probably increase the risk of stress fracture which in line with the higher complication rates of second metatarsal stress fracture in clinical findings.

Effective interventions are expected to remedy the pain, impaired functions, and quality of life because of the disease or problems, even though surgery may interfere natural anatomy and physiology resulting in complications and other negative outcomes. Biomechanical information provides additional information for physicians to understand the limitations or potential consequences of an intervention and support their decision-making process.

4 Biomechanical Study of Calcaneal Fracture Mechanism

Summary
Calcaneus fracture comprises 1–2% of all fractures and about 60% of those affecting the foot, with approximately 75% as intra-articular fractures. Fractures of the calcaneus are typically produced by axial compressive force yet relevant research using cadavers demonstrated variations in experimental design and outcome. Biomechanical tolerance of calcaneus towards axial collision impact also remains unclear. Finite element (FE) analysis provides a versatile platform to estimate the internal features of the calcaneus in a controlled environment. In this study, a comprehensive FE analysis was adopted to evaluate the influence of axial impact on the risk of calcaneal fractures. An impact at 5.0 m/s induced a maximum stress (von Mises) of 3.21 MPa and 2.41 MPa, respectively, for the calcaneus and talus trabecular, in addition to maximum shear stress (Tresca) of 3.46 and 2.55 MPa. Approximately one-fifth of the volume surpassed the yielding point of compressive stress and more than 80% exceeded that of the shear stress. These volumes were centered at the talocalcaneal articulation and the inferior calcaneal tuberosity that resembled common sites of fracture. This study can provide insights into injury prevention and fracture management for high energy trauma.

4.1 Background

Calcaneus plays an important role in the foot by its unique morphology and its various connections to other soft tissue attachment. It sustains the pulling force of the plantar fascia, tendon, and ligaments during weight-bearing and forming a tensegrity structure to facilitate the stability of the longitudinal arch and lateral column of

the foot [80]. Besides, calcaneus transmits majority of the body weight to the ground and acts as a strong lever for the greatest plantarflexor of the foot during propulsion.

Calcaneus is the most common fracture site of the hindfoot, and the consequence could be devastating. Calcaneal fractures occur during the high-energy events, such as a car crash or a fall from height. The annual incidence was 11.5 in every 100,000 population and males had a 2.4 times higher occurrence than females [81]. In males, the annual incidence was 16.5 in every 100,000 population, with a peak incidence of 21.6 in the age group 20–29. In females, the overall incidence was 6.26, with a more evenly distributed rate across the age cohorts and showing a gradual increase towards the post-menopause.

Calcaneal fracture is difficult to treat and requires a lengthy recovery period. Treatment involves both conservative and surgical interventions to reconstruct the normal anatomy of the heel and restore mobility so that patients can return to normal activity [82]. But even with appropriate treatment, some fractures may result in long-term complications, such as pain, swelling, loss of motion, and arthritis. Many complications can be prevented and treated with the considerations of biomechanics during surgical planning.

4.2 Biomechanical Research of Calcaneal Fractures

The ankle joint that encompassed the calcaneus and talus stands close to the load line. Therefore, the calcaneus is more vulnerable to high axial compressive force that leads to calcaneal fracture [83, 84]. From the biomechanical point of perspective, it is worth knowing the detailed mechanism of the fracture, while relevant studies examined the influence of collision impact during an accident and the tolerance of the foot and ankle [83]. The fracture was induced to cadaveric specimens with a prescribed impact velocity or energy [85], while some mimicked a pedal impact using different pre-dorsiflexed ankle position, as well as different impact forces and velocities [86–89].

Among hindfoot fracture, calcaneus was one of the most frequent sites of injury, followed by talus and ankle fracture [84]. Despite, cadaveric studies in support to this fact reported mixed results probably due to the variation in research protocols. One study envisaged an extremely high impact velocity at 12 m/s to simulate a pedal impact upon a landmine explosion on the vehicle [87]. Different loading profiles were also considered in quasi-static scenarios [88]. Even though within a single study, the reports of fracturing load on different specimens can range from 3.7 to 8.3 kN [84].

Computational simulation provides an alternative to evaluate the potential of calcaneal fracture upon impact otherwise difficult to be conducted ethically using physical experiments [90]. The advantage of the finite element (FE) method included the assessment of internal biomechanical environment of complex structures in well-controlled conditions which support different designs and clinical applications [91–94]. Previous studies had also utilized dynamic analyses in applications such as

car crash, landing, and running [2, 3, 95]. A pedal impact on the forefoot was also simulated using a foot-shank model complex by Shin et al. and his colleagues [96].

The aim of this research was to study how different impact velocity attenuate the stress of the heel and thus the risk of fracture by means of FE analysis. Prior to the dynamic simulation, we constructed an anatomically detailed FE model of the foot and ankle complex and performed a validation. The outcome measure of the simulation included the reaction forces and the volume fraction of the yielding bone upon different impact velocities.

4.3 Mechanism of Calcaneal Fracture

4.3.1 Model Reconstruction

We recruited a healthy female (age 28; height 165 cm; body mass 54 kg) to participate in the study. She did not reported any musculoskeletal pain, disorder or previous foot surgeries. The coronal magnetic resonance (MR) images of the right foot was scanned using A 3.0-T scanner (TrioTim, Siemens Medical Solutions, Erlangen, Germany) at neutral position and under no weight-bearing. The clinical images were processed in an image segmentation software (Mimics 10, Materialise, Leuven, Belgium) where 30 bones and the encapsulated tissue were segmented and further optimized in another software (Rapidfrom XOR2, INUS technology Ltd., Seoul, Korea). The calcaneus and talus bones were further segmented into the cortical layer and the trabecular core according to the settings of Sabry et al. [97]. Since the cartilage was difficult to identify in the clinical images, we simplified the layer geometry into a nonlinear contact stiffness [65] along with a frictionless behavior [98]. The ligaments, tendons, and fascia were constructed using trusses, surfaces, and connectors jointing the insertion points on the constructed osseous geometry which was further confirmed by anatomy expert. The model was an extension to our previous work in which the validation process using both plantar pressure measurement and cadavers, and the mesh convergence test were conducted [99]. The reconstructed finite element model of the foot and ankle complex is shown in Fig. 10.19.

4.3.2 Material Properties

The material properties of the model parts were all sourced from literature as shown. The calcaneus and talus were segmented into trabecular and cortical core and assumed linearly elastic with a Young's modulus of 0.4 MPa and 17 GPa, and the Poisson's ratio of 0.3 [100] while that of the other bones without segmentation were assigned 7.3 GPa [40]. Hyperelastic material property was assigned to the encapsulated soft tissue and skin using the constitutive equation of the second order polynomial strain energy potential and first-order Ogden model, respectively [41, 101]. The suggested average elasticity of rearfoot ligament from literature

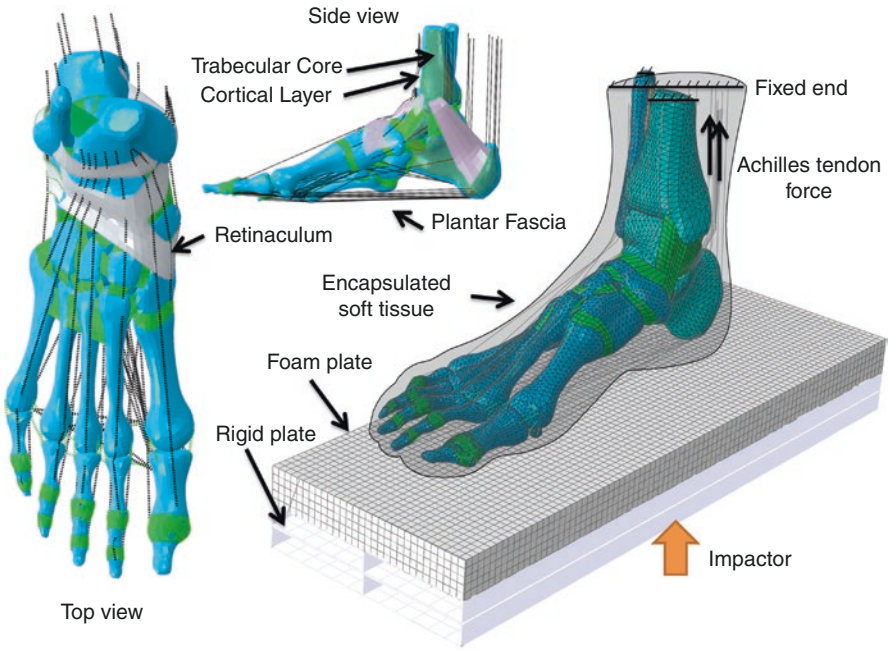

Fig. 10.19 Finite element model of the foot and ankle complex. Finite element model of the foot and ankle complex showing the top and side view of the parts geometry and demonstrating the boundary and load conditions used in the simulation. (*Reprinted from PlosOne, Wong et al., Finite Element Analysis of Foot and Ankle Impact Injury: Risk Evaluation of Calcaneus and Talus Fracture, e0154435 (2016), under CC-BY*)

was assigned to our model with a value of 264.8 MPa [42, 102]. The forefoot ligaments were assumed as truss and assigned with a cross-sectional area of 18.4 mm^2 [63], while the other ligaments modelled with shell surface have a thickness of 1.5 mm [43, 98]. The footplate was regarded as a 19-mm thick foam padding with a higher elastic modulus (15 MPa) sticking on top of another plate with rigid definition [84].

4.3.3 Boundary and Loading Conditions

The simulation was carried out using commercially available finite element package (Abaqus 6.11, Dassault Systèmes, RI, USA). The coefficient of friction bounded by the encapsulated soft tissue and the ground plate was set to 0.6 [47] and the bones were tied to the encapsulated soft tissue.

Firstly, two sets of simulations were conducted for model validation which attempted to resemble the two sets of conditions in a cadaveric study [84]. According to the study protocol. The encapsulated bulk tissue and the proximal end of tibial and fibular were encastré. As shown in Fig. 10.22, a foot pedal was driven by an impact plate striking at 5.0 m/s such that the pedal would eventually meet the

plantar foot surface [84]. The mass of the impactor was assigned 7 kg while that of the foot pedal was 4.5 kg and comprised one deformable and one rigid layer [86]. On the other hand, a vertical ground reaction force resembling half body weight of a 54 kg person was applied on the pedal in superior direction once the foot came into contact. The second load case for validation presented the same settings as the first load case, except that the Achilles tendon would be loaded 1940 N. Immediately after the simulation for validation, a parametric analysis with different impact velocities from 2.0 to 7.0 m/s would be conducted based on the aforementioned boundary and loading conditions for validation.

4.3.4 Data Analysis

Ground reaction force (GRF; as computed by the contact between the plantar foot and pedal) and tibial reaction force (TRF) would be evaluated on the two scenarios (i.e., with and without Achilles tendon load). TRF is the predicted reaction force to maintain the fixture of the proximal tibial end.

By varying the impact velocity at 1.0 m/s interval from 2.0 to 7.0 m/s, we investigated the influence on GRF, TRF, as well as the maximum von Mises stress and shear (Tresca) stress of the calcaneal and talar trabecular core. The volume fraction of bone exceeding yield in compression and shear would be regarded as the risk indicator for bone fracture. The compressive and shear yield was 1.8 MPa and 0.79 MPa, respectively [103, 104].

4.4 Biomechanical Evaluation of Impact Injury on the Calcaneus

4.4.1 Model Validation

Figure 10.20 illustrates the GRF and TRF under impact with and without Achilles tendon load and compared the outcome between our FE predictions and existing study [84]. Regarding GRF, the differences between prediction and experiment findings were approximately 10% under both the conditions with and without Achilles tendon load. FE analysis found that the GRFs were 7400 and 6000 N with and without Achilles tendon load conditions. Besides, the differences of TRF between simulation and experiment were relatively prominent (27.5%) under the condition with Achilles tendon, while the difference (600 N) was less without the Achilles tendon load.

4.4.2 Ground Reaction Force and the Tibial Reaction Force

Figure 10.21 suggests that an increase in impact velocity resulted in increases in both GRF and TRF, while the slope of increase for GRF was larger. The GRF was nearly two times than TRF in baseline, and they reached 11.53 kN and 7.78 kN,

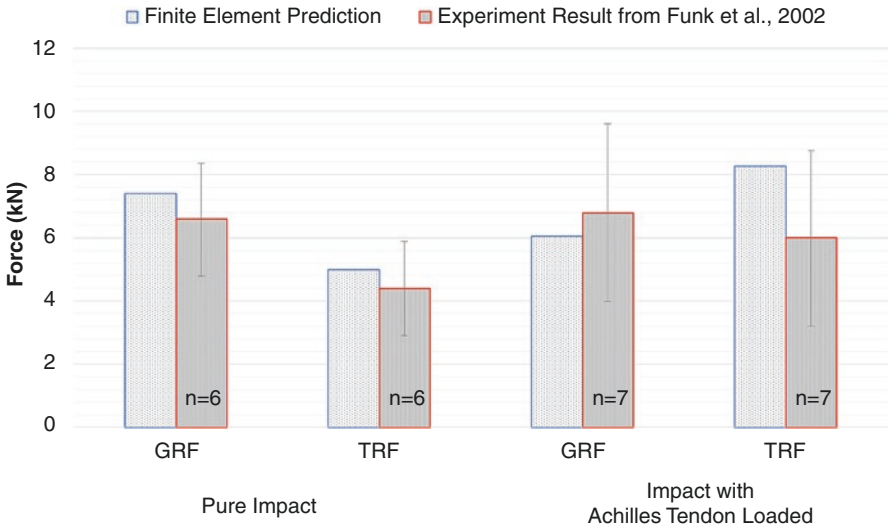

Fig. 10.20 Validation of finite element model by comparing the prediction results to existing literature. Comparison of finite element prediction and cadaveric experiment results from Funk et al. [84] on the ground reaction force (GRF) and tibial reaction force (TRF) under pure impact and impact with Achilles tendon loading. (*Reprinted from PlosOne, Wong et al., Finite Element Analysis of Foot and Ankle Impact Injury: Risk Evaluation of Calcaneus and Talus Fracture, e0154435 (2016), under CC-BY*)

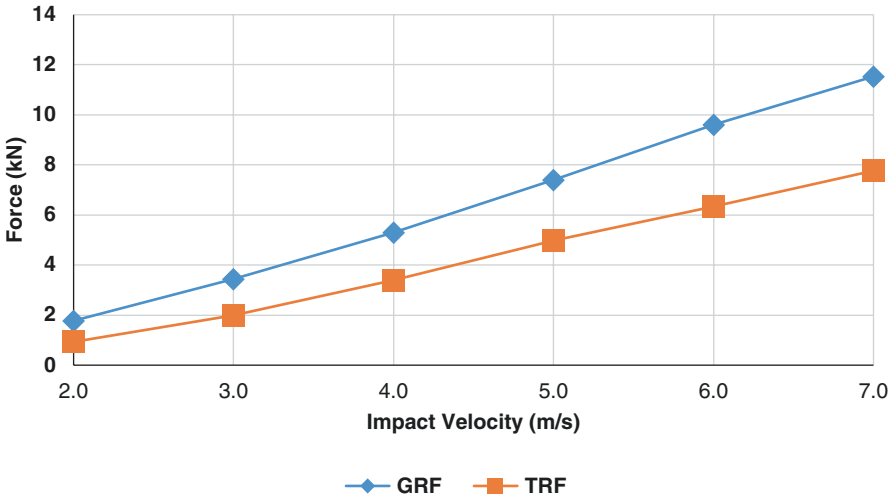

Fig. 10.21 Ground reaction force (GRF) and tibial reaction force (TRF) under different impact velocity (2.0–7.0 m/s). (*Reprinted from PlosOne, Wong et al., Finite Element Analysis of Foot and Ankle Impact Injury: Risk Evaluation of Calcaneus and Talus Fracture, e0154435 (2016), under CC-BY*)

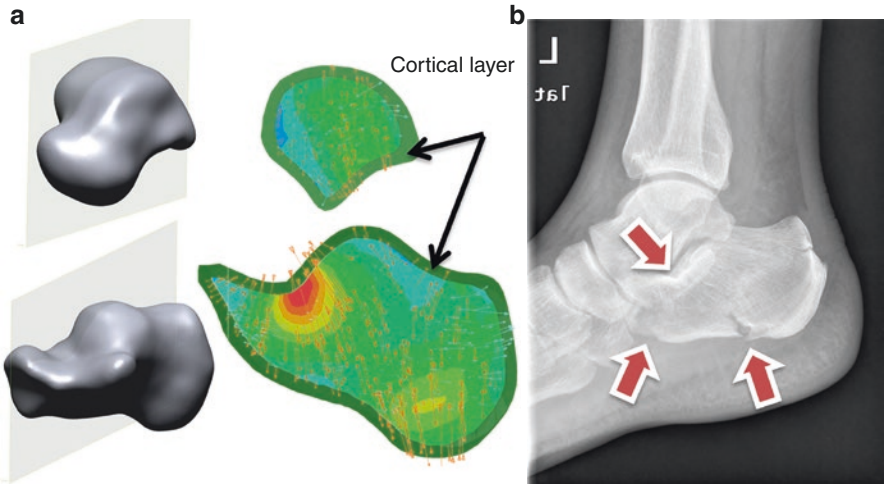

Fig. 10.22 Von Mises stress of calcaneus and talus. (**a**) Cross section view of von Mises stress of the calcaneus and talus at 5.0 m/s impact velocity. Orange arrows indicate compressive stress. Cyan arrows indicate tensile stress. (**b**) X-ray of a typical patient with a compressive fracture of the calcaneus. Arrows indicate regions of fractures. (*Reprinted from PlosOne, Wong et al., Finite Element Analysis of Foot and Ankle Impact Injury: Risk Evaluation of Calcaneus and Talus Fracture, e0154435 (2016), under CC-BY*)

respectively, at the highest impact velocity. Their differences ranged from 33% to 47% in the study range of impact velocities.

4.4.3 Stress and Tresca

Figure 10.22a displays the von Mises stress of the calcaneus and talus. In addition, as shown in Figure 10.22b, the fracture sites of one typical patient presented similar pattern to that of the location of the peak stress. Figures 10.24 and 10.25 suggested that the increase of impact velocity resulted in the increase of both the maximum von Mises stress and Tresca stress. The Tresca stress was 7% higher than the maximum von Mises stress at 2.0 m/s impact and the difference was enlarged with increasing impact velocity. At 7.0 m/s impact velocity, the maximum von Mises stress was 5.06 MPa compared to 5.47 MPa of Tresca stress.

Figures 10.23 and 10.24 illustrates the volume fraction of the trabecular bone of calcaneus that was higher than the yielding point. Interestingly, the yielding was dominant by shear stress. Nearly 80% of the bone experienced yielding at 4.0 m/s and nearly total fraction exceeded shear yield at 7.0 m/s. The trabecular bone experienced less yield and only two-third of the volume exceeded compressive yield at 7.0 m/s.

The volume of trabecular calcaneus that exceeded yield is presented in Fig. 10.24. The trabecular calcaneus underwent shear yielding predominantly compared to compressive yield. The volume of bone with shear yielding increased considerably

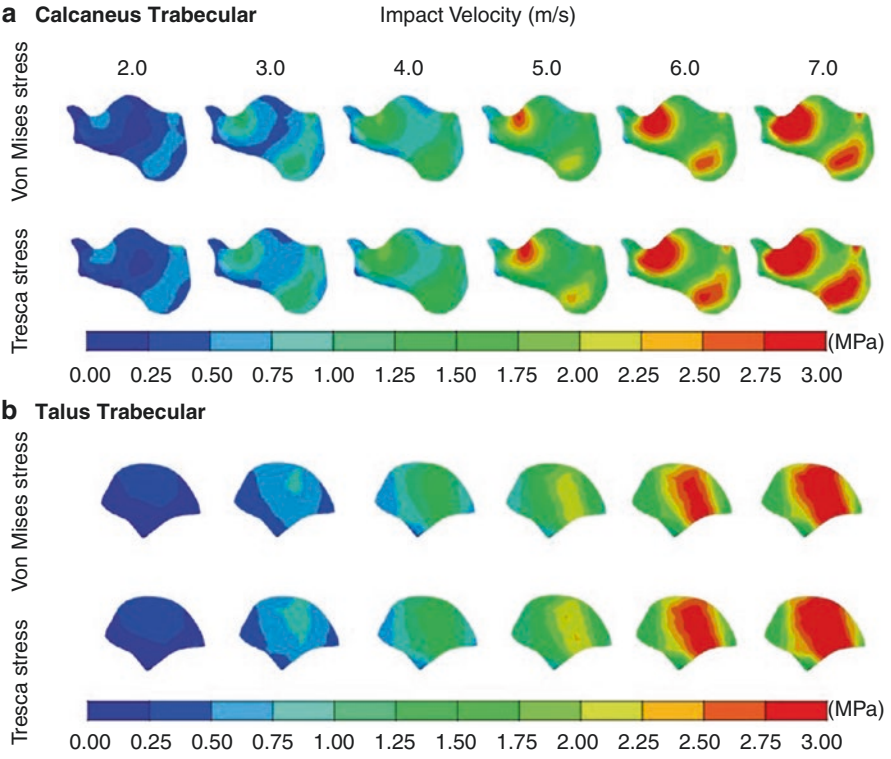

Fig. 10.23 Von Mises and Tresca stresses of the (**a**) calcaneus trabecular and (**b**) talus trabecular at different impact velocities. (*Reprinted from PlosOne, Wong et al., Finite Element Analysis of Foot and Ankle Impact Injury: Risk Evaluation of Calcaneus and Talus Fracture, e0154435 (2016), under CC-BY*)

from 36.2% at 3.0 m/s impact to 79.7% at 4.0 m/s. Nearly all trabecular bone of the calcaneus exceeded the yielding point of shear at 7.0 m/s impact. The trabecular bone that exceeded the compressive strength was relatively mild. About one-fifth and two-thirds of the volume reached the compressive yield at 5.0 m/s and 7.0 m/s impact, respectively (Fig. 10.24).

The maximum stress and Tresca of trabecular talus are demonstrated in Figs. 10.23 and 10.25. The line of shear stress was consistently larger than that of the von Mises stress, while both parameters increased with increasing impact velocity. The stresses were 0.48 and 0.55 MPa for the maximum von Mises and Tresca at 2.0 m/s impact and were increased to 3.68 and 3.90 MPa, respectively, at 7.0 m/s. Nearly one-fifth of the bone volume experienced a compressive yield which was then increased to half from 5.0 to 7.0 m/s.

Figure 10.23 shows that both the peak of von Mises stress and shear (Tresca) were located at the inferior calcaneal tuberosity and talus articulation, which was generally agreeable with the findings of cadaveric study and common fracture sites [84, 87]. The stress concentration at the posterior talocalcaneal articulation, as well as the superior side of the talar trochlea suggested that talus was also susceptible to fracture during compressive impact [87]. Lateral malleolar articulation and

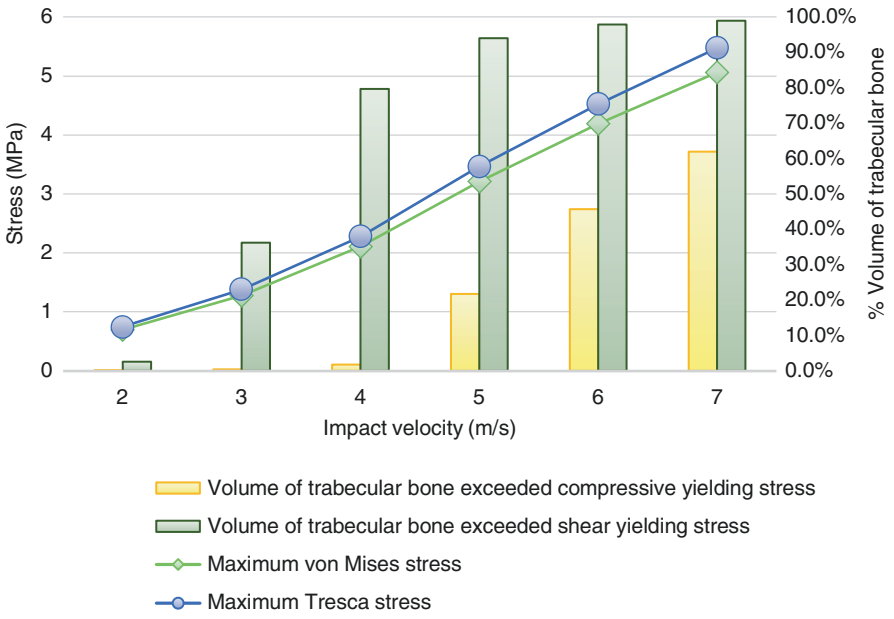

Fig. 10.24 Maximum von Mises and Tresca stress with yielding volume of trabecular calcaneus against impact velocity. (*Reprinted from PlosOne, Wong et al., Finite Element Analysis of Foot and Ankle Impact Injury: Risk Evaluation of Calcaneus and Talus Fracture, e0154435 (2016), under CC-BY*)

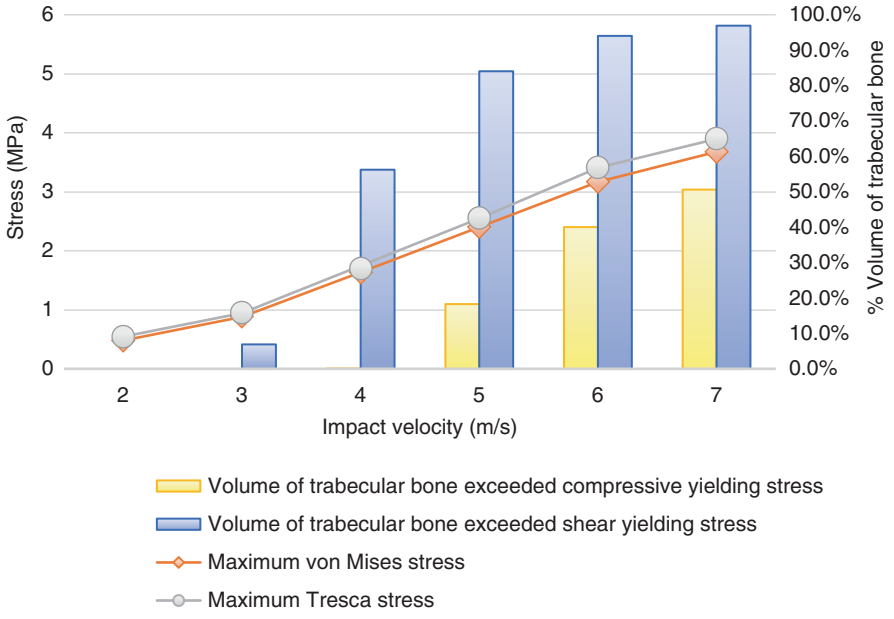

Fig. 10.25 Maximum von Mises and Tresca stress with yielding volume of trabecular talus against impact velocity. (*Reprinted from PlosOne, Wong et al., Finite Element Analysis of Foot and Ankle Impact Injury: Risk Evaluation of Calcaneus and Talus Fracture, e0154435 (2016), under CC-BY*)

talocalcaneal articulation fracture could be followed by the calcaneal fracture and displaced talus. The volume of yielding trabecular bone of the calcaneus and talus was similar in both compression and shear, despite that the maximum stress of the talus was smaller. The material was assumed linearly elastic in the simulation. Therefore, the prediction may overestimate the risk of fracture. It shall be improved with elasto-plastic behavior [105].

4.5 Conclusion

An axial compressive impact (5.0 m/s) induced yielding to the trabecular bone of the heel which predisposes potential fracture. Our prediction showed that the fracture could be dominant by shear failure and compounded by compression. Future study shall consider the sensitivity of different loading patterns on fracture which could provide additional insights to design measures for injury prevention and intervention for fracture management.

In the future, this computational platform can investigate the relationship between different loading modes and fracture pattern/mechanism that could support design for the prevention of injury, as well as management of the fracture.

Acknowledgments The work of this chapter was supported by the Key R&D Program granted by the Ministry of Science and Technology of China (2018YFB1107000), NSFC granted by the National Natural Science Foundation of China (11732015), and General Research Fund granted by the Hong Kong Research Grant Council (PolyU152065/17E).

References

1. Abhishek A, Roddy E, Zhang W, Doherty M. Are hallux valgus and big toe pain associated with impaired quality of life? A cross-sectional study. Osteoarthr Cartil. 2010;18(7):923–6.
2. Cho JR, Park SB, Ryu SH, Kim SH, Lee SB. Landing impact analysis of sports shoes using 3-d coupled foot-shoe finite element model. J Mech Sci Technol. 2009b;23(10):2583–91.
3. Cho NH, Kim S, Kwon DJ, Kim HA. The prevalence of hallux valgus and its association with foot pain and function in a rural korean community. J Bone Joint Surg Br. 2009a;91b(4):494–8.
4. Menz HB, Roddy E, Thomas E, Croft PR. Impact of hallux valgus severity on general and foot-specific health-related quality of life. Arthritis Care Res Hoboken. 2011;63(3):396–404.
5. Meyr AJ, Adams ML, Sheridan MJ, Ahalt RG. Epidemiological aspects of the surgical correction of structural forefoot pathology. J Foot Ankle Surg. 2009;48(5):543–51.
6. Wu D, Louie L. Does wearing high-heeled shoe cause hallux valgus? A survey of 1,056 chinese females. Foot Ankle Online J. 2010;3(5):3.
7. Bonney G, McNab L. Hallux valgus and hallux rigidus—a critical survey. J Bone Joint Surg Br. 1952;34-B(3):366–85.
8. Roddy E, Zhang W, Doherty M. Prevalence and associations of hallux valgus in a primary-care population. Ann Rheum Dis. 2006;65:403–4.

9. Coughlin MJ, Shurnas PS. Hallux valgus in men. Part II: first ray mobility after bunionectomy and factors associated with hallux valgus deformity. Foot Ankle Int. 2003a;24(1):73–8.
10. Ferrari J, Hopkinson DA, Linney AD. Size and shape differences between male and female foot bones: is the female foot predisposed to hallux abducto valgus deformity? J Am Podiatr Med Assoc. 2004;94(5):434–52.
11. Wilkerson RD, Mason MA. Differences in men's and women's mean ankle ligamentous laxity. Iowa Orthop J. 2000;20:46.
12. Coughlin MJ, Jones CP. Hallux valgus and first ray mobility. A prospective study. J Bone Joint Surg Am. 2008;90(5):1166–7.
13. Owoeye BA, Akinbo SR, Aiyegbusi AL, Ogunsola MO. Prevalence of hallux valgus among youth population in Lagos, Nigeria. Nigerian Postgrad Med J. 2011;18(1):51–5.
14. Menz HB, Lord SR. The contribution of foot problems to mobility impairment and falls in community-dwelling older people. J Am Geriatr Soc. 2001;49(12):1651–6.
15. Thompson FM, Coughlin MJ. The high price of high-fashion footwear. J Bone Joint Surg Am. 1994;76a(10):1586–93.
16. Access Economics. The economic impact of podiatric surgery. In: Report for the Australasian College of Podiatric Surgeons. Sydney: Access Economics Pty Ltd; 2008.
17. Australian Bureau of Statistics. Australian National Accounts: national income, expenditure and product. Canberra: Australian Bureau of Statistics; 2008.
18. Courtney TK, Matz S, Webster BS. Disabling occupational injury in the us construction industry, 1996. J Occup Environ Med. 2002;44(12):1161–8.
19. Mathers CD, Vos ET, Stevenson CE, Begg SJ. The burden of disease and injury in Australia. Bull World Health Organ. 2001;79(11):1076–84.
20. Caminear DS, Addis-Thomas E, Brynizcka AW, Saxena A. Revision hallux valgus surgery. In: Saxena A, editor. International advances in foot and ankle surgery. London: Springer-Verlag; 2012. p. 71–82.
21. Lehman DE. Salvage of complications of hallux valgus surgery. Foot Ankle Clin. 2003;8(1):15–35.
22. Coughlin MJ, Mann RA. Hallux valgus. In: Coughlin MJ, Saltzman CL, Mann RA, editors. Surgery of the foot and ankle. 8th ed. Pennsylvania: Mosby Elsevier; 2012.
23. Faber FWM, Kleinrensink GJ, Mulder PGH, Verhaar JAN. Mobility of the first tarsometatarsal joint in hallux valgus patients: a radiographic analysis. Foot Ankle Int. 2001;22(12):965–9.
24. Glasoe WM, Allen MK, Saltzman CL, Ludewig PM, Sublett SH. Comparison of two methods used to assess first-ray mobility. Foot Ankle Int. 2002;23(3):248–52.
25. Kim JY, Park JS, Hwang SK, Young KW, Sung IH. Mobility changes of the first ray after hallux valgus surgery: clinical results after proximal metatarsal chevron osteotomy and distal soft tissue procedure. Foot Ankle Int. 2008;29(5):468–72.
26. Smith BW, Coughlin MJ. The first metatarsocuneiform joint, hypermobility, and hallux valgus: what does it all mean? Foot Ankle Surg. 2008;14(3):138–41.
27. Klaue K, Hansen ST, Masquelet AC. Clinical, quantitative assessment of first tarsometatarsal mobility in the sagittal plane and its relation to hallux valgus deformity. Foot Ankle Int. 1994;15(1):9–13.
28. Hillstrom HJ, Song JS, Kraszewski AP, et al. Foot type biomechanics part 1: structure and function of the asymptomatic foot. Gait Posture. 2013;37(3):445–51.
29. Stokes IAF, Hutton WC, Stott JRR, Lowe LW. Forces under the hallux valgus foot before and after surgery. Clin Orthop Relat Res. 1979;142:64–72.
30. Kernozek TW, Elfessi A, Sterriker S. Clinical and biomechanical risk factors of patients diagnosed with hallux valgus. J Am Podiatr Med Assoc. 2003;93(2):97–103.
31. Martínez-Nova A, Cuevas-García JC, Sánchez-Rodríguez R, Pascual-Huerta J, Sánchez-Barrado E. Study of plantar pressure patterns by means of instrumented insoles in subjects with hallux valgus. Rev Esp Cir Ortop Traumatol (Engl Ed). 2008;52(2):94–8.
32. Mickle KJ, Munro BJ, Lord SR, Menz HB, Steele JR. Gait, balance and plantar pressures in older people with toe deformities. Gait Posture. 2011;34(3):347–51.

33. Wen JM, Ding QC, Yu ZY, Sun WD, Wang QN, Wei KL. Adaptive changes of foot pressure in hallux valgus patients. Gait Posture. 2012;36(3):344–9.
34. Mittal D, Raja S, Geary NPJ. The modified mcbride procedure: clinical, radiological, and pedobarographic evaluations. J Foot Ankle Surg. 2006;45(4):235–9.
35. Saro C, Andrén B, Felländer-Tsai L, Lindgren U, Arndt A. Plantar pressure distribution and pain after distal osteotomy for hallux valgus: a prospective study of 22 patients with 12-month follow-up. Foot. 2007;17(2):84–93.
36. Dhukaram V, Hullin MG, Senthil Kumar C. The Mitchell and scarf osteotomies for hallux valgus correction: a retrospective, comparative analysis using plantar pressures. J Foot Ankle Surg. 2006;45(6):400–9.
37. Cheung JT-M, Nigg BM. Clinical applications of computational simulation of foot and ankle. Sports Orthop Traumatol. 2008;23(4):264–71.
38. Yu J, Cheung JTM, Fan YB, Zhang Y, Leung AKL, Zhang M. Development of a finite element model of female foot for high-heeled shoe design. Clin Biomech. 2008;23:S31–8.
39. Kai T, Wang C-T, Wang D-M, Wang X. Primary analysis of the first ray using a 3-dimension finite element foot model. Paper read at Engineering in Medicine and Biology Society, 2005. In: 27th Annual International Conference of the IEEE-EMBS 2005. 2006.
40. Nakamura S, Crowninshield RD, Cooper RR. An analysis of soft tissue loading in the foot—a preliminary report. Bull Prosthet Res. 1981;10:27–34.
41. Lemmon D, Shiang TY, Hashmi A, Ulbrecht JS, Cavanagh PR. The effect of insoles in therapeutic footwear—a finite element approach. J Biomech. 1997;30(6):615–20.
42. Siegler S, Block J, Schneck CD. The mechanical characteristics of the collateral ligaments of the human ankle joint. Foot Ankle. 1988a;8(5):234–42.
43. Milz P, Milz S, Steinborn M, Mittlmeier T, Putz R, Reiser M. Lateral ankle ligaments and tibiofibular syndesmosis—13-MHz high-frequency sonography and mri compared in 20 patients. Acta Orthop Scand. 1998;69(1):51–5.
44. Arnold EM, Ward SR, Lieber RL, Delp SL. A model of the lower limb for analysis of human movement. Ann Biomed Eng. 2010;38(2):269–79.
45. Froberg A, Komi P, Ishikawa M, Movin T, Arndt A. Force in the achilles tendon during walking with ankle foot orthosis. Am J Sports Med. 2009;37(6):1200–7.
46. Perry J, Davids JR. Gait analysis: normal and pathological function. J Pediatr Orthop. 1992;12(6):815.
47. Zhang M, Mak AFT. In vivo friction properties of human skin. Prosthetics Orthot Int. 1999;23(2):135–41.
48. Coughlin MJ. Instructional course lectures, the american academy of orthopaedic surgeons-hallux valgus. J Bone Joint Surg. 1996;78(6):932–66.
49. Valderrabano V, Horisberger M, Russell I, Dougall H, Hintermann B. Etiology of ankle osteoarthritis. Clin Orthop Relat Res. 2009;467(7):1800–6.
50. Goldberg AJ, MacGregor A, Dawson J, et al. The demand incidence of symptomatic ankle osteoarthritis presenting to foot & ankle surgeons in the United Kingdom. Foot. 2012;22(3):163–6.
51. Glazebrook M, Daniels T, Younger A, et al. Comparison of health-related quality of life between patients with end-stage ankle and hip arthrosis. J Bone Joint Surg. 2008;90(3):499–505.
52. Slobogean GP, Younger A, Apostle KL, et al. Preference-based quality of life of end-stage ankle arthritis treated with arthroplasty or arthrodesis. Foot Ankle Int. 2010;31(7):563–6.
53. Coester LM, Saltzman CL, Leupold J, Pontarelli W. Long-term results following ankle arthrodesis for post-traumatic arthritis. J Bone Joint Surg Am. 2001;83a(2):219–28.
54. Fuchs S, Sandmann C, Skwara A, Chylarecki C. Quality of life 20 years after arthrodesis of the ankle—a study of adjacent joints. J Bone Joint Surg Br. 2003;85b(7):994–8.
55. Mazur JM, Schwartz E, Simon SR. Ankle arthrodesis - long-term follow-up with gait analysis. J Bone Joint Surg Am. 1979;61(7):964–75.
56. Thomas R, Daniels TR, Parker K. Gait analysis and functional outcomes following ankle arthrodesis for isolated ankle arthritis. J Bone Joint Surg Am. 2006;88a(3):526–35.

57. Muir DC, Amendola A, Saltzman CL. Long-term outcome of ankle arthrodesis. Foot Ankle Clin. 2002;7(4):703–8.
58. Beyaert C, Sirveaux F, Paysant J, Mole D, Andre JM. The effect of tibio-talar arthrodesis on foot kinematics and ground reaction force progression during walking. Gait Posture. 2004;20(1):84–91.
59. Flavin R, Coleman SC, Tenenbaum S, Brodsky JW. Comparison of gait after total ankle arthroplasty and ankle arthrodesis. Foot Ankle Int. 2013;34(10):1340–8.
60. Piriou P, Culpan P, Mullins M, Cardon JN, Pozzi D, Judet T. Ankle replacement versus arthrodesis: a comparative gait analysis study. Foot Ankle Int. 2008;29(1):3–9.
61. Ramlee MH, Kadir MRA, Murali MR, Kamarul T. Finite element analysis of three commonly used external fixation devices for treating type iii pilon fractures. Med Eng Phys. 2014;36(10):1322–30.
62. Vazquez AA, Lauge-Pedersen H, Lidgren L, Taylor M. Finite element analysis of the initial stability of ankle arthrodesis with internal fixation: flat cut versus intact joint contours. Clin Biomech. 2003;18(3):244–53.
63. Cheung JTM, Zhang M, Leung AKL, Fan YB. Three-dimensional finite element analysis of the foot during standing - a material sensitivity study. J Biomech. 2005;38(5):1045–54.
64. Cheung JTM, Zhang M. A 3-dimensional finite element model of the human foot and ankle for insole design. Arch Phys Med Rehabil. 2005;86(2):353–8.
65. Athanasiou KA, Liu GT, Lavery LA, Lanctot DR, Schenck RC. Biomechanical topography of human articular cartilage in the first metatarsophalangeal joint. Clin Orthop Relat Res. 1998;348:269–81.
66. Gefen A, Megido-Ravid M, Itzchak Y, Arcan M. Biomechanical analysis of the three-dimensional foot structure during gait: a basic tool for clinical applications. J Biomech Eng Trans ASME. 2000;122(6):630–9.
67. Wright DG, Rennels DC. A study of the elastic properties of plantar fascia. J Bone Joint Surg. 1964;46(3):482–92.
68. Dul J. Development of a minimum-fatigue optimization technique for predicting individual muscle forces during human posture and movement with application to the ankle musculature during standing and walking. Ph.D. thesis, Vanderbilt University. 1983.
69. Kim K-J, Kitaoka HB, Luo Z-P, et al. In vitro simulation of the stance phase in human gait. J Musculoskelet Res. 2001;5(02):113–21.
70. Eleftheriou KI, Rosenfeld PF, Calder JDF. Lisfranc injuries: an update. Knee Surg Sports Traumatol Arthrosc. 2013;21(6):1434–46.
71. Arastu MH, Buckley RE. Tarsometatarsal joint complex and midtarsal injuries. Acta Chir Orthop Traumatol Cechoslov. 2012;79(1):21–30.
72. Desmond EA, Chou LB. Current concepts review: Lisfranc injuries. Foot Ankle Int. 2006;27(8):653–60.
73. Watson TS, Shurnas PS, Denker J. Treatment of lisfranc joint injury: current concepts. J Am Acad Orthop Surg. 2010;18(12):718–28.
74. Ghate SD, Sistla VM, Nemade V, Vibhute D, Shahane SM, Samant AD. Screw and wire fixation for lisfranc fracture dislocations. J Orthop Surg. 2012;20(2):170–5.
75. Lakin RC, DeGnore LT, Pienkowski D. Contact mechanics of normal tarsometatarsal joints. J Bone Joint Surg Am. 2001;83a(4):520–8.
76. Wang Y, Li Z, Zhang M. Biomechanical study of tarsometatarsal joint fusion using finite element analysis. Med Eng Phys. 2014;36(11):1394–400.
77. Keyak JH, Rossi SA. Prediction of femoral fracture load using finite element models: an examination of stress-and strain-based failure theories. J Biomech. 2000;33(2):209–14.
78. Weatherall JM, Chapman CB, Shapiro SL. Postoperative second metatarsal fractures associated with suture-button implant in hallux valgus surgery. Foot Ankle Int. 2013a;34(1):104–10.
79. Weatherall JM, Chapman C, Shapiro S. Comment on “postoperative second metatarsal fractures associated with suture-button implant in hallux valgus surgery” response. Foot Ankle Int. 2013b;34(6):919–20.

80. Epstein N, Chandran S, Chou L. Current concepts review: intra-articular fractures of the calcaneus. Foot Ankle Int. 2012;33(1):79–86.
81. Mitchell MJ, McKinley JC, Robinson CM. The epidemiology of calcaneal fractures. Foot. 2009;19(4):197–200.
82. Lim EVA, Leung JPF. Complications of intraarticular calcaneal fractures. Clin Orthop Relat Res. 2001;391:7–16.
83. Forman JL, Lopez-Valdes FJ, Duprey S, et al. The tolerance of the human body to automobile collision impact–a systematic review of injury biomechanics research, 1990–2009. Accid Anal Prev. 2015;80:7–17.
84. Funk JR, Crandall JR, Tourret LJ, et al. The axial injury tolerance of the human foot/ankle complex and the effect of achilles tension. J Biomech Eng Trans ASME. 2002;124(6):750–7.
85. Gallenberger K, Yoganandan N, Pintar F. Biomechanics of foot/ankle trauma with variable energy impacts. Ann Adv Automot Med. 2013;57:123.
86. Crandall JR, Portier L, Petit P, et al. Biomechanical response and physical properties of the leg, foot, and ankle. SAE Technical Paper. 1996.
87. McKay BJ, Bir CA. Lower extremity injury criteria for evaluating military vehicle occupant injury in underbelly blast events. Stapp Car Crash J. 2009;53:229.
88. Parenteau CS, Viano DC, Petit PY. Biomechanical properties of human cadaveric ankle-subtalar joints in quasi-static loading. J Biomech Eng Trans ASME. 1998;120(1):105–11.
89. Yoganandan N, Pintar FA, Kumaresan S, Boynton M. Axial impact biomechanics of the human foot-ankle complex. J Biomech Eng. 1997;119:433–7.
90. Chang CY, Rupp JD, Kikuchi N, Schneider LW. Development of a finite element model to study the effects of muscle forces on knee-thigh-hip injuries in frontal crashes. Stapp Car Crash J. 2008;52(52):475–504.
91. Cheung JT-M, Yu J, Wong DW-C, Zhang M. Current methods in computer-aided engineering for footwear design. Footwear Sci. 2009;1(1):31–46.
92. Telfer S, Erdemir A, Woodburn J, Cavanagh PR. What has finite element analysis taught us about diabetic foot disease and its management. A systematic review. PLoS One. 2014;9(10):e109994.
93. Wang Y, Li ZY, Wong DWC, Zhang M. Effects of ankle arthrodesis on biomechanical performance of the entire foot. PLoS One. 2015;10(7):e0134340.
94. Wang Y, Wong DWC, Zhang M. Computational models of the foot and ankle for pathomechanics and clinical applications: a review. Ann Biomed Eng. 2016;44(1):213–21.
95. Farhang B, Araghi FR, Bahmani A, Moztarzadeh F, Shafieian M. Landing impact analysis of sport surfaces using three-dimensional finite element model. Proc Inst Mech Engrs P J Sports Eng Technol. 2016;230(3):180–5.
96. Shin J, Yue N, Untaroiu CD. A finite element model of the foot and ankle for automotive impact applications. Ann Biomed Eng. 2012;40(12):2519–31.
97. Sabry FF, Ebraheim NA, Mehalik JN, Rezcallah AT. Internal architecture of the calcaneus: implications for calcaneus fractures. Foot Ankle Int. 2000;21(2):114–8.
98. Wong DWC, Zhang M, Yu J, Leung AKL. Biomechanics of first ray hypermobility: an investigation on joint force during walking using finite element analysis. Med Eng Phys. 2014;36(11):1388–93.
99. Wong DWC, Wang Y, Zhang M, Leung AKL. Functional restoration and risk of non-union of the first metatarsocuneiform arthrodesis for hallux valgus: a finite element approach. J Biomech. 2015;48(12):3142–8.
100. Morales-Orcajo E, Bayod J, de Las Casas EB. Computational foot modeling: scope and applications. Arch Comput Methods Eng. 2016;23(3):389–416.
101. Gu YD, Li JS, Ren XJ, Lake MJ, Zeng YJ. Heel skin stiffness effect on the hind foot biomechanics during heel strike. Skin Res Technol. 2010;16(3):291–6.
102. Siegler S, Chen J, Schneck CD. The effect of damage to the lateral collateral ligaments on the mechanical characteristics of the human ankle joint. In: Proceedings of the annual interna-

tional conference of the IEEE Engineering in Medicine and Biology Society, Pts 1–4, 1988b. p. 622–3.
103. Mittra E, Rubin C, Gruber B, Qin YX. Evaluation of trabecular mechanical and microstructural properties in human calcaneal bone of advanced age using mechanical testing, mu ct, and dxa. J Biomech. 2008;41(2):368–75.
104. Sanyal A, Gupta A, Bayraktar HH, Kwon RY, Keaveny TM. Shear strength behavior of human trabecular bone. J Biomech. 2012;45(15):2513–9.
105. Kelly N, McGarry JP. Experimental and numerical characterisation of the elasto-plastic properties of bovine trabecular bone and a trabecular bone analogue. J Mech Behav Biomed Mater. 2012;9:184–97.

Chapter 11
Biomechanics of Human Motion

Rongshan Cheng, Zhongzheng Wang, Cong Wang, Fuping Li, Yifei Yao, Yan Yu, and Tsung-Yuan Tsai

Abstract In contemporary orthopedics, biomechanics of human motion has come to reflect the investigation of the joint's mechanical properties throughout joint motion. This involves the stresses in the joint throughout motion, the limits of and to motion, and the interaction between these two during joint function. This chapter will discuss these properties with regard to each joint. As such, an appreciation and understanding of joint kinematics, including the native joint, the diseased joint, and the replaced joint is critical for the next stage of improvements in joint arthroplasty. This chapter will outline and discuss the current understanding of how joint kinematics change throughout common pathologies as well as following joint arthroplasty.

Keywords Hip joint · Knee joint · Spine joint · Kinematic · Common pathologies Joint arthroplasty

1 Biomechanics of Hip Joint Motion

Studies on the hip biomechanics about hip movement or structure can be valuable to underpin the understanding of joint function, etiology, and treatment of hip-related diseases. Although ongoing endeavors to improve arthroplasty materials are of value in increasing longevity of implants, component positioning and dynamic

R. Cheng · Z. Wang · C. Wang · Y. Yao · T.-Y. Tsai (✉)
Clinical Translational R&D Center of 3D Printing Technology, Department of Orthopaedic Surgery, Shanghai Ninth People's Hospital, Shanghai Jiao Tong University School of Medicine, School of Biomedical Engineering, Shanghai Jiao Tong University, Shanghai, China
e-mail: tytsai@sjtu.edu.cn

F. Li · Y. Yu
Department of Spine Surgery, Tongji Hospital, Tongji University School of Medicine, Shanghai, China

C.-K. Cheng, S. L-Y. Woo (eds.), *Frontiers in Orthopaedic Biomechanics*,
https://doi.org/10.1007/978-981-15-3159-0_11

function have gained attention as significant factors affecting joint mobility, stability, and survivorship after total hip arthroplasty. Thus, it is critical to understand and appreciate hip kinematics on the normal hip, the diseased hip, and the replaced hip for the improvement of hip disease treatment in orthopedics. The following sections will discuss the structural factors contributing to the balance between hip stability and mobility throughout the healthy status, common pathologies, as well as hip arthroplasty follow-ups.

1.1 Fundamentals of Hip Joint Motion

The hip joint connects the femur and acetabulum of the pelvis. The hip joint plays an important role to dynamically sustain and transmit the rotational moment, the gravitational force of the body, and the ground reaction force of the lower extremities throughout an extensive range of motion. The hip joint has to maintain balance and stability of the body in an erect position during standing. While moving, a combination of both static and dynamic stabilizers helps to prevent joint dislocation and to maintain mechanical efficiency.

1.1.1 Stability

The acetabulum results from the triradiate cartilage growth center of the pelvic innominate bone at the union of the ilium, ischium, and pubic bones. Though the acetabular cup appears to have a hemispherical shape, it is spherical only in the upper 1/3rd or in the dome, allowing the required maximal distribution of force in areas for weight-bearing during upright stance. As mentioned above, the inclined acetabulum gives an acetabular index (slope of the acetabulum on an anterior-posterior (AP) radiograph) an average of 38° in males and 40° in females allowing for increased abduction but decreased adduction (Fig. 11.1a) [1]. The osseous structure on the femoral side of the joint also contributes to joint stability during static or dynamic loading. The femoral head is semispherical in shape, ranging from hemispherical to 2/3rds of a full sphere. The head quickly tapers into the femoral neck that connects to the body of the femur. The distance between the center of the femoral head and the anatomic axis of the femur represents the “head-neck offset” and is directly associated with the moment arm and efficiency of the hip abductors. Similar to the anteversion of the acetabulum, the femoral head/neck is anteverted relative to the anatomic axis by approximately 10–20° in adults (Fig. 11.1b).

Though the spherical acetabular design imparts a high degree of stability and additional ligamentous support to the hip joint, acting as checkrein to all 6 degrees of freedom during hip motion, the extra-articular ligaments consist of band-like thickenings of the capsule that allow for hip motion within a certain range of arc. Cadaveric studies have demonstrated some variability and controversy regarding the exact nature and discrete nomenclature of these bands [1]. However, it is gener-

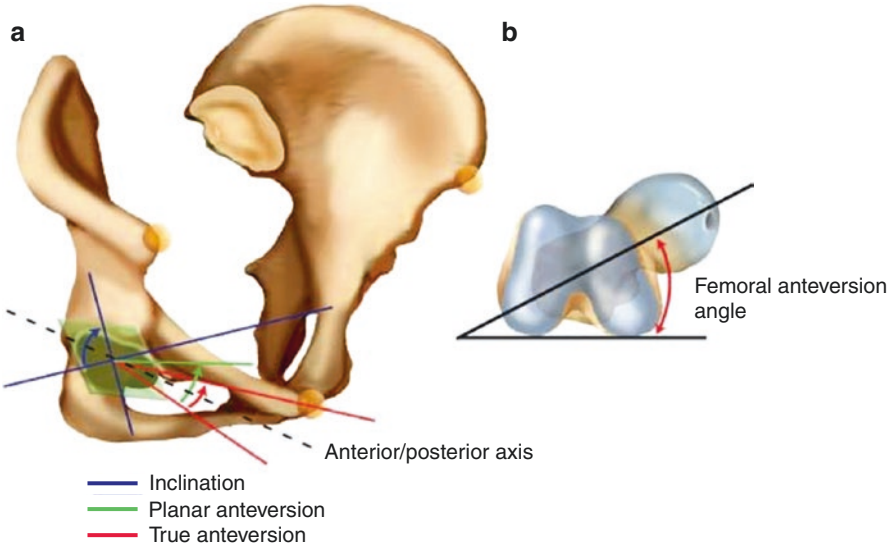

Fig. 11.1 Pelvic and femoral version. (**a**) True acetabular anteversion is the angle between the anterior/posterior axis and the interception line of transverse plane and the cup opening plane. Planar anteversion is the complement to the angle between the normal axis of the cup opening plane and the anterior/posterior axis. Inclination is the angle of the cup rotating along the anterior/posterior axis with respect to the medial/lateral axis. The anterior/posterior axis is perpendicular to the frontal pelvic plane formed by two ASIS and pubic symphysis. (**b**) Femoral anteversion is the inclination of the femoral neck axis with reference to the retrocondylar line. With the long axis determined by the best-fit cylinder of the femoral shaft, the neck axis is defined as the centerline of the femoral head and neck model. The retrocondylar line is determined from the postfemoral condyles (Reprinted with permission from Wolters Kluwer Health)

ally described that the capsule has four extra-capsular ligaments consisting of longitudinal fibers of the iliofemoral, the ischiofemoral, the pubofemoral ligaments as well as the annular fibers of the zona orbicularis. These ligaments play a crucial role in different joint positions during hip motion, which is supported by the change in motion after removal of the ligaments.

Dynamic stabilizers of the hip joint include flexors, extensors, internal and external rotators, abductors, and adductors. Similar to the rotator cuff stabilizing shoulder, antagonist function from dynamic stabilizers help to maintain the femoral head within the acetabulum. However, the interactions among muscle groups in the hip are much less well understood compared to that among the muscles of the rotator cup. Conceptually, it is assumed that antagonistic muscle groups help to counter each other's motion to lead to a hip rotation with minimal translation, as mentioned above. For example, with gluteus minimus and medius function during hip abduction, the adductor complex eccentrically contracts to help translate the femoral head back into the center of the acetabulum, thereby maintaining concentric and primarily rotatory motion. However, since the insertion points on hip abductors and the abductor complex are not directly located opposite on the femur, the resulting

difference in lever arms and moments results in a more complex intermuscular relationship than, say, that of the subscapularis and infraspinatus. Moreover, additional dynamic stabilizers also participate in direct stabilization of the hip joint, acting as physical blocks to femoral head escape. In particular, muscles that pass directly over or even attach to the hip capsule may physically confine the translation of the femoral head with applied loads.

1.1.2 Mobility

Motions of the lower extremities mostly require a combination of both translational and rotational changes in the hip joint. The rotation is the primary biomechanical degree of freedom in the hip motion, while the exception is flexion/extension in neutral abduction and external rotation. In this position and within this arc of motion, the centers of the femoral head and acetabulum are maintained in an overlapping position by balanced forces from hip flexors and adductors. Outside of this arc of motion, an associated translation due to rotation of the femoral head must be countered by opposing static or dynamic stabilizers to maintain a stable joint [2].

Experimental results for the normal range of motion of the native hip are provided in Table 11.1. The range of motion in the hip during life's activities has large variance between patients. Nevertheless, a minimum range of motion is required for daily activities such as sitting, standing, climbing stairs or walking. Thus, the evaluation of the range of motion can improve the assessment of functional limitations. In general, Heller et al. demonstrated that the hip requires a smaller arc of motion with a flexion/extension arc of 40°, abduction/adduction arc of 10°, and 10° rotational arc during walking without assistance on level ground, compared to other activities such as uneven surface ambulation, running, or raising from a chair which require a much greater range of motion [3]. It is the osseous structures that determine the absolute limits of the joint motion while the soft tissue components determine the in vivo range of motion during activities.

The hip joint is constrained by the mechanical boundaries of the bones composing the joint so that there is osseous impingement at the motion extremes. The osseous anatomy may change in pathological situations (i.e., osteoarthritis, trauma, osteonecrosis), while it is the soft tissues (ligaments, muscles, labrum, etc.) that determine the in vivo range of motion. Soft tissues either restrain or block a motion by interposition and impingement. Turley et al. [5] investigated this phenomenon by comparing the ranges of motion in the hips of subjects through a series of daily living activities. They found a significantly decreased range of functional motion as

Table 11.1 Normal motion ranges for the adult native hip at rest and observed during level surface gait

		Normal range	Level surface gait range
Adduction/abduction	(x-axis)	25°/50°	5°/5°
Internal/external rotation	(y-axis)	90°/70°	5°/5°
Flexion/extension	(z-axis)	140°/30°	30°/10°

Data from Heller et al. [3, 4]

compared to the osseous range of motion particularly in extension and flexion with adduction (Fig. 11.2). Conversely, Turley et al. [5] found that osseous impingement occurred in vivo at the extremes of adduction in an upright stance as well as abduction at 90 degrees of flexion corresponding to impingement of the lesser trochanter

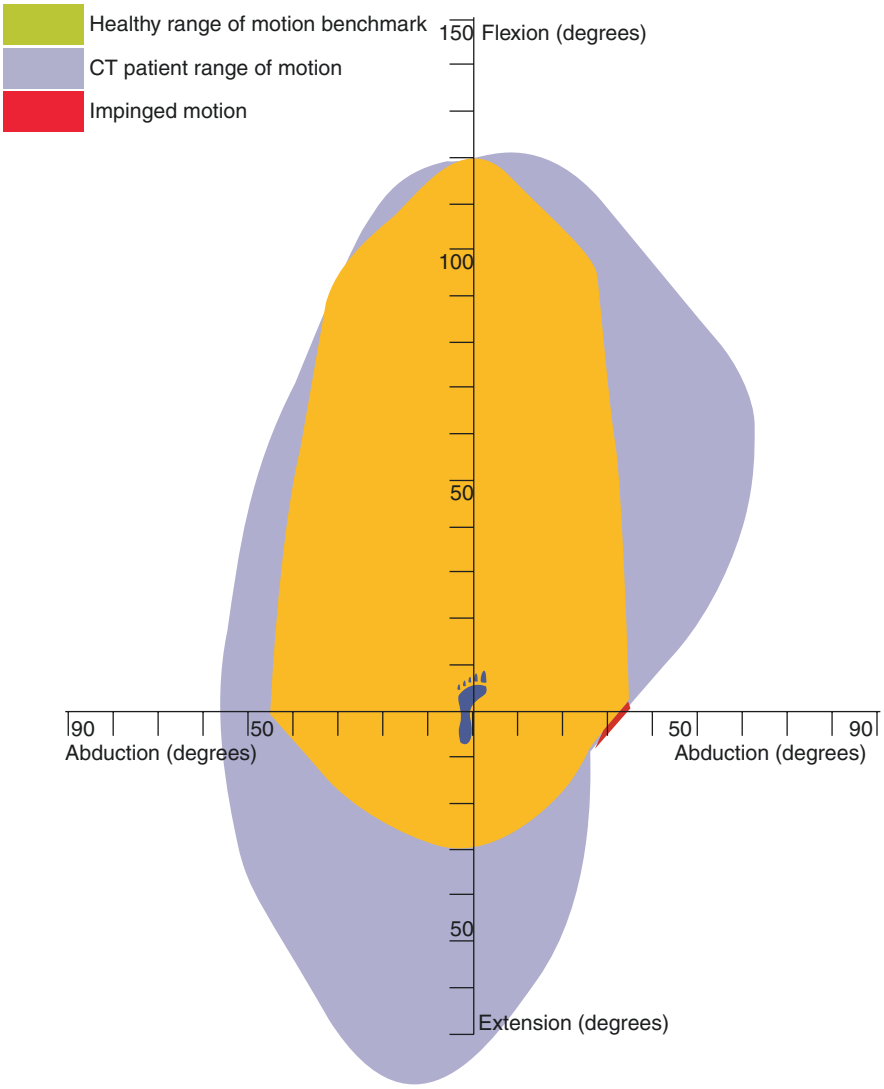

Fig. 11.2 The difference in the hip range of motion is presented between the predicted and realized motions. Flexion/extension and abduction/adduction motion differences between predicted models of motion based on osseous factors versus motion observed from the in vivo measurements. The yellow area corresponds to a range of motion observed in vivo from patients during a series of motions involved in activities of daily living. Purple areas correspond to the predicted range of hip motion based on osseous factors alone. Red areas correspond to in vivo hip motions where osseous impingement limits further motion (Reprinted with permission from Springer Nature)

on the pubis and the greater trochanter on the lateral acetabular rim. This is particularly salient with regard to total hip replacement because an implant or osseous impingement versus soft tissue impingement presumably puts the patient at higher risk of dislocation and earlier wear/failure.

1.1.3 ROM and Gait

The human gait cycle has long been studied using high-speed cameras. Observational studies on gait analysis were conducted, particularly in injured or weakened patients. We will discuss the hip functions in the gait cycle. The human gait comprises two main phases, stance phase corresponding to 60% of gait and swing phase, making up the rest 40%. The simplification of the stride pattern observed in humans serves as a blueprint for analyzing the position of the hip and the points at which static and dynamic factors are involved throughout the gait cycle.

The main role of the hip is to support the weight of the body, transferring this weight force through the pelvis and into the lower extremities throughout the gait cycle. However, the hip must transfer force through a dynamic range, depending on the combination of static and dynamic stabilizers not only to maintain concentric alignment of the joint but also to facilitate the transition in the gait cycle and locomotion. At the beginning of the gait cycle, the hip is flexed, slightly externally rotated, and in neutral adduction centering the femoral head in the acetabulum, which allows for a large degree of the femoral head coverage. After heel strike, the hip extends when the gait progresses towards toe-off. Just before toe-off, the hip begins to flex and abduct to allow for the leg to swing through during the swing phase and clear the ground. This meets with internal rotation through the acceleration phase followed again by external rotation at the end of swing phase to maintain a centered femoral head as the leg passes from the behind the body to the front of the body.

At any given point of the gait cycle, the forces on the hip are the sum of both moment forces produced by hip musculature and loading forces distributed from the head, arms, and thorax. The net sum of these forces is the total amount of force across the joint, also known as joint reactive force. The direction and magnitude of the hip joint reactive force vector change through the gait cycle, ranging from 3.5 to 5 times the subject's total body weight [6]. It is the interplay between concentrically contracting muscles and dynamic and static stabilizers that are dramatically altered in some pathologic conditions of the hip and following the surgical solutions.

1.2 In Vivo Hip Kinematics

Imaging modalities and diagnostic criteria of hip pathology nowadays are frequently based on static findings (i.e., radiographs, lab values). Still, it is important to note that all pathologies of the hip involve dynamic scenarios and that disease development cannot occur without eventual effects on motion. Moreover, past and current innovations for THA have only focused on improving fixation methods and bearing

surfaces, so that the current challenges with the contemporary THA involve in vivo dynamic phenomena such as edge loading, impingement, and dislocation. Thus, a kinematic understanding of the hip is critical for evaluating the etiology of hip pathology as well as improving the restoration of hip function through arthroplasty.

1.2.1 Local Coordinate System

The hip is a synarthrodial spheroidal joint comprising a near-spherical femoral head and a complementary acetabular cup resulting in a soild and stable multiaxial ball-and-socket synovial joint. In the discussion of the kinematics and biomechanics of the hip joint, it is important to establish the planes of motion in which the joint moves. The hip has motion with 6 degrees of freedom, which means it can rotate and translate along three axes perpendicular to each other. The rotational axes are described in terms of abduction/adduction or rotation along the anterior/posterior axis (*x*-axis), internal/external rotation or rotation along the cephalad/caudal axis (*y*-axis), and flexion/extension or rotation along the medial/lateral axis (*z*-axis) (Fig. 11.3) [7].

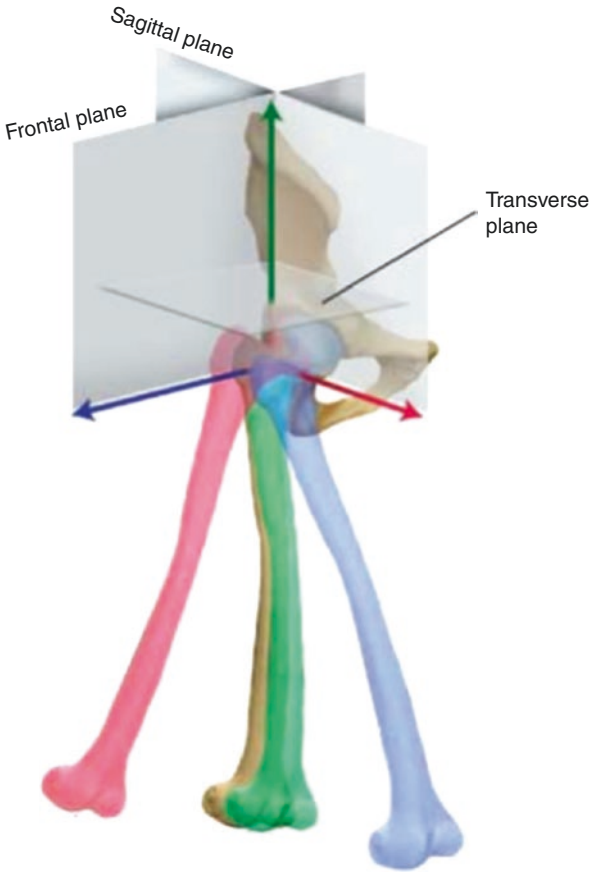

Fig. 11.3 The 3D image demonstrates anatomic planes and the axes of motion about the hip. Rotation about the *x*-axis is shown in red. It corresponds to abduction/adduction, rotation about the *y*-axis is shown in green and corresponds to internal/external rotation, and rotation about the *z*-axis is shown in blue, corresponding to flexion/extension. The red, green, and blue femurs of the right hip show examples of abduction, internal rotation, and flexion, respectively (Reprinted with permission from Wolters Kluwer Health)

Similarly, translational motion is described in terms of translation along each of these axes (i.e., anterior translation, lateral translation). Though the motion of the hip occurs largely as the rotation of the femoral head within the acetabulum, it represents the combination of both rotational motions and balanced translations. Consequently, throughout the hip's arc of motion, the main rotational components with slight translational motions are all coupled through a series of static and dynamic stabilizers.

With regard to the constraints of motion and anatomy of the pelvis, the acetabular cup has both inclination and anteversion, meaning that the cup of the right hip is both negatively rotated about the *x*-axis (abducted) and positively rotated, or anteverted, about the *z*-axis (flexed). The degree of inclination and anteversion has classically been determined with regard to the body's axis and ranging between 35–45° of inclination and 15–25° of anteversion (flexion) during upright stance. However, it is important to note that the orientation of the pelvis changes with various positions and throughout the gait cycle [8]. As a result, depending on the pelvic tilt, the acetabulum may appear to be more or less anteverted or inclined. To address this, the International Society of Biomechanics recommended a standardized pelvic coordinate system [7].

1.2.2 Kinematic Measurement Methods

Over the past decade, the development and implementation of 2D/3D registration techniques have been employed to address the growing need for higher accuracy in human kinematic and implant wear measurements. These techniques evaluate a single fluoroscopic image of the hip using a stored 3D model of the same prosthetic implant to match the orientation of components to the silhouette on fluoroscopy. The position of the components can be reconstructed by doing so. Through evaluating a series of sequential images, the implant motions and relationship between implants and bones can be evaluated. These methods have provided initial advancements to our current understanding of THA motion in vivo, particularly with regard to femoral head/cup separation during gait and abduction activities, intraoperative stability assessment, and position during extremes of motion [9–12]. However, the accuracy of such methods has been significantly inferior to other methods of measurement, namely RSA, thus limiting the use for further kinematic evaluation, particularly during motion [12].

Most recently, methods that employ the combination of orthogonal fluoroscopic images, as well as 2D/3D registration techniques, have been developed, known as dual fluoroscopic imaging system (DFIS) [13]. This technique involves an initial CT image of the patient's hip that is subsequently used to generate a 3D adaptive global surface model of the femur, pelvis, and any implanted components [14, 15]. As a result, a patient-specific model of osseous geometry is generated and allows for more accurate measurements than previous techniques that relied on generalized implant models (Fig. 11.4). Patients are then imaged at a rate of 30 Hz through-

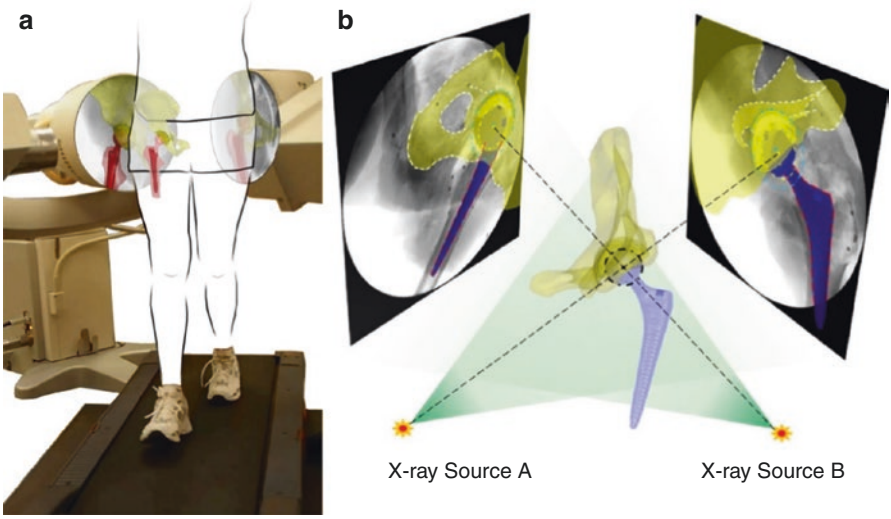

Fig. 11.4 Dual fluoroscopic imaging system imaging registration. (**a**) Experimental setup of measurement of a subject walking on a treadmill using DFIS. (**b**) An example of a total hip arthroplasty registered to images in the computer-simulated dual fluoroscopic imaging system (DFIS). (Redrawn from Tsai, T.-Y., J.-S. Li, et al. A novel dual fluoroscopic imaging method for determination of THA kinematics: in-vitro and in-vivo study. Journal of biomechanics, 2013. 46(7): 1300–1304)

out the activity of interest, for example, gait, with two fluoroscopic images positioned orthogonally to one another (Fig. 11.4a). The fluoroscopes obtain images synchronously, producing a tandem view of the hip from orthogonal positions and reducing the artifacts from parallax and beam scatter otherwise experienced by single beam methods [13]. These images are then processed in conjunction with the 3D CT images, which virtually position the 3D models to match the exact positions of the patient's pelvis, femur, and implants observed in the orthogonal X-ray images (Fig. 11.4b). All images in the series from fluoroscopy are analyzed in the way mentioned above to generate a series of 3D images that depict the exact motion of the patient's pelvis, femur, and implants during gait. This provides solid information about the hip motion in all 6 degrees of freedom as well as allows for predictions of angular momentum, force, and even wear characteristics. DFIS has provided the exciting potential for more accurately measuring small perturbations in components separation and also in vivo motion trajectory without the need for invasive markers as in RSA [16]. The accuracy of DFIS is comparable to RSA and able to measure translational and rotational changes with a measurement error of 0.2 ± 0.3 mm and $0.2 \pm 0.8°$, respectively [17]. However, although DFIS is a non-invasive tool, it does inherently increase radiation exposure beyond prior 2D/3D registration or RSA techniques but remains on the order of 5–6 mSv with current methods [16].

1.3 Hip Kinematics in Common Pathologies

The hip geometry and its kinematics represent the summation of complex interactions between the static and dynamic stabilizers. The most common changes to this function can be attributed to alterations in anatomy originating with the acetabular shape and position (i.e., pincer lesion, DDH) or changes in the femoral head and neck shapes (i.e., cam lesion, Perthes, SCFE, altered femoral version). Frequently these changes are reciprocal, and both femoral and acetabular effects must be evaluated, respectively. Though many of these changes originate in infancy or childhood, the effects of these changes can often go unrecognized or even undiagnosed well into adulthood. Consequently, the adult hip can represent the response to a lifetime's worth of altered hip kinematics that must be recognized and accounted for by the arthroplasty surgeon.

1.3.1 Femoroacetabular Impingement and Labral Injury

The most common anatomic changes affecting native hip kinematics are cam and pincer lesions. Cam lesions represent additional bony contours to the femoral head, typically over the superior lateral base of the femoral head. The resulting loss in overall head sphericity results in a functional decrease in the head-neck offset of the hip [18]. As previously mentioned, this offset is critical for the hip range of motion and results in a contracted arc of abduction. At the extremes of motion (i.e., flexion and abduction), the flattened head-neck junction impinges on the acetabular labrum and eventually osseous rim [19]. Known as femoroacetabular impingement (FAI), the constant cycling of the labrum between the misshapen femoral head and acetabulum results in accelerated wear and deterioration of the labrum. This cyclical damage also results in consequent changes, including cysts, sclerosis, and microfracture, in the underlying bone. Similarly, the pincer lesion represents an overgrowth of the acetabular rim, particularly in the anterosuperior quadrant. The resulting functional overcovering of the femoral head again can lead to a contracted arc of motion due to impingement.

Regardless of the etiology of labral pathology, the loss of labral integrity results in a breakdown of the articular seal and significantly increases the joint reactive forces. Among other actions, the labrum acts as a gasket to seal the hip joint throughout the motion. Upon loading, articular cartilage extrudes synovial fluid at a rate determined by the adhesive and cohesive properties of the fluid and cartilage, the pressure in the system, and the rate of loading [20]. The intact labrum allows the pressure in the articular system to increase through a hydraulic effect providing a transfer and dispersion of the applied force to the entire joint and joint fluid. Consequently, loss of the labral seal results in a leak of the synovial fluid leading to a significant decrease in the fluid pressure and causing increase in cartilage loading rates, creep rates (i.e., extrusion of synovial fluid), and overall joint reactive forces [21, 22]. Biomechanical modelings predict that the loss of labral integrity increases

the contact stresses on the weight-bearing articular cartilage of the hip by up to 90% [21]. Moreover, the loss of the hydraulic effect with labral pathology shifts the peak pressures of the system laterally, resulting in an increase in overall joint reactive force primarily over the lateral acetabular edge [21].

1.3.2 Total Hip Arthroplasty

As we continue to elicit more details about the kinematics of the native hip, how arthroplasty or resurfacing alters the mechanics of the hip remains largely unknown and controversial. Current arthroplasty techniques require not only substitution of the natural hip mechanics for those interjected by artificial implants but also alterations in much other static and even dynamic stabilizers of the hip. Dramatic changes in both dynamic and static stabilizers result from the surgical approach for THA. However, many of the same factors that can affect native hip function also plague the total arthroplasty function. Factors such as femoral neck offset to prevent impingement, over- and under-coverage of the femoral head by the acetabular component to prevent escape and dislocation, and also soft tissue balancing to prevent translation and edge loading are all even more critical factors regarding to total hip arthroplasty.

The hip is critical for some parameters of the gait cycle and is important in determining stride length, leg progression, and single-leg stance stability. Previous investigations utilizing external skin markers to evaluate primarily gait efficiency and cadence demonstrated significantly reduced gait velocities as well as stride lengths following THA. Kyriazis and Rigas [23] demonstrated that among 20 females with severe hip OA, gait velocity and stride lengths were significantly lower than healthy age-matched controls both before and after THA using external markers and force plate analysis. However, they not only found a significant improvement in these metrics in patients post THA compared to pre THA, but there was continued improvement such that at 8–10 years follow-up, gait velocity and stride length approached but did not reach that of healthy controls. In a similar vein, Wykman et al. [24] reported a significant improvement of overall gait velocity, stride length, and duration of single-leg stance of the affected hip following THA compared to preoperation. They made the further distinction that this improvement was most pronounced in patients with bilateral hip involvement though this benefit was most notably observed after the second hip was replaced. Together, these studies suggest that after THA, the affected hip has a significantly increased range of motion leading to the overall increase in the duration of the gait cycle and overall mechanical efficiency. However, after THA, the significant improvement providing more efficient hip mechanics and lower energy expenditures perhaps never quite reaches that of the age-matched native hip [25, 26].

Though these studies provide intriguing information about the gait alterations following THA, they are limited in part by the methods of obtained data; namely surface mounted markers. More recently, Tsai et al. [16] describe THA kinematics with the use of DFIS, directly evaluating implant position throughout the gait cycle.

Initial findings demonstrate similar increases in maximum hip extension as well as increases in overall hip abduction after THA [16]. Meanwhile, Tsai et al. [27] investigated the in vivo 3D kinematics of the hip in unilateral THA patients during gait. Initial results demonstrated that there was 3D motion asymmetry of the hip and pelvis in unilateral THA patients during gait (Fig. 11.5). Regardless, these studies offer exciting new steps towards a better and more accurate depiction of how the arthroplasty hip functions and how small changes in implant positioning or muscle tensioning can affect wear and prosthetic life span.

As previously mentioned, the hip capsule and labral tissues play a critical role in stabilizing the native hip throughout its arc of motion, namely with regard to translation as well as rotation by shear and compressive forces. Replacement causes interruption of the capsular components leading to the need for considerations of capsular repair and postoperative motion restrictions. Perhaps one of the most dramatic procedures is the resection of the hip labrum in order to ensure appropriate sizing and seating of the acetabular component. This excision also helps to prevent the interposition of the labral and associated capsular tissues behind the prosthetic components or during motion of the replaced hip. However, the lack of labral function eliminates the gasket and hydraulic effects on the joint itself, thereby increasing joint reactive forces and even increasing the translation of the components throughout motion. Though dynamic stabilizers help to retain the femoral head particularly during gait, other activities of daily living and hip motions can result in dramatic translation of the femoral head and even put the joint at risk of dislocation. In vivo imaging studies have demonstrated the separation of the femoral head component of THAs by as much as 0.5–1 mm particularly during activities that require extensive internal or external rotation such as pivoting and shoe tying in asymptomatic patients [28]. Further investigations into this phenomenon have suggested that this translation results in increased loading as the head returns from its displaced position in addition to increased soft tissue stretch and risk for dislocation events at the extremes of displacement [10].

The orientation of hip arthroplasty components including the acetabular cup, femoral neck length, femoral neck ankle head sizes, etc., also dramatically affect the kinematics of the hip. With regard to kinematics, the placement and orientation of implants help to determine the range of motion and overall stability of the joint. Soft tissue impingement, restriction, and laxity as well as osseous impingement affect the total range of motion and stability of the native hip. Similarly, these factors also affect the hip motion following THA. Femoral head size is a critical component of hip stability and motion following arthroplasty. Several comparisons of head size and dislocation rate following THA have globally demonstrated that the larger the femoral head, the greater the jump distance and the lower the risk of dislocation [29, 30]. Of course, hip motion requires static and dynamic stabilizers, and while femoral head size is important, the role of soft tissue stabilizers cannot be underestimated. Another critical component to THA motion is the orientation and position of the acetabular components. Experimental modelings demonstrate that cup anteversion and inclination (abduction) relationship, as well as femoral anteversion, play an interrelated balance between the range of motion and stability. D'Lima et al. [31] demonstrated that in general 45–55° of acetabular abduction provides the optimal

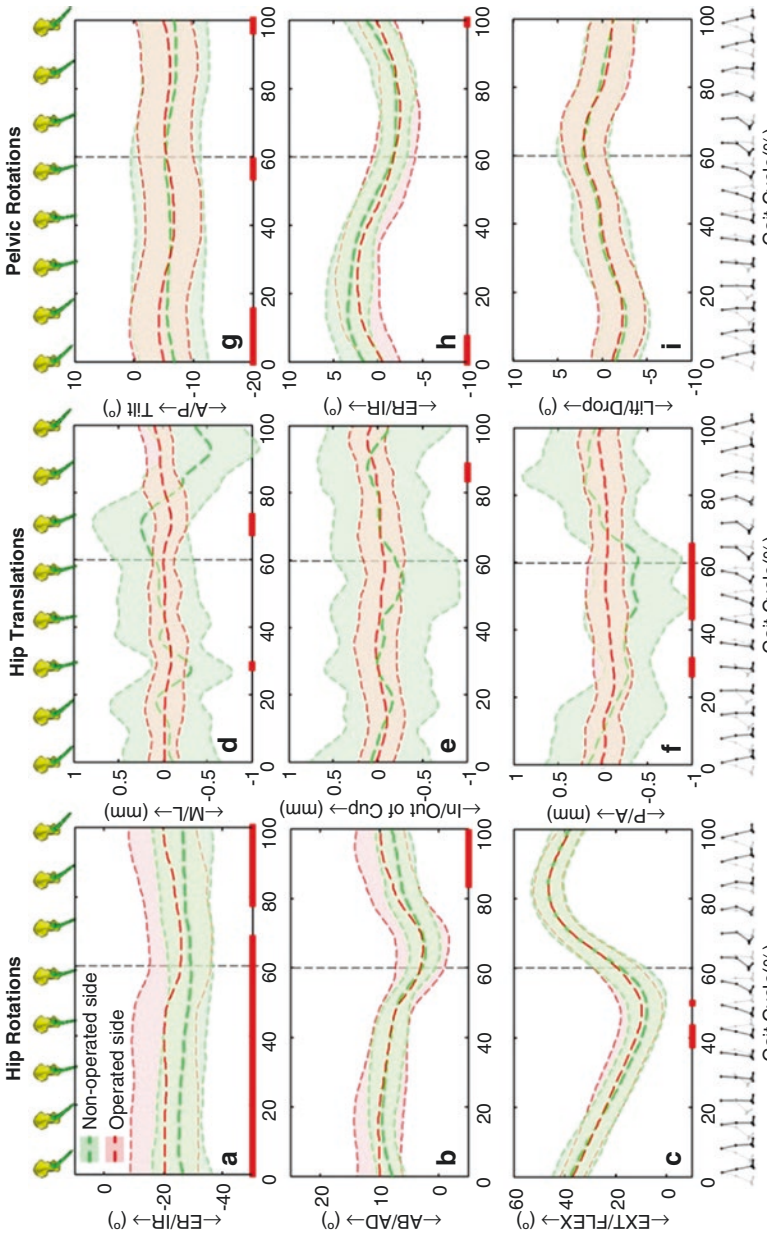

Fig. 11.5 Average and standard deviation of hip kinematics for the operated and nonoperated hips in unilateral THA patients during gait. Significant differences in hip rotations, hip translations, and pelvic A/P tilt were observed. (Redrawn from Tsai, T.-Y., J.-S. Li, et al. Does component alignment affect gait symmetry in unilateral total hip arthroplasty patients? Clinical Biomechanics, 2015. 30(8): 802–807)

situation of the maximal range of motion with maximal stability. Tsai et al. [32] demonstrated that an average 5.1° increase in the internal rotation was observed in the implanted hip than the contralateral non-implanted hip and internal rotation was significantly correlated with a linear combination of the increase of cup anteversion, medial cup translation, and leg-lengthening.

2 Biomechanics of Knee Joint Motion

The knee joint comprises two distinctly separate joints/articulations, the tibiofemoral (TF) joint and the patellofemoral (PF) joint. The main functions of the knee joint are (1) to allow locomotion with (a) minimum energy requirements from the muscles and (b) stability, accommodating for different terrains, and (2) to transmit, absorb, and redistribute forces caused during the activities of daily life [33].

2.1 Fundamentals of Knee Joint Motion

2.1.1 The Tibiofemoral Joint Motion

The tibiofemoral joint motion is movement with 6 degrees of freedom (DOF), three in rotation, and three in translation. The three degrees of freedom in rotation are flexion–extension (F–E) in the sagittal plane (primary), varus–valgus (V–V) (or adduction–abduction) in the frontal plane and internal–external (I–E) rotation in the horizontal plane. The three degrees of freedom in translation are anterior–posterior (A–P) movement, mediolateral (M–L) translation, and compression. The 6 DOF movement could be described in a clinical joint coordinate system (Fig. 11.6) [34]. Full extension (i.e., zero-degree flexion) is usually defined when the long axis of the tibia and femur are aligned in the sagittal plane [33].

Flexion–Extension

The F–E axis has a different definition from many researchers. Morrison assumed that a fixed axis of rotation was coincident with the axis of rotation of the knee joint in the position of full extension [35]. The line through the center of medial and lateral femoral condyles are defined as the F–E axis. Some surgeons used the transepicondylar axis (TEA) as the F–E rotation axis in total knee arthroplasty (TKA). Berger defined surgical TEA as a line connecting the sulcus of the medial epicondyle and the lateral epicondylar prominence [36]. The angle between the surgical TEA and the posterior condylar line is defined as the posterior condylar angle. Another TEA definition is called clinical TEA. It is defined as a line connecting the medial and lateral epicondylar prominence by Yoshioka [37].

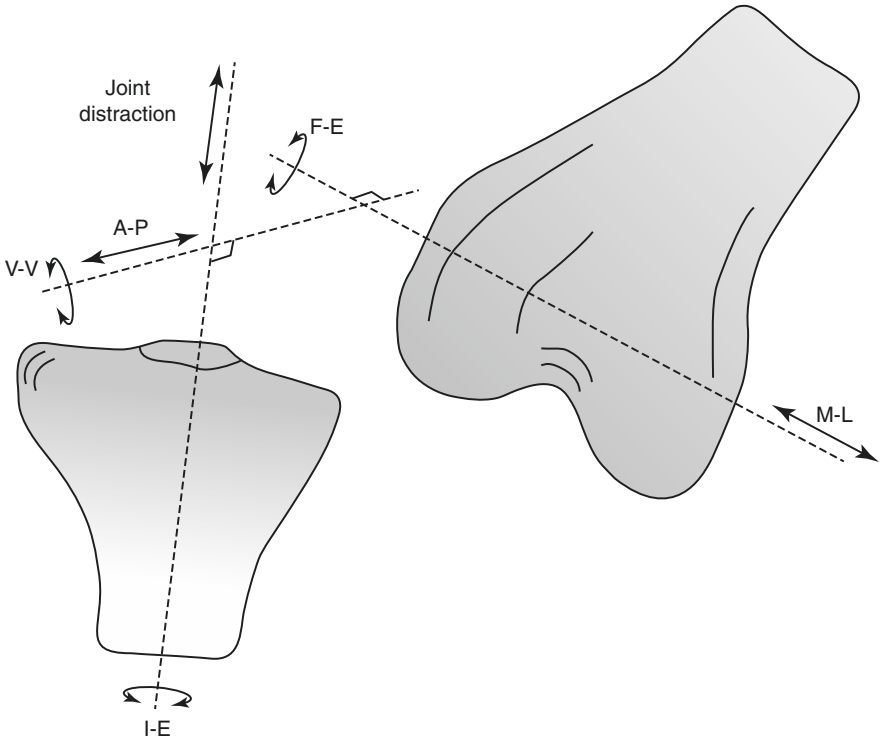

Fig. 11.6 The six DOF of TF joint motion expressed in a clinical joint coordinate system. M–L translation and F–E occur along and about an epicondylar femoral axis. Joint distraction and (I–E) rotation occur along and about a tibial long axis. A–P translation and V–V rotation occur along and about a floating axis, which is perpendicular to both femoral epicondylar and tibial long axes (Reprinted with permission from Elsevier: Masouros, S., A. Bull, and A. Amis, (i) Biomechanics of the knee joint. Orthopaedics Trauma, 2010. 24(2):84–91)

Internal–External Rotation

Many studies have shown that the I–E rotation axis is located near the center of the medial tibial plateau. Wang et al. used human knee joint specimens to study the effect of flexion and rotation on the length patterns of the ligaments of the knee. Their results showed that the I–E rotation axis was located slightly posterior to the center of the medial plateau for mid-flexion angles (30°, 60°, 90°), but at 0 and 120° flexion, this axis passed through the mid-point of the medial spine of tibial eminence [38]. These results were in line with Shaw and Murray's research experimentally showing that the I-E rotation axis passes through the medial spine of the intercondylar eminence [39].

Varus–Valgus

Varus–valgus occurs at about the center of the femoral condyles. Crowninshield et al. found that abduction occurs at about the lateral condyle while adduction occurs at about the medial condyle [40]. Based on their results, Pennock and Clark chose the V–V axis which intersects the transepicondylar line at the mid-point between the epicondyles and so that it bisects the angle between the projection of the femoral condyles on the transverse plane [41].

2.1.2 The Patellofemoral Joint Motion

Patella is the largest sesamoid bone in the human body. It is embedded in quadriceps tendon and its function is to increase the mechanical leverage of the quadriceps. At full knee extension, the patella contacts femur at the distal end of the patella (Fig. 11.7a). As the flexion angle increases, the patella engages into the femoral trochlear groove and the contact area spreads across the width of the patella and moves proximally (Fig. 11.7b) [34]. The increase of PF contact area with knee flexion is a clever mechanism that controls the magnitude of stresses by spreading the increasing PF joint load with knee flexion over a larger area.

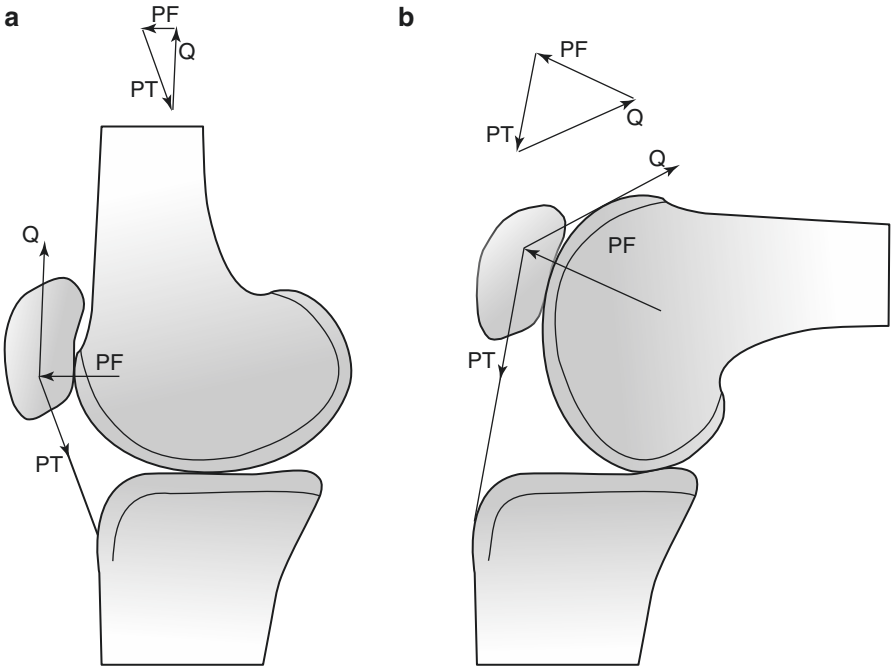

Fig. 11.7 PF joint force at (**a**) extension and (**b**) 90° flexion, showing geometrically the increase of PF joint force with flexion. (*PT* patellar tendon, *Q* quadriceps muscles, *PF* patellofemoral, *TF* tibiofemoral) (Reprinted with permission from Elsevier: Masouros, S., A. Bull, and A. Amis, (i) Biomechanics of the knee joint. Orthopaedics Trauma, 2010. 24(2): 84–91)

2.1.3 Soft Tissue Balance

The soft tissues in the knee joint provide dynamic stability. The muscles stabilize the joint according to the movement and provide stability of the joint. Ligaments and meniscus provide passive stability. The ligament elongates as a response to external force, and thus maintain the joint stability.

Two cruciate ligaments, anterior cruciate ligament (ACL) and posterior cruciate ligament (PCL) are arranged in a crossed formation in the knee joint. The primary function of ACL is to prevent excessive tibial anterior translation. The primal function of PCL is to restrain posterior tibial translation. Two cruciate ligaments act together to control the A-P rolling and sliding of TF joint during F–E [42].

In the M–L direction, the two collateral ligaments stabilize the knee joint by restraining the V–V and I–E rotation [34]. The medial collateral ligament (MCL) is the primary restraint to valgus and internal tibial rotation [43]. The lateral collateral ligament (LCL) is the primary restraint to varus angulation but slackens with knee joint flexion, which reduces its restraining capability [44].

The main ligament in PFJ is medial patellofemoral ligament (MPFL). It acts as the primary passive restraint to lateral patellar displacements and assists in controlling patellar motion, especially guiding the patella into the trochlear groove in early knee flexion.

2.2 In Vivo Healthy Knee Kinematics

Gait analysis is based on an optical motion tracking system and is widely used in investigating in vivo joint kinematics and kinetics. Gait cycle could be divided into two phases, stance phase and swing phase. The stance phase is defined as the period between heel strike and toe off. Swing phase is defined as the period between toe off and next heel strike. In gait analysis, healthy knee joint motion features a large sagittal plane range of motion (ROM), small rotation in the horizontal plane and frontal plane. The knee joint kinematics of healthy adults is shown in Fig. 11.8 [45].

For F–E angles, there are two peaks in one gait cycle. The first peak is smaller and in the mid-stance phase, which has a value of 20° flexion. The second peak is larger and in the early stage of the stance phase, which has a value of 60° flexion.

In the frontal plane, knee joint movements involve both abduction and adduction. During the stance phase, the knee joint undergoes abduction. After the start of the swing phase, the knee joint transform to adduction. At the end of the swing phase, the knee joint turns back to the abduction. Overall, the abduction/adduction angle is small during the gait cycle.

In the horizontal plane, at the beginning of the stance phase, tibia has a slight external rotation according to the femur. After heel strike, both femur and tibia undergo internal rotation. The tibia has a faster speed of internal rotation. As a result, the knee joint has an internal rotation in the stance phase. After the middle-stance phase, both femur and tibia undergo external rotation and keep external rotating until the middle-swing phase.

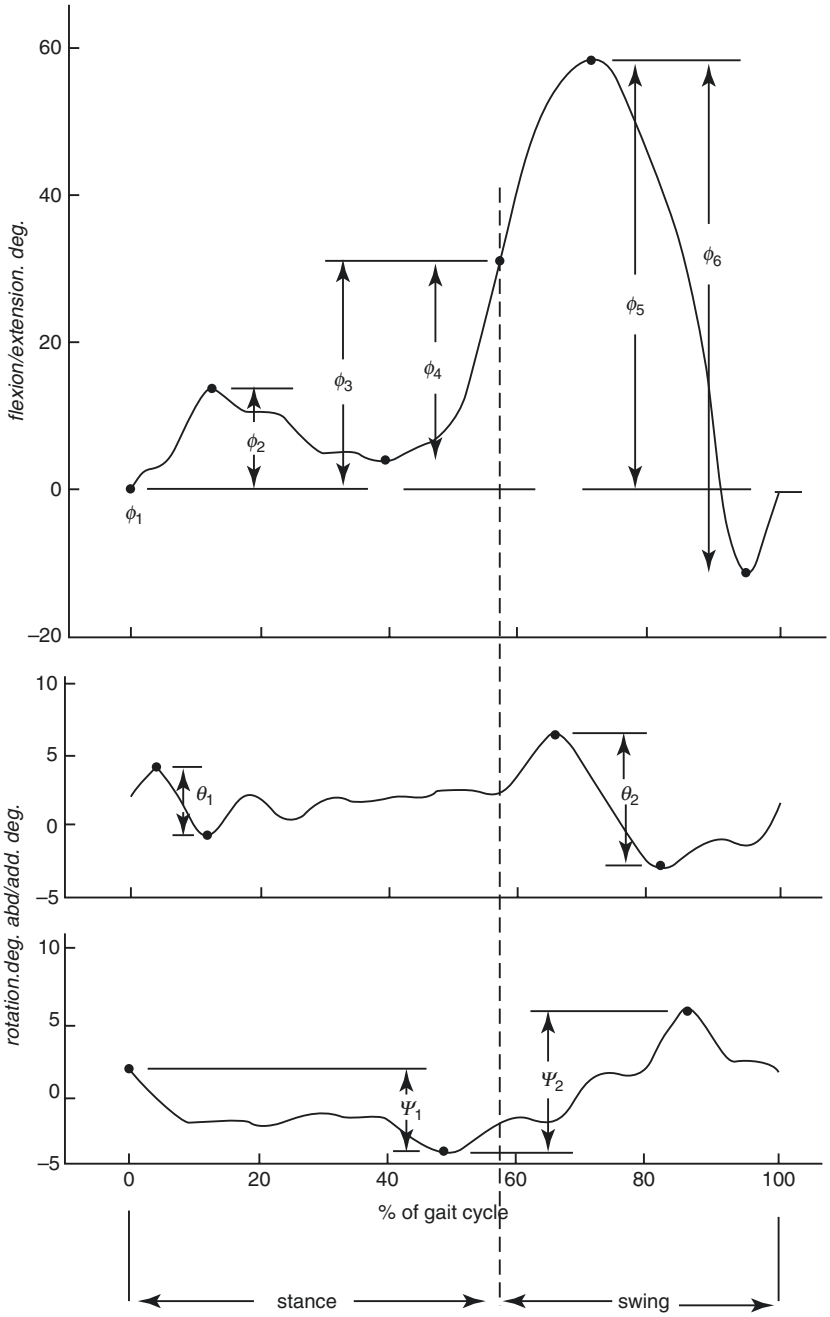

Fig. 11.8 Chao et al. evaluated 148 subjects' lower limb gait. All the subjects were allowed to walk at their preferred speed and wore shoes [45] (Reprinted with permission from Elsevier: Chao, E., R. Laughman, et al. Normative data of knee joint motion and ground reaction forces in adult level walking. 1983. 16(3): 219–233)

2.3 Knee Kinematics in Common Pathologies

2.3.1 Osteoarthritis and Total Knee Arthroplasty

Knee Osteoarthritis

Osteoarthritis (OA) is one of the most common sources of locomotor disability and musculoskeletal pain worldwide, and the prevalence is as high as over 40% in older adults [46]. Factors that may increase the risk of osteoarthritis include older age, sex, obesity, joint injuries, and deformities. Accepted by most surgeons, knee OA patients are classified into two categories: (1) idiopathic: those with no presently known prior event or disease related to the OA; and (2) secondary: those with known events or disease associated with OA. The knee OA patients can be further divided into five stages: (1) stage 0: no radiographical signs or pain; (2) stage 1: minor bone spur growth in X-rays of knee joints; (3) stage 2: greater bone spur growth and healthy size of cartilage; (4) stage 3: damaged cartilage and minor narrow space between bones; and (5) stage 4: the cartilage is completely gone and the joint space between bones is dramatically reduced. Osteoarthritis symptoms often develop slowly and worsen over time. Knee OA patients always have signs of tenderness, loss of flexibility, grating sensation, stiffness, and pain. The biomechanical behavior of knee OA joints is correspondingly changed compared to normal knees, especially in end-stage knee OA patients. Kinematics and kinetics parameters are crucial for the evaluation of osteoarthritis severity and treatment outcomes.

Kinematics Characteristic of KNEE OA Patients

Kinematics analysis mainly studies the variation of spatiotemporal parameters of knee joints. The range of motion, walking speed, stride length, and the gait cycle period of knee OA patients all show abnormal changes compared to that of normal knees. Moreover, one explanation of that is individuals with severe knee osteoarthritis and great pain are hypothesized to adopt neuromuscular strategies to increase knee joint stiffness, decrease joint movement, and alter movement patterns to shift or reduce tissue loads and thus limit pain [47]. Previous studies reported that end-stage knee OA patients walked at a lower speed than healthy subjects and the knee flexion angle reduced before heel strike. Reduced range of motion, slower stride cadence, and shorter stance phase were reported in the knee OA patients [48–51], which is called an antalgic type of gait. Taking analgesic may relief severe joint pain and increase the stride velocity, but the anomalous gait will aggravate osteoarthritis [50]. Knee OA patients at different stages showed different gait characteristics and kinematics parameters, which should be taken into consideration when rehabilitation and treatment programs were designed accordingly.

Knee kinematics of different stage of knee OA patients have been investigated in the past decades. All the patients showed a reduction of flexion at the early stage of stance phase, and extension insufficiency develops with the pro-

gression of osteoarthritis. The decreases of hip internal rotation and ankle dorsiflexion angle from late stance to early swing were also found in the progression of knee OA [52].

Kinetics Characteristic of KNEE OA Patients

The change of joint loading has a crucial effect on articular cartilage. Native joint stress should be homogeneously distributed under proper lubrication. The increase of joint loading and repeated impact of joint are considered to induce joint wear and decide the severity of knee OA. Uneven stress distribution may cause the damage and loss of articular cartilage and the secondary degeneration of knee osteoarthritis. External knee adduction moment, especially the mid-stance knee adduction moment, is a key parameter, which is closely associated with joint loading. Two knee adduction moment peaks showed in the early and late stance phase. The first knee adduction moment peak is of great clinical significance because it is correlated with cartilage thickness and joint loading [53]. In the past decade, the mid-stance knee adduction moment attracted more and more attention, which is not dependent on the stride velocity and is taken as an ideal indication for knee OA diagnosis. Expect for the operative management; gait retraining is an effective treatment for correct knee adduction moment. So far, several gait patterns were reported to reduce the adduction moment, such as toe-out gait, slow velocity, stride length reduction, side swing, and so on [54–56].

Total Knee Arthroplasty

Through the progression of knee OA, conservative treatment would have few effects on the patients with tremendous pain, deformities, and disabilities. Total knee arthroplasty (TKA) is the most effective surgical interventions for pain relief and functional recovery in patients with advanced degenerative arthritis or rheumatoid arthritis [57]. Aging of the society has led to increase in the prevalence of arthritis and the incidence of TKA for end-stage arthritis. With the development of TKA techniques and design, the demand for TKA increased in the past 20 years, and over 1300,000 patients took TKA procedures annually [58]. TKA has three components: femoral components, tibial components, and patellar components. Following different criteria, TKA prosthesis can be classified as (1) cruciate retaining, and posterior stabilized prosthesis; (2) mobile-bearing and fixed bearing prosthesis; (3) cemented and uncemented prosthesis. The knee prosthesis can be further divided into medial pivot, single radius, and multi-radius based on geometric design.

Although total knee arthroplasty has been developed for many years, complication rates are still high after primary TKA procedure [59]. John Insall proposed that total knee arthroplasty should meet the following requirements: (1) correct alignment axes; (2) equivalent joint gap during flexion and extension; (3) balanced collateral ligament tension; (4) –3° to 130° of knee flexion; (5) 3 mm changes of joint line; and (6) balanced patellar trajectories. These biomechanical factors should be taken into consideration to avoid secondary complication like polyethylene wear,

periprosthetic fractures, loss of flexion, joint instability, and infection. Different choices of prosthesis play an important role in postoperative kinematics behavior. In this section, two major types of TKA prosthesis, cruciate retaining (CR) and posterior stabilized (PS) prosthesis, will be discussed in the following literature. With or without the posterior cruciate ligament (PCL) retaining, different in-vivo kinematics and kinetics characteristics were investigated by researchers.

Cruciate Retaining Prosthesis

With the retaining of the PCL, CR prosthesis is considered to restore normal knee biomechanical function compared to PS prosthesis. PCL retention in total knee replacement has the advantages of enhanced inherent stability, a greater range of motion, improved proprioception, and increased rollback associated with the native PCL retention and joint line. Tsai et al. investigated the articular cartilage contact kinematics of the knee before and after a cruciate retaining arthroplasty. In their study, the distances between medial and lateral contact locations in TKA knees were significantly larger than those of the OA knees (Fig. 11.9) [60]. Further, the

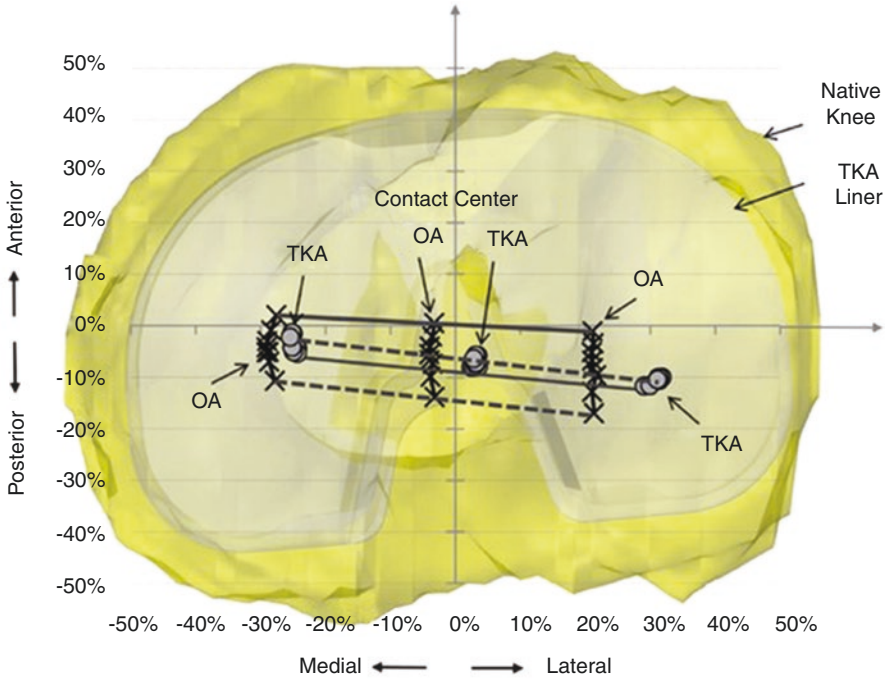

Fig. 11.9 Average medial and lateral articular contact locations and the center points between medial and lateral contacts of the knees before and after TKA operations were depicted. The solid and dotted lines represent the distances between medial and lateral contact locations at full extension and maximal flexion, respectively (Reprinted with permission from John Wiley and Sons: Li, C., A. Hosseini, T.Y. Tsai, et al. Articular contact kinematics of the knee before and after a cruciate retaining total knee arthroplasty. J Orthop Res, 2015. 33(3):349–358)

contact points on the medial and lateral compartments were more laterally located than those of the OA knees. The centers of medial and lateral contact locations have shifted from the medial side of the tibial plateau of the OA knees to the lateral side of the TKA knees. The bearing surface design of polyethylene liner has been recognized as a major factor that could affect the postoperative kinematics and contact patterns of the knee. Failure of polyethylene liner has been reported to account for approximately 50% of CR-TKA revision procedures. The small contact locations in the TKA knees found in postoperative patients imply that the contact forces induced by repeated sliding and rolling during knee motion were localized in these small medial and lateral contact areas, which may induce unfavorable surface fatigue wear.

In the normal knees, the medial and lateral femoral condyles roll backward to assist further knee flexion as the degree of flexion increases. However, CR prosthesis was reported to show evidence of the paradoxical anterior femoral movement during mid-flexion [61]. Improved CR prosthesis with femoral component oversizing and reducing femoral radius can control the paradoxical anterior femoral movement efficiently [62]. The survivorship of improved CR prosthesis was up to 94% after 10 years follow-ups [63].

Posterior Stabilized Prosthesis

For the patients with injured/contracted/degenerated PCL, over 20° of flexion contracture. Without the cruciate ligament retaining, the PS total knee arthroplasty is more applicable in advanced stage patients. Due to the reduction in the difficulty of surgery, the PS prosthesis is widely used in the clinical field. The PCL substituted with a post-cam device, which constrains the posterior femoral offset at 70° of knee flexion and helps the knee joint to roll back during flexion. The PS prosthesis is easier to realize gap balance and allow minor changes of joint line, for which the prosthesis wear can be reduced. Tsai et al. compared the in vivo kinematics of the knee after a posterior cruciate-substituting total knee arthroplasty between Caucasian and South Korean patients. Paradoxical anterior translation of contact points was observed from 45° to 90° of flexion in the Caucasian patients, whereas contact points of the South Korean patients moved posteriorly from full extension to 60° of flexion and then remained relatively constant until 90° of flexion. South Korean TKA patients had more anterior contact points on the medial compartment, more lateral contact points on the lateral compartment, and bicondylar femoral posterior translation rather than medial pivot pattern compared to the Caucasian TKA patients. Different tibiofemoral articular contact kinematics should be considered for the design of bearing articular surface in Asian patients (Fig. 11.10).

2.3.2 Ligament Deficiency and Reconstruction

Four important ligaments stabilize the knee joint, including the anterior cruciate ligament (ACL), posterior cruciate ligament (PCL), medial collateral ligament (MCL), and lateral collateral ligament (LCL). Each separate ligament prevents

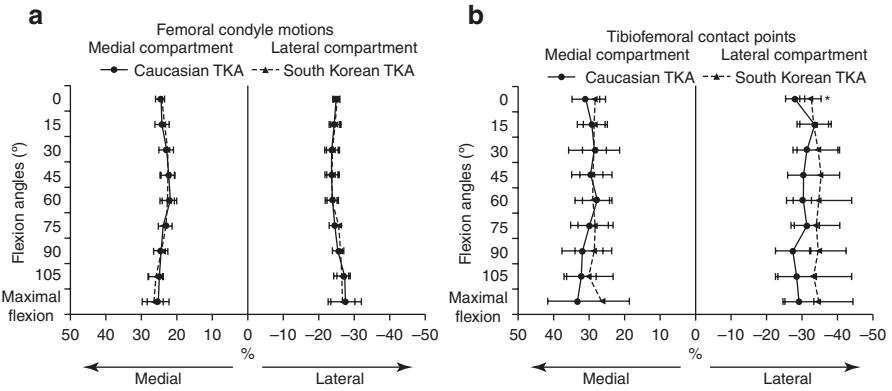

Fig. 11.10 Contact kinematics of Caucasian and South Korean total knee arthroplasty (TKA) knees in a mediolateral translation. (**a**) Normalized femoral condylar motions. (**b**) Normalized tibiofemoral contact kinematics. Positive values mean medial translation. $*p < 0.05$ (Reprinted with permission from The Knee Surgery and Related Research: Bae, J. H., et al. In vivo Kinematics of the Knee after a Posterior Cruciate-Substituting Total Knee Arthroplasty: A Comparison between Caucasian and South Korean Patients. Knee surgery & related research, 2016. 28(2): 110–117)

excessive motion of the knee. When some of the ligament was damaged, the knee would become unstable in the direction that the injured ligament stabilized. Different types of physical tests in clinical practice (anterior drawer test, posterior drawer test, etc.) are based on the abnormal behavior of knee after ligament injuries. The most common injured ligaments in the clinical field are ACL and PCL. This section will focus on the kinematics and kinetics characteristics after ACL/PCL injury and reconstruction.

ACL Deficiency and Reconstruction

ACL is one of the major knee stabilizers, which constrains not only the anterior tibial translation but also the internal-external rotation stability. Zhao et al. investigated the kinematics of ACL-deficient patients and healthy subject in the Chinese population. In their study, individuals with ACL deficiency exhibit greater knee internal rotation during higher demand activities, such as ascending and descending steps or jogging. Compared to Caucasian population, Asian patients showed smaller tibial varus [64]. An anomalous tibial rotation will change the loading distribution on the meniscus and cause secondary meniscal damage. Zhang et al. reported that ACL deficiency with meniscal injury would alter the kinematics when compared to isolated ACL injury [65].

Previous studies showed that after ACL tear more than 50% of individuals showed radiographic evidence of osteoarthritis 10–12 years post-injury [66, 67]. An ACL reconstruction is one of the standard treatments for ACL injury. Operative treatment showed superior outcomes for knee symptoms and function, and in knee-specific and health-related quality of life, compared to patients who chose nonsurgi-

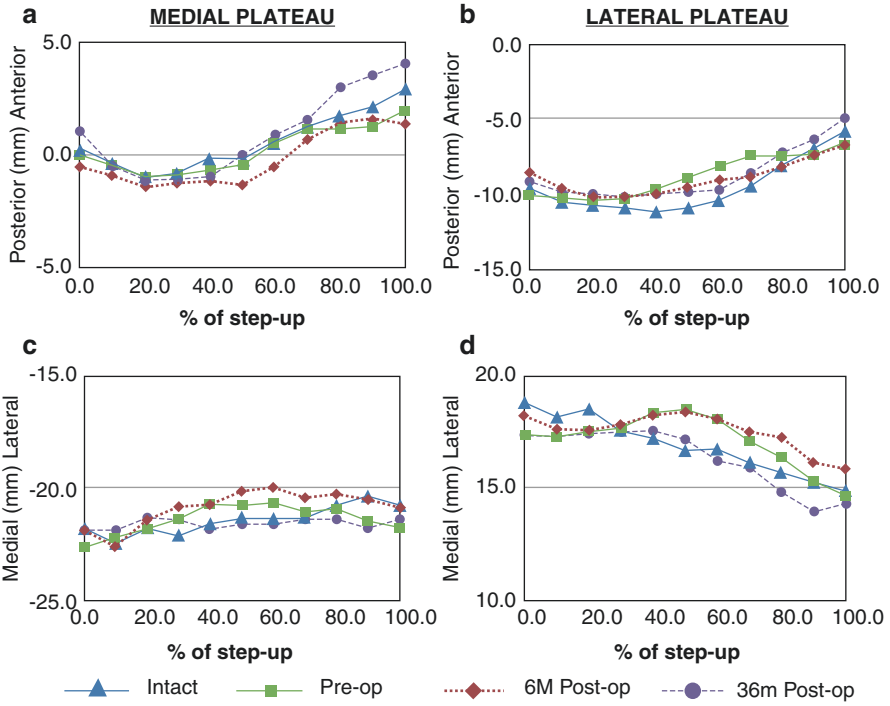

Fig. 11.11 Cartilage contact locations after ACL reconstruction during the step-up motion. Anterior-posterior translation of cartilage contact locations on the (**a**) medial and (**b**) lateral tibial plateau; Medial-lateral translation of the cartilage contact locations on (**c**) medial and (**d**) lateral tibial plateau (Reprinted with permission from Elsevier: Lin, L., J.-S. Li, W.A. Kernkamp, A. Hosseini, C. Kim, P. Yin, L. Wang, T.-Y. Tsai, et al. Postoperative time-dependent tibiofemoral articular cartilage contact kinematics during step-up after ACL reconstruction. Journal of biomechanics, 2016. 49(14): 3509–3515)

cal treatment [68]. Tsai et al. measured the articular cartilage contact kinematics after ACL reconstruction (Fig. 11.11) [69]. This study showed that the tibiofemoral cartilage contact locations of the knee changes with time after ACL reconstruction. Li also measured the tibiofemoral cartilage contact biomechanics in patients after ACL reconstruction. These research revealed that the abnormal posterior and lateral shift of cartilage contact location to smaller regions of thinner cartilage seen in ACL-deficient knees persisted in the ACL-reconstructed knees around 0° and 15°, resulting in a persistent increase of cartilage contact deformation at those flexion angles [70]. Kernkamp WA et al. predicted the isometry and strain for ACL reconstruction, and an area of least anisometry was found in the proximal-distal direction just posterior to the intercondylar notch (Fig. 11.12). Moving the femoral socket positions in the anterior-posterior direction affected the theoretical ACL strains significantly. Posterior femoral attachments resulted in decreased lengths with increasing flexion angles, whereas anterior-distal grafts increased in length with increasing flexion angles.

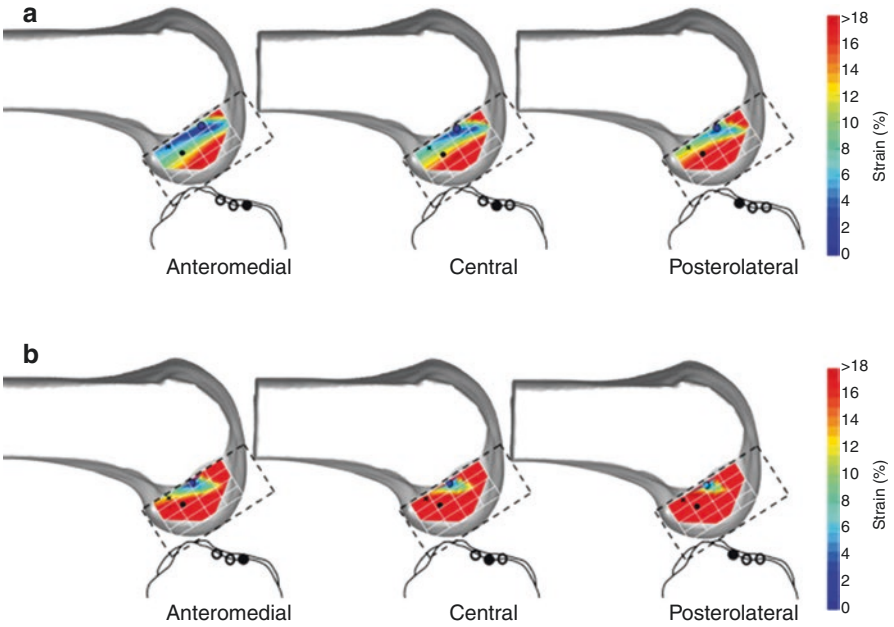

Fig. 11.12 Medial view of a 3D femur model in 90° of flexion. The "heat map" illustrates the isometry distribution (mean maximum strain-minimum strain) over the medial aspect of the lateral femoral condyle for single point-to-point curves when connected to the anteromedial, central, or posterolateral tibial attachment during the dynamic step-up (**a**) and sit-to-stand motion (**b**). The darkest blue area on the femur represents the most isometric attachment area, whereas the red areas highlight those with a high degree of anisometry. Specifically, the circle represents the most isometric attachment. The black cross (×) on the femur shows the "over the top" position as would be achieved by transtibial drilling; the black dot shows the center of the ACL footprint as described by Parkar et al. (Reprinted with permission from Elsevier: Kernkamp, W.A., A.J.T. Jens, N.H. Varady, E.R.A. van Arkel, et al. Anatomic is better than isometric posterior cruciate ligament tunnel placement based upon in vivo simulation. Knee Surg Sports Traumatol Arthrosc, 2018)

PCL Deficient and Reconstruction

PCL injuries occupy up to 44% of all acute knee injuries, but the prevalence of isolated PCL injuries (PCL injuries in which no other ligamentous injuries require repair and reconstruction) was reported as little as 3.5% [71, 72]. In vivo and in vitro drawer tests reported that PCL is the primary restraint to the posterior translation of the knee [73, 74]. Li performed an in vivo kinematics study on PCL-deficient knees compared with contralateral knees, data of which demonstrated that PCL injuries caused an increase of about 5 mm posterior tibial translation through all the flexion angle and an increase of about 1 mm lateral tibial translation at 90° of knee flexion [75]. Anatomic studies showed that PCL orientated anteromedially on femur through the whole range of knee flexion. This structure implies that PCL injury is not only a loss of posterior stabilizer but also

a medial-lateral stabilizer. The abnormal contact pattern along with the ACL-deficient kinematics characteristics will yield secondary joint degeneration when treated nonoperatively.

Isolated PCL injuries have been treated nonoperatively and often have good functional results, but the 5-year incidence of osteoarthritis in nonsurgically treated PCL-deficient knees has been reported to be up to 80% and 50% on the medial femoral condyle and patella, respectively [76–78]. Tunnel selection is a crucial parameter for PCL reconstruction to restore native PCL function. Kernkamp et al. simulated the PCL elongation with in vivo kinematics and found that too proximal (i.e., nonanatomical) femoral attachments are unable to replicate anatomical graft length changes [79]. However, recent studies reported that isolated PCL reconstruction could not restore either anteroposterior or rotational stability compared to the healthy knee. A supplemental surgical technique is required to overcome residual external rotation instabilities, varus laxity [80].

3 Biomechanics of Spine Motion

3.1 Fundamentals of Spine Joint Motion

The spine is made up of the vertebrae and the intervertebral discs, facet joints, and ligaments, forming the central axis of the human body, and transmitting the load as well as protecting the spinal cord. The spine provides motion functions for trunk such as three-dimensional physiological activities.

3.1.1 Vertebral Body

The vertebral body is mainly composed of cancellous bone, and the surface is a thin layer of cortical bone [81, 82]. It presents as a short cylinder with a slightly thin central portion and a large expansion at both ends. The upper and lower sides are rough and can be divided into two areas: the central part is concave and porous, filled by the cartilage onto the edge; the edge part bulges and is cortical bone, firmly attached to the intervertebral disc. The vertebral body is a complicated structure composed of cartilage endplates, cancellous bones, and cortical bones. The function of these different ingredients contributes to their unique biomechanical properties. Vertebrae rely on their natural structure to resist various stresses. Mainly, the vertebrae are almost composed of cancellous bone (net structure) entirely, but a hard shell covers the outer part. Since the axial stress of the vertebra presents the largest, the trabecular bone along the vertical direction exhibits the hardest. The trabecular bones are arranged along the direction of the normal stress (axial force) to exert their biological function as much as possible. The horizontal trabecular bone acts as a lateral bracket to prevent vertical deformation of the trabecular bone.

The vertebral body primarily sustains compressive forces. As the weight of the vertebral body increases from top to bottom, the vertebral body also becomes larger from top to bottom. For example, the shape of the lumbar vertebral body is thicker and broader than that of the thoracic and the cervical vertebrae and is sustained by a larger load. The mechanical properties of the vertebral body are related to the anatomical features and bone masses.

3.1.2 Intervertebral Disc

The intervertebral disc is located between adjacent vertebral bodies, and the adjacent vertebral bodies are firmly connected aiming to maintain the arrangement of the vertebral canals [81, 83]. The thickness of the intervertebral disc is about one-fourth of the total length of the spine above the sacrum. Intervertebral disc is a kind of solid viscoelastic material, which has the characteristics of creep, relaxation, and hysteresis, and can absorb the energy of vibration. Under a slight load, the deformation disappears after unloading. If the load is too excessive, the irreversible deformation will occur. The intervertebral disc consists of three parts: nucleus pulposus, fibrous annulus, and cartilage endplate. The nucleus pulposus is a liquid mass located in the center of the intervertebral disc. The lower lumbar vertebra is more backward. It contains a large amount of hydrophilic glucosamine and present as gelatinous tissue. Its water content varies greatly with age and load. When young, the water content is up to 90%, but with the aging of people, the water content decreases gradually. Under compression load, water in nucleus pulposus seeps through the endplate, and the volume of nucleus pulposus decreases. When the load decreases, water returns and the volume of nucleus pulposus recovers. A fibrous annulus is composed of fibrocartilage tissue. There are many intersecting collagen bundles in fibrocartilage. The unique alignment of annular fibers helps the intervertebral disc maintain a certain degree of torsion resistance. The posterior part of the fibrous ring is woven by the posterior longitudinal ligament (PLL). The cartilage endplate between the vertebral body and the intervertebral disc is composed of hyaline cartilage.

It is an essential biomechanical function of an intervertebral disc that it can bear and distribute the loads and restrict excessive activity. Compression load acts on nucleus pulposus and annulus fibrosus through the end plate. Hydraulic pressure generated inside the nucleus pulposus causes annulus fibrosus to expand outward. The outer annulus fibrosus bears the maximum tensile stress. The inner annulus fibrosus bears less tensile stress than the outer one, but it bears a part of compressive stress.

3.1.3 Pedicle and Facet Joint

The type of the spinal segment motion depends on the direction of the articular surface of the intervertebral joint, and the direction of the articular surface varies among the whole spinal vertebrae [81, 83]. The joint plane of the lower cervical

spine is parallel to the coronal plane and 45° to the horizontal plane. It allows the cervical spine to flex forward, extend backward, bend laterally, rotate, and extend to a certain extent. The articular surface of the lumbar spine is perpendicular to the horizontal plane and 45° to the coronal plane, allowing flexion, extension, and lateral bending, but limiting rotation.

In addition to guiding segmental motion, the facet joints also bear different kinds of loads, such as compressive force, tensile force, shear force, and torsion force. The amount of loads they bear vary with the different movements of the spine. The load on the facets of the joints is the greatest at extension, accounting for 30% of the total load (another 70% of the load from the intervertebral disc). The load on the facet joint is also higher when flexion and rotation occur. The tensile loading of facet joints mainly occurs as the lumbar forward bending. When the lumbar forward bending reaches the maximum limitation, 39% of the tension load is borne by facet joints.

3.1.4 Ligament

The main components of the ligament are collagen fibers and elastic fibers [81]. The collagen fibers give the ligaments a certain strength and rigidity, and the elastic fibers give the ligaments the ability to extend under the loading. Most of the fibers of the ligament are nearly parallel [83, 84], so their functions are more specific and often only bear the loading along a single direction. The function of the spinal ligaments is to provide a proper physiological activity for adjacent spines, as well as maintain the stability of the spine. The specimen of the spine in vitro still maintains a certain intervertebral disc pressure under the traction load. The prestress is derived from the tension of the ligament and is most prominent in the ligament flavum. All ligaments possess the ability to resist tension, but they are fatigued quickly under compressive forces. The ligament strength is closely related to the cross-sectional area of the ligament.

The ligaments of the spine bear most of the distraction loads of the spine. They act like rubber bands. When the load direction is consistent with the fiber direction, the ligaments have the strongest bearing capacity. When the spinal motion segments are applied by different forces and moments, the corresponding ligaments are stretched and stabilized for the motion segments.

It is generally believed that the anterior longitudinal ligament (ALL) is the toughest, and together with the PLL, can prevent the spine from excessive flexion and extension, but the effect of limiting axial rotation and lateral flexion is not obvious. The facet joint capsule ligament plays a key role in resisting torsion and lateral flexion. The main function of the interspinous ligament is to stabilize the spine by limiting the ability to flex.

3.1.5 Muscle

The dynamic stability of the spine is correlated with the function of the complete paraspinal muscle during activities. The muscles associated with the spinal activity can be divided into the front and back groups according to their locations [85]. The

muscles located behind the lumbar vertebrae can be further categorized into three groups: the deep layer, the middle layer, and the superficial layer [81, 83, 84]. The deep muscles include the interspinous muscles that end at the adjacent spinous processes, the intertransverse muscles that start at the adjacent transverse processes, and the rotator muscles that start and end at the transverse processes and spinous processes. The middle layer muscles mainly refer to the multifidus muscles of the transverse process and the spinous process of the upper vertebral body. The superficial muscles can be divided into three groups: iliocostalis, longissimus, and spinalis.

3.2 In Vivo Spine Kinematics

In vitro biomechanical studies can describe the displacement patterns of spinal motion under different loads. However, it is not possible to establish normal spinal motion because the load generated in the body muscle cannot be simulated in vitro studies. Therefore, some methods have been developed to quantitatively study the movement of the spine in the body.

In the past, flexion/extension dynamic X-ray films have been widely used to measure the abnormal motion of the spine. X-ray films suggest signs of instability of the segments including narrowing of the intervertebral space, formation of osteophyte, and spondylolisthesis. However, these can only provide two-dimensional images. Because the true spine motion is three-dimensional and unstable, X-ray films do not reflect accurate spine motion.

In 1974, in order to avoid the error caused by the bony landmark, Aronson built a biocompatible metal mark into the bone of the subject and performed X-ray stereoscopic imaging [86]. The measurement accuracy can reach 0.1–0.2 mm. This method becomes the gold standard for assessing bone image measurements. However, this method is invasive and cannot be a routine clinical examination. Later, based on this technology, the dual plane fluorescence imaging technique (DFIS) combined with the computed tomography imaging technique for bone modeling, after the later registration, can accurately simulate the three-dimensional motion data [87].

A large number of spine-related in vivo studies have been carried out based on DFIS combined CT (Fig. 11.13). In studies of the normal cervical spine in vivo, the anterior portion of the intervertebral disc experienced large changes in traction/compression deformation and shear deformation between functional maximum flexion and neck extension [88]. Higher level discs experience a higher range of disc deformation. No significant differences were found in the deformation range of the posterior areas of all the discs. The range of disc deformation depends on the level of the disc, and in addition to the C6/7 intervertebral disc, the deformation of the anterior region is greater than the central and posterior regions. The position of center of rotation (COR) during dynamic extension-flexion-extension (EFE) motion and axial left-right-left (LRL) rotation is shown as segment-specific and neck motion-related. The intervertebral segments CORs of C45 and C56 are closer to the geometric center than C34 and C67 are. The ROM is larger during EFE exercise

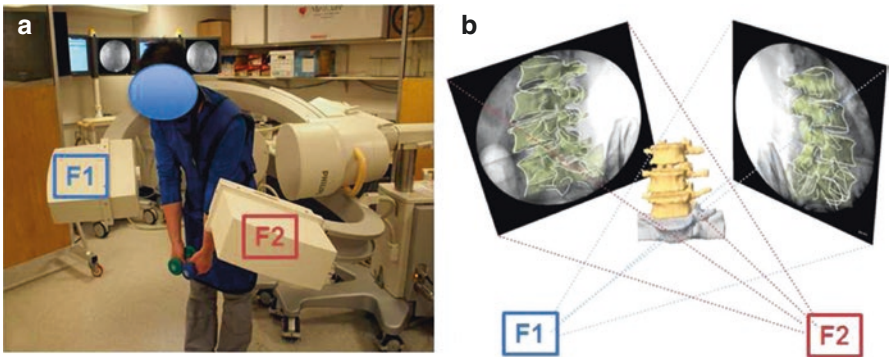

Fig. 11.13 (**a**) Experimental set-up of dynamic in vivo imaging using the DFIS. (**b**) Virtual DFIS used to recreate intervertebral kinematics throughout the dynamic motion (Reprinted with permission from Elsevier: Zhong, W., S.J. Driscoll, T.Y. Tsai, et al. In vivo dynamic changes of dimensions in the lumbar intervertebral foramen. Spine J, 2015. 15(7): 1653–9)

than during the LRL rotation at each intervertebral level. During LRL rotation, the later COR corresponds to a smaller ROM. The data obtained from this study can provide insight into the improvement of motor-preserving prosthesis design and surgical implantation techniques designed to restore normal neck function and prevent adjacent segmental degenerative cervical surgery.

In vivo studies of the lumbar spine showed that during weightlifting, L4-5 and L5-S1 of lower lumbar segments showed larger anterior-posterior (AP) and proximal-distal (PD) translations than higher vertebral segments, respectively [89, 90]. Body and lumbar foramen size showed segmental characteristics during dynamic weightlifting. Also, the movement behavior of the upper lumbar facet joints (L2-L3 and L3-L4) was similar but different from that of the lower lumbar joints (L4-L5).

3.3 Spine Kinematics in Common Pathologies

3.3.1 Herniated Disc Symptoms and Spondylolisthesis

Spinal degenerative diseases are most common among all spinal diseases, and disc herniation caused by degenerative disc disease is the most common cause of pain in the lower back and neck [91, 92].

Degenerative disc disease's symptom is usually lower back or neck pain caused by aging and wear of the disc. When the herniated disc tissue compresses the spinal nerves or the spinal cord, it can also cause weakness in the arms or legs, numbness and burning shot pain (radicular pain) [93, 94]. Cervical and lumbar vertebrae undergo maximum exercise and pressure and are most susceptible to disc degeneration, so there is a high probability of painful disc degeneration. Disc degeneration is not a disease and usually does not cause long-term disability, and most cases can be

treated with nonsurgical approach. Degenerative disc disease varies in nature and severity. Degenerative discs do not always cause pain or other symptoms. Because the intervertebral disc itself is short of innervation, it causes or accelerates the onset of other spinal disorders when the degenerated disc affects other structures in the spine, such as muscles, joints, or nerve roots.

Discogenic pain usually results from two main factors: One is inflammation. When the disc is degraded, inflammatory factors from the interior of the disc may leak, causing swelling of the surrounding spine. Therefore, inflammation causes muscle tension, muscle spasm, and tenderness in the back or neck. Pain and numbness may radiate to the arms and shoulders (the symptom of cervical radiculopathy), or into the buttocks or legs (the symptom of lumbar disc herniation), due to inflamed nerve roots.

The other is unstable micro-motion. When the outer layer (fibrous ring) of the disc degrade, the cushioning and support of the intervertebral disc usually reduce, resulting in small, unnatural movements between the vertebrae. Unstable spinal segments can induce micro-motions and cause tension and irritation in the surrounding muscles, joints, and nerve roots, leading to recurrent severe pain episodes. In most cases, however, the disc herniation itself is not painful, but the tissue leaking from the intervertebral disc, inflaming or stimulating nearby nerves, causes nerve root pain. Leg pain from sensitive nerves is often referred to as sciatica.

Spondylolisthesis is a forward translation of a vertebral segment below which a vertebral segment is located. Typical symptoms are an activity-related history of low back pain and painful spinal activity and hamstring tension without radiculopathy sign and imaging. Plain films, computed tomography, and single photon emission computed tomography are useful in determining the diagnosis. The best way to treat the symptomatic stress response of the spinal joint or adjacent vertebral structures is to immobilize the spine and activity restriction.

3.3.2 Spinal Fusion

The spinal surgery usually applies a rigid internal fixation device to secure the spine, aiming to correct deformities, relieve pain, stabilize the spine, and protect the nerves [95, 96]. Spinal fusion surgery includes a variety of surgical procedures: for example, lumbar fusion, cervical fusion, and OLF [91]. Although each surgery is different, they are all designed to help relieve pain or neurological symptoms caused by the intervertebral joints, depending on whether the patient is undergoing surgery for degenerative disc disease, lumbar spondylolisthesis, or other diseases. During spinal fusion surgery, two adjacent vertebrae are combined to eliminate the underlying mechanism of pain. Fusion of joints eliminate instability of the spinal segments and reduce pain caused by micro-motion, muscle tension, and inflammation. Moreover, the most important thing is that fusion can solve the nerve compression problem completely. Fusion surgery establishes a mechanism of bone growth that occurs months after surgery. For this reason, the complete recovery process for fusion surgery can last up to a year, although most patients return to normal activity within 6 weeks.

It is recommended to use a back or neck brace to keep the spine stable and to minimize painful movements that may disrupt the healing process after surgery. Also, rehabilitation (physical therapy for example) is often recommended to modulate the muscles to support the spine better and to provide painkillers to control postoperative pain when necessary [97].

References

1. Fuss FK, Bacher A. New aspects of the morphology and function of the human hip joint ligaments. Am J Anat. 1991;192(1):1–13.
2. Levangie PK, Norkin CC. Joint structure and function: a comprehensive analysis. 3rd ed. Philadelphia: F.A. Davis Company; 2000.
3. Heller MO, Bergmann G, Deuretzbacher G, Durselen L, Pohl M, Claes L, Haas NP and Duda GN. Musculo-skeletal loading conditions at the hip during walking and stair climbing. J Biomech. 2001;34:883–93.
4. Heller MO, Bergmann G, Deuretzbacher G, Claes L, Haas NP, Duda GN. Influence of femoral anteversion on proximal femoral loading: measurement and simulation in four patients. Clin Biomech. 2001;16(8):644–9.
5. Turley GA, Williams MA, Wellings RM, Griffin DR. Evaluation of range of motion restriction within the hip joint. Med Biol Eng Comput. 2013;51(4):467–77.
6. Crowninshield RD, Johnston RC, Brand RA, Pedersen DR. Pathologic ligamentous constraint of the hip. Clin Orthop Relat Res. 1983;(181):291–7.
7. Wu G, Siegler S, Allard P, Kirtley C, Leardini A, Rosenbaum D, Whittle M, D'Lima DD, Cristofolini L, Witte HJJob. ISB recommendation on definitions of joint coordinate system of various joints for the reporting of human joint motion—Part I: ankle, hip, and spine. J Biomech. 2002;35(4):543–8.
8. Dandachli W, Islam SU, Richards R, Hall-Craggs M, Witt JJHI. The influence of pelvic tilt on acetabular orientation and cover: a three-dimensional computerised tomography analysis. Hip Int. 2013;23(1):87–92.
9. Ferguson S, Bryant JT, Ganz R, Ito K. An in vitro investigation of the acetabular labral seal in hip joint mechanics. J Biomech. 2003;36(2):171–8.
10. Lombardi AV Jr, Mallory TH, Dennis DA, Komistek RD, Fada RA, Northcut EJ. An in vivo determination of total hip arthroplasty pistoning during activity. J Arthroplast. 2000;15(6):702–9.
11. Tanino H, Ito H, Harman MK, Matsuno T, Hodge WA, Banks SA. An in vivo model for intraoperative assessment of impingement and dislocation in total hip arthroplasty. J Arthroplast. 2008;23(5):714–20.
12. Koyanagi J, Sakai T, Yamazaki T, Watanabe T, Akiyama K, Sugano N, Yoshikawa H, Sugamoto K. In vivo kinematic analysis of squatting after total hip arthroplasty. Clin Biomech. 2011;26(5):477–83.
13. Li G, Wuerz TH, DeFrate LE. Feasibility of using orthogonal fluoroscopic images to measure in vivo joint kinematics. J Biomech Eng. 2004;126(2):313–8.
14. Gronenschild E. The accuracy and reproducibility of a global method to correct for geometric image distortion in the X-ray imaging chain. Med Phys. 1997;24(12):1875–88.
15. Gronenschild E. Correction for geometric image distortion in the X-ray imaging chain: local technique versus global technique. Med Phys. 1999;26(12):2602–16.
16. Tsai T-Y, Li J-S, Wang S, Lin H, Malchau H, Li G, Rubash H, Kwon Y-M. A novel dual fluoroscopic imaging method for determination of THA kinematics: in-vitro and in-vivo study. J Biomech. 2013;46(7):1300–4.

17. Lin H, Wang S, Tsai T-Y, Li G, Kwon Y-M. In-vitro validation of a non-invasive dual fluoroscopic imaging technique for measurement of the hip kinematics. Med Eng Phys. 2013;35(3):411–6.
18. Ito H, Song Y, Lindsey DP, Safran MR, Giori NJ. The proximal hip joint capsule and the zona orbicularis contribute to hip joint stability in distraction. J Orthop Res. 2009;27(8):989–95.
19. Bedi A, Lynch EB, Sibilsky Enselman ER, Davis ME, DeWolf PD, Makki TA, Kelly BT, Larson CM, Henning PT, Mendias CL. Elevation in circulating biomarkers of cartilage damage and inflammation in athletes with femoroacetabular impingement. J Bone Joint Surg. 2013;41(11):2585–90.
20. Soltz MA, Ateshian GA. Experimental verification and theoretical prediction of cartilage interstitial fluid pressurization at an impermeable contact interface in confined compression. J Biomech. 1998;31(10):927–34.
21. Ferguson S, Bryant J, Ganz R, Ito K. The acetabular labrum seal: a poroelastic finite element model. Clin Biomech. 2000;15(6):463–8.
22. Ferguson S, Bryant J, Ganz R, Ito K. The influence of the acetabular labrum on hip joint cartilage consolidation: a poroelastic finite element model. J Biomech. 2000;33(8):953–60.
23. Kyriazis V, Rigas C. Temporal gait analysis of hip osteoarthritic patients operated with cementless hip replacement. Clin Biomech. 2002;17(4):318–21.
24. Wykman A, Olsson E. Walking ability after total hip replacement. A comparison of gait analysis in unilateral and bilateral cases. J Bone Joint Surg. 1992;74(1):53–6.
25. Arborelius MM, Carlsson A, Nilsson B. Oxygen intake and walking speed before and after total hip replacement. Clin Orthop Relat Res. 1976;121:113–5.
26. Bennett D, Humphreys L, O'brien S, Kelly C, Orr J, Beverland D. Gait kinematics of age-stratified hip replacement patients—a large scale, long-term follow-up study. Gait Posture. 2008;28(2):194–200.
27. Tsai T-Y, Dimitriou D, Li J-S, Nam KW, Li G, Kwon Y-M. Asymmetric hip kinematics during gait in patients with unilateral total hip arthroplasty: in vivo 3-dimensional motion analysis. J Biomech. 2015;48(4):555–9.
28. Blumenfeld TJ, Glaser DA, Bargar WL, Langston GD, Mahfouz MR, Komistek RDJO. In vivo assessment of total hip femoral head separation from the acetabular cup during 4 common daily activities. Orthopedics. 2011;34(6):e127–32.
29. Kung PL, Ries MD. Effect of femoral head size and abductors on dislocation after revision THA. Clin Orthop Relat Res. 2007;465:170–4.
30. Nevelos J, Johnson A, Heffernan C, Macintyre J, Markel DC, Mont MA. What factors affect posterior dislocation distance in THA? Clin Orthop Relat Res. 2013;471(2):519–26.
31. D'lima DD, Urquhart AG, Buehler KO, Walker RH, Colwell CW. The effect of the orientation of the acetabular and femoral components on the range of motion of the hip at different head-neck ratios. J Bone Joint Surg. 2000;82(3):315–21.
32. Tsai T-Y, Li J-S, Dimitriou D, Kwon Y-M. Does component alignment affect gait symmetry in unilateral total hip arthroplasty patients? Clin Biomech. 2015;30(8):802–7.
33. Masouros S, Bull A, Amis A. Biomechanics of the knee joint. Orthopaed Trauma. 2010;24(2):84–91.
34. Wu G, Cavanagh PR. ISB recommendations for standardization in the reporting of kinematic data. J Biomech. 1995;28(10):1257–61.
35. Morrison J. The mechanics of the knee joint in relation to normal walking. J Biomech. 1970;3(1):51–61.
36. Berger RA, Rubash HE, Seel MJ, Thompson WH, Crossett LS. Determining the rotational alignment of the femoral component in total knee arthroplasty using the epicondylar axis. J Clin Orthopaed Relat Res. 1993;(286):40–7.
37. Yoshioka Y, Siu D, Cooke T. The anatomy and functional axes of the femur. J Bone Joint Surg Am. 1987;69(6):873–80.
38. Wang C-J, Walker PS, Wolf B. The effects of flexion and rotation on the length patterns of the ligaments of the knee. J Biomech. 1973;6(6):587–96.

39. Shaw JA, Murray DG. The longitudinal axis of the knee and the role of the cruciate ligaments in controlling transverse rotation. J Bone Joint Surg Am. 1974;56(8):1603–9.
40. Crowninshield R, Pope M, Johnson R. An analytical model of the knee. J Biomech. 1976;9(6):397–405.
41. Pennock G, Clark K. An anatomy-based coordinate system for the description of the kinematic displacements in the human knee. J Biomech. 1990;23(12):1209–18.
42. Butler D, Noyes F, Grood E. Ligamentous restraints to anterior-posterior drawer in the human knee. J Bone Joint Surg Am. 1980;62(2):259–70.
43. Robinson JR, Bull AM, Thomas RR dW, Amis AA. The role of the medial collateral ligament and posteromedial capsule in controlling knee laxity. Am J Sports Med. 2006;34(11):1815–23.
44. Davies H, Unwin A, Aichroth P. The posterolateral corner of the knee: anatomy, biomechanics and management of injuries. Injury. 2004;35(1):68–75.
45. Chao E, Laughman R, Schneider E, Stauffer R. Normative data of knee joint motion and ground reaction forces in adult level walking. J Biomech. 1983;16(3):219–33.
46. Ma VY, Chan L, Carruthers KJ. Incidence, prevalence, costs, and impact on disability of common conditions requiring rehabilitation in the United States: stroke, spinal cord injury, traumatic brain injury, multiple sclerosis, osteoarthritis, rheumatoid arthritis, limb loss, and back pain. Arch Phys Med Rehabil. 2014;95(5):986–995.e1.
47. Boyer KA, Hafer JF. Gait mechanics contribute to exercise induced pain flares in knee osteoarthritis. BMC Musculoskelet Disord. 2019;20(1):107.
48. Kaufman KR, Hughes C, Morrey BF, Morrey M, An KN. Gait characteristics of patients with knee osteoarthritis. J Biomech. 2001;34(7):907–15.
49. Baliunas AJ, Hurwitz DE, Ryals AB, Karrar A, Case JP, Block JA, Andriacchi TP. Increased knee joint loads during walking are present in subjects with knee osteoarthritis. Osteoarthr Cartil. 2002;10(7):573–9.
50. Lewek MD, Scholz J, Rudolph KS, Snyder-Mackler L. Stride-to-stride variability of knee motion in patients with knee osteoarthritis. Gait Posture. 2006;23(4):505–11.
51. Hurwitz DE, Ryals AB, Case JP, Block JA, Andriacchi TP. The knee adduction moment during gait in subjects with knee osteoarthritis is more closely correlated with static alignment than radiographic disease severity, toe out angle and pain. J Orthop Res. 2002;20(1):101–7.
52. Astephen JL, Deluzio KJ, Caldwell GE, Dunbar MJ, Hubley-Kozey CL. Gait and neuromuscular pattern changes are associated with differences in knee osteoarthritis severity levels. J Biomech. 2008;41(4):868–76.
53. Chehab EF, Favre J, Erhart-Hledik JC, Andriacchi TP. Baseline knee adduction and flexion moments during walking are both associated with 5 year cartilage changes in patients with medial knee osteoarthritis. Osteoarthr Cartil. 2014;22(11):1833–9.
54. Charlton JM, Hatfield GL, Guenette JA, Hunt MA. Toe-in and toe-out walking require different lower limb neuromuscular patterns in people with knee osteoarthritis. J Biomech. 2018;76:112–8.
55. Cheung RTH, Ho KKW, Au IPH, An WW, Zhang JHW, Chan ZYS, Deluzio K, Rainbow MJ. Immediate and short-term effects of gait retraining on the knee joint moments and symptoms in patients with early tibiofemoral joint osteoarthritis: a randomized controlled trial. Osteoarthr Cartil. 2018;26(11):1479–86.
56. Lin C-J, Lai K-A, Chou Y-L, Ho C-S. The effect of changing the foot progression angle on the knee adduction moment in normal teenagers. Gait Posture. 2001;14(2):85–91.
57. Jüni P, Reichenbach S, Dieppe P. Osteoarthritis: rational approach to treating the individual. Best Pract Res Clin Rheumatol. 2006;20(4):721–40.
58. Kurtz SM, Ong KL, Lau E, Widmer M, Maravic M, Gómez-Barrena E, de Fátima de Pina M, Manno V, Torre M, Walter WL, de Steiger R, Geesink RGT, Peltola M, Röder C. International survey of primary and revision total knee replacement. Int Orthop. 2011;35(12):1783–9.
59. Baldini A, Castellani L, Traverso F, Balatri A, Balato G, Franceschini V. The difficult primary total knee arthroplasty: a review. Bone Joint J. 2015;97-b(10 Suppl A):30–9.
60. Li C, Hosseini A, Tsai TY, Kwon YM, Li G. Articular contact kinematics of the knee before and after a cruciate retaining total knee arthroplasty. J Orthop Res. 2015;33(3):349–58.

61. Vince K. Mid-flexion instability after total knee arthroplasty: woolly thinking or a real concern? Bone Joint J. 2016;98-b(1 Suppl A):84–8.
62. Donadio J, Pelissier A, Boyer P, Massin P. Control of paradoxical kinematics in posterior cruciate-retaining total knee arthroplasty by increasing posterior femoral offset. Knee Surg Sports Traumatol Arthrosc. 2015;23(6):1631–7.
63. Duffy GP, Berry DJ, Rand JA. Cement versus cementless fixation in total knee arthroplasty. Clin Orthop Relat Res. 1998;356:66–72.
64. Zhao C, Lin C, Wang W, Zeng C, Fang H, Pan J, Cai D. Kinematics of anterior cruciate ligament-deficient knees in a Chinese population during stair ascent. J Orthop Surg Res. 2016;11(1):89.
65. Zhang Y, Huang W, Yao Z, Ma L, Lin Z, Wang S, Huang H. Anterior cruciate ligament injuries alter the kinematics of knees with or without meniscal deficiency. Am J Sports Med. 2016;44(12):3132–9.
66. Oiestad BE, Engebretsen L, Storheim K, Risberg MA. Knee osteoarthritis after anterior cruciate ligament injury: a systematic review. Am J Sports Med. 2009;37(7):1434–43.
67. Lohmander LS, Englund PM, Dahl LL, Roos EM. The long-term consequence of anterior cruciate ligament and meniscus injuries: osteoarthritis. Am J Sports Med. 2007;35(10):1756–69.
68. Ardern CL, Sonesson S, Forssblad M, Kvist J. Comparison of patient-reported outcomes among those who chose ACL reconstruction or non-surgical treatment. Scand J Med Sci Sports. 2017;27(5):535–44.
69. Lin L, Li J-S, Kernkamp WA, Hosseini A, Kim C, Yin P, Wang L, Tsai T-Y, Asnis P, Li G. Postoperative time dependent tibiofemoral articular cartilage contact kinematics during step-up after ACL reconstruction. J Biomech. 2016;49(14):3509–15.
70. Hosseini A, Van de Velde S, Gill TJ, Li G. Tibiofemoral cartilage contact biomechanics in patients after reconstruction of a ruptured anterior cruciate ligament. J Orthop Res. 2012;30(11):1781–8.
71. Fanelli GC, Giannotti BF, Edson CJ. The posterior cruciate ligament arthroscopic evaluation and treatment. Arthroscopy. 1994;10(6):673–88.
72. Shelbourne KD, Davis TJ, Patel DV. The natural history of acute, isolated, nonoperatively treated posterior cruciate ligament injuries. A prospective study. Am J Sports Med. 1999;27(3):276–83.
73. Gupte CM, Bull AM, Thomas RD, Amis AA. The meniscofemoral ligaments: secondary restraints to the posterior drawer. Analysis of anteroposterior and rotary laxity in the intact and posterior-cruciate-deficient knee. J Bone Joint Surg Br. 2003;85(5):765–73.
74. Noyes FR, Stowers SF, Grood ES, Cummings J, VanGinkel LA. Posterior subluxations of the medial and lateral tibiofemoral compartments. An in vitro ligament sectioning study in cadaveric knees. Am J Sports Med. 1993;21(3):407–14.
75. G L, R P, M L, J B, KW N, D A, T G. Effect of posterior cruciate ligament deficiency on in vivo translation and rotation of the knee during weightbearing flexion. Am J Sports Med. 2008;36(3):474–9.
76. Patel DV, Allen AA, Warren RF, Wickiewicz TL, Simonian PT. The nonoperative treatment of acute, isolated (partial or complete) posterior cruciate ligament-deficient knees: an intermediate-term follow-up study. HSS J. 2007;3(2):137–46.
77. Strobel MJ, Weiler A, Schulz MS, Russe K, Eichhorn HJ. Arthroscopic evaluation of articular cartilage lesions in posterior cruciate ligament—deficient knees. Arthroscopy. 2003;19(3):262–8.
78. Parolie JM, Bergfeld JA. Long-term results of nonoperative treatment of isolated posterior cruciate ligament injuries in the athlete. Am J Sports Med. 1986;14(1):35–8.
79. Kernkamp WA, Jens AJT, Varady NH, van Arkel ERA, Nelissen R, Asnis PD, LaPrade RF, Van de Velde SK, Li G. Anatomic is better than isometric posterior cruciate ligament tunnel placement based upon in vivo simulation. Knee Surg Sports Traumatol Arthrosc. 2019;27(8):2440–9.
80. Lee D-Y, Park Y-J, Kim D-H, Kim H-J, Nam D-C, Park J-S, Hwang S-C. The role of isolated posterior cruciate ligament reconstruction in knees with combined posterior cruciate ligament and posterolateral complex injury. Knee Surg Sports Traumatol Arthrosc. 2018;26(9):2669–78.

81. Jastrow H, Vollrath L. Anatomy online: presentation of a detailed WWW atlas of human gross anatomy--reference for medical education. Clin Anat. 2002;15(6):402–8.
82. Bland JH, Boushey DR. Anatomy and physiology of the cervical spine. Semin Arthritis Rheum. 1990;20(1):1–20.
83. Turinsky AL, Fanea E, Trinh Q, Dong X, Stromer JN, Shu X, Wat S, Hallgrimsson B, Hill JW, Edwards C, Grosenick B, Yajima M, Sensen CW. Integration of genomic and medical data into a 3D atlas of human anatomy. Stud Health Technol Inform. 2008;132:526–31.
84. Pait TG, Elias AJ, Tribell R. Thoracic, lumbar, and sacral spine anatomy for endoscopic surgery. Neurosurgery. 2002;51(5 Suppl):S67–78.
85. Baaj AA, Papadimitriou K, Amin AG, Kretzer RM, Wolinsky JP, Gokaslan ZL. Surgical anatomy of the diaphragm in the anterolateral approach to the spine: a cadaveric study. J Spinal Disord Tech. 2014;27(4):220–3.
86. Aronson AS, Hoist L, Selvik G. An instrument for insertion of radiopaque bone markers. Radiology. 1974;113(3):733–4.
87. Zhu Z, Li G. An automatic 2D-3D image matching method for reproducing spatial knee joint positions using single or dual fluoroscopic images. Comput Methods Biomech Biomed Engin. 2012;15(11):1245–56.
88. Yu Y, Mao H, Li JS, Tsai TY, Cheng L, Wood KB, Li G, Cha TD. Ranges of cervical intervertebral disc deformation during an in vivo dynamic flexion-extension of the neck. J Biomech Eng. 2017;139(6):0645011–7.
89. Zhong W, Driscoll SJ, Tsai TY, Wang S, Mao H, Cha TD, Wood KB, Li G. In vivo dynamic changes of dimensions in the lumbar intervertebral foramen. Spine J. 2015;15(7):1653–9.
90. Wu M, Wang S, Driscoll SJ, Cha TD, Wood KB, Li G. Dynamic motion characteristics of the lower lumbar spine: implication to lumbar pathology and surgical treatment. Eur Spine J. 2014;23(11):2350–8.
91. Heider FC, Mayer HM. Surgical treatment of lumbar disc herniation. Oper Orthop Traumatol. 2017;29(1):59–85.
92. Truumees E. A history of lumbar disc herniation from Hippocrates to the 1990s. Clin Orthop Relat Res. 2015;473(6):1885–95.
93. Karademir M, Eser O, Karavelioglu E. Adolescent lumbar disc herniation: impact, diagnosis, and treatment. J Back Musculoskelet Rehabil. 2017;30(2):347–52.
94. Corniola MV, Tessitore E, Schaller K, Gautschi OP. Lumbar disc herniation—diagnosis and treatment. Rev Med Suisse. 2014;10(454):2376–82.
95. Sonntag VK, Marciano FF. Role of spinal instrumentation in fusion for degenerative disease of the lumbosacral spine. West J Med. 1995;162(3):262–3.
96. Frymoyer JW. Low back pain. The role of spine fusion. Neurosurg Clin N Am. 1991;2(4):933–54.
97. Greenwood J, McGregor A, Jones F, Mullane J, Hurley M. Rehabilitation following lumbar fusion surgery: a systematic review and meta-analysis. Spine (Phila Pa 1976). 2016;41(1):E28–36.

Chapter 12
Biomechanics of the Fracture Fixation

Yingze Zhang, Hongde Wang, Tianrui Wang, Wei Chen, and Yanbin Zhu

Abstract Biomechanical factors is an important aspect that affects bone healing directly. Although some biologic etiologies of fixation failure can be directly affected by the physician, there are only minimally under the surgeon's control. The surgeon should do their best to preserve soft tissue, vessel, and the zone of injury. Skillful surgical technique, tight wound closure, and appropriate antibiotic therapy could decrease the risk of infection and reduce the risk of fixation failure. If failure occurs suddenly or prior to the expected time when fracture healing would occur, a mechanical issue is usually the primary cause. Biomechanics study the role of force and energy in biological systems. The fracture fixation should follow the principle of biomechanics. Excessive stress concentration and fatigue, leading to increased pressure load and bending load, results in internal fixation failure. Understanding the biomechanical principles underlying stable fixation and failure fixation could help the surgeon determine the appropriate investigation and intervention. Appropriate biomechanical fixation technology will promote fracture healing, accelerate rehabilitation of patients, and reduce nonunion of fracture. Biomechanical study can help the design of the internal fixation and also plays an important role on the improved clinical effects; furthermore, it will help clinicians to choose reasonable diagnosis and treatment strategies.

Keywords Biomechanics · Innovation · Orthopedics trauma · Fixation principle Fixation devices

Y. Zhang (✉)
Department of Orthopaedic Surgery, The Third Hospital, Hebei Medical University, Shijiazhuang, Hebei, People's Republic of China

Key Laboratory of Biomechanics of Hebei Province, Shijiazhuang, Hebei, People's Republic of China

Chinese Academy of Engineering, Beijing, People's Republic of China

H. Wang · T. Wang · W. Chen · Y. Zhu
Department of Orthopaedic Surgery, The Third Hospital, Hebei Medical University, Shijiazhuang, Hebei, People's Republic of China

Key Laboratory of Biomechanics of Hebei Province, Shijiazhuang, Hebei, People's Republic of China

C.-K. Cheng, S. L-Y. Woo (eds.), *Frontiers in Orthopaedic Biomechanics*,
https://doi.org/10.1007/978-981-15-3159-0_12

1 Introduction

Biologic and mechanical problems are the two underlying problems, when fracture implants fail prior to fracture union [1–3]. Patient's systemic biology as biologic factors including chronic diseases, smoking, medications, and many other causes may cause delayed union and fixation failure [4–6]. Many biologic etiologies of fixation failure can be treated by the physician, but there are still many biologic etiologies beyond the surgeon's control [7, 8]. Therefore, surgeons should make many efforts to preserve soft tissue and vascularity, and respect the zone of injury [9]. Meticulous surgical technique, wound closure, and appropriate perioperative antibiotic therapy can all reduce the risk of infection and treatment failure. Mechanical problems are usually the main cause, when failure occurs acutely or prior to the expected time that fracture healing [10–13]. To determine the appropriate investigation and intervention, surgeons should understand biomechanical principles underlying the stable fixation and fixation failure.

2 Pin and Wire Fixation

There are some biomechanical differences among pins, rods, and nails used for fracture fixation. Pins only resist alignment changes, rods resist deviations in alignment and translation, and nails resist changes in alignment, translation, and rotation. Kirschner wires and Steinmann pins are often used for both provisional and definitive fracture fixation. Due to its poor bending resistance, it should be used in conjunction with bracing or casting. They are usually inserted as final fixation with limited open reduction or percutaneously. They should be inserted slowly and stop drilling frequently. To prevent thermal damage to bone and soft tissues. To make their removal easier after fracture healing, we recommend using smooth wires.

Threaded wires can better fix the fractures compared with temporary fixation, but the fracture fragments must be fixed together when insertion wire to avoid distraction. If the cortical bone is hard, there is a risk of pin breakage. For small fragments in metaphyseal and epiphyseal regions, especially in the fracture of distal foot, forearm, and hand, such as Colles fracture, and in displaced metacarpal and phalangeal fracture after closed reduction, pin or wire fixation is usually sufficient [14, 15]. In most cases, pins are inserted under the control of an image intensifier. This can protect the soft tissues from further damage, theoretically allowing for maximum bone regeneration; however, it must be noted that nerves and tendons are not wound around the pin during insertion. Wire fixation is used alone or in combination with other implants for definitive fixation of some metaphyseal fractures, such as in the cervical spine, proximal humerus, and patella [16]. The wire should not be notched as it may reduce the fatigue life of the implant. It is rare touse wire alone to provide adequate stability for functional rehabilitation of the extremity [17].

For some intra-articular fractures, simple rigid fixation using screws or plates for a long time might result in some complications such as articular degeneration,

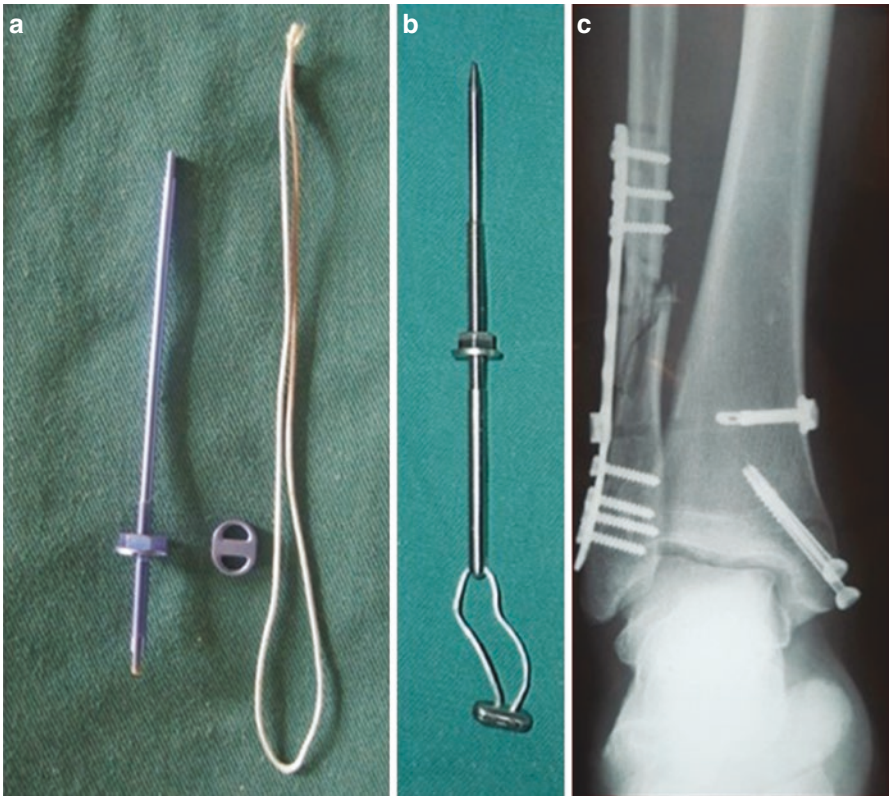

Fig. 12.1 (**a**) Components of the elastic bionic fixation; (**b**) Assembly of the fixation device; (**c**) Post-operative X ray film of the fixation device

arthritis, and the limited articular mobility. Given that, our research team used the biomechanical principle to invent an elastic fixation device for treatment of ankle fracture combined with distal tibiofibular syndesmosis (DTS). As presented, the elastic bionic fixation device included elastic cable, a bolt, and a button (Fig. 12.1), which could provide both rigid and elastic fixation, and therefore reduce the possible intra-articular issues, compared to the traditional rigid fixation. With this device, we treated 17 cases of ankle fracture combined with DTS, and at the final follow-up all of them obtained excellent and good outcomes according to the AOFAS score.

3 Screw Fixation

Screws are made up of four parts: head, shaft, thread, and tip. The head of a screw acts as an attachment for the screwdriver and can be hexagonal, cruciate, slotted, or Phillips. The head also acts as a reaction, and the pressure generated by the screw acts on the bone. The shaft or shank is the smooth portion of the screw between the

head and the threaded portion. The thread is defined by its root (or core) diameter, its thread (or outside) diameter, its pitch (or distance between adjacent threads), and its lead (or distance it advances into the bone with each complete turn). The root area determines the resistance of the screw to pullout forces and relates to the area of the bone at the thread interface and the root area of the tapped thread. The cross-sectional design usually is a buttress (ASIF screws) or V-thread (usually used in machine screws). The tip of the screw is either round (require spretapping) or self-tapping (fluted or trocar). Clinically, if it is necessary to consider pulling out from the screw because of soft bone, it is more inclined to use a larger thread diameter, and if the bone is stronger and more fatigue is needed, the screw with a wider root diameter has a higher anti-fatigue failure ability. Screws also usually are divided into machine-type screws and ASIF screw.

The use of screws to convert torque forces into compressive forces through a fracture is a valuable technique. Its success requires the application of a screw in such a way that the proximal portion of the screw is allowed to slide in the near bone and the thread is formed in the opposite cortex so that the head of the screw can exert load and forces the fracture to heal. Careful selection of the angle of the screw corresponding to the fracture is necessary to prevent the fracture fragments from slipping when compressed.

Screw Breakage by Shearing During Insertion

A screw is a mechanical device that is used to convert rotary load (torque) into compression between a plate and a bone or between bone fragments. The basic components of a screw are shown in Fig. 12.2. As shown in Fig. 12.3, when the thread of the screw is released from the shaft, it is actually a slope or a slope, and the lower bone is pulled toward the fixing plate, causing compression between the bone and the bone. In order to achieve this effect, the screw head and shaft should rotate freely within the steel plate; otherwise, the compressive force generated may be limited. The locking screw passes through the plate hole; although this fixed interface is beneficial in some clinical situations, it prevents compression between the plate and the bone.

In the cortical bone, a tap is necessary so that the torque applied by the surgeon translates into compression rather than cutting the thread, thereby overcoming the friction between the screw thread and the bone (Fig. 12.3) that it is being driven into (Fig. 12.4). In some cases such as inserting screw into a dense bone or inserting a smaller diameter screw, using a separate tap and then inserting the screw, the screw can be pushed into the bone. Most modem screw designs have self-tapping screw tips that cuts the path of the thread when the screw is inserted. Screws with multiple cutting flutes at the up of the screw appear to be the easiest to insert and have a greater grip. Tapping in cancellous bone is less advantageous because tapping reduces the pullout strength of the screw. In some cases, it may beneficial to tap the cancellous bone. A clinical example is when treating a femoral neck fracture with a physiologically older patient versus a younger patient; you may need to use a tap to make a thread in the denser bone of a younger patient. The reason for using tap in the dense bone is to prevent the frictional force from causing femoral head to rotate

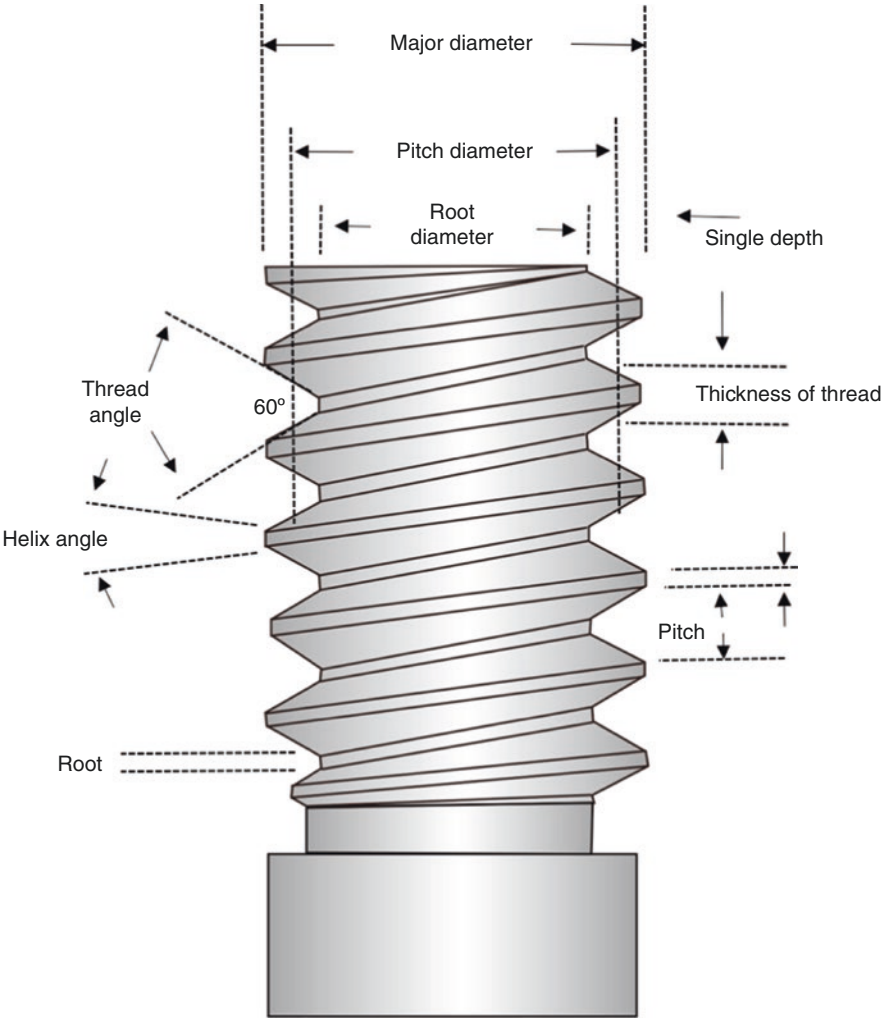

Fig. 12.2 Nomenclature of screws. The root diameter is the inner diameter of the screw and the pitch defines the distance between threads

during the insertion of screw resulting malreduction. In particularly hard bones the frictional forces become so great that it becomes difficult to advance the screw [18].

One problem with the placement of the screw is that the shear failure of the screw, the head twisting off usually, making it difficult to remove the shaft from the bone. This can occur especially if the tap is not used before insertion, or when a smaller (less than 4-mm diameter) screw is inserted into the dense bone. The stiffness and strength of the screw are related to the fourth power of its radius (the effect of moment of inertia for screws of the same material). The 6-mm diameter screw is

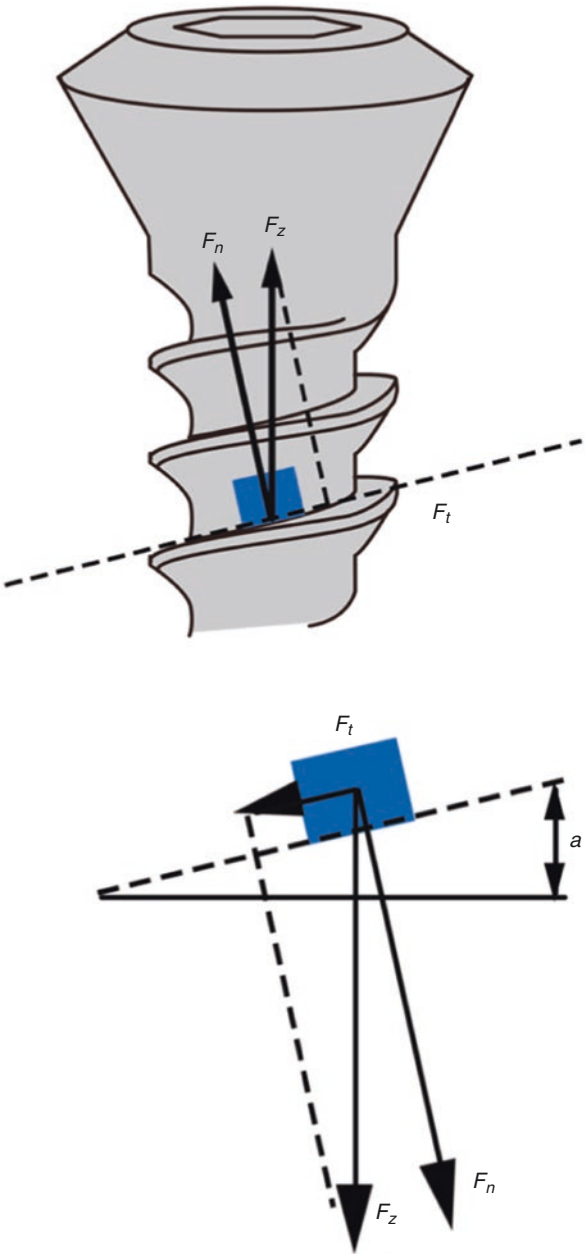

Fig. 12.3 A screw is a mechanical device that converts torque into compression between objects. The screw thread is actually an inclined plane that slowly pulls the objects it is embedded into together (F_n normal or compressive force acting against the screw head; F_t tangential or frictional force acting along the screw thread; F_z resultant of the two forces; α angle of the screw thread. The smaller the angle α [finer thread] the lower the frictional force)

about five times stiffer than a 3-mm diameter screw and 16 times more resistant to shear damage than a 3 mm diameter screw. The junction of the screw head and threaded portion of the screw is the transition point of shape and size. Therefore, it acts as a stress concentrator, usually where the screw breaks.

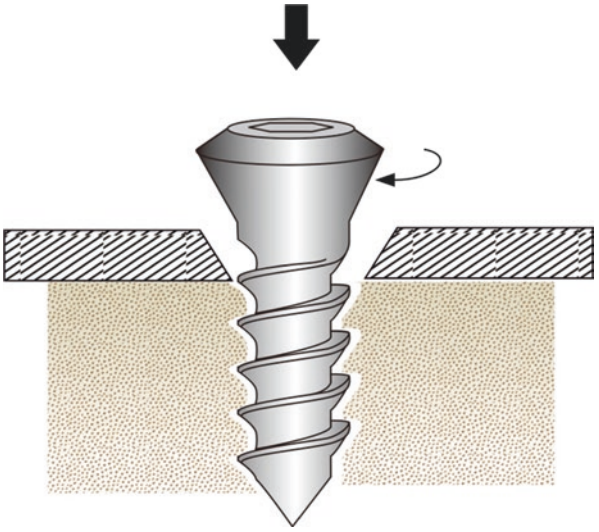

Fig. 12.4 Schematic diagram showing the approximate distribution of torque acting on a screw placed into cortical bone. With a pre-tapped hole, about 65% of the applied torque goes to produce compression and 35% to overcome the friction associated with driving the screw. When the hole is not tapped, only about 5% of the torque is used to produce compression, the rest going to overcome friction and to cut threads in bone. These observations do not apply in cancellous bone

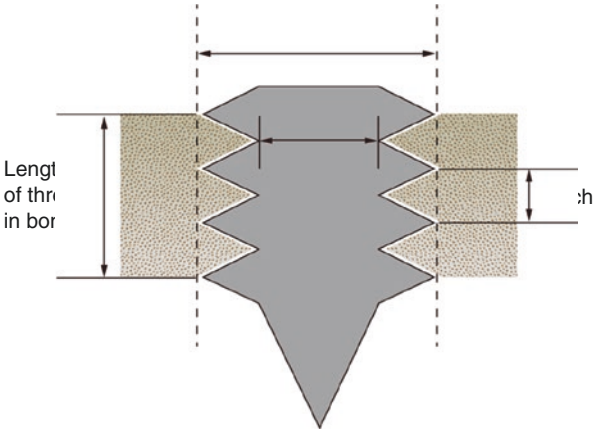

Fig. 12.5 The factors that determine the pullout strength of a screw are its outer diameter and length of engagement (this defines the dimensions of a cylinder of bone that is carried in the threads and is sheared out as the screw is pulled out of the bone) and the shear strength of bone at the screw-bone interface, which is directly related to its density. A finer pitch screw produces a small gain in purchase

Screw Pullout

Especially, in cancellous bone, the maximum force that a screw can withstand along its axis. The pullout force depends on the size of the screw and the density of the bone placed. As shown in Fig. 12.5, when the force acting on the screw exceeds its pullout strength, the screw will be pulled out or "stripped" out of the hole, and the sheared bone will be placed in thread, greatly reducing the nail holding force and fixing force. The larger the diameter of the screw, the larger the number of threads per unit length, and the longer the insertion length of the screw shaft, the greater the pulling force. And a greater density of the bone it is placed into. The diameter and length of the embedded screw can be considered to define the outer surface of a cylinder along that screw shears. Given a maximum stress that bone of a particular

density can withstand, increasing the surface area of the screw cylinder increases the pullout force (because force = stress multiplied by the area over which it acts). In order to enhance screw purchase, it is conceivable to insert the screw of largest diameter into the bone of the highest density with the length of the implant as long as possible. However, placing screws of as large a diameter as possible has disadvantages. Larger screws occupy a larger volume in small fracture fragments, limiting the number of possible fixation sites and propagating adjacent fracture lines.

In cancellous bone, the extraction of the screw becomes a more important problem because the porosity of cancellous bone reduces its density and thus the shear strength. Drilling preparation, especially drilling, rather than tapping, can increase the pullout strength of cancellous bone (such as pedicle screws in the vertebral body). The reason why the cancellous bone is knocked down is that the tap is removed from the hole or placed in the hole, which can effectively increase the diameter of the hole and reduce the amount of bone material that interacts with the thread. When the bone density is reduced, the tapping is more harmful, and the pullout strength can be reduced from 8 to 27%. The pullout strength can also be related to the time after insertion. As the bone heals, it can remodel around the screw, possibly doubling its initial pullout strength [19].

Recent research has focused on whether pullout strength is an appropriate measure of screw performance in cancellous bone. In nonlocking steel and screw constructions, the stability of most structures comes from the friction created by compression between the plate and the bone. When the screw is inserted into the bone, if it is able to generate high values of insertional torque, the compression of the steel plate to the bone is increased, and the stability is increased. As the maximum insertional torque is reached and then exceeded, the screw will then "strip out" and lose its supporting force in the bone. Although there is a relationship between maximum insertional torque, screw pitch, and compression forces, it has been found that the pullout strength has no correlation with either the maximum insertional torque or screw pitch. Therefore, this may be a better way to measure screw performance and optimize screw characteristics.

Screw Breakage by Cyclic Loading

Once screw is successfully inserted and the construction is completed, the screw will be subjected to cyclic bending forces as the patient begins to mobilize (Fig. 12.6). Ideally, a nonlocking screw initially tightens the plate to achieve the maximal torque, which is translated into the maximum compression between the plate and the bone (Fig. 12.4). The screw on the bone portion is in frictional contact, depending on the friction generated between the plate and the bone. The frictional force is directly dependent on the compressive force generated by the screws. If a slip occurs between the plate and the bone, the bending load will be transferred from the screw head into the plate, at which point the screw comes into contact with the plate. The bending load perpendicular to the axis of the screw, coupled with possible stress corrosion and fretting corrosion, may cause the screw to fail rapidly in fatigue. Zand et al.'s research shows that when the screw is fastened to the steel plate, it is subjected to a maximum load of less than 1000 loading cycles due to bending

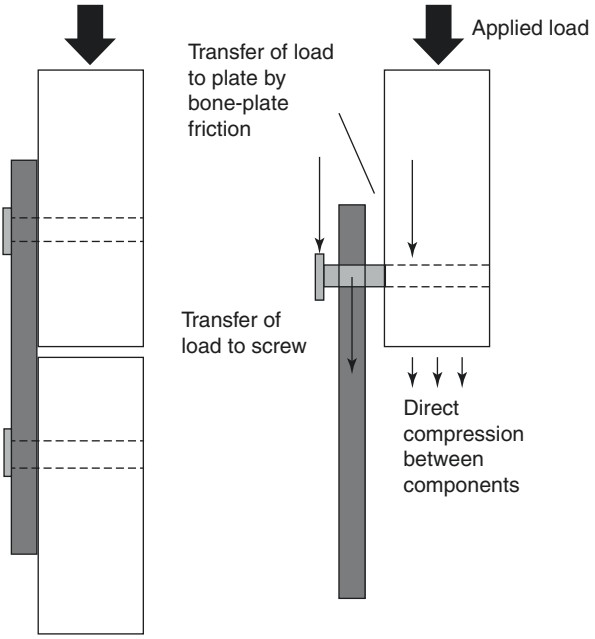

Fig. 12.6 A mechanism for rapid failure of screws in cyclic bending occurs when the screw has not been tightened sufficiently to keep the plate from sliding along the bone surface (the plate-bone gap shown here is exaggerated for clarity). The results is that bending loads are applied transverse to the long axis of the screw, which in combination with fretting corrosion caused by the screws rubbing against the plate results in early failure of the screw

fatigue, compared to a fully fastened screw capable of withstanding more than 2.5 million loading cycles. The load is less than 10–15% of the maximum load. This emphasizes the clinical importance of ensuring screw tightness during the fixation of the plate.

Locking the screws on the board can reduce the problem, since the problem is less subjective when the screw head is fully fastened to the plate hole. Small-fragment screws (3.5- to 4-mm outer diameter) can fatigue because of their small core diameters. Although the use of locking screws with a larger core diameter and shallower thread can reduce the possibility of fatigue failure, a smaller core diameter and deeper thread can increase purchase strength in the bone. Screws with smaller core diameters are more likely to fatigue than larger ones. The fatigue strength of the screw must be weighed against the purchasing power of the screw and the size of the screw associated with the size of the bone fragment. The surgeon sometimes must make a decision between a screw with a large core diameter with shallower thread, which maximizes fatigue strength, and a smaller core diameter screw with deeper threads, which maximizes purchase power.

Cannulated screws are used for fixation when the insertion of a guide wire is helpful to guide the future path of the screw. However, as the bone density increases and the diameter of the guide wire increases, the drilling accuracy of the guide wire decreases. Cannulated screws follow the same mechanical principles as solid screws, but material must be removed from the center of the screw to accommodate the passage of the guidewire. Manufacturers commonly increase the diameter of the screw at the base of the thread to fit the loss of this central material. The same size

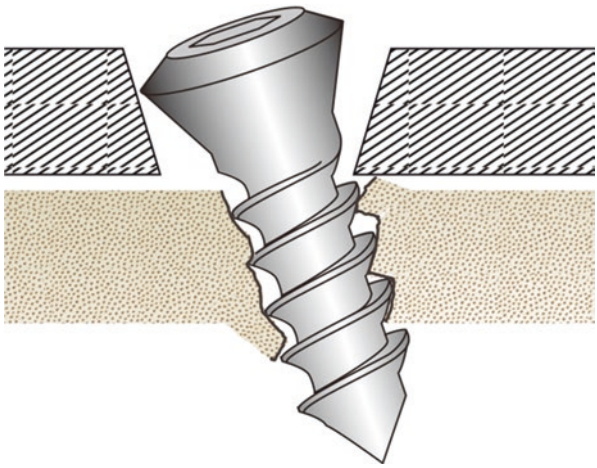

Fig. 12.7 Using a fully threaded lag screw causes the threads to engage in bone on both sides of the fracture. This inhibits the screw from compressing the bone fragments together

of cannulated screws usually has less thread depth than solid screws. The result depends on the size of screw, rather than pullout strength. For screws with a diameter of 4 mm, the tensile strength of the cannulated screws of the same outer diameter is about 16% lower. Alternatively, to maintain the same thread depth, the outer diameter of the screw may be increased. Another consideration is that the cannulated screw is much more expensive than the solid screw [20].

Fully Threaded Lag Screws

The lag screw is a very effective device which can produce amount of pressure across fracture fragments and the fracture site. The head of the screw and upper portion of the shaft must be allowed to glide in the near broken pieces to pull the far broken fragments toward it, thereby creating compression on the fracture surface. As shown in Fig. 12.7, a fully threaded lag screw can prevent the gliding action between the two fracture fragments. The fully and partly threaded lag screws were used to compare the compressive forces across the fracture site. The results showed that the average compressive force at the opposite cortex (i.e., the force in the screw itself) was about 50% greater when a partly threaded screw was used.

3.1 Machine Screws

The machine screws are threaded throughout the length and can be self-tapping or threaded before insertion. Most are self-tapping; there is a cutting flute that cuts the screw threads as the screw is inserted. Machine screws are mainly used to fix the hip compression screw on the femoral shaft. The size of the machine screw holes is critical. A hole that is too large can cause the thread to be unsafe, and a hole that is too small can cause the screw to be inserted or fractured during insertion. The drill bit selected should be slightly smaller than the screw after the screw minus the

thread. For a self-tapping screw, the drill point is used to drill holes in soft bone. The size of the screw and drill tip should be checked before surgery.

3.2 Asif Screws

Screws developed by the Swiss ASIF Group for bone fixation techniques and principles are widely used. The threads are more horizontal than the machine screws, and these screws rarely seldom self-tapping; the drill must be tapped with a cutting tapper before inserting the screws. ASIF screws are available in cortical, cancellous, and malleolar designs. Mini screws for fixation of small fragments and small bones, and the standard cancellous and cortical screws, come in multiple lengths and diameters. Standard cancellous and cortical screw heads have a hexagonal recess for a special screwdriver, while the smaller screws have a Phillips head.

3.2.1 Cortical Screws

The full length thread of the cortical ASIF screw is available in a variety of diameters (4.5, 3.5, 2.7, 2.0, and 1.5 mm). If the hole in the near cortex is drilled too deep, the cortical screws can be used as a positional or lag screws for inter-fragmentary compression.

3.2.2 Cancellous Screws

These screws have larger threads that provide more support for soft cancellous bone, making them more suitable for use on the metaphyseal areas. The cancellous screws are available in 6.5- and 4.0-mm diameters with thread lengths of 16 and 32 mm, respectively. Regardless of the lengths of the screw, both lengths are threaded. The malleolar 4.5-mm screw is also included in this group, but it is unique in that it has a self-tapping thread. Choosing the right drill size and tapping the hole is the key to a safe purchase. Plastic and metal washers are commonly used with these types of screws to reattach ligament tears or to increase compression between the fragments by providing a larger cortical surface area for screw head.

3.2.3 Self-Tapping, Self-Drilling Screws

The self-tapping screws are the same sizes as cortical screws. A small portion of the ends of these screws are used to remove bone fragments. Self-tapping screws have a lower pullout strength due to their structure. These screws are preferably used for external fixation pins [21].

3.2.4 Locking Screws

The locking screw is a self-tapping screw with a locking screw at the head. These screws require accurate predrilling so that the locking plate is tightly attached to the locking plate and requires a special screw drivers for implantation.

4 Plate and Screw Fixation

Pauwels et al. firstly defined and applied the tension band principle to fix fractures and nonunion. This engineering principle applies to the transformation of the tensile force into a compressive force on the convex side of an eccentrically loaded bone. This is accomplished by placing a tension band (bone plate) across the fracture on the tension (or convex) side of the bone. The tension is counteracted by the tension band at this position and converted into a compressive force. If the plate is applied to the compression (or concave) side of the bone, it is likely to bend, fatigue, and fail [22]. Therefore, a basic principle of tension band plating is that it must be applied to the tension, and the bone itself will get a compressive force, so the tension band device does not require a heavy and rigid tension band principle and is also used for some olecranon and patellar fractures. Tension bands and axial compression are often combined when using plates and screws [23–25].

We have found that almost all plate hole breaks occur at the plate hole near fracture area [26]. Therefore, the hole area seems to be the weakest part of the board, and naturally it is a place for improvement. We only widened the locking compression plate (LCP) in the hole area to make it a gourd-shaped LCP to increase the strength of the plate and reduce the plate breakage (Fig. 12.8) [27, 28]. After a series of axial loading single cycle to failure test, torsion single cycle to failure test, four-

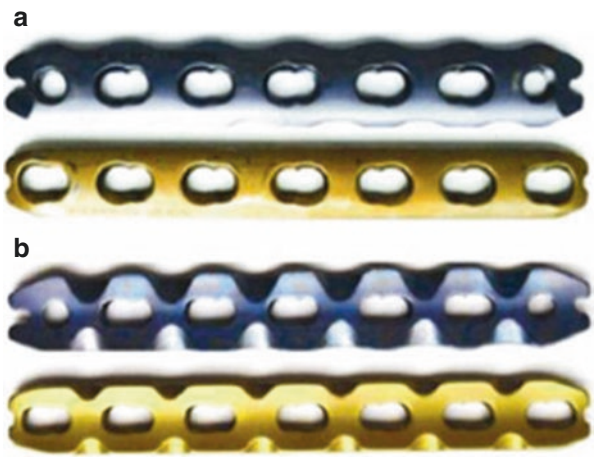

Fig. 12.8 Gourd-shaped LCP designed to enhance the plate strength in order to reduce plate breakage. (**a**) The Gourd-shaped LCP (up) and LCP (down) viewed from above; (**b**) Gourd-shaped LCP (up) and LCP (down) viewed from below

point bending single cycle to failure test, and dynamic four-point bending test, it is concluded that the gourd-shaped LCP structure has greater stiffness, strength, and longer fatigue life than LCP. This may be a more reasonable LCP that can reduce the rate of clinical breaks [29].

Our team used a new anatomical plate and compression bolt fixation technique, combined with a small incision of the posterior foot, to treat intra-articular calcaneal fractures and achieved good or excellent clinical results, and had fewer soft-tissue problems (Fig. 12.9) [30]. Compared to the conventional plate and cancellous screws technique, our fixation technique requires higher loads to cause structural failure, which may be related to the design of the implant. According to the measurement of the calcaneus specimen and the data of the three-dimensional CT image of the calcaneus, the anatomical steel plate and the compression bolt were designed. The use of conventional anatomical plates and cancellous screws to fix a calcaneal fracture is characterized by compression of the plate to the lateral wall of the calcaneus. The actual stability lies in the friction between the plate and the bone, which

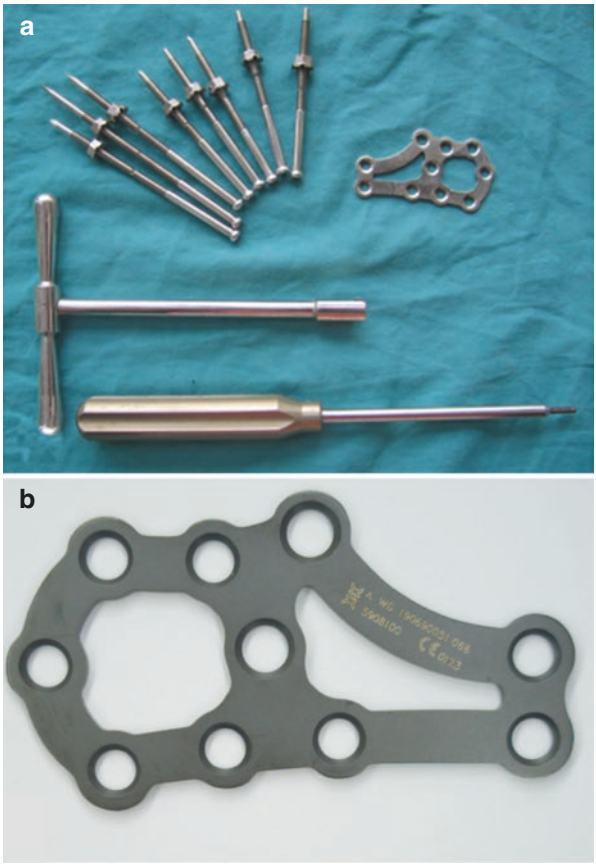

Fig. 12.9 (**a**) components of the calcaneal fracturefixation system; (**b**) the anatomical steel plate viewed from up; (**c**) post-operative lateral and posteroanterior radiograph; (**d**) post-operative CT images

Fig. 12.9 (continued)

can easily be achieved by our anatomic plate and compression bolts. Putting the compression bolts together can be seen as another piece of plate that is compressed onto the inner side wall of the bone specimen to provide higher friction and restore the width of the calcaneus.

Another example was the application of compression bolt in the treatment of Schatzker type II–VI tibial plateau fractures (Fig. 12.10), in which joint surface widening and collapse are commonly accompanied [31, 32]. The traditional metal plates and screw fixation of fractures of such types are commonly associated with a high rate of postoperative reduction loss, which likely result in the development of traumatic arthritis. Our preliminary reports of using this compression bolt presented the favorable results, both in biomechanics and clinical effectiveness.

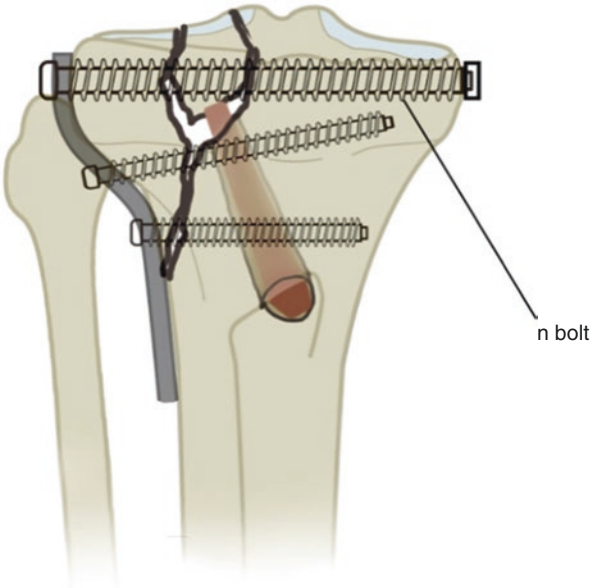

Fig. 12.10 Application of compression bolt in the treatment of Schatzker type II–VI tibial plateau fractures

4.1 Locking Plates

Locking plates are a combination of steel plate technology and percutaneous bridge plating technology using locking screws as fixed angle devices [33]. Locking steel plates provide a stronger, longer lasting fix than nonlocking steel plates [34]. They have been proven to allow for greater loads bearing than regular plates. The Less Invasive Stabilization System (LISS) (Synthes, Inc., West Chester, PA) uses unicortical locking screws that allow for greater elastic deformation than conventional plating systems. The locking plate can also be used in combination with locking and unlocking screws, mechanically similar to a pure locking structure. The locking plate works best on osteoporotic bones, where pulling out the steel plate is problematic. They also provide sufficient load-bearing strength to avoid the distal femur, proximal humerus, and medial and lateral plates of the tibial plateau. However, the locking plate structure also has an inherent that inhibits the movement of the fracture site, making it insufficient to stimulate callus formation. Therefore, the locking plate of the distal femoral fracture can result in insufficient and asymmetrical ankle formation, with minimal deposits in the proximal cortex. A recent study of locking plates for distal femoral fractures confirmed this and showed a nonhealing rate of 10–23% and a reoperation rate of open fractures of 31%.

5 Intramedullary Nail Fixation

Satisfactory stable intramedullary fixation of the fracture is possible under the following conditions:

1. When a non-comminuted fracture occurs in the narrowest part of the medullary canal, it can be considered to unlock the intramedullary nail; not only the lateral force and shear force are eliminated, but also the rotational force is controlled. If the medullary canal of one fragment is much larger than the other, it often results in poor control of the rotational force; in these cases, interlocking techniques are required. In general, the interlocking screws should be placed at least 2 cm from the fracture to provide sufficient stability for postoperative functional activity. Axially unstable fractures are best treated with static or double-locked nails.
2. The curvature of the bone must be taken into consideration when selecting the type of staple and determining the degree of reaming necessary. Biomechanically, unlocked nails achieves stability by a curvature mismatch in curvature between the bone and the nail, resulting in a longitudinal interference fit. If curvature mismatch is large, more reaming will be required. The entry portal is critical for all nails and should be in areas where the insertion force is minimized. In the femur, this is a straight nail that conforms to the medullary canal in the piriform fossa, or a nail that is curved at the proximal trochanter with a slightly lateral proximal bend. For the tibia and humerus, the offset between the entrance and the alignment of the tube create a powerful force on the posterior and medial cortex, respectively. The humeral head of the nail begins to reduce the insertion of the force into the tibia.
3. Sufficient diameter and continuity of the medullary canal are prerequisites for intramedullary nail techniques. Excessive reaming should be avoided as it significantly weakens the bone and increases the risk of thermal necrosis. We recommend reaming until the cortical "chatter" is encountered, i.e., "reaming to accommodate," but never insert a nail larger than the diameter of the tube. In general, we use nails 0.5 or 1.0 mm smaller than the largest reamer.
4. The locking intramedullary nailing technique should allow the fracture to be nailed into the joint 2–4 cm. These techniques require the use of locking screws or tightening screws. These techniques require the use of blocking screws or "Poller" screws. A new design of an intramedullary nail with an oblique distal locking screw and a screw that can be locked into the incision to form a fixed angle can increase the stability of these metaphyseal fractures.

A perfect intramedullary nail has not yet been designed. Different bone contours make this nail impossible, but improvements in the design of the intramedullary nail continue. Special nails may be designed for each bone, all types of fractures, fractures or the same bones in different areas. The intramedullary nails should meet the following requirements:

1. It should be strong enough to provide sufficient stability to maintain alignment and position, including preventing rotation; it should include the necessary interlocking screws only.
2. It should be constructed so that contact-compression forces can impact the fracture surfaces, an ideal physiological stimulus.
3. It should be easy to remove when placed; accessories are provided for easy movement.

Before selecting this technique, surgeons should be aware that intramedullary fixation, like other internal fixations, may present complications. This is not a technique that can be used at will. We recommend the following considerations:

1. Adequate preoperative planning must ensure that the fracture can be fully stabilized within the working area.
2. The patient should be able to tolerate a major surgical procedure. Patients with severe pulmonary injury should be taken special consideration, because the added fat emboli from the procedure may intensify pulmonary problems.
3. The proper length and diameter of the nail must be available before the [35–37] surgery is determined.
4. Appropriate equipment, well-trained assistants, and optimal hospital conditions are necessary for successful insertion of an intramedullary nail.
5. A metal nail is not a substitute for the union and if subjected to excessive will also bend or break the strain during the recovery period.
6. Closure nailing techniques should be used whenever possible, using these techniques to improve healing rates and reduce infection; [38–41] however, surgeons must be familiar with both open and closed techniques. As more experience is gained with closed techniques, fewer and fewer fractures are needed for open reduction [42, 43]. However, limited open reduction is better than accepting a poor closed reduction. This situation most frequently occurs in high-energy subtrochanteric femoral fractures, traction does not adequately correct flexion and abduction.

5.1 Types of Intramedullay Nails

Just as plate, intramedullary nail has an anatomic and functional name. The central body nail is inserted into the bone in a straight line with the medullary canal. It interferes longitudinally with the bone through multiple points of contact [44–49]. They rely on restoring bone contact and stability to avoid axial deformation of the fracture during rotation [50, 51]. The classic Küntscher cloverleaf and Sampson nails are examples of centromedullary nails. The condylocephalic nails enter the bone of the condyles of the metaphysis and usually enter the opposite metaphyseal-epiphyseal area. They are usually inserted into groups to increase rotational stability. Ender and Hackenthall pins are examples of condylocephalic nails. Cephalomedullary nails have a centromedullary portion but it is also allowed to be fixed to the femoral head. The Küntscher Y-nail and Zickel subtrochanteric nail are examples of this type [52, 53].

Interlocking techniques further improves these classics by adding interlocking centromedullary and interlocking cephalomedullary nails [54–56]. Interlocking nails allow longer working length of the interlocking nail screw axial and rotational deformation resistance of fracture. Modney first designed the first interlocking nail. Küntscher also designed an interlocking nail (the detensor nail), which was modified by Klemm and Scheilman and later modified by Kempf et al. These pioneers

developed techniques and implants that form the basis of some designs and techniques used today. Cephalomedullary interlocking nails, designed to treat complex fractures and the proximal femur, were axially and rotationally unstable, such as complex subtrochanteric fractures, pathologic fractures, and ipsilateral hip and shaft fractures. These nails can be secured with bolts, nails, and special lag screws such as Russell-Taylor reconstruction nails, Williams y nails, and Uniflex nails [57]. The current intramedullary nails for femoral fixation design reflect regional internal fixation nails. Antegrade femoral nails can be performed through the piriformis or trochanteric inlet. The retrograde femoral nail passes through the entrance between the femoral condyles [58, 59].

Interlocking fixation is defined as a dynamic, static, and double lock. Dynamic fixation controls bending and rotational deformation but allows axial load transfer of the bone. Axial stable fractures and partial nonunion can be fixed by power. Static fixation controls the rotation, bending, and axial load, so that the implant has more bearing potential and reduce the fatigue life of the equipment. It is particularly useful in crushing, nonisthmal fractures of the femur and tibia. The double-locked mode controls bending, rotational forces, and some axial deformation, but some shortening occurs due to the ability of the screw to translate axially within the nail. This type of fixation is often used for humerus fracture with delayed union and not healing.

The dynamics of the interlocking nails were originally designed to avoid fracture healing, [60] as it is theoretically believed that static interlocking will stop the repair of the fracture. This technique involves conversion of the static mode to a dynamic mode by removing the screws from the longest fragment. Dynamization increases the fatigue life of the nail by reducing the load-carrying capacity of the nail while increasing the compressive force at the break point; however, if there is insufficient cortical stability or bone regeneration before exercise, shrinkage may occur [45, 61, 62].

5.2 Reamed Versus Unreamed Intramedullary Nailing

For patients with multiple fractured long bone fractures, the need for reaming for intramedullary nailing has been controversial [63]. Physicians who support non-reamed nails emphasize the lack of physiological effects of reaming, such as fat embolism in the lungs [64, 65]. Experimental evidence suggests that reaming has an adverse effect on lung function. This adverse effect does not appear to be apparent in most clinical patients; however, some authors believe that the development of pulmonary complications may be related to the severity of the associated chest injury, rather than to the reaming of the medullary cavity. Studies supporting the reaming nail showed no statistically significant difference in the incidence of pulmonary complications in patients with and without reaming [66]. Due to various factors leading to the development of adult lung failure syndrome, it is difficult to determine which patients' lung expansion may be harmful. Whether the long bone

reaming nail increases the frequency of infection is another controversial area. Current clinical data show no significant difference in infection rates between reamed and non-reamed intramedullary nail.

6 External Fixation

External fixation is accepted in trauma management, ranging from damage control to final treatment. External fixation requires more careful clinical and radiographic monitoring than internal fixation, but the general application and management principles are absolutely straightforward, [67, 68] and its versatility allows it to be used in a variety of fractures [69, 70]. However, external fixation is not suitable for all fractures; [71–73] when other forms of fixation, such as screws, plates, or nails, are more suitable, it should not be used [74].

External fixator should be used when the other methods of fracture fixation are not applicable, although the external fixation will cause inconvenience to the patient and is highly likely to cause surface needle infection, it fills the clinical vacancy [75–77]. After high energy trauma with open injuries, plates and intramedullary nails are sometimes considered an unacceptable risk of deep infection. Although the degree of comminution and the extent of involvement sometimes lead to inherent instability of the fracture morphology, the external fixator can even better mechanically control the fracture through the joint. Unlike plates and most intramedullary nails, external fixator provides an opportunity for postoperative correction. The adjustability of the external fixator has been unique until recently, partly explaining why they continue to play an important role in musculoskeletal wound care. External fixation has become the preferred method for treating some of the most challenging bone pathological diseases encountered in the clinic [78]. Although there are alternative treatments, it is still an important factor in limb salvage in early and late bone remodeling of severe limb injuries [79]. This is currently the only system that allows surgeons to control fixation flexibility during bone healing. External fixtures have undergone tremendous changes, from the most primitive combination of wood plywood design to the modern design of widely used metals and composites. The development of these devices has brought many complications and it has become a more technically demanding process. Despite these factors, many surgeons around the world continue to use external fixators to treat complex fractures, segmental defects, and congenital malformations. The work of many clinicians, researchers, and engineers around the world is responsible for the current external fixture design [80]. For example, the dispersion and compression mechanisms of modern equipment are attributed to Lambret in 1911. In 1931, Pitkin and Black field first proposed a double cortical pins to connect two external fixation clips as a bilateral frame to promote fracture healing. Anderson et al. published a series of papers from 1933 to 1945, outlining the application of half-pins and transfixation pins in various long bone fractures, arthrodesis, and limb lengthening surgery [81]. These incre-

mental improvements have resulted in currently available designs, providing three main configurations of external fixtures [82].

Professor Gavril A. Ilizarov's contribution to the modern design of unilateral and circular external fixes should be recognized [83–85]. He also invented methods for limb salvage and bone extension by distraction osteogenesis. Distraction osteogenesis is a fixture for us to use mechanical force to stimulate the bone regeneration process clinically. This is achieved by a special form of external fixture called an annular fixture. Ilizarov found that these external frames can be used in a variety of applications, including post-traumatic and congenital limb reconstruction, treatment of osteomyelitis, regeneration of bone defects, deformity correction, and complex arthrodesis. These devices take advantage of Ilizarov's principle of stretch tissue, relying on a special type of low energy osteotomy to preserve local blood vessels. Ideally, only cortical bone fractures are made, while the medullary vessels and periosteum remain intact at the metaphysis. The initial incubation period allows the osteotomy to begin healing before the fixture is periodically adjusted to achieve a controlled gradual mechanical stretch. When the anchor is slowly extended, new bone is formed in the gap created in the osteotomy by the now familiar distraction osteogenesis process. For example, this process considers bone reconstruction through bone transport across segmental defects, using small tensioned Kirschner wires (K-wires) and circumferential ring supports. When new bone growth occurs at the metaphysis, a healthy bone gradually shifts to the defect. When the new bone grows out of the metaphysis, the normal bone gradually shifts to the defect. During the development of similar stretched tissue, the tension generated by mechanical stretch stimulates new bone formation, skin, blood vessels, peripheral nerves, and muscles. This impressive process, bone elongation and regeneration occurs at a rate of about 1 cm per month. The Ilizarov technique is important in the treatment of nonunion by mechanical stimulation and regulation of callus and can be used to reconstruct segmental defects that can be reliably filled far beyond the iliac bone graft. More importantly, this technology has produced limb salvage with superior quality of regenerative normal bone.

The circular frame contains the basic components of the rings, the tensioned wires, and the connected threaded rods. The stability of the frame depends on the configuration of the components, which will affect the local mechanical environment around the regenerated bone, and also determining the type, rate, and quality of the tissue formed. For example, the stability of the structure will change depending on the type and size of the rings (full ring, partial ring, or arches). Full ring provides the greatest stability, partially intermediate, and arches the least. The complete ring provides maximum stability, partial middle, and arch. At the very least, the diameter of the ring is also important, and the smaller ring is more stable than the larger ring of the same thickness. Stability will also depend on the distance between the rings, as well as the type and number of ring connectors, such as wires, rods, and Shantz pins. In clinical cases, different combinations of the circular frame components are used depending upon the intended application and required stability.

6.1 *Biomechanical Aspects of Fracture Fixation in Specific Location*

6.1.1 Fixation in the Proximal Femur

Fixation of the proximal femur fracture is particularly challenging because during normal activity, the pressure through the femoral head can reach four to eight times the body weight [86–89]. This force acts through an important forearm (the length of the femoral neck) that exerts a large bending load on the fixation hardware [90]. In addition, many of these fractures occur in the elderly, who may have trabecular bone of low density and poor mechanical quality. In addition, it is generally not possible to obtain a screw in the cortical bone of the femoral head [91–93].

The major force acting in a basicervical fracture of the femoral neck, fixed with a sliding hip screw, is the joint reaction force through the femoral head, derived from body weight and the force generated by muscle movement during walking [94–96]. The joint reaction force can be divided into two parts. One (Fig. 12.11) is perpendicular to the axis of the sliding screw, causing the fracture surfaces to shear along the fracture line, which results in inferior displacement and varus angulation of the femoral head, and increases the resistance of the screw to sliding. The other parties parallel to the screw, and the surfaces are joined together by friction and

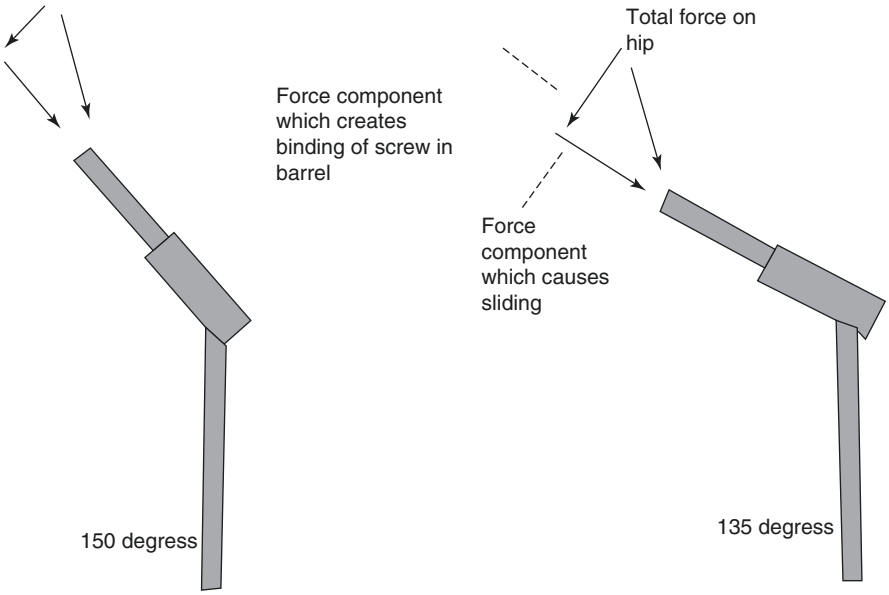

Fig. 12.11 The joint reaction force in the femoral head can be divided into two major components. The one parallel to the axis of the femoral neck produces sliding and impaction of the fracture components and the other, transverse to the femoral neck, causes the screw component of the femoral hip screw to bind, resisting sliding. The higher-angle hip screw has a screw axis more closely aligned with the joint reaction force so the force component that produces sliding is larger whereas the transverse force component resisting sliding is smaller

mechanical interlocking for improved stability. Therefore, the goal of the femoral neck fixation system is to use the component of the joint force parallel to the femoral neck to encourage the fracture surfaces to slide together. This is the basic principle for selecting high angle hip screw when possible.

The following points regarding the sliding hip screw device also apply to the nail/tension screw device. When the screw slips, since the structure is staggered by the fracture, the screw is supported by the barrel to prevent the femoral head from bending down. Adhering to two basic mechanical principles will increase the ability of the screw to slide within the side plates or nail holes. As mentioned above, higher angle hip screws are more effective in adjusting slip [97–101]. In addition, the screw should engage as deep as possible within the barrel. For the force acting on the femoral end of the screw, if the internal force of the screw in contact with the barrel is small, the remaining amount of the screw shaft in the barrel is small, and the internal force in the barrel is increased. This is because the moment (bending load) generated by the force acting transversely on the screw axis at the femoral head (Fig. 12.12) acts on the longer force arm or the vertical distance L (the force x is perpendicular to the edge of the barrel, i.e. the fulcrum)). The balance arm L_b is shorter because there are fewer screws left in the barrel. Since F_h acts on a longer arm and F acts on a shorter arm, F_b increases. When the screw is in contact with the barrel, its internal force F_b produces greater frictional resistance, which requires more friction to overcome the friction and allow slippage. Sliding hip screws with two- or four-hole side plates seems to provide an equivalent anti-physiological compression load. There are several factors that affect the fixation strength of the femoral neck using multiple screws, but the number of screws used (3 or 4) is not a significant factor.

Factors that increase this type of fixed strength include more long-axis screws with transverse fracture lines, larger femoral skull mass density in the position of the screw, and less comminuted fractures, shorter arm loads on the arm (shorter The distance from the center of the femoral head fracture line). However, the most important factor is the quality of the reduction because of the importance of cortical support in reducing fracture displacement. Under physiological load, several mechanisms of fixed failure were observed (Fig. 12.13). In some cases, the screw bends downwards, especially when it is unable to support a fracture surface below the screw due to fracture comminution. If a washer is not used to distribute the screw load to the bone, when the cortex is thin, the screw head will pass through the cortex near the greater trochanter. Finally, if the screws do not support well down through the fracture, they may rotate downwards, causing the femoral head to invert. Supporting the hypodermis with at least one screw is a mature clinical technique that may help prevent this from happening.

6.1.2 Fixation Around the Metaphyseal Region of the Knee

Both supracondylar fractures of the femur and tibial plateau fractures are challengingly stable because they usually involve the fixation of multiple small cancellous bones [102–104]. Mechanically comparable alternative methods for supraorbital

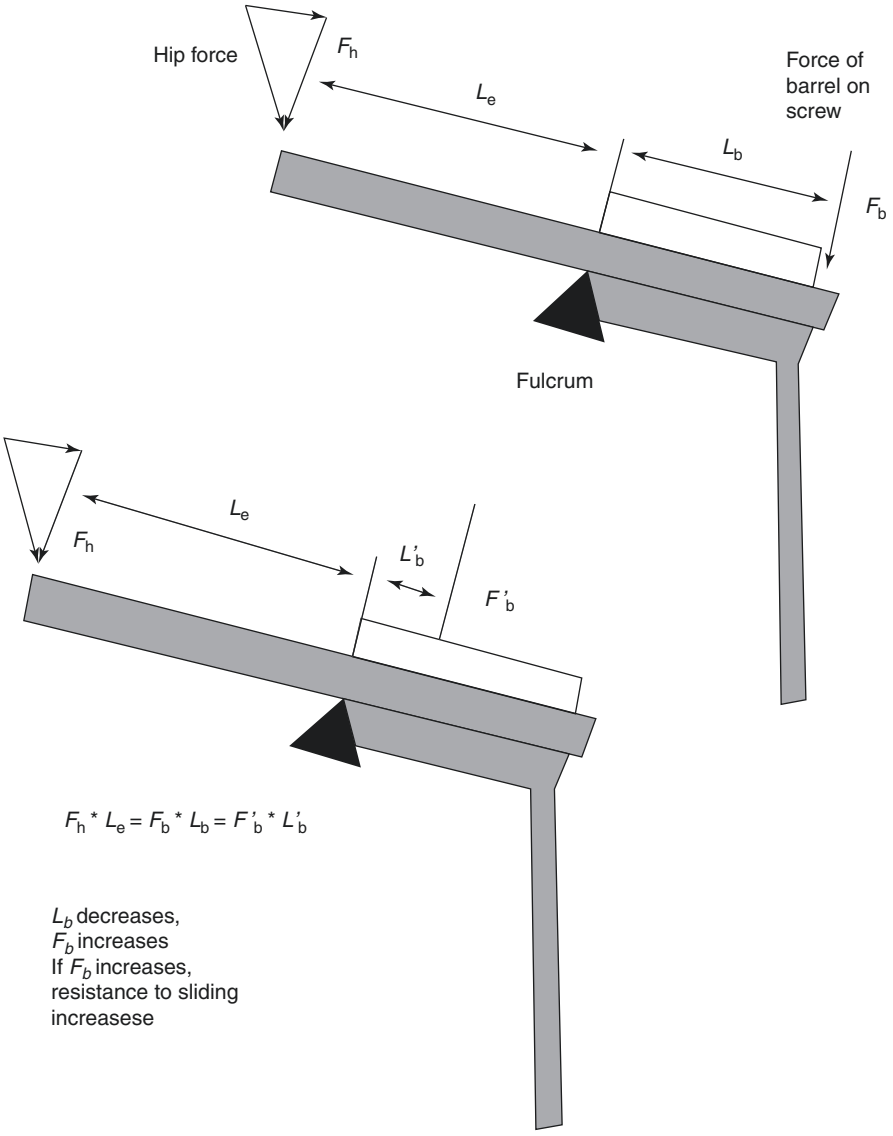

Fig. 12.12 The greater the length of the sliding screw within the barrel, the lower its resistance to sliding. In this diagram F_h is the component of the joint reaction force perpendicular to the axis of the screw. The inferior edge of the proximal end of the barrel is the location of the fulcrum in bending. An internal force, F_b from the surface of the barrel acts against the screw to counteract F_h. For equilibrium, the moments produced by $F_h(F_h \times L_e)$ and $F_b(F_b \times L_b)$ must be equal. If L_b, the distance from the point of application of internal force F_b to the fulcrum, decreases, F_b must increase to therefore the resistance to screw sliding will increase (L_e is the length of the screw beyond the barrel)

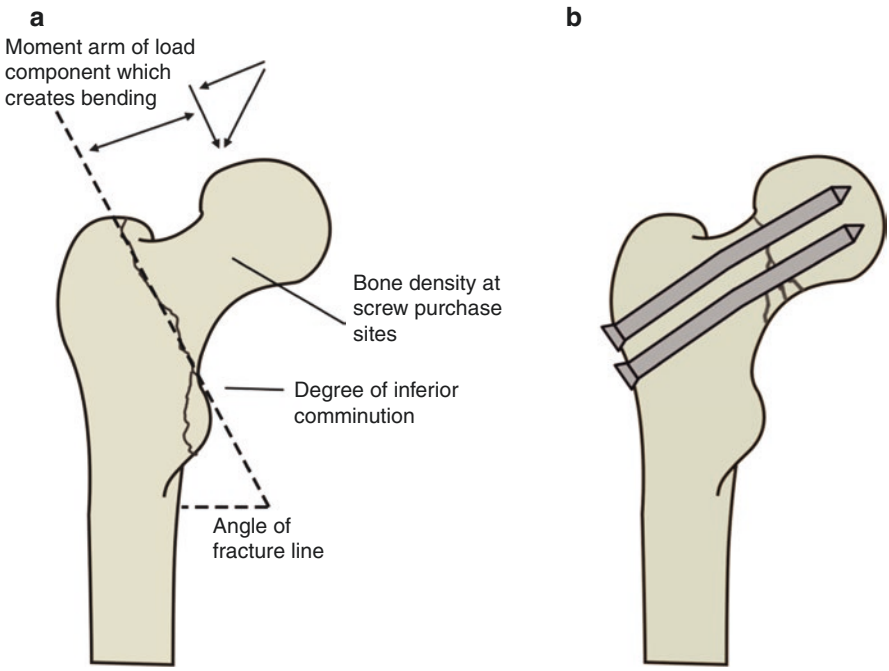

Fig. 12.13 (**a**) Some factors that decrease the strength of femoral neck fracture fixation include decreased bone density, a more vertical fracture surface (which reduces buttressing against bending), and a longer moment arm or distance of the center of the femoral head to the fracture line. (**b**) Observed mechanisms of failure of femoral neck fixation using screws include bending of the pins, displacement of the screw heads through the thin cortex of the greater trochanter, especially if washers are not used, and rotation of the screws inferiorly through the low-density cancellous bone of the Ward triangle area until they settle against the inferior cortex

fixation include condylar plates, plates and plates that use lag screws at the fracture site. All equipment tests seem to provide similar structural stiffness [105–108]. The most important factor in determining plate fixation is to maintain contact at the cortex opposite the fixture. A fixed structure without cortical contact is only 20% harder than a fixed structure with cortical support. It has been found that the use of a retrograde IM supracondylar nail results in a 14% reduction in axial compression strength and a 17% reduction in torsional strength compared to fixed-angle side panels. However, longer nails (36 cm) enhance fixation stability compared to shorter nails (20 cm). Several new fixation systems have been described as stable for supracondylar fractures of the femur. The Minimally Invasive Stabilization System (LISS) uses a low profile plate with a single cortical screw distal end, which is also locked to the plate. Compared to a conical screw or a support plate, the LISS plate produces a structure with greater elastic deformation and less sedimentation.

The tibial plateau fracture is difficult to stabilize [109–111]. Given the patient's prognosis, risk factors for reduced reduction have been shown to include patients older than 60 years, premature weight bearing, fracture comminution, and severe

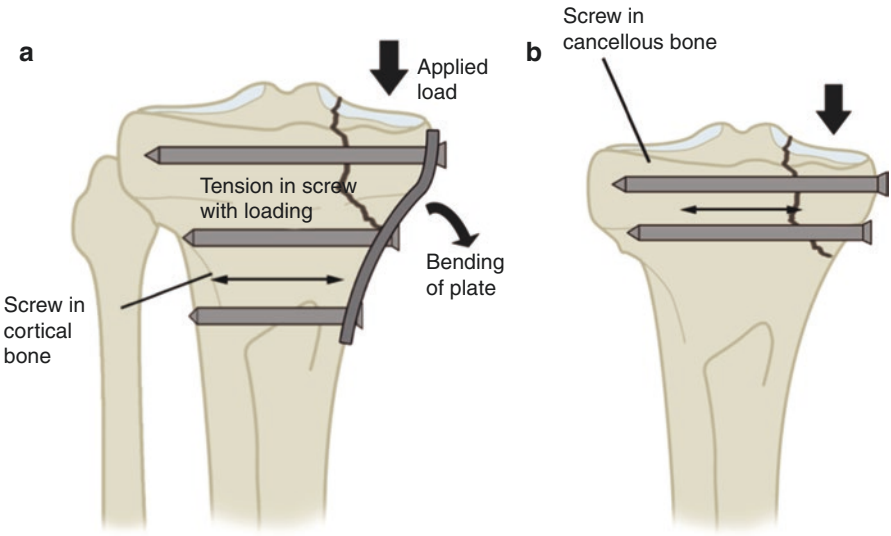

Fig. 12.14 Two alternative methods of fixation of tibial plateau fractures: (**a**) transverse screws combined with a buttress plate and (**b**) transverse screws alone. The buttress plate provides additional support in bending as the tibial fracture component is loaded in an inferior direction and allows the screws to engage the thicker, more distal cortical bone

osteoporosis [112–114]. Different fixing methods include using a wire or screw alone (Fig. 12.14), [115, 116] or placing a screw through an L-shaped or t-shaped plate to support the cortex. Wires of various shapes have been tested and the results show that the stiffness of the structure increases with the number of wires, regardless of the direction of the wires. As shown in Fig. 12.14, when the screw is used alone and the tibia fragments are pressed to the distal end through the joint, the screw needs to resist the bending force. By adding plates, not only the load is distributed to the plate, but also additional screws can be placed at the distal end of the cortical bone, which is stronger at the metaphysis of the humerus. One disadvantage of the support plate is that it requires peeling off the soft tissue during application, [117–120] which may compromise the blood supply [121–124]. Regardless of the specific configuration of the screw, the I-plate and screw fixing are most resistant to axial compression loads. Studies of different plate configurations have found that for bilateral tibial plateau fractures, bilateral (outer and medial) plates can reduce sag by about 50% under axial loading compared to single-sided locking plates. For the medial platform fracture, the medial support plate directly supports the load, and its mechanical properties are significantly better than the outer locking plate. A new option is the proximal humerus staple with multiple interlocking screws. Under the combined action of axial load, bending and rotation, the stability of the nail is equivalent to double steel plate, which is higher than the use of locking steel plate, external fixator or traditional tibial nail. The device can be used in cases without significant proximal (joint) comminution [125, 126].

6.1.3 Fixation of the Humerus

Proximal humerus fractures fixed with a locking plate provided greater stability against torsional loading, but is similar to blade plate structure when bent, as both fixation devices are loaded as tension bands in bending [127]. When comparing different types of blade plate structures, the hardest structure uses an eight-hole, low-contact dynamic compression plate that is shaped into the shape of the blade and secured with a diagonal screw that is triangular to the end of the blade. This arrangement is quite harder than other blade plates or T-plate and screw structures. A potential problem is the screw penetration of the subchondral bone in patients with osteoporosis. Due to the stiffness of the locking plate-screw structure, if there is any "settling" in the fracture site, the locking screw may penetrate the joint. The incidence of intra-articular screw penetration in the proximal humeral locking plate was significantly higher than that of conventional implants [14].

6.1.4 Fixation of Spine

For the treatment of spinal fractures, the goals are to reduce the fracture, protect the neurological function, and accelerate functional recovery [128]. The theory of 3-column model is the basis of the treatment rationale in spinal fractures [129]. Injuries that represent 3-column instability require operative stabilization even if there is no neurological deficit. The attachments of spinal fixation system consist of hooks, wires and screws, which produce different types of holding force [130, 131]. Wires could resist tension, hooks could resist driving force against the bone, while screws could resist forces from all directions except rotation. Therefore, screws are widely used for spinal fixation because of the superiority.

Posterior internal fixation system with pedicle screws has become popular for the treatment of spinal fracture. When applying lumbar spinal fixation, some principles can be considered. Screws are vulnerable to toggling when they are placed into pedicles. The screw tends to toggle about the base of the pedicle because of the cortical bone. In order to reduce toggling, the screw head should be locked to the rod of plate (Fig. 12.15).

Longer fixation could reduce forces acting on the screws because of the effect of the greater lever arm of a longer rod along with more vertebrae. Whereas it is not beneficial for a clinical perspective because the reduced spinal motion. It is also important to add a fusion cage to reduce forces in the fixation. Coupler bars could connect the fixation rods to form an *H* configuration, and prevent the rods from rotating medially or laterally, as shown in (Fig. 12.16). The coupler bars could significantly enhance the torsional and lateral bending stability of the implant.

6.1.5 Fixation for Pelvic Fractures

68.3% of pelvic fractures are unstable fractures, which are serious injuries, and the mortality rate is up to 19%. The stability of the pelvis is mainly related to the integrity of posterior pelvic ring. There are many methods available, including iliosacral

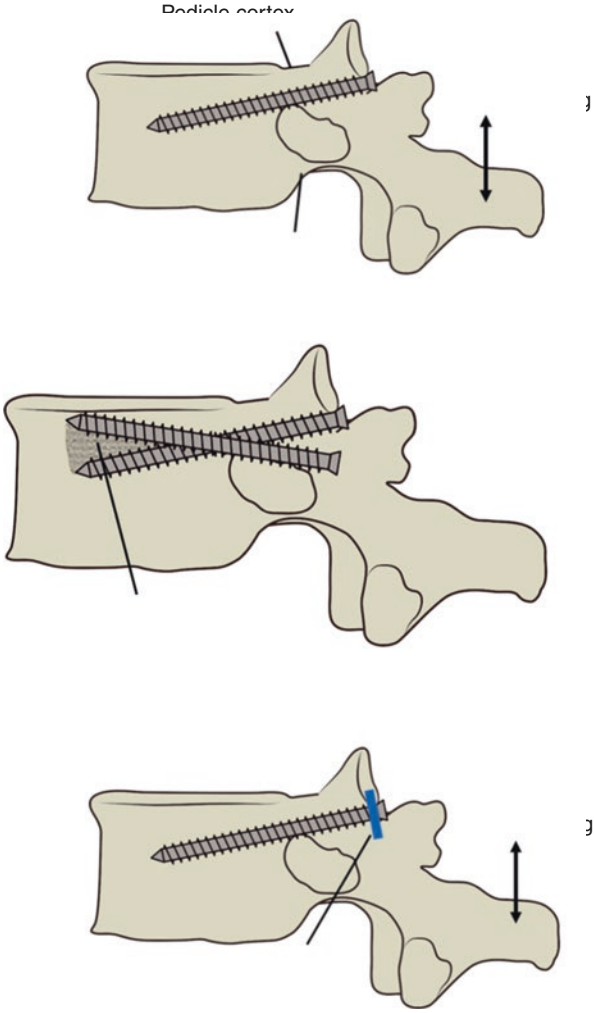

Fig. 12.15 (**a**) The mechanism of toggling of a single pedicle screw subjected to a caudocephalad loading. (**b**) The fulcrum is at the base of the pedicle, the narrowest region with little cancellous bone. The screw toggle compresses the bone within the vertebral body. (**c**) Toggling is reduced if the plate or rod to which the screw connects contacts the vertebra over a wide surface, which prevents it from rotating, whereas the screw head is locked to the plate or rod

(IS) screws, sacral bars, tension band plate (TBP), triangular osteosynthesis, and so on. IS screw fixation is a well-recognized technique for treating the posterior pelvic ring disruption. It is implanted in the supine or prone position and has such merits as short operative time, slight trauma, and minimal invasion. However, it remains a technically demanding procedure, and both doctors and patients are exposed to large amounts of radiation as continuous fluoroscopic or computerized tomography (CT) guidance for appropriate screw insertion. In addition, higher rates of iatrogenic injury is one of the disadvantages, seriously affecting the clinical use of this technology. To avoid these limitations, our team developed a novel minimally invasive adjustable plate (MIAP) (Fig. 12.17). This MIAP is designed according to the anatomy of the pelvic ring and simulated the sacroiliac complex structure of "bridge." It can be better attached the posterior aspect of the sacroiliac joint without bending and adjusted the length of the connecting rod to pressure or separation of

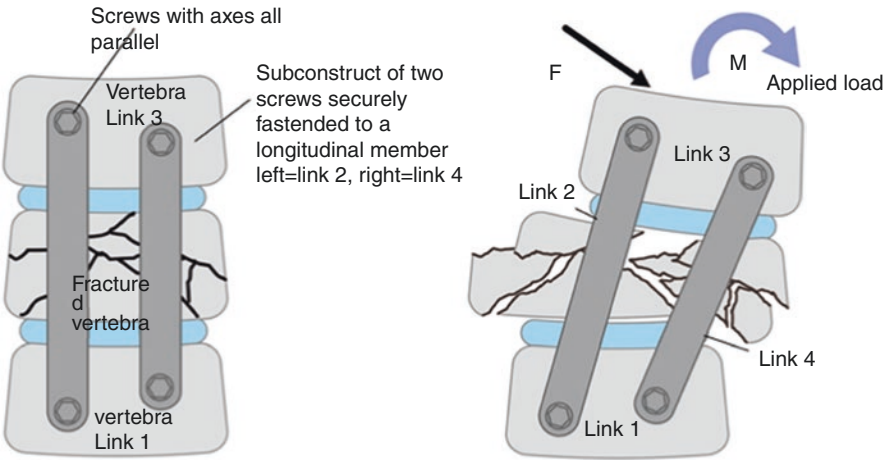

Fig. 12.16 Without a coupler bar between two longitudinal rods (left), they can rotate when a lateral moment or axial torsion is applied (right). A coupler connecting the rods to form an *H* configuration reduces this effect

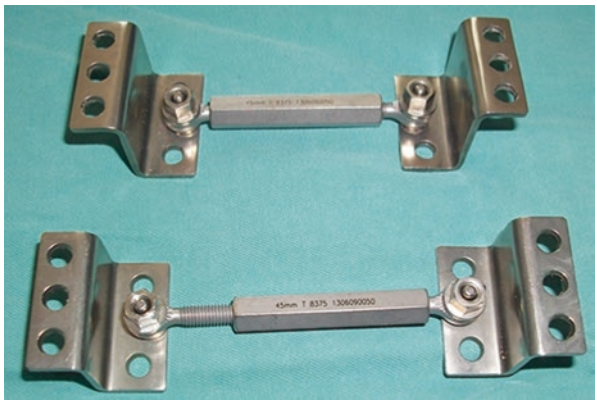

Fig. 12.17 Structure of MIAP for posterior pelvic ring injury

fracture end. Moreover, during the operation, two small incision were made for placing the MIAP, which can effectively reduce the blood loss and shortened the operation time.

6.1.6 Fixation for Tibiofibular Syndesmosis Injuries

Operative fixation and anatomic reconstruction of the distal tibiofibular syndesmosis is important to achieving an optimal outcome. An ideal implant to stabilize the tibiofibular syndesmosis should allow early mobilization for weight-bearing and be strong enough to maintain reduction in the syndesmosis. The screw fixation has been considered the standard management which can provide rigidity of the distal tibiofibular syndesmosis and easily be performed. However, this rigid fixation may reduce the physiologic motion of the syndesmosis and the screw breakage may

occur. In recent years, the suture button as a flexible fixation has been applied. The suture button allows physiologic motion in the tibiofibular joint and maintains the reduction of the ankle. However, the suture between buttons can gradually release under daily motion. To avoid these drawbacks, our team developed a novel technique called "bionic fixation" (Fig. 12.18). The screw segment may afford an improved rigidity and stability. The high strength non-absorbable suture located between the

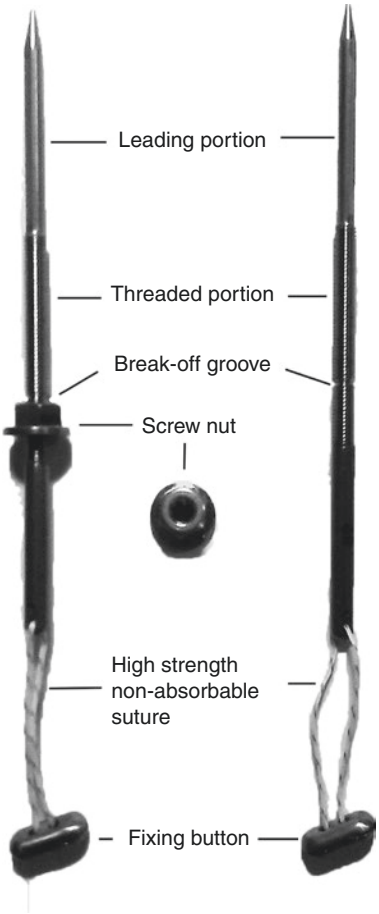

Fig. 12.18 (**1**): Schematic diagrams showing the bionic fixation construct (**2**): Schematic diagrams showing the three techniques for fixation of the tibiofibular syndesmosis. (*a*) A hole was drilled with a 2.8-mm drill bit from posterolateral fibula to anteromedial tibia. (*b*, *c*) A 3.5-mm cortical screw was then inserted through the hole from the fibular side. (*d*) After the cortical screw was removed, the hole was over-drilled with a 4.0-mm drill bit. (*e*) A 3.5-mm main screw was passed through the hole from the fibular side and the fixing button of the screw-tail was tightly attached to the fibula, then the screw nut was installed and adjusted on the tibial side to make the construct tightened properly. (*f*) The exposed leading portion of the screw was broken off. (*g*) The bionic fixation construct was removed. (*h*) The non-absorbable suture of the fixing construct was pulled from the fibular side to the tibial side. (*i*) The suture was threaded into the tibial button, looped, traversed through and securely tied over the fibular button. This process was repeated until there were three independent groups of sutures in the channel

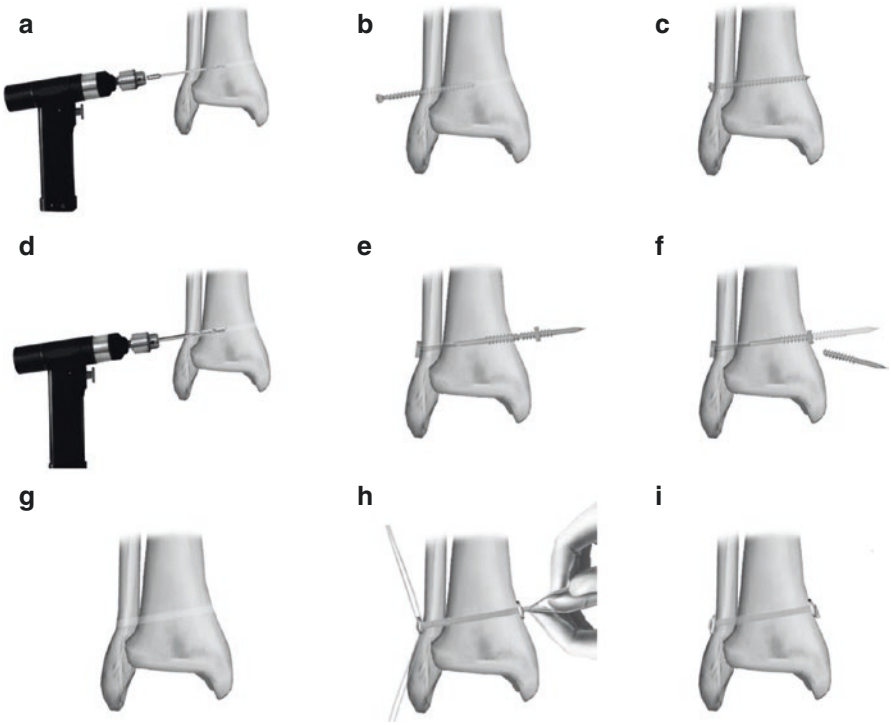

Fig. 12.18 (continued)

tibia and fibula may retain the motion of the syndesmosis to the maximum degree. Comparing with the Endo button fixation, the bionic fixation can provide more stable fixation force and retaining the motion function of syndesmosis. Besides, this technique has a low cost and is easy to perform.

6.1.7 Fixation for Posterior Column Acetabular Fractures

Operative reduction and internal fixation is the standard treatment for unstable posterior column acetabular fractures to allow early mobilization and decrease the risk of posttraumatic arthritis. The conventional methods of fixation involve lag screws and reconstruction plates, or both in combination. Conventional fixation depends on the structure of the acetabulum and the surgical technique because of the specific anatomy of posterior column of acetabulum. The conventional reconstruction plates need to be bended based on the size of the size of the acetabulum. Using screws and two reconstruction plates to obtain better fixation is a potentially serious traumatic complication. Our team designed a W-shaped acetabular angular plate (WAAP) for posterior columns of the acetabulum fractures (Fig. 12.19). This novel fixation includes a W-shaped locking plate and the guide apparatus. Comparing with other

Fig. 12.19 The W-shaped acetabular angular plate. *R* right, *L* left

reconstruction plates, the WAAP provides some advantages. First, the WAAP is anatomically pre-contoured and could match the surface of the posterior acetabulum column properly. Second, the extended fixation range spans from the greater sciatic notch to the rim of the posterior acetabulum. Third, the WAAP has locking holes which can achieve angular stability.

References

1. Agel J, Rockwood T, Barber R, Marsh JL. Potential predictive ability of the orthopaedic trauma association open fracture classification. J Orthop Trauma. 2014;28:300–6.
2. Centers for Disease Control and Prevention. Fatalities and injuries from falls among older adults—United States, 1993–2003 and 2001–2005. MMWR Morb Mortal Wkly Rep. 2006;55:1221–4.
3. Glatt V, Bartnikowski N, Quirk N, Schuetz M, Evans C. Reverse dynamization: influence of fixator stiffness on the mode and efficiency of large-bone-defect healing at different doses of rhBMP-2. J Bone Joint Surg Am. 2016;98:677–87.
4. Bonyun M, Nauth A, Egol KA, et al. Hot topics in biomechanically directed fracture fixation. J Orthop Trauma. 2014;28(Suppl 1):S32–5.
5. Carter DR, Blenman PR, Beaupre GS. Correlations between mechanical stress history and tissue differentiation in initial fracture healing. J Orthop Res. 1988;6:736–48.
6. Carter DR, Wong M. The role of mechanical loading histories in the development of diarthrodial joints. J Orthop Res. 1988;6:804–16.
7. Crichlow RJ, Andres PL, Morrison SM, Haley SM, Vrahas MS. Depression in orthopaedic trauma patients. Prevalence and severity. J Bone Joint Surg Am. 2006;88:1927–33.
8. Giorgi M, Verbruggen SW, Lacroix D. In silico bone mechanobiology: modeling a multifaceted biological system. Wiley Interdiscip Rev Syst Biol Med. 2016;8:485–505.
9. Boerckel JD, Uhrig BA, Willett NJ, Huebsch N, Guldberg RE. Mechanical regulation of vascular growth and tissue regeneration in vivo. Proc Natl Acad Sci U S A. 2011;108:E674–80.
10. Arazi M, Yalcin H, Tarakcioglu N, Dasci Z, Kutlu A. The effects of dynamization and destabilization of the external fixator on fracture healing: a comparative biomechanical study in dogs. Orthopedics. 2002;25:521–4.
11. Augat P, Burger J, Schorlemmer S, Henke T, Peraus M, Claes L. Shear movement at the fracture site delays healing in a diaphyseal fracture model. J Orthop Res. 2003;21:1011–7.
12. Augat P, Simon U, Liedert A, Claes L. Mechanics and mechano-biology of fracture healing in normal and osteoporotic bone. Osteoporos Int. 2005;16(Suppl 2):S36–43.

13. Bizzarri M, Palombo A, Cucina A. Theoretical aspects of systems biology. Prog Biophys Mol Biol. 2013;112:33–43.
14. Adamczyk MJ, Riley PM. Delayed union and nonunion following closed treatment of diaphyseal pediatric forearm fractures. J Pediatr Orthop. 2005;25:51–5.
15. Anderson R. A new method of treating fractures in the distal third of the femur. Can Med Assoc J. 1935;32:625–9.
16. Bassuener SR, Mullis BH, Harrison RK, Sanders R. Use of bioabsorbable pins in surgical fixation of comminuted periarticular fractures. J Orthop Trauma. 2012;26:607–10.
17. Flannery W, Balts J, McCarthy JJ, Swick J, Noonan KJ, Olson J. Are terminally threaded guide pins from cannulated screw systems dangerous? Orthopedics. 2011;34:e374–7.
18. Bottlang M, Doornink J, Fitzpatrick DC, Madey SM. Far cortical locking can reduce stiffness of locked plating constructs while retaining construct strength. J Bone Joint Surg Am. 2009;91:1985–94.
19. Barber FA, Dockery WD. Long-term absorption of poly-L-lactic acid interference screws. Arthroscopy. 2006;22:820–6.
20. Downey MW, Kosmopoulos V, Carpenter BB. Fully threaded versus partially threaded screws: determining shear in Cancellous bone fixation. J Foot Ankle Surg. 2015;54:1021–4.
21. De Bastiani G, Aldegheri R, Renzi Brivio L. The treatment of fractures with a dynamic axial fixator. J Bone Joint Surg Br. 1984;66:538–45.
22. Claes L, Augat P, Suger G, Wilke HJ. Influence of size and stability of the osteotomy gap on the success of fracture healing. J Orthop Res. 1997;15:577–84.
23. Aalto K, Holmstrom T, Karaharju E, Joukainen J, Paavolainen P, Slatis P. Fracture repair during external fixation. Torsion tests of rabbit osteotomies. Acta Orthop Scand. 1987;58:66–70.
24. Chrisovitsinos JP, Xenakis T, Papakostides KG, Skaltsoyannis N, Grestas A, Soucacos PN. Bridge plating osteosynthesis of 20 comminuted fractures of the femur. Acta Orthop Scand Suppl. 1997;275:72–6.
25. Harbacheuski R, Fragomen AT, Rozbruch SR. Does lengthening and then plating (LAP) shorten duration of external fixation? Clin Orthop Relat Res. 2012;470:1771–81.
26. Stoffel K, Dieter U, Stachowiak G, Gachter A, Kuster MS. Biomechanical testing of the LCP—how can stability in locked internal fixators be controlled? Injury. 2003;34(Suppl 2):B11–9.
27. Xu GH, Liu B, Zhang Q, et al. Biomechanical comparison of gourd-shaped LCP versus LCP for fixation of comminuted tibial shaft fracture. J Huazhong Univ Sci Technol Med Sci. 2013;33(2):250–7.
28. Xu G, Chen W, Zhang Q, et al. Flexible fixation of syndesmotic diastasis using the assembled bolt-tightrope system. Scand J Trauma Resusci Emerg Med. 2013;21(1):1–9.
29. Gautier E, Sommer C. Guidelines for the clinical application of the LCP. Injury. 2003;34(Suppl 2):B63–76.
30. Wang H, Yang Z, Wu Z, et al. A biomechanical comparison of conventional versus an anatomic plate and compression bolts for fixation of intra-articular calcaneal fractures. J Huazhong Univ Sci Technol Med Sci. 2012;32(4):571–5.
31. Uhthoff HK, Finnegan M. The effects of metal plates on post-traumatic remodelling and bone mass. J Bone Joint Surg Br. 1983;65:66–71.
32. Uhthoff HK, Poitras P, Backman DS. Internal plate fixation of fractures: short history and recent developments. J Orthop Sci. 2006;11:118–26.
33. Lujan TJ, Henderson CE, Madey SM, Fitzpatrick DC, Marsh JL, Bottlang M. Locked plating of distal femur fractures leads to inconsistent and asymmetric callus formation. J Orthop Trauma. 2010;24:156–62.
34. Eichinger JK, Herzog JP, Arrington ED. Analysis of the mechanical properties of locking plates with and without screw hole inserts. Orthopedics. 2011;34:19.
35. Nahm NJ, Como JJ, Wilber JH, Vallier HA. Early appropriate care: definitive stabilization of femoral fractures within 24 hours of injury is safe in most patients with multiple injuries. J Trauma. 2011;71:175–85.

36. Schreiber VM, Tarkin IS, Hildebrand F, et al. The timing of definitive fixation for major fractures in polytrauma—a matched-pair comparison between a US and European level I centres: analysis of current fracture management practice in polytrauma. Injury. 2011;42:650–4.
37. Stannard JP, Lopez-Ben RR, Volgas DA, et al. Prophylaxis against deep-vein thrombosis following trauma: a prospective, randomized comparison of mechanical and pharmacologic prophylaxis. J Bone Joint Surg Am. 2006;88:261–6.
38. Kempf I, Grosse A, Beck G. Closed locked intramedullary nailing. Its application to comminuted fractures of the femur. J Bone Joint Surg Am. 1985;67:709–20.
39. Lottes JO. Blind nailing technique for insertion of the triflange medullar nail: report of three hundred nailing for fractures of the shaft of the tibia. J Am Med Assoc. 1954;155:1039–42.
40. Ly TV, Travison TG, Castillo RC, Bosse MJ, MacKenzie EJ, Group LS. Ability of lower-extremity injury severity scores to predict functional outcome after limb salvage. J Bone Joint Surg Am. 2008;90:1738–43.
41. Makridis KG, Tosounidis T, Giannoudis PV. Management of infection after intramedullary nailing of long bone fractures: treatment protocols and outcomes. Open Orthop J. 2013;7:219–26.
42. Sassoon A, Riehl J, Rich A, et al. Muscle viability revisited: are we removing Normal muscle? A critical evaluation of dogmatic debridement. J Orthop Trauma. 2016;30:17–21.
43. Slobogean GP, O'Brien PJ, Brauer CA. Single-dose versus multiple-dose antibiotic prophylaxis for the surgical treatment of closed fractures. Acta Orthop. 2010;81:256–62.
44. Acker JH, Murphy C, D'Ambrosia R. Treatment of fractures of the femur with the Grosse-Kempf rod. Orthopedics. 1985;8:1393–401.
45. Basumallick MN, Bandopadhyay A. Effect of dynamization in open interlocking nailing of femoral fractures. A prospective randomized comparative study of 50 cases with a 2-year follow-up. Acta Orthop Belg. 2002;68:42–8.
46. Patton MS, Lyon TD, Ashcroft GP. Levels of systemic metal ions in patients with intramedullary nails. Acta Orthop. 2008;79:820–5.
47. Qin YX, Kaplan T, Saldanha A, Rubin C. Fluid pressure gradients, arising from oscillations in intramedullary pressure, is correlated with the formation of bone and inhibition of intracortical porosity. J Biomech. 2003;36:1427–37.
48. Tornetta P 3rd, Collins E. Semiextended position of intramedullary nailing of the proximal tibia. Clin Orthop Relat Res. 1996;328:185–9.
49. Tran W, Foran J, Wang M, Schwartz A. Postsurgical bleeding following treatment of a chronic Morel-Lavallee lesion. Orthopedics. 2008;31:814.
50. Rose DM, Smith TO, Nielsen D, Hing CB. Expandable intramedullary nails in lower limb trauma: a systematic review of clinical and radiological outcomes. Strategies Trauma Limb Reconstr. 2013;8:1–12.
51. Betz A, Baumgart R, Schweiberer L. [First fully implantable intramedullary system for callus distraction—intramedullary nail with programmable drive for leg lengthening and segment displacement principles and initial clinical results]. Chirurg. 1990;61:605–9.
52. Bong MR, Kummer FJ, Koval KJ, Egol KA. Intramedullary nailing of the lower extremity: biomechanics and biology. J Am Acad Orthop Surg. 2007;15:97–106.
53. Brumback RJ, Uwagie-Ero S, Lakatos RP, Poka A, Bathon GH, Burgess AR. Intramedullary nailing of femoral shaft fractures. Part II: fracture-healing with static interlocking fixation. J Bone Joint Surg Am. 1988;70:1453–62.
54. Utvag SE, Korsnes L, Rindal DB, Reikeras O. Influence of flexible nailing in the later phase of fracture healing: strength and mineralization in rat femora. J Orthop Sci. 2001;6:576–84.
55. Utvag SE, Reikeras O. Effects of nail rigidity on fracture healing. Strength and mineralisation in rat femoral bone. Arch Orthop Trauma Surg. 1998;118:7–13.
56. Uzer G, Thompson WR, Sen B, et al. Cell mechanosensitivity to extremely low-magnitude signals is enabled by a LINCed nucleus. Stem Cells. 2015;33:2063–76.
57. Uhthoff HK, Dubuc FL. Bone structure changes in the dog under rigid internal fixation. Clin Orthop Relat Res. 1971;81:165–70.

58. Cole JD, Justin D, Kasparis T, DeVlught D, Knobloch C. The intramedullary skeletal kinetic distractor (ISKD): first clinical results of a new intramedullary nail for lengthening of the femur and tibia. Injury. 2001;32(Suppl 4):SD129–39.
59. Cullinane DM, Fredrick A, Eisenberg SR, et al. Induction of a neoarthrosis by precisely controlled motion in an experimental mid-femoral defect. J Orthop Res. 2002;20:579–86.
60. Tigani D, Fravisini M, Stagni C, Pascarella R, Boriani S. Interlocking nail for femoral shaft fractures: is dynamization always necessary? Int Orthop. 2005;29:101–4.
61. Claes L, Blakytny R, Besse J, Bausewein C, Ignatius A, Willie B. Late dynamization by reduced fixation stiffness enhances fracture healing in a rat femoral osteotomy model. J Orthop Trauma. 2011;25:169–74.
62. Foxworthy M, Pringle RM. Dynamization timing and its effect on bone healing when using the Orthofix dynamic axial fixator. Injury. 1995;26:117–9.
63. Court-Brown CM, Gustilo T, Shaw AD. Knee pain after intramedullary tibial nailing: its incidence, etiology, and outcome. J Orthop Trauma. 1997;11:103–5.
64. Dietch ZC, Petroze RT, Thames M, Willis R, Sawyer RG, Williams MD. The “high-risk” deep venous thrombosis screening protocol for trauma patients: is it practical? J Trauma Acute Care Surg. 2015;79:970–5; discussion 975
65. Study to Prospectively Evaluate Reamed Intramedullary Nails in Patients with Tibial Fractures Investigators, Bhandari M, Guyatt G, et al. Randomized trial of reamed and unreamed intramedullary nailing of tibial shaft fractures. J Bone Joint Surg Am. 2008;90:2567–78.
66. Keating JF, O’Brien PJ, Blachut PA, Meek RN, Broekhuyse HM. Locking intramedullary nailing with and without reaming for open fractures of the tibial shaft. A prospective, randomized study. J Bone Joint Surg Am. 1997;79:334–41.
67. Klein P, Opitz M, Schell H, et al. Comparison of unreamed nailing and external fixation of tibial diastases—mechanical conditions during healing and biological outcome. J Orthop Res. 2004;22:1072–8.
68. Oh JK, Hwang JH, Sahu D, Jun SH. Complication rate and pitfalls of temporary bridging external fixator in periarticular communited fractures. Clin Orthop Surg. 2011;3:62–8.
69. Eggers GW. Internal contact splint. J Bone Joint Surg Am. 1948;30A:40–52.
70. Gerber C, Mast JW, Ganz R. Biological internal fixation of fractures. Arch Orthop Trauma Surg. 1990;109:295–303.
71. Lebel E, Blumberg N, Gill A, Merin O, Gelfond R, Bar-On E. External fixator frames as interim damage control for limb injuries: experience in the 2010 Haiti earthquake. J Trauma. 2011;71:E128–31.
72. Lenarz C, Bledsoe G, Watson JT. Circular external fixation frames with divergent half pins: a pilot biomechanical study. Clin Orthop Relat Res. 2008;466:2933–9.
73. Lerner A, Fodor L, Soudry M. Is staged external fixation a valuable strategy for war injuries to the limbs? Clin Orthop Relat Res. 2006;448:217–24.
74. Eijer H, Hauke C, Arens S, Printzen G, Schlegel U, Perren SM. PC-fix and local infection resistance—influence of implant design on postoperative infection development, clinical and experimental results. Injury. 2001;32(Suppl 2):B38–43.
75. Paffrath T, Lefering R, Flohe S, TraumaRegister DGU. How to define severely injured patients?—an injury severity score (ISS) based approach alone is not sufficient. Injury. 2014;45(Suppl 3):S64–9.
76. Pape HC, Tornetta P 3rd, Tarkin I, Tzioupis C, Sabeson V, Olson SA. Timing of fracture fixation in multitrauma patients: the role of early total care and damage control surgery. J Am Acad Orthop Surg. 2009;17:541–9.
77. Park SH, O’Connor K, Sung R, McKellop H, Sarmiento A. Comparison of healing process in open osteotomy model and closed fracture model. J Orthop Trauma. 1999;13:114–20.
78. Gomez-Benito MJ, Garcia-Aznar JM, Kuiper JH, Doblare M. A 3D computational simulation of fracture callus formation: influence of the stiffness of the external fixator. J Biomech Eng. 2006;128:290–9.
79. Siguier T, Glorion C, Langlais J, Rouvreau P, Pouliquen JC. External fixation in fractures of the lower limb in children. Rev Chir Orthop Reparatrice Appar Mot. 1995;81:157–62.

80. Marsh JL, Nepola JV, Wuest TK, Osteen D, Cox K, Oppenheim W. Unilateral external fixation until healing with the dynamic axial fixator for severe open tibial fractures. J Orthop Trauma. 1991;5:341–8.
81. Paley D. PRECICE intramedullary limb lengthening system. Expert Rev Med Devices. 2015;12:231–49.
82. Gardner TN, Evans M, Kenwright J. The influence of external fixators on fracture motion during simulated walking. Med Eng Phys. 1996;18:305–13.
83. Huang C, Ogawa R. Mechanotransduction in bone repair and regeneration. FASEB J. 2010;24:3625–32.
84. Ilizarov GA. The principles of the Ilizarov method. Bull Hosp Jt Dis Orthop Inst. 1988;48:1–11.
85. Ilizarov GA, Frankel VH. The Ilizarov external fixator, a physiologic method of orthopaedic reconstruction and skeletal correction. A conversation with Prof. G. A. Ilizarov and Victor H. Frankel. Orthop Rev. 1988;17:1142–54.
86. Gandhi RR, Overton TL, Haut ER, et al. Optimal timing of femur fracture stabilization in polytrauma patients: a practice management guideline from the eastern Association for the Surgery of trauma. J Trauma Acute Care Surg. 2014;77:787–95.
87. Gillespie WJ, Walenkamp GH. Antibiotic prophylaxis for surgery for proximal femoral and other closed long bone fractures. Cochrane Database Syst Rev. 2010;(3):CD000244.
88. Ozaki A, Tsunoda M, Kinoshita S, Saura R. Role of fracture hematoma and periosteum during fracture healing in rats: interaction of fracture hematoma and the periosteum in the initial step of the healing process. J Orthop Sci. 2000;5:64–70.
89. Pacicca DM, Moore DC, Ehrlich MG. Physiologic weight-bearing and consolidation of new bone in a rat model of distraction osteogenesis. J Pediatr Orthop. 2002;22:652–9.
90. Wu CC. The effect of dynamization on slowing the healing of femur shaft fractures after interlocking nailing. J Trauma. 1997;43:263–7.
91. Domb BG, Sponseller PD, Ain M, Miller NH. Comparison of dynamic versus static external fixation for pediatric femur fractures. J Pediatr Orthop. 2002;22:428–30.
92. Farouk O, Krettek C, Miclau T, Schandelmaier P, Tscherne H. Effects of percutaneous and conventional plating techniques on the blood supply to the femur. Arch Orthop Trauma Surg. 1998;117:438–41.
93. Glatt V, Evans CH, Matthys R. Design, characterisation and in vivo testing of a new, adjustable stiffness, external fixator for the rat femur. Eur Cell Mater. 2012;23:289–98.. discussion 299
94. Glatt V, Miller M, Ivkovic A, et al. Improved healing of large segmental defects in the rat femur by reverse dynamization in the presence of bone morphogenetic protein-2. J Bone Joint Surg Am. 2012;94:2063–73.
95. Glatt V, Tepic S, Evans C. Reverse dynamization: a novel approach to bone healing. J Am Acad Orthop Surg. 2016;24:e60–1.
96. Nickerson TP, Zielinski MD, Jenkins DH, Schiller HJ. The Mayo Clinic experience with Morel-Lavallee lesions: establishment of a practice management guideline. J Trauma Acute Care Surg. 2014;76:493–7.
97. Verkerke GJ, Schraffordt Koops H, Veth RP, et al. Design of a lengthening element for a modular femur endoprosthetic system. Proc Inst Mech Eng H. 1989;203:97–102.
98. Wang L, Li JY, Zhang XZ, et al. Involvement of p38MAPK/NF-kappaB signaling pathways in osteoblasts differentiation in response to mechanical stretch. Ann Biomed Eng. 2012;40:1884–94.
99. Wang Q, Huang C, Xue M, Zhang X. Expression of endogenous BMP-2 in periosteal progenitor cells is essential for bone healing. Bone. 2011;48:524–32.
100. Weyts FA, Bosmans B, Niesing R, van Leeuwen JP, Weinans H. Mechanical control of human osteoblast apoptosis and proliferation in relation to differentiation. Calcif Tissue Int. 2003;72:505–12.
101. Wolf S, Janousek A, Pfeil J, et al. The effects of external mechanical stimulation on the healing of diaphyseal osteotomies fixed by flexible external fixation. Clin Biomech (Bristol, Avon). 1998;13:359–64.

102. Haas N, Hauke C, Schutz M, Kaab M, Perren SM. Treatment of diaphyseal fractures of the forearm using the point contact fixator (PC-fix): results of 387 fractures of a prospective multicentric study (PC-fix II). Injury. 2001;32(Suppl 2):B51–62.
103. Hak DJ, Toker S, Yi C, Toreson J. The influence of fracture fixation biomechanics on fracture healing. Orthopedics. 2010;33:752–5.
104. Hake ME, Young H, Hak DJ, Stahel PF, Hammerberg EM, Mauffrey C. Local antibiotic therapy strategies in orthopaedic trauma: practical tips and tricks and review of the literature. Injury. 2015;46:1447–56.
105. Goodship AE, Kenwright J. The influence of induced micromovement upon the healing of experimental tibial fractures. J Bone Joint Surg Br. 1985;67:650–5.
106. Klein P, Schell H, Streitparth F, et al. The initial phase of fracture healing is specifically sensitive to mechanical conditions. J Orthop Res. 2003;21:662–9.
107. Klein-Nulend J, Bakker AD, Bacabac RG, Vatsa A, Weinbaum S. Mechanosensation and transduction in osteocytes. Bone. 2013;54:182–90.
108. Konda SR, Lack WD, Seymour RB, Karunakar MA. Mechanism of injury differentiates risk factors for mortality in geriatric trauma patients. J Orthop Trauma. 2015;29:331–6.
109. Gorman SC, Kraus KH, Keating JH, et al. In vivo axial dynamization of canine tibial fractures using the Securos external skeletal fixation system. Vet Comp Orthop Traumatol. 2005;18:199–207.
110. Grundnes O, Reikeras O. Effects of instability on bone healing. Femoral osteotomies studied in rats. Acta Orthop Scand. 1993;64:55–8.
111. Haller JM, Holt D, Rothberg DL, Kubiak EN, Higgins TF. Does early versus delayed spanning external fixation impact complication rates for high-energy Tibial plateau and plafond fractures? Clin Orthop Relat Res. 2016;474:1436–44.
112. Young H, Topliss C. Complications associated with the use of a titanium tibial nail. Injury. 2007;38:223–6.
113. Zucman J, Maurer P. Two-level fractures of the tibia. Results in thirty-six cases treated by blind nailing. J Bone Joint Surg Br. 1969;51:686–93.
114. Wang L, Zhang Y, Song Z, et al. A novel method of using elastic bionic fixation device for distal tibiofibular syndesmosis injury. Int Orthop. 2018;42(9):2219–29.
115. Tejwani SG, Cohen SB, Bradley JP. Management of Morel-Lavallee lesion of the knee: twenty-seven cases in the national football league. Am J Sports Med. 2007;35:1162–7.
116. Thompson WR, Rubin CT, Rubin J. Mechanical regulation of signaling pathways in bone. Gene. 2012;503:179–93.
117. Marsh JL, Slongo TF, Agel J, et al. Fracture and dislocation classification compendium—2007: orthopaedic trauma association classification, database and outcomes committee. J Orthop Trauma. 2007;21:S1–133.
118. Marumo K, Sato Y, Suzuki H, Kurosaka D. MRI study of bioabsorbable poly-L-lactic acid devices used for fixation of fracture and osteotomies. J Orthop Sci. 2006;11:154–8.
119. Morgan EF, Gleason RE, Hayward LN, Leong PL, Palomares KT. Mechanotransduction and fracture repair. J Bone Joint Surg Am. 2008;90(Suppl 1):25–30.
120. Wang B, Zheng Z, Liu H, et al. The preliminary clinical application of Zhang' compression bolt for treatment of tibial plateau fracture. J Hebei Med Univ. 2018;
121. Farouk O, Krettek C, Miclau T, Schandelmaier P, Guy P, Tscherne H. Minimally invasive plate osteosynthesis: does percutaneous plating disrupt femoral blood supply less than the traditional technique? J Orthop Trauma. 1999;13:401–6.
122. Jansen JH, Weyts FA, Westbroek I, et al. Stretch-induced phosphorylation of ERK1/2 depends on differentiation stage of osteoblasts. J Cell Biochem. 2004;93:542–51.
123. Kato M, Namikawa T, Terai H, Hoshino M, Miyamoto S, Takaoka K. Ectopic bone formation in mice associated with a lactic acid/dioxanone/ethylene glycol copolymer-tricalcium phosphate composite with added recombinant human bone morphogenetic protein-2. Biomaterials. 2006;27:3927–33.

124. Kelly DJ, Jacobs CR. The role of mechanical signals in regulating chondrogenesis and osteogenesis of mesenchymal stem cells. Birth Defects Res C Embryo Today. 2010;90:75–85.
125. Hente R, Cordey J, Rahn BA, Maghsudi M, von Gumppenberg S, Perren SM. Fracture healing of the sheep tibia treated using a unilateral external fixator. Comparison of static and dynamic fixation. Injury. 1999;30(Suppl 1):A44–51.
126. Huang Z, Wang B, Chen F, et al. Fast pinless external fixation for open tibial fractures: preliminary report of a prospective study. Int J Clin Exp Med. 2015;8:20805–12.
127. Gardner MJ, Griffith MH, Demetrakopoulos D, et al. Hybrid locked plating of osteoporotic fractures of the humerus. J Bone Joint Surg Am. 2006;88:1962–7.
128. Garwe T, Cowan LD, Neas B, Cathey T, Danford BC, Greenawalt P. Survival benefit of transfer to tertiary trauma centers for major trauma patients initially presenting to nontertiary trauma centers. Acad Emerg Med. 2010;17:1223–32.
129. Tanno M, Furukawa KI, Ueyama K, Harata S, Motomura S. Uniaxial cyclic stretch induces osteogenic differentiation and synthesis of bone morphogenetic proteins of spinal ligament cells derived from patients with ossification of the posterior longitudinal ligaments. Bone. 2003;33:475–84.
130. Yacoub AR, Joaquim AF, Ghizoni E, Tedeschi H, Patel AA. Evaluation of the safety and reliability of the newly-proposed AO spine injury classification system. J Spinal Cord Med. 2017;40:70–5.
131. Yanagisawa M, Suzuki N, Mitsui N, Koyama Y, Otsuka K, Shimizu N. Effects of compressive force on the differentiation of pluripotent mesenchymal cells. Life Sci. 2007;81:405–12.

Chapter 13
Biomechanical Principles in Designing Custom-Made Hip Prosthesis

Jia Hua

Abstract Total hip replacement has increasingly become popular in treating osteoarthritis, relieving pain, restoring joint function and correcting the deformities. However, due to the wide variations of the anatomy in femoral bone between individuals, the commonly used off-the-shelf standard hip stems cannot consistently achieve the good fit, thus the clinical outcome is compromised. On the other hand, an increasing demand for restoring the normal life quality after total hip replacement including play sports and other activities, especially with the coming era of the precision medicine and digital orthopaedics, and the availability of the advanced surgical navigation systems and 3-D printing technologies, the patient-specific hip prostheses have become ever favourable.

The rationale for using the custom stem is not only for the complex cases, but also for the routine cases in order to achieve better clinical outcomes and longer survivorship. This chapter will focus on how to design a custom hip stem for an individual patient based on the bone geometry, deformities and pathological conditions. The advantages and disadvantages of each design options are considered and analysed.

Keywords Hip joint arthroplasty · Total hip replacement · Design of hip stem
Custom hip stem · Osteoarthritis

1 Introduction

Constantly on the rise in quantities and qualities, total hip arthroplasty (THA) has become ever popular in the treatment of hip diseases, and in relieving pain, restoring function and correcting deformities [1]. THA is now one of the most successful surgical intervention in the century for improving life quality of the patients.

J. Hua (✉)
Department of Natural Science, Faculty of Science and Technology, Middlesex University, London, UK
e-mail: j.hua@mdx.ac.uk

C.-K. Cheng, S. L-Y. Woo (eds.), *Frontiers in Orthopaedic Biomechanics*,
https://doi.org/10.1007/978-981-15-3159-0_13

According to the 14th Annual Report of the National Joint Registry, over a hundred thousand hip surgeries were performed in 2016 across the UK except for Scotland, a 3.5% increase from the previous year, 90% of which were for the treatment of osteoarthritis [2]. The joint registry data from the USA showed that 443,219 hip surgeries have been reported between 2012 and 2017; among them revision surgeries accounted for 10.7% [3]. One of the concerns is that some of the revision surgeries were performed at very early stages after the first procedure, meaning that the revision patients are no longer old and inactive; some of them now fall into the physically active group, while the clinical results for revision THR are still inferior to that for primary THR [4]. In the past, most cases are performed using standard off-the-shelf hip stems; only a few of the very difficult cases have used the custom designed prosthesis to correct deformities and provide best stem fixation and better hip functions.

However, due to wide variations of anatomy in femoral bone and increasing demand for the normal function of the hip including sports activity, especially with the availability of the 3D printing technology, the patient-specific custom designed hip prostheses have become more favourable. This chapter will focus on how to design a custom hip stem for an individual patient based on their unique bone geometry, deformities and pathological conditions. For those readers who are not designing hip stems such as surgeons and researchers, may probably find the information in this chapter can also be very useful.

2 Design Consideration of a Custom Stem

2.1 Determination of Cortical Boundary from Images

In order to design a stem that can exactly fit with the femoral cavity, accurately determining the boundary of cortical bone from the images, either from normal X-rays or CT scan, is crucially important. Some of the factors can affect the determination of the boundary.

1. For normal plain X-ray images, it should normally include the pelvis and down to the knee joint on AP and lateral views, with the scaled ruler placed on the side of the femur at the level of the bone. The opposite side is ideally also included for comparison. This allows the designer to assess the leg length discrepancy, orientation of the knee and fixed deformities of the lumbar spine and the knee joint, as these may affect reconstruction of the new centre of the hip.
2. The images should be clear with adequate contrast, brightness and resolution in order for designers to identify the boundary, which involves proper adjustment of kV and exposure time. However, for digital X-rays that have now been exclusively used, the contrast and brightness can be manipulated on the screen; thus,

the line of boundary showed on the images could be altered as a result, which may not reflect the true boundary of the cortex. For using of CT scan, the determination of cortical boundary become critical.

3. Some of the other factors that could also affect the determination of the boundary are the nature of the diseases and the density of the bone. For example, young and active patients with osteoarthritis usually have hard bone, especially for a band of trabecular bone adjacent to the cortex, which are sometimes too hard to remove. On the other hand, for rheumatoid arthritis, the bone is quite softer, especially for those under treatment of steroids. Therefore, the cavity can easily be overreamed and the stem should be designed slightly tighter than normal. All these should be considered when assessing the boundary of cortex for designing custom hip stems.

2.2 Stem Design Inside Medullary Canal (Implant Fixation)

2.2.1 Fit and Fill of the Stem Inside the Cavity

To design a hip stem that achieves the best fit with the cavity is always considered to be of critical importance in order to obtain a long-term success of the surgery. This requires the geometry of the stem to match that of the femoral cavity. However, for a stem to reach 100% fill of the cavity is unpractical in which the stem will not be able to be inserted. Therefore, the designer should not only focus on which part of the bone the stem should fit with but also assess whether the stem can be inserted or not. In principle, the proximal medial curve of the femur in calcar region is regarded as the most priority region which requires an exact fit in order to achieve immediate stability of the stem and physiological stress transfer to the bone (Fig. 13.1). However, this design mostly depends on the condition of the bone being strong enough to carry the load.

The cortical bone on the lateral side of the femur is equally thick and strong as that on the medial side due to the tensile stress across this region when the bone is loaded. The lateral curve can provide stem with additional axial stability due to its wedge effect and avoid stem from valgus tilt over time. However, one of the considerations is how far should the stem follow the curve. This really depends on the position of the greater trochanter and how wide is the opening at the neck resection. If the greater trochanter is too medialized or the opening of the neck resection is too narrow, the lateral flare of the stem needs to be reduced in order to facilitate the insertion of the stem.

For the anterior part of the femur, the stem geometry should not completely follow the curve of the femur; otherwise the stem will be too thick to be inserted. Nevertheless, the anterior curve of the stem is very useful in enhancing the torsional stability when comparing with the thin and symmetrical design.

The design of the posterior part of the stem is simple; basically it is straight.

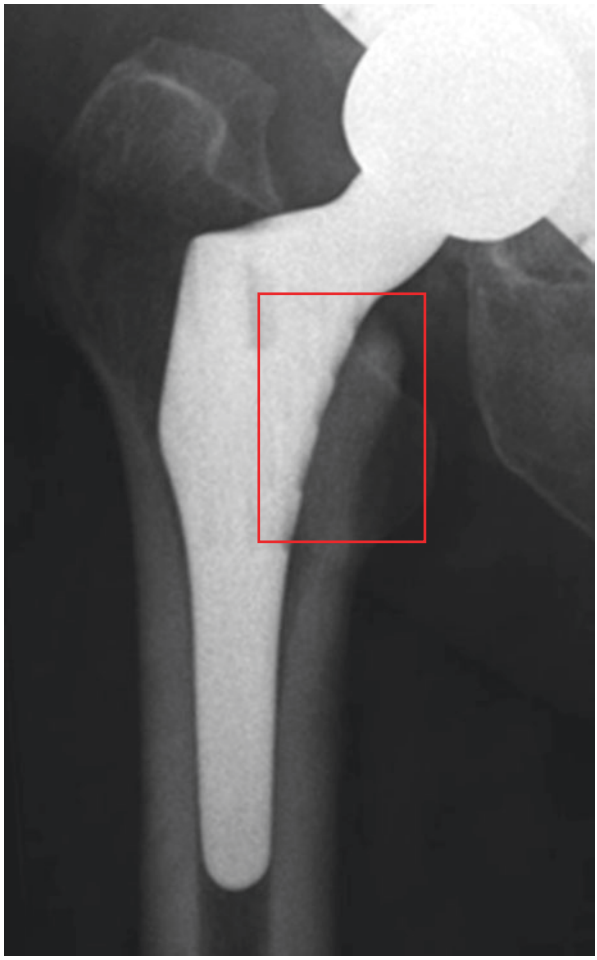

Fig. 13.1 Radiographic image shows the calcar region that a stem should always fit with in total hip replacement

2.2.2 The Length of Femoral Stems

From biomechanical and clinical points of view, the stem length should be as short as possible in order for the femoral cavity being least disturbed. The longer the stem, the more damage to the bone can occur, which leaves revision surgery more difficult. However, when the stem being too short it can cause instability and high stress concentration on the lateral bone at the tip of the stem. In most cases, if the stem geometry can match the normal proximal medial curve of the bone, a total length of 90–100 mm (around 2 cm below the lesser trochanter) should be adequate to provide stem stability as well as the physiological distribution of the stresses. This is because when the proximal stem is properly supported by the medial calcar bone, the stem tip will not be tilted under load and distribute lower contact stresses

to the bone. In this regard, the design of the short stem is adequate. However, if the stem fit in the calcar region is not appropriate or uncertain, then the length of the stem should be increased to engage more cavity in diaphyseal region to avoid stress concentration on the bone at the tip of the stem.

2.2.3 Determination of Stem Diameters

In most of the cases, to determine the diameter of the stem should be straightforward, which simply follows the diameter of the femoral canal. However, sometimes the diameter needs to be adjusted in certain circumstances. The reason for this is that the shape of the femoral cavity in the diaphyseal region is more likely oval, but the distal stem is usually in round shape, so that cross-section of the distal stem will not completely fit with the canal. Therefore, the diameter of the stem can be customized depending on how much bone can be overreamed on the narrow side.

In some unusual situations where the canal diameter is too small such as less than 6 mm while the patient has normal body weight, the stem diameter designed accordingly could cause a fracture. In this case, a deliberately overream of the bone may become necessary in order to increase the diameter of the stem, should the thickness of the cortical wall and quality of the bone be allowed. If in certain cases that the increase of the stem diameter being impossible which could cause weakness of the bone, reducing offset of the neck or changing the material of the implant such as using Cobalt Chrome instead become an alternative option.

On the other hand, if the diameter of the canal being too large such as over 16 mm, then the distal stem designed for may be too stiff that could lead to stress shielding of the bone. In order to reduce the stiffness of the stem, a few methods can be applied. One of the common methods is to make a slot in the middle of the stem, or to remove part of the metal on the medial side towards to distal so that the shape of the distal stem looks like a half-moon. Both designs can equally fulfil the purpose, but offer different biomechanical benefits, so which method should be applied depend on the actual cases.

2.3 Stem Design Outside Medullary Canal (Function of the Hip)

The design of the stems outside the medullary canal is basically to determine the centre of the femoral head that mainly involves the height, offset and angle of the femoral stem neck. Different stem neck angle can influence the range of motions of the hip joint and impingement between the neck of the stem and acetabular cup or pelvic bone. The neck angle for the standard implants are usually around 45°, or 135° in neck-shaft angle. However, the neck angle for a custom implant can vary, which depends on the anatomy of the particular patient and surgical requirement, so

that the height and offset of the femoral neck are adjusted in each case to suit for the patients. Nowadays, the modular femoral heads have been exclusively used; therefore if the angle of the neck is more vertical, then any plus heads will increase the height more than increasing the offset, and vice versa.

2.3.1 Height of the Femoral Head

One of the challenges in designing custom hip stem is to determine the height of the femoral head. It is always attempted to either maintain or equalize the leg length. In most of the cases, the contralateral side of the femoral head can be referenced for the affected side in order to make both leg lengths equal. However, if the leg length discrepancy is too large, then only partial correction may be possible in order to prevent overstretches of the nerves and vessels. For some of the cases, the soft tissues and joint capsule may need to be extensively released during surgery to allow for pulling down the leg and reducing the hip joint. In revision total hip replacements, the leg can normally be pulled down by 2.5 cm roughly; but in the situation such as developmental dysplasia of the hip (DDH), only limited leg length can be corrected due to long-lasting dislocation of the hip and shortening of the nerves, vessels and soft tissues. In some situations, if the cup needs to be placed into the true anatomical acetabulum to restore anatomical and biomechanical normality, conducting a sub-trochanteric osteotomy and removing a segment of the bone may become necessary.

2.3.2 Offset of the Femoral Head

Often less attention has been paid to adjust and optimize the offset of the femoral neck when designing a hip stem. However, it can be of paramount importance in affecting the hip joint biomechanically and functionally. The change of the neck offset directly affects the forces across the hip joint. If the offset is increased, the forces across the hip joint will decrease in a single leg stance, because the forces from the abductor muscles are reduced. This can be calculated based on the balance of the moments from two sides—the centre of the body weight and the force from the abduct muscles. However, increasing the offset will increase the bending force across the hip stem. If the stem diameter is too small, the stem fracture will cause for concern; then the patients' body weights need to be taken into consideration.

In the situation that the diameter of the stem cannot be increased due to small cavity of the femur and overream of the bone is not attempted, in order to avoid stem fracture, reducing offset of the femoral neck can be one of the choices to reduce bending force across the hip stem. To do so, the distance of the lever arm of the abductor muscles is decreased, in which more forces will be generated from the muscle contraction in order to balance the moment of the hip joint when the patient is in single leg stance. Therefore, the forces across the hip joint will be increased, which subsequently increase the wear particles from the bearing surface of the joint.

3 Stress Distribution over the Bone

Stress shielding of the bone following total hip replacements has caused major concerns over the past, and many research projects have been carried out to study the stem geometries that can distribute the normal stresses over the bone [5]. According to Wolff's law, if the bone is under-stresses, bone resorption will occur [6]. The clinical follow-up study showed that 20% of reduction in bone density at the calcar region has been observed at 1 year after total hip replacements [7]. This may further lead to bone fracture or loosening of the implants.

A number of factors can contribute to the stress shielding of the bone following THR. One of the main reasons is the mismatch of the material modulus between the implant and the bone so that most of the loads are carried by the implant rather than the femoral bone. The higher Young's modulus of elasticity for the implant materials (110 GPa for Titanium alloy; and 230 GPa for Cobalt Chrome) comparing with the bone (17 GPa for cortical bone at mid-shaft of the femur under compression load) seem making this occurrence of stress shielding inevitable. In the past, some of the hip stems have been designed with lower Young's modulus such as Identifit implant, but the clinical results were very disappointing, with 17% of revision rates over the 2 years [8]. The reason for this is that reducing the stiffness of the implant will increase interface micromotion between the stem and bone, which will inhibit the bone ingrowth into the stem. Some of the other factors such as stem fails to closely contact with the bone in the calcar region resulting in less stress transfer to the bone also play a critical role. Therefore, the match of the stem geometry with the bone in order to achieve a line-to-line fit and maintain long-term bone qualities is of the most importance.

However, some researches have shown a wide variation in the geometry of the femur between individuals, in which three types of femoral shape have been summarized. The three shapes include normal, stovepipe and champagne bottle, which represent different ratios in width between proximal and distal canals [9]. For this reason, the off-the-shelf standard hip stems cannot consistently provide an optimal fit for each patient.

In the occurrence of loading carried by the distal stem, where the distal fit is too tight but the proximal bone contact is not achieved, the proximal stem will transfer less stresses onto the bone. Over the time, the proximal part of the bone will undergo stress shielding and bone resorption while the distal part will show the formation of the para-prosthetic pedestal bone [10].

On the contrary, the custom designed hip stem can reliably provide the best fit and transfer close to normal load onto the bone. A clinical follow-up of custom hip stems showed that the bone densities measured by DEXA scan at 2 years postoperatively were maintained at 97% when compared with that measured immediately after surgery [11].

Therefore, in most of the cases for uncemented fixation, the distal stems should only be designed for sliding fit to avoid distal loading, in which the function of the distal stems is only served to prevent the stems from tilting.

4 Stem Stability (Relative Motion and Migration)

Among all other factors that may have detrimental effects to the survivorship of the hip implants, failing to obtain immediate fixation of the stem is the most critical. In situations where the proximal bone is too poor to load, distal fixation should always be regarded as an alternative. Primary factors relating to the stability of the stems include relative motion between stem and bone, and migration of the stem over time.

Relative motion is defined as a recoverable relative position of a component relative to its host bone after a cyclic loading (Fig. 13.2). This is due to elastic or plastic deformation of the materials or geometric mismatch between bone and component. The amount of relative motion for uncemented stems can vary but should be around 10–150 μm. It can occur either in localized areas or over the entire interface. If the motion is over 150 μm, osseointegration and biological fixation of the stem will unlikely take place [12]. This phenomenon is due to higher tolerance of fibrous tissue to strain energy in the interface than that of bone tissue. Furthermore, the relative motion can induce more shear stresses and strains in the bone, which is not favourable to bone tissue ingrowth.

Therefore, in order to achieve long-term stability and biological fixation of the stem through osteointegration, immediate mechanical fixation of the stem with the bone is of critical importance. This to large degrees relies on the geometry of the stem designed to match the medullary canal. To fit stem in the proximal medial region of the canal has always been regarded by many designers as the priority for achieving immediate fixation of the stems.

Migration is defined as a permanent change of position or subsidence of a component relative to its host bone after many cyclic loadings over a period of time (Fig. 13.2), in which the distance between the final position and initial position of the stem is measured. This can similarly be due to elastic or plastic deformation, but the geometric mismatch between bone and component plays large roles. In situations that stems have been in situ for many years, progressive bone resorption and

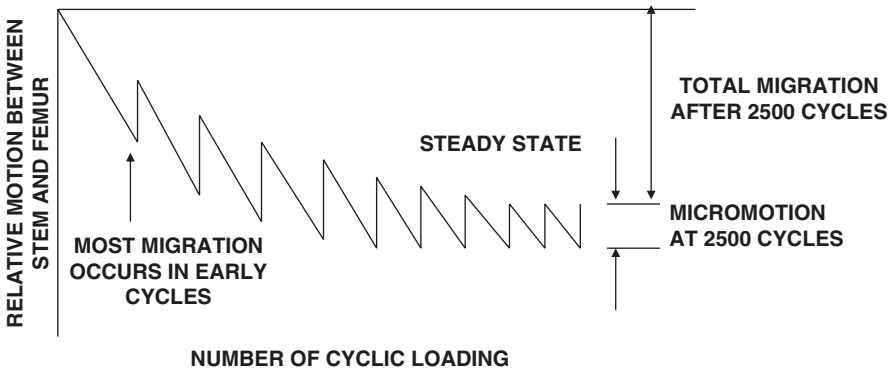

Fig. 13.2 Diagram shows axial migration and micromotion of the hip stem in relation to the femoral bone

extensive osteolysis can also lead to considerable migration of the stem, eventually causing aseptic loosening and failure of the stems.

Previously a number of studies have shown that early migration of the stem correlates with the long-term clinical success. If the stems were initially stable and only migrated less than 2 mm within 2 years, they were likely to be successful in long term; otherwise if the stems were not stable at beginning and migrated over 2 mm in 2 years, these stems were likely to fail [13–15]. In general, uncemented stems need more time to stabilize which could take up to 1–3 months after surgery. Therefore the uncemented stems may be migrated more at early stage which mostly depends on the geometry of the stem, and also how tightly the stem has been impacted during surgery. Once the stem has settled, the uncemented stem should be as stable as the cemented stem for the initial stage. With porous and hydroxyapatite coating for most of the uncemented stems, bone ingrowth and long-term biological fixation will take place. Progressive migration of the stems for both cemented and uncemented fixation indicates that a failure of the stem will soon occur.

The custom-made hip stems have achieved superior results for both relative motion and migration when compared with the standard stems. A laboratory testing showed that relative axial motion for custom-made stems was 11 μm in average after 2500 cyclic loading, while for standard stems was 19 μm [16]. In a clinical follow-up study, the migration for custom-made primary and revision stems were less than 2 mm in 2 years, which were more stable than the standard stems [17].

Both relative motion and migration of the stem are three-dimensional referred to the axis systems in the medullary canal. Relative motion can basically only be measured in vitro using LVTDs mounted onto the bone and attached to the stem. The relative motion of the stem along the long axis of the femur, the horizontal motion at the tip of the stem on both medial-lateral and anterior-posterior direction and the rotational motion at the neck of the stem are usually measured. The differences in reading before and after loading in a single cycle are calculated as the magnitude of the relative motion. A number of cyclic loadings to pre-set the stem into the position are necessary in order to achieve a stable and consistent reading and to reflect the true value of relative motion. To measure relative motion after the stem is inserted into patients is normally impossible, unless two X-rays are taken in a sequence. The first X-ray is taken when the patient is standing on the effected leg (in loading situation) and the second X-ray is taken when the patient is standing on the alternative leg (in off-loading situation). The distance between the stem and bone before and after the leg is loaded can be measured and compared on the images, and the amount of difference can be calculated as the value for relative motion.

Migration of the stem can be measured both in vitro using LVTDs and in vivo using medical images. There are basically three types of methods that can be applied to measure the migration.

1. Using the pen to mark the landmarks on the stem and the bone and measure them by the ruler on plain X-rays. This method is simple and no additional equipment is required. However, the accuracy is low, which can only be used in clinical for a gross comparison and general assessment.

2. Applying a digitize technique on the plain X-rays either on the digitize table or on the computer screen with a specially developed software. This method is more accurate than using the ruler and pen. A previous study showed that the accuracy of the method can be up to 0.25 mm if the landmarks on the stem and bone can be clearly defined [15]. The most benefits of using this method are not only that it can be more accurate but also that it can be applied for a retrospective study. This means that all clinical plain X-rays taken in the past years can be used for the study. However, this method can only measure the axial migration of the stem, other axes such as rotation and varus-valgus tilt of the stem will not be able to measure due to the two-dimensional views of the images.
3. Application of Radiostereometric analysis (RSA) is currently the most accurate technique to measure the migration of the stems. The study showed that the accuracy of the method can reach to 0.15 mm. Moreover, it can also measure the migration of the stem in three-dimensional planes using plain X-rays [18], so that it can more truly reflect the status of the stem in situ. However, this method requires special equipment, technical expertise and analysing software. Therefore it can only be applied in special centres. The RSA techniques involve injecting a number of tantalum beads into stem and bone during surgery as specially defined reference marks for the measurements, and the radiograph has to be taken using the special method of dual X-ray tubes placed at diagonal planes [19]. In this way, any studies measuring the migration of the stems using RSA techniques has to be pre-planned and set up prospectively, so that the study will take long times to complete.
4. A most recently developed method of measuring migration of the stem using CT scan has been studied [20]. The method also relies on the injection of the tantalum beads as reference marks for the measurements; thus, it can only be used for a prospective study. Instead of using dual X-ray tubes, it measures the reference marks from the CT scan images. From the study, the femoral head was used as the reference marks for the stem and the different lengths of the femoral heads (−3.0, 0.0, 2.5, 5.0, 7.5 and 10 mm) were regarded as the migration of the stem related to the bone. The accuracy of the method was claimed to be 0.11 mm [20], even better than the RSA method. However, this method has only been validated on the cadaveric bone, its real value for clinical application needs further evaluation.

5 Selecting the Sizes of Femoral Heads

The 28 mm diameter of the femoral head has been mostly used in the past. However, larger sizes of the femoral heads such as 32 and 36 mm have become more favourable for some of the surgeons. According to the report from American Joint Replacement Registry, 36 mm femoral heads had become the most popular size, followed by 32 mm [1]. This is because large femoral heads have the advantages of providing stable joints, being less likely to dislocate, and potentially offering more

range of motion of the hip. It can also increase the bearing surfaces and lead to decreased contact stresses and thus reduced linear wear; but on the other hand, large femoral heads cause more volumetric wear and number of wear particles.

Small femoral heads such as 22 mm diameter are usually only used due to the restriction of the small size of the acetabular cups. However, small femoral heads do provide biomechanical advantages such as producing lower friction between the femoral head and the acetabular cup, offering shorter travel distance for the same range of motion, and thus generating fewer wear particles.

6 Range of Motion of the Hip (Head/Neck Ratio)

Restoring range of motion of the hip should always be part of the design objectives for the hip replacement. Although how the acetabular cup being placed can affect the range of motion, the diameter of the femoral heads in relation to the sizes of the stem neck can be one of the determining factors. In general, the bigger the size of the femoral head, the more the range of the motion it can achieve, but this is not always true. Strictly speaking, the range of motion of the hip is only associated with the head/neck ratio. While for most of the cases where the size of the neck is constant, the bigger size of the head will obtain more range of the motion. However, for a small head such as 22.2 mm, it can achieve the same range of flexion and extension as that for 28 mm head as long as a mini spigot on the anterior and posterior side of the neck is produced, which make head/neck ratio the same as for 28 mm head.

7 Design Consideration for Developmental Dysplasia of the Hip (DDH)

Among other complex cases, developmental dislocation of the hip (DDH) is one of the most challenge cases to design a hip stem for, due to its unusual bone geometry, with excessive anteversion of the femoral neck, and often accompanied by a maldeveloped acetabular socket. The disease usually started when the baby is born, gradually further developed and deteriorated over time. If the proper treatment is not undertaken in time, the hip joint becomes so deformed that severely affect the hip functions, and finally requires a total hip replacement. One of the difficulties in designing a DDH stem is that the proximal medial part of the stem needs to be gradually anteverted to follow the deformity of the femoral canal, while the stem neck needs to be retroverted in order for the femoral head to match the normal orientation of the acetabular cup (Fig. 13.3). With this design, the hip can be reduced and the further dislocation of the hip can be avoided; but the full function of the hip has still not been restored, because the greater trochanter and abductor muscle are still at the posterior side of the hip.

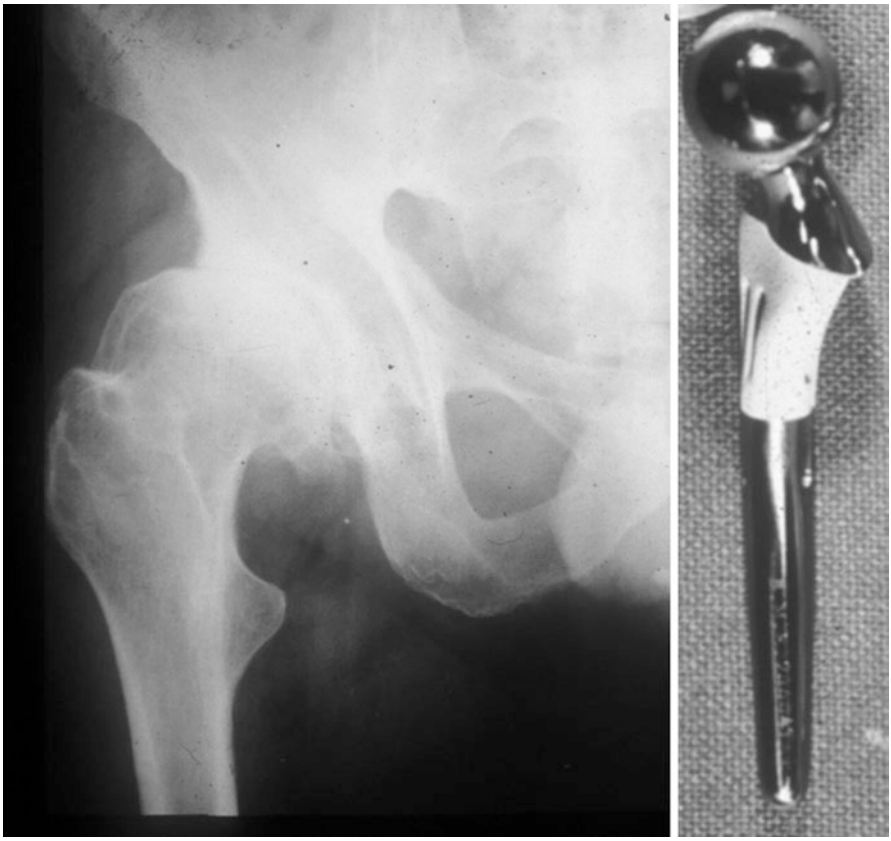

Fig. 13.3 Hip stem designed for DDH case. The stem follows the geometry of the femoral cavity and the femoral neck retroverted to the normal position of the acetabular cup

An alternative design is to carry out a de-rotational sub-trochanteric osteotomy, in which the proximal part of the bone will be rotated internally so that the greater trochanter and abductor muscle can move laterally to their normal anatomical positions. This design is specially suitable for the anteversion of the hip over 60°, where a simple retroverted neck may not be able to fully adjust the deformity of the hip. When the de-rotational osteotomy being performed, the function of the hip should be significantly improved and the gait pattern should become more normal [21]. Unfortunately, none of the studies has been carried out to prove this due to unavailability of the resources in gait analysis at time to compare patient's gait before and after operation.

In spite of these advantages in de-rotational osteotomy, some of the concerns have greatly restricted the wide use of this design. One of the main concerns is the uncertainty of whether the osteotomy site can be union or not, especially for those with poor bone qualities and old patients. If the non-union of the osteotomy had happened, the clinical results could be largely compromised and the revision surgery might be inevitable.

Another concern is how to secure the stem with the cavity below the osteotomy site. The proximal and the distal part of the bones need to be held together tightly by the stem, so bone rotation around the stem will occur after the stem undergoes torsional loading. A stem with distal cutting flutes is usually designed to provide the torsional stability for the distal stem, while the proximal stability is normally achieved by the geometry fit with the bone. Sometimes, the transverse screws through the distal bone and stem can be used to provide the torsional stability, provided the diameter of the stem is large enough for the hole. However, this option has been less favourable because it may cause destruction and weakness for both bone and stem. If the diameter of the femoral canal in the diaphyseal region is too small, both designs may not be suitable. In this situation, two-stage surgeries, with derotational and bone shortening osteotomy performed first followed by total hip replacement, may be the choice.

8 Design Consideration for Revision Stems

In overall, the design for revision stems are more complicated than that for primary stems because there are large variations on the quality of the remaining bone, as well as the different locations of the bone defects. However, the principles for designing a revision stem should be kept the same as that for a primary stem, in which to achieve the initial stability of the stem is the priority. In revision situations, the design rationales for each case can be different, which are mostly determined by the condition of the remaining bone. From previous experience of designing custom-made hip prostheses, the design rationales for each revision stem have been summarized into four types [12], which were correspondent to Paprosky's classification of cavitary defects in revision situation [22].

- **Type 1:** The quality of the bone is uniformly preserved along the entire femoral canal. The density of the bone especially in the calcar region is normal which can be used for load bearing. In this case, the revision stem can be designed short just like a usual primary stem, regardless of the length of the original stem. The fixation can be relied on the calcar and metaphyseal bone.
- **Type 2A and B:** The proximal bone is reasonably maintained. The implant can be fully or partially supported by the metaphysis. The diaphyseal bone is mostly intact but there are localized osteolytic lesions, particularly around the previous distal stem. For this situation, proximal fixation is still obtainable, but the stem should be designed longer in order to bypass the defects. The optimal length of stem to bypass the defect should be 2.5–3.0 times the canal diameter in order to avoid the distally concentrated stresses further weakening the defect and causing bone fracture. The stress concentration caused by the tip of the stem is mostly around the lateral side. Therefore, the stem should pass more if the defect is on the lateral side of the bone.

- **Type 2C and Type 3:** There is further destruction of the bone, leaving an enlarged proximal cavity with an irregular and thin cortical wall. The distal cortex beyond the level of the original stem has reasonable quality and thickness. In cases involving a second or even third revision, the length of the bone destruction may be extended due to the previous use of long stems. Owing to the compromised quality of the proximal femur, fixation and load-bearing are limited, and stem fixation is primarily achieved in the region below the defective bone. The distal cutting flutes are usually designed for the stem to enhance the fixation and provide additional torsional stability. Nevertheless, the proximal part of the implant is still designed to closely fit (not press-fit) the cavity. Together with the hydroxyapatite coating, regeneration of bone and long-term stem/bone osteointegration could be achievable. These design features aim to obtain the maximum possible fixation in both regions, but initial fixation is obtained by the distal stem.
- **Type 4:** This situation is rare but severe, in which the cortical bone has severely been destructed along the proximal and middle parts of the cavity, usually resulting from previous multiple revisions involving long-stem implants. The only portion of the good bone which is good enough for load bearing is in the distal where the bone shape has flared out. Therefore uncemented fixation of the stem in this region is intractable. To solve this problem, a long stem reached to femoral condyle can be designed with distally cemented fixation to obtain immediate stability in conjunction with a large HA-coated proximal section, with nonconforming spaces filled with grafted material. This stem was also suitable when the femur was longitudinally split for removal of the previous stem.

9 Clinical Results of Custom Hip Implants

Comparing with the clinical results of the standard hip implants, the information for custom hip implants are much less published. Furthermore, the evaluation of the clinical results for custom hip stems is more difficult because none of the implants is designed the same, especially if the stems are designed from the different companies. In overall, most of the clinical results for custom hip stems are excellent.

A clinical follow-up study of the primary custom hip stems designed by the author and produced by Stanmore Implants Worldwide (SIW) showed that among the 114 consecutive CAD-CAM custom-made primary hip stems, inserted by a single surgeon from one hospital, the survivorship was 100% with the average 13.2 years of follow-up (ranged from 10 to 17 years) and mean age of 46.2 years old (range from 24 to 62 years old), although after 12 years, some cases have changed the acetabular liner and femoral head but none of the femoral stems need replacement. A radiographic study showed no aseptic loosening around the stem [23, 24]. Also, a study of the 158 consecutive revision custom hip stems with minimal 10 years follow-up showed that all femoral components were well fixed radiologically, with 97% survivorship at 10 years. Among the revised cases, some were not related to the femoral components [23, 24]. One of the observation from the radio-

graphic study showed that there were very little osteolysis occurring, even after some of the femoral heads and acetabular liners being revised. This suggests that the close geometric fit of the stem with the cavity may have additional benefits of achieving layers of osteointegration thus seal the stem-bone interface. If this can happen, the wear particles generated from the bearing surface will be prevented from travelling into the femoral cavity, furthermore prevent the macrophages and osteoclasts from reacting to the wear particles. As a result, osteolysis can be avoided.

10 Disadvantages of Using Custom Stems

Apart from many benefits of using custom stems, some of the disadvantages should also be considered, which could be the main reasons to prevent the custom stems from being widely used. However, with the advance of the new technologies, some of the issues may be able to solve. From surgical point of view, one of the major disadvantages is that no sequence of the tools can be used to prepare the femoral cavity and to facilitate insertion of individual implant. Usually only the final shape-matched custom reamer and rasp can be provided for each case. Therefore, some of the surgeons may find difficulty to insert a custom hip stem, because all the custom stems are designed to have line-to-line fit with the cavity, any misalignment at the initial insertion point will cause the implant jam inside the cavity. With the advance and wide use of the surgical navigation system, the surgical procedures can be more precise, accurate and easier. Another disadvantage of using custom stem could be that the stem may not fit with the bone, in which the stem may be unable to be inserted. A number of factors can cause this happen. One of the common factors is the quality of the images makes the boundary of the cortical bone not well defined or misinterpreted. Other factors could also be possible such as the time between the images taken and surgery is too long so that the bone geometry has changed since. Other disadvantages related to the custom stems such as costing and delivery timing should not be the restricting factors now because the increasingly popular 3D printing technology can make manufacture process of custom stems more quickly, efficiently and economically.

11 Summary

In total hip replacements, the standard stems have been playing a major role for a long time. However, since individual patients have significantly different requirements, such as bone conditions, anatomy, pathologies, clinical problems, and expectations for hip functions/activities/quality of life, custom stems are becoming ever more popular and demanding in performance. This is true not only for the complex cases, but also for the routine cases to achieve better clinical outcomes and longer survivorship. While we are expecting the coming era of precision medicine and

digital orthopaedics, advanced surgical navigation systems and 3-D printing technologies are paving the way for using patient specific custom stems to solve patient specific clinical problems. Although the advanced and rapid development of future science and technology will change people's view and expectation on total hip replacements, the basic principles of implant design will remain the same. I would be very pleased if this chapter can be of some contribution and useful to those dedicated to the design of hip stems.

References

1. Berry D. In: Fourth American Joint Replacement Registry (AJRR) 2017 annual report on hip and knee arthroplasty data, Rosemont, IL. ISSN 2375-9100 (print) and ISSN 2375-9119 (online). 2017.
2. Green M, Howard P, Porter MWilkinson M and Wishart N. In: 14th annual report National Joint Registry for England, Wales, Northern Ireland and the Isle of Man, Surgical data to 31 December 2016; ISSN 2054-1821 (print). 2017.
3. Bozic K. In: Fifth American Joint Replacement Registry (AJRR) 2018 annual report on hip and knee arthroplasty data, Rosemont, IL. ISSN 2375-9100 (print) and ISSN 2375-9119 (online). 2018.
4. Postler AE, Beyer F, Wegner T, Lützner J, Hartmann A, Ojodu I, Günther KP. Patient-reported outcomes after revision surgery compared to primary total hip arthroplasty. Hip Int. 2017;27(2):180–6.
5. Behrens BA, Wirth CJ, Windhagen H, et al. Numerical investigations of stress shielding in total hip prostheses. Proc Inst Mech Eng H. 2008;222(5):593–600.
6. Chamay A, Tschantz P. Mechanical influences in bone remodeling. Experimental research on Wolff's law. J Biomech. 1972;5(2):173–80.
7. Tapaninen T, Kröger H, Venesmaa P. Periprosthetic BMD after cemented and uncemented total hip arthroplasty: a 10-year follow-up study. J Orthop Sci. 2015;20(4):657–62.
8. Robinson RP, Clark JE. Uncemented press-fit total hip arthroplasty using the identifit custom-molding technique. J Arthroplast. 1996;11(3):247–54.
9. Dorr LD, Faugere MC, Mackel AM, et al. Structural and cellular assessment of bone quality of proximal femur. Bone. 1993;14(3):231–42.
10. Agathangelidis F, Boutsiadis A, Petsatodis G. Pedestal sign in cementless total hip replacement. Hippokratia. 2014;18(4):378.
11. Hua J, Walker PS, Muirhead-Allwood SK, Engelhardt F, Bentley G. Custom uncemented revision stems based on a femoral classification. Hip Int. 2010;20:18–25.
12. Soballe K, Brockstedt-Rasmussen H, Hansen ES, Bunger C. Hydroxyapatite coating modifies implant membrane formation. Controlled micromotion studied in dogs. Acta Orthop Scand. 1992;63:128–40.
13. Freeman MAR, Plante-Bordeneuve P. Early migration and late aseptic failure of proximal femoral prostheses. J Bone Joint Surg Br. 1994;76-B:432–8.
14. Walker PS, Mai SF, Cobb AG, Bentley G, Hua J. Prediction of clinical outcome of THR from migration measurements on standard radiographs: a study of cemented Charnley and Stanmore femoral stems. J Bone Joint Surg Br. 1995;77-B:705–14.
15. Hua J, Walker PS. Relative motion of hip stems under load: an in vitro study of symmetrical, asymmetrical and custom asymmetrical designs. J Bone Joint Surg. 1994;76-A(1):95–103.
16. Walker PS, Culligan S, Hua J, Muirhead-Allwood S, Bentley G. Stability and bone preservation in custom designed revision hip stems. Clin Orthop. 2000;373:164–73.
17. Alfaro-Adrian J, Gill HS, Murray DW. Cement migration after THR: a comparison of Charnley Elite and Exeter femoral stems using RSA. J Bone Joint Surg Br. 1999;81(1):130–4.

18. Chung VWJ. Leveraging the use of existing C-arms for roentgen stereophotogrammetric analysis. University of British Columbia; 2015.
19. Boettner F, Sculco P, Lipman J, Renner L, Faschingbauer M. A novel method to measure femoral component migration by computed tomography: a cadaver study. Arch Orthop Trauma Surg. 2016;136(6):857–63.
20. Zadeh HG, Hua J, Walker PS, Muirhead-Allwood SK. Uncemented total hip replacement with subtrochanteric derotational osteotomy in hip joint osteoarthritis with concomitant severe femoral anteversion. J Arthroplast. 1999;14(6):682–8.
21. Paprosky WG, Lawrence J, Cameron H. Femoral defect classification: clinical application. Orthop Rev. 1990;19(Suppl):9–15.
22. Muirhead-Allwood S, Sandiford N, Skinner JA, Hua J, Kabir C, Walker PS. Uncemented custom computer-assisted design and manufacture of hydroxyapatite-coated femoral components—survival at 10 to 17 years. J Bone Joint Surg Br. 2010a;92-B(8):1079–84.
23. Muirhead-Allwood S, Sandiford NA, Skinner JA, Hua J, Muirhead W, Kabir C, Walker PS. Uncemented computer-assisted design-computer-assisted manufacture femoral components in revision total hip replacement: a minimum follow-up of ten years. J Bone Joint Surg Br. 2010b;92(10):1370–5.
24. Hua J, Walker PS. Closeness of fit of uncemented stems improves the strain distribution in the femur. J Orthop Res. 1995;13(3):339–46.

Chapter 14
Biomechanics of Orthopedic Rehabilitation

Ayman A. Mohamed, Yih-Kuen Jan, Ian M. Rice, Fang Pu, and Cheng-Kung Cheng

Abstract This chapter discusses four main areas that clinicians should understand to improve the effectiveness of orthopedic rehabilitation. The first part is about the biomechanical factors that affect orthopedic rehabilitation process. The second part is about the types of exercises during orthopedic rehabilitation and their underlying biomechanical principles. The third part is about how to apply these biomechanical principles to manage common orthopedic disorders. The fourth part is about the biomechanical guidelines for the use of assistive devices during orthopedic rehabilitation.

Keywords Assistive devices · Biomechanics · Exercise · Musculoskeletal Orthopedic · Rehabilitation

Biomechanics is defined as the use of the mechanical principles to understand functions and structures of the biological systems and how these biological systems can mechanically react to applied forces or loads in both normal and

A. A. Mohamed
Rehabilitation Engineering Lab, Department of Kinesiology and Community Health, University of Illinois at Urbana-Champaign, Champaign, IL, USA

Department of Basic Science and Biomechanics, Faculty of Physical Therapy, Beni-Suef University, Beni Suef, Egypt

Y.-K. Jan (✉) · I. M. Rice
Rehabilitation Engineering Lab, Department of Kinesiology and Community Health, University of Illinois at Urbana-Champaign, Champaign, IL, USA
e-mail: yjan@illinois.edu

F. Pu
Advanced Innovation Center for Biomedical Engineering, School of Biological Science and Medical Engineering, Beihang University, Beijing, China

C.-K. Cheng
School of Biomedical Engineering, Shanghai Jiao Tong University, Shanghai, China
e-mail: ckcheng2020@sjtu.edu.cn

C.-K. Cheng, S. L-Y. Woo (eds.), *Frontiers in Orthopaedic Biomechanics*,
https://doi.org/10.1007/978-981-15-3159-0_14

abnormal circumstances. The application of biomechanics to orthopedic rehabilitation aims to maximize treatment effectiveness while shortening recovery time. Biomechanically driven therapies can be applied either during an acute, recovery, or functional stage of orthopedic rehabilitation [1, 2].

Learning Objectives
After reading this chapter, the readers will be able to:

1. Understand the biomechanical factors of the musculoskeletal tissues (muscles, tendons, and ligaments) in the human body that can help to improve orthopedic rehabilitation
2. Understand the biomechanical principles of common exercise types in orthopedic rehabilitation
3. Recognize the advantages of applying biomechanical principles to improve effectiveness of orthopedic rehabilitation
4. Know the common orthopedic disorders of the upper and lower joints and how biomechanical principles can improve their interventions during orthopedic rehabilitation
5. Use the biomechanical principles to prescribe appropriate assistive devices (splints, walkers, crutches, and canes) to improve orthopedic rehabilitation.

1 The Biomechanical Factors Affecting Orthopedic Rehabilitation

There are several biomechanical factors that should be well understood when performing orthopedic rehabilitation to the human musculoskeletal tissues. This part discusses the factors that clinicians should understand when applying different rehabilitation therapies. We provide examples of key factors to clarify the role of these factors during orthopedic rehabilitation.

1.1 The Viscoelasticity

Viscoelasticity is the main mechanical property of musculoskeletal tissues [3]. It is defined as the property of any material that exhibits both viscous and elastic characteristics when a stress is applied to it. Viscoelastic materials have time-dependent or frequency-sensitive stress–strain relations which are dependent on the magnitude, period of application, and velocity of an applied load. Understanding the viscoelastic characteristics of the musculoskeletal tissues gives us a better understanding of how the musculoskeletal tissues as viscoelastic materials respond to different types of the rehabilitation modalities. This section discusses two main phenomena (the creep [4–6] and the hysteresis [7]) and two main relationships (the stress–relaxation relationship [8, 9] and the force–velocity relationship [10]).

1.1.1 The Creep Phenomenon

The creep phenomenon is the first common viscoelastic property that the musculoskeletal tissues follow when they are subjected to stress. The creep phenomenon is defined as the gradual lengthening (shortening) of a viscoelastic material with time when a constant tensile (compressive) stress is placed on it. When a constant tension is placed on a muscle for a period of time, this tension is distributed on all of the sarcomeres in an equal manner. An increase (decrease) in one sarcomere length due to this tension produces a change in its isometric tension. This causes a lengthening (shortening) of this sarcomere at a fixed speed that matches the amount of applied tension (speed of sarcomere change is proportionate to the magnitude of applied tension). For example, use of splints for stretching shortened musculoskeletal tissues (lengthening effect) functions primarily through the creep phenomena. These tissues change their shape after a period of time in response to the constant tension of the applied splint.

1.1.2 The Hysteresis Phenomenon

The hysteresis is the second common viscoelastic property that the musculoskeletal tissues follow when they are subjected to stress. The hysteresis can be defined as the energy loss in the form of heat. It is considered a recovery process after the removal of a certain load. The amount of energy loss as heat is based on the rate of applied strain to deform the body tissues. The continual loading and unloading can explain the increase in the temperature of the viscoelastic material during loading and unloading (Fig. 14.1). For example, when a shortened ligament is repetitively stretched with a constant stretching force (stretch then relax then stretch), hysteresis is developed and the ligament length limit increases with each cycle. Thus, an extra ligament length occurs in the same session by performing a repetitive stretching manner.

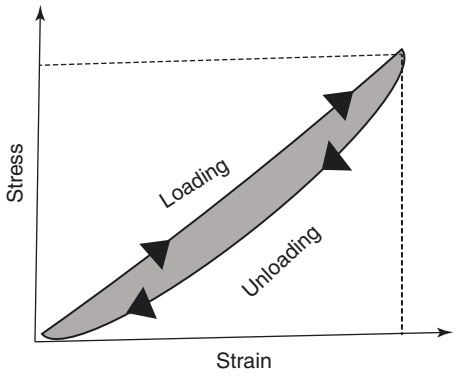

Fig. 14.1 The hysteresis. When a viscoelastic material is stretched (loading) and returns to its original length (unloading), it (unloading phase) does not return to the same manner as when it is stretched (loading phase). The process losses energy in the form of heat

1.1.3 The Stress–Relaxation Relationship

The stress–relaxation relationship is the third common viscoelastic property that the musculoskeletal tissues follow when they are subjected to stress. The stress–relaxation relationship can be defined as the reduction in the stress due to the same degree of strain produced in the viscoelastic tissues. To explain this, when musculoskeletal tissues (viscoelastic materials) are held under tensile stress for a prolonged time, there is an increase in this stress over time. Thus, the stress should be increased to produce the same required strain (Fig. 14.2). For example, in static stretching, when a constant stretch (strain) is applied on a muscle for a prolonged time, the magnitude of the stretching force (stress) is less than the firstly applied stretching force.

1.1.4 The Force–Velocity Relationship

The force–velocity relationship is the fourth common viscoelastic property that the musculoskeletal tissues exhibit when they are subjected to stress. The force–velocity relationship can be defined as the amount of muscle force in relation to the velocity of motion or vice versa. Based on this relationship, the maximum possible tension occurs with the eccentric contraction (Fig. 14.3). This clarifies why it is easier to lower a load and stop it than lifting it and why it is easier to descend from a certain height and land than to jump up to the same height.

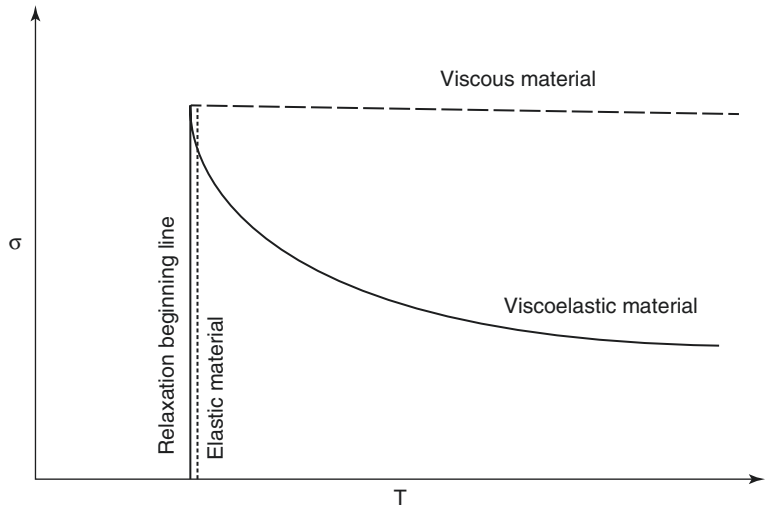

Fig. 14.2 The stress relaxation curve. There are differences in the relaxation behaviors for the viscous, elastic, and viscoelastic materials in the stress–relaxation curve (σ = stress, T = time). The elastic material returns immediately to its original state after relaxation. The viscoelastic material exhibits some changes in the return way, loses some energy in the form of heat and an alteration in its original state occurs. The viscous material continues in the state developed by the stress and does not relax

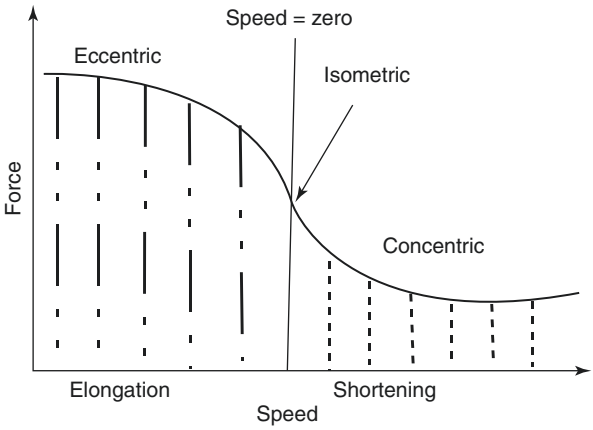

Fig. 14.3 The force–velocity relationship. In concentric contraction, as the load increases, there is a decrease in the velocity of contraction. In concentric contraction, as the load increases, there is an increase in the velocity of contraction

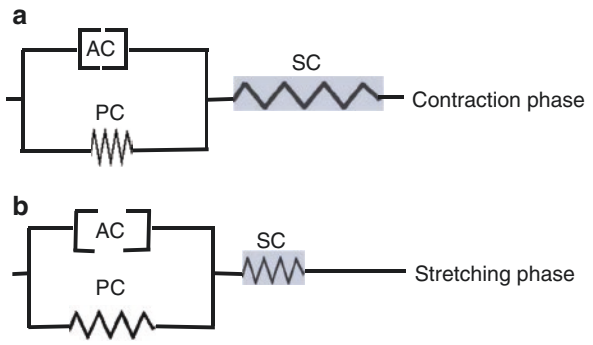

Fig. 14.4 The Hill's muscle model. (**a**) The contraction phase, the parallel component (PC) and active component (AC) are contracted, while the elastic component (EC) is stretched. (**b**) The stretching phase, PC and AC are stretched, while the EC is contracted

1.2 The Hill's Muscle Model

The Hill's muscle model is another biomechanical factor that can help us to understand which muscle tissues are responsible for developing each type of the muscle tension. The Hill's muscle model demonstrates that there are two sources participated in the development of the muscle tension (active and passive). The active tension is developed by the interaction of actin and myosin filaments in the muscle, while the passive tension is developed by the connective tissue components (fascia and tendon) in the muscle when the muscle length exceeds its resting length. The Hill's muscle model demonstrates that the active and passive tensions are depending on each other and each of them cannot be considered as a separate structural element of the muscle because the connective tissue matrix of the muscle is relatively complex and connected to each other (within and between the muscles) [11] (Fig. 14.4).

2 The Biomechanics of the Therapeutic Exercises

The most common exercise types during orthopedic rehabilitation are stretching, strengthening, ROM, and mobilization exercise.

2.1 Stretching Exercise

Stretching exercise is a critical part of any rehabilitation program applied to increase the joint range of motion (ROM) and improve the muscle-tendon flexibility. The application of biomechanical principles into stretching therapies enables orthopedic rehabilitation team to improve stretching exercise effectiveness, reduce the likelihood of injury, and customize the stretching program to better meet the needs of the client. Creep, hysteresis, and stress relaxation are all concepts which give us a better understanding of why the late effect or the prolonged stretch is better than the acute or short stretch in gaining a stretching effect. This section discusses the biomechanical effects of the stretching exercise, including the immediate [12, 13] and the late biomechanical effects [11, 14, 15] and the types of the stretching exercise [16].

2.1.1 The Biomechanical Effects of the Stretching Exercise

The Immediate Effects of the Stretching Exercise

The immediate effect of stretching is mainly dependent on two relationships. The first relationship is the stress–relaxation relationship. The stress–relaxation relationship causes an immediate decrease in the passive tension of the muscle at a particular joint angle. Stretching a muscle for 20–30 s can result in a decrease in the passive tension of the muscle because the most percentage of the strain to reduce the stress effect occurs in the first 20 s of the stretching exercise (stress–relaxation principle). The stretching exercise can give an immediate 10–30% reduction in the passive muscle tension. The second relationship is the force–length relationship. The force–length relationship demonstrates how the force magnitude can be increased by increasing the prior length of the contracted muscle. When a shortened muscle is stretched before contraction, the produced force rises considerably. The background behind the long-lasting rise in the force may be due to alteration in the sarcomere length that is developed through the activation and after the stretch.

The Late Effects of the Stretching Exercise

The late effects of stretching exercise are much better than the immediate effects. The first effect is due to the prolonged stretch that causes a significant improvement (8–12° or 5–31%) in the ROM after 12 weeks of training. This effect is attributed to

the sarcomere myogenic response. The sarcomere myogenic response demonstrates that when a muscle is stretched, two possible mechanisms occur. An elongation of each muscle fiber itself to its maximum resting length until the whole sarcomeres are fully elongated. Then, a stretch of the connective tissues around it occurs. To explain this, when the stretching tension increases, the collagen fibers in the connective tissue line up themselves with the same line of force according to the direction of the applied tension. Thus, prolonged stretching can improve the muscular functions as it aids in the rearrangement of any disorganized muscle fibers (sarcomeres and connective tissues).

The second effect, according to the American Council on Exercise [15], stretching exercise can improve the overall body flexibility. When the stretching exercise is performed as a daily habit, connective tissues show some elongation. After a period of time, this elongation in the musculoskeletal tissues increases the ROM for all body joints. This improvement in the flexibility of muscles and connective tissues reduces the risk of joint degeneration and relieve muscle stiffness. Adding a stretch after strength training session is significantly effective in maintaining normal range of motion because it acts as an extra overload stimulus that increases the strength gain.

2.1.2 Types of the Stretching Exercise

There are three types of muscle stretching exercise commonly performed in orthopedic rehabilitation (static, dynamic, and pre-contraction). The first type, static stretching exercise, is most common and regularly used. In static stretching, the stretching force is constant and includes two subtypes, passive and self-stretching. Passive stretching exercise occurs when the stretch force is applied by the therapist or another person. In contrast, self-stretching exercise requires the patient to apply the stretch force independently.

The second type is the dynamic stretching exercise that occurs when the stretching force is not constant and includes two subtypes, active and ballistic stretching. The active stretching exercise is usually applied by moving the limb repeatedly until the end of the available ROM. The ballistic stretching exercise is conducted by quick, alternating stretching motions or “bouncing” performed at the end of the available ROM. This technique is not recommended as there is an increased incidence of the injury to the stretched tissues.

2.2 Strengthening Exercise

A strengthening exercise program should be designed based on the training goals [17]. This includes the selection of the type of the strengthening exercise, strengthening progression features, and injury avoidance. The strengthening exercise should also be adapted to the stage of the healing status of injured tissues and to the overall

muscle strength of the patient. This section discusses two biomechanical principles of strengthening exercise [18] and lever systems [19].

2.2.1 Types of Strengthening Exercise

There are three types of the strengthening exercise (isometric, isotonic, and isokinetic types). The isometric strengthening exercise is a static type of the strengthening exercise. During isometric strengthening, muscles contract without any noticeable alteration in either its length or the joint ROM. Although there is no movement, the amount of force and tension developed can be measured. The second type is the isotonic strengthening exercise. Isotonic strengthening is a dynamic type of the strengthening exercise in which muscle contraction occurs with joint movement and excursion. It includes two subtypes, the concentric type, in which the muscle force is produced through contraction (muscle shortening), and the eccentric type, in which the force is produced during muscle lengthening. The third type, isokinetic strengthening exercise, is a dynamic type of strengthening exercise in which muscle contraction occurs about a joint moving at a fixed velocity.

The maximum force generated with eccentric strengthening contraction is more than during isometric or concentric contraction due to two causes [20]. First, when a muscle is stretched before contraction, more cross-bridges are included, and thus more tension is developed than when muscle contracts from a shortened position. Second, the cross-bridges cycling interaction can occur with less adenosine triphosphate (ATP) hydrolysis than in concentric contractions. However, the eccentric contractions are accompanied by a lesser energy cost and high force output and have a higher tension production that leads to a damage to the muscle-tendon system. Thus, using the eccentric contraction during orthopedic rehabilitation should be performed with caution because of a high incidence of injury.

2.2.2 The Lever System

The lever can be defined as a semirigid or rigid segment that moves on a stationary point (axis) when a force is applied to this segment (not passing through its axis point) [19]. The lever has a capability to assist or resist the muscle contraction. This capability is based mainly on its mechanical advantage. The mechanical advantage of the lever equals the proportion of muscular force to the resistance force. Levers are classified into three categories by the relative locations of the axis, muscular force, and resistance. They include three classes.

For the first class, the axis is located between the force and the resistance. Thus, the force arm can be greater, equal, or less than the resistance arm. For an example, in the extension of the neck. The axis (the atlantooccipital joint) is positioned between the resistance (head weight) and the force (deep cervical extensors). The mechanical advantage may be higher than, less than, or equivalent to 1

depending on the distance of the head to the joint. Thus, the assistance or resistance to the muscle contraction depends on which the lever arm is larger (Fig. 14.5a).

For the second class, the resistance is located between the force and the axis. Thus, the force arm is always bigger than the resistance arm. For an example, the resistance (body weight) is positioned between the axis (the metatarsophalangeal joints) and the force (calf muscle) during standing on the toes. The mechanical advantage of the second class is constantly larger than the first class because the resistance arm is less than the force arm. Thus, it causes an increase in the force production. It is also called the force multiplier lever (Fig. 14.5b).

For the third class, the force is located between the resistance and the axis. Thus, the resistance arm is always bigger than the force arm. For an example, the force (biceps brachii muscle) is positioned between the axis (the elbow joint) and the resistance (forearm weight) during elbow flexion. The mechanical advantage is constantly less than the first class because the force arm is lesser than the resistance arm. Thus, it causes an increase in the speed of movement. It is also called the speed multiplier lever (Fig. 14.5c).

Using lever systems to graduate the strengthening exercise is considered a safe and effective way during orthopedic rehabilitation. For an example, during strengthening exercise for weak shoulder flexors, the strengthening exercise with elbow flexion is easier than with elbow extension while the weight of the upper limb is fixed. This is because when the elbow is flexed the resistance arm is only to the elbow joint; while, when the elbow is extended the resistance arm is to the fingers. Increasing the lever arm of the resistance increases the demand on the muscle to counteract this increase.

2.3 Range of Motion Exercise

Range of motion (ROM) exercise is considered to be an important element of orthopedic rehabilitation and is performed in nearly all orthopedic conditions [21]. The primary aim of ROM exercise is to maintain or increase the joint ROM to prevent the development of joint contractions. Joint contractures can be defined as the limitation in the passive joint range of motion due to a shortening of the muscles and periarticular connective tissues. Joint contractures often occur after fractures due to prolonged immobilization. Joint contractures can limit the passive and active range of motion in one plane or multiple planes. It is important during the application of the ROM exercise to understand the type of the joint movements that the ROM exercises performed through, the fundamental planes and axes of these movements and the type of the ROM exercise that is used. This section discusses the types of joint movements and which type is used during ROM exercises [22], fundamental planes and axes of movements [22] and types of ROM exercise [23].

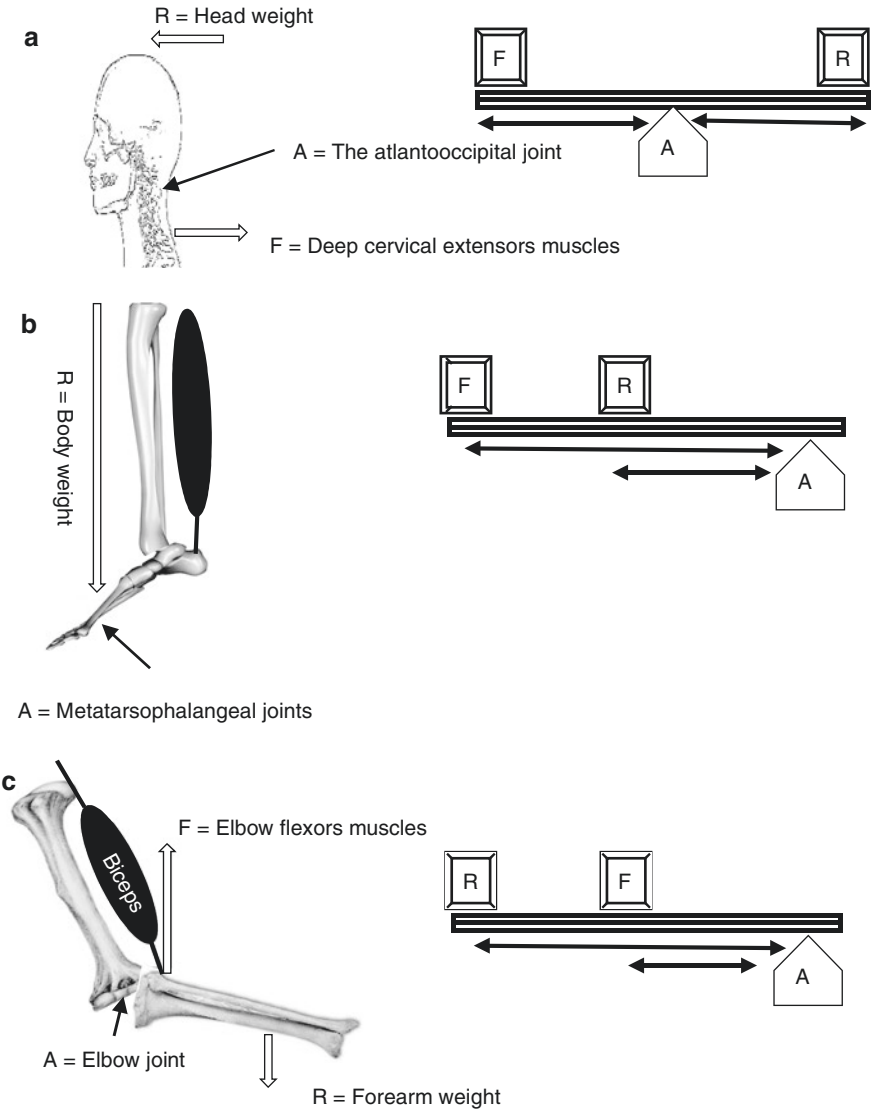

Fig. 14.5 Types of lever systems. (**a**) First class lever. As in the action of the deep cervical extensors muscles. The force is performed by cervical deep extensors muscles to overcome the resistance which is applied by the weight of the head, and the axis is the atlantooccipital joint. (**b**) Second class lever. As in the action of the calf muscle when standing on the toes. The force is performed by the calf muscle to overcome the resistance which is applied by the weight of the body, and the axis is the metatarsophalangeal joints. (**c**) Third class lever. As in the action of the biceps muscle when it flexes the elbow joint. The force is performed by the biceps muscle to overcome the resistance which is applied by the weight of the forearm, and the axis is the elbow joint. *F* muscular force, *R* resistance, *A* axis

2.3.1 Types of Joint Movements

Two primary types of movements occur within joints and there are specific exercises for each movement. The first joint movement is the physiological movement, which is defined as the movement of the two joint bone segments outside the joint through the available ROM. The second joint movement is the accessory movement; it is defined as the movement of the two joint segments inside the joint capsule through the available ROM "joint play" motion. In the ROM exercises the focus is on the physiological movement, while the mobilization exercise focuses on accessory movements.

2.3.2 Fundamental Planes and Axes of Movements

There are three fundamental planes and axes in which physiological movements occur and orthopedic rehabilitation team should be aware of which physiological movement plane is limited such that a ROM exercise plan can be formulated. The first plane is the sagittal plane; it intersects the body into anterior and posterior halves. The axis perpendicular to the sagittal plan in which movements occur is known as the frontal axis. The primary movements of the sagittal plane are flexion and extension. The second plane is the frontal plane which intersects the body into medial and lateral halves and its movement axis is the sagittal axis. Primary movements occurring in the frontal plane are adduction and abduction. The third type is the transverse plane, which intersects the body into upper and lower halves and its movement axis is the vertical axis. The movements occurring in the transverse plane are rotation, elevation, and depression.

2.3.3 Types of ROM Exercise

There are three main types of ROM exercise commonly used during orthopedic rehabilitation. The first type is passive ROM exercise, in which no voluntary contraction occurs and an external force is used to move the segment through the available ROM. The external force can be the other limb, gravity, a machine, or a therapist. The second type is active ROM exercise, in which no external assistance is used and the segment is moved through the available ROM with active voluntary contraction created by the muscles crossing that joint. The third type is the active-assistive ROM; it is a combination of both passive and active ROM. In which the first part of the ROM is actively performed and the second part is passively performed because the agonist muscles cannot complete the whole ROM alone due to its weakness.

2.4 Mobilization Exercise

Mobilization exercise can be defined as a force applied to move the articular surfaces inside a joint. It is performed to improve the joints mobility, ROM or to reduce accompanying pain associated with joint structures via passive or manual accessory joint movement [6]. In order to perform a successful mobilization exercise, the rehabilitation team should know three main aspects. The first aspect is understanding how the accessory movements work to form the mobilization exercise. The second aspect is the biomechanics of the articular surfaces of the treated joint including the convex–concave rule and the loose- and close-packed positions of this joint and the grades for this mobilization exercise. The third aspect is the grades of the mobilization exercise and the indications for each. This section discusses types of joint play movements [24], the convex–concave rule [25], close- and loose-packed positions [26], and grades of the mobilization exercise [27].

2.4.1 Types of Joint Play Movements

The accessory or joint play movements, in which the mobilization exercise is applied, consists of five types. The first type is the rolling movement, in which a new point on one of the two joint bone surfaces contacts new points on the other bone surface. The second type is the gliding movement, in which the same point on one of the two joint bone surfaces contacts new points on the other bone surface. The third type is the traction movement, in which there is a vertical linear separation of the joint surfaces away from the treatment plane. The fourth type is the compression movement, in which there is a vertical linear approximation of the joint surface toward the treatment plane. The fifth type is the spinning movement, in which there is a rotation of one joint surface around a stationary axis. This occurs in either clockwise or counterclockwise directions (Fig. 14.6).

2.4.2 The Convex–Concave Rule

MacConaill is one of the pioneers of kinesiology; he described the convex–concave rule for any moving joint. He demonstrated that the convex–concave rules are based on the shape of the articular surfaces. It includes two conditions depending on which joint surface moves on the other. The first condition, when the convex surface is moving on the concave surface, rolling occurs in the same direction as the movement, while sliding movement occurs in the opposite direction. For an example, during shoulder (glenohumeral) abduction, the humeral head (convex) rolls superior to the glenoid fossa (concave). To perform a successful mobilization exercise to increase the shoulder abduction, the mobilization force should be in the inferior direction (opposite direction) (Fig. 14.7a). The second condition, when the concave surface is the moving on the convex surface, both the rolling and sliding movements occur in the same direction. For an example, during distal radioulnar

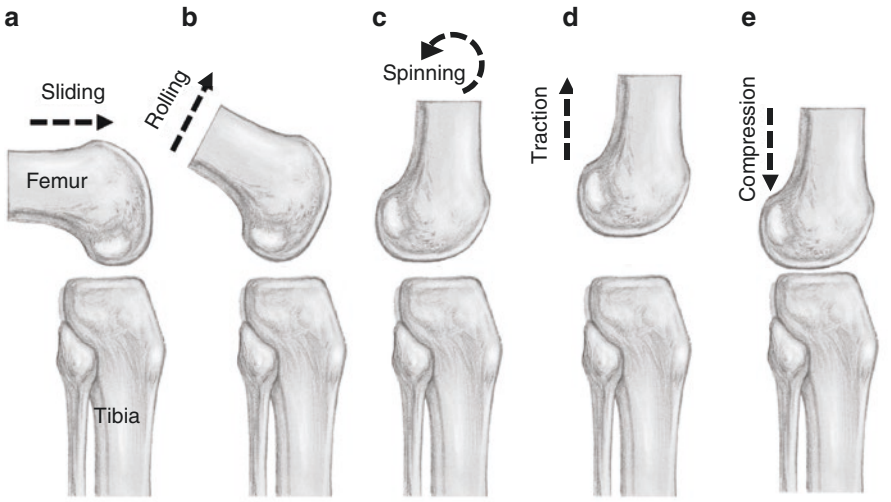

Fig. 14.6 Types of accessory movements. (**a**) Gliding movement, in which the same point on one of the two joint bony surfaces contacts new points on the other bone surface. (**b**) Rolling movement, in which the new point on one of the two joint bony surfaces contacts new points on the other bone surface. (**c**) Spinning movement, in which one joint bony surface rotates around a stationary axis in clockwise or counterclockwise direction. (**d**) Traction movement, in which there is an increase in the vertical linear separation between both joint surfaces away from the treatment plane. (**e**) Compression movement, in which there is a decrease in the vertical linear separation between the joint surfaces away from the treatment plane

joint supination, the radius (concave) moves on the ulna (convex). To perform a successful mobilization exercise to increase distal radioulnar joint supination, the mobilizing force should be in a posterior direction (same direction) (Fig. 14.7b).

2.4.3 The Close- and Loose-Packed Positions

There are two common positions for any joint. The first position is the close-packed position; it is a joint position in which the capsule ligaments are taut and there is a maximum contact between the two contacting bones. It is the most congruent position of the joint. The second position is the loose-packed position; it is a joint position in which the capsule ligaments are loose and there is a minimum contact between the two contacting bones. It the loosest position of the joint. The mobilization exercise should be performed in the loose-packed position, not in the close-packed position, because a greater movement can be achieved in this position.

2.4.4 Grades of the Mobilization Exercise

The grades of the mobilization exercise depend on several biomechanical factors including speed, movement amplitude, and oscillations degree. The mobilization exercise has five grades based on the previous factors. Grade 1 is a low speed, small

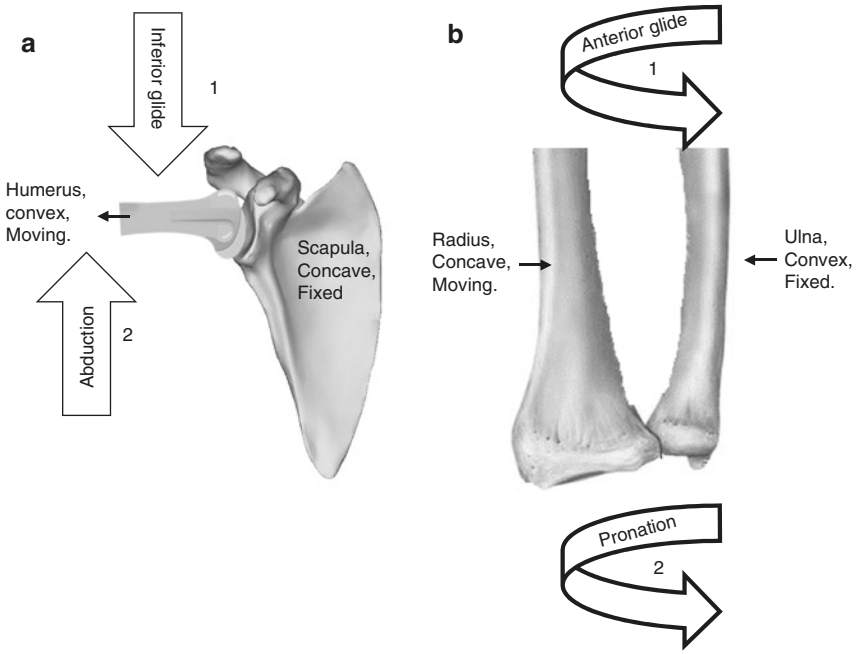

Fig. 14.7 The convex–concave rule. (**a**) Mobilizing force. (**b**) Movement direction. (**a**) The mobilizing force for increasing shoulder abduction is performed in an opposite direction to the desired movement (inferior glide) because the convex humeral head moves on the concave glenoid cavity of the scapula (convex on concave rule). (**b**) The mobilizing force for increasing the pronation in the distal radioulnar joint is performed in a same direction of the desired movement (the anterior glide) because the concave ulnar notch on the radius moves on the convex ulnar head (concave on convex rule). *1*: mobilization force direction and *2*: direction of desired movement

oscillations and small amplitude movements are performed at only the beginning of the available ROM. It is mainly used to decrease pain. Grade II is a low speed, small oscillations and large amplitude movements are performed near the middle of the available ROM. It is mainly used to decrease pain. Grade III is a low speed, small oscillations and large amplitude movements are performed near the end of the available ROM. It is mainly used to increase the ROM. Grade IV is a low speed, small oscillations, and small amplitude movements are performed at the end of the available ROM. It is mainly used to increase the ROM. Grade V is a high speed, large oscillations and small amplitude movements are performed beyond the end of the available ROM. It is called manipulation.

3 Biomechanical Concepts in Orthopedic Rehabilitation

The application of the biomechanical principles in orthopedic rehabilitation helps the rehabilitation team to perform the rehabilitation of orthopedic disorders in a more effective and safe manner and to decrease the recovery time for these disorders.

This part discusses common biomechanical concepts applied to orthopedic rehabilitation strategies for upper and lower limb joints.

3.1 The Upper Limbs

The upper limbs consist of several joints, including the shoulder, elbow, wrist, and hand joints. Upper limb functions typically consist of activities that require a high degree of mobility.

3.1.1 The Shoulder Girdle

The shoulder girdle is responsible for complex movements which are important for functional activities. To perform optimally, the shoulder girdle must work together in a synchronized and coordinated manner in order to perform overhead activities, such as hair brushing and reaching to a high shelf [28]. This section discusses the common biomechanical principles utilized in orthopedic rehabilitation for management of shoulder joint stiffness [29, 30], shoulder joint dislocations, and subluxations [31, 32].

Shoulder Joint Stiffness

Prolonged immobilization or pain in the shoulder joint often produces shoulder joint stiffness which limits overhead movements. These complications are often related to not only stiffness in the glenohumeral joint but also reduced upward rotation of the scapula. To treat the upward rotation limitation of the scapula, the rehabilitation team should strengthen all the muscular forces that produce this movement. The normal scapular rotation movements include two force couples which rotate about an axis (center of the scapula); each rotation is performed by three muscles. The upward rotation of the scapula occurs when the glenoid fossa turns upward and the inferior angle of the scapula move superolaterally away from the spinal column. Upward rotation of the scapula is performed by the upper fiber of trapezius, lower fibers of trapezius, and the serratus anterior muscles (Fig. 14.8a). The downward rotation of the scapula occurs when the inferior angle of the scapula moves inferomedially toward the spinal column and the glenoid fossa returns to its normal position. Downward rotation of the scapula is performed by the levator scapula, rhomboids, and pectoralis minor muscles (Fig. 14.8b).

The upward rotation moment of the scapula can be calculated by equation of moments as follows (Eq. (14.1)):

$$\Delta M = M_1 + M_2 + M_3 \tag{14.1}$$

$$M = F \times \mathrm{ma} \tag{14.2}$$

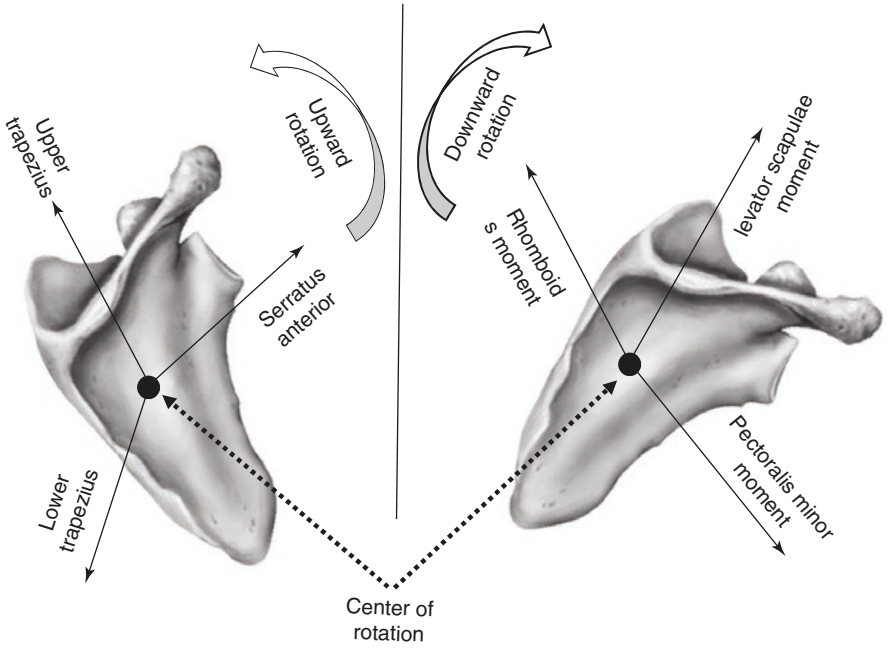

Fig. 14.8 The muscular forces included in upward and downward rotations of the scapula. (**a**) Upward rotation of the scapula is performed by action of three moments rotate around a fixed axis of rotation (center of the scapula). These moments include upper trapezius, lower trapezius and the serratus anterior moments. (**b**) Downward rotation of the scapula also is performed by action of three moments rotate around a fixed axis of rotation (center of the scapula). These moments include levator scapula, rhomboids, and pectoralis minor moments

$$\Delta M = \left(F_1 \times \mathrm{ma}_1\right) + \left(F_2 \times \mathrm{ma}_1\right) + \left(F_3 \times \mathrm{ma}_3\right) \tag{14.3}$$

where M: moment, F: force, and ma: moment arm from the center of scapula (center of rotation).

According to the previous equations, to increase the upward rotation of the scapula during orthopedic rehabilitation, the rehabilitation team should increase the force of all three muscles responsible for upward rotation of the scapula. Because theses muscles act together from different directions to induce rotation, any decrease in the force production due to weakness or pathology can affect scapular rotation.

Shoulder Joint Dislocations or Subluxations

In orthopedic rehabilitation of the shoulder dislocations or subluxations, the orthopedic rehabilitation team should focus on strengthening the deltoid muscle to minimize the recurrence of shoulder dislocation or subluxation because the deltoid muscle circles the shoulder joint from three directions, superiorly, medially, and laterally. The deltoid

muscle is a multipennate muscle which is advantageous because pennate muscles possess more muscle fibers oriented in parallel which allows for more force production than any other type of the skeletal muscle. In pennate muscle, considering the physiological cross-sectional area (PCSA) is more accurate than the anatomical cross sectional-area (ACSA) because the ACSA in these muscles does not represent all muscle fibers (Fig. 14.9). The PCSA is increased in length with the increase in the pennation angle and with muscle length. In a pennate muscle, PCSA is always larger than ACSA. It can be calculated by the following equation [Eq. (14.4)].

$$\text{PCSA} = \text{muscle volume} / \text{fiber length} \tag{14.4}$$

In pennate muscles, muscle force can be calculated by these equations Eqs. (14.5) and (14.6)

$$\text{Total force} = \text{PCSA} \times \text{specific tension} \tag{14.5}$$

$$\text{Muscle force} = \text{Total force} \times \cos\Theta\left(\text{angle of pennation}\right) \tag{14.6}$$

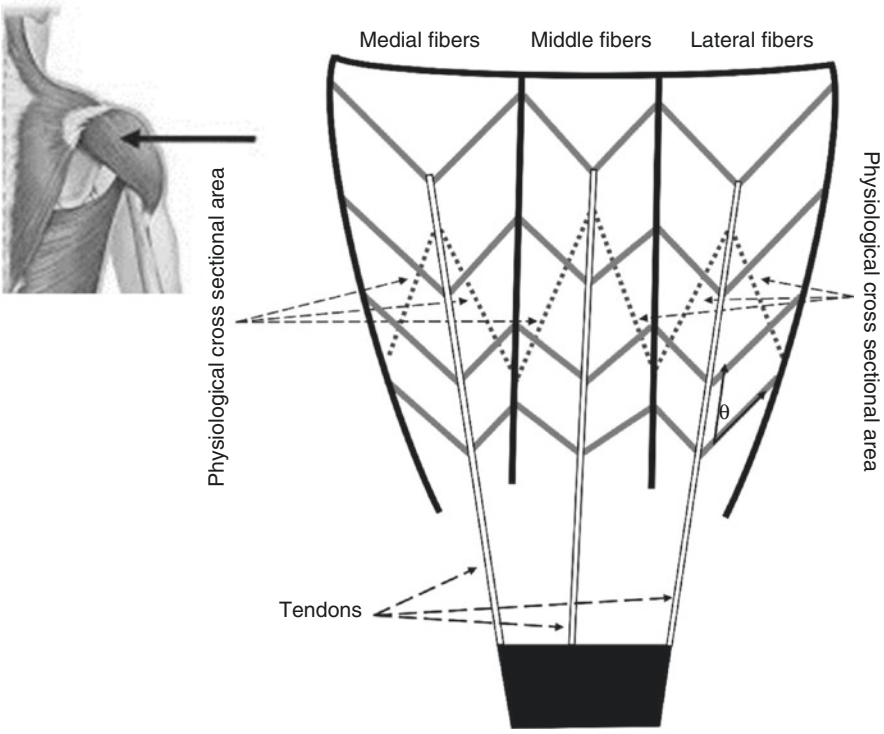

Fig. 14.9 The Deltoid muscle. It is a multipennate muscle that contain several muscle fiber orientations. PCSA is more accurate than the ACSA in the presentation of all its muscle fibers. The pennation angle (Θ) is the angle between the tendon and the fiber orientation. Its force production equals the summation of all forces generated in it, thus its force production is high

The deltoid muscle is also composed of three types of fibers, including anterior, middle, and posterior. Thus, deltoid muscle force production is greater than the unipennate muscles. This increases its force production as well. In the case of a dislocated or subluxated shoulder joint, therapists should prescribe deltoid strengthening to increase the compression force inside the glenohumeral joint. Ultimately, compression force inside the glenohumeral joint increases and glenohumeral joint stability improves.

3.1.2 The Elbow Joint

The elbow joint consists of three bones, including humerus, ulna, and radius bones. The articulations between these bones form the elbow complex. The elbow complex consists of four joints, the humeroulnar (main elbow joint), humeroradial, superior radioulnar, and inferior radioulnar joints. The orthopedic rehabilitation protocol for the elbow ligaments injuries should focus on offering the injured ligament to be healed maximally while minimizing the hazards of joint stiffness, residual instability, and posttraumatic arthritis [33]. This section discusses common biomechanical principles applied to orthopedic rehabilitation specific to the elbow joint collateral ligaments, the medial (ulnar) [34, 35] and lateral (radial) [36, 37].

Medial (Ulnar) Collateral Ligament

MCL exercise should be performed with the forearm in pronation. Elbow flexion from a pronated position increases the force production of the biceps muscle and increases the axial compressive force inside the elbow joint. Biceps brachii muscle inserts into the radial tuberosity. With forearm pronation, the radial tuberosity moves away and this increases the length of the biceps muscle. This increases the compression force between the trochlear notch of the ulna and the trochlea of the humerus. Also, during elbow flexion exercise, this lengthening in the biceps brachii before its contraction causes an increase in its force production that increases the level of the compression force inside the elbow joint during exercises.

Passive mobilization of the deficient MCL should be performed when the forearm is in supination because the forearm supination generates an external rotation moment on the ulna that closes the medial side of the elbow effectively and this increases the stability of the elbow joint. The movements of the radius and ulna are related to each other and it takes place around an axis that passes from the center of the head of the radius to the base of the styloid process of the ulna. External rotation of the ulna takes place with forearm supination and internal rotation of the ulna takes place with forearm pronation. In a forearm supination, the external rotation moment pulls the ulna medially inside the elbow joint; this increases the pull on the ulna inside the joint and gives a more elbow stability (Fig. 14.10).

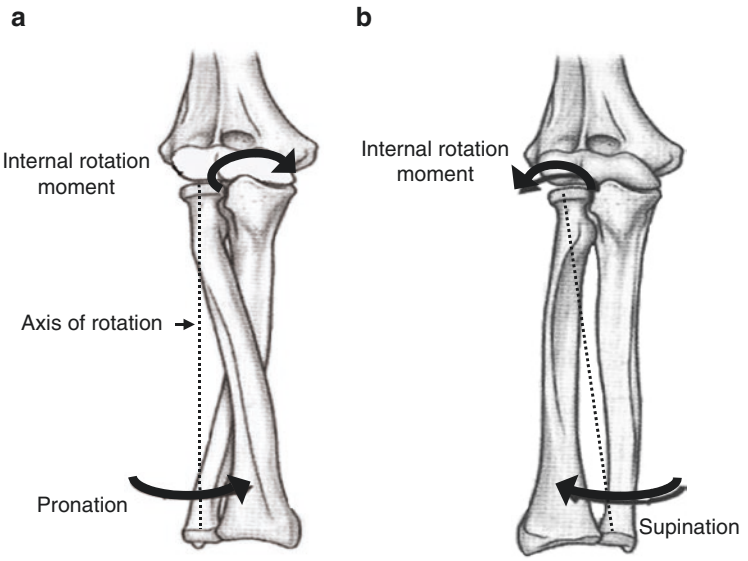

Fig. 14.10 Types of moments placed on the ulna during elbow supination and pronation. The movements of the radius and ulna are related to each other and they take place around an axis that passes from the center of the head of the radius to the base of the styloid process of the ulna. External rotation of the ulna takes place with forearm supination and internal rotation of the ulna takes place with forearm pronation. In a forearm supination, the external rotation moment pulls the ulna medially inside the elbow joint; this increases the pull on the ulna inside the joint and gives a more elbow stability

The Lateral (Radial) Collateral Ligament

The LCL is a key stabilizer which resists both the varus stresses and the rotational instabilities which prevents elbow joint laxity. Forearm pronation helps to stabilize the LCL lacking while the arm is passively flexed in a vertical orientation because the internal rotational torque placed on the wrist to keep the forearm in a pronation causes the ulna to be hinged over the intact soft tissues on the medial side of the elbow. This overlapping closes the valgus stress on the lateral side of the elbow. Thus, patients with acute posterolateral rotatory instability can be actively and passively mobilized early by keeping the elbow in a full pronation.

Patients with LCL injuries should exercise with the arm positioned in a gravity-loaded overhead position, because in this position, the gravity and contraction of the biceps brachii, brachialis, and triceps brachii increase axial compression, congruency, and stability of the elbow joint. When elevating the arm above head, the gravity and these previous muscles that connect the humerus to the ulna or radius apply downward forces. These forces help to approximate the joint surface and increase the compression force inside the elbow joint and consequently improve its stability.

3.1.3 Wrist and Hand Joints

Wrist and hand are complicated structures that contain high numbers of joints to allow performance of several fine motor activities such as writing, painting, and grasping. All of these joints are inter-related and must work together in harmony to achieve optimal functioning at the hand and wrist. Good understanding of the biomechanics of the hand and wrist joints is crucial to treat these injuries. This section discusses common biomechanical concepts applied to wrist injuries [38] and in the carpal tunnel syndrome [39, 40].

Splints for Treatment of the Wrist Injuries

Splinting is an effective rehabilitation tool for treatment of wrist injuries. Splints usually follow the rule of the first-class lever systems through use of three points of pressure techniques. The first force is located on the wrist joint and the two other forces are located proximally (forearm component) and distally (palmar component) to the wrist joint. These proximal and distal force components provide a counterforce against the opposing applied middle force. The forearm component represents the force arm, and the palmar aspect represents the resistance arm (the weight of the hand). Before applying the splints to the wrist joint, the three points of pressure must always be well defined. The force applied on the proximal end of the wrist splint can be calculated by measuring the length of the forearm component, the length of the palmar component, and the average weight of the hand.

$$F \times \mathrm{Fa} = R \times \mathrm{Ra} \tag{14.7}$$

Thus,

$$F = \left(R \times \mathrm{Ra}\right) / \mathrm{Fa} \tag{14.8}$$

The mechanical advantage,

$$\mathrm{Fa} / \mathrm{Ra} \tag{14.9}$$

where F: Force applied by the splint, Fa: length of the forearm component, R: weight of the hand, and Ra: the length of the palmar component (Fig. 14.11).

According to the previous equations, increase in forearm component length is recommended to decrease the stress on the healing tissues and to increase the patient's comfort level. Increasing the forearm component length decreases the force required to counteract the weight of the hand to support the splint, and consequently the resultant stress applied to the healing tissues is less. Reduced stress on the healing tissues has been associated with increased comfort and decreased pain.

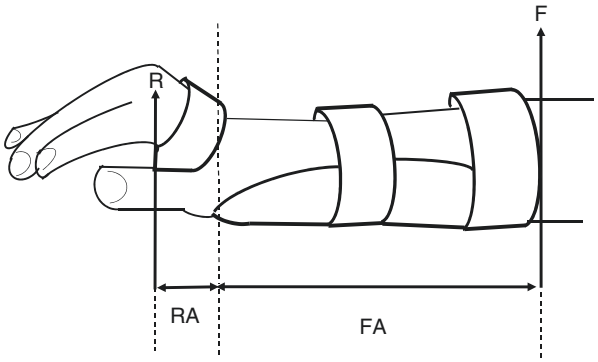

Fig. 14.11 The wrist splint. Wrist splint is considered as the first class lever. The forearm piece should be large to increase the lever arm of the force. This decreases the force needed to overcome the hand weight of the hand. F splint force, F_A force arm, R resistance (hand weight), R_A resistance arm

Splints for Treatment of the Carpal Tunnel Syndrome

Carpal tunnel syndrome is one of the most common injuries to the wrist joint in which the median nerve is narrowed across the carpal tunnel between the radial and ulnar bursa and the synovial membranes of the extrinsic finger flexor tendons. Extension or flexion of the wrist increases the contact stress and motion friction between the tendons on the palmar and dorsal surfaces of the carpal tunnel. The dorsal surface includes the distal head of the radius and the carpal bones. While the volar surface includes the median nerve and the flexor retinaculum.

In carpal tunnel syndrome, the rehabilitation team should focus on relieving the stress on the median nerve. The median nerve is more compressed during wrist flexion than extension because it is located more on the volar side of the carpal tunnel. The resultant compression force on the median nerve during flexion can be calculated by assuming the tendons and nearby structures as a low friction pulley-belt mechanism (Fig. 14.12). The load distribution for the contacting surfaces, F_L, is related to tendon load, F_t, and the anatomical pulley radius, r:

$$F_L = F_t / r$$

Thus, the resultant force, F_R, on the pulley construction is connected to the tendon load and angle of contact between the pulley and the tendon [41].

$$F_R = 2F_t \sin\left(\theta / 2\right) \tag{14.10}$$

Based on the previous equations, wrist splints should be adjusted at angles of "neutral" to 20° of wrist extension to avoid the higher pressure presented on the median nerve during flexion.

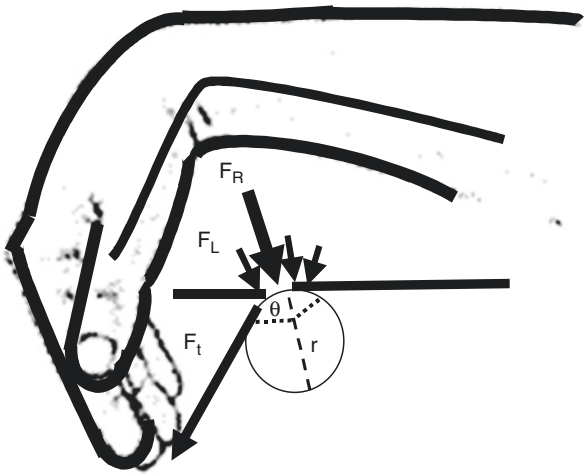

Fig. 14.12 Calculations of the forces applied on the median nerve during wrist flexion. If the tendons and nearby structures are considered as a low friction pulley-belt mechanism, the resultant force F_R is calculated by measuring the load distribution for the contacting surfaces (F_L), the related tendon load (F_t), the anatomical pulley radius (r) and the angle of inclination (θ)

3.2 The Lower Limbs

The main function of the lower limbs is the locomotion and body weight support. Thus, orthopedic rehabilitation should focus on providing more strength to support the body weight. The lower limb consists of several joints the hip, knee joints, and ankle and foot joints.

3.2.1 The Hip Joint

The hip joint has special biomechanical characteristics; it is formed by the articulation between the acetabulum and the femoral head. The acetabulum is deep in order to apply more stability to the hip joint to enable it to carry the weight of the body. Osteoarthritis of the hip joint is commonly due to weight-bearing [42]. Total hip arthroplasty can be a treatment to overcome the severe pain and degeneration with severe hip osteoarthritis. This section discusses common biomechanical concepts that should be applied during orthopedic rehabilitation after total hip arthroplasty [43–45].

The main aims of orthopedic rehabilitation after total hip arthroplasty are to minimize the pain, return function, and decrease possible deformities in the hip joint. The hip abductor peak moment reduction is one of the problems occurring with the total hip arthroplasty that can affect stride length and gait pattern. There are three elements which can cause a decrease in the hip abduction peak moment at the hip.

The first one is the muscle strength related to soft tissue damage. The second one is the surgical approach, as it is supposed that the posterior approach leads to fewer damage to the hip abductor muscles and consequently improved postoperative gait. The third one is the vertical distance between the point of action of the abduction force and the axis of hip rotation.

In total hip arthroplasty, the rehabilitation team must increase the strength of the hip abductors because during walking it counteracts three times the weight of the body during normal standing. To maintain the body in equilibrium during any phase of waking, the muscular moment should counteract the weight of the body moment, according to the equilibrium equation of moments.

In normal standing,

$$\left(M_{\mathrm{R}} \times M_{\mathrm{ma}}\right) + \left(M_{\mathrm{L}} \times M_{\mathrm{ma}}\right) = W \times W_{\mathrm{ma}} \tag{14.11}$$

In single limb support,

$$\left(M \times M_{\mathrm{ma}}\right) = W \times W_{\mathrm{ma}} \tag{14.12}$$

where M_{R}: the muscular force of the right hip abductors, M_{L}: the muscular force of the left hip abductors, M_{ma}: muscle moment arm, W: body weight force, and W_{ma}: is the weight moment arm. The moment arm is defined as the line between the force and the center of the affected hip joint.

Both hip abductors contract to counteract the body weight during the double leg support. In single limb support, the hip abductors of the supporting limb should increase its force to compensate for the other hip abductor force and movement of the weight line of action away from the supporting limb. Thus, the hip abductor of the supporting limb counteracts approximately three times greater body weight than the body weight that placed on it during normal standing. The other element is the distance of the vertical distance between the hip abductors and the center of the hip joint. According to Eq. (14.11), decreased femoral offset decreases the hip abductor moment arm, and consequently increases the hip abductors force to counteract the weight of the body. Thus, in orthopedic rehabilitation after total hip arthroplasty, if the femoral offset is smaller than the normal femoral neck, the rehabilitation team should increase the strength of the affected hip abductors muscles to counteract the decrease in the femoral offset (Fig. 14.13).

3.2.2 The Knee Joint

The knee joint consists of two joints, the tibiofemoral and the patellofemoral joints. The rehabilitation exercise for the knee joint is mainly conducted in two forms, an open kinetic chain (OKC) and a closed kinetic chain (CKC) exercises. The OKC exercise is described as the movement of the knee joint in which the distal segment (tibia and fibula) is freely moving. Non-weight-bearing exercise is considered a

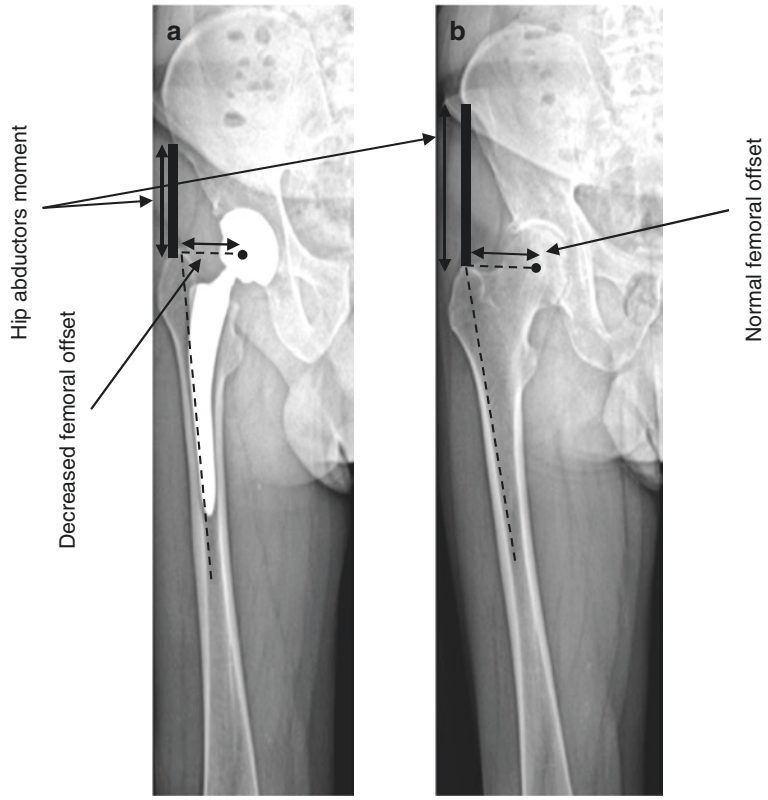

Fig. 14.13 The difference in femoral offset effect on the hip abductors. A decreased femoral offset decreases the hip abductor moment arm. This increases the work required from the hip abductor muscles. (**a**) Decreased the femoral offset. (**b**) Normal femoral offset

regular OKC exercises, such as knee extension from seating on a leg extension machine. The CKC exercise is described as the movement of the knee joint in which the proximal segment (femur) is moving or the movement in which the distal segment of the joint encounters significant resistance. The weight-bearing exercise is considered a typical CKC exercise such as a squat or step-up. This section discusses the effect of these two exercises on the stability of the tibiofemoral and patellofemoral joints [46].

The Tibiofemoral Joint

The tibiofemoral joint is formed by the articulation of the femur and the tibia. This section discusses the effect of these two types of exercises on the anterior cruciate ligament (ACL) [46–48] and posterior cruciate ligament (PCL) injuries and reconstructions [45, 49].

Orthopedic Rehabilitation of ACL Injuries or Reconstruction Surgery

In orthopedic rehabilitation after ACL injuries or reconstruction surgery, OKC and CKC should be performed correctly to avoid applying overloads on the healing ACL or on ACL graft. During OKC knee extension, OKC exercise should not be performed in the last 45° of knee extension. The OKC exercise is provided by contraction of the quadriceps muscles, which causes an anterior translation of the tibia. When a load is conducted vertically to the distal region of the leg, a resultant posterior shear movement of the femur (anterior shear of the tibia) occurs. The anterior cruciate ligament (ACL) resists about 85% of the restrictive force to this anterior tibial shear movement. The stress on the ACL increases during the last 45° of knee extension due to an increase in the anterior tibial translation in this range. Thus, any exercise in this range should be avoided following ACL reconstruction as it places an adverse effect on the ACL graft or on the injured ACL. After 45°, the tibial translation is decreased at 60° and 75° of knee flexion because the patellar tendon exerts approximately a vertical torque (0°) on the tibia in an upward direction (Fig. 14.14). Thus, in this range, quadriceps contraction cannot cause either an anterior or posterior tibial translation.

The degree of strain applied on the ACL during the OKC exercise depends in addition to the angle of knee flexion, also on the level of quadriceps activity. Isometric OKC contraction of the quadriceps at 15° and 30° causes an average peak of a strain of 4.4% and 2.7%, respectively, whereas at 60° and 90° of knee flexion there is no ACL strain. Therefore, it is recommended to use the exercises that produce no to low strain on the ACL. This exercise involves quadriceps muscle strengthening with a flexed knee at 60° or higher, or unloaded knee movement amid 35° and 90° of flexion. The healing graft of ACL is susceptible to be failed if exercises are aggressive.

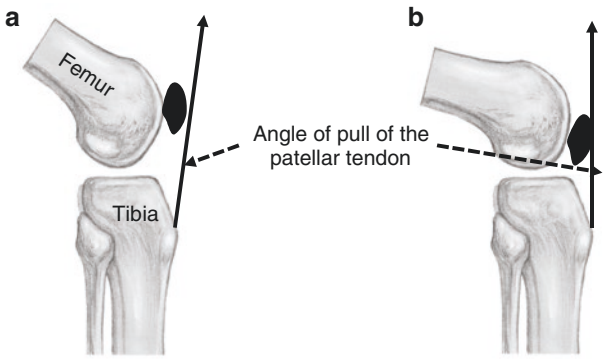

Fig. 14.14 The anterior tibial translation during 45° and 75°. (**a**) At 45° of knee flexion, there is a large anterior transition tension which is not recommended during early ACL rehabilitation. (**b**) At 75° of knee flexion there is a decrease in the anterior transition force because the patellar tendon exerts approximately a vertical torque (0°) on the tibia in an upward direction

OKC of knee flexion is produced by the contraction of the hamstrings muscle. During OKC isometric hamstring contractions there is no to low strain on the ACL. Thus, all OKC knee flexion exercises produce insignificant stress on the ACL and should be utilized carefully during the rehabilitation after ACL injury or reconstruction.

CKC exercise is commonly prescribed by clinicians after ACL injuries or reconstruction surgery because CKC exercise decreases the tibiofemoral shear stress by raising the joint compression and muscular co-contraction between the hamstring and the quadriceps. This decreases the stress on the injured ACL. During CKC, the line of force is positioned more centrally in comparative to the tibia. This minimizes the axial compression and the shear forces on the ACL. Consequently, the joint displacement is minimized. Weight-bearing exercise causes a small anterior tibial displacement in comparative to non-weight-bearing exercise. All squat types (power, front, and lunge) produce a back tibiofemoral shear stress. The effect of load on the injured or reconstructed ACL is nonsignificant during weight-bearing exercise because the total anteroposterior translation is decreased by about 50–66% in healthy ACL and by about 42–71% in unhealthy ACL. During squatting, both quadriceps and hamstring contract to resist the flexion moment. The quadriceps muscle resists the flexion moment at the knee and the hamstrings contracts to resist it at the hip joint.

CKC exercises can be performed without co-contraction between the quadriceps and hamstring muscles. In squats with straight leg, the body is located posterior to the knee joint. So, quadriceps must resist the increase in knee flexion moment. In contrast, in the upright squat, the body is located somewhat back to the knee, Thus, a co-contraction is raised among the quadriceps and hamstring muscles. Also, bicycling is considered a type of CKC exercise. Throughout bicycling the values of mean peak ACL strain were relatively low (1.7%). Thus, bicycling can be used for increase thigh musculature strength without harming ACL.

Orthopedic Rehabilitation of PCL Injuries or Reconstruction

PCL injuries are less common than ACL injuries. During OKC knee flexion, the contraction of the hamstring causes a posterior translation of the tibia; this exerts a stress on PCL. The posterior translation of the tibia is minimum at full extension and progressively increases with increasing the knee flexion angle to be 11.4 mm at 90° of knee flexion. The posterior shear force exerted on the tibiofemoral joint throughout the entire range of flexion reaches its peak at 75° of knee flexion. The isometric OKC exercise of flexion should be performed at full knee extension or it should be avoided in the earlier periods of PCL injuries or reconstruction.

The synchronized knee and hip extension in CKC exercise, when it is performed from a flexed position makes two actions, elongates the rectus femoris across the hip joint and shortens it across the knee joint. However, the hamstring elongates across the knee and shortens across the hip; the resultant eccentric and concentric contraction at the origin and insertion of the muscle produce a “pseudo isometric contraction” which is called “concurrent shift.” This type of contraction is useful for

functional activities such as gait, run, stair climb, and jump and cannot be regenerated by isolated OKC exercises. Thus, CKC exercises are safely related to anterior shearing forces placed on the tibia and it can be performed safely in the early phase of orthopedic rehabilitation following PCL surgery.

The Patellofemoral Joint

The patellofemoral joint is composed of the articulation between the femur (proximal) and the patella (distal). The stability of this joint is based mainly on the active and passive restraints within the knee. The main passive restraints include the lateral patellar and the medial patellofemoral ligaments. It accounts for about 60% of the whole restrictive force. The lateral retinaculum accounts for 10% and the medial patellomeniscal ligament accounts for 13% of the resistive components to the lateral displacement of the patella. While for medial patellar translation, the main passive resistive components to it are the structures that make the profound and superficial lateral retinaculum. The deep retinaculum is made by the lateral patellofemoral ligament, the lateral patellotibial ligament, and the deep fibers of the iliotibial band. The superficial retinaculum is made by fibers from the iliotibial band and vastus lateralis.

In knee flexion training, during CKC flexion training, with the increase in the flexion, the knee flexion moment arm increases. This requires a high quadriceps and patellar tendon tension to offset the increase of the flexion moment arm. This leads to a higher patellofemoral joint reaction force (PFJRF) with knee flexion. During gait, the PFJRF is equal to the half of the body weight. In ascending and descending stairs, the PFJRF is about 3–4 times the body weight. In squatting, the PFJRF is about 7–8 times the body weight. This data can illustrate the increase in patellofemoral pain with activities that include progressive knee flexion with weight-bearing.

During OKC extension, there is an increase in the knee flexion moment arm with a decrease in the patellar extension moment arm. This increases the request for the quadriceps force to make the knee extension, particularly at full range. This illustrates the extensor lag that occurs with quadriceps weakness as in poliomyelitis.

In OKC knee extension, the peak PFJRF at 36° of flexion is 4 times of the weight of the body. It is decreased to half of the weight of body with full extension. Thus, the straight leg raise and short arc quadriceps exercises are recommended to perform from 20° to 0° during the initial phase of orthopedic rehabilitation. The PFJRF and patellofemoral contact stress are higher with OKC leg extension exercise in comparison with the leg press from 0° to 45° knee flexion. While, from 50° to 90° knee flexion, the PFJRF and contact stress were higher for the leg press in comparison with the OKC leg extension exercise.

In knee extension training, with OKC exercises, the forces across the patella are minimum at 90° knee flexion. With knee extension from 90° of flexion, the PFJRF rises, and there is a decrease in the patellofemoral contact area. This causes more contact stress with knee extension until about 20° because the patella is non-contacting the trochlea. With CKC exercise, there are minimum

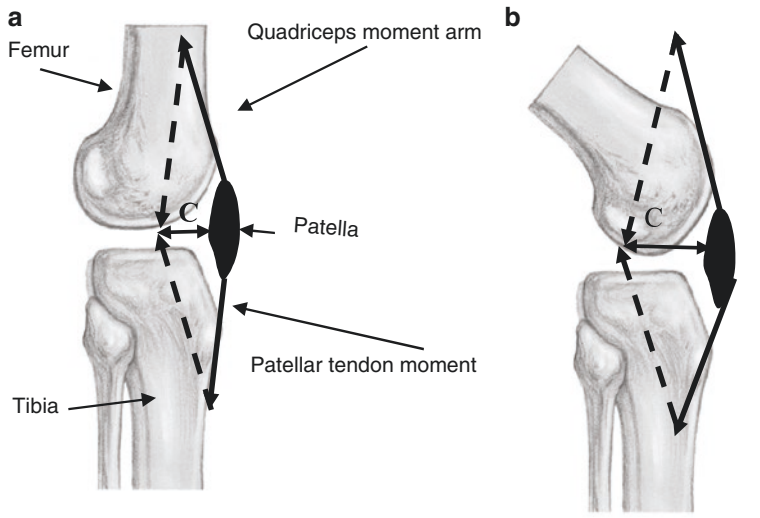

Fig. 14.15 The patellofemoral resultant compression force. The compression force on the patella increases with the increase in knee flexion (**a**). Thus, in the painful proximal lesion of the patella, exercises should be avoided from 60° to 90° of flexion (**b**). (**c**) Resultant compression force

forces across the patella at 0° of extension. With knee flexion, PFJRF increases with an increase in the patellofemoral contact area. This initial increase in the PFJRF causes a reduction in contact stress, then, the contact stress increases with flexion progression subordinate to the increase in joint reaction force (Fig. 14.15).

Both CKC and OKC exercises are performed to treat the patients with patellofemoral pain if conducted in the pain-free range. CKC exercises for the patellofemoral joint are better tolerated during 0–45° of knee flexion. During this range, CKC exercise includes leg presses, step-ups, and mini-squats. In contrast to CKC exercises, OKC training for the patellofemoral joint is better tolerated in the ranges during 20–0° and 90–50° of knee flexion. During these ranges, exercises may include straight leg raises, quadriceps sets, multiple angle isometrics, and short arc isotonic. The aim of the exercising in these previous ranges is to load the quadriceps muscles with lower degrees of the stress exerted on the patella.

3.2.3 The Ankle Joint

Ankle and foot articulations are considered as a closed chain system, in which each bone segments are interdependent and interrelated on each other, and thus their functions are dependent on each other and cannot move autonomously of the others. Hypomobility at any joint affects the whole movement of all joints through a compound sequence of compensations that disturb all other joints.

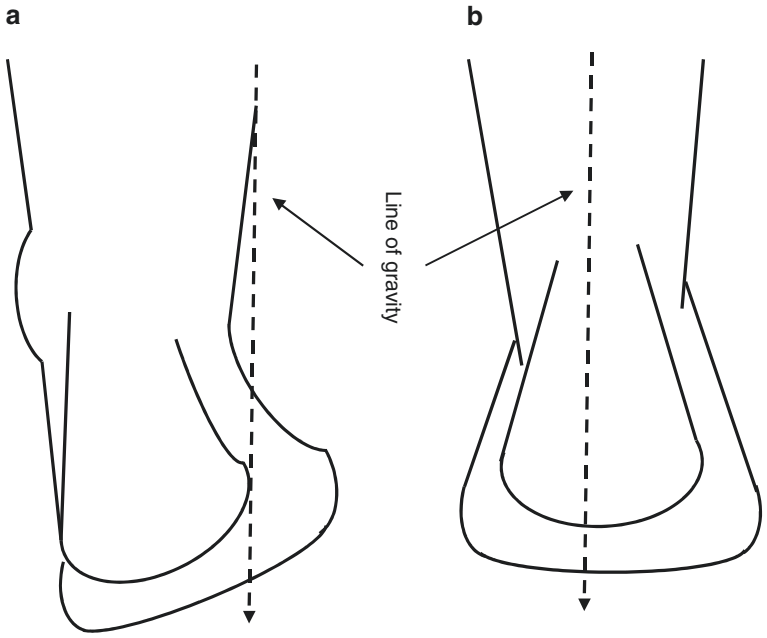

Fig. 14.16 The line of gravity course with normal and supinated foot (posterior view). During supination, the line of gravity moves medially, this increases the stress applied to the lateral side of the ankle and causes a lateral ankle sprain. (**a**) Supinated foot. (**b**) Normal foot

Lateral collateral ligament sprain is a common ankle injury [50]. It results from an increase in the supination moment across the subtalar joint, which results from increasing the magnitude of the upright ground reaction time during initial foot contact. At this position, if the center of plantar pressure deviates more medially to the axis of the subtalar joint, a higher moment arm occurs across the subtalar joint axis. Thus, more supination moment is occurred due to sudden aggressive ankle supination. When the foot is plantarflexed, the initial touch is performed with the forefoot. This increases the moment arm between the resultant joint torque and the subtalar joint axis. Consequently, the sudden aggressive twisting movement results; this causes ankle sprain injury. Thus, during the rehabilitation, ankle taping or bracing for correcting the ankle joint position at stance phase provides more ankle mechanical support [51] (Fig. 14.16). Ankle taping or bracing should apply a varus stress to reduce the stress on the healing tissues and increase the patient comfort.

4 Biomechanics of Assistive Devices

This part discusses assistive devices that are mainly used for ambulation in patients with lower limbs orthopedic disorders. Early ambulation is an essential component to orthopedic rehabilitation because it decreases postoperative complications and

length of stay. Thus, the rehabilitation team should have a complete understanding of assistive device prescription and the biomechanical advantages associated with each. The rehabilitation team should prescribe an appropriate assistive device for each patient in accordance with his/ her abilities and needs and at the correct time during orthopedic rehabilitation. Assistive devices can also be used to decrease pain, decrease inflammation, and compensate for muscle weakness in the lower limbs. The assistive devices include the wheelchairs, walkers, crutches and canes.

4.1 Wheelchairs

The main goal of any orthopedic rehabilitation program is to make patients as independent as possible. Wheelchairs are the main way of ambulation for patients who are unable to ambulate because of both lower limbs amputations. There are several patterns of wheelchair propulsion that patients can use. This section discusses guidelines for wheelchair prescription [52] and biomechanical concepts associated with wheelchair use [53–55].

4.1.1 Guidelines for Wheelchair Prescriptions

Wheelchair prescriptions significantly rely on the relationship between three variables, including the wheelchair user (abilities, needs, and preferences), wheelchair technology (light or heavy), and the environment (home, work, or study) in which the wheelchair is utilized. Numerous factors must be considered when selecting a wheelchair. Firstly, the chair width should be narrow but without applying compression against the hips. A wheelchair which is too tight fitting laterally increases the pressure on the patient hips and waist while a wheelchair that is too wide may increase the side-to-side movement of the patients inside. This increases the friction between the patient and chair. Secondly, the chair length should usually be 5 cm from the back of the chair to knee in order to provide enough length to support the legs. This distributes the weight on a larger surface area, thus decreasing the pressure on the ischial tuberosity and preventing the development of pressure sores. Pressure is calculated by dividing the force (weight of the body) over the area on which the patient sits (chair length) [Eq. (14.13)].

$$P = F / a \tag{14.13}$$

where P pressure, F body weight, and a chair length.

Thirdly, chair back height should be 2 cm beneath the inferior angle of the scapula to allow the scapula to move easily while supporting the back maximally. Fourthly, the patient's head should be in the middle between both shoulders and hips, knees, and ankles at right angles to prevent the development of back deformities as a result of changing the line of gravity to adapt alterations in their positions. Fifthly, the feet

should be supported to avoid overwork of the dorsiflexors which works to keep the feet in a horizontal position and to prevent planterflexor contractures.

4.1.2 Biomechanical Concept of Wheelchair Propulsions

Wheelchair propulsion includes two phases, including the push (stroke, drive) and the recovery phases. The push phase (the force production phase) occurs when the hands are in contact with the hand rims. The second phase is the recovery phase (the non-propulsive phase), in which the hands are repositioned to start the push phase again.

The wheelchair propulsion pattern is mainly determined via the recovery phase during the push phase because the upper limbs are moving in a closed kinematic chain. Movement patterns are mainly two patterns, namely "semicircular" or "pumping" patterns. The semicircular push pattern occurs when the hand passes below the push rim through the recovery phase, producing a semicircular movement. The pumping push pattern occurs when the hands only pass slightly below push rim during the recovery phase. There are two additional propulsion patterns identified, including single loop over (SL) and double loop over (DL). The SL pattern occurs when the hands rise above push rim through the recovery phase. The DL pattern occurs when the hands rise above push rim and then cross over and drop under the push rim through the recovery phase (Fig. 14.17).

Understanding propulsion pattern is important because it can help maximize an individual's quality of life through repetitive strain injury minimization and performances optimization. Importantly, the semicircular propulsion pattern is

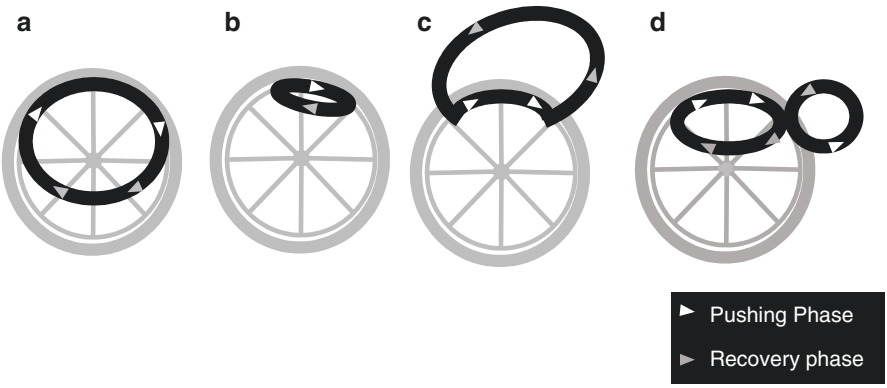

Fig. 14.17 Wheelchair propulsion patterns. (**a**) The semicircular push pattern occurs when the hands pass below the push rim through the recovery phase. (**b**) The pumping push pattern occurs when the hands only pass slightly below push rim during the recovery phase. (**c**) The single loop over (SL) pattern occurs when the hands rise above push rim through the recovery phase. (**d**) The double loop over pattern occurs when the hands rise above push rim and then cross over and drop under the push rim through the recovery phase

thought to be superior to the other population patterns because it is associated with larger push angles. Increased push angles lends to a higher effective force, reduced force loading, and reduced stroke frequency. Ultimately, these biomechanical characteristics may protect from overuse injuries.

4.2 Walkers

Walkers are the most stable assistive devices used for gait training and usually orthopedic rehabilitation begins with it. Walkers have several advantages over crutches and canes, including increasing the patient base of support, anterior stability, and lateral stability and decreasing the weight-bearing and joint reaction forces. This section discusses the main guidelines for walker description [56] and the main biomechanical concepts in weaker-assisted gait [54, 56].

4.2.1 Guidelines for Walker Prescriptions

Walkers' height should be adjusted by the alignment of the top of the frame with the ulnar styloid process. This technique has been shown to provide between 20° and 30° of elbow flexion. This slight elbow flexion permits the patients for a powerful downward push on the walker. This downward push permits patients to bear some of the body weight through the upper limbs. Extended elbow (no flexion angle) causes a decrease in the downward push force. Excessive elbow flexion angle causes the patient to excessively bend at trunk anteriorly. Anterior bending of the trunk can prevent hip extension during the stance phase of gait by moving the center of gravity anterior to the hip joints (Fig. 14.18).

4.2.2 Biomechanical Concept of Walker-Assisted Gait

Strengthening of the elbow extensors should be prescribed by clinicians for all patients that use walker-assisted gait because maximum elbow extension moment far exceeds those at the shoulder or wrist joints. Shoulder flexors and adductors should be strengthened too. The eccentric moment of the shoulder flexors is needed because this represents the eccentric demand on the shoulder flexors to control the deceleration and downward movement of the walker frame. While shoulder adductors counteract the shoulder abduction moment, this abduction moment increases the distal to proximal moment arm away from joint centers and increasing the influence of distal joint forces.

Walker-assisted gait should be explained by clinicians to patients because going too much into the walker during the gait moves the center of gravity backward and increases the tendency to fall backward. The proper technique for walker use involves the patients moving the walker slightly forward first followed by movement of the affected leg forward and finally movement of the unaffected leg comes forward to meet the affected leg.

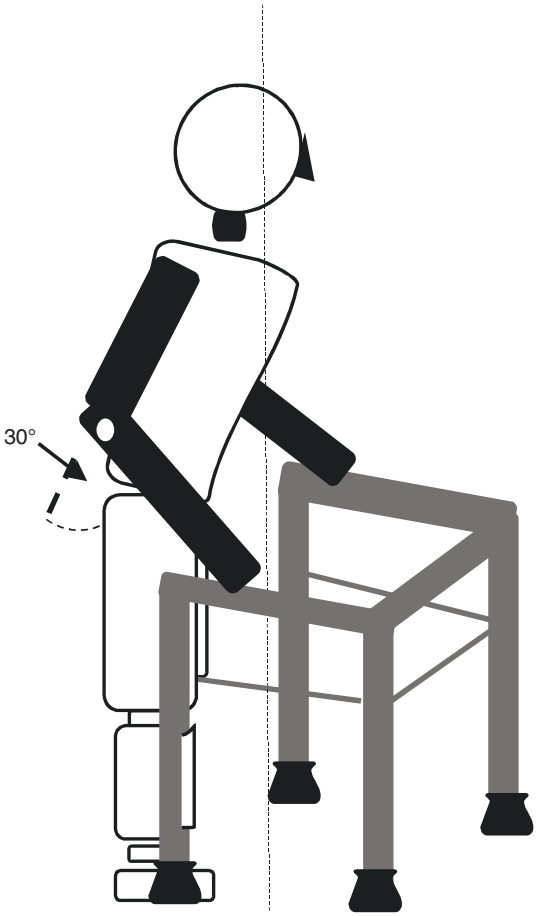

Fig. 14.18 Guidelines for walker prescriptions. Elbows should be flexed about 30°. A slight trunk bending forward is required to move the center of rotation anteriorly to prevent falling backward. Too anterior bending of the trunk could also prevent the hip extension during the stance phase of gait. The patient should avoid going too much into the walker, as this moves the center of gravity backward and increase the tendency to fall backward

4.3 Crutches

Crutches are commonly used in couples. Crutches are commonly used to assist locomotion by decreasing the load on injured tissue, compensating for the loss of muscular control or alleviating pain. This section discusses the guidelines for crutches prescription [54] and the common biomechanical concepts in crutch-assisted gait [57, 58].

4.3.1 Guidelines of Crutch Prescriptions

The main types of crutches are the axillary, triceps, platform, and forearm crutches. The first type is the axillary crutch which is the most common type. In axillary crutches, the patient must avoid complete weight-bearing on the crutch over the axilla during walking to avoid excess pressure on the blood vessels and superficial nerves. This excessive pressure increases incidence of injuries. This excessive

pressure can be decreased by two considerations. Firstly, the upper end of the crutch must be two to three fingers widths under the patient's axilla when the patient is standing with a 30° of elbow flexion. Secondly, putting a sponge rubber to cover the upper end of the crutch to minimize stress against the user's chest. The design of the crutch should include a longer upper end than the lower end to increase the support area on the chest and reduce energy consumption in the initial few minutes of walking. The lower end of the crutch should be padded with a rubber to prevent patient slippage during walking. The crutch should be adjusted to that the lower end of the crutch to be 15 cm from the outside of the patient's feet to avoid the ankle trauma caused by the contact of the crutch with the patient legs during gait (Fig. 14.19).

The other types are less common and each one has a particular purpose. The second type is the triceps crutches. They are prescribed by clinicians for patients with paralyzed shoulder muscles. The proximal part has lateral and medial supports merged with a couple of posterior bands. These supports perform the same action of the triceps muscle to maintain the elbow in extension. The third type is platform

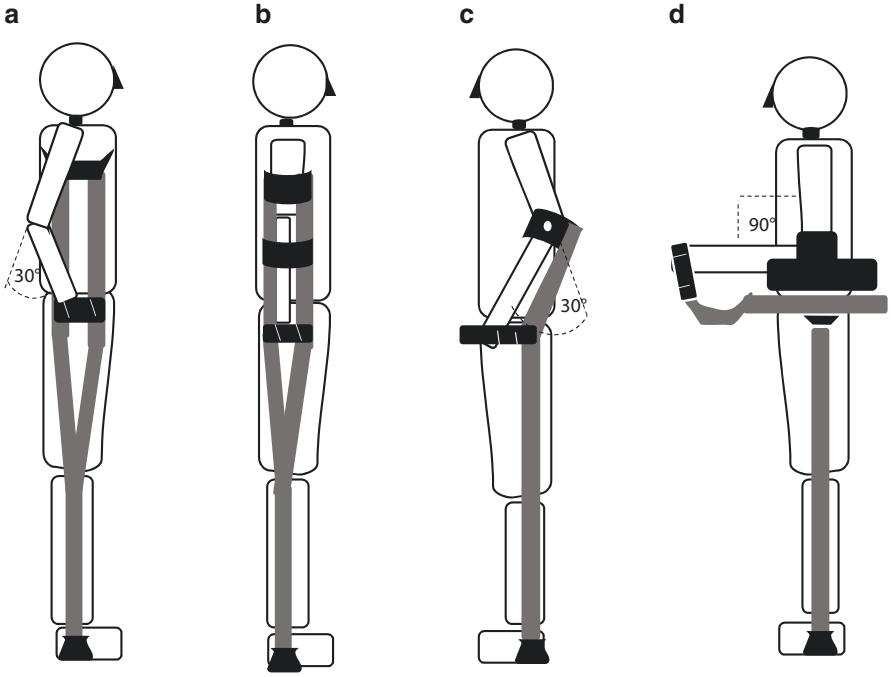

Fig. 14.19 Different types of crutches. All types should be well padded and include a sponge lower tip to prevent the slippage during gait. (**a**) Axillary crutch is the common ones, in which elbow angle is 30°. (**b**) Triceps crutch is used to help the weak triceps muscles, in which elbow angle is 0°. (**c**) Forearm crutch is used when a partial weight bearing only is required, in which elbow angle is 30°. (**d**) Platform crutch has a flat support for loading the weight on the forearm, in which elbow angle is 90°

crutches; they have a flat support for loading the weight on the forearm. These crutches are prescribed for patients with the inability to bear weight transmission over the hand, wrist, or forearm. The fourth type is the forearm crutch, they are prescribed by clinicians to patients who have mild orthopedic problems and need only a partial weight-bearing gait.

4.3.2 Biomechanical Concept of Crutch-Assisted Gait

Crutches should be prescribed by clinicians to adequately fit the crutch to the patients' needs and abilities. There are four patterns of crutche-assisted gait, including 2 points, 3 points, 4 points, swing-through and swing-to patterns. The commonly used patterns are swing-through and 3 point patterns.

Through the swing-through crutch gait, the energy requirements for crutch walking are more than the normal gait. The partial weight-bearing crutch gait demands about 33% more energy than normal gait, and the non-weight-bearing crutch gait demands about 78% more energy. The external flexion moment that acted around the elbow during crutch gait is counteracted by an extension moment provided by the upper arm muscles, particularly the elbow extensors. The mechanical work through the swing-through crutch gait was almost the same as in normal gait; however a higher percentage of this work is done by the upper extremities. The upper limbs muscles are fatigued more quickly than the lower limbs muscles because they are not functionally designed to support the weight of the body. Thus, strengthening exercise to the upper limb muscle particularly elbow and shoulder extensors should be prescribed by clinicians before the use of axillary crutches to avoid early and quick fatigue of these muscles.

Energy consumption of the upper limb during swing-through crutch-assisted gait is greater than during normal gait. This increased energy consumption results in health problems in patients due to crutch-assisted gait, such as upper-limb joint degeneration or nervous system injuries like bilateral ulnar nerves neuropraxia. The possible mechanism to reduce these health problems is to decrease the vertical movement between the body and the crutch tip to make the motion to be performed with less difficulty.

Through the three-point crutch-assisted gait, a decrease in the energy consumption occurs because of the useful kinematic alterations that occur due to adaptation to the crutch-assisted gait. These kinematic alterations include a decrease in the trunk and pelvis rotation and lateral movements, hip flexion and adduction, knee flexion, and ankle plantarflexion at the toe-off. In contrast, the unaffected side exhibits a slight increase in hip abduction and external rotation, and knee flexion. This is because of the movement of the center of gravity away from the affected side slightly to the affected side. Thus, strengthening exercise for both lower limbs should be prescribed by the clinician, not just the affected lower limb, to accommodate the required increase in the unaffected lower limb force.

Three-point crutch-assisted gait is commonly prescribed by clinicians because it offers for different levels of weight-bearing ranging from non-weight-bearing to

full-weight-bearing. In three-points gait pattern, both crutches are moved forward simultaneously, then the affected side is moved and lastly the unaffected side is then moved. The swing-through gait pattern includes moving the crutch forward; then both legs are moved together forward to a point slightly anterior to the crutches.

4.4 Canes

Canes are considered the simplest assistive devices used for ambulation. It is commonly used by older people or people with lower limb osteoarthritis. This section discusses the main guidelines for cane prescription [54, 59, 60] and the biomechanical concepts in cane-assisted gait [61, 62].

4.4.1 Guidelines of Cane Prescriptions

Canes are available with several kinds of handles. The basic one is the inverted U shape which allows patients to suspend the cane on a forearm or back of a chair while it is not in use. Other handle designs include the pistol grip handles which are designed to increase the contact area, thus decreasing the pressure on the hand [Eq. (14.13)]. This design helps to increase comfort and decrease pain. The shaft of the cane can be folded, height adjusted, depending on the subject height. The cane's base should be rubbered with broad deep grooves to prevent its slippage. It should be kept clean to offer ultimate traction. The base can be single or quadruped. The quadruped base increases the base of support and gives more stability to the patients.

The cane should be grasped as its handle's height should permit semi-flexed elbow about 30°. The cane's tip should be at a distance of 15 cm forward and 5–10 cm lateral to the foot. Prolonged use of the cane causes a backward bend of the subject or can interfere with a proper weight that should the cane alleviates. Canes which are too short cause excessive anterior bending in patients. For canes with a wide base, the clinicians should ensure that the base edge of the cane is laterally away from the foot enough to avoid hitting the ankle by the cane base through the swing phase of gait.

4.4.2 Biomechanical Concept of Cane-Assisted Gait

People with lower-limb instability usually use the cane on their ipsilateral side, while people with muscle weakness or pain use the cane on their unaffected side (contralateral). The contralateral use of the cane decreases the hip contact forces more efficiently and encourages the normal reciprocal gait pattern. The decrease in hip contact forces during cane-assisted gait is mainly argued to the increase in the moment arm of the cane which decreases the demand on the abductor muscles of the affected side (Fig. 14.20). The hip abductor muscle force is required

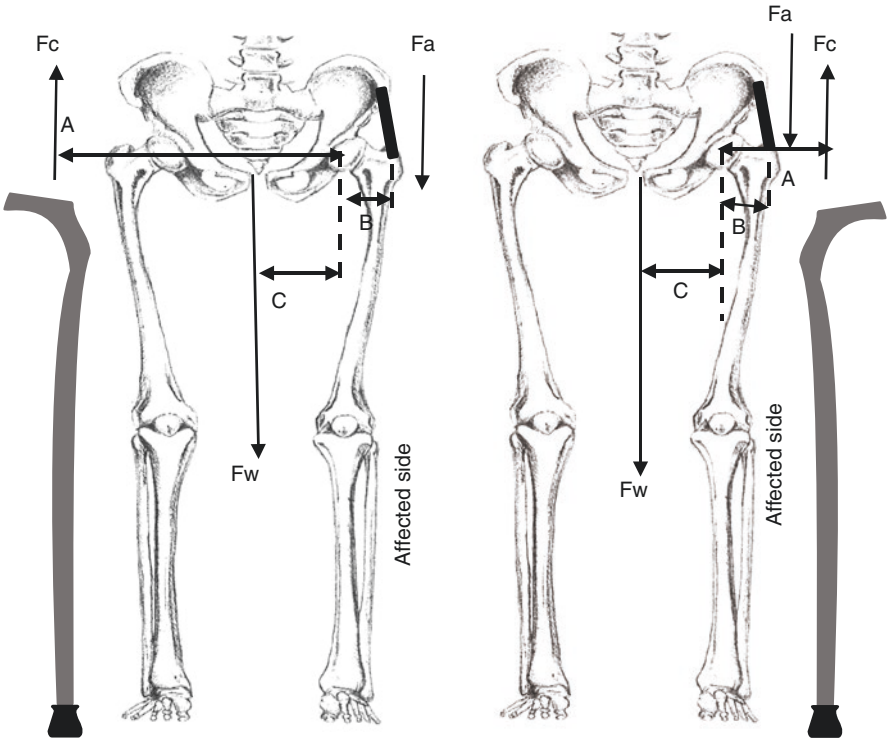

Fig. 14.20 The side of holding a cane in a person with an affected hip joint. The cane should be held in the contralateral side to decrease pain of the affected hip and increase the force of the hip abductor muscle on the affected side. Using the cane on the contralateral side increases the moment arm of the cane and decreasing the need of the affected hip abductors. F_c force of the cane, A moment arm of the cane, F_w force of the body weight, C moment arm of the body weight, F_a force of affected hip abductor muscle and B moment arm of hip abductor muscle

to balance the pelvis during unilateral stance. When the cane is grasped on the affected side, the force of the hip abductor muscles can be calculated by the following equation.

$$F_w \times C = \left(F_c \times A\right) + \left(F_a \times B\right)) \tag{14.14}$$

where F_a: hip abductor force, F_c: cane force, F_w: body weight, A: moment arm of cane, and B: moment arm of the hip abductor and C: moment arm of the body weight. By increasing (A) there is an increase in the (F_a); this leads to a decrease in the demand on the hip abductors to produce high force.

It is shown that the hip contact forces can be decreased up to 56% and the gluteus medius moment can be decreased up to 31.1% with using the cane on the contralateral side in comparison with the normal gait. Thus, clinicians should prescribe the use of the cane on the unaffected side during cane-assisted gait because the use of

the cane on the uninvolved side significantly decreases demands on the hip abductors and consequently decreases compression forces inside the hip joint accompanied with hip adductors contraction.

References

1. Kassab GS. Biomechanics of the cardiovascular system: the aorta as an illustratory example. J R Soc Interface. 2006;3(11):719–40.
2. Koontz AM, McCrory JL, Cham R, Yang Y, Wilkinson M. Rehabilitation biomechanics. In: Wiley encyclopedia of biomedical engineering. 2006.
3. Zhang G. Evaluating the viscoelastic properties of biological tissues in a new way. J Musculoskelet Neuronal Interact. 2005;5(1):85–90.
4. Saldana RP, Smith DA. Four aspects of creep phenomena in striated muscle. J Muscle Res Cell Motil. 1991;12(6):517–31.
5. Knudson D. Fundamentals of biomechanics. 2nd ed. New York: Springer; 2007.
6. Manske RC. Fundamental orthopedic management for the physical therapist assistant. 4th ed. Mosby/Elsevier: St. Louis, MI; 2016.
7. Özkaya N, Nordin M, Goldsheyder D, Leger D. Fundamentals of biomechanics. 3rd ed. New York: Springer; 2012.
8. Magnusson SP, Simonsen EB, Dyhre-Poulsen P, Aagaard P, Mohr T, Kjaer M. Viscoelastic stress relaxation during static stretch in human skeletal muscle in the absence of EMG activity. Scand J Med Sci Sports. 1996;6(6):323–8.
9. Knudson D. Mechanics of the musculoskeletal system. In: Fundamentals of biomechanics. 2nd ed. New York: Springer; 2007. p. 343.
10. Lin DC. Force–velocity relationship of skeletal muscle. In: Encyclopedia of neuroscience. Berlin: Springer; 2009. p. 1611–5.
11. Knudson D. The biomechanics of stretching. J Exerc Sci Physiother. 2006;2:3–12.
12. Duong B, Low M, Moseley AM, Lee RYW, Herbert RD. Time course of stress relaxation and recovery in human ankles. Clin Biomech. 2001;16(7):601–7.
13. Minozzo FC, Baroni BM, Correa JA, et al. Force produced after stretch in sarcomeres and half-sarcomeres isolated from skeletal muscles. Sci Rep. 2013;3:77–86.
14. Decoster LC, Cleland J, Altieri C, Russell P. The effects of hamstring stretching on range of motion: a systematic literature review. J Orthop Sports Phys Ther. 2005;35(6):377–87.
15. Shrier I. Does stretching improve performance? A systematic and critical review of the literature. Clin J Sport Med. 2004;14(5):267–73.
16. Page P. Current concepts in muscle stretching for exercise and rehabilitation. Int J Sports Phys Ther. 2012;7(1):109–19.
17. Haskell WL, Lee I-M, Pate RR, et al. Physical activity and public health: updated recommendation for adults from the American College of Sports Medicine and the American Heart Association. Circulation. 2007;116(9):1081–93.
18. Kisner C and Colby L. Resistance exercise for impaired muscle performance. In: Theraputic exercise foundations and techniques. 6th ed. Philadelphia, PA: F.A. Davis Company; 2012. p. 157–240.
19. Davidovits P. Static forces. In: Physics in biology and medicine. 4th ed. Academic Press; 2012. p. 8–10.
20. Pasquet B, Carpentier A, Duchateau J, Hainaut K. Muscle fatigue during concentric and eccentric contractions. Muscle Nerve. 2000;23(11):1727–35.
21. Clavet H, Hébert PC, Fergusson D, Doucette S, Trudel G. Joint contracture following prolonged stay in the intensive care unit. CMAJ. 2008;178(6):691–7.
22. Macdermid J. Evidence-based orthopaedics: the best answers to clinical questions. 1st ed. In: Wright JG, editor. Philadelphia, PA: Elsevier Saunders; 2009.

23. Kisner C, Colby L. Range of motion. In: Theraputic exercise founsations and techniques. 6th ed. Philadelphia, PA: F.A. Davis Company; 2012. p. 52.
24. Weigel JP, Arnold G, Hicks DA, Millis DL. Biomechanics of rehabilitation. Vet Clin North Am - Small Anim Pract. 2005;35(6):1255–85.
25. Neumann DA. The convex-concave rules of Arthrokinematics: flawed or perhaps just misinterpreted? J Orthop Sport Phys Ther. 2012;42(2):53–5.
26. Michael Aloysius MacConaill JB. Muscles and movements: a basis for human kinesiology. Baltimore: Williams & Wilkins; 1969.
27. Kisner C, Colby L. Peripheral joint mobilization/manipulation. In: Therapeutic exercise foundations and techniques. 6th ed. Philadelphia, PA: F.A. Davis Company; 2012. p. 119–156.
28. Müntener M. Functional anatomy of the shoulder girdle. Helv Chir Acta. 1982;48(5): 523–32.
29. Ludewig PM, Cook TM. Alterations in shoulder kinematics and associated muscle activity in people with symptoms of shoulder impingement. Phys Ther. 2000;80(3):276–91.
30. Ludewig Paula MJPB. Shoulder impingement: biomechanical considerations in Rehabilitation. Man Ther. 2011;16(1):33–9.
31. Wilk KE, Macrina LC, Reinold MM. Non-operative rehabilitation for traumatic and atraumatic glenohumeral instability. N Am J Sports Phys Ther. 2006;1(1):16–31.
32. Rosso C, Mueller AM, McKenzie B, et al. Bulk effect of the deltoid muscle on the glenohumeral joint. J Exp Orthop. 2014;1(1):14.
33. Alolabi B, Gray A, Ferreira LM, Johnson JA, Athwal GS, King GJW. Rehabilitation of the medial- and lateral collateral ligament-deficient elbow: an in vitro biomechanical study. J Hand Ther. 2012;25(4):363–73.
34. Morrey BF, AK-N TS. Valgus stability of the elbow: a definition of primary and secondary constraints. Clin Orthop Relat Res. 1991;26(5):187–195.
35. Armstrong AD, Dunning CE, Faber KJ, Duck TR, Johnson JA, King GJW. Rehabilitation of the medial collateral ligament-deficient elbow: an in vitro biomechanical study. J Hand Ther. 2000;25(6):1051–7.
36. Patterson SD, Johnson JA, King GJW. Muscle forces and pronation stabilize the lateral ligament deficient elbow. Clin Orthop Relat Res. 2001;388:118–24.
37. Manocha RHK, Kusins JR, Johnson JA, King GJW. Optimizing the rehabilitation of elbow lateral collateral ligament injuries: a biomechanical study. J Shoulder Elb Surg. 2017;26(4):596–603.
38. Duncan RM. Basic principles of splinting the hand. Phys Ther. 1989;69(12):1104–16.
39. Walker WC, Metzler M, Cifu DX, Swartz Z. Neutral wrist splinting in carpal tunnel syndrome: a comparison of night-only versus full-time wear instructions. Arch Phys Med Rehabil. 2000;81(4):424–9.
40. Page MJ, Massy-Westropp N, O'Connor D, Pitt V. Splinting for carpal tunnel syndrome. Cochrane Database Syst Rev. 2012;7(7):CD010003.
41. Armstrong T. Development of a biomechanical hand model for study of manual activities. In: Ronald Easterby KHE, Kroemer DBC, editors. Anthropometry and biomechanics: theory and application. New York: Plenum Press; 1982. p. 188–9.
42. Baker-LePaina JC, Lane NE. Relationship between joint shape and the development of osteoarthritis. Curr Opin Rheumatol. 2010;22(5):538–43.
43. Madsen MS, Ritter MA, Morris HH, et al. The effect of total hip arthroplasty surgical approach on gait. J Orthop Res. 2004;22(1):44–50.
44. Ewen AM, Stewart S, St Clair Gibson A, Kashyap SN, Caplan N. Post-operative gait analysis in total hip replacement patients-a review of current literature and meta-analysis. Gait Posture. 2012;36(1):1–6.
45. Shiba N, Tagawa Y, Nakashima Y, et al. Biomechanical effect and clinical application of the hip joint moment reduction brace. Clin Orthop Relat Res. 1998;351:149-157.
46. McGinty G, Irrgang JJ, Pezzullo D. Biomechanical considerations for rehabilitation of the knee. Clin Biomech (Bristol, Avon). 2000;15(3):160–6.

47. Beynnon BD, Fleming BC, Johnson RJ, Nichols CE, Renstrom PA, Pope MH. Anterior cruciate ligament strain behavior during rehabilitation exercises in vivo. Am J Sports Med. 1995;23(1):24–34.
48. Fleming BC, Beynnon BD, Renstrom PA, Peura GD, Nichols CE, Johnson RJ. The strain behavior of the anterior cruciate ligament during bicycling. Am J Sports Med. 1998;26(1):109–18.
49. Lutz GE, Palmitier RA, An KN, Chao EY. Comparison of tibiofemoral joint forces during open-kinetic-chain and closed-kinetic-chain exercises. J Bone Joint Surg Am. 1993;75(5):732–9.
50. Lin C-WC, Hiller CE, de Bie RA. Evidence-based treatment for ankle injuries: a clinical perspective. J Man Manip Ther. 2010;18(1):22–8.
51. Fong DT, Chan Y-Y, Mok K-M, Yung PS, Chan K-M. Understanding acute ankle ligamentous sprain injury in sports. Sports Med Arthrosc Rehabil Ther Technol. 2009;1(1):14.
52. Di Marco A, Russell M, Masters M. Standards for wheelchair prescription. Aust Occup Ther J. 2003;50(1):30–9.
53. Vanlandewijck Y, Theisen D, Daly D. Wheelchair propulsion biomechanics: implications for wheelchair sports. Sports Med. 2001;31(5):339–67.
54. Edelstein J. Assistive devices for mobility: canes, crutches, walkers and wheelchairs. In: Michelle H, Cameron LM, editors. Physical rehabilitation: evidence-based examination, evaluation, and intervention. 1st ed: Saunders; 2007. p. 877–96.
55. Koontz AM, Roche BM, Collinger JL, Cooper RA, Boninger ML. Manual wheelchair propulsion patterns on natural surfaces during start-up propulsion. Arch Phys Med Rehabil. 2009;90(11):1916–23.
56. Bachschmidt RA, Harris GF, Simoneau GG. Walker-assisted gait in rehabilitation: a study of biomechanics and instrumentation. IEEE Trans Neural Syst Rehabil Eng. 2001;9(1):96–105.
57. Li S, Armstrong CW, Cipriani D. Three-point gait crutch walking: variability in ground reaction force during weight bearing. Arch Phys Med Rehabil. 2001;82(1):86–92.
58. Carpentier C, Font-Llagunes JM, Kövecses J. Dynamics and energetics of impacts in crutch walking. J Appl Biomech. 2010;26(4):473–83.
59. Dean E, Ross J. Relationships among cane fitting, function, and falls. Phys Ther. 1993;73(8):494–500-4.
60. Kumar R, Roe MC, Scremin OU. Methods for estimating the proper length of a cane. Arch Phys Med Rehabil. 1995;76(12):1173–5.
61. Ajemian S, Thon D, Clare P, Kaul L, Zernicke RF, Loitz-Ramage B. Cane-assisted gait biomechanics and electromyography after total hip arthroplasty. Arch Phys Med Rehabil. 2004;85(12):1966–71.
62. Bateni H, Maki BE. Assistive devices for balance and mobility: benefits, demands, and adverse consequences. Arch Phys Med Rehabil. 2005;86(1):134–45.

Chapter 15
Biomechanics of Osteo-Synthetics

Chia-Ying James Lin, Heesuk Kang, and Scott J. Hollister

Abstract Osteo-synthetics play critical roles in skeletal tissue regeneration by supporting mechanical integrity as well as enhancing cell–tissue interaction to facilitate tissue formation. These roles can be fulfilled by the functional design of porous architectures to provide proper load bearing and mass transportation for the *neo* tissue formation. These require a simultaneous design for mechanical and mass transport properties. In this chapter, trends for introducing osteo-synthetics in the clinical setting, design parameters for capable implants, and influence of implant physical characteristics on osteointegration are extensively reviewed, followed by introduction of a novel numerical approach to integrate all these factors. We applied a homogenization-based topology optimization scheme to design the three-dimensional unit microstructures for the desired scaffolds. The target effective bulk modulus and isotropic diffusivity are obtained by the optimized porous microstructure. Cross-property bounds between the desired bulk moduli and diffusivities are adapted to determine the defined targets for a given porosity.

Keywords Osseointegration · Multifunctional microstructure · Homogenization Topology optimization · Cross-property bounds

1 Trends in Osteo-Synthetics

Osseointegration occurs when a direct structural and functional connection between ordered, living bone and the surface of a load-carrying implant takes place. However, osseointegration is particularly challenging in traumatic injury and spinal

C.-Y. J. Lin (✉)
Department of Orthopaedic Surgery, University of Cincinnati, Cincinnati, OH, USA
e-mail: chia-ying.lin@uc.edu

H. Kang
Ford Motor Company, Dearborn, MI, USA
e-mail: hkang11@ford.com

S. J. Hollister
Department of Biomedical Engineering, Georgia Institute of Technology, Atlanta, GA, USA
e-mail: scott.hollister@bme.gatech.edu

C.-K. Cheng, S. L-Y. Woo (eds.), *Frontiers in Orthopaedic Biomechanics*,
https://doi.org/10.1007/978-981-15-3159-0_15

arthrodesis where excessive instrumentations are normally required. Spine arthrodesis or fusion has been performed to manage pathological spine disorders and vertebral instability. The number of the procedures increases dramatically to nearly one million cases performed each year [1]. An extensive study in 2001 [2] revealed that in the United States alone, approximately 360,000 patients underwent certain types of spinal arthrodesis. Indications for spine arthrodesis are mostly low back pain, spondylosis and spondylolisthesis, rheumatoid instabilities, postdiscectomy, unstable fractures, trauma, and other lesions. Each of the aforementioned presents different challenges for surgeons in improving the solid integrity as permanent fixation with successful osseointegration to immobilize the interfered motion segments.

Efforts have been made with various approaches to achieve successful bone union. Although autologous bone grafting still remains as the gold standard, ongoing efforts have been pursued to improve healing and decrease the morbidity created during bone harvesting. New design and fabrication techniques with compliant biocompatible or biodegradable materials create less rigid but still mechanically sound systems. Additionally, porous architecture has been incorporated in implants to scaffold ingrown tissue while promoting specific biological interactions to enhance bony reunion. Gene transfer, recombinant protein delivery, and therapeutic cell-based transplantation also provide novel opportunities to replace conventional grafting strategies. All the attempts have collectively pushed the new development of osteo-synthetics that will contribute to successful osseointegration .

2 Potential Design Variable Modifications for Osteo-Synthetics Development

The primary function of osteo-synthetics is to provide immediate stability to the motion segment until arthrodesis is complete so that the existing mechanical deformation will be corrected.

Porous implants made with osteo-synthetics are typically designed with an external shape, surface topography, and pore dimension. These parameters in turn determine the overall performance including mechanical integrity and the integration of tissue ongrowth and ingrowth. Besides the dimensional factors of design, the limitations of the base material presents another big concern. Stress shielding, migration of the implant, and pseudoarthrosis of the motion segment lead to complications that result in problems in osseointegration. The highlight in this chapter is to magnify the request of the rigidity and stability without sacrificing essential compliance as the favorable stimulation for tissue regeneration. A further attempt is to create the implant to be a porous-matrix-like structure as a scaffold to increase osteoconduction and achieve biofactor delivery as bone graft substitutes, such as genes, proteins, growth factors, and/or cells. In all, the goal herein is to develop a triplet construct with osteo-synthetics to maintain segmental stability, deliver therapeutic biofactors, and therefore enhance bone union.

2.1 Motion, Ingrowth, and Stability

Functional osseointegration is highly related to the local mechanical environment at the footprint of implants on bone. Indeed, the way by which the induced motion perform will determine the patterns of the tissue formation. Cuillinane et al. [3] conducted a precisely controlled motion in an experimental mid-femoral defect and reported that the defect of mechanical treatment group failed to achieve union, but instead the neoarthroses formed. The structural composition of molecular components within the newly formed tissue are influenced by their local mechanical environment, which has been investigated with a deep-to-superficial polarity on subcondral bone arcades and a flattened morphology in the midline. This pattern was directed by the applied symmetrical bending motion, which mimicked the mechanical environment in utero join development. Pilliar et al. and Simmons et al. [4–6] pioneered the limited movement between the implant and the surrounding tissue within as a necessary criterion for bone formation onto implants with porous surface. They have then elucidated the morphological change of the tissue-implant interface from radiographs and animal models.

An early report [7] from the group in 1981 showed that excessive movement prevents the calcification of the tissue within the pores and resulted in implant attachment by fibrous tissue only. However, they suggested that the implant fixation supported by fibrous tissue ingrowth can be adequate. In the follow-up studies [5, 6], they concluded different bone formation patterns corresponded to respective local mechanical environment. Appositional bone formation occurred when the strain components at the tissue-host bone interface were less than 8%, while localized, de novo bone formation occurred when the distortional tissue strain is approximately <3%. The studies illustrated that controlled motion in devices with adjacent bone tissue provide some extent of manipulation of bone formation patterns and new construct stability.

2.2 Stress

The bone tissue structure significantly contributes to bone mechanical properties. Bone structure, on the other hand, can be altered to respond stress as described by Julius Wolff [8]. In Wolff's law, the structure will align along the direction of principal stress and the orientation could change if there is a change in mechanical stress direction. This discovery revealed the bone adaptation to mechanical environment. Essentially, Wolff's law implied that bone tissue continues to self-optimize by the remodeling process, attempting to obtain maximum mechanical efficiency with minimum mass.

During fracture healing, the tissue differentiation is related to mechanical stimulus accompanied through the fracture healing history, as postulated by Carter et al [9]. The relation of mechanical stimulus to tissue growth, remodeling, and healing

is based upon the level of vascularity. Earlier, the group also developed an osteogenic index and applied the theory on the numerical models to judge the occurrence of bone, cartilage, and fibrous tissue [10].

Followed by the healing, stress still plays an determinant role in bone remodeling. As noted in the Wolff's law, the bone structure still undergo an optimization to fit in the demand of mechanical requirement without redundancy in the intricate architecture. Guldberg et al. developed an in vivo model of hydraulic bone chamber in their canine metaphyseal trabecular bone and found convincing evidence of microstructural adaptation during trabecular bone repair form microcomputed tomography images [11]. The microstructural adaptation within the bone chamber was similar to that observed in the spinal cage during bony bridge formation. Therefore, if the designed internal architecture of osteo-synthetics could provide a controlled and predictable mechanical stimulation, more reliable construct strength would be obtained.

Implants can share the load applied to bone, and hence stress on the tissue is reduced. This phenomenon is known as stress shielding. According to the Wolff's law, bone would adapt itself by reducing its mass, either by becoming more porous (internal remodeling) or by making the structure thinner (external remodeling), to respond to the decreased load. During spinal fusion, it remains unclear whether the bone quality of the developing interbody fusion mass will be affected due to the shield-stress, and if so, what the threshold of the adequate mechanical load would be required to prevent bone mass loss over the long period. In a more than 8-year postoperative investigation, Cunningham et al. showed the histological composition of cervical interbody fusion in thoroughbred horses and they discovered significant decrease in bone mineral density at the fusion site within the cage compared with the adjacent vertebral bodies [12]. Similarly, a series of clinical reports showed resorption in a manner of reduced cortical thickness and increased porosity were observed in most patients who received noncemented total hip arthroplasty. On the contrary, van Dijk et al. showed that reduced stiffness of cage contributed to the rate of lumber interbody fusion [13]. The group used polymeric material poly(L-lactic acid) (PLLA), which possess an apparently lower elastic modulus (4.2 GPa) compared to titanium (110 GPa), to fabricate a cage with an identical geometry. They found reduced stiffness significantly enhanced interbody fusion as compared with titanium cages after 6 months. The results from their large quadrupedal animal models showed significant improvement in the arthrodesis rate and the quality of trabecular bone in the new constructs [13–15]. This result implied that reduced stiffness of the cage compensates the loss of strain energy to bone tissues.

The relationship between the change of bone density and strain energy was successfully quantified in a remodeling algorithm propose by Huiskes et al. [16]. The model included the idea of a lazy or homeostatic zone where a certain threshold interval exists. Bone mass increases when the strain energy density is above a certain level inferring to the modeling from stress fractures. Below a certain threshold, there is excessive remodeling or absorption of bone; in between these levels is maintenance of bone structure. Therefore, the reduction of shielded stress would

ensure bone tissue adjacent to the implant to acquire sufficient energy to maintain bone mineral density when the rigidity requirement is still placed first in the priority.

2.3 Porosity

In tissue regeneration, porosity, pore size, and interconnectivity of the scaffolding constructs as the factors are critical for nutrient supply to transplanted cells. Large void volume is favorable to vascularization, extracellular matrix deposition, and maximal cell population. Internal pore connection increases diffusion rates to and from the center of the scaffold and enhances the vascularization that improves the mass transportation such as metabolic waste removal and nutrient supply. It has been postulated that bone tends to infiltrate into the pores of an inert porous system [17]. Hence, by creating a highly porous scaffold, bone ingrowth will be more augmented to stabilize the construct of bone and implants. Designing high porous structure for spinal cages would facilitate fusion rate and restabilize the affected segment, especially when cellular grafting is performed as an alternative biological component.

3 Implantology and Osteoconduction

3.1 Influence of Implant Surface Geometry on Osseointegration

It has been shown earlier in series of in vivo studies that implant surface geometry as a design variable significantly influences long-term implant performance [18–20]. Early in 1979, Bobyn and colleagues examined the optimal pore size for the fixation of porous surfaced metal implants by the bone ingrowth [21]. The pore size was investigated to influence the rate of bone ingrowth and the retained maximum fixation strength. They concluded that in the shortest period (8 weeks) a pore size range of approximately 50–400 μm ended up to provide the optimum or maximum fixation strength of 17 MPa. In an earlier report, the group also showed the surface configuration played as an additional role affecting the tensile strength of fixation of implants by bone ingrowth [22]. The results indicated implants with the multiple particle layer surface configuration develop a greater tensile strength of fixation than that provided by implants with the single particle layer surface configuration. Also, they suggested this fixation strength develops more quickly if the cortical bone is petaled prior to implantation. In a more microscopic investigation, Simmons et al. reported the differences in osseointegration caused by surface geometry can be attributed to the alteration of local tissue strains [6]. In their computational modeling, local tissue strain was predicted in two different designs of plasma-sprayed and

porous-surfaced. The result indicated that porous surface structure provided a larger secure region that experienced low distortional and volumetric strains, whereas the plasma-sprayed implant provided little local strain protection to the healing tissue. Coincident with Pilliar's study, low distortional and volumetric strains are believed to favor osteogenesis.

In a more cellular-based study, Carter and Giori suggested that proliferation and differentiation of the mesenchymal cells responsible for surrounding tissues formation of implants are regulated by the local mechanical environment [19]. Put together, the mesenchymal cells tend to be more osteogenic when experiencing low distortional strain and low compressive hydrostatic stress, provided under an adequate vascularity.

3.2 Porous Material

To regenerate tissues and organs with high vascularity, porous structure has been considered as a desirable feature of scaffolds because of high void ratio and surface area. Many biomaterials have been fabricated into porous structures with defined global and local pore sizes as well as interconnected pore network. In 1972, Hulbert and the colleagues investigated the tissue reaction with porous ceramics versus nonporous ones [23]. Tissue around discs of porous ceramics healed faster and presented a thinner fibrous encapsulation than the impervious implants. Blood vessels invasion were more rapid in those discs with pore size of 100 to 150 μm, constituting a richer blood supply.

Currently biodegradable polymers such as poly(lactic-co-glycolic acid) have been prevalently used in tissue engineering. Peter et al. developed porous, polymeric bone flaps with attached vascular pedicle to reconstruct defects and found blocks of vascularized bone were formed 6 weeks after implantation [7]. Hacking et al. also showed complete tissue ingrowth throughout a porous tantalum implant. Tissue ingrowth and sufficient vascularity were noted over time and the attachment strength was three- to sixfold greater compared to a similar study where the implant was treated with porous beads [24].

4 New Design Strategy: Topology Optimization

4.1 Introduction of Topology Optimization and Homogenization Theory

The multiple factors in osteo-synthetics that can be determinant for osseous integration suggest that new synthetic implants can be optimized to concurrently enhance stability, biofactor delivery, and mechanical tissue stimulation. Modern structural optimization can be traced back to 1940s, when the discipline was initially developed

in the aerospace industry. In order to design with light-weighting aircraft structural components with possibly maximal stiffness, the researchers developed a variety of optimization approaches for simple as well as complex structures, based on analytical procedures to a specified type of geometry. Until 1960s when modern computers and finite element method (FEM) became more available, the structural analysis with mathematical programming embedded became possible. The structural optimization, however, was still limited to size and shape optimization of the structure during the period. A more generalized and nonparametric optimization method which can simultaneously select the best geometric layout and topological configuration was not available until late 1980s. Such an optimization method named "topology optimization" (or layout optimization) is more superior in saving significant amount of materials to avoid redundancy over those designed by the size and the shape optimizations.

4.2 Topology Optimization

Structural topology optimization, which is a generous design method to find the optimal structural layouts in a nonparametric fashion, is truly a milestone for mechanic structural design. It involves simultaneous optimization of the topology and the shape of internal boundaries in porous composite continua. The topology optimization is based on the image-based representation that consists of a macroscopic variation of solid material and void in a fixed reference design domain. It is also called material distribution approach or black-and-white design since the density of structure is given by either 0 or 1, representing void or solid.

Ever since the epochal contribution by Bendsøe and Kikuchi [25] in 1988, the topology optimization method has progressed with a significant breakthrough from theoretical into practice. A FE-based numerical topology optimization scheme was implemented to solve structural design problem with a homogenization-based method. Many practical engineering problems have been successfully addressed with the breaking algorithm over the past decades. Neves et.al [26] presented two computational models to design the periodic microstructure of lattice materials with optimal elastic properties. Kikuchi et al. [27] furthered the approach to design the optimal layout and microstructure of composite materials. Topology optimization method is now leading to a well-acceptable methodology in many industrial applications.

4.3 Homogenization Theory

The homogenization theory allows the effective properties of periodic composite materials to be calculated without enforcing the restriction on the geometry of the given composite structure. The mathematical formulation assumes that the

composite is composed of the periodic microstructures, and the microscopic scale is much smaller compared to the global dimension, namely the macroscopic domain. Hence, from the macroscopic view, the composite looks like a "homogeneous" material. The homogenization theory is a key foundation to conduct topology optimization [25].

The homogenization theory was established by a school of French mathematicians in 1970s [28]. They cooperated homogenization method with the G-convergence theory and solved many mechanical problems in linear elasticity, heat, and wave equations. Sanchez-Palencia addressed the fluid flow in porous media, elasticity, electromagnetism, and vibration of solid mechanics by using the theory [29]. Later, a numerical homogenization method for elasticity was implemented by Guedes and Kikuchi [30] using an adaptive finite element method. The homogenization-based topology optimization was considered a building block in structural optimization field, and was wildly implemented in different disciplines and applications.

5 Materials for Osteo-Synthetics

5.1 Metals

Metals are perhaps the most common materials used in modern orthopedics. Among the metals, stainless steel and titanium have been prevalently used for instruments, particularly when load bearing and mechanical integrity of the new constructs are required. In spinal applications, anterior interbody cages are often titanium cylinders that are placed in the intervertebral disc space. The cages made of titanium offer a superior rigidity, and therefore in most single-level fusion cases, additional instrumentation (e.g., pedicle screws) or postoperative back braces for support are not needed.

Although biocompatible metals provide desired load bearing, the dense material has also created certain obstacles in the real practice . Potential image artifacts have been observed in the vicinity of the cage during magnetic resonance imaging (MRI) and computed tomographic (CT) scanning [31, 32]. Although the CT images with titanium or titanium, aluminum, and vanadium (Ti-6Al-4V) alloy present a better result, the amount of MR image artifacts is still comparable to that with stainless steel [33, 34]. How, lesser field strength and the use of fast spin–echo techniques have been found to effectively remedy the problem [35–37].

The second concern with these materials is that solid fusion cannot be easily and definitely determined from simple radiographic analysis alone. The devices made of metals are not radiolucent and thus bring the difficulty to determine whether solid osseous fusion has occurred (osseous trabeculation, evidence of bone formation in and around the device) on radiographs. Complementary histological examinations

of the tissue obtained in the hollow spaces from retrieved cages in the studies of Lange et al. [38] and Carvi et al. [39] confirmed sufficient bone growth in these areas. However, the reexamination is not feasible in the real practice.

Like the common complication with the use of any metallic device, stress shielding significantly contributes to the relatively high incidence of cage subsidence. Stress shielding in the segmental fusion achieved by rigid stabilization techniques with transpedicular screws has been noticed to be associated with disuse osteopenia in fused vertebra in dog models [40–45]. This osteopenia will likely lead to screw loosening and instrumentation failures [41]. The mechanically shielded environment resulted from thick wall or cylindrical thread in conventional cage designs allows lower intracage pressure propagation [46], which leads to significant bone mineral density decrease in long term [12]. Consequently, increased incidence of postoperative complications has been reported such as stress-shielding, the migration or dislodgement of the cage, pseudarthrodesis, or the combined adverse symptoms [14].

5.2 Allograft

Allogenic grafts using corticocancellous blocks [47, 48], corticocancellous dowels [49, 50], and femoral ring allografts [51] have been commonly integrated in the segmental reconstruction. Biological contents such as growth factors are well preserved after dementalization process. To the context, allografts have been tailored to accommodate the existing fusion systems. O'Brien et al. devised a hybrid interbody graft consisting of a biological fusion cage (femoral cortical allograft ring) packed with autogenous cancellous bone graft [51]. It was thought that the femoral allograft ring provides the instant stability of the fusion construct, while the autogenous cancellous bone graft help induce long-term stability achieved by later complete arthrodesis. Femoral cortical dowels have been fabricated using cadaveric femurs that is machined in a dowel formation with a hollow intramedullary region for grafting bone [52]. They are cut along the weight-bearing axis of the bone to provide structural stability. Because the femoral cortical dowels are not metallic, fusion can be assessed radiographically. The device have also been shown to have osteoconductive properties. The intramedullary region can be filled with autogenous cancellous bone or bone morphogenetic protein (BMP) allowing the hybrid to be osteoinductive. The two components synergistically stimulate proper bone ingrowth within the graft and the ongrowth over a resorptive surface that is integrated with adjacent bone to form bony union. The femoral cortical dowels provide adequate mechanical strength as they have been shown to withstand forces of up to 25,000 N. It should be noted that although cases are extremely rare with current screening techniques, using femoral dowel is with risks of pathogen propagation and disease transmission.

5.3 Carbon Fiber Reinforced Polymer

To overcome the major problems of image distortions in the postoperative assessment and stress-shielding induced complications commonly observed with the use metallic cages as previously described, a family of implants made of a carbon fiber reinforced polymer (CFRP), PEEK-Optima (Invibio Inc., Greenville, SC) derived from polyetheretherketone, have been developed since the mid-1980s by Dr. John Brantigan [53]. The Brantigan CFRP cage is radiolucent, allowing postoperative visualization of the bone graft healing. The more compliant stiffness close to native bone properties decreases the incidence of complications resulted from stress shielding, and a series of clinical reports have shown favorable outcomes [54, 55]. However, it should be noted that device made with PEEK alone does not provide sufficient fixation and therefor additional posterior pedicle screws are normally necessary.

5.4 Biodegradable Polymers

In order to address the complications associated with excessive stiffness aforementioned, biodegradable/bioabsorbable polymers, when used to fabrication implants, should possess several advantageous characteristics compared to their metallic counterparts. First, the immediate stability should be still acquired in the segment where the device is implanted, with the stiffness retained through the degradation. Second, the implant should be radiolucent without postoperative image interference as presented in the metallic counterpart. The biodegradable implant should also be capable of transferring stress during tissue formation by a dynamic equilibrium that as the implant degrades and its mechanical properties decline, the compromised strength must be compensated by the tissue regenerate. This main advantage of a degradable/resorbable material confers initial and intermediate stability without long-term complications, e.g., stress shielding or migration, of metallic implants. Finally, the metabolites by implant breakdown should be able to be incorporated into normal cellular processes without inciting a metabolic derangement that possesses mutagenic or immunogenic properties to their host cells [56]. A number of adverse effects with the use of bioabsorbable implants have been reported, including synovitis, osteolysis, hypertrophic fibrous encapsulation, and sterile sinus tract formation. These have brought up concerns with bioabsorbable implants to incite aseptic inflammatory reactions during the resorption process [57–60].

The class of bioabsorbable materials that has been most studied is alpha-poly hydroxyl esters. These include the two mostly used polymers in biomedical applications, poly(glycolic acid) (PGA) and poly(lactic acid) (PLA). Both materials have been shown with complete absorption in bone [61–63]. However, different degradation byproducts and inflammatory reactions were found with the two polymers. PGA has been shown to induce more inflammatory tissue reactions than PLA

[64, 65]. In addition, degradation patterns and half-lives are also different for stereoisomers belonging to the same compound [63, 66, 67].

The idea to incorporate bioabsorbable polymers in the surgical implants was first introduced by Kulkarni et al. [68]. A variety of other applications were then invented, including sutures, repair of craniofacial defects, appendicular fracture fixation, and soft-tissue repair [59, 61, 62, 67, 69–73]. A recent attempt also included to fabricate a PLA interbody fusion cage with the same geometry from the titanium [14, 74, 75].

The use of bioabsorbable materials in skeletal reconstruction has aroused significant interests in clinic. The dynamic load transition has been show to lead to higher bone formation rates, further improving clinical outcomes in specific applications. Clinical studies are currently underway to evaluate the feasibility to extend their use in more practice of orthopedic surgery.

6 Osteo-Synthetics with Designed Architecture Possessing Solid–Fluid Bi-phasic Properties of Native Bone

6.1 Introduction

The effects of how porous features of a scaffold such as pore size, pore shape, and interconnectivity affect tissue regenerates have been well studied. These microstructural parameters are correlated with mechanical and mass transport properties of the scaffolds. One delicate way to achieve a viable tissue regenerate is to find optimal microstructures that achieve prescribed mechanical and mass transport properties.

To obtain the overarching aim, hierarchical scaffold design appears to be an adapting optimization scheme to include all these diverse design goals [76]. In the hierarchical scaffold design scheme, unit microstructures, or unit cells (structural unit, not biological cells) are selected from unit cell libraries and assembled to form a scaffold with a global shape that fits into anatomical geometries. The mechanical and fluidic properties of the scaffold are calculated using the homogenization theory based on double-scale asymptotic expansion [77, 78]. Furthermore, the pore architectures can be designed with predefined geometries such as three orthogonal cylindrical pores or spherical pores. Hollister et al. optimized pore diameters of scaffolds with three orthogonal cylindrical pores using the homogenization method and empirically fitted polynomials that relate pore diameters and the effective stiffness tensor [79]. The requirements for mass transport were considered by applying a lower-bound constraint to the porosity.

In more general cases, new microstructures with target properties can be created using topology optimization [80–82]. Topology optimization distributes material within a unit microstructure with compose of the final, global architecture that fulfills the targeted performances. Lin et al. adapted the topology optimization to find scaffold microstructures that reach the targeted anisotropic elastic constants [83].

Hollister and Lin further extended the method by introducing effective permeability to the optimization scheme to design scaffolds with the maximized permeability [84]. However, in that initial attempt, the permeability was not coupled with the mechanical property in the optimization procedure, so that maximizing permeability could affect the mechanically optimized microstructure.

Recently, several multifunctional material design schemes based on the topology optimization have been reported. Guest and Prevost illustrated a general 3D microstructure design scheme using the topology optimization method to achieve maximized bulk modulus and isotropic permeability [85]. They optimized microstructures by differentially weighting mechanical and transport terms in the objective, allowing designers to tailor the material properties. de Kruijf et al. found optimal structures with maximized bulk modulus and thermal conductivity by minimizing both mechanical and thermal compliance in 2D [86]. The authors explored Pareto optimality by varying weights for mechanical and transport properties. Challis et al. presented the design of isotropic unit structures with maximized bulk modulus and isotropic conductivity by a level set method [87]. The authors also explored changes in design with different combinations of weighting factors.

The design approaches of multifunctional material structures with maximized properties have gained increasing interests in many engineering fields. Tissue engineering scaffolds, for example, have been tailored to meet a wide range of mechanical and mass transport properties, including cross property relationships that fall well within the cross-property bounds. For instance, cartilage needs low mass transport and mechanical properties, which lay well within the interior of the mass transport and mechanical cross-property bounds [88].

Thus, in order to design microstructures with ranges of mechanical and mass transport properties, we adapted a local microstructure topology optimization scheme based on the SIMP method for target optimization. The target properties were selected within defined cross-property bounds connecting effective bulk modulus and isotropic diffusivity. Various microstructures were designed and utilized within the tissue engineering scaffolds. A porous biodegradable interbody fusion cage was designed as a biomedical application of multifunctional microstructures by integrating the layout from the global topology optimization with the local optimized microstructure. The final integrated structures were then built using solid free-form fabrication techniques.

6.2 Tailoring Scaffold Properties

6.2.1 Material Interpolations

Microstructure topology optimization computes the optimal topology of a scaffold microstructure by distributing material density within the unit cell domain under design objectives and constraints. The design domain is discretized with the finite elements assigned with density values, ranging from 0 through 1. In this relaxed problem,

material laws should be defined to relate element densities and local material properties. In addition, the intermediate density values are penalized to have a final discrete design. The most common local material law is the Solid Isotropic Microstructure with Penalization (SIMP) [89]. We utilized the SIMP method for elasticity:

$$C_{ijkl} = \rho^{p} C_{ijkl}^{\text{base}}, \quad (p > 1)$$

where C_{ijkl} is the element stiffness tensor, ρ is the element density, p is a penalization factor, and C_{ijkl}^{base} is the stiffness tensor for the base material. For the diffusivity, a SIMP-like material law can be applied to the interpretation of the intermediate densities with penalization,

$$D_{ij} = (1-\rho)^{p} D_{ij}^{\text{base}}, \quad p > 1$$

where D_{ij} is the element diffusivity tensor, ρ is the element density, p is a penalization factor, and D_{ij}^{base} is the free diffusivity tensor for the fluid phase. With the local material laws defined for both stiffness and diffusivity, the objective function and sensitivity derivatives are derived with respect to material density ρ, and the optimization problem can be solved by updating ρ at each iteration.

For the phase base material, we used unit isotropic diffusivity, $D = 1$ for the void phase. For the base material solid phase, we chose Poisson's ratio equal to 1/3 with a Young's modulus of 1, which yields a bulk modulus of 1. In this case, the designed properties could be easily compared within the cross-property bounds normalized to base material properties.

6.2.2 Problem Statement for Target Optimization

In order to tailor the material properties directly, the optimization problem was defined to minimize the error between the target and the effective bulk moduli and diffusivities, with constraints on porosity:

$$\begin{aligned} &\textit{minimize} \quad f = w_1 \left(\frac{K^{\text{H}}}{K^{*}} - 1 \right)^2 + w_2 \left(\frac{D^{\text{H}}}{D^{*}} - 1 \right)^2 + w_3 f_{\text{cubic}} \\ &\text{subject to} \quad \phi_{\text{lb}} \le \sum_{i=1}^{N} \frac{1-\rho_i}{N} \le \phi_{\text{ub}}, \\ &\qquad\qquad 0 < \rho_i \le 1 \end{aligned}$$

where K^{H} is the homogenized bulk modulus, K^{*} is the target bulk modulus, D^{H} is the homogenized isotropic diffusivity, D^{*} is the target isotropic diffusivity, f_{cubic} is the cubic error function and w_i (i = 1, …, 3) are weighting factors, ϕ_{lb} and ϕ_{ub} are the upper and lower bounds of porosity, ρ_i is ith element density, and N is the total number of elements.

Imposing isotropic or cubic symmetric material microstructures, the effective bulk modulus was converted from elastic stiffness tensor components assuming isotropic/cubic symmetry in the final result.

$$K^{\mathrm{H}} = \frac{1}{3}\left(\frac{C^{\mathrm{H}}_{1111} + C^{\mathrm{H}}_{2222} + C^{\mathrm{H}}_{3333}}{3} + \frac{2\left(C^{\mathrm{H}}_{1122} + C^{\mathrm{H}}_{2233} + C^{\mathrm{H}}_{1133}\right)}{3} \right)$$

In the same way, the effective diffusivities were evaluated as average of the diagonal terms in diffusivity tensor.

$$D^{\mathrm{H}} = \frac{D^{\mathrm{H}}_{11} + D^{\mathrm{H}}_{22} + D^{\mathrm{H}}_{33}}{3}$$

The cubic error function is defined to minimize the differences among three normal components, three off-diagonal terms, and three shear terms in the stiffness tensor components, respectively.

$$\begin{aligned} f_{\mathrm{cubic}} = &\left(\frac{C^{\mathrm{H}}_{2222}}{C^{\mathrm{H}}_{1111}} - 1 \right)^2 + \left(\frac{C^{\mathrm{H}}_{3333}}{C^{\mathrm{H}}_{2222}} - 1 \right)^2 + \left(\frac{C^{\mathrm{H}}_{1111}}{C^{\mathrm{H}}_{3333}} - 1 \right)^2 \\ &+ \left(\frac{C^{\mathrm{H}}_{2233}}{C^{\mathrm{H}}_{1122}} - 1 \right)^2 + \left(\frac{C^{\mathrm{H}}_{1133}}{C^{\mathrm{H}}_{2233}} - 1 \right)^2 + \left(\frac{C^{\mathrm{H}}_{1122}}{C^{\mathrm{H}}_{1133}} - 1 \right)^2 \\ &+ \left(\frac{C^{\mathrm{H}}_{1313}}{C^{\mathrm{H}}_{2323}} - 1 \right)^2 + \left(\frac{C^{\mathrm{H}}_{1212}}{C^{\mathrm{H}}_{1313}} - 1 \right)^2 + \left(\frac{C^{\mathrm{H}}_{2323}}{C^{\mathrm{H}}_{1212}} - 1 \right)^2 \end{aligned}$$

where C^{H}_{ijkl} are the components of the homogenized stiffness tensor. This multi-objective formulation can be easily converted to a formulation in which one of the target properties is optimized while the other is constrained.

6.2.3 Implementation

Topology optimization, in its relaxed formulation, still requires additional treatments to avoid known numerical instabilities such as checkerboard patterns and mesh dependencies [90]. We applied a nonlinear filtering scheme to the sensitivity derivatives to prevent checkerboard patterns and mesh dependency as proposed by Sigmund [91]. Assuming unit cell size of 1 mm in each direction, a filter radius of 3 elements was chosen to maintain a minimum physical feature size (0.15 mm) for the $40 \times 40 \times 40$ element unit cells. When the mesh resolution was increased to $60 \times 60 \times 60$, the filter radius was increased to 4 elements to maintain the minimum physical feature size (0.13 mm). Finally, to solve the optimization problem, the Method of Moving Asymptotes (MMA) was adopted to provide greater efficiency in solving problems with a large number of variables and a small number of constraints [92].

6.3 Design Results

Our results demonstrate that the properties of the microstructures can be tailored to meet various scaffold requirements such as stiffness and mass transport using topology optimization with SIMP interpolation and sensitivity filtering. Target design points were chosen close to the cross-property upper bounds. Figure 15.1 illustrates various microstructural architectures obtained in this study and the achieved properties are presented in Table 15.1. The mesh resolution for microstructures (a), (c), (e), (g), and (f) was $60 \times 60 \times 60$, and the mesh resolution for the other microstructures

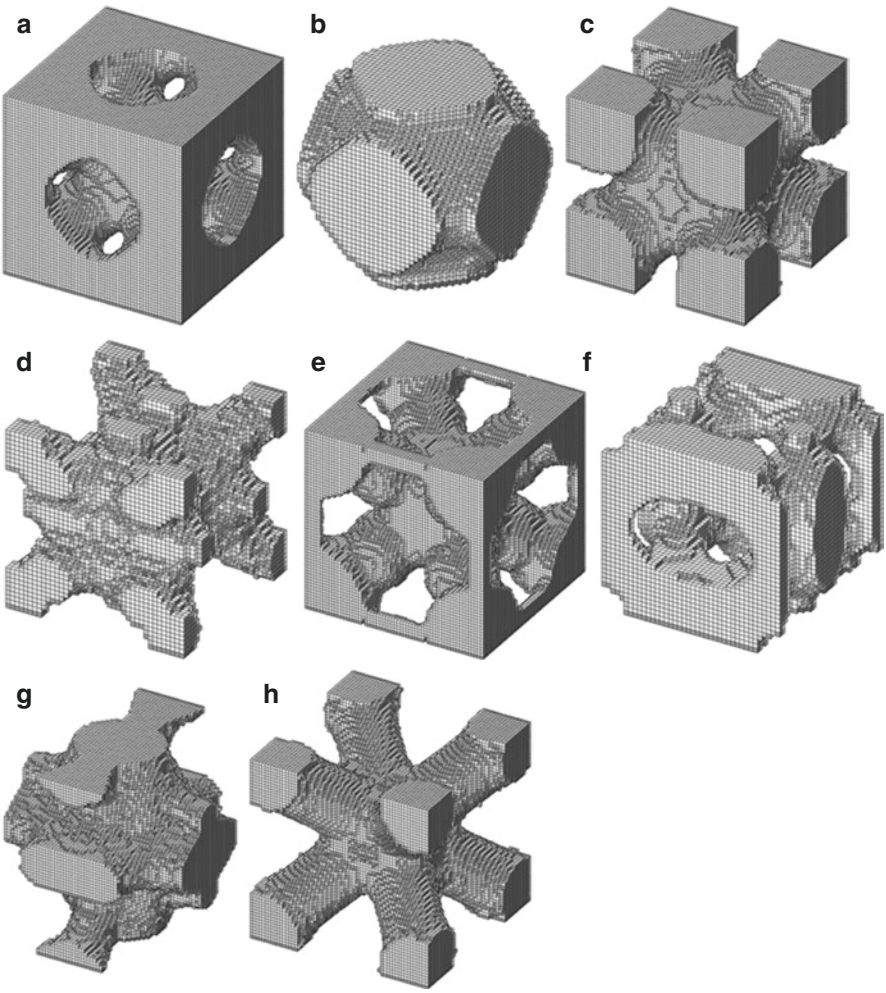

Fig. 15.1 Microstructures obtained by targeting bulk modulus and diffusivity close to the upper cross-property bounds, for 30% porosity (**a**, **b**, and **c**), 50% porosity (**d**, **e**, and **f**), and 60% porosity (**g**, **h**). (With permission from "Structural and Multidisciplinary Optimization", Springer Nature)

Table 15.1 Properties of microstructures tailored with target bulk moduli and diffusivities (With permission from "Structural and Multidisciplinary Optimization", Springer Nature)

Microstructures	Porosity	Diffusivity[a]	Bulk modulus[a]	Young's modulus[a]	Poisson's ratio
A	0.2825	0.1276	0.3734	0.4875	0.2824
B	0.3030	0.1340	0.3565	0.5273	0.2535
C	0.2935	0.1616	0.3317	0.4277	0.2851
D	0.4831	0.3016	0.1512	0.2258	0.2511
E	0.4828	0.3156	0.1624	0.1955	0.2994
F	0.5037	0.3330	0.1522	0.2251	0.2535
G	0.5802	0.3556	0.1246	0.2442	0.1734
H	0.5882	0.4164	0.1114	0.0973	0.3544

[a]The values are normalized to the base material properties

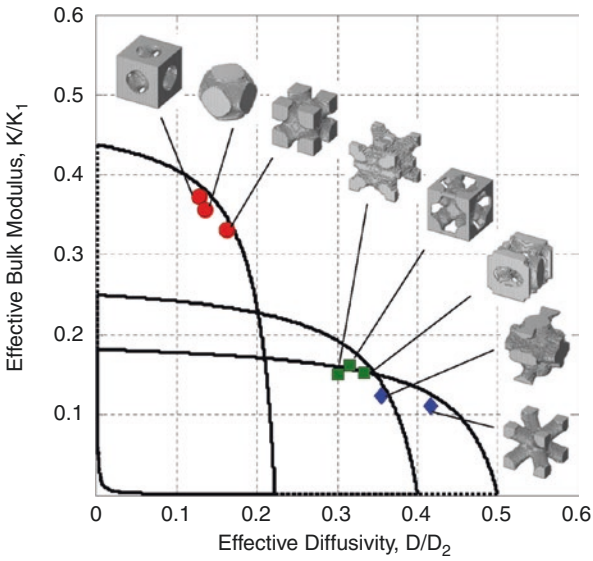

Fig. 15.2 Microstructures designed to achieve properties close to the upper cross-property bounds are specified within the cross-property bounds. (With permission from "Structural and Multidisciplinary Optimization", Springer Nature)

was 40 × 40 × 40. The designed microstructures were identified within the cross-property bounds in Fig. 15.2.

Note that the porosities of the designed microstructures satisfied the constraints despite the lack of an exact match in the corresponding cross-property bounds. This is because the porosity constraints were set at a small range around the target porosity. For example, the porosity constraints were set less than 52% and greater than 48% for the design of 50% porosity microstructures. Nonetheless, there was excellent agreement between the target and designed bulk moduli and diffusivities (Fig. 15.3).

Because of the theoretical cross-property bounds for 50~60% porosities, the maximum normalized diffusivities are 0.4 and 0.5, respectively. Thus, we may consider diffusivity over 0.3 as high diffusivity for 50~60% porosity materials.

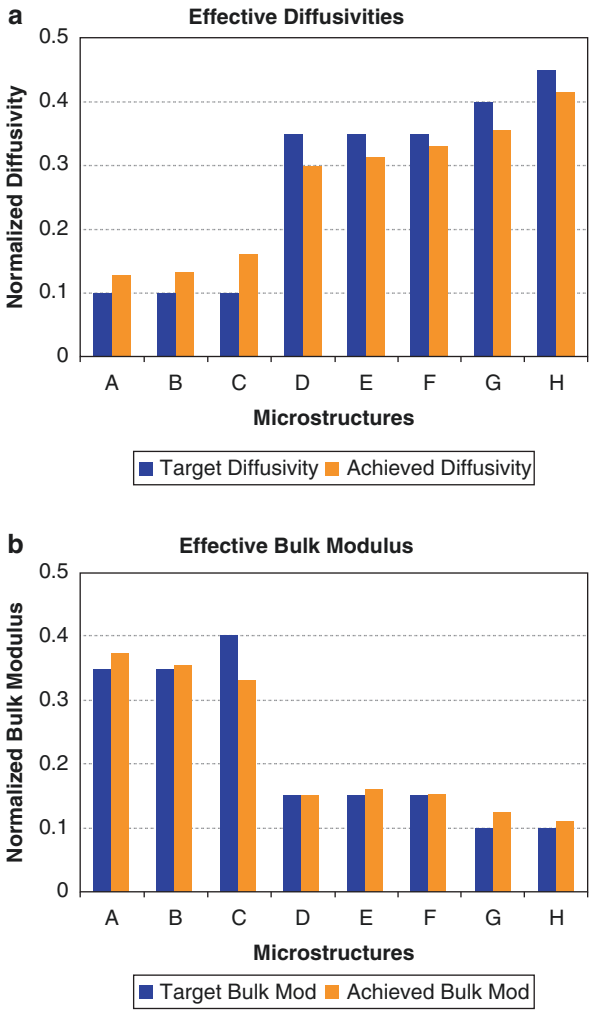

Fig. 15.3 The achieved diffusivities (**a**) and bulk moduli (**b**) were compared with target properties for the mirostructures presented in Fig. 15.1 (**a**–**h**, respectively). (With permission from "Structural and Multidisciplinary Optimization", Springer Nature)

6.3.1 Microstructures with High Diffusivity

Microstructures with relatively high diffusivity designed for either 50% or 60% porosity approached the cross-property upper bound, as depicted in Fig. 15.1d–h. The properties of the microstructures illustrated in these figures were isotropic. It should be noted that the designed microstructures have different topologies while the achieved properties were close to each other. Interestingly, the property pair of the microstructure in Fig. 15.1f is the closest to the cross-property upper bound, implying that the structure is optimal. Furthermore those microstructures designed to have 60% porosity showed lower bulk modulus of approximately 0.1 of that of the solid phase. When the structures were specified within cross-property bounds,

both structures again have near optimal properties because the properties are close to the upper bounds (Fig. 15.2).

6.3.2 Microstructures with Low Diffusivity

Microstructures targeted a low diffusivity for 30% porosity were also near the corresponding cross-property upper bounds (Fig. 15.1a–c). The optimized structures have thick diagonal in the unit cell domain to obtain a high bulk modulus and small pore diameter to decrease diffusivity. The normalized diffusivities of these microstructures were between 0.12 and 0.17 (Table 15.1). These low diffusivity structures were also close to the upper cross-property bounds due to high bulk moduli (Fig. 15.2).

6.3.3 Microstructure Targeting Low Diffusivity and Low Bulk Modulus

For cartilage tissue engineering applications, microstructures with low modulus and low diffusivity are desired. Such microstructures lie within the interior of the cross property bounds, distant from the upper limits that are more often targets of other multiphysics microstructural topology optimizations. These targets present significant challenges as the increase of material will increase bulk modulus while decreasing diffusivity, reaching the opposite end of the design goal.

To eliminate the intermediate densities, we used a post processing technique. We designed a microstructure with a low diffusivity of 0.1 and a low bulk modulus of 0.1, respectively. However, the result of the post processing had changed the initial properties set as targets. The intermediate density values were interpolated using the SIMP model. After applying a threshold, the properties shifted toward cross-property upper bounds.

One interpretation for intermediate densities were generated is that the algorithm converged to a local minimum before all densities were penalized. We employed the convention of Sigmund's continuation method to avoid convergence to a local minimum [82]. However as expected, this essentially heuristic approach could not sufficiently penalize the intermediate densities: the final mechanical and transport properties were with a diffusivity of 0.12 and a bulk modulus of 0.1, which were not a totally satisfactory solution to the problem. The full structure and 1/eighth of the structure are shown in Fig. 15.4a, b, respectively. In addition, representative cross-sectional view of the density distribution are illustrated in Fig. 15.4c. There are significant amounts of gray elements at convergence, which may indicate local minima. There are very weak connections between large spheres at the corners.

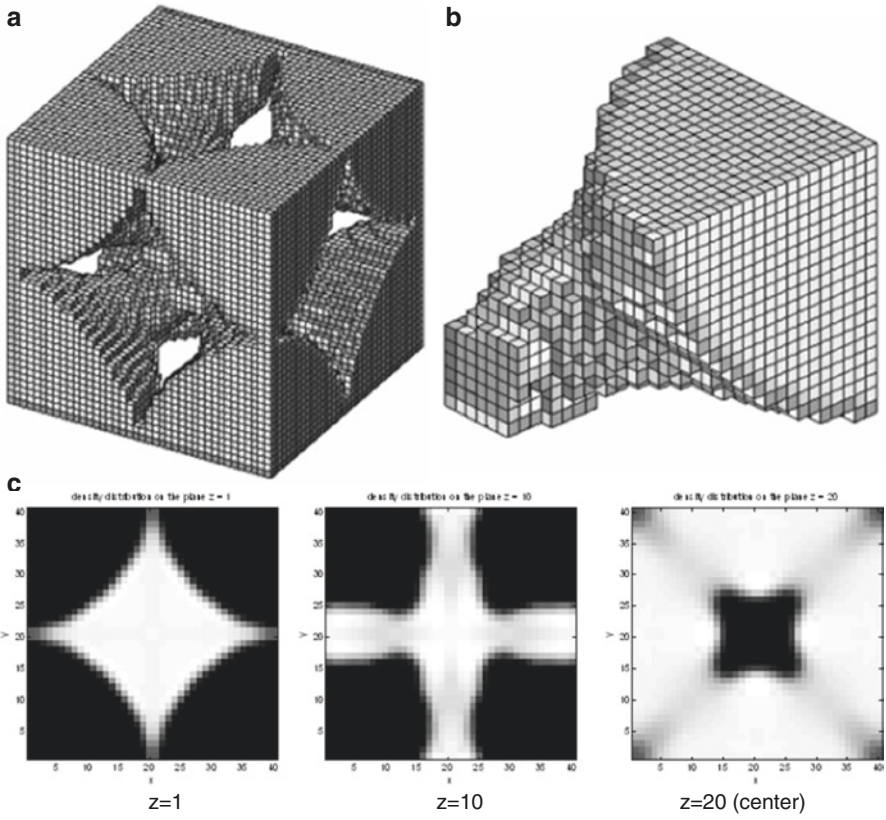

Fig. 15.4 (**a**) Microstructures with low diffusivity and low bulk modulus, (**b**) 1/8 of the designed microstructure, and (**c**) representative cross-sectional view of the structure. (With permission from "Structural and Multidisciplinary Optimization", Springer Nature)

6.3.4 Microstructures with the Same Porosity But Different Bulk Modulus and Diffusivity

A particular strength of the targeted optimization is the capability to create microstructures of the same porosity, but with a range of bulk moduli and diffusivities. Here, we demonstrated a series of microstructures that were successfully designed with 45~50% porosity with diffusivities ranging from 16 to 33% and effective bulk moduli ranging from 12 to 24% of the base properties, respectively (Fig. 15.5). This endorses the argument that our developed algorithms is capable of distributing the same amount of material in different layouts to dramatically retain different effective mechanical and mass transport properties. The microstructures in Fig. 15.5 can be experimentally tested to evaluate the effect of material distribution on load bearing and mass transport without changing the porosities.

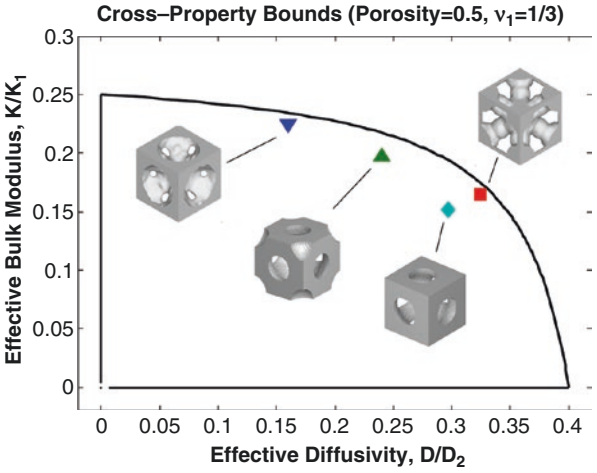

Fig. 15.5 Microstructure designs with ranges of diffusivities for 50% porosity. (With permission from "Structural and Multidisciplinary Optimization", Springer Nature)

6.3.5 Comparison of Designed Properties with Experimental Measurements

Using SFF technique, we fabricated the designed scaffolds with PCL/HA composites for compression tests. Because the scaffold microstructures were represented using voxel elements, a three-dimensional version of pixels, the geometry of the optimized scaffolds was generated by simply repeating the corresponding voxels using an image-based modeling technique. The dimension of the specimens tested were 8 mm × 8 mm × 16 mm, with unit microstructures of 2.67 mm × 2.67 mm × 2.67 mm, which represents 3 × 3 × 6 units of microstructures. The voxel representation of the specimens was then converted to STL files to accommodate the SFF technique.

A selective laser sintering technique was utilized to fabricate the specimens by sintering PCL and HA in a powder bed. As shown in Fig. 15.6, the specimens (a)~(h) corresponds to microstructures (a)~(h) in Fig. 15.1. Compression tests were conducted with the fabricated specimens and the results were compared to the designed properties. MTS Alliance RT30 electromechanical test frame (MTS Systems Corp., MN) was used with a strain rate of 1 mm/min under a preload of 1 lb. TestWorks4 software (MTS Systems Corp., MN) was used to collect load-displacement responses. Average stress was obtained from the recorded load divided by the undeformed cross-sectional area of the specimen (~64 mm^2). In the similar manner, average strain was calculated from the displacement divided by the undeformed height (~16 mm).

The stress–strain curve is presented in Fig. 15.7. The experimental modulus was then calculated based on the slope of a line that connects the origin and 1% strain point. The moduli obtained by the average stress and strain were compared with the designed Young's modulus, which was calculated from bulk modulus and Poisson's ratio because the optimized microstructures were all cubic symmetric (Table 15.2).

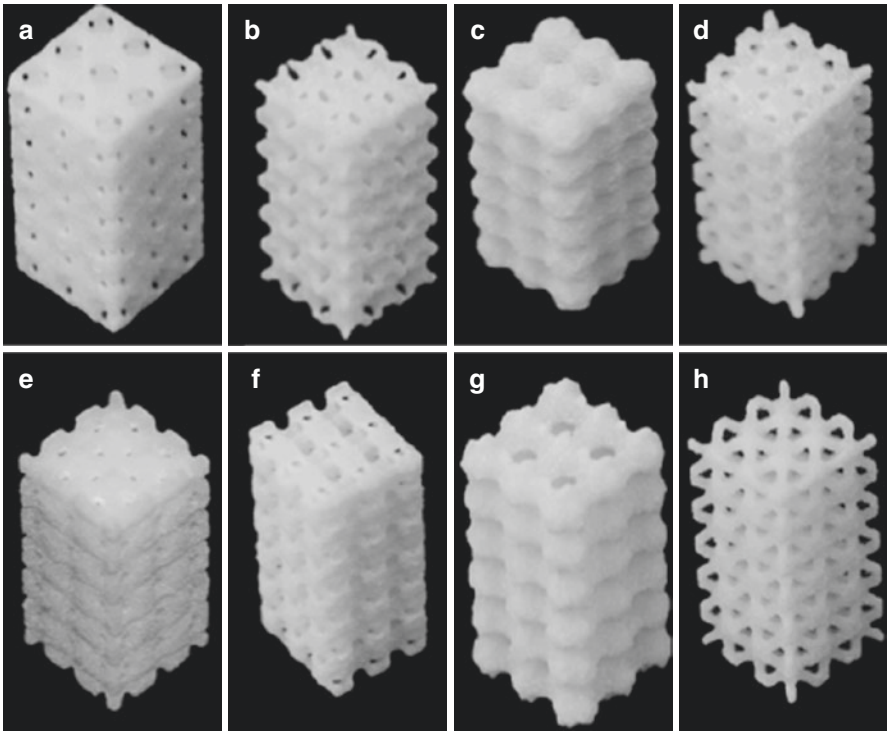

Fig. 15.6 Scaffolds with optimal microstructures illustrated in Fig. 15.1 (**a**–**h**, respectively) were designed and fabricated using SFF

Fig. 15.7 Stress–strain curves obtained from compression tests of the fabricated scaffolds designed with the optimal microstructures

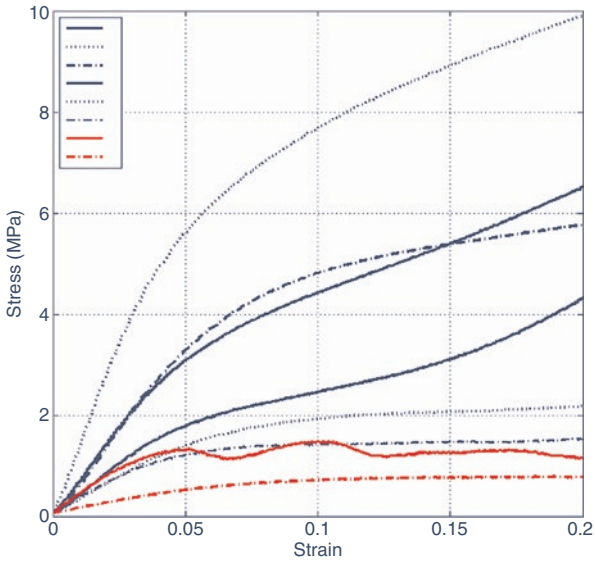

Table 15.2 Comparison of theoretical Young's modulus calculated from the homogenization method, and experimental Young's modulus measured compression tests

Microstructures	Theoretical Young's modulus[a]	Experimental Young's modulus[b]
A	0.4875	0.2167
B	0.5273	0.4424
C	0.4277	0.2479
D	0.2258	0.1284
E	0.1955	0.2186
F	0.2251	0.1373
G	0.2442	0.1509
H	0.0973	0.0571

[a]Values are normalized to the base material Young's modulus

[b]Experimental Young's moduli are normalized to experimental Young's moduli of bulk specimen (295 MPa)

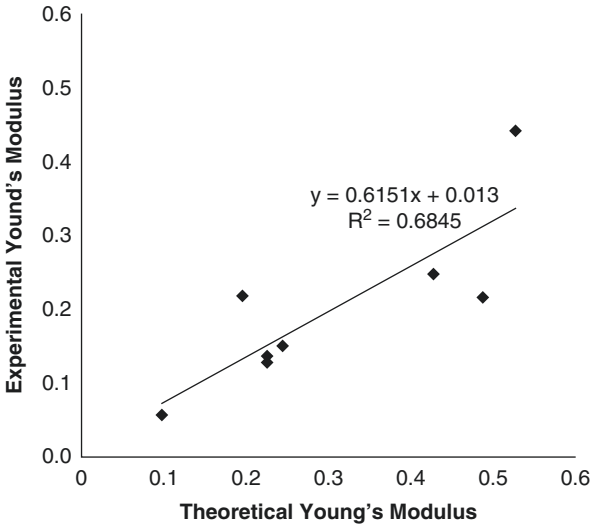

Fig. 15.8 Theoretical Young's modulus was correlated to experiments

As shown in Fig. 15.8, the theoretical Young's moduli were correlated to experimental Young's moduli, although the latter were lower than the former. It should be noted that small geometric features such as struts and pores in the microstructures were not accurately fabricated in some cases. For example, disconnected struts were identified between unit microstructures in Figs. 15.6, 15.7, and 15.8. In the selective laser sintering process, the laser beam scanning speed and particle size of the powder have been found to affect the energy exposure at a spot, which determines the minimal curing path size. Geometric features, smaller than the minimum path size, were skipped based on the preset accuracy of the machine. Considering these manufacturing defects, the theoretically designed properties seemed to provide upper bound for the experimental properties.

6.4 Discussion

It is hypothesized that scaffolds should provide mechanical and mass transport properties as close as possible to native tissues to enhance tissue regeneration [93]. As an active component, scaffolds should be able to provide a proper mechanical withstanding to maintain structural integrity at the defect site as well as transpass appropriate mechanical stimuli to newly generated tissues [94–96]. In addition, scaffolds should provide appropriate mass transportation that can support cellular functions, tissue ingrowth, and supply of nutrition [93, 97]. However, it is still unclear what optimal properties the scaffold should possess in order to obtain the best outcome of tissue regeneration. For example, there have been inconsistent suggestions from different prior studies on the optimal pore size or porosities for tissue regeneration. Moreover, different levels of fluidities have been also shown to result in different cell differentiations [98].

In order to rigorously investigate correlations between functional environments and tissue regeneration, the ability to design scaffolds with controlled mechanical and mass transport properties is essential. In this study, we demonstrated a developed approach to tailor these properties using topology optimization. Cross-property bounds provide a favorable yet also feasible domain in the intersection of the bulk modulus and diffusivity. Thus, topology optimization with cross-property bounds make it a powerful design tool for creating microstructures with desirable, precise controls.

To avoid numerical instabilities inherent to the process, we introduced a nonlinear sensitivity filter proposed by Sigmund [91]. Filtering techniques are known to avoid known instabilities such as checkerboard patterns and mesh dependence. The downside of the technique is that the final structure often contains intermediate densities spanning solid-void boundaries due to the blurring effect of the filter. However, in our case, we found 0 and 1 were successfully distinguished with the nonlinear sensitivity filter. We measured the convergence of the intermediate densities toward 0 or 1 by:

$$R_{\text{conv}} = \frac{1}{N}\sum_{i=1}^{N}\frac{\left|\rho_i - 0.5\right|}{0.5}$$

R_{conv} approaches 1 as the intermediate densities are penalized toward either 0 or 1. With the SIMP topology optimization and sensitivity filter, we were able to obtain microstructures with an R_{conv} index over 0.95, which can be considered converged.

If R_{conv} is less than 0.95, the designed properties may shift toward upper cross-property bounds after the post-processing. From a practical viewpoint, this could be beneficial because the premature solution still serves as a design choice. However, achieving a discrete solution is more desirable in terms of tailoring the material properties and creating a manufacturable design. In this regard, other techniques can be applied such as density filtering with a Heaviside step function [99] or addition of a nonlinear diffusion term to the objective function [100].

Several studies for microstructure design have shown the composite or porous structures that are near or on the cross-property upper bounds [85–87]. In these previous works, two competing properties were maximized simultaneously. However, one of our main interests in this study was to design microstructures whose properties are far from the upper bounds.

In particular, our main interest was the design of microstructures with low diffusivity and low bulk modulus. As presented in the result, our design converged to a minimum. Typically the R_{conv} index was less than 0.8. If we targeted a design point far from the upper cross-property bounds, the R_{conv} index became even smaller. To evaluate the difficulty of achieving this inner design point, we tested three design points: (1) $K = 0.2$ and $D = 0.3$, (2) $K = 0.15$ and $D = 0.2$, and (3) $K = 0.1$ and $D = 0.15$. We used the same problem statement and control parameters for filtering until convergence at a local minimum was achieved.

The outer point or the point on the upper bounds was easily achieved with an R_{conv} index of almost 0.99. For the middle design point, the R_{conv} index was 0.93, which means the final design contained a blurry solid-void boundary. However, for the innermost design point case, the R_{conv} index was 0.71 and the structure exhibited a clear gray layer in addition to the black solid structure. This can be noticed in the histogram as shown in Fig. 15.9 where the number of elements with given densities were plotted in bins. The case with the inner design point generated a large amount of elements containing around 0.3–0.4. One possibility was that the presence of the gray regions represented sub-microstructures were with higher degrees of freedom in reaching the interior targets than the distinct 0 or 1. This would be more relevant in the hierarchical structure of biologic tissues, where the feature sizes can range from the nanometer to centimeter scale.

Another important factor is the practical aspect for manufacturing. Particularly for the designs with low diffusivities designs, small holes would become the case that in turn limits the overall diffusivity. Considering the size of unit cells (typically around 1 mm) in the skeletal tissue scaffolds, the small holes may not be manufacturable due to the default resolution of the machine.

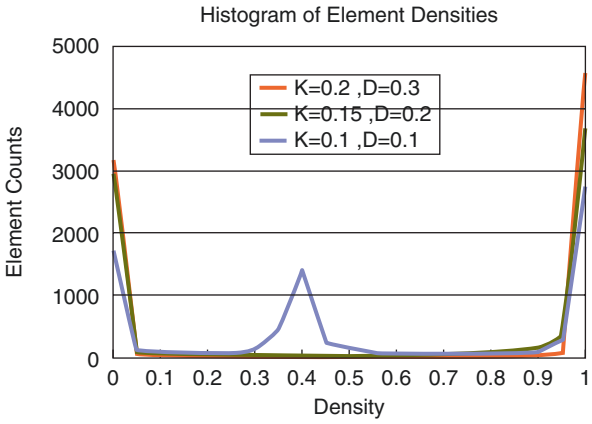

Fig. 15.9 Histograms of densities of three microstructure designs targeting $K = 0.2$ and $D = 0.3$, $K = 0.15$ and $D = 0.2$, and $K = 0.1$ and $D = 0.1$

In our study, diffusivity was considered in our design process because the characteristics of diffusion in the scaffold can affect many critical cellular behaviors, such as migration. The property will also influence mass transportation such as oxygen and nutrient delivery as well as metabolic waste removal. Mathematical models of cell migration and tissue regeneration have adapted diffusion in the simulations [101, 102]. In addition, diffusivity and permeability of scaffolds are well correlated [103]. There are also known cross-property bounds on the effective diffusivity and bulk modulus, suggesting the necessity to include them as design characteristics.

As a temporary substitute for the extracellular matrix, scaffolds are expected to provide a favorable milieu to promote new tissue formation. More experimental data are warranted to elucidate what are considered as optimal conditions to augment tissue regeneration as ambiguities have been noticed in different observations. For example, conflicting findings have been reported regarding the effect of oxygen diffusion on cartilage regeneration [97]. In this regard, the method of microstructural topology optimization emerges as a new platform tool to further this type of studies and help explore the most relevant scaffold properties.

References

1. Liberman JR, Daluiski A, Einhorn TA. The role of growth factors in the repair of bone. Biology and clinical application. J Bone Joint Surg. 2002;84-A:1032–44.
2. Sanhu HS. Anterior lumbar interbody fusion with osteoinductive growth factors. Clin Orthop Relat Res. 2000;371:56–60.
3. Cullinane DM, Fredrick A, Eisenberg SR, Pacicca D, Elman MV, Lee C, et al. Induction of a neoarthrosis by precisely controlled motion in an experimental mid-femoral defect. J Orthop Res. 2001;20(2002):579–86.
4. Pilliar RM, Cameron HU, Welsh RP, Binnington AG. Radiographic and morphologic studies of load-bearing porous-surfaced structured implants. Clin Orthop Relat Res. 1981;156:249–57.
5. Simmons CA, Meguid SA, Pilliar RM. Mechanical regulation of localized and appositional bone formation around bone-interfacing implants. J Biomed Mater Res. 2001;55:63–71.
6. Simmons CA, Meguid SA, Pilliar RM. Differences in osseointegration rate due to implant surface geometry can be explained by local tissue strains. J Orthop Res. 2001;19(2001):187–94.
7. Peter SJ, Miller MJ, Yasko AW, Yaszemski MJ, Mikos AG. Polymer concepts in tissue engineering. J Biomed Mater Res. 1998;43:442–27.
8. Wolff J. Das gaesetz der transformation der knochen. A. Hirchwild: Berlin; 1982.
9. Carter DR, Blenman PR, Beaupre GS. Correlations between mechanical stress history and tissue differentiation in initial fracture healing. J Orthop Res. 1988;6:734–48.
10. Carter DR. Mechanical loading history and skeletal biology. J Biomech. 1987;20: 1095–109.
11. Guldberg RE, Caldwell NJ, Guo XE, Goulet RW, Hollister SJ, Goldstein SA. Mechanical stimulation of tissue repair in the hydraulic bone chamber. J Bone Miner Res. 1997;12(8):1295–302.
12. Cunningham BW, Ng JT, Haggerty CJ. A quantitative densitometric study investigating the stress-shiedling effects of interbody spinal fusion devices: emphasis on long-term fusions in thoroughbred racehorses. Trans Orthop Res Soc. 1998;23:250.

13. van Dijk M, Smith TH, Suglihara S, Burger EH, Wuisman PI. The effect of cage stiffness on the rate of lumbar interbody fusion: an in vivo model using poly(L-lactic acid) and titanium cages. Spine. 2002;27:682–8.
14. van Dijk M, Smit TH, Burger EH, Wuisman PI. Bioabsorbable poly-L-lactic acid cages for lumbar interbody fusion: three-year follow-up radiographic, histologic, and histomorphometric analysis in goats. Spine. 2002;27(23):2706–14.
15. van Dijk M, Tunc DC, Smit TH, Higham P, Burger EH, Wuisman PI. In vitro and in vivo degradation of bioabsorbable PLLA spinal fusion cages. J Biomed Mater Res. 2002;63(6):752–9.
16. Huiskes R, Weinan H, Grootenboer HJ, Dalstra M, Fudala B, Slooff TJ. Adaptive bone-remodeling theory applied to prosthetic-design analysis. J Biomech. 1987;20:1135–50.
17. Smith L. Ceramic plastic material as a bone substitute. Arch Surg. 1963;87:653.
18. Buser D, Schenk RK, Steinemann S, Fiorellini JP, Fox CH, Stich H. Influence of surface characteristics on bone integration of titanium implants. A histomorphometric study in miniature pigs. J Biomed Mater Res. 1991;25:889–902.
19. Carter DR, Giori NJ. Effect of mechanical stress on tissue differentiation in the bony implant bed. In: Davies JE, editor. The bone-biomaterial interface. Toronto: U. Toronto Press; 1989.
20. Maniatopoulos C, Pilliar RM, Smith DC. Threaded versus porous-surfaced designs for implant stabilization in bone-endodontic implant model. J Biomed Mater Res. 1986;20:1309–33.
21. Bobyn J, Pilliar R, Cameron H, Weatherly G, Kent G. The effect of porous surface configuration on the tensile strength of fixation of implants by bone ingrowth. Clin Orthop Relat Res. 1980;149:291–8.
22. Bobyn JD, Pilliar RM, Cameron HU, Weatherly GC. The optimum pore size for the fixation of porous-surfaced metal implants by the ingrowth of bone. Clin Orthop Relat Res. 1980;150:263–70.
23. Hulbert SF, Morrison SJ, Klawitter JJ. Tissue reaction to three ceramics of porous and nonporous structures. J Biomed Mater Res. 1972;6:347–74.
24. Hacking SA, Bobyn JD, Toh KK, Tanzer M, Krygier JJ. Fibrous tissue ingrowth and attachment to porous tantalum. J Biomed Mater Res. 2000;52:631–8.
25. Bensoe MP, Kikuchi N. Generating optimal yopologies in structural design using a homogenization method. Comput Methods Appl Mech Eng. 1988;71:197.
26. Neves M, Rodrigues H, Guedes J. Optimal design of periodic linear elastic microstructures. Comput Struct. 2000;76:421.
27. Kikuchi N. Design optimization method for compliant mechanisms and material microstructure. Comput Math App Mech Eng. 1998;151:401.
28. Cioranescu D, Donato P. An introduction to homogenization. Oxford: Oxford University Press; 1999.
29. Scachez-Palencia E, Zaoui A. In: Araki H, Kyoto J, et al., editors. Homogenization techniques for composite media. New York: Springer; 1987.
30. Guedes JM, Kikuchi N. Preprocess and postprocess for material based on the homogenization method with adaptive finite element methods. Comput Methods Appl Mech Eng. 1989;83:143.
31. Laakman RW, Kaufman B. Han JS. MRI imaging in patients with metallic implants. Radiology. 1985;157:711–4.
32. Mechlin M, Thickman D, Kressel HY, Gefter W, Joseph P. Magmetic resonance imaging of postoperative patients with metallic implants. Am J Radiol. 1984;143(6):1281–4.
33. Levi AD, Choi WG, Keller PJ, Heiserman JE, Sonntag VK, Dickman CA. The radiographic and imaging characteristics of porous tantalum implants within the human cervical spine. Spine. 1998;23(11):1245–50; discussion 51
34. Wang JC, Yu WD, Sandhu HS, Tam V, Delamarter RB. A comparison of magnetic resonance and computed tomographic image quality after the implantation of tantalum and titanium spinal instrumentation. Spine. 1998;23(15):1684–8.
35. Farahani K, Sinha U, Sinha S. Effect of field strength onsusceptibility artifacts in magnetic resonance imaging. Comput Med Imaging Graph. 1990;14:409–13.

36. Ortiz O, Pait TG, McAllister P. Postoperative magnetic resonance imaging with titanium implants of the thoracic and lumbar spine. Neurosurgery. 1996;38:741–5.
37. Tartaglino LM, Flanders AE, Vinitski S. Metallic artifactson MR images of the postoperative spine: reduction with fastspin-echo techniques. Radiology. 1994;190:565–9.
38. Lange M, Philipp A, Fink U. Anterior cervical spine fusion using RABEA-Titan-Cages avoiding iliac crest spongiosa: first experiences and results. Neurol Neurochir Pol. 2000;34(suppl 6):64–9.
39. Carvi y Nievas MN, Pollath A, Haas E. Cervical discectomy: bone graft or cage fusion? In: Brock M, Schwarz W, Wille C, editors. First interdisciplinary world congress on spinal surgery and related disciplines. Monduzzi Editore: Bologna; 2000. p. 123–8.
40. Craven TG, Carson WL, Asher MA, Robinson RG. The effects of implant stiffness on the bypassed bone mineral density and facet fusion stiffness of the canine spine. Spine. 1994;19(15):1664–73.
41. Dalenberg DD, Asher MA, Robinson RG, Jayaraman G. The effect of a stiff spinal implant and its loosening on bone mineral content in canines. Spine. 1993;18(13):1862–6.
42. Farey ID, McAfee PC, Gurr KR, Randolph MA. Quantitative histologic study of the influence of spinal instrumentation on lumbar fusions: a canine model. J Orthop Res. 1989;7(5):709–22.
43. Kandziora F, Kerschbaumer F, Starker M, Mittlmeier T. Biomechanical assessment of transoral plate fixation for atlantoaxial instability. Spine. 2000;25(12):1555–61.
44. McAfee PC, Farey ID, Sutterlin CE, Gurr KR, Warden KE, Cunningham BW. The effect of spinal implant rigidity on vertebral bone density. A canine model. Spine. 1991;16(6 Suppl):S190–7.
45. Shirado O, Zdeblick TA, McAfee PC, Cunningham BW, DeGroot H, Warden KE. Quantitative histologic study of the influence of anterior spinal instrumentation and biodegradable polymer on lumbar interbody fusion after corpectomy. A canine model. Spine. 1992;17(7):795–803.
46. Kanayama M, Cunningham BW, Haggerty CJ, Abumi K, Kaneda K, McAfee PC. In vitro biomechanical investigation of the stability and stress-shielding effect of lumbar interbody fusion devices. J Neurosurg. 2000;93:259–65.
47. Hodgson AR, Stock FE. Anterior spinal fusion. Br J Surg. 1956;44:226–75.
48. Hodgson AR, Stock FE. Anterior spine fusion for the treatment of tuberculosis of the spine. J Bone Joint Surg. 1960;42:295–310.
49. Harmon PH. Anterior excision and vertebral body fusion operation for intervertebral disc syndromes of the lower lumbar spine. Clin Orthop Relat Res. 1963;26:107–27.
50. Sacks S. Anterior interbody fusion of the lumbar spine. J Bone Joint Surg. 1965;47B:211–23.
51. O'Brien JP, Dawson MH, Heard CW. Simultaneous combined anterior and posterior fusion. Clin Orthop Relat Res. 1986;203:191–5.
52. Lowery G, Kulkarni S, Pennisi AE. Use of autologous growth factors in lumbar spinal fusion. Bone. 1999;25:47S–50S.
53. Brantigan JW, Steffee AD, Lewis ML, Quinn LM, Persenaire JM. Lumbar interbody fusion using the Brantigan I/F cage for PLIF and the VSP pedicle screw system: two year results of a Food and Drug Administration IDE clinical trial. In: Intersomatique du Rachis Lumbaire. 1996.
54. Hashimoto T, Shigenobu K, Kanayama M, Harada M, Oha F, Ohkoshi Y, et al. Clinical results of single-level posterior lumbar interbody fusion using the Brantigan I/F carbon cage filled with a mixture of local morselized bone and bioactive ceramic granules. Spine. 2002;27:258–62.
55. Molinari RW, Gerlinger T. Functional outcomes of instrumented posterior lumbar interbody fusion in active-duty US servicemen: a comparison with nonoperative management. Spine J. 2001;1:215–24.
56. Ciccone WJ, Motz C, Bentley C, Tasto JP. Bioabsorbable implants in orthopaedics: new developments and clinical applications. J Am Acad Orthop Surg. 2001;9:280–8.
57. Bergsma JE, de Bruijn WC, Rozema FR, Bos RRM, Boering G. Late degradation tissue response to poly (L-lactide) bone plates and screws. Biomaterials. 1995;16:25–31.

58. Bergsma JE, Rozema FR, Bos RRM, de Bruijn WC. Foreign body reactions to resorbable poly (L-lactide) bone plates and screws used for the fixation of unstable zygomatic fractures. J Oral Maxillofac Surg. 1993;51:666–70.
59. Bostman O, Hirvensalo E, Makinen J, Rokkanen P. Foreign-body reactions to fracture fixation implants of biodegradable synthetic polymers. J Bone Joint Surg. 1990;72:592–6.
60. Tegnander A, Engebretsen L, Bergh K, Eide E, Holen KJ, Iversen OJ. Activation of the complement system and adverse effects of biodegradable pins of polylactic acid (Biofix) in osteochondritis dissecans. Acta Orthop Scand. 1994;65:472–5.
61. Christel P, Chabot F, Leray JL, Morin C, Vert M. Biodegradable composites for internal fixation. Biomaterials. New York: Wiley; 1980. p. 271–80.
62. Cutright DE, Hunsuck EE. The repair of fractures of the orbital floor using biodegradable polylactic acid. Oral Surg. 1972;33:28–34.
63. Miller RA, Brady JM, Cutright DE. Degradation rates of oral resorbable implants: rate modification with changes in PLA/PGA copolymer ratios. J Biomed Mater Res. 1977;11:711–9.
64. Cutright DE, Hunsuck EE. Tissue reaction to the biodegradable polylactic acid suture. Oral Surg Oral Med Oral Pathol. 1971;31:134.
65. Van der Elst M, Klein CP, Blieck-Hogervorst JM, Patka P, Haarman HJ. Bone tissue response to biodegradable polymers used for intramedullary fracture fixation: a long-term in vivo study in sheep femora. Biomaterials. 1999;20:121.
66. Hollinger JO, Battistone GC. Biodegradable bone repair materials. Synthetic polymers and ceramics. Clin Orthop Relat Res. 1986;207:290.
67. Vert M, Christel P, Chabot F, Leray J. Bioresorbable plastic materials for bone surgery. In: Hastings GW, Ducheyne P, editors. Macromolecular biomaterials. Boca Raton: CRC Press; 1984. p. 119–42.
68. Kulkarni RK, Pani KC, Neuman C, Leonard F. Polylactic acid for surgical implants. Arch Surg. 1966;93:839.
69. Bucholz RW, Henry S, Henley MB. Fixation with bioabsorbable screws for the treatment of fractures of the ankle. J Bone Joint Surg. 1994;76:319–24.
70. Caborn DNM, Coen M, Neef R, Hamilton D, Nyland J, Johnson DL. Quadrupled semitendinous-gracilis autograft fixation in the femoral tunnel: a comparison between a metal and a bioabsorbable interference screw. Arthroscopy. 1998;14:241–5.
71. Cohen B, Tasto J. Meniscal arrow. Tech Orthop. 1998;13:164–9.
72. Cordewener FW, Bos RR, Rozema FR, Houtman WA. Poly(L-lactide) implants for repair of human orbital floor defects: clinical and magnetic resonance imaging evaluation of long-term results. J Oral Maxillofac Surg. 1996;54:9–13.
73. Warme WJ, Arciero RA, Savoie FHI, Uhorchak JM, Walton M. Nonabsorbable versus absorbable suture anchors for open Bankart repair: a prospective, randomized comparison. Am J Sports Med. 1999;27:742–6.
74. Kandziora F, Pflugmacher R, Kleemann R, Duda G, Wise DL, Trantolo DJ, et al. Biomechanical analysis of biodegradable interbody fusion cages augmented with poly(propylene glycol-co-fumaric acid). Spine. 2002;27(15):1644–51.
75. Toth JM, Estes BT, Wang M, Seim HB 3rd, Scifert JL, Turner AS, et al. Evaluation of 70/30 poly (L-lactide-co-D,L-lactide) for use as a resorbable interbody fusion cage. J Neurosurg. 2002;97(4 Suppl):423–32.
76. Hollister SJ. Porous scaffold design for tissue engineering. Nat Mater. 2005;4(7):518–24.
77. Bensoussan A, Lions JL, Papanicolaou G. Asymptotic analysis for periodic structures. Amsterdam: North-Holland Pub. Co sole distributors for the U.S.A. and Canada, Elsevier North-Holland; 1978.. xxiv, 700 p
78. Sanchez-Palencia E, Zaoui A, CISM International Center for Mechanical Sciences. In: Homogenization techniques for composite media: lectures delivered at the CISM International Center for Mechanical Sciences, Udine, Italy, July 1–5, 1985. Berlin: Springer; 1987. ix, 397 p.

79. Hollister SJ, Maddox RD, Taboas JM. Optimal design and fabrication of scaffolds to mimic tissue properties and satisfy biological constraints. Biomaterials. 2002;23(20):4095–103.
80. Bendsoe MP, Kikuchi N. Generating optimal topologies in structural design using a homogenization method. Comput Methods Appl Mech. 1988;71(2):197–224.
81. Sigmund O. Tailoring materials for specific needs. J Intel Mater Syst Struct. 1994;5(6):736–42.
82. Sigmund O. Tailoring materials with prescribed elastic properties. Mech Mater. 1995;20(4):351–68.
83. Lin CY, Kikuchi N, Hollister SJ. A novel method for biomaterial scaffold internal architecture design to match bone elastic properties with desired porosity. J Biomech. 2004;37(5):623–36.
84. Hollister SJ, Lin CY. Computational design of tissue engineering scaffolds. Comput Methods Appl Mech. 2007;196(31–32):2991–8.
85. Guest JK, Prevost JH. Optimizing multifunctional materials: design of microstructures for maximized stiffness and fluid permeability. Int J Solids Struct. 2006;43(22–23):7028–47.
86. de Kruijf N, Zhou SW, Li Q, Mai YW. Topological design of structures and composite materials with multiobjectives. Int J Solids Struct. 2007;44(22–23):7092–109.
87. Challis VJ, Roberts AP, Wilkins AH. Design of three dimensional isotropic microstructures for maximized stiffness and conductivity. Int J Solids Struct. 2008;45(14–15):4130–46.
88. Kemppainen JM, Hollister SJ. Differential effects of designed scaffold permeability on chondrogenesis by chondrocytes and bone marrow stromal cells. Biomaterials. 2010;31(2):279–87.
89. Bendsoe MP, Sigmund O. Material interpolation schemes in topology optimization. Arch Appl Mech. 1999;69(9–10):635–54.
90. Sigmund O, Petersson J. Numerical instabilities in topology optimization: a survey on procedures dealing with checkerboards, mesh-dependencies and local minima. Struct Optimiz. 1998;16(1):68–75.
91. Sigmund O. Design of material structures using topology optimization. Technical University of Denmark; 1994.
92. Svanberg K. The method of moving asymptotes—a new method for structural optimization. Int J Numer Methods Eng. 1987;24(2):359–73.
93. Hollister SJ, Liao EE, Moffitt EN, Jeong CG, Kemppainen JM. Defining design targets for tissue engineering scaffolds. Berlin: Springer; 2009. p. 521–37.
94. Thomson RC, Yaszemski MJ, Powers JM, Mikos AG. Fabrication of biodegradable polymer scaffolds to engineer trabecular bone. J Biomater Sci Polym Ed. 1995;7(1):23–38.
95. Hutmacher DW. Scaffold design and fabrication technologies for engineering tissues—state of the art and future perspectives. J Biomater Sci Polym Ed. 2001;12(1):107–24.
96. Simmons CA, Meguid SA, Pilliar RM. Differences in osseointegration rate due to implant surface geometry can be explained by local tissue strains. J Orthopaed Res. 2001;19(2):187–94.
97. Malda J, Woodfield TBF, van der Vloodt F, Kooy FK, Martens DE, Tramper J, et al. The effect of PEGT/PBT scaffold architecture on oxygen gradients in tissue engineered cartilaginous constructs. Biomaterials. 2004;25(26):5773–80.
98. Malda J, Martens DE, Tramper J, van Blitterswijk CA, Riesle J. Cartilage tissue engineering: controversy in the effect of oxygen. Crit Rev Biotechnol. 2003;23(3):175–94.
99. Guest JK, Prevost JH, Belytschko T. Achieving minimum length scale in topology optimization using nodal design variables and projection functions. Int J Numer Methods Eng. 2004;61(2):238–54.
100. Wang MY, Zhou S, Ding H. Nonlinear diffusions in topology optimization. Struct Multidiscip Optim. 2004;28(4):262–76.
101. Adachi T, Osako Y, Tanaka M, Hojo M, Hollister SJ. Framework for optimal design of porous scaffold microstructure by computational simulation of bone regeneration. Biomaterials. 2006;27(21):3964–72.
102. Anderson ARA, Chaplain MAJ. A mathematical model for capillary network formation in the absence of endothelial cell proliferation. Appl Math Lett. 1998;11(3):109–14.
103. Hollister SJ, Lin C-Y, Kang H, Adachi T. Computational design and simulation of tissue engineering scaffolds; 2008. p. 113–27. https://link.springer.com/chapter/10.1007/978-0-387-68831-2_6.